CONTRIBUTING FACTORS TO RENAL DYSFUNCTION: FETAL PROGRAMMING, HORMONES AND EPIGENETIC

EDITED BY: Guiomar Nascimento Gomes, Minolfa C. Prieto, Karina Thieme and H. Della Coletta Francescato

PUBLISHED IN: Frontiers in Physiology

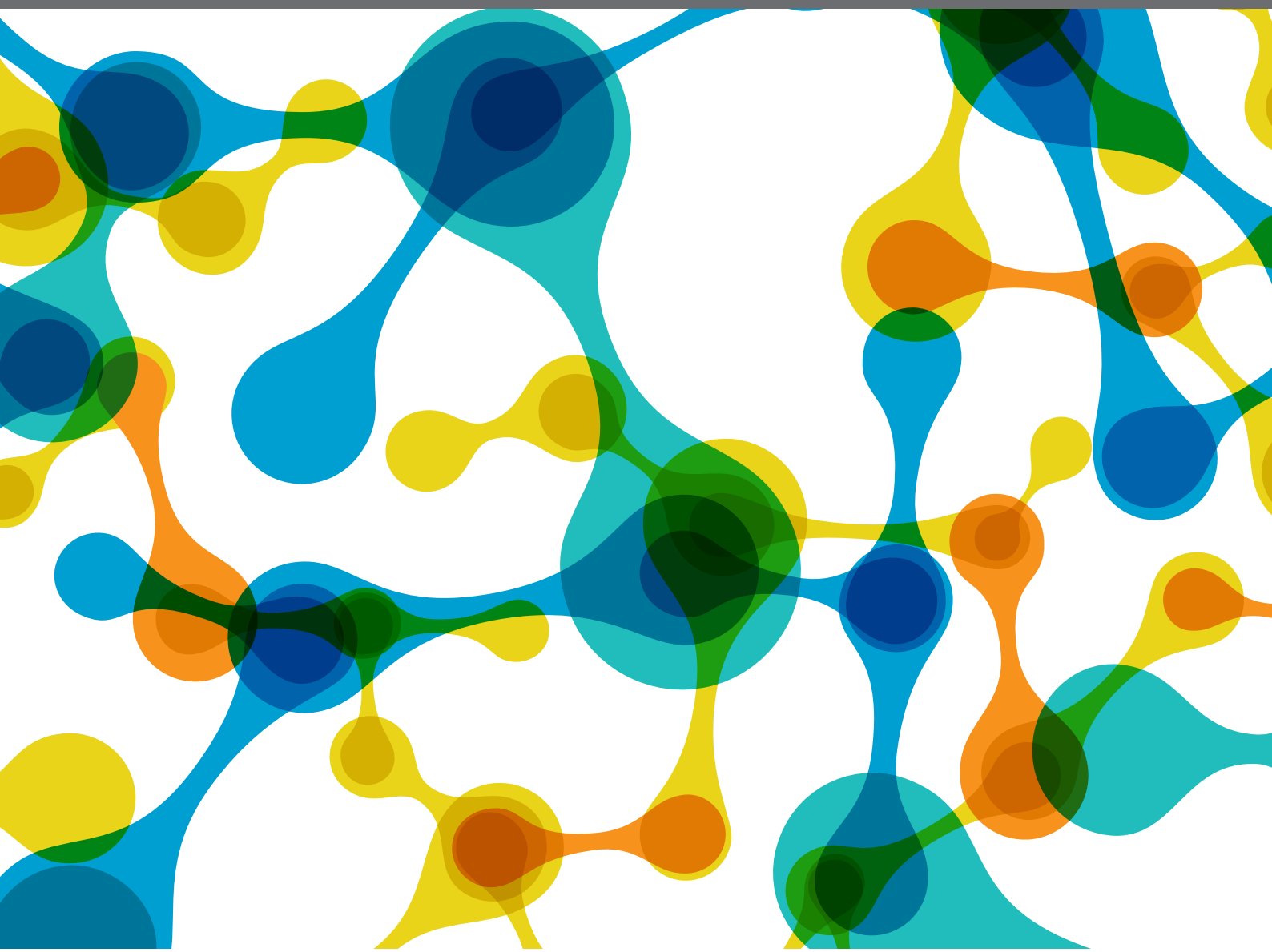

frontiers Research Topics

frontiers

ISSN 1664-8714
ISBN 978-2-88974-130-4
DOI 10.3389/978-2-88974-130-4

About Frontiers

Frontiers is more than just an open-access publisher of scholarly articles: it is a pioneering approach to the world of academia, radically improving the way scholarly research is managed. The grand vision of Frontiers is a world where all people have an equal opportunity to seek, share and generate knowledge. Frontiers provides immediate and permanent online open access to all its publications, but this alone is not enough to realize our grand goals.

Frontiers Journal Series

The Frontiers Journal Series is a multi-tier and interdisciplinary set of open-access, online journals, promising a paradigm shift from the current review, selection and dissemination processes in academic publishing. All Frontiers journals are driven by researchers for researchers; therefore, they constitute a service to the scholarly community. At the same time, the Frontiers Journal Series operates on a revolutionary invention, the tiered publishing system, initially addressing specific communities of scholars, and gradually climbing up to broader public understanding, thus serving the interests of the lay society, too.

Dedication to Quality

Each Frontiers article is a landmark of the highest quality, thanks to genuinely collaborative interactions between authors and review editors, who include some of the world's best academicians. Research must be certified by peers before entering a stream of knowledge that may eventually reach the public - and shape society; therefore, Frontiers only applies the most rigorous and unbiased reviews.
Frontiers revolutionizes research publishing by freely delivering the most outstanding research, evaluated with no bias from both the academic and social point of view. By applying the most advanced information technologies, Frontiers is catapulting scholarly publishing into a new generation.

What are Frontiers Research Topics?

Frontiers Research Topics are very popular trademarks of the Frontiers Journals Series: they are collections of at least ten articles, all centered on a particular subject. With their unique mix of varied contributions from Original Research to Review Articles, Frontiers Research Topics unify the most influential researchers, the latest key findings and historical advances in a hot research area! Find out more on how to host your own Frontiers Research Topic or contribute to one as an author by contacting the Frontiers Editorial Office: frontiersin.org/about/contact

CONTRIBUTING FACTORS TO RENAL DYSFUNCTION: FETAL PROGRAMMING, HORMONES AND EPIGENETIC

Topic Editors:
Guiomar Nascimento Gomes, Federal University of São Paulo, Brazil
Minolfa C. Prieto, Tulane University, United States
Karina Thieme, University of São Paulo, Brazil
H. Della Coletta Francescato, University of São Paulo, Brazil

Citation: Gomes, G. N., Prieto, M. C., Thieme, K., Francescato, H. D. C., eds. (2022). Contributing Factors to Renal Dysfunction: Fetal Programming, Hormones and Epigenetic. Lausanne: Frontiers Media SA. doi: 10.3389/978-2-88974-130-4

Table of Contents

frontiers in Physiology

EDITORIAL
published: 06 December 2021
doi: 10.3389/fphys.2021.793730

Editorial: Contributing Factors to Renal Dysfunction: Fetal Programming, Hormones, and Epigenetic

Guiomar Nascimento Gomes[1]*, *Minolfa C. Prieto*[2], *Karina Thieme*[3] and *Heloisa Della Coletta Francescato*[4]

[1] Department of Physiology, Federal University of São Paulo, São Paulo, Brazil, [2] Department of Physiology, Tulane University School of Medicine, New Orleans, LA, United States, [3] Department of Physiology and Biophysics, University of São Paulo, São Paulo, Brazil, [4] Department of Physiology, Faculty of Medicine of Ribeirão Preto, University of São Paulo, Ribeirao Preto, Brazil

Keywords: fetal programming, renal dysfunction, miRNA—microRNA, renin–angiotensin–aldosterone system, renal fibrosis

Editorial on the Research Topic

Contributing Factors to Renal Dysfunction: Fetal Programming, Hormones, and Epigenetic

Over the past few decades, many advances led to a better understanding of the mechanisms involved in renal development and function. Even so, kidney disease is still one of the most prevalent complications in chronic conditions, including cardiovascular diseases, diabetes, and obesity. Thus, it is timely and essential to deepen knowledge about the underlying factors predisposing to renal dysfunction, such as fetal programming, epigenetic, hormonal, or nutritional interferences.

Recently, the interest in the link between *in utero* fetal stressors, epigenetics, and the risk of later in life diseases has surged. Evidence have demonstrated that early *in utero* maladaptation may have repercussion on health outcomes in adulthood. However, most of the involved mechanisms remain unclear, and developments are underway.

In this collection, an extensive review of recent evidence and discoveries highlighting contemporary understanding of this intriguing and sometimes controversial relationship.

The appraisal of fetal programming is introduced through the review article: "Programmed kidney disease in adults: importance of the fetal environment" (Argeri et al.). The authors describe the impact of adverse conditions during pregnancy on the fetal kidneys, focusing on the mechanisms underlying epigenetic events, and the components/functions of the renin–angiotensin–aldosterone system (RAAS). Still, in the field of fetal programming, Barros Sene et al. present the role of specific miRNAs involved in molecular modulations during nephrogenesis. The kidneys from low-protein-intake offspring on the 17th gestational day reveal changes in miRNAs and the molecular pathways, reducing the reciprocal interaction between the metanephric cap and the ureter bud. Additionally, the renal structural and functional modifications found in the fetal programming model of protein restriction during gestation and lactation are detailed (Lamana et al.).

Epigenetics was also explored in its relationship with the role of extracellular vesicles in the context of tuberous sclerosis complex (TSC) disease. Tuberous sclerosis complex-associated renal phenotypes show considerable variability, adding another layer of complexity to the diagnosis and proper treatment. Thus, studying other mechanisms associated with this disease pathogenesis

OPEN ACCESS

Edited and reviewed by:
Carolyn Mary Ecelbarger, Georgetown University, United States

***Correspondence:**
Guiomar Nascimento Gomes
guiomar.gomes@unifesp.br

Specialty section:
This article was submitted to Renal and Epithelial Physiology, a section of the journal Frontiers in Physiology

Received: *12 October 2021*
Accepted: *16 November 2021*
Published: *06 December 2021*

Citation:
Gomes GN, Prieto MC, Thieme K and Francescato HDC (2021) Editorial: Contributing Factors to Renal Dysfunction: Fetal Programming, Hormones, and Epigenetic. Front. Physiol. 12:793730. doi: 10.3389/fphys.2021.793730

also offers new therapeutic avenues. In this sense, using mouse inner medullary collecting duct (mIMCD) cells with the Tsc1 (T1G cells) or Tsc2 (T2J cells) gene disrupted by CRISPR/CAS9 Kumar et al. demonstrated that miR-212-3p/mTORC1 and mIR-99a-5p/mTORC1 axis could be a novel therapeutic target or biomarker for TSC.

Besides epigenetics, new genetic and molecular aspects involved in the development of kidney disease are also discussed in this special issue. Epithelial–mesenchymal transition (EMT) is essential for the progression of kidney fibrosis. However, tubular epithelial cells (TEC) can first undergo partial EMT, secreting chemokines and cytokines to promote fibrogenesis and inflammation, leading to kidney fibrosis. The review by Sheng and Zhuang emphasizes the most recent findings related to the process of "partial epithelial–mesenchymal transition (pEMT)" and its contribution to renal fibrogenesis, including cell cycle arrest, metabolic alternation of epithelial cells, infiltration of immune cells, epigenetic regulation, as well as new signaling pathways that mediate this altered epithelial–mesenchymal communication. Furthermore, the participation of the transcription factor Tisp40 in the process of the TEC pyroptosis after the renal ischemia-reperfusion injury is detailed by Xiao et al. Likewise, Li et al. showed that α-lipoic acid acts as a protective molecule in folic acid-induced kidney damage, reducing tubular cell death mainly by inhibiting ferropotosis.

Acute crystalline nephropathy is usually associated with damage to the tubulointerstitial compartment. Few studies have investigated glomerular injuries in this condition. De Araújo et al. unveil aspects of glomerular and tubulointerstitial injury in an experimental model of crystalline-induced acute kidney injury, with kidney function decline and reduction in podocyte markers, nephrin, and WT1, possibly leading to a podocyte loss.

The role of renal sympathetic nerves in hypertension has been explored in the last decades. However, the role of the renal afferent innervation is still poorly understood. In a well-designed study, the role of renal afferent nerves on GABAergic signaling on the paraventricular nucleus of the hypothalamus (PVN) was investigated in the 2-kidney 1-clip (2K1C) renovascular hypertensive rat model (Milanez et al.). The selective removal of renal sensory innervation enhanced GABAergic inputs into the PVN, which may have contributed to the decrease in blood pressure and sympathetic excitation, as well as improvement in renal function and proteinuria, as indicated previously.

Addressing the use of angiotensin-converting enzyme inhibitor or angiotensin receptor blocker, alone or in combination in arterial hypertension, a significant antiproteinuric effect in hypertensive individuals was observed. To better understand this effect, Corrêa et al. evaluated in 2K1C rats the result of the RAAS double blockade on the expression of filtration barrier components as well as components involved in proximal protein transport. The double blockade restored the expression of podocin, cubillum, and ClC5, likely related to the antiproteinuric effect. On the other hand, the double blockade of the RAAS, due to an exacerbated negative regulation of the active form of the alpha epithelial sodium channel (α-ENaC), lead to hyperkaliemia.

The role of AT1R-associated protein (ATRAP) on potassium transport in distal nephron was explored by Polidoro et al. This protein attenuates the inhibition of ROMK channels by angiotensin II in collecting duct cells, probably by decreasing c-Src activation and blocking ROMK internalization.

In sum, chronic kidney disease (CKD) is a worldwide public health problem with an increasing prevalence. Studies directed to understand better the events related to CKD are imperative with the development of strategies to minimize the progression of this disease. In this way, the present collection of articles brings relevant contributions to molecular and epigenetic mechanisms modulating nephrogenesis under the influence of the intrauterine environment and recent advances related to the pathophysiology of renal fibrosis. Also, the emergent experimental strategies carry a better understanding and in the management of arterial hypertension.

AUTHOR CONTRIBUTIONS

All listed authors contributed equally to the elaboration of the manuscript and approved its final format for publication.

ACKNOWLEDGMENTS

We thank to all authors who contributed to this Research Topic and the reviewers who indisputably helped to elaborate on this Research Topic.

Conflict of Interest: The authors declare that the research was conducted in the absence of any commercial or financial relationships that could be construed as a potential conflict of interest.

Publisher's Note: All claims expressed in this article are solely those of the authors and do not necessarily represent those of their affiliated organizations, or those of the publisher, the editors and the reviewers. Any product that may be evaluated in this article, or claim that may be made by its manufacturer, is not guaranteed or endorsed by the publisher.

frontiers in Physiology

ORIGINAL RESEARCH
published: 13 August 2020
doi: 10.3389/fphys.2020.00906

Tisp40 Induces Tubular Epithelial Cell GSDMD-Mediated Pyroptosis in Renal Ischemia-Reperfusion Injury via NF-κB Signaling

Chengcheng Xiao[1†], Haijun Zhao[1], Hai Zhu[1], Yingyu Zhang[2], Qiuju Su[2], Feng Zhao[1] and Renhe Wang[2†]*

[1] Department of Urology, Qingdao Municipal Hospital, Qingdao University, Qingdao, China, [2] Department of Traditional Chinese Medicine, Qingdao Municipal Hospital, Qingdao University, Qingdao, China

Renal ischemia-reperfusion injury (IRI) is a major cause of acute kidney injury (AKI). As a transcription factor, the Transcript induced in spermiogenesis 40 (Tisp40) has been found to be involved in renal IRI. However, the role of Tisp40 in tubular epithelial cell (TEC) pyroptosis of renal IRI remains unknown. In this study, we investigated effects of Tisp40 on Gasdermin D (GSDMD)-mediated TEC pyroptosis in renal IRI and underlying molecular mechanisms in I/R-induced kidney by hematoxylin and eosin (HE) staining, Terminal deoxynucleotidyl transferase dUTP nick-end labeling (TUNEL) assay,immunohistochemistry (IHC), reverse transcription-quantitative PCR (RT-qPCR) and western blot analysis *in vivo* and oxygen-glucose deprivation/reoxygenation (OGD/R)-stimulated TCMK-1 cells by lactate dehydrogenase (LDH) release assay, CCK-8 assay,enzyme-linked immunosorbent assay (ELISA), flow cytometric analysis, immunofluorescence staining,RT-qPCRand western blot analysis *in vitro*. We found that the levels of Tisp40 and GSDMD-N expression increased gradually, and peaked at 30 min ischemia/24 h reperfusion *in vivo* and 24 h OGD/R/6 h reoxygenation *in vitro*, simultaneously, the levels of TEC pyroptosis and renal injury were correspondingly increased. The data of Pearson's correlation analysis showed that the expression of Tisp40 and GSDMD-N was positively correlated. Furthermore, Tisp40 overexpression aggravated TEC pyroptosis rate and increased the expressions of related proteins, including GSDMD-N, NLRP3, caspase-1, IL-1β, and IL-18 in the OGD/R-stimulated TCMK-1 cell line, whereas the opposite occurred in cells treated with small interfeing RNA (siRNA) targeting Tisp40. Tisp40-deficient mice showed attenuated renal IRI and pyroptosis compared with wild-type mice. In addition, Tisp40 knockout remarkably decreased the levels of GSDMD-N, IL-1β, IL-18, NLRP3, and caspase-1 expression, and alleviated renal pyroptosis induced by I/R. Importantly, Tisp40 overexpression significantly increased TECs pyroptosis via p-p65 activation, however, the effects of Tisp40 overexpression were partially blocked by parthenolide (PTL). Collectively, our findings provide insight into the mechanism of how Tisp40 regulated GSDMD-mediated pyroptosis in renal IRI.

Keywords: renal ischemia-reperfusion injury, Tisp40, pyroptosis, tubular epithelial cell, NF-κB signaling

OPEN ACCESS

Edited by:
Karina Thieme,
University of São Paulo, Brazil

Reviewed by:
Tao-Tao Tang,
Zhongda Hospital Southeast University, China
Qingjun Pan,
Affiliated Hospital of Guangdong Medical College Hospital, China

***Correspondence:**
Renhe Wang
doc_wangrh@163.com

† These authors have contributed equally to this work

Specialty section:
This article was submitted to Renal and Epithelial Physiology, a section of the journal Frontiers in Physiology

Received: *07 May 2020*
Accepted: *06 July 2020*
Published: *13 August 2020*

Citation:
Xiao C, Zhao H, Zhu H, Zhang Y, Su Q, Zhao F and Wang R (2020) Tisp40 Induces Tubular Epithelial Cell GSDMD-Mediated Pyroptosis in Renal Ischemia-Reperfusion Injury via NF-κB Signaling. Front. Physiol. 11:906. doi: 10.3389/fphys.2020.00906

INTRODUCTION

Acute kidney injury (AKI) is a common complication in clinical inpatients and shows a morbidity and mortality of approximately 5% and 50–80%, respectively. (Gill et al., 2005; Perico and Remuzzi, 2015). Approximately 2 million patients die from ischemic AKI every year worldwide (Tao et al., 2013). Continuous inflammatory stimulation of the tubule interstitium significantly increases the risk of chronic kidney disease (CKD) and end-stage renal disease (ESRD) in surviving patients (Chawla et al., 2014). Currently, no effective prevention or cure measures for AKI have been established in clinical practice (Arai et al., 2016). Renal ischemia-reperfusion injury (IRI) is one of the main causes of AKI (Jha et al., 2013) and is secondary to various clinical conditions, including kidney transplantation, cardiopulmonary and aortic aneurysm surgeries, severe hemorrhagic shock, and endotoxin sepsis (Gill et al., 2005; Bastin et al., 2013; Noh et al., 2015). Tubular epithelial cells (TECs) are likely injured by high metabolic activity and hypoxia (Al-Bataineh et al., 2016). Determining the underlying mechanism of TEC injury is critical for better understanding the progression of renal IRI and preventing AKI and its evolution to CKD and ESRD.

As a form of programmed cell death, pyroptosis is characterized by excessive cell death and inflammation (Miao et al., 2010). Gasdermin D (GSDMD) is a key downstream effector in cell pyroptosis (Kovacs and Miao, 2017). It forms pores in the plasma membrane that ultimately cause cell swelling, membrane lysis, and inflammatory cytokines release (Shi et al., 2015). GSDMD-mediated pyroptosis of renal TECs is an essential process in renal ischemia-reperfusion (I/R) injury (Diao et al., 2019; Tajima et al., 2019; Liu et al., 2020). Thus, studies are needed to determine the biological networks involved in GSDMD-mediated pyroptosis in TEC injury induced by renal IR.

The transcript induced in spermiogenesis 40 (Tisp40), also named CREB3L4, AIbZIP, and ATCE1, belongs to the CREB/ATF family (Velpula et al., 2012). As a transcription factor, Tisp40 is involved in initiation of the transcription of multiple genes by binding to various response elements, such as the CRE response element, nuclear factor (NF)-κB response element, and unfolded protein response element (Asada et al., 2011). Tisp40 has been reported to be involved in the pathogenesis of renal IRI, and Tisp40 deficiency inhibits and delays IRI (Qin et al., 2017, 2018; Xiao et al., 2017). In this study, we further investigated the potential molecular mechanism of Tisp40 and whether it is involved in regulating TEC pyroptosis in renal IRI.

MATERIALS AND METHODS

Animals and Surgical Protocols

All surgical procedures were conducted according to the Guide for the Care and Use of Laboratory Animals and approved by the Institutional Animal Care and Use Committee of Qingdao Municipal Hospital. C57BL/6 mice (Male, 8 week-old, 20–25 g) were purchased from Beijing Huafukang bioscience Co., Inc (Beijing, China). Tisp40-knockout mice (RIKEN BioResource Center, Stock NO. RBRC01942) with a C57BL/6 background had been described previously (Xiao et al., 2017). According to random number table, the mice were assigned into four groups: (1) wild-type sham-operated; (2) Tisp40-knockout sham-operated; (3) wild-type renal I/R; and (4) Tisp40-knockout renal I/R (n = 6 per group). The mice were intraperitoneally anesthetized with 2% sodium phenobarbital (50 mg/kg). The mice, whose desired depth of surgical anesthesia were judged by loss of righting reflex, were bedded onto a homeothermic table to keep a rectal temperature of 38°C approximately. Bilateral pedicles were exposed entirely, and ischemia was induced by pedicels clamping. After 30 min, the clips were removed, and kidneys were collected after 0, 6, 12, 24, and 48 h of reperfusion. The sham animals were subjected to above operation without pedicels clamping. After experiment, the mice were sacrificed by pentobarbital sodium overdose. The left kidneys were removed, and then snap-frozen in liquid nitrogen and stored at −80°C or fixed in 4% paraformaldehyde for biochemical analysis and pathological evaluation.

Cell Culture

TCMK-1 cells (no. CCL-139) were purchased from American Type Culture Collection. A total of 1.5×10^6 cells/ml cells for group comparison was cultured in complete medium under a 95% air and 5% CO_2 condition. Cells in OGD/R groups were stimulated with glucose-free medium under hypoxic conditions for 24 h. Then the cells were cultured in complete medium under normal conditions for 0, 2, 4, 6, and 8 h. To knockdown Tisp40, cells were intervened with siRNA-Tisp40 (100 nM, forward, 5′-AGUAGAAGUUGGCCACUUCCAUGGG-3′, reverse, 5′-CCCAUGGAAGUGGCCAACUUCUACU-3′), whose inhibitory effect had been confirmed previously (Xiao et al., 2017) or a scrambled siRNA (forward, 5′-CCUACGCCACCAAUUUCGUdTdT-3′, reverse, 5′-ACGAAAU UGGUGGCGUAGGdTdT-3′) for 12 h using Lipofectamine RNA iMAX (Invitrogen).

Establishment of Tisp40-Overexpression Cell Line

TCMK-1/Tisp40 (Tisp40-overexpression group) and TCMK-1/vector (empty vector group) cells were obtained as described previously (Xiao et al., 2017). In brief, pUC57-Tisp40 and pLVX-mCMV-ZsGreen-IRES-Puro (Wuhan Viral therapy Technologies Co., Ltd.) were digested by EcoRI and SpeI (NEB), and the products were connected by T4 DNA Ligase (BM121, Transgen BioTech). Then, an Agarose Gel Extraction Kit (D2500, Omega) was used to retrieve fragments. JM109 (Wuhan Viral therapy Technologies Co., Ltd.), which was transfected with the ligation product, was inoculated and amplificated, and the sequencing primer CMV-F, whose primer sequence is 5′-CGCAAATGGGCGGTAGGCGTG-3′, was used to verify the bacterial fluid. rLV-Tisp40 and rLV-ShRNA2 containing the target gene was obtained in 293T cells co-transfected with recombinant plasmid or control plasmid using a Lentiviral Packaging Kit (R003, Wuhan Viral therapy Technologies Co., Ltd.). TCMK-1 cells were transfected with

rLV-Tisp40 and rLV-ShRNA2 on the basis of MOI = 20. Two days after transfection, lentivirus-infected TCMK-1 cells were cultured normally.

HE Staining

Four percent paraformaldehyde was used to fix kidney tissues. The fixed tissues were paraffin embedded and cut into 5-μm-thick sections. Sections were stained using hematoxylin and eosin (HE Kit; Beyotime), according to Kit instructions. Five images were randomly selected under a microscope (×400) to analyze pathological changes. Tubule injury scores were referred to the percentage of tubules affected as follows: 0 ≤ 10%, 1 = 10–25%, 2 = 26–50%, 3 = 51–75%, and 4 ≥ 75%.

Terminal Deoxynucleotidyl Transferase dUTP Nick-End Labeling (TUNEL) Assay

A total of 5 μm thick sections were stained using a TUNEL kit (Roche). The brown stained cell nuclei were identified as Tunel-positive. Five images were randomly selected under a microscope (×400) to analyze cell apoptosis level. The numbers of the TUNEL-positive TECs in the five fields of renal cortex region for each section were counted at ×400 magnification.

CCK-8 Assay

Cell viability was measured using a CCK-8 assay kit (C0038, Beyotime) according to the manufacturer's instructions. The absorbance at 450 nm was measured using a microplate reader (Molecular Devices).

Lactate Dehydrogenase (LDH) Release Assay

The cells were inoculated into 96-well plates and the culture supernatants were collected. Then, the levels of LDH release were examined using a LDH release assay kit (Beyotime) following the instructions. The absorbance at 495 nm was measured using a microplate reader.

Reverse Transcription-Quantitative PCR (RT-qPCR)

Total RNA from renal samples and TCMK-1 cells were isolated with TRIzol reagent (Invitrogen). Then Revert Aid First Strand cDNA Synthesis kit (cat. no. K1622; Invitrogen) was used to quantify total RNA and reverse transcribe into cDNA, according to the manufacturer's instructions. The real-time quantitative PCR for β-actin, Tisp40, NLRP3 and caspase-1 were carried out using the following primers to amplify genes:Tisp40 forward, 5′- TACCTGAAGCCCCAACTACAAA -3′ and reverse, 5′- GTGCCCTGCCACATGATAAA -3′; NLRP3 forward, 5′- ATGCTGCTTCGACATCTCCT -3′ and reverse, 5′- AACCAATGCGAGATCCTGAC -3′; caspase-1 forward, 5′- CACAGCTCTGGAGATGGTGA -3′ and reverse, 5′- TCTTTCAAGCTTGGGCACTT -3′; β-actin forward, 5′- CTGAGAGGGAAATCGTGCGT-3′ and reverse, 5′- CCACAGGATTCCATACCCAAGA-3′. The relative mRNA expression levels were determined using the 2-ΔΔCq method (Livak and Schmittgen, 2001).

Enzyme-Linked Immunosorbent Assay (ELISA)

The levels of Interleukin (IL)-1β and IL-18 expression in the medium were detected using IL-1β and IL-18 ELISA kits (IL-1β, cat. no.ab197742; IL-18, cat. no.ab216165, Abcam), according to the manufacturer's instructions. The absorbance at 495 nm was measured using a microplate reader, and ELISA signal was read with a plate reader.

Flow Cytometric Analysis of Apoptosis

After treatment, the cells were stained with Annexin V, followed by an additional stain with propidium iodide using the Annexin V-FITC Apoptosis Detection kit (BD Biosciences). Subsequently, apoptotic cells were analyzed by flow cytometry (BD Biosciences).

Immunohistochemistry (IHC)

After deparaffinized and hydrated, the 5-μm-thick sections were blocked with 3% hydrogen peroxide. Then sections were treated with 10% normal goat serum (cat. no. 16210072; Gibco; Thermo Fisher Scientific, Inc.), and incubated overnight following antibodies targeting pro-IL-1β(1:100; cat no. ab205924), IL-1β(1:100;cat no. ab9722) and IL-18 (1:200; cat. no. ab71495). After that, sections were incubated with horseradish peroxidase (HRP)-conjugated goat anti-rabbit secondary antibodies (1:400; cat. no. A32731; Invitrogen). The slides were subsequently stained with DAB to develop the color. The images (magnification, ×400) were captured with a microscope. The percentage of area stained represents the ratio of the summed absolute areas of staining versus the total tissue.

Immunofluorescence Staining

Four percent paraformaldehyde were used to fix TCMK-1 cells, afterward which were permeabilized with 0.1% Triton X-100, followed by blocked in 10% donkey serum (Sigma-Aldrich). Next, the cells were incubated using following antibodies against GSDMD-N (1:200bs-14287R, Bioss) overnight. The cells were incubated with a secondary antibody (1:400; cat. no. A32731; Invitrogen). DAPI (Roche) was used to nuclei staining. The images (magnification, ×400) were captured with a fluorescent microscope (Leica).

Western Blotting

Proteins from kidney tissues or cultured TCMK-1 cells were extracted using a Nuclear-Cytosol Extraction Kit (KGP150, Nanjing KeyGen Biotech. Co., Ltd.). Total protein levels were quantified with a BCA assay kit (Invitrogen). The expressions of Tisp40, GSDMD-N, NLRP3, Caspase-1, p65,p-p65 and β-actin was measured. The membranes were incubated overnight with the following antibodies: anti-Tisp40 (1: 100; sc-54800; Santa), anti-GSDMD-N (1:100,bs-14287R, Bioss), anti-NLRP3 (1:200; cat. no. ab214185, Abcam), anti-Caspase-1 (1:200; cat. no. ab138483, Abcam), anti-p65 (1:200; cat. no. ab32536, Abcam), anti-p-p65 (1:200; cat. no. ab86299, Abcam) and β-actin (1:500; cat. no. ab8224, Abcam). Subsequently membranes were incubated with HRP-conjugated secondary antibodies (1:500; cat.

no. ab6789, Abcam). Protein bands were visualized and detected using Odyssey Infrared Imaging system Model 9120 (LI-COR Biotechnology).

Statistical Analysis

Statistical analysis was conducted using the SPSS version 22.0 software, and all data were presented as the mean ± standard deviation (SD). Linear correlation between variables was tested by pearson's correlation. All experiments were performed ≥3 times. Analysis of variance was used to evaluate statistical significance. *P*-values <0.05 was considered to show a statistically significant difference.

RESULTS

Tisp40 Was Closely Related to in GSDMD-Mediated Pyroptosis in I/R-Induced Kidney and OGD/R-Stimulated TECs

Our previous study showed that Tisp40 is upregulated in the kidney of I/R-induced mice (Xiao et al., 2017) and oxygen oxygen-glucose deprivation/reoxygenation (OGD/R)-induced TECs (Qin et al., 2017). To investigate if Tisp40 is involved in GSDMD-mediated TECs pyroptosis, samples were collected and assayed at 0, 6, 12, 24, or 48 h of reperfusion after 30 min of ischemia *in vivo*, and at 0, 2, 4, 6, and 8 h of reoxygenation after 24 h of OGD *in vitro*. As shown in **Figure 1A**, the loss of brush border detachment, interstitial congestion, and tubular cell death were aggravated, and TUNEL-positive TECs increased gradually with reperfusion time. At 30 min ischemia/24 h reperfusion, large numbers of renal tubules severely damaged, and most TECs were TUNEL-positive (**Figures 1B,C**). The expression of Tisp40 and GSDMD-N were evaluated in mice samples by western blotting, and Tisp40 was assessed using qRT-PCR. The results showed that Tisp40 and GSDMD-N expression increased gradually, peaked at 24 h, and was maintained until 48 h of reperfusion compared to the sham group (**Figures 1D–F,H**, $n = 6$ per group). As shown in **Figure 2A**, data from the CCK-8 assay demonstrated that OGD/R reduced the viability of TCMK-1 cells, which continuously decreased to approximately 40% at 6 h of reoxygenation and showing a significant difference compared to the Con group. OGD/R treatment stimulated significantly higher LDH release compared with the Con group; LDH release increased gradually over time, peaking at 6 h of reoxygenation in TCMK-1 cells (**Figure 2B**). Consistently in *in vivo* experiments, TCMK-1/wt cells treated with OGD/R also showed gradually elevated expression of Tisp40 and GSDMD-N, which peaked at 6 h and was maintained until 8 h of reperfusion compared to the Con group (**Figures 2C–E,G**, $n = 3$ per group). Furthermore, the data of pearson's correlation analysis showed that the expression of Tisp40 and GSDMD-N was positively correlated in I/R-induced kidney and OGD/R-stimulated TECs (**Figures 1G**, **2F**). These results indicate that Tisp40 is critical for GSDMD-mediated TEC pyroptosis.

Tisp40 Enhanced Inflammasome Activation and Inflammatory Factors Release in Cultured OGD/R-Stimulated TCMK-1 Cells

To further evaluate the functions of Tisp40 protein in pyroptosis, the effects of Tisp40 on NLRP3 inflammasome activation and IL-1β and IL-18 release were assessed in cultured OGD/R-stimulated TCMK-1 cells. A Tisp40-overexpressing cell line (TCMK-1/Tisp40) and si-Tisp40 were used to upregulate or downregulate Tisp40 *in vitro*, as described in our previous study (Xiao et al., 2017). Following treatment with OGD/R, LDH release increased significantly in cultured TCMK-1/Tisp40 cells compared to those in the control and empty vector groups (**Figure 3A**), but decreased significantly after Tisp40 silencing (**Figure 4A**). IL-1β and IL-18 were examined using ELISA, and NLRP3 and caspase-1 were measured using qPT-PCR and western blotting. Exposure of the cells to OGD/R resulted in an increase in the levels of IL-1β, IL-18, NLRP3, and caspase-1, which was aggravated by Tisp40 overexpression compared to that in the control and empty vector groups (**Figures 3B–H**), and relieved by Tisp40 silencing compared to that in the scramble group (**Figures 4B–H**). These results indicate that Tisp40 enhanced NLRP3 inflammasome activation and promoted the release of IL-1β and IL-18 in cultured OGD/R-stimulated TCMK-1 cells, supporting that Tisp40 is critical in pyroptosis of TECs.

Tisp40 Knockout Protects Against Inflammasome Activation and Inflammatory Factors Release in I/R-Induced Kidney

After determining the effects of Tisp40 on OGD/R-stimulated inflammasome activation and inflammatory factor release *in vitro*, we investigated the protective effect of Tisp40 deficiency on NLRP3 inflammasome activation and release of IL-1β and IL-18 using Tisp40-knockout ($Tisp40^{-/-}$) and wild-type ($Tisp40^{+/+}$) mice for *in vivo* analysis. We confirmed that Tisp40 was not expressed in the kidneys of $Tisp40^{-/-}$ mice (Xiao et al., 2017). We compared renal pathologic changes in renal IRI of both genotypes induced by I/R. HE staining suggested that Tisp40 knockout could not change renal structures without the treatment of I/R. The kidneys of wild-type mice exhibited significantly elevated renal tubular damages, which in Tisp40-/- mice were markedly attenuated (**Figures 5A,B**). IHC staining revealed that the levels of pro-IL-1β, IL-1β, and IL-18 in kidneys were higher in I/R-induced mice than in sham-operation mice. There was no difference in pro-IL-1β in I/R-induced kidneys between Tisp40-/- mice and wild type mice, but both IL-1β and IL-18 were significantly inhibited in I/R-induced kidneys of Tisp40-/- mice. (**Figures 5A,C–E**). Furthermore, the qRT-PCR and western blotting results showed that NLRP3 and caspase-1 were significantly inhibited in the kidneys of $Tisp40^{-/-}$ mice induced by I/R (**Figures 5F–J**).

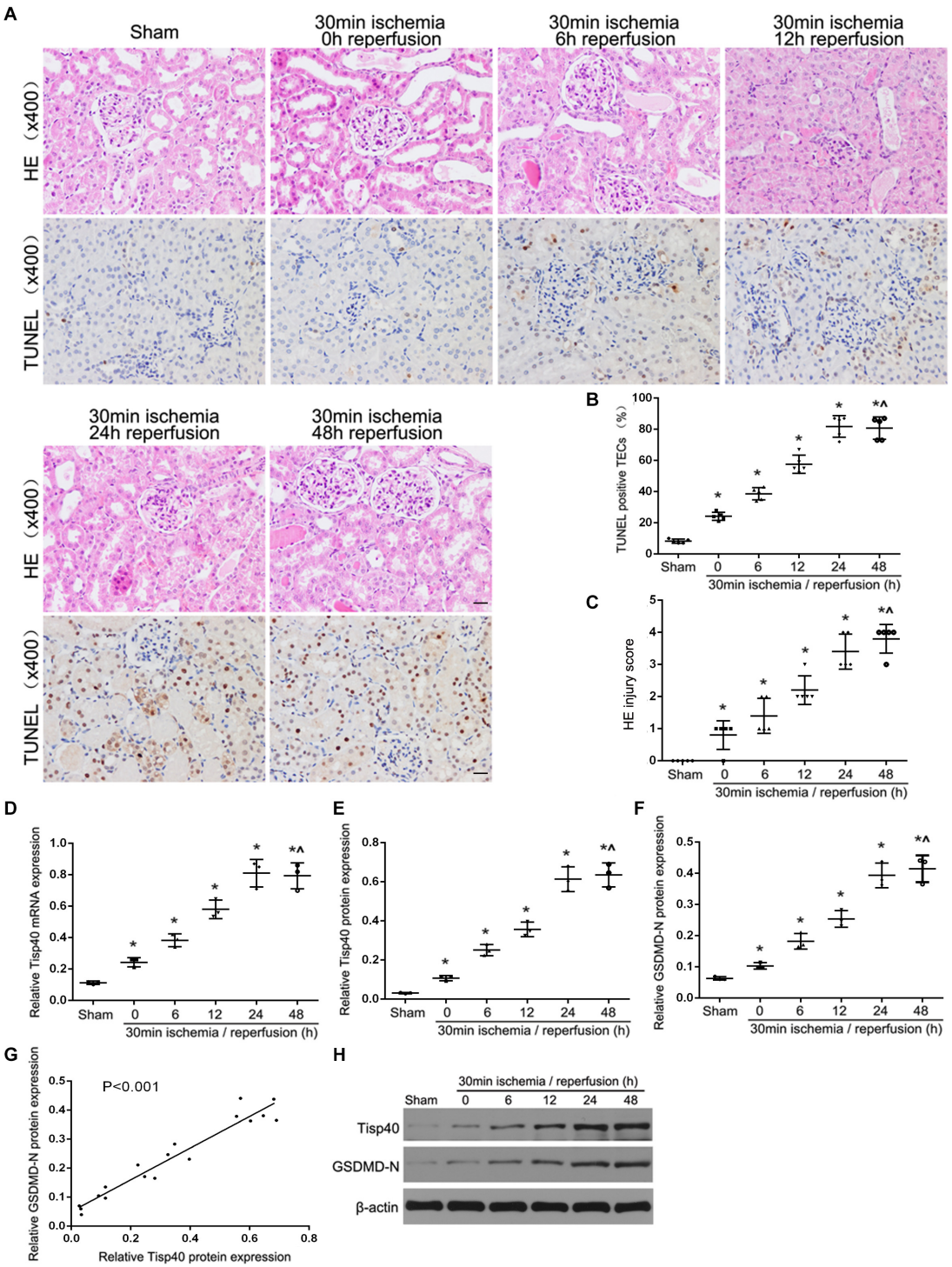

FIGURE 1 | Tisp40 and GSDMD-mediated pyroptosis of TECs were induced in I/R-induced kidney. **(A)** Representative photomicrographs of tubular cell injury in mouse kidney tissue sections with HE and TUNEL staining, 400×, scale bar = 20 μm. **(B)** Statistical analysis showed the percentage of TUNEL positive TECs in the kidney tissues exposed to 30 min ischemia followed by reperfusion of different durations. **(C)** Statistical quantification analysis showed the injury score of HE staining in the kidney tissues exposed to 30 min ischemia followed by reperfusion of different durations. **(D,E,H)** qRT-PCR and western blot analysis of Tisp40 expression at different reperfusion times after 30 min ischemia in kidney samples. **(F,H)** Western blot analysis of GSDMD-N protein expression at different reperfusion times after 30 min ischemia in kidney samples. **(G)** The correlation between the protein expression of Tisp40 and GSDMD-N was analyzed by Pearson's correlation analysis in the kidney tissues. Data are expressed as the mean ± SD. $n = 6$ per group. $^{*}P < 0.05$ vs. sham, $^{\wedge}P > 0.05$ vs. 30 min ischemia and reperfusion of 24 h, one-way ANOVA.

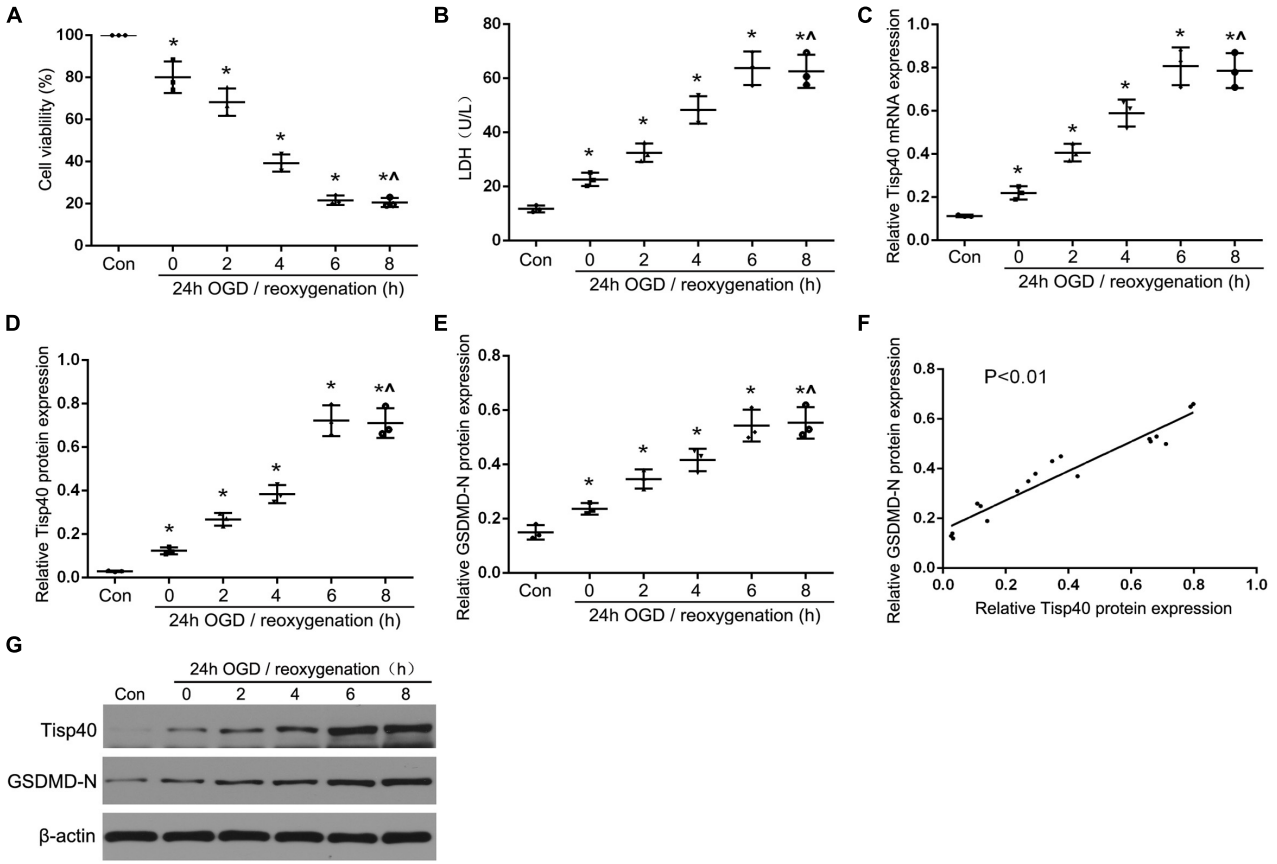

FIGURE 2 | Tisp40 and GSDMD-mediated pyroptosis were induced in OGD/R-stimulated TCMK-1 cell. **(A)** Cell viability was detected by CCK-8 assay. **(B)** The LDH release was detected by activity assays. **(C,D,G)** qRT-PCR and western blot analysis of Tisp40 expression at different durations of reoxygenation after 24 h OGD in TCMK-1 cells; **(E,G)** Western blot analysis of GSDMD-N protein expression at different durations of reoxygenation after 24 h OGD in TCMK-1 cells. **(F)** The correlation between the protein expression of Tisp40 and GSDMD-N was analyzed by Pearson's correlation analysis in TCMK-1 cells. Data are expressed as the mean ± SD. $n = 5$ per group. $^*P < 0.05$ vs. con, $^\wedge P > 0.05$ vs. 24 h OGD and reoxygenation of 6 h, one-way ANOVA.

Tisp40 Is an Essential Regulator of GSDMD-Mediated Pyroptosis in TECs

We next investigated the effect of Tisp40 on GSDMD-mediated pyroptosis in TECs. Flow cytometry data showed that TCMK-1 cell pyroptosis was induced by 24 h of OGD/6 h of reoxygenation and that Tisp40 overexpression markedly promoted cell pyroptosis in TCMK-1/Tisp40 compared to those in the control and empty vector groups (**Figures 6A,B**). The level of GSDMD-N was examined using western blotting, which showed that the expression of OGD/R-stimulated GSDMD-N in TCMK-1/Tisp40 cells was markedly higher than those in the control and empty vector groups (**Figures 6C,D**). The TUNEL assay revealed no obvious pyroptosis of TECs in the sham group. Compared to the Tisp40$^{+/+}$ group, Tisp40 knockout obviously decreased the number of TUNEL-positive TECs induced by I/R (**Figures 6E,F**). In addition, GSDMD-N was significantly inhibited in the I/R-induced kidneys of Tisp40-knockout mice compared to that in the wild-type mice (**Figures 6G,H**). Based on the role of Tisp40 in regulating inflammasome activation and inflammatory factors release in I/R induced mice and OGD/R stimulated TCMK-1 cells, it is further illustrated that Tisp40 is an essential regulator of GSDMD-mediated TEC pyroptosis.

Tisp40 Regulated GSDMD-Mediated TECs Pyroptosis via NF-κB Pathway

Studies have shown that the NF-κB signaling pathway can activate GSDMD-related pyroptosis in tubular cells (Wang et al., 2019). As shown in **Figures 7A,B**, we found parthenolide (PTL, NF-κB inhibitor) alleviated cell pyroptosis in the TCMK-1/Tisp40 group. To further evaluate the signal transduction pathways involved, we confirmed that the levels of p-p65 and caspase-1 were higher in the OGD/R-induced TCMK-1/Tisp40 group than in the control group. However, the effect of Tisp40 overexpression on p-p65 and caspase-1 abundance was partially blocked by PTL (**Figures 7C–G**). Additionally, PTL reduced OGD/R-induced GSDMD-N expression in TCMK-1/Tisp40 cells according to immunofluorescence analysis. These results indicate that Tisp40 regulates GSDMD-mediated pyroptosis in TECs via the NF-κB pathway.

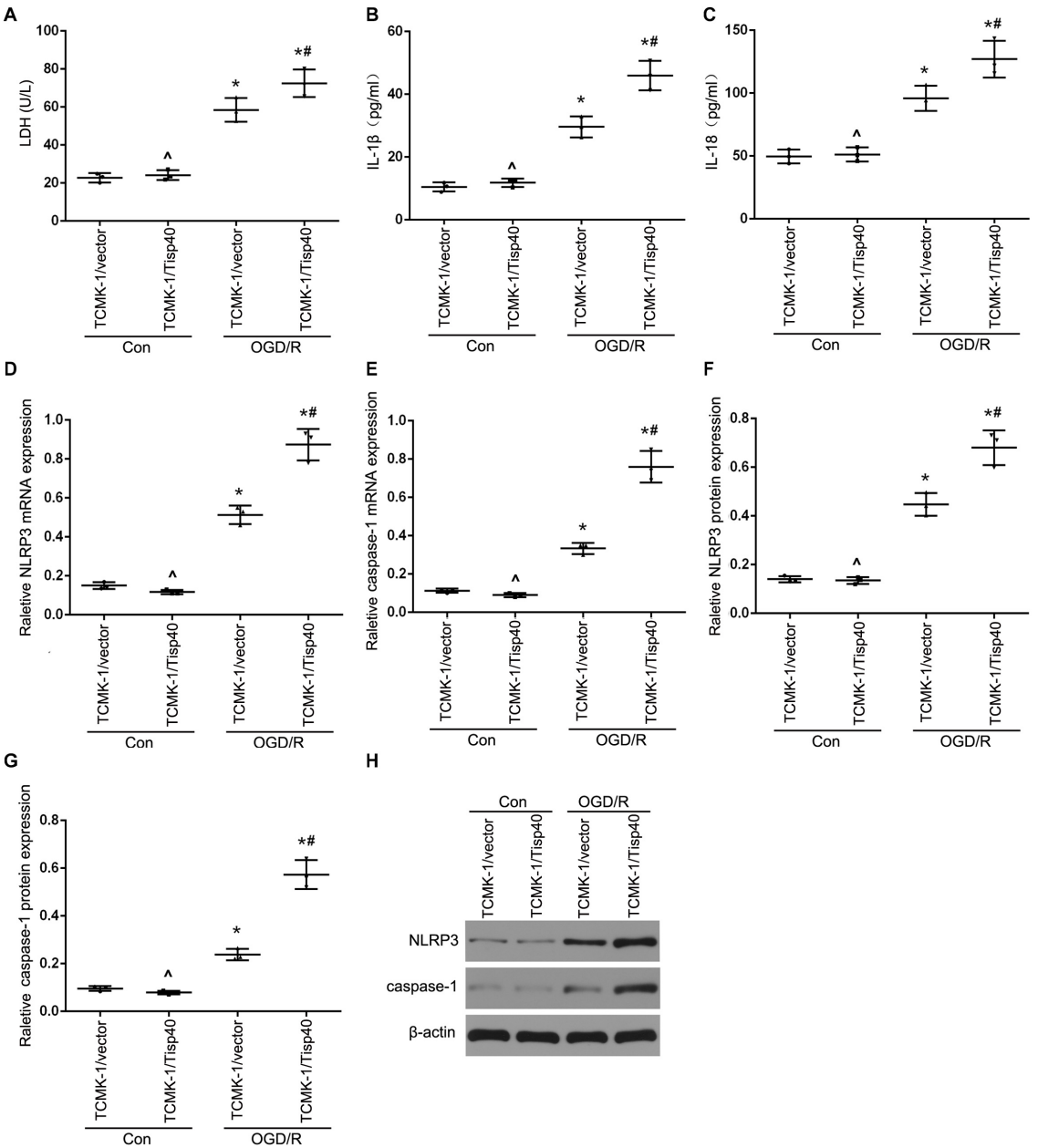

FIGURE 3 | Tisp40 enhanced NLRP3 inflammasome activation in cultured OGD/R-stimulated TCMK-1 cells. **(A)** The LDH release was detected by activity assays. IL-1β **(B)** and IL-18 **(C)** contents were measured by using ELISA kits. **(D–H)** The expression of NLRP3 and caspase-1 were analyzed by qRT-PCR and western blot. Data are expressed as the mean ± SD. $n = 5$ per group. $^{*}P < 0.05$ vs. corresponding control groups (Con). $^{\wedge}P > 0.05$ vs. TCMK-1/vector in con group. $^{\#}P < 0.05$ vs. the group of TCMK-1/vector cells induced by OGD/R, one-way ANOVA.

The renal IRI induces the increased expression of Tisp40, which leads to the phosphorylation of NF-κB p65. Subsequently, p-p65 triggers the assembly of NLRP3 inflamamsome. The activation of NLRP3 inflammasome binds procaspase-1 and adapter protein ASC, after which procaspase-1 is converted into catalytic caspase-1, which promotes the maturation of IL-1 β and IL-18, triggering a strong inflammatory response. In addition, GSDMD is cleaved by catalytic caspase-1, and GSDMD-N domains oligomerizes to generate membrane pores, leading to cell swelling and inflammatory factors releasing (**Figure 8**).

DISCUSSION

Renal IRI is a common cause of AKI and easily develops into CKD and ESRD, creating societal and personal economic burdens (Tao et al., 2013; Chawla et al., 2014). No effective

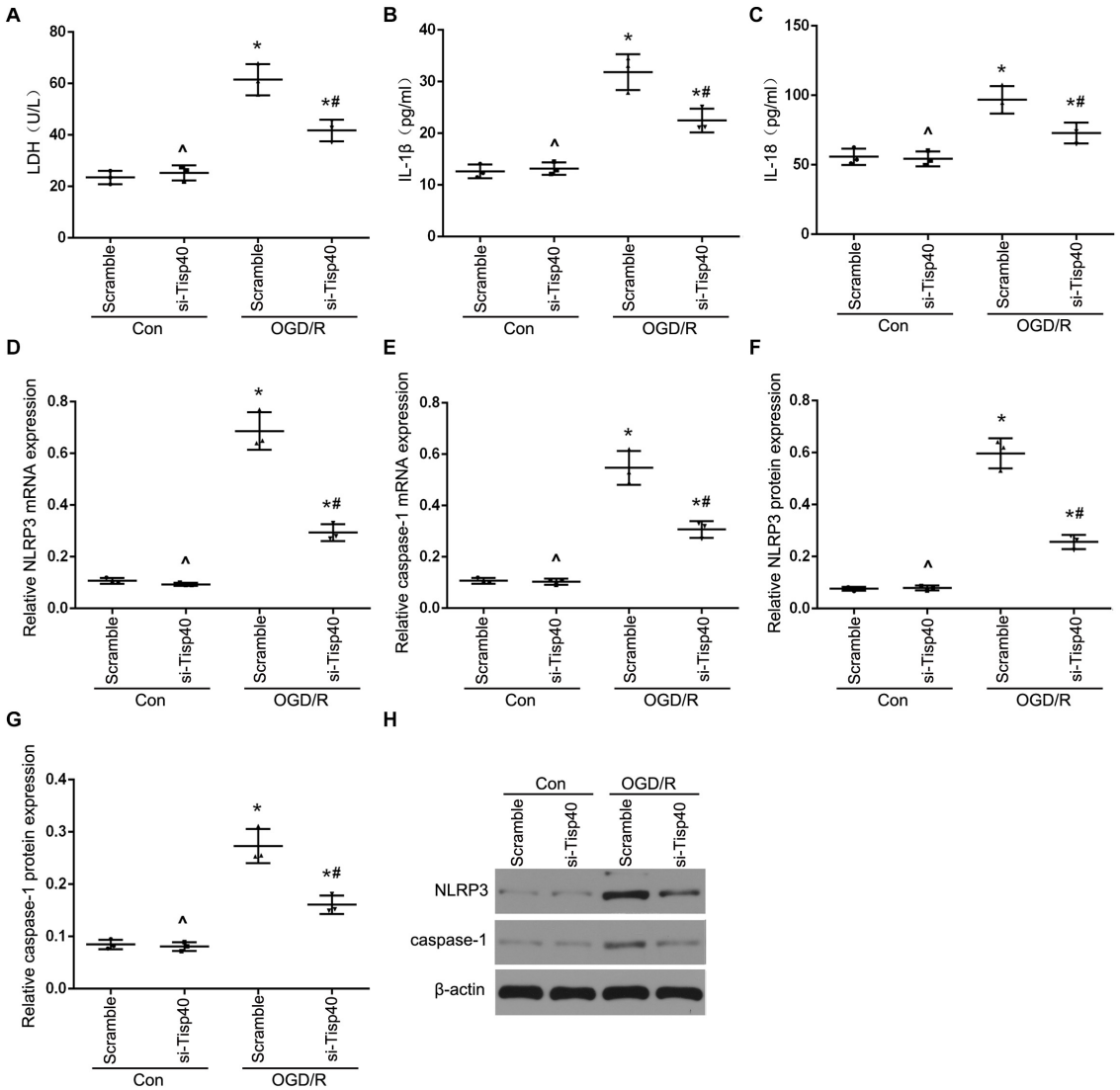

FIGURE 4 | Tisp40 inhibitor alleviated NLRP3 inflammasome activation in cultured OGD/R-stimulated TCMK-1 cells. **(A)** The LDH release was detected by activity assays. IL-1β **(B)** and IL-18 **(C)** contents were measured by using ELISA kits. **(D–H)** The expression of NLRP3 and caspase-1 were analyzed by qRT-PCR and western blot. Data are expressed as the mean ± SD. $n = 5$ per group. $^{*}P < 0.05$ vs. corresponding control groups (Con). $^{\wedge}P > 0.05$ vs. scramble con group. $^{\#}P < 0.05$ vs. the group of Scramble induced by OGD/R, one-way ANOVA.

drugs or related treatment strategies are available except for renal replacement therapy to prolong survival (Kaushal and Shah, 2014). Determining the underlying mechanism of renal IRI is important for developing treatments for AKI (Agarwal et al., 2016). Various mechanisms are involved in renal IRI, including oxygen radicals, intracellular calcium overload, inflammatory response, and apoptosis (Linkermann et al., 2014); however, the mechanism of pyroptosis in renal IR is poorly understood. We examined the function of the Tisp40 gene and its regulatory relationship in the pyroptosis of renal IRI. We found that Tisp40 was closely related to GSDMD-mediated pyroptosis in TECs, and Tisp40 deficiency inhibited GSDMD-mediated pyroptosis by inhibiting NLRP3, caspase1, IL-1β, and IL-18 via the NF-κB pathway in I/R-induced kidneys and OGD/R-induced TECs.

We and others reported that Tisp40 was a regulator in injury of TECs induced by I/R, and Tisp40 knockout effectively alleviated I/R-induced renal fibrosis, apoptosis and inflammation (Qin et al., 2017, 2018; Xiao et al., 2017). Under physiological conditions, Tisp40 is mainly located on the endoplasmic reticulum. When stimulated by external stimuli, Tisp40 is transferred by Golgi body site 1 protease to the nucleus to regulate downstream target genes (Nagamori et al., 2005). In concurrence with the development of renal tubular injury, Tisp40 expression was gradually elevated and peaked at 30 min ischemia/24 h reperfusion. This not only illustrated that renal IRI model was established successfully, also showed Tisp40 gene expression could be an important molecular event in renal IRI and play a role in regulating biological behavior of TECs. Further

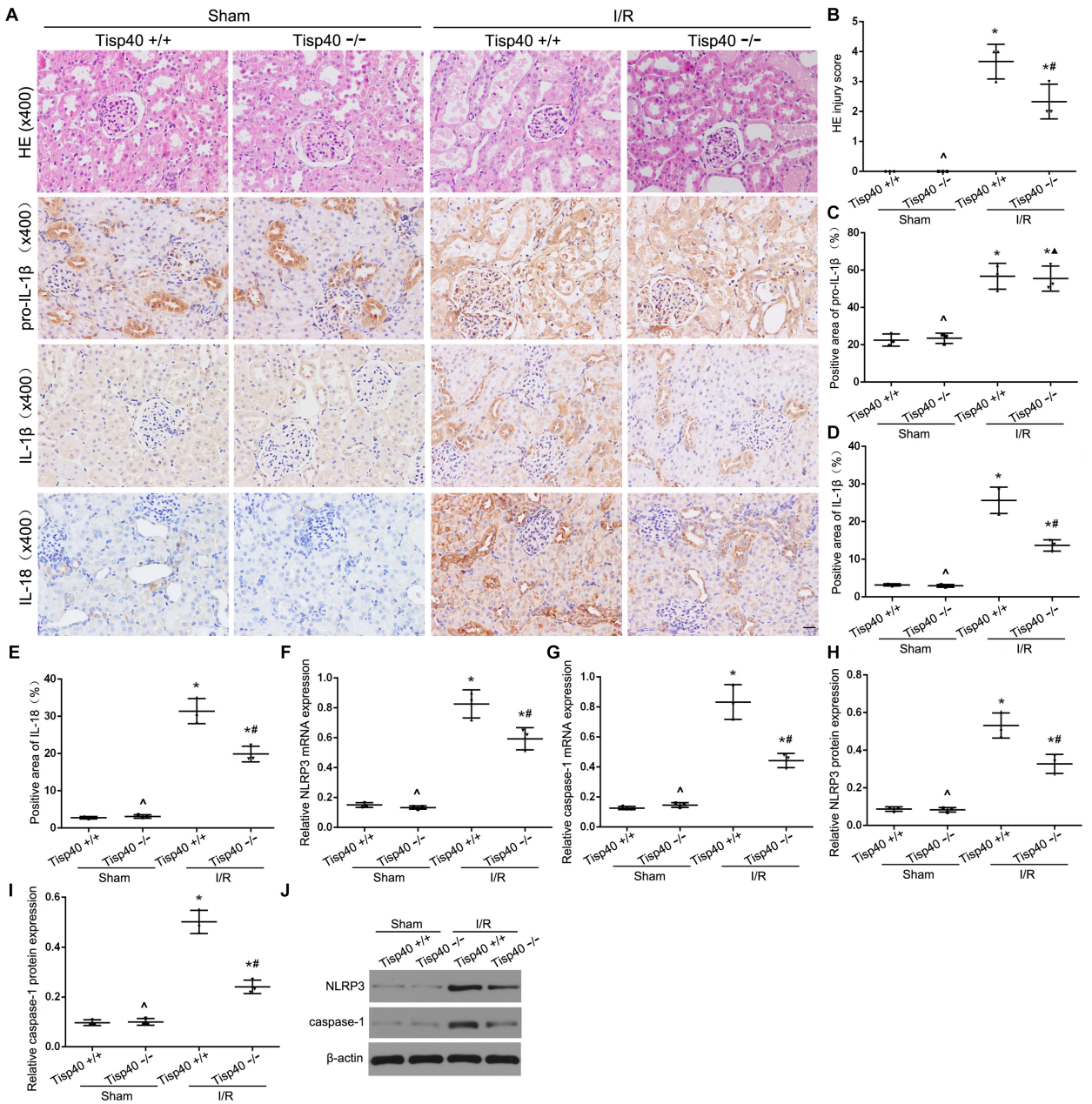

FIGURE 5 | Tisp40 knockout protects against NLRP3 inflammasome activation in I/R-induced kidney. **(A)** Representative photomicrographs of tubular cell injury in mouse kidney tissue sections with HE staining and representative photomicrographs of pro- IL-1β, IL-1β, and IL-18 expression in mouse kidney tissue sections by immunohistochemistry, 400×, scale bar = 20 μm. **(B)** Statistical quantification analysis showed the injury score of HE staining in the kidney tissues **(C,D,E)** Statistical analysis showed the positive area of pro- IL-1β, IL-1β, and IL-18 in the kidney tissues. **(F–J)** The expression of NLRP3 and caspase-1 were analyzed by qRT-PCR and Western blot. Data are expressed as the mean ± SD. $n = 6$ per group. $^{*}P < 0.05$ vs. corresponding sham-operation groups (Sham). $^{\wedge}P > 0.05$ vs. Tisp40$^{+/+}$ in sham groups. $^{\#}P < 0.05$, $^{\blacktriangle}P > 0.05$ vs. the group of I/R-induced Tisp40$^{+/+}$ mice. one-way ANOVA.

results showed the exposure to OGD/R led to an abundance of Tisp40 in TEC.

Pyroptosis, characterized by excessive cell death and inflammation, is a specific cell death program distinct from apoptosis and necrosis (Miao et al., 2010). In this study, we found the injury induced by I/R and OGD/R resulted in excessive TEC death, which always went with pyroptosis in renal IRI (Tajima et al., 2019; Wang et al., 2019; Liu et al., 2020). As the main executor of cell pyroptosis, GSDMD, is widely expressed in different cells and tissues (Shi et al., 2015; Liu et al., 2016). During pyroptosis, the N-terminal domain of GSDMD (GSDMD-N) and cell membrane combine, leading to the formation of cell membrane pores, which causes the cells to swell and disrupt, releasing inflammatory factors,

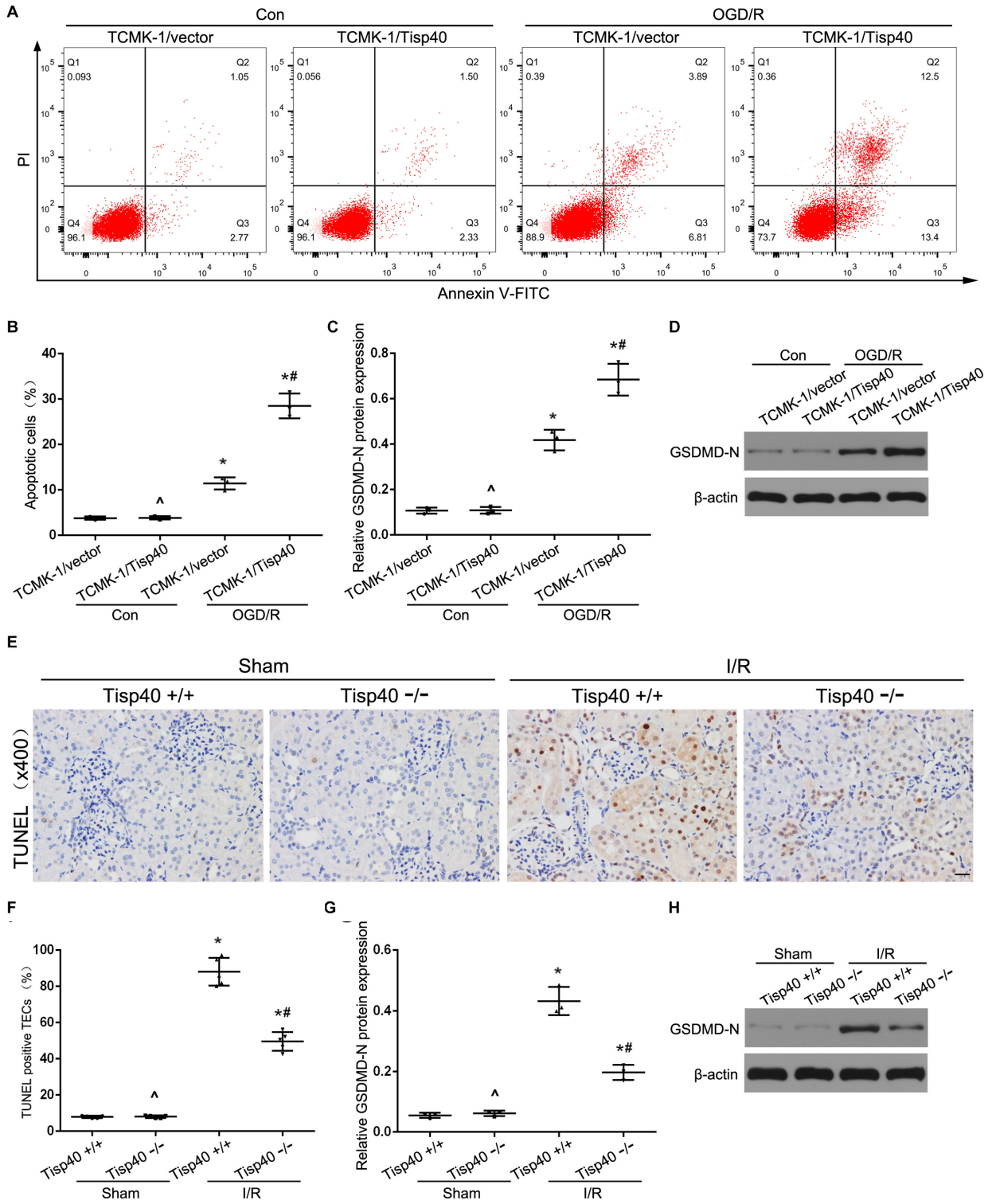

FIGURE 6 | Tisp40 was an essential regulator of GSDMD-mediated TECs pyroptosis. **(A)** Flow cytometry assays were performed to show the cell pyroptosis. **(B)** Statistical analysis was used to show pyroptosis cells. **(C,D)** The expression of GSDMD-N in TCMK-1 cells were analyzed by Western blot. **(E)** Representative photomicrographs of tubular cell injury in mouse kidney tissue sections with TUNEL staining, 400×, scale bar = 20 μm. **(F)** Statistical analysis showed the percentage of TUNEL positive TECs in the kidney tissues exposed to sham or I/R. **(G,H)** The expression of GSDMD-N in kidneys were analyzed by Western blot. Data are expressed as the mean ± SD. $n = 5$ per group *in vitro* and $n = 6$ per group *in vivo*. ^P>0.05 vs. TCMK-1/vector cells in con group or. Tisp40$^{+/+}$ mice in sham group. *$P < 0.05$ vs. corresponding control groups (Con) or sham-operation groups (Sham). $^{\#}P < 0.05$ vs. TCMK-1/vector cells in OGD/R group or Tisp40$^{+/+}$ I/R group, one-way ANOVA.

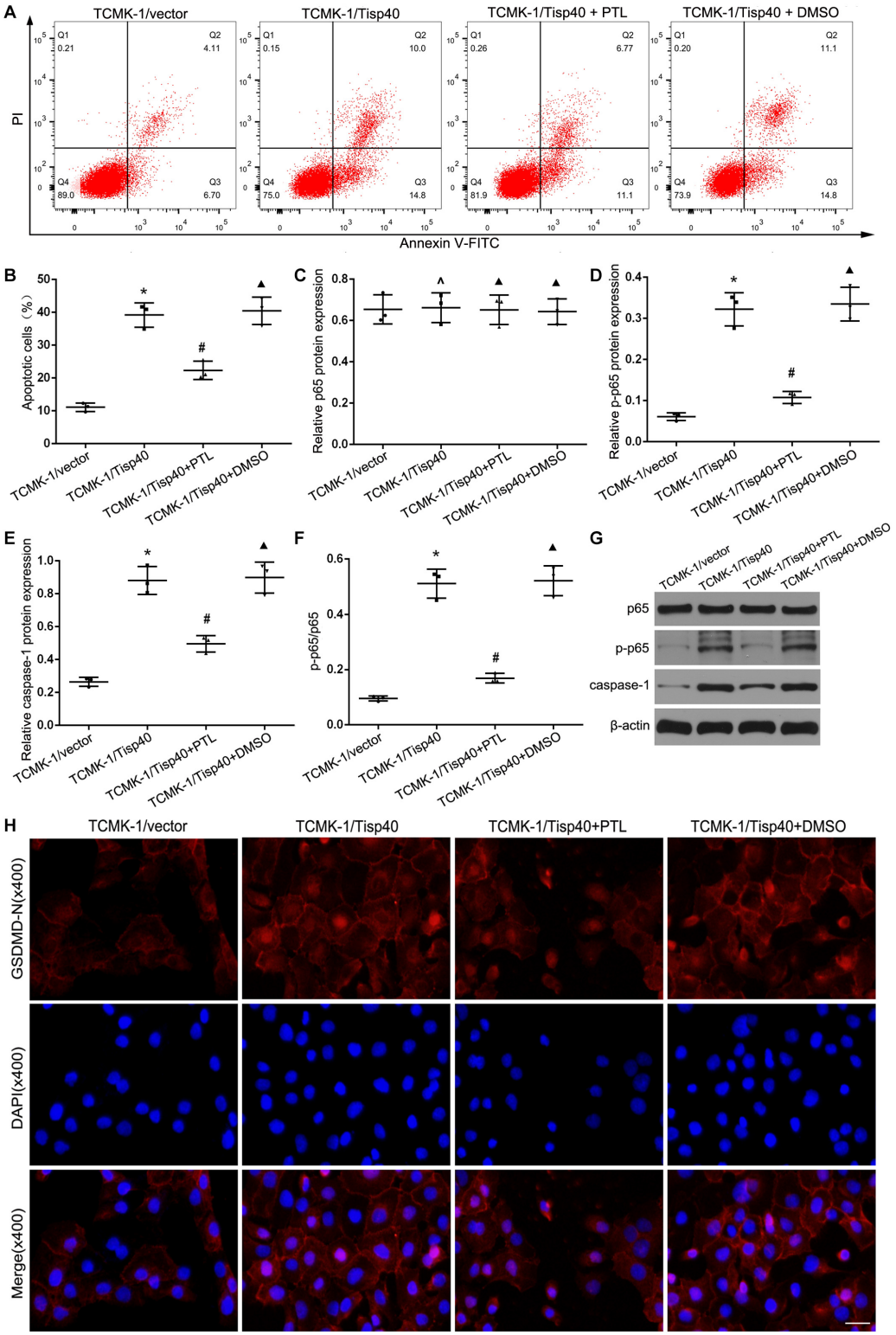

FIGURE 7 | Tisp40 regulated GSDMD-mediated pyroptosis via NF-κB pathway in OGD/R stimulated TCMK-1 cell. **(A)** Flow cytometry assays were performed to show the cell pyroptosis. **(B)** Statistical analysis was used to show pyroptosis cells. **(C,D,E,G)** The expression of p65,p-p65 and caspase1 were analyzed by Western blot. **(F)** The ratio of p-p65 to p65 reflect phosphorylation level of p65. **(H)** Representative photomicrographs of GSDMD-N expression in TCMK-1 cells by Immunofluorescence, 400×, scale bar = 20 μm. Data are expressed as the mean ± SD. $n = 5$ per group. $^{*}P < 0.05$, $^{\wedge}P > 0.05$ vs. TCMK-1/vector group. $^{\#}P < 0.05$, $^{\blacktriangle}P > 0.05$ vs. TCMK-1/Tisp40 group, one-way ANOVA.

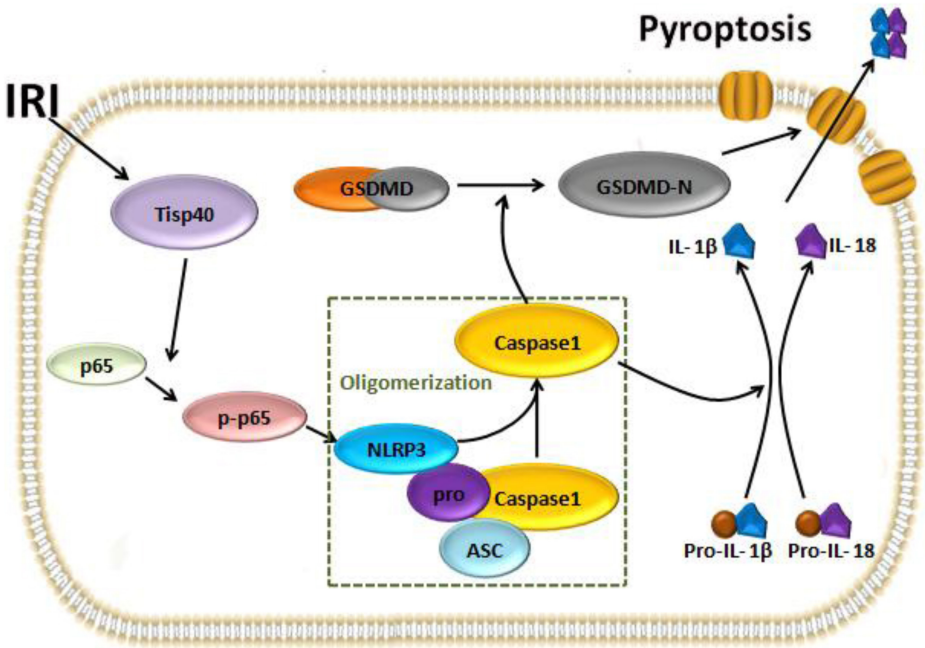

FIGURE 8 | The pathway that Tisp40 regulates Ischemia-reperfusion induced pyroptosis in kidney.

such as LDH (Byrne et al., 2013; Shi et al., 2015; Whitfield et al., 2017). In our study, GSDMD-N expression increased gradually with injury of TECs. Simultaneously, the level of LDH release was correspondingly increased in cultured TCMK-1 cells. We suggest that TEC pyroptosis appeared at early stage of renal IRI. In addition, the levels of GSDMD-N expression and LDH release peaked at 30 min ischemia/24 h reperfusion in *in vivo* and 24 h OGD/R/6 h reoxygenation *in vitro*. These results indicated TECs pyroptosis was an efficient and speedy cell death program. We also provided a method for model establishment of TEC pyroptosis in renal IRI. Besides, the expressions of Tisp40 and GSDMD-N were positively correlated, which revealed Tisp40 might be involved in GSDMD-mediated TEC pyroptosis.

Pyroptosis, marked by inflammasome formation and requires caspase-1 activation, is an adaptive immune in response to intra- and extracellular stimuli (Shi et al., 2016). As an inflammatory molecule, NLRP3 (nod-like receptor protein-3) is activated by binding to the precursor of caspase-1 (procaspase-1) and adapter protein ASC, after which procaspase-1 is converted into catalytic caspase-1, which promotes the maturation and release of IL-1β and IL-18, triggering a strong inflammatory response (Miao et al., 2010; Xi et al., 2016). Notably, we observed the characteristic hallmarks of pyroptosis in renal IRI, including increased activation of NLRP3 inflammasome and caspase-1, and the release of IL-1β and IL-18. We further explored the mechanism of Tisp40's involvement in TEC pyroptosis. We found Tisp40 overexpression aggravated the expressions of NLRP3 and caspase-1, and the release of LDH, IL-1β and IL-18, whereas the opposite occurred in TECs treated with siRNA targeting Tisp40. These findings was further confirmed *in vivo*. Interesting, we found that there was no change in the expression of pro-IL-1β between Tisp40-deficient mice and wild-type mice, which suggests that the protective effect of Tisp40 deficiency might suppress the inflammatory factors mature, rather than inhibit the expressions of inflammatory cytokines precursors. Subsequently, the nature of cell death was monitored by flow-cytometry analyze *in vitro* and TUNEL staining *in vivo*. Tisp40 overexpression markedly promoted pyroptosis in TECs induced by OGD/R, and Tisp40 knockout alleviated TEC pyroptosis in I/R-induced kidney. Furthermore, the expression of GSDMD-N was detected to verify the role of Tisp40 in pyroptosis. We found that Tisp40 overexpression markedly promoted the expression of GSDMD-N in TECs induced by OGD/R, and Tisp40 knockout alleviated the expression of GSDMD-N in I/R-induced kidney. Collectively, it is confirmed that Tisp40 has transcriptional regulation function on GSDMD-midiated pyroptosis in renal IRI.

As a nuclear transcription factor commonly present in the cytoplasm in the form of a homo- or hetero dimer, NF-κB is a key regulator of TEC pyroptosis by activating the NLRP3 inflammasome and promoting proinflammatory responses (Gordon et al., 2011; Yang et al., 2014). In addition, NF-κB activated GSDMD-related pyroptosis in tubular cells (Wang et al., 2019). Moreover, Tisp40 deficiency limits renal inflammation by inhibition of phosphorylation NF-κB (Qin et al., 2018). Therefore, we predicted that the NF-κB was a bridge between Tisp40 and TEC pyroptosis. As expected, Tisp40 overexpression significantly increased the expression of p-p65 in OGD/R-stimulated cells, while the effects of Tisp40 overexpression on GSDMD-mediated pyroptosis were partially

blocked by parthenolide (an inhibitor of NF-κB). These results demonstrate that Tisp40 regulate GSDMD-mediated TECs pyroptosis via phosphorylation of p65.

CONCLUSION

In conclusion, our study indicates Tisp40 is an essential regulator of GSDMD-mediated pyroptosis in TECs via nuclear factor-κB p65 activation, and Tisp40 inhibition protects against tubular epithelial cell GSDMD-mediated pyroptosis in renal ischemia-reperfusion injury (**Figure 8**). Combined with our previous research results, this study further confirms that Tisp40 may be a promising therapeutic target for preventing AKI and its evolution to CKD and ESRD.

DATA AVAILABILITY STATEMENT

The raw data supporting the conclusions of this article will be made available by the authors, without undue reservation.

ETHICS STATEMENT

The animal study was reviewed and approved by the Institutional Animal Care and Use Committee of Qingdao Municipal Hospital.

AUTHOR CONTRIBUTIONS

CX and RW designed the research, analyzed the data, and drafted the manuscript. HZo and QS performed the experiments. CX, HZu, and YZ helped with data acquisition and discussion. CX and RW analyzed the data and prepared the figures. All authors contributed to manuscript writing and editing.

FUNDING

This work was financially supported by the National Natural Science Foundation of China (81470923).

REFERENCES

Agarwal, A., Dong, Z., Harris, R., Murray, P., Parikh, S. M., Rosner, M. H., et al. (2016). Cellular and molecular mechanisms of AKI. *J. Am. Soc. Nephrol.* 27, 1288–1299. doi: 10.1681/ASN.2015070740

Al-Bataineh, M. M., Kinlough, C. L., Poland, P. A., Pastor-Soler, N. M., Sutton, T. A., Mang, H. E., et al. (2016). Muc1 enhances the beta-catenin protective pathway during ischemia-reperfusion injury. *Am. J. Physiol. Renal Physiol.* 310, F569–F579. doi: 10.1152/ajprenal.00520.2015

Arai, S., Kitada, K., Yamazaki, T., Takai, R., Zhang, X., Tsugawa, Y., et al. (2016). Apoptosis inhibitor of macrophage protein enhances intraluminal debris clearance and ameliorates acute kidney injury in mice. *Nat. Med.* 22, 183–193. doi: 10.1038/nm.4012

Asada, R., Kanemoto, S., Kondo, S., Saito, A., and Imaizumi, K. (2011). The signalling from endoplasmic reticulum-resident bZIP transcription factors involved in diverse cellular physiology. *J. Biochem.* 149, 507–518. doi: 10.1093/jb/mvr041

Bastin, A. J., Ostermann, M., Slack, A. J., Diller, G. P., Finney, S. J., and Evans, T. W. (2013). Acute kidney injury after cardiac surgery according to Risk/Injury/Failure/Loss/End-stage, Acute kidney injury network, and Kidney disease: improving global outcomes classifications. *J. Crit. Care* 28, 389–396. doi: 10.1016/j.jcrc.2012.12.008

Byrne, B. G., Dubuisson, J. F., Joshi, A. D., Persson, J. J., and Swanson, M. S. (2013). Inflammasome components coordinate autophagy and pyroptosis as macrophage responses to infection. *mBio* 4:e00620-12. doi: 10.1128/mBio.00620-12

Chawla, L. S., Eggers, P. W., Star, R. A., and Kimmel, P. L. (2014). Acute kidney injury and chronic kidney disease as interconnected syndromes. *N. Engl. J. Med.* 371, 58–66. doi: 10.1056/NEJMra1214243

Diao, C., Chen, Z., Qiu, T., Liu, H., Yang, Y., and Liu, X. (2019). Inhibition of PRMT5 attenuates oxidative stress-induced pyroptosis via activation of the Nrf2/HO-1 signal pathway in a mouse model of renal ischemia-reperfusion injury. *Oxid. Med. Cell. Longev.* 2019:2345658. doi: 10.1155/2019/2345658

Gill, N., Nally, J. J., and Fatica, R. A. (2005). Renal failure secondary to acute tubular necrosis: epidemiology, diagnosis, and management. *Chest* 128, 2847–2863. doi: 10.1378/chest.128.4.2847

Gordon, J. W., Shaw, J. A., and Kirshenbaum, L. A. (2011). Multiple facets of NF-kappaB in the heart: to be or not to NF-kappaB. *Circ. Res.* 108, 1122–1132. doi: 10.1161/CIRCRESAHA.110.226928

Jha, V., Garcia-Garcia, G., Iseki, K., Li, Z., Naicker, S., Plattner, B., et al. (2013). Chronic kidney disease: global dimension and perspectives. *Lancet* 382, 260–272. doi: 10.1016/S0140-6736(13)60687-X

Kaushal, G. P., and Shah, S. V. (2014). Challenges and advances in the treatment of AKI. *J. Am. Soc. Nephrol.* 25, 877–883. doi: 10.1681/ASN.2013070780

Kovacs, S. B., and Miao, E. A. (2017). Gasdermins: effectors of pyroptosis. *Trends Cell Biol.* 27, 673–684. doi: 10.1016/j.tcb.2017.05.005

Linkermann, A., Chen, G., Dong, G., Kunzendorf, U., Krautwald, S., and Dong, Z. (2014). Regulated cell death in AKI. *J. Am. Soc. Nephrol.* 25, 2689–2701. doi: 10.1681/ASN.2014030262

Liu, H., Chen, Z., Weng, X., Chen, H., Du, Y., Diao, C., et al. (2020). Enhancer of zeste homolog 2 modulates oxidative stress-mediated pyroptosis *in vitro* and in a mouse kidney ischemia-reperfusion injury model. *FASEB J.* 34, 835–852. doi: 10.1096/fj.201901816R

Liu, X., Zhang, Z., Ruan, J., Pan, Y., Magupalli, V. G., Wu, H., Lieberman, J., et al. (2016). Inflammasome-activated gasdermin D causes pyroptosis by forming membrane pores. *Nature* 535, 153–158. doi: 10.1038/nature18629

Livak, K. J., and Schmittgen, T. D. (2001). Analysis of relative gene expression data using real-time quantitative PCR and the 2(-Delta Delta C(T)) method. *Methods* 25, 402–408. doi: 10.1006/meth.2001.1262

Miao, E. A., Leaf, I. A., Treuting, P. M., Mao, D. P., Dors, M., Sarkar, A., et al. (2010). Caspase-1-induced pyroptosis is an innate immune effector mechanism against intracellular bacteria. *Nat. Immunol.* 11, 1136–1142. doi: 10.1038/ni.1960

Nagamori, I., Yabuta, N., Fujii, T., Tanaka, H., Yomogida, K., and Nojima, H. (2005). Tisp40, a spermatid specific bZip transcription factor, functions by binding to the unfolded protein response element via the Rip pathway. *Genes Cells* 10, 575–594. doi: 10.1111/j.1365-2443.2005.00860.x

Noh, M. R., Kim, J. I., Han, S. J., Lee, T. J., and Park, K. M. (2015). C/EBP homologous protein (CHOP) gene deficiency attenuates renal ischemia/reperfusion injury in mice. *Biochim. Biophys. Acta* 1852, 1895–1901. doi: 10.1016/j.bbadis.2015.06.004

Perico, N., and Remuzzi, G. (2015). Acute kidney injury: more awareness needed, globally. *Lancet* 386, 1425–1427. doi: 10.1016/S0140-6736(15)00425-0

Qin, C., Li, M., Bai, T., Yang, K., Xu, T., and Zhang, J. (2018). Tisp40 deficiency limits renal inflammation and promotes tubular cell proliferation in renal ischemia reperfusion injury. *Exp. Cell Res.* 371, 255–261. doi: 10.1016/j.yexcr.2018.08.019

Qin, C., Xiao, C., Su, Y., Zheng, H., Xu, T., Lu, J., et al. (2017). Tisp40 deficiency attenuates renal ischemia reperfusion injury induced apoptosis of tubular epithelial cells. *Exp. Cell Res.* 359, 138–144. doi: 10.1016/j.yexcr.2017.07.038

Shi, J., Gao, W., and Shao, F. (2016). Pyroptosis: gasdermin-mediated programmed necrotic cell death. *Trends Biochem. Sci.* 42, 245–254. doi: 10.1016/j.tibs.2016.10.004

Shi, J., Zhao, Y., Wang, K., Shi, X., Wang, Y., Huang, H., et al. (2015). Cleavage of GSDMD by inflammatory caspases determines pyroptotic cell death. *Nature* 526, 660–665. doi: 10.1038/nature15514

Tajima, T., Yoshifuji, A., Matsui, A., Itoh, T., Uchiyama, K., Kanda, T., et al. (2019). beta-hydroxybutyrate attenuates renal ischemia-reperfusion injury through its anti-pyroptotic effects. *Kidney Int.* 95, 1120–1137. doi: 10.1016/j.kint.2018.11.034

Tao, L. P., Burdmann, E. A., and Mehta, R. L. (2013). Acute kidney injury: global health alert. *Int. J. Organ Transplant. Med.* 4, 1–8. doi: 10.1016/j.hkjn.2013.03.001

Velpula, K. K., Rehman, A. A., Chigurupati, S., Sanam, R., Inampudi, K. K., and Akila, C. S. (2012). Computational analysis of human and mouse CREB3L4 Protein. *Bioinformation* 8, 574–577. doi: 10.6026/97320630008574

Wang, Y., Zhu, X., Yuan, S., Wen, S., Liu, X., Wang, C., et al. (2019). TLR4/NF-kappaB signaling induces GSDMD-related pyroptosis in tubular cells in diabetic kidney disease. *Front. Endocrinol.* 10:603. doi: 10.3389/fendo.2019.00603

Whitfield, N. N., Byrne, B. G., and Swanson, M. S. (2017). Mouse macrophages are permissive to motile Legionella species that fail to trigger pyroptosis. *Infect. Immun.* 78, 423–432. doi: 10.1128/IAI.00070-09

Xi, H., Zhang, Y., Xu, Y., Yang, W. Y., Jiang, X., Sha, X., et al. (2016). Caspase-1 inflammasome activation mediates homocysteine-induced pyrop-apoptosis in endothelial cells. *Circ. Res.* 118, 1525–1539. doi: 10.1161/CIRCRESAHA.116.308501

Xiao, C. C., Zhang, J., Luo, P. C., Qin, C., Du, Y., Ning, J. Z., et al. (2017). Identification of Tisp40 as an essential regulator of renal tubulointerstitial fibrosis via TGF-beta/Smads pathway. *Cell. Physiol. Biochem.* 42, 697–712. doi: 10.1159/000477887

Yang, J. R., Yao, F. H., Zhang, J. G., Ji, Z. Y., Li, K. L., Zhan, J., et al. (2014). Ischemia-reperfusion induces renal tubule pyroptosis via the CHOP-caspase-11 pathway. *Am. J. Physiol. Renal Physiol.* 306, F75–F84. doi: 10.1152/ajprenal.00117.2013

Conflict of Interest: The authors declare that the research was conducted in the absence of any commercial or financial relationships that could be construed as a potential conflict of interest.

frontiers in Physiology

ORIGINAL RESEARCH
published: 25 August 2020
doi: 10.3389/fphys.2020.01076

Sodium Oxalate-Induced Acute Kidney Injury Associated With Glomerular and Tubulointerstitial Damage in Rats

*Larissa de Araújo, Juliana Martins Costa-Pessoa†, Mariana Charleaux de Ponte† and Maria Oliveira-Souza**

Laboratory of Renal Physiology, Department of Physiology and Biophysics, Institute of Biomedical Sciences, University of São Paulo, São Paulo, Brazil

Acute crystalline nephropathy is closely related to tubulointerstitial injury, but few studies have investigated glomerular changes in this condition. Thus, in the current study, we investigated the factors involved in glomerular and tubulointerstitial injury in an experimental model of crystalline-induced acute kidney injury (AKI). We treated male Wistar rats with a single injection of sodium oxalate (NaOx, 7 mg·100 g^{-1}·day^{-1}, resuspended in 0.9% NaCl solution, i.p.) or vehicle (control). After 24 h of treatment, food and water intake, urine output, body weight gain, and renal function were evaluated. Renal tissue was used for the morphological studies, quantitative PCR and protein expression studies. Our results revealed that NaOx treatment did not change metabolic or electrolyte and water intake parameters or urine output. However, the treated group exhibited tubular calcium oxalate (CaOx) crystals excretion, followed by a decline in kidney function demonstrated along with glomerular injury, which was confirmed by increased plasma creatinine and urea concentrations, increased glomerular desmin immunostaining, nephrin mRNA expression and decreased WT1 immunofluorescence. Furthermore, NaOx treatment resulted in tubulointerstitial injury, which was confirmed by tubular dilation, albuminuria, increased Kim-1 and Ki67 mRNA expression, decreased megalin and Tamm–Horsfall protein (THP) expression. Finally, the treatment induced increases in CD68 protein staining, MCP-1, IL-1β, NFkappaB, and α-SMA mRNA expression, which are consistent with proinflammatory and profibrotic signaling, respectively. In conclusion, our findings provide relevant information regarding crystalline-induced AKI, showing strong tubulointerstitial and glomerular injury with a possible loss of podocyte viability.

Keywords: sodium oxalate, crystalline nephropathy, acute kidney injury, glomerular and tubulointerstitial injury, albuminuria, inflammation

OPEN ACCESS

Edited by:
H. Della Coletta Francescato, Faculty of Medicine of Ribeirão Preto, University of São Paulo, Brazil

Reviewed by:
Xiao-Ming Meng, Anhui Medical University, China
Zhanjun Jia, Nanjing Medical University, China

***Correspondence:**
Maria Oliveira-Souza
souza@icb.usp.br

†These authors have contributed equally to this work

Specialty section:
This article was submitted to Renal and Epithelial Physiology, a section of the journal Frontiers in Physiology

Received: *06 April 2020*
Accepted: *05 August 2020*
Published: *25 August 2020*

Citation:
de Araújo L, Costa-Pessoa JM, de Ponte MC and Oliveira-Souza M (2020) Sodium Oxalate-Induced Acute Kidney Injury Associated With Glomerular and Tubulointerstitial Damage in Rats. Front. Physiol. 11:1076. doi: 10.3389/fphys.2020.01076

INTRODUCTION

Oxalate is an end product of hepatic metabolism of glyoxylate, amino acids and carbohydrates (Gambardella and Richardson, 1977; Poore et al., 1997; Knight et al., 2011). In addition, exogenous oxalate is supplied by a diet composed especially of green leafy vegetables, seeds and roots (Noonan and Savage, 1999). Intestinal oxalate absorption is predominantly passive and paracellular. In

addition, transcellular transport of oxalate is mediated by SLC26 anion exchangers expressed on both apical and basolateral membranes of intestinal epithelial cells (Efe et al., 2019; Knauf et al., 2019). In healthy humans, the plasma oxalate levels are fairly low (1–6 μmol/L) (Kasidas and Rose, 1986; Hoppe et al., 2009). Oxalate is primarily excreted by the kidneys via glomerular filtration and tubular secretion, the last one being mediated by the SLC26A anion exchanger expressed in the basolateral membrane (Robijn et al., 2011) and the Cl^-/oxalate exchanger SLC26A6 expressed mainly in the brush-border membrane of proximal tubule cells (Bergsland et al., 2011; Knauf et al., 2019) and in the apical membrane of distal nephron cells (Kujala et al., 2005).

Studies have demonstrated that an internal oxalate imbalance results in hyperoxaluria (Pfau and Knauf, 2016), which predisposes to the formation of renal stone. In fact, it is a common and multifactorial disease, occurring in 8% of the population and considered related to environmental factors and diseases such as metabolic syndrome, diabetes mellitus, obesity and kidney disease progression (Meydan et al., 2003; Carbone et al., 2018; Waikar et al., 2019). Hyperoxaluria leads to urinary calcium oxalate (CaOx) supersaturation, resulting in the formation of crystals in the kidney parenchyma and tubules, consistent with nephrolithiasis or nephrocalcinosis (Sayer et al., 2004).

During the acute supersaturation phase, CaOx complexes are the most common type of kidney stone, which was initially referred to as type 2 crystalline nephropathy (Mulay et al., 2018). Under this condition, tubular injury is associated with crystals and/or Tamm–Horsfall protein (THP) complexes, apoptotic and inflammatory responses consistent with acute kidney injury (AKI), in addition to the risk for recurrence and/or chronic kidney disease (CKD) progression (Lorenz et al., 2014; Pfau and Knauf, 2016; Fox et al., 2018; Mulay et al., 2018; Efe et al., 2019). However, clinical evidence and experimental models of ischemia-reperfusion have revealed that frequently, the recovery of renal function after AKI is incomplete and accompanied by proteinuria, tubular injury and glomerular filtration rate (GFR) decline, leading to end-stage renal disease (ESRD) (Hingorani et al., 2009; Basile et al., 2012). Furthermore, other studies using animal models of ischemia-reperfusion and glomerulosclerosis have identified podocyte injury as an etiological factor of progressive proteinuria and kidney function decline (Hara et al., 2015; Chen et al., 2019).

In the clinical context of nephrolithiasis, the investigation of factors involved with crystalline-induced AKI is essential to understand the relationship between AKI events and CKD progression with or without recurrence. Compared to humans, rodent present a special resistance to crystal retention (Khan and Glenton, 2010). However, the animal models can provide a deeper insight into the molecular mechanisms involved in the renal injury. In view of these findings, in the current study, we used a crystalline-related AKI model induced by a single injection of sodium oxalate solution (NaOx). We sought to explore the factors involved in glomerular and tubulointerstitial injury associated with the intrarenal CaOx crystal formation in this rodent model.

MATERIALS AND METHODS

Animal Study Design

Male Wistar rats aged 60 days (n = 15, weighing 150–250 g) were obtained from the animal care facility of the Department of Physiology and Biophysics, Institute of Biomedical Sciences, the University of São Paulo (São Paulo, Brazil). The experimental protocols were conducted in accordance with the ethical standards approved by the Institutional Animal Care and Use Committee of the University of São Paulo (Protocol no. 9276140518). All animals were housed at the department facility under standard conditions (constant temperature of 22°C, 12:12-h light-dark cycle, 60% relative humidity, fed standard rat chow and water *ad libitum*). The animals were randomly allocated into the following two groups: (1) control rats (n = 7), which received a single vehicle injection of 237 μL/100g of 0.9% NaCl solution (i.p.); (2) sodium oxalate-treated rats (n = 8), which received a single injection of NaOx (7 mg·100 g^{-1}·day^{-1}) (Khan et al., 1992; Khan and Glenton, 2010), resuspended in 237 μL/100g of 0.9% NaCl solution (i.p.) (Synth, Diadema, SP, Brazil). Just after the injection, the animals were placed individually in metabolic cages (Techniplast, Milan, Italy) for 24 h. The food (g/day) and water (mL/day) intake as well as urine output (μL/min) were analyzed. At the end of 24 h of treatment, the animals were anesthetized with ketamine (75 mg/kg i.p.) and xylazine (4 mg/kg i.p., Virbac, Jurubatuba, São Paulo, Brazil), placed on a warm table to maintain body temperature and prepared surgically for cannulation of the distal aorta using a PE-50 catheter (Clay Adams Company, Inc., Parsippany, NJ, United States) for blood sample collection followed by kidney perfusion with PBS (0.15 M NaCl containing 10 mM sodium phosphate buffer, pH 7.4) at 20 mL/min using a peristaltic perfusion pump, BP600 (Milan Scientific Equipment, Colombo, PR, Brazil) as previously described (Casare et al., 2016; de Ponte et al., 2017). Euthanasia was performed by exsanguination. One kidney was isolated, removed, weighed and snap frozen for further quantitative PCR and protein expression studies. The remaining kidney was fixed in 4% paraformaldehyde solution, dehydrated and embedded in paraffin for morphological studies.

Plasma and Urine Analysis

Urine sediment (30 μL) was examined under a light microscope (Eclipse 80i, Nikon, Tokyo, Japan) to confirm the occurrence of crystals. Plasma osmolality was measured using an osmometer (Precision Systems, Natick, MA, United States) and sodium concentration was determined by flame photometry (9180 Electrolyte Analyzer; Roche, Basel, Switzerland) as previously described (Casare et al., 2016; de Ponte et al., 2017). Plasma urea and creatinine as well as urine creatinine levels were evaluated using colorimetric tests (Labtest, Lagoa Santa, MG Brazil). The creatinine clearance was calculated using the following formula: $[C = (Urine_{Cr} \cdot V)/Plasma_{Cr}]$, where C is clearance, Cr is

creatinine, and V represents urinary flow. The urinary albumin excretion was determined using a SilverQuest Silver Staining Kit (Thermo Fisher Scientific, Waltham, MA, United States) by the modified Oakley method (Oakley et al., 1980). Briefly, urine samples (volume corresponding to 5 μg creatinine) from the metabolic cages were separated by SDS polyacrylamide gel electrophoresis (10%). Next, silver staining was performed on the gel, and albumin bands were identified using a molecular weight marker (bovine serum albumin – BSA, 66 kDa). The bands were analyzed by optical densitometry using ImageJ software [National Institutes of Health (NIH), Bethesda, MD, United States].

Total Renal Tissue mRNA Expression Studies

The isolated kidney was cut into two sections, which were quickly frozen and pulverized in liquid nitrogen. As previously described (de Ponte et al., 2017) and summarized here, frozen kidney sections were exposed to TRIzol LS Reagent (Life Technologies, Carlsbad, CA, United States) for RNA isolation. Then, 2 μg of total RNA was used to obtain cDNA (High-Capacity cDNA Reverse Transcription Kit; Life Technologies) and real-time PCR was performed using a StepOnePlus (Life Technologies) machine and TaqMan assay system (Life Technologies). The following TaqMan probes were used: nephrin (*NPHS1*), Rn00674268_m1; kidney injury molecule-1 (Kim-1) (*Havcr1*), Rn00597703_m1; Ki67 (*Mki67*), Rn01451446_m1; monocyte chemoattractant protein-1 (MCP-1) (*Ccl2*), Rn00580555_m1; interleukin 1 beta (*Il1b*), Rn00580432_m1; nuclear factor kappa B 1 (*Nfkb1*), Rn01399572_m1; α-SMA (*Acta2*), Rn01759928_g1; and glyceraldehyde-3-phosphate dehydrogenase (*Gapdh*), Rn01775763_g1 (reference gene). All qPCRs were performed using 20 ng cDNA and all samples were assayed in duplicate. The comparative cycle threshold ($2^{\Delta\ \Delta\ Ct}$) method was used for data analysis. The data were normalized to *Gapdh* expression and are shown as the fold change relative to the control group.

Immunoblotting Studies

Total protein was extracted from the remaining kidney section using ice-cold PBS with protease inhibitors (Roche Brazil, São Paulo, Brazil) and centrifugation (3,000 × *g* for 10 min at 4°C). As previously described (Costa-Pessoa et al., 2014; Gonçalves et al., 2018) and summarized here, immunoblot analysis was performed on 50-μg protein aliquots resolved by 4 or 10% SDS-PAGE. Then, the protein samples were transferred to a polyvinylidene fluoride (PVDF) membrane. The blots were blocked and incubated with the following primary antibodies: mouse anti-THP (1:1000), goat anti-megalin (1:1000) (Santa Cruz Biotechnology, SC, CA, United States) and mouse anti-β-actin (1:5000, Abcam, Cambridge, United Kingdom). A horseradish peroxidase-conjugated secondary antibody (Jackson ImmunoResearch Laboratories, Baltimore, MD, United States) was used and the blots were treated with enhanced chemiluminescence (ECL) reagent (GE HealthCare, Aurora, OH, United States). The bands were quantified by optical densitometry using ImageJ software (National Institutes of Health) and protein expression was analyzed relative to the endogenous control β-actin. The values are presented as protein expression relative to the control group.

Morphological Studies and Immunostaining

As previously described (Thieme and Oliveira-Souza, 2015) and summarized here, fixed 4-μm kidney sections were deparaffinized for histological studies. Next, the histological sections were stained with hematoxylin and eosin (HE) and examined under a light microscope (Eclipse 80i, Nikon) to evaluate tubular morphology, interstitial conditions and tubular crystal formation. Additionally, deparaffinized 4-μm kidney sections were subjected to immunohistochemical staining with rabbit anti-desmin (1:200, Abcam), mouse anti-CD68 (ED-1) (1:50, AbD Serotec, Oxford, United Kingdom) and mouse anti-THP (1:400, Santa Cruz Biotechnology) primary antibodies. Non-specific protein binding was first blocked by incubation with 10% goat serum in TBS + BSA 1% for 60 min and then the sections were incubated with primary antibodies overnight at 4°C. The reaction products were detected using avidin-biotin-peroxidase complex (Vector Labs, Burlingame, CA, United States) and the sections were counterstained with methyl green (Amresco, Ohio, United States), dehydrated and mounted with Permount (Fisher Scientific, Fair Lawn, NJ, United States). The immunostained proteins were analyzed using a computerized morphometry program (NIS-Elements, Nikon) with 20 and 40× objectives. THP staining was qualitatively analyzed using a light microscope (Eclipse 80i, Nikon). The number of CD68-positive infiltrating cells was counted in 30 fields (107172, 99 μm^2) and the mean of the control and treated groups were compared. Glomerular desmin staining was quantified using Aperio ImageScope software version 12.3.2

TABLE 1 | Metabolic parameters.

Parameters	CTL (*n* = 6–7)	NaOx (*n* = 7–8)	*p*-value
Food intake (g/day)	47.00 ± 4.51	48.17 ± 1.26	0.8765
Water intake (mL/day)	15.00 ± 3.10	15.14 ± 1.26	0.6435
Urinary flow (μL/min)	16.51 ± 1.89	13.61 ± 1.39	0.2810
Kidney weight/body weight (mg/g)	3.84 ± 0.12	4.16 ± 0.16	0.1520
Plasma sodium (mEq/L)	135.80 ± 1.86	133.30 ± 1.40	0.2646
Plasma osmolality (mOsmol/kg H_2O)	308.80 ± 5.44	317.70 ± 4.57	0.1352

Values are mean ± SE, number of animals (n) per group is indicated in parenthesis.

(Leica Biosystems, Buffalo Grove, IL, United States) and protein staining is expressed as the total intensity of the positive signal. Fluorescence measurements were performed as previously reported with minor modifications (Cardoso et al., 2018). Four-micrometer deparaffinized kidney sections were blocked with 3% BSA in PBS for 1 h at room temperature before being incubated overnight at 4°C with rabbit anti-WT1 (1:200) and goat anti-megalin (1:200) primary antibodies (Thermo Fisher Scientific). Next, the kidney sections were washed three times with PBS, incubated with Alexa Fluor 594-conjugated *F*(ab′) goat anti-rabbit (1:200) and Alexa Fluor 488-conjugated *F*(ab′) rabbit anti-goat (1:200) secondary antibodies (Thermo Fisher Scientific) for 1 h at room temperature in the dark, and mounted with Fluoroshield (Sigma Aldrich). Megalin staining was analyzed using a Zeiss LSM 510 confocal microscope equipped with a 63× objective and laser excitation at 488 nm. Tubular megalin fluorescence signal was quantified using the ImageJ (National Institute of Mental Health, Bethesda, MD, United States) and the equation: *Corrected total cells fluorescence = integrated density* − (*area of selected cells* × *means fluorescence background*). The numbers of positive tubules were counted in three areas per animal and the means of the control and treated groups were compared. For WT1, kidney sections were analyzed using a fluorescence microscope (Eclipse 80i, Nikon, Tokyo, Japan) equipped with a 40× objective and laser excitation at 546 nm for Alexa Fluor 594 and 405 nm for DAPI. The number of WT1-positive cells and DAPI-positive cells were counted in 10 glomeruli per animal. Then, the WT1/DAPI ratio was calculated and the mean of the control and treated groups were compared. All morphological analyses were performed blindly by one independent investigator.

Statistical Analysis

Comparisons between two groups were performed using a non-parametric Mann–Whitney test using GraphPad Prism Software (GraphPad Software, Inc., San Diego, CA, United States). The results are expressed as the mean ± standard error of the mean (SE) and $p < 0.05$ was considered significant.

RESULTS

Metabolic Parameters

As shown in **Table 1**, NaOx treatment did not change the food and water intake, urinary flow, kidney weight, plasma sodium concentration or osmolality in comparison to the control group.

Kidney Function

To confirm the establishment of the experimental model of NaOx-induced acute crystalline nephropathy, hematoxylin and eosin staining was performed and the staining revealed medullary casts and CaOx crystals, which were also confirmed by urinary sediment analysis (**Figure 1A**). Plasma levels of creatinine and urea were significantly increased after acute NaOx treatment (**Figures 1B,C** and **Table 2**). In addition, urinary creatinine concentration and creatinine clearance were decreased in comparison to those in the control group (**Table 2**), although urinary flow remained unchanged as showed in **Table 1**.

Glomerular Injury

Next, we evaluated glomerular conditions in both the control and treated groups. NaOx treatment induced a significant increase in glomerular desmin immunostaining (**Figures 2A,B**), decreased

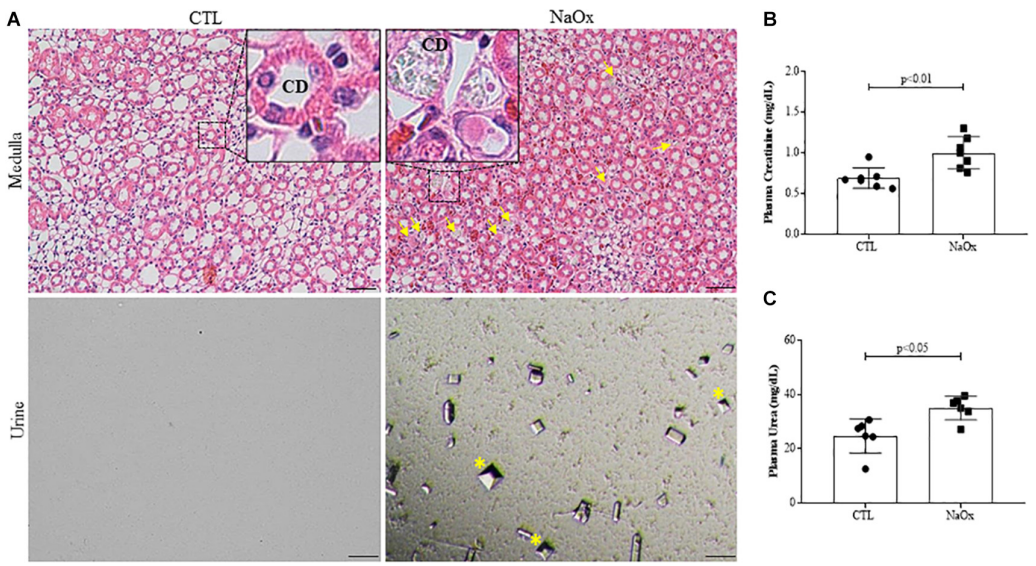

FIGURE 1 | Representative photomicrographs of renal tissue illustrating the medullar area and urinary sediment in control and treated rats. Kidney sections (4-μm thick) were stained with hematoxylin and eosin (HE). **(A)** Standardized images were captured using a morphometric program (NIS-Elements, Nikon) with a 20× objective, and magnified images captured with a 40× objective are shown at the top. The arrows indicate crystal formations and protein casts in collecting ducts (CD), and the asterisks indicate urinary CaOx crystals. The effects of NaOx treatment on plasma creatinine **(B)** and urea **(C)** levels. The values are the means ± SEs (n = 6–8). Bar = 100 μm. CTL, control; NaOx, sodium oxalate.

the WT1 immunofluorescence signal (**Figures 2C,D**) and increased nephrin mRNA expression (**Figure 2E**) in comparison to the control group. The mean values are shown in **Table 2**.

Tubular Injury

To determine if treatment with NaOx induces morphological changes in the kidneys, 4-μm hematoxylin and eosin-stained kidney sections were evaluated, and the results indicated that there was prominent tubular dilation in the treated group in comparison to the control group (**Figure 3A**). Furthermore, NaOx treatment induced albuminuria (**Figures 3B,C**) and a significant increase in Kim-1 and Ki67 mRNA expression (**Figures 3D,E**). The mean values are shown in **Table 2**.

Tubular injury in the NaOx-treated group occurred concomitantly with a decrease in total megalin protein expression and proximal tubular megalin distribution in comparison to those observed in the control animals (**Figures 4A–D**). The mean values are shown in **Table 2**.

THP Expression

Since distal nephron segments showed protein casts in the treated group, as reported before, we investigated THP expression and its tubular distribution. The results demonstrated that NaOx treatment induced a significant decrease in the total of THP protein expression and distribution in both cortical and medullary regions of the kidney in comparison to those observed in the control group (**Figures 5A–C** and **Table 2**).

Proinflammatory and Profibrotic Factors

We performed immunohistochemistry for CD68 (ED1), a monocyte/macrophage marker. Treatment with NaOx induced a significant increase in CD68 protein staining, indicating the infiltration of macrophages in the kidney (**Figures 6A,B**). Next, we investigated the gene expression of the proinflammatory and profibrotic factors. We observed that NaOx treatment induced a significant increase in MCP-1, IL-1β, NFkappaB, and α-SMA mRNA expression, in comparison to that in the control group (**Figures 6C–F** and **Table 2**).

DISCUSSION

In the current study, a single intraperitoneal injection of NaOx in male rats induced CaOx crystal and luminal cast formation in the medullary tubules, observed 24 h after treatment. This experimental model was characterized by Khan et al. (1979, 1982, 1992), who reported an increase in urinary excretion of oxalate after a single NaOx injection, followed by its decrease

TABLE 2 | Differences among experimental group.

Parameters	**CTL (*n* = 6–7)**	**NaOx (*n* = 6–8)**	***p*-value**
Plasma creatinine (mg/dL)	0.69 ± 0.05	1.00 ± 0.07	0.0041**
Urinary creatinine (mg/dL)	42.37 ± 2.01	31.56 ± 1.43	0.0159*
Creatinine clearance (mL/min)	1.08 ± 0.06	0.56 ± 0.05	0.0007***
Plasma urea (mg/dL)	24.71 ± 2.61	35.03 ± 1.77	0.0152*
Parameters	**CTL (*n* = 5–6)**	**NaOx (*n* = 5–6)**	***p*-value**
Glomerular desmin expression (intensity signal)	27926 ± 4673	77566 ± 6440	0.0079**
WT-1/DAPI (ratio)	0.49 ± 0.01	0.42 ± 0.02	0.0143**
Nephrin (*Nphs1*) mRNA expression *(Fold Change)*	1.00 ± 0.05	1.27 ± 0.06	0.0152*
Parameters	**CTL (*n* = 6–7)**	**NaOx (*n* = 6–8)**	***p*-value**
Alb/Cr ratio (AU)	48.71 ± 4.95	89.49 ± 4.97	0.0005***
Kim-1 (*Havcr1*) mRNA expression *(Fold Change)*	0.96 ± 0.20	278.00 ± 126.60	0.0022**
Ki67 (*Mki67*) mRNA expression *(Fold Change)*	1.06 ± 0.14	4.04 ± 1.20	0.0012**
Parameters	**CTL (*n* = 4–6)**	**NaOx (*n* = 4–7)**	***p*-value**
Relative megalin protein expression	6.13 ± 0.65	1.85 ± 0.87	0.0286*
Corrected tubular fluorescence for megalin	5.73 ± 0.73	1.87 ± 0.27	0.0026**
Relative THP expression	1.09 ± 0.11	0.59 ± 0.07	0.0082**
Parameters	**CTL (*n* = 5–6)**	**NaOx (*n* = 5–8)**	***p*-value**
CD68 positive cells/field	6.80 ± 1.80	24.00 ± 3.97	0.0065**
MCP-1 (*Ccl2*) mRNA expression *(Fold Change)*	1.02 ± 0.08	3.16 ± 0.43	0.0007***
IL-1β (*Il1b*) mRNA expression *(Fold Change)*	0.95 ± 0.19	2.44 ± 0.37	0.0159*
NFkappaB mRNA expression *(Fold Change)*	1.00 ± 0.03	1.41 ± 0.11	0.0043**
α-SMA (*Acta2*) mRNA expression *(Fold Change)*	1.01 ± 0.07	1.53 ± 1.12	0.0047**

*Values are mean ± SE, number of animals (n) per group is indicated in parenthesis. *p < 0.05, **p < 0.01, ***p < 0.001 versus control (CTL); NaOx, sodium oxalate. Alb/Cr, albumin/creatinine; A. U, arbitrary units; THP, Tamm–Horsfall protein.*

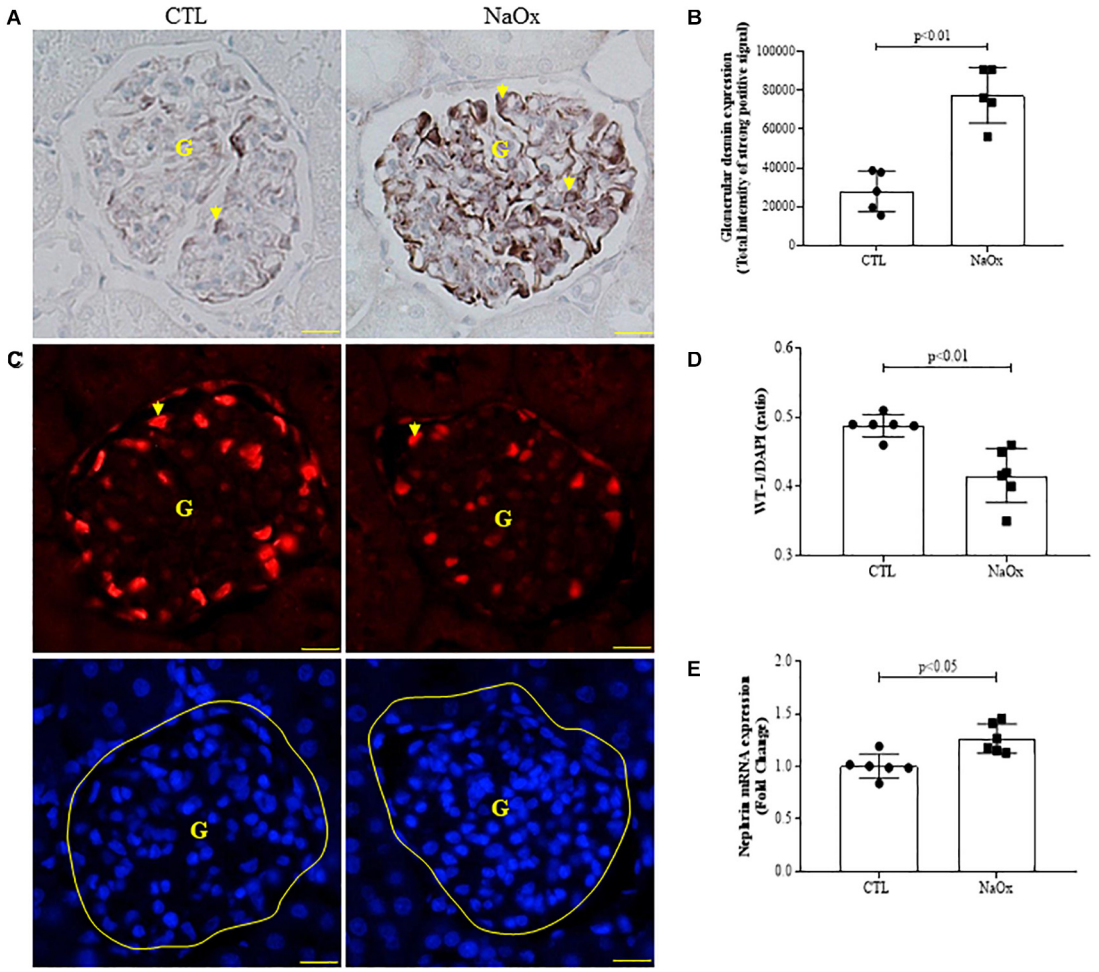

FIGURE 2 | Effect of NaOx treatment on desmin staining **(A,B)**, WT1/DAPI ratio **(C,D)**, and nephrin mRNA expression **(E)**. The values represent the mean ± SE (n = 5–6/group). Images were captured using a morphometric program (NIS-Elements, Nikon) with a 40× objective. The arrows indicate desmin and WT1 staining, and G indicates the glomerulus. Bar = 50 μm. CTL, control; NaOx, sodium oxalate.

within the next 12 h. In our study we observed a still prominent excretion of crystals in 24 h. Here, we focused on the factors involved in crystalline-induced AKI and consequent changes in renal function and morphology in 24 h.

In our study, although the metabolic parameters were similar between the groups, we observed a significant decline in kidney function in rats treated with NaOx, since under this condition the animals showed increased plasma level of creatinine followed by reduced creatinine clearance. It is known that serum creatinine level is a suboptimal marker of glomerular injury, since it depends of many factors, including the new glomerular filtration rate (GFR), tubular secretion rate and urine volume (Moran and Myers, 1985; Arai et al., 2016). Thus, in the current study we also evaluated different factors related to glomerular injury. Our results demonstrate increased plasma level of urea, enhanced glomerular desmin staining intensity, decreased podocyte WT1 staining, increased nephrin mRNA expression in the NaOx-treated group. Together, our results indicate consistent glomerular injury in crystalline-induced AKI.

Our findings corroborate other studies that demonstrated that tubular casts formed by crystals and/or necrotic cell debris can transiently obstruct the tubular lumen, resulting in decline of glomerular filtration rate (GFR) (Arai et al., 2016). Podocytes are terminally differentiated and non-proliferative glomerular epithelial cells that are situated on the outer surface of the glomerular capillary basement membrane (GBM) (Qian et al., 2019). Under healthy conditions, podocyte foot processes are connected to each other by slit diaphragms (SDs), which are organized by cross-linking molecules such as nephrin, podocin, Neph1, CD2AP and cytoskeleton proteins (Faul et al., 2007; Feliers, 2015; Garg, 2018). In addition, WT1 is a transcription factor that regulates the differentiation state of podocytes and is highly expressed in mature podocytes (Guo et al., 2002). It has been documented that injured podocytes re-enter the cell cycle, leading to dedifferentiation, podocyte damage and a loss of ultrafiltration barrier function, resulting in proteinuria (Greka and Mundel, 2012), which is the major risk factor for progressive chronic kidney disease. The increased nephrin mRNA expression

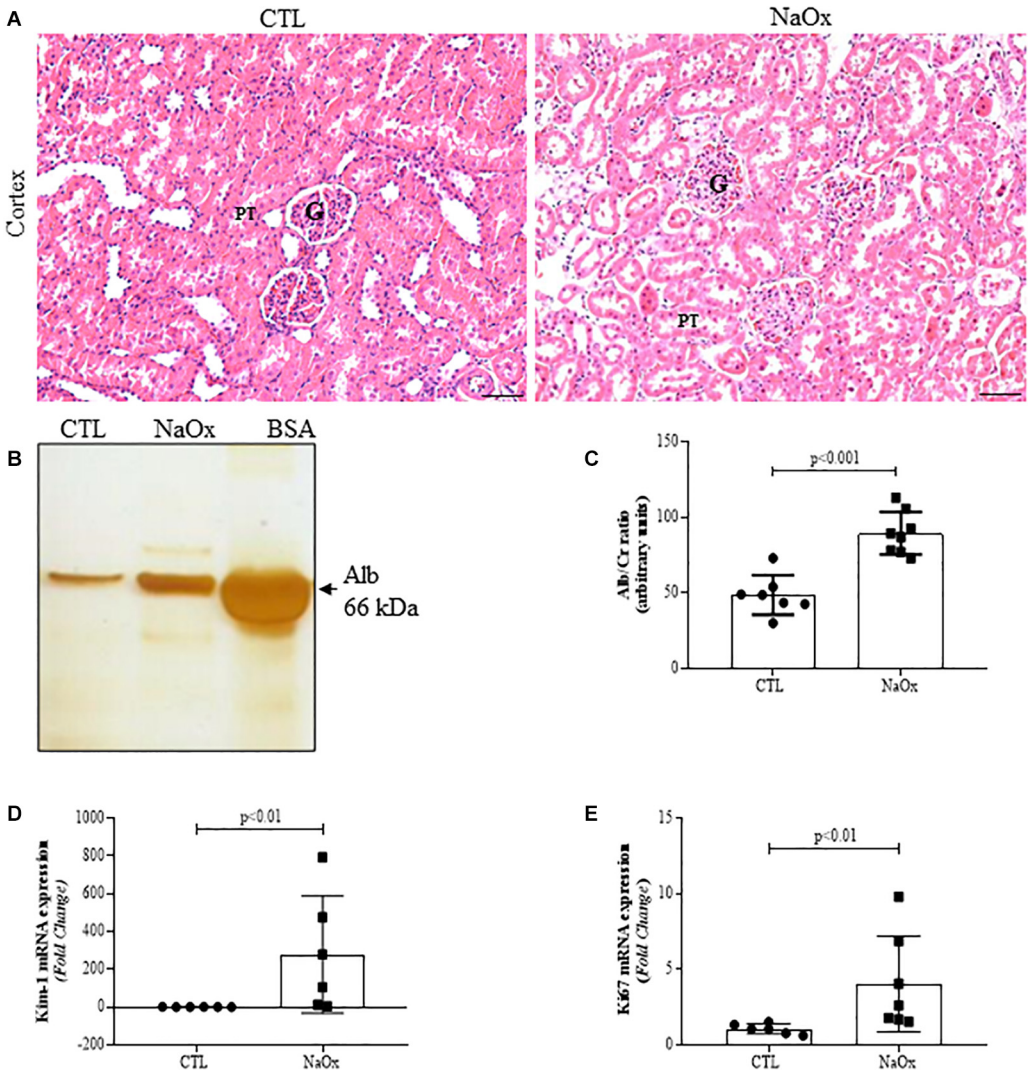

FIGURE 3 | Effect of NaOx treatment on cortical changes, including tubular injury, as demonstrated by HE staining **(A)**. Urine samples from control and treated rats were resolved on 10% SDS page gels followed by gel staining with a protein-sensitive SilverQuest Silver Staining Kit. Statistical analysis of albumin excretion in both the control and treated groups was performed **(B,C)**. The mRNA expression levels of Kim-1 **(D)** and Ki67 **(E)**. The values are mean ± SE (n = 6–8). Bar = 100 μm. CTL, control; NaOx, sodium oxalate; G glomerulus; PT, proximal tubule.

observed in our study suggests a compensatory strategy of podocytes against the possible loss of damaged cells.

In healthy glomeruli, desmin is distributed mainly in mesangial cells. However, in different experimental models of mice and rats with glomerular disease, increased glomerular desmin staining is recognized as a marker of podocyte dedifferentiation and injury (Crowley et al., 2009; Casare et al., 2016; Xie et al., 2019) and is followed by decreased nuclear WT1 expression and loss of slit diaphragm proteins (Greka and Mundel, 2012).

Considering the relevance of podocyte injury to progressive proteinuria previously demonstrated in ischemia-reperfusion and glomerulosclerosis animal models (Hara et al., 2015; Chen et al., 2019), we also evaluated whether acute crystalline-related glomerular injury contributes to proteinuria. Indeed, we observed significant albuminuria in treated animals in comparison to the control group. However, this result was not exclusively attributable to podocyte injury since we found increased tubular injury factors mRNA expression, as discussed below. Thus, we extended our observations from the glomerulus to the renal tubules.

It is established that in kidney crystalline diseases, intraluminal crystals deposition leads to tubular obstruction, followed by crystals endocytosis through tubular cells. Under these conditions, sensitized tubular cells release damage-associated molecular patterns (DAMPs) to the interstitial compartment. DAMPs activate proteins such as NACHT, LRR and PYD domains-containing protein 3 (NLRP3) inflammasome in renal dendritic cells. In addition, intraluminal crystals can be translocated to the interstitial compartment, where are

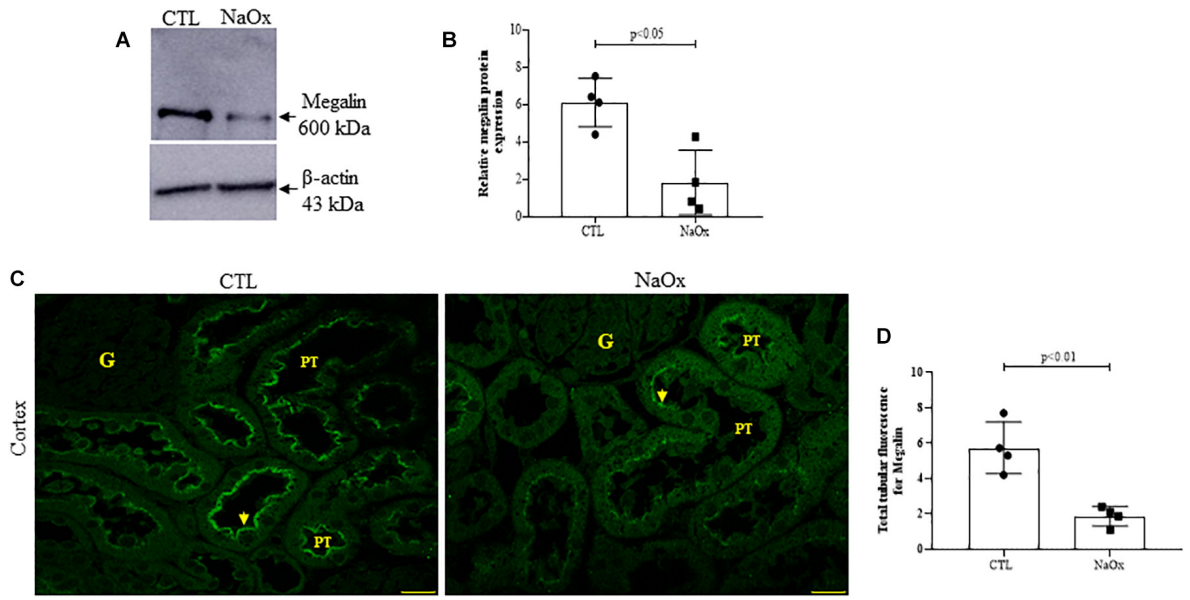

FIGURE 4 | Effect of NaOx treatment on total megalin protein expression. **(A,B)** Immunoblot analysis was performed on 50-μg protein aliquots resolved by 4% SDS-PAGE. The values are presented as the mean ± SE (n = 4/group) and β-actin was used as an internal control. Megalin staining in the proximal tubule (PT) **(C)** is indicated by the arrows. Images of megalin immunofluorescence were captured using a Zeiss LSM 510 confocal microscope equipped with a 63× objective. Statistical analysis of megalin immunofluorescence in both the control and treated groups was performed **(D)**. CTL, control; NaOx, sodium oxalate; G, glomerulus. Bar = 50 μm.

phagocytized by dendritic cells and macrophages, resulting in activation of NLRP3 inflammasome and consequent secretion of IL-1β (Mulay et al., 2013; Mulay and Anders, 2017). In turn, IL-1β induces numerous inflammatory responses.

Relative to proximal tubule (PT), its epithelium has a remarkable capacity to repair itself since it has potent ability to replace lost cells through proliferation (Bonventre, 2003). Notably, proximal tubule cells express kidney injury molecule 1 (Kim-1), which is highly upregulated after acute kidney injury (Ichimura et al., 1998; Sabbisetti et al., 2014), acts as a marker of cell differentiation and proliferation (Han et al., 2002), and mediates the phagocytosis of oxidized lipids and apoptotic bodies, including luminal cellular debris (Ichimura et al., 2008). It has been established that in addition to Kim-1, Ki67 is used as a marker of tubular regeneration and renal repair after AKI (Lazzeri et al., 2018; Zhou et al., 2018). Severe AKI could result in incomplete repair and a persistent increase in Kim-1 and Ki67 expression in tubular cells leads to AKI-to-CKD transition (Dong et al., 2019). In the current study, the proximal tubular injury was associated to a decreased megalin protein expression. Megalin is a large glycoprotein (∼600 kDa) expressed mainly in PT cells that acts as an endocytic receptor; it accumulates in clathrin-coated pits and is involved in the reabsorption of various molecules, including albumin and other low-molecular-weight proteins from glomerular filtrates (Cui et al., 1996).

We also evaluated whether THP is involved in crystalline-induced AKI. THP, or uromodulin, is a multifunctional renal-specific glycoprotein produced by the epithelial cells of the thick ascending limb (TAL) of Henle's loop, targeted to the apical domain through its glycosylphosphatidylinositol (GPI) anchor site and subsequently cleaved by the serine protease and released in the lumen (Brunati et al., 2015). In the urine, THP tends to assemble in multimeric networks through its Zona Pellucida (ZP) domain to form a dense matrix of high-molecular weight polymers constituting hyaline casts, which are increased in AKI (Devuyst et al., 2017). Although predominantly secreted into the urine, THP is also released at the basolateral membrane as a monomeric form toward the interstitial compartment, where it mediates a protective crosstalk between TAL and S3 segments of the proximal tubules, downregulating inflammatory cytokines such as MCP-1and TNF-α mainly during AKI recovery (Safirstein et al., 1991; Rampoldi et al., 2011; Heitmeier et al., 2014). El-Achkar group and other investigators using renal ischemia-reperfusion injury (IRI), but not crystalline-experimental models, observed that the THP mRNA and protein expression were reduced at the peak of injury (24 h), and recovered 72 h and 6 days after the surgery (Safirstein et al., 1991; El-Achkar et al., 2008; El-Achkar et al., 2013; Micanovic et al., 2018). Our results corroborate these findings, since we observed a relevant decrease in total THP protein expression in the kidney as well as a decrease in tubular THP protein staining in crystalline-induced AKI.

It is known that in crystalline-induced AKI, a rapid and diffuse crystallization contribute to kidney injury in several ways, including crystal-induced cytotoxicity triggers inflammation (Mulay and Anders, 2017). However, the mechanisms involved in these processes have not been elucidated. Considering the macrophage phenotypes, it is well described that pro-inflammatory M1 macrophage releases cytokines such as IL-1,

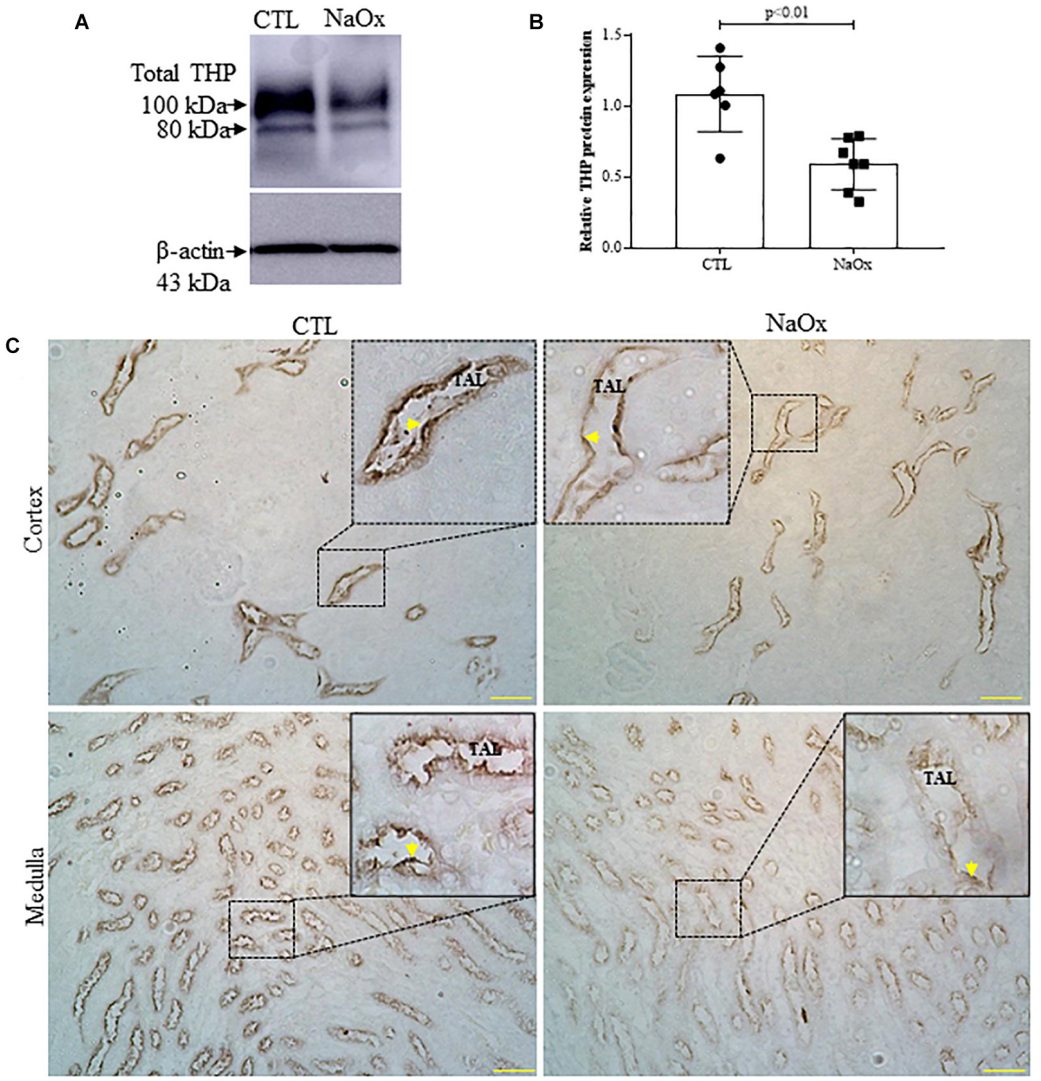

FIGURE 5 | Tamm–Horsfall protein (THP) expression and distribution. Total THP expression in the kidney **(A,B)**. Immunoblot analysis was performed on 50-μg protein aliquots resolved by 10% SDS-PAGE. The values represent the mean ± SE (*n* = 6–7/group) and β-actin was used as an internal control.
(C) Immunohistochemical images of THP staining in the cortex and medulla. Standardized images were captured using a morphometric program (NIS-Elements, Nikon) with a 20× objective and magnified images captured with a 40× objective are shown at the top. The arrows indicate THP staining in the cortex and thin ascending limb (TAL). Bar = 100 μm. CTL, control; NaOx, sodium oxalate.

IL-6, TNF-α, and MCP-1, which in turn promotes macrophage recruitment and activation during kidney injury (Kanda et al., 2006; Ricardo et al., 2008; Tesch, 2008; Dias et al., 2017). In addition to activating macrophages, IL-1β can also activate NFkappaB p65 (Shi and Berger, 2018). Activated NFkappaB p65 exacerbate the transcription of inflammatory mediators such IL-1β and MCP-1 (Anders, 2016). In contrast, M2 macrophages seems to be anti-inflammatory and profibrotic, secreting IL-10, fibronectin, TGF-β and other ECM proteins, triggering the accumulation of myofibroblasts that express smooth muscle α-actin (αSMA) (Tang et al., 2019). Consistent with these findings, our results revealed that crystalline-induced AKI resulted in an increased expression of interstitial CD68, a macrophages marker, MCP-1, IL-1β and NFkappaB mRNA, suggesting a relevant signal crosstalk between inflammatory response and cellular injury. In addition to inflammatory condition, we found profibrotic signal, highlighting the contribution of both macrophage subtypes in crystalline-induced AKI.

FUTURE PERSPECTIVE AND DIRECTIONS FOR RESEARCH

It is now becoming clear that in crystalline-induced AKI, inflammatory factors contribute to renal pathology, including a possible crosstalk between tubulointerstitial compartment and the glomerulus. However, considering the acute condition of the current study, we cannot confirm all biological events related

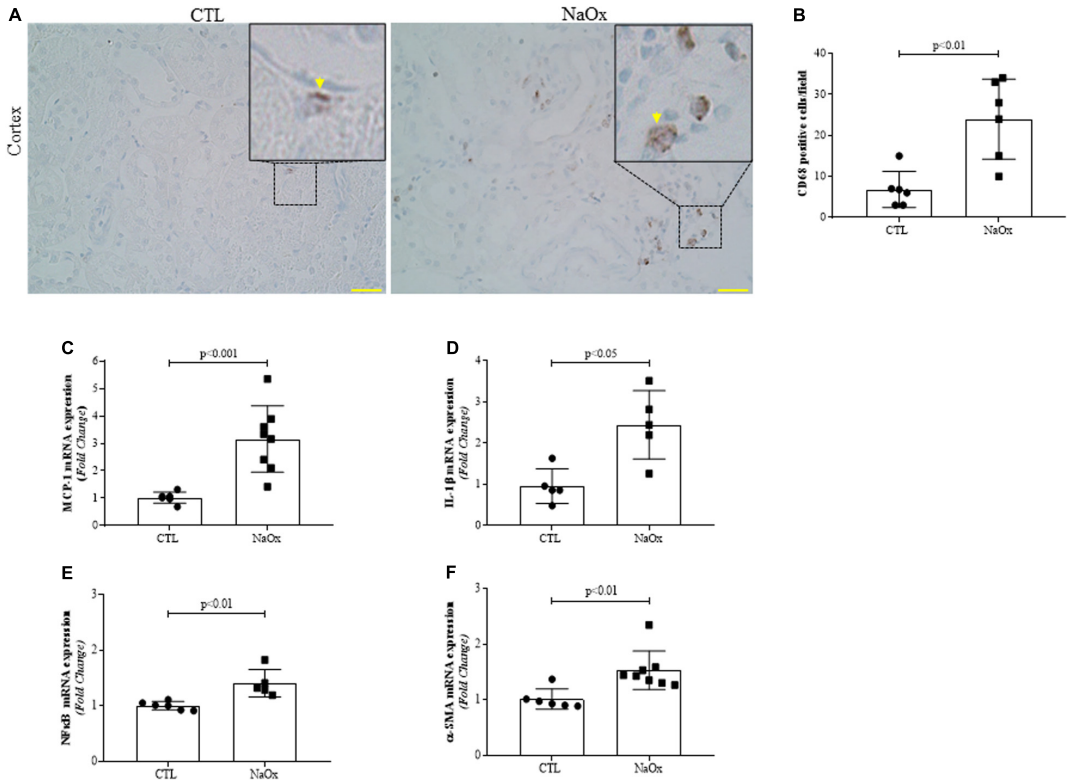

FIGURE 6 | Representative photomicrographs of the renal cortex illustrating tubulointerstitial CD68-positive cells (indicated by arrows) by immunohistochemistry. Images were captured using a morphometric program (NIS-Elements, Nikon) with a 20× objective and magnified images shown at the top were captured with a 40× objective. The values represent the mean ± SE **(A,B)**. Bar = 100 μm. In addition, MCP-1 **(C)**, IL-β1 **(D)** NFkappaB **(E)** and α-SMA **(F)** mRNA expression levels are shown as the mean ± SE (*n* = 5–8/group). CTL, control; NaOx, sodium oxalate.

to glomerular injury. On the other hand, our data are relevant and open perspectives for understanding of the crystalline-induced CKD. A deeper knowledge about the temporal events in the kidney will certainly provide a better understanding of crystalline nephropathies.

CONCLUSION

Renal pathology is the result of different cellular programming pathways, whose responses involve risks that depend on the host defense and tissue repair upon injuries. Taken together, our results suggest that acute crystalline nephropathy induces glomerular injury with a loss of podocyte viability in addition to strong tubulointerstitial injury. Thus, we believe that our findings will contribute to understanding of crystal biology and help to improve patient outcomes by defining novel cellular and molecular targets to limit nephron loss and to maintain renal function.

DATA AVAILABILITY STATEMENT

The raw data supporting the conclusions of this article will be made available by the authors, without undue reservation, to any qualified researcher.

ETHICS STATEMENT

The animal study was reviewed and approved by Institutional Animal Care and Use Committee of the University of São Paulo (Protocol no. 9276140518).

AUTHOR CONTRIBUTIONS

LA designed and performed all the experiments, analyzed the data, helped to writing, and reviewed the manuscript. JC-P helped with animals treatment, metabolic parameters analysis, immunoblotting, immunohistochemistry, immunofluorescence, and mRNA expression experiments. MP helped with animal treatments, kidney function analysis, and gene and protein expression experiments. MO-S supported and supervised the study and contributed with the writing of the manuscript. All authors approved the final manuscript.

FUNDING

This work was supported by the Fundação de Amparo a Pesquisa do Estado de São Paulo (FAPESP) to MO-S (17/02020-0),

by the Conselho Nacional de Desenvolvimento Científico e Tecnológico (CNPq) and Fundação de Amparo a Pesquisa do Estado de São Paulo (FAPESP) to LA (CNPq, 145098/2018-4 and FAPESP, 2019/06358-0), and Fundação de Amparo a Pesquisa do Estado de São Paulo (FAPESP) to MP (2016/12354-0).

ACKNOWLEDGMENTS

The authors thank Karina Thieme for helping with the writing review, Adilson da Silva Alves for assistance with the Confocal Microscope, and William Tadeu Lara Festucia for allowing the use of the Nanodrop instrument.

REFERENCES

Anders, H. J. (2016). Of inflammasomes and alarmins: IL-1β and IL-1α in kidney disease. *J. Am. Soc. Nephrol.* 27, 2564–2575. doi: 10.1681/asn.2016020177

Arai, S., Kitada, K., Yamazaki, T., Takai, R., Zhang, X., Tsugawa, Y., et al. (2016). Apoptosis inhibitor of macrophage protein enhances intraluminal debris clearance and ameliorates acute kidney injury in mice. *Nat. Med.* 22, 183–193. doi: 10.1038/nm.4012

Basile, D. P., Anderson, M. D., and Sutton, T. A. (2012). Pathophysiology of acute kidney injury. *Compr. Physiol.* 2, 1303–1353.

Bergsland, K. J., Zisman, A. L., Asplin, J. R., Worcester, E. M., and Coe, F. L. (2011). Evidence for net renal tubule oxalate secretion in patients with calcium kidney stones. *Am. J. Physiol. Renal Physiol.* 300, F311–F318.

Bonventre, J. V. (2003). Dedifferentiation and proliferation of surviving epithelial cells in acute renal failure. *J. Am. Soc. Nephrol.* 14(Suppl. 1), S55–S61.

Brunati, M., Perucca, S., Han, L., Cattaneo, A., Consolato, F., Andolfo, A., et al. (2015). The serine protease hepsin mediates urinary secretion and polymerisation of Zona Pellucida domain protein uromodulin. *eLife* 4:e08887.

Carbone, A., Al Salhi, Y., Tasca, A., Palleschi, G., Fuschi, A., De Nunzio, C., et al. (2018). Obesity and kidney stone disease: a systematic review. *Minerva Urol. Nefrol.* 70, 393–400.

Cardoso, V. G., Gonçalves, G. L., Costa-Pessoa, J. M., Thieme, K., Lins, B. B., Casare, F. A. M., et al. (2018). Angiotensin II-induced podocyte apoptosis is mediated by endoplasmic reticulum stress/PKC-δ/p38 MAPK pathway activation and trough increased Na. *BMC Nephrol.* 19:179. doi: 10.1186/s12882-018-0968-4

Casare, F. A., Thieme, K., Costa-Pessoa, J. M., Rossoni, L. V., Couto, G. K., Fernandes, F. B., et al. (2016). Renovascular remodeling and renal injury after extended angiotensin II infusion. *Am. J. Physiol. Renal Physiol.* 310, F1295–F1307.

Chen, Y., Lin, L., Tao, X., Song, Y., Cui, J., and Wan, J. (2019). The role of podocyte damage in the etiology of ischemia-reperfusion acute kidney injury and post-injury fibrosis. *BMC Nephrol.* 20:106. doi: 10.1186/s12882-019-1298-x

Costa-Pessoa, J. M., Damasceno, R. S., Machado, U. F., Beloto-Silva, O., and Oliveira-Souza, M. (2014). High glucose concentration stimulates NHE-1 activity in distal nephron cells: the role of the Mek/Erk1/2/p90 and p38MAPK signaling pathways. *Cell Physiol. Biochem.* 33, 333–343. doi: 10.1159/000356673

Crowley, S. D., Vasievich, M. P., Ruiz, P., Gould, S. K., Parsons, K. K., Pazmino, A. K., et al. (2009). Glomerular type 1 angiotensin receptors augment kidney injury and inflammation in murine autoimmune nephritis. *J. Clin. Invest.* 119, 943–953.

Cui, S., Verroust, P. J., Moestrup, S. K., and Christensen, E. I. (1996). Megalin/gp330 mediates uptake of albumin in renal proximal tubule. *Am. J. Physiol.* 271, F900–F907.

de Ponte, M. C., Casare, F. A. M., Costa-Pessoa, J. M., Cardoso, V. G., Malnic, G., Mello-Aires, M., et al. (2017). The role of β-adrenergic overstimulation in the early stages of renal injury. *Kidney Blood Press Res.* 42, 1277–1289. doi: 10.1159/000485931

Devuyst, O., Olinger, E., and Rampoldi, L. (2017). Uromodulin: from physiology to rare and complex kidney disorders. *Nat. Rev. Nephrol.* 13, 525–544. doi: 10.1038/nrneph.2017.101

Dias, C. B., Malafronte, P., Lee, J., Resende, A., Jorge, L., Pinheiro, C. C., et al. (2017). Role of renal expression of CD68 in the long-term prognosis of proliferative lupus nephritis. *J. Nephrol.* 30, 87–94. doi: 10.1007/s40620-015-0252-7

Dong, Y., Zhang, Q., Wen, J., Chen, T., He, L., Wang, Y., et al. (2019). Ischemic duration and frequency determines AKI-to-CKD progression monitored by dynamic changes of tubular biomarkers in IRI Mice. *Front. Physiol.* 10:153. doi: 10.3389/fphys.2019.00153

Efe, O., Verma, A., and Waikar, S. S. (2019). Urinary oxalate as a potential mediator of kidney disease in diabetes mellitus and obesity. *Curr. Opin. Nephrol. Hypertens.* 28, 316–320. doi: 10.1097/mnh.0000000000000515

El-Achkar, T. M., McCracken, R., Liu, Y., Heitmeier, M. R., Bourgeois, S., Ryerse, J., et al. (2013). Tamm-Horsfall protein translocates to the basolateral domain of thick ascending limbs, interstitium, and circulation during recovery from acute kidney injury. *Am. J. Physiol. Renal Physiol.* 304, F1066–F1075.

El-Achkar, T. M., Wu, X. R., Rauchman, M., McCracken, R., Kiefer, S., and Dagher, P. C. (2008). Tamm-Horsfall protein protects the kidney from ischemic injury by decreasing inflammation and altering TLR4 expression. *Am. J. Physiol. Renal Physiol.* 295, F534–F544.

Faul, C., Asanuma, K., Yanagida-Asanuma, E., Kim, K., and Mundel, P. (2007). Actin up: regulation of podocyte structure and function by components of the actin cytoskeleton. *Trends Cell Biol.* 17, 428–437. doi: 10.1016/j.tcb.2007.06.006

Feliers, D. (2015). Epigenetic control of podocyte differentiation: a new target of the renin-angiotensin system in kidney disease. *Kidney Int.* 88, 668–670. doi: 10.1038/ki.2015.224

Fox, B., Saxena, N., Schuppener, L., and Maursetter, L. (2018). Combining acute kidney injury with gastrointestinal pathology: a clue to acute oxalate nephropathy. *Case Rep. Nephrol.* 2018:8641893.

Gambardella, R. L., and Richardson, K. E. (1977). The pathways of oxalate formation from phenylalanine, tyrosine, tryptophan and ascorbic acid in the rat. *Biochim. Biophys. Acta* 499, 156–168. doi: 10.1016/0304-4165(77)90238-0

Garg, P. (2018). A review of podocyte biology. *Am. J. Nephrol.* 47(Suppl. 1), 3–13. doi: 10.1159/000481633

Gonçalves, G. L., Costa-Pessoa, J. M., Thieme, K., Lins, B. B., and Oliveira-Souza, M. (2018). Intracellular albumin overload elicits endoplasmic reticulum stress and PKC-delta/p38 MAPK pathway activation to induce podocyte apoptosis. *Sci. Rep.* 8:18012.

Greka, A., and Mundel, P. (2012). Cell biology and pathology of podocytes. *Annu. Rev. Physiol.* 74, 299–323. doi: 10.1146/annurev-physiol-020911-153238

Guo, J. K., Menke, A. L., Gubler, M. C., Clarke, A. R., Harrison, D., Hammes, A., et al. (2002). WT1 is a key regulator of podocyte function: reduced expression levels cause crescentic glomerulonephritis and mesangial sclerosis. *Hum. Mol. Genet.* 11, 651–659. doi: 10.1093/hmg/11.6.651

Han, W. K., Bailly, V., Abichandani, R., Thadhani, R., and Bonventre, J. V. (2002). Kidney injury molecule-1 (KIM-1): a novel biomarker for human renal proximal tubule injury. *Kidney Int.* 62, 237–244. doi: 10.1046/j.1523-1755.2002.00433.x

Hara, S., Kobayashi, N., Sakamoto, K., Ueno, T., Manabe, S., Takashima, Y., et al. (2015). Podocyte injury-driven lipid peroxidation accelerates the infiltration of glomerular foam cells in focal segmental glomerulosclerosis. *Am. J. Pathol.* 185, 2118–2131. doi: 10.1016/j.ajpath.2015.04.007

Heitmeier, M., McCracken, R., Micanovic, R., Khan, S., and El-Achkar, T. M. (2014). The role of tumor necrosis factor alpha in regulating the expression of Tamm-Horsfall Protein (uromodulin) in thick ascending limbs during kidney injury. *Am. J. Nephrol.* 40, 458–467. doi: 10.1159/000369836

Hingorani, S., Molitoris, B. A., and Himmelfarb, J. (2009). Ironing out the pathogenesis of acute kidney injury. *Am. J. Kidney Dis.* 53, 569–571. doi: 10.1053/j.ajkd.2009.01.002

Hoppe, B., Beck, B. B., and Milliner, D. S. (2009). The primary hyperoxalurias. *Kidney Int.* 75, 1264–1271.

Ichimura, T., Asseldonk, E. J., Humphreys, B. D., Gunaratnam, L., Duffield, J. S., and Bonventre, J. V. (2008). Kidney injury molecule-1 is a phosphatidylserine receptor that confers a phagocytic phenotype on epithelial cells. *J. Clin. Invest.* 118, 1657–1668. doi: 10.1172/jci34487

Ichimura, T., Bonventre, J. V., Bailly, V., Wei, H., Hession, C. A., Cate, R. L., et al. (1998). Kidney injury molecule-1 (KIM-1), a putative epithelial cell adhesion molecule containing a novel immunoglobulin domain, is up-regulated in renal cells after injury. *J. Biol. Chem.* 273, 4135–4142. doi: 10.1074/jbc.273.7.4135

Kanda, H., Tateya, S., Tamori, Y., Kotani, K., Hiasa, K., Kitazawa, R., et al. (2006). MCP-1 contributes to macrophage infiltration into adipose tissue, insulin resistance, and hepatic steatosis in obesity. *J. Clin. Invest.* 116, 1494–1505. doi: 10.1172/jci26498

Kasidas, G. P., and Rose, G. A. (1986). Measurement of plasma oxalate in healthy subjects and in patients with chronic renal failure using immobilised oxalate oxidase. *Clin. Chim. Acta* 154, 49–58. doi: 10.1016/0009-8981(86)90087-2

Khan, S. R., Finlayson, B., and Hackett, R. L. (1979). Histologic study of the early events in oxalate induced intranephronic calculosis. *Invest. Urol.* 17, 199–202.

Khan, S. R., Finlayson, B., and Hackett, R. L. (1982). Experimental calcium oxalate nephrolithiasis in the rat. Role of the renal papilla. *Am. J. Pathol.* 107, 59–69.

Khan, S. R., and Glenton, P. A. (2010). Experimental induction of calcium oxalate nephrolithiasis in mice. *J. Urol.* 184, 1189–1196. doi: 10.1016/j.juro.2010.04.065

Khan, S. R., Shevock, P. N., and Hackett, R. L. (1992). Acute hyperoxaluria, renal injury and calcium oxalate urolithiasis. *J. Urol.* 147, 226–230. doi: 10.1016/s0022-5347(17)37202-6

Knauf, F., Velazquez, H., Pfann, V., Jiang, Z., and Aronson, P. S. (2019). Characterization of renal NaCl and oxalate transport in Slc26a6. *Am. J. Physiol. Renal Physiol.* 01, F128–F133.

Knight, J., Assimos, D. G., Callahan, M. F., and Holmes, R. P. (2011). Metabolism of primed, constant infusions of [1,2-^{13}łC_2] glycine and [1-^{13}łC_1] phenylalanine to urinary oxalate. *Metabolism* 60, 950–956. doi: 10.1016/j.metabol.2010.09.002

Kujala, M., Tienari, J., Lohi, H., Elomaa, O., Sariola, H., Lehtonen, E., et al. (2005). SLC26A6 and SLC26A7 anion exchangers have a distinct distribution in human kidney. *Nephron Exp. Nephrol.* 101, e50–e58. doi: 10.1159/000086345

Lazzeri, E., Angelotti, M. L., Peired, A., Conte, C., Marschner, J. A., Maggi, L., et al. (2018). Endocycle-related tubular cell hypertrophy and progenitor proliferation recover renal function after acute kidney injury. *Nat. Commun.* 04:1344.

Lorenz, G., Darisipudi, M. N., and Anders, H. J. (2014). Canonical and non-canonical effects of the NLRP3 inflammasome in kidney inflammation and fibrosis. *Nephrol. Dial. Transplant.* 29, 41–48. doi: 10.1093/ndt/gft332

Meydan, N., Barutca, S., Caliskan, S., and Camsari, T. (2003). Urinary stone disease in diabetes mellitus. *Scand. J. Urol. Nephrol.* 37, 64–70. doi: 10.1080/00365590310008730

Micanovic, R., Khan, S., Janosevic, D., Lee, M. E., Hato, T., Srour, E. F., et al. (2018). Tamm-horsfall protein regulates mononuclear phagocytes in the kidney. *J. Am. Soc. Nephrol.* 03, 841–856.

Moran, S. M., and Myers, B. D. (1985). Course of acute renal failure studied by a model of creatinine kinetics. *Kidney Int.* 27, 928–937. doi: 10.1038/ki.1985.101

Mulay, S. R., and Anders, H. J. (2017). Crystal nephropathies: mechanisms of crystal-induced kidney injury. *Nat. Rev. Nephrol.* 04, 226–240. doi: 10.1038/nrneph.2017.10

Mulay, S. R., Kulkarni, O. P., Rupanagudi, K. V., Migliorini, A., Darisipudi, M. N., Vilaysane, A., et al. (2013). Calcium oxalate crystals induce renal inflammation by NLRP3-mediated IL-1β secretion. *J. Clin. Invest.* 123, 236–246. doi: 10.1172/jci63679

Mulay, S. R., Shi, C., Ma, X., and Anders, H. J. (2018). Novel insights into crystal-induced kidney injury. *Kidney Dis. (Basel).* 4, 49–57. doi: 10.1159/000487671

Noonan, S. C., and Savage, G. P. (1999). Oxalate content of foods and its effect on humans. *Asia Pac. J. Clin. Nutr.* 8, 64–74. doi: 10.1046/j.1440-6047.1999.00038.x

Oakley, B. R., Kirsch, D. R., and Morris, N. R. (1980). A simplified ultrasensitive silver stain for detecting proteins in polyacrylamide gels. *Anal. Biochem.* 105, 361–363. doi: 10.1016/0003-2697(80)90470-4

Pfau, A., and Knauf, F. (2016). Update on nephrolithiasis: core curriculum 2016. *Am. J. Kidney Dis.* 12, 973–985. doi: 10.1053/j.ajkd.2016.05.016

Poore, R. E., Hurst, C. H., Assimos, D. G., and Holmes, R. P. (1997). Pathways of hepatic oxalate synthesis and their regulation. *Am. J. Physiol.* 272, C289–C294.

Qian, T., Hernday, S. E., Bao, X., Olson, W. R., Panzer, S. E., Shusta, E. V., et al. (2019). Directed differentiation of human pluripotent stem cells to podocytes under defined conditions. *Sci. Rep.* 9:2765.

Rampoldi, L., Scolari, F., Amoroso, A., Ghiggeri, G., and Devuyst, O. (2011). The rediscovery of uromodulin (Tamm-Horsfall protein): from tubulointerstitial nephropathy to chronic kidney disease. *Kidney Int.* 80, 338–347. doi: 10.1038/ki.2011.134

Ricardo, S. D., van Goor, H., and Eddy, A. A. (2008). Macrophage diversity in renal injury and repair. *J. Clin. Invest.* 118, 3522–3530. doi: 10.1172/jci36150

Robijn, S., Hoppe, B., Vervaet, B. A., D'Haese, P. C., and Verhulst, A. (2011). Hyperoxaluria: a gut-kidney axis? *Kidney Int.* 80, 1146–1158. doi: 10.1038/ki.2011.287

Sabbisetti, V. S., Waikar, S. S., Antoine, D. J., Smiles, A., Wang, C., Ravisankar, A., et al. (2014). Blood kidney injury molecule-1 is a biomarker of acute and chronic kidney injury and predicts progression to ESRD in type I diabetes. *J. Am. Soc. Nephrol.* 25, 2177–2186. doi: 10.1681/asn.2013070758

Safirstein, R., Megyesi, J., Saggi, S. J., Price, P. M., Poon, M., Rollins, B. J., et al. (1991). Expression of cytokine-like genes JE and KC is increased during renal ischemia. *Am. J. Physiol.* 261, F1095–F1101.

Sayer, J. A., Carr, G., and Simmons, N. L. (2004). Nephrocalcinosis: molecular insights into calcium precipitation within the kidney. *Clin. Sci. (Lond).* 106, 549–561. doi: 10.1042/cs20040048

Shi, H., and Berger, E. A. (2018). Characterization of site-specific phosphorylation of NF-. *Mediators Inflamm.* 2018:3020675.

Tang, P. M., Nikolic-Paterson, D. J., and Lan, H. Y. (2019). Macrophages: versatile players in renal inflammation and fibrosis. *Nat. Rev. Nephrol.* 03, 144–158. doi: 10.1038/s41581-019-0110-2

Tesch, G. H. (2008). MCP-1/CCL2: a new diagnostic marker and therapeutic target for progressive renal injury in diabetic nephropathy. *Am. J. Physiol. Renal Physiol.* 294, F697–F701.

Thieme, K., and Oliveira-Souza, M. (2015). Renal hemodynamic and morphological changes after 7 and 28 days of leptin treatment: the participation of angiotensin II via the AT1 receptor. *PLoS One* 10:e0122265. doi: 10.1371/journal.pone.0122265

Waikar, S. S., Srivastava, A., Palsson, R., Shafi, T., Hsu, C. Y., Sharma, K., et al. (2019). Association of urinary oxalate excretion with the risk of chronic kidney disease progression. *JAMA Intern. Med.* 179, 542–551.

Xie, K., Xu, C., Zhang, M., Wang, M., Min, L., Qian, C., et al. (2019). Yes-associated protein regulates podocyte cell cycle re-entry and dedifferentiation in adriamycin-induced nephropathy. *Cell Death Dis.* 10:915.

Zhou, D., Fu, H., Xiao, L., Mo, H., Zhuo, H., Tian, X., et al. (2018). Fibroblast-specific. *J. Am. Soc. Nephrol.* 29, 1257–1271.

Conflict of Interest: The authors declare that the research was conducted in the absence of any commercial or financial relationships that could be construed as a potential conflict of interest.

frontiers in Physiology

REVIEW
published: 15 September 2020
doi: 10.3389/fphys.2020.569322

New Insights Into the Role and Mechanism of Partial Epithelial-Mesenchymal Transition in Kidney Fibrosis

Lili Sheng[1] *and Shougang Zhuang*[1,2]*

[1] Department of Nephrology, Shanghai East Hospital, Tongji University School of Medicine, Shanghai, China, [2] Department of Medicine, Rhode Island Hospital and Alpert Medical School, Brown University, Providence, RI, United States

Epithelial-mesenchymal transition (EMT) is described as the process in which injured renal tubular epithelial cells undergo a phenotype change, acquiring mesenchymal characteristics and morphing into fibroblasts. Initially, it was widely thought of as a critical mechanism of fibrogenesis underlying chronic kidney disease. However, evidence that renal tubular epithelial cells can cross the basement membrane and become fibroblasts in the renal interstitium is rare, leading to debate about the existence of EMT. Recent research has demonstrated that after injury, renal tubular epithelial cells acquire mesenchymal characteristics and the ability to produce a variety of profibrotic factors and cytokines, but remain attached to the basement membrane. On this basis, a new concept of "partial epithelial-mesenchymal transition (pEMT)" was proposed to explain the contribution of renal epithelial cells to renal fibrogenesis. In this review, we discuss the concept of pEMT and the most recent findings related to this process, including cell cycle arrest, metabolic alternation of epithelial cells, infiltration of immune cells, epigenetic regulation as well as the novel signaling pathways that mediate this disturbed epithelial-mesenchymal communication. A deeper understanding of the role and the mechanism of pEMT may help in developing novel therapies to prevent and halt fibrosis in kidney disease.

Keywords: renal fibrosis, myofibroblast, epithelial-mesenchymal transition, partial epithelial-mesenchymal transition, chronic kidney disease

OPEN ACCESS

Edited by:
Guiomar Nascimento Gomes, Federal University of São Paulo, Brazil

Reviewed by:
Youhua Liu, University of Pittsburgh, United States
Danilo Candido De Almeida, Federal University of São Paulo, Brazil

***Correspondence:**
Shougang Zhuang
shougang_zhuang@brown.edu

Specialty section:
This article was submitted to Renal and Epithelial Physiology, a section of the journal Frontiers in Physiology

Received: *03 June 2020*
Accepted: *26 August 2020*
Published: *15 September 2020*

Citation:
Sheng L and Zhuang S (2020) New Insights Into the Role and Mechanism of Partial Epithelial-Mesenchymal Transition in Kidney Fibrosis. Front. Physiol. 11:569322. doi: 10.3389/fphys.2020.569322

INTRODUCTION

The progress of renal fibrosis – glomerulosclerosis and tubulointerstitial fibrosis – is characterized by an excessive deposition of extracellular matrix (ECM) components in the tubular interstitium. Fibrosis in the short term is an adaptive mechanism for repairing tissue damage, whereas persistent fibrosis after severe or repetitive injury eventually leads to renal failure as functional renal parenchyma is replaced by connective tissue (Farris and Colvin, 2012; Kaissling et al., 2013; Ovadya and Krizhanovsky, 2015; Djudjaj and Boor, 2018). Up to now, there is no specific therapy to halt progression of renal fibrosis. Moreover, the cellular and molecular mechanisms mediating fibrosis are still not well understood. A better understanding of the complex mechanisms and related cellular mediators of kidney fibrosis is urgently needed to develop new therapeutic approaches to prevent chronic kidney disease (Djudjaj and Boor, 2018).

During the pathogenesis of renal fibrosis, activated fibroblasts or myofibroblasts are generally thought of as the major type of matrix-producing cells (LeBleu et al., 2013). Similar to smooth muscle cells, myofibroblasts express α-SMA and secrete a pericellular matrix containing collagen and glycosaminoglycans. The origin of myofibroblasts in the kidney remains uncertain, but is considered to be derived from various sources: proliferation of resident fibroblasts (LeBleu et al., 2013), differentiation from local fibroblasts or pericytes (Lin et al., 2008; Humphreys et al., 2010), direct and complete transition from resident endothelial or epithelial cells through endothelial-mesenchymal transition (EndoMT) and epithelial-mesenchymal transition (EMT) (Carew et al., 2012). Some studies have suggested that bone marrow derived fibroblasts also contribute to the myofibroblast population (LeBleu et al., 2013). One of major controversies over renal interstitial fibrosis revolves around the relative contribution of activated tubular epithelial cells to the total myofibroblast pool.

EMT of tubular epithelial cells has been long considered a mechanism that promotes renal fibrosis. During that process, injured epithelial cells are activated and undergo a phenotypic conversion, acquiring the features of matrix-producing fibroblasts or myofibroblasts (Liu, 2010; Lee and Nelson, 2012). EMT was primarily identified in the kidney in a landmark article published in 1994 (Nadasdy et al., 1994) in which cells in renal interstitium with immunohistochemical features of tubular cells were found in end-stage kidney disease. In all tissues including kidney, key events during the process of EMT are summarized as follows (Kalluri and Weinberg, 2009; Fragiadaki and Mason, 2011; Prunotto et al., 2012; Lamouille et al., 2014; Loeffler and Wolf, 2015; Tennakoon et al., 2016): (1) dissolution of epithelial cell junctions and loss of cell polarity; (2) downregulation of epithelial proteins expression such as E-cadherin, zonula occludens-1 (ZO-1), and upregulation of mesenchymal marker expression including α-smooth muscle actin (α-SMA), vimentin, fibroblast-specific protein-1 (FSP1), and fibronectin (Gonzalez and Medici, 2014; Liu et al., 2018; Zhou et al., 2018); (3) reorganization of the cytoskeletal architecture and changes in cellular morphology with increased cell protrusions and motility; (4) acquisition of the ability to secrete factors to degrade extracellular matrix and exhibit invasive behavior (Liu, 2004; Lamouille et al., 2014; Loeffler and Wolf, 2015). Most studies applied co-immunostaining for markers of epithelial cells and, fibroblasts to detect the alternation of EMT transcriptional program. This does not, however, provide direct evidence of EMT (Iwano et al., 2002; Humphreys et al., 2010; Zeisberg and Neilson, 2010; LeBleu et al., 2013). Moreover, the exact percentage of fibroblasts that derive from tubular epithelial cells in a diseased kidney is entirely uncertain and remains under debate.

The controversy over the relative contribution of EMT to the total fibroblast or myofibroblast pool lasted many years. A study in 2013 used multiple genetically engineered mice to track the source of myofibroblasts. It was found that the source of myofibroblasts is split, with 50% arising from proliferation of local resident fibroblasts, 35% through differentiation from bone marrow, 10% from endothelial-to-mesenchymal transition. The contribution of EMT only occupies 5% of the total myofibroblast pool (LeBleu et al., 2013). Although a complete phenotype alternation from renal tubular epithelial cell to myofibroblast is rare, most studies provide evidence for a large population of tubular epithelial cells that co-express epithelial and mesenchymal markers. Recent studies found that the dedifferentiated TECs remain attached to the basement membrane after renal injury (LeBleu et al., 2013; Lovisa et al., 2016). This type of renal epithelial cells is considered to have undergone partial EMT (Grande et al., 2015; Lovisa et al., 2015). In this review article, we will discuss advances in our understanding of the role and mechanism of partial EMT in kidney fibrosis.

IDENTIFICATION OF PARTIAL EPITHELIAL-MESENCHYMAL TRANSITION IN THE KIDNEY

In an early review examining the EMT hypothesis (Kalluri and Weinberg, 2009), it was suggested that epithelial cells undergo a "partial EMT" to acquire some of the phenotypic characteristics fibroblasts rather than converting to a "fully fibroblastic phenotype" (Kriz et al., 2011; Hajarnis et al., 2018). In 2015, two studies offered new perspective into the potential role of partial EMT in the development and progression of renal fibrosis (Grande et al., 2015; Lovisa et al., 2015). Both studies demonstrated that during the process of fibrosis, TECs expressed both markers of epithelial and mesenchymal cells while remaining attached to the basement membrane during fibrosis. Grande et al. (2015) demonstrated that *Snail1* induced partial EMT of renal tubular cells, which produces fibrogenic cytokines to promote myofibroblasts proliferation and macrophage recruitment. Lovisa et al. (2015) showed that the partial EMT program is associated with p21-mediated G2/M cell cycle arrest in proximal TECs. And inhibition of the EMT program by conditional deletion of *Twist1* or *Snai1* resulted in the maintenance of TEC integrity, decrease of immune cell infiltration and attenuation of interstitial fibrosis. These two observations demonstrated that without a complete conversion to fibroblast, a partial EMT is enough to induce TEC dysfunction by triggering cell cycle arrest, thereby promoting the secretion of profibrogenic cytokines and fibrosis.

PHENOTYPIC ALTERATIONS OF RENAL TUBULAR CELLS WITH PARTIAL EMT

During the process of partial EMT in kidney, epithelial cells experience series of changes, including cell-cycle arrest, metabolic alternation, and inflammation, that result in disturbed epithelial-mesenchymal crosstalk, leading to renal fibrosis.

Cell-Cycle Arrest – Defective Repair and Regeneration

The cell cycle consists of four phases (G1, S, G2, M), each of which has specific characteristics. Cell division starts with the G1 phase.

In the G2 phase, the cell prepares itself for mitosis by genetic material replication and protein synthesis. Genetic material and cellular components are distributed to two daughter cells during the M phase (Moonen et al., 2018). In G2/M arrest, cells are blocked from entering mitosis unless DNA replication or repair is complete, a cell size is large enough to divide and the cell has enough energy.

In acute kidney injury (AKI) models, such as ischemic reperfusion, acid toxic nephropathy, and obstructive mouse models, proximal TECs usually undergo G2/M phase cell-cycle arrest (Yang et al., 2010; Cianciolo et al., 2013; Canaud and Bonventre, 2015; Kumar, 2018). Chronic kidney disease is also associated with inappropriate cell cycle progression in TECs (Yang et al., 2010; Canaud and Bonventre, 2015). The number of tubular cells that undergo G2/M arrest is correlated with the degree of fibrosis (Yang et al., 2010; Kishi et al., 2019). Proximal tubular cells in G2/M arrest activate c-jun NH2-terminal kinase (JNK) signaling and upregulate profibrotic cytokine generation. The cells at G2/M phase have higher levels of COL4A1, ACTA2, TGF-β1, and CTGF expression (Yang et al., 2010; Canaud and Bonventre, 2015). Activation of signaling pathways such as TGF-β1 also triggers epithelial arrest at the G2/M phase of the cell cycle (Wu et al., 2013). Reversal of G2/M arrest rescues cells from the fibrogenic effects. This observation was further confirmed by several other groups (Cianciolo et al., 2013; Tang J. et al., 2013; Bonventre, 2014; Jenkins et al., 2014). In the setting of EMT, Lovisa et al. (2015) showed that after a fibrotic injury, TECs undergo a pEMT program and G2/M cell cycle arrest, which impairs cell regeneration and halts tissue repair, resulting in chronic fibrosis. Inhibition of pEMT in TECs protects kidney function by promoting cell cycle-dependent repair of the injured kidney. Therapeutic strategies targeting the G2/M check point are thought to be quite promising. Canaud and Bonventre (Canaud and Bonventre, 2015) suggested several approaches targeting cell cycle arrest. These include prevention of cells from activating downstream checks that trigger G2/M arrest, helping cells overcome G2/M checkpoints, facilitating apoptosis or selective depletion of senescent cells, and blocking pathways that are involved in production of profibrotic cytokines.

Metabolic Alternation

The renal tubular epithelial cell is one of the most metabolically active cells in the body, and investigators are increasingly looking into the metabolic changes that occur during kidney fibrosis. Injured epithelial cells display dramatic metabolic rearrangements that affect their capacity to regenerate and influence fibrogenesis. Tubular cells have a high energy demand, producing ATP mostly by fatty acid oxidation (FAO) (Simon and Hertig, 2015). However, fibrotic kidneys exhibit lower expression of key regulators of FAO and higher intracellular lipid deposition in human and mouse models. Dysregulated FAO results in intracellular lipid accumulation and, inflammatory cell infiltration and cytokine secretion, and acceleration of interstitial fibrosis (Lovisa et al., 2016; Zhou and Liu, 2016). Lipid accumulation also promoted glucose-induced morphological changes of tubular epithelial cell, as well as the cytoskeletal switch including loss of E-cadherin and acquisition of α-SMA (Simon and Hertig, 2015). These results suggest that the decrease of FAO along with accumulation of lipids may promote development of EMT.

Currently, there is still no direct evidence indicating that the EMT results in metabolic alterations in the kidney. Nevertheless, Kang et al. (2015) demonstrated that TGF-β1 can induce remarkable depression of FAO through Smad3-mediated repression of the expression of PPARGC1a, one of the key FAO transcription factors in fibrotic kidneys. Given that TGFβ1-induced activation of Smad3 is also a key signaling event leading to EMT, this study also suggests that FAO depression may occur secondary or in parallel to EMT. Supporting this, it has been reported that upregulation of *Snail*, a major regulator of EMT, correlated with the downregulation of critical genes involved in FAO expression in hepatocellular carcinomas (Tanaka et al., 2013); pharmacological inhibition of FAO reverses Snail-mediated metabolic reprogramming *in vivo* and progression of breast cancer (Yang et al., 2020). Future studies are needed to elucidate the role of EMT in the regulation of FAO or other metabolic alteration in the kidney after fibrotic injuries.

Pathological Secretome

Inflammation is widely described as a key promotor of kidney fibrosis. It is initiated as a protective response to acute injury. But when it persists, inflammation may contribute to fibrotic progression. Tubulointerstitial inflammation is observed in the early stage of different renal diseases. Apart from inflammatory cell infiltration, damaged TECs can be transformed into a secretory phenotype and act as proinflammatory mediators. The inflammatory response of TECs to injury is likely to be a key determinant in the development of interstitial fibrosis (Liu et al., 2018).

An early study (Abbate et al., 2002) explored the interactions between activated proximal tubular cells expressing the myofibroblast markers and peritubular cells, especially inflammatory cells. In remnant kidney models, α-SMA expression became evident in tubular epithelial cells at day 30, correlating with the $ED1^+$ macrophages co-localization in peritubular areas in kidneys. This result suggests a relation between phenotype transition of epithelial cells and inflammatory cell recruitment. Grande et al. (2015) and Lovisa et al. (2015, 2016) examined the relationship between inflammation and EMT. They found that in fibrotic kidney, the immune response was attenuated after EMT inhibition with downregulated inflammatory cytokines. Lovisa et al. found that EMT inhibition resulted in a distinct reduction in immune cell infiltration in renal interstitium such as $CD3^+$ T cells, $CD8^+$ T cells, $CD11c^+$ dendritic cells and macrophages. Grande et al. (2015) also observed a reduction in the presence of F4/80 macrophages, as well as lower levels of pNF-κB, cytokines and chemokines in tubular cells after EMT inhibition by deletion of *Snail*. In particular, the levels of M2-type macrophages, which are thought to be pro-fibrogenic during tissue repair, decreased evidently. Taken together, this suggests that blocking EMT could halt the related secretome of TECs and inhibit subsequent inflammation, serving as a potential approach to reduce fibrosis.

CONTRIBUTION OF pEMT TO RENAL FIBROSIS

Tubulointerstitial fibrosis is commonly seen during CKD progression (Fine et al., 1993; Eddy and Neilson, 2006; Zeisberg and Neilson, 2010). Studies showed that the phenotypic changes suggesting EMT correlate with the progression of kidney fibrosis. One study enrolled 83 kidney transplant recipients who had undergone allograft biopsies at 3 and 12 months after transplantation. Patients with vimentin and β-catenin expression in more than 10% of tubules at 3 months had much more severe interstitial fibrosis at 1 year. In addition, the presence of early phenotypic changes in TECs was associated with poorer graft function 18 month after transplantation (Hertig et al., 2008). These data suggest that epithelial phenotypic changes represent an "activated state" of the tubular cells that can lead to fibrosis.

The fibrotic interstitium is characterized by fibroblast and myofibroblast proliferation, inflammatory cell infiltration and tubular cell atrophy, as well as excessive accumulation of ECM (Prunotto et al., 2012). Historical data suggest that the progression of renal fibrosis might be the result of an altered epithelial-mesenchymal cellular crosstalk (Lewis et al., 1996; Johnson et al., 1998; Abbate et al., 2002; Yang et al., 2010). Well-balanced crosstalk between tubular epithelial cells and mesenchymal cells or inflammatory cells is essential to maintain a normal and healthy tubulointerstitium.

Experiments in the early 1990s showed the role of disturbed crosstalk between different cells during fibrogenesis. In the study of Johnson et al. (1998), cultured proximal tubule cells were found to be capable of stimulating fibroblast proliferation, collagen synthesis and MMP activity. This may occur through paracrine mechanisms that involve TEC-derived growth factors such as PDGF and TGF-β1. In cultured kidney epithelial cells, TGF-β1 stimulated profibrotic cytokines production and then promoted the proliferation and transition of pericytes to myofibroblasts (Wu et al., 2013). Bielesz et al.'s (2010) showed that activation of the Notch1 pathway in TECs contributes to tubulointerstitial fibrogenesis. TGF-β1 treated TECs induced Notch1 pathway activation, which not only promoted epithelial dysfunction, but also stimulated interstitial cell proliferation including myofibroblast proliferation. These results provide compelling evidence that TECs could regulate the behavior of neighboring myofibroblasts and fibroblasts in the interstitium. Disturbance of normal epithelial-mesenchymal unit crosstalk may be an initial cause of fibroblast and myofibroblast activation in the course of renal fibrosis.

Grande et al. (2015) showed that after partial EMT program activation, tubular epithelial cells were still integrated in the tubules and could express epithelial-related genes. The incomplete EMT program was still able to promote proliferation and activation of interstitial fibroblasts (Grande et al., 2015; Lovisa et al., 2015). This suggests that tubular cells undergoing partial EMT may produce some profibrotic cytokines/growth factors to induce renal fibroblast activation. In this regard, it has been reported that TGF-β1 treatment can induce cultured kidney epithelial cells to express several profibritic cytokines that stimulate the proliferation and transition of pericytes to myofibroblasts (Wu et al., 2013). Therefore, the fibrogenic response of EMT activation may not need complete transition of epithelial cells into myofibroblasts, and the cell with partial EMT acquire the ability to produce profibrotic cytokines/growth factors to induce renal fibroblast activation and renal fibrosis.

Increasing evidence indicates that the occurrence of EMT in renal tubular cells is associated with cellular senescence. Cellular senescence is mainly characterized by growth arrest and formation of a senescence-associated secretory phenotype that produces numerous profibrotic cytokines/growth factors, including TGF-β1 (Sosa Peña et al., 2018; Docherty et al., 2019). As mentioned, some growth factors and TGF-β1 not only induce renal fibroblast activation, but also stimulate the EMT response. Thus the cellular senescence-initiated EMT program may contribute to renal fibrosis. On the other hand, TGF-β1-induced partial EMT can also promote renal epithelial cells arrest at the G2/M phase of cell cycle and parenchymal damage in renal fibrosis. Therefore, it seems that EMT and senescence of renal tubular cells are intrinsically linked, leading to a vicious cycle in promoting chronic fibrosis. Currently, a causative link between these two processes and molecular mechanisms related to their reciprocal regulation in the fibrotic kidney are not yet been fully understood. It has been reported that induction of Twist or Snai1 expression in renal epithelial cells is sufficient to induce EMT and promote prolonged TGF-β1–induced cell cycle arrest in G2/M phase (Lovisa et al., 2015), suggesting that activation of these two transcriptional factors may play an essential role in mediating these two processes. Further studies are required to identify the signaling pathways that regulate senescence and EMT cross-talk as well as their potential co-targets.

NEW SIGNALS THAT MEDIATE pEMT AND SUBSEQUENT RENAL FIBROBLAST ACTIVATION

Defective crosstalk between epithelial cell and mesenchymal cell might involve multiple pathways of injury and repair. Epithelial cells communicate with interstitial fibroblasts by promoting activation and excitation of growth factors, such as TGF-β, CTGF, EGF, and FGF (Prunotto et al., 2012). In injured tubular epithelial cells, regular signaling pathways are disrupted and irregular pathways, such as Wnts and sonic hedgehog (SHH) (Kramann et al., 2015a,b), are activated. Activation of these irregular pathways could produce ligands of developmental pathways in pericytes or fibroblasts and trigger cell proliferation and fibrosis.

Sonic Hedgehog (SHH) Signaling

Sonic hedgehog (SHH) signaling plays an important role in embryonic development, tissue regeneration and organogenesis. The disturbed activation of this pathway leads to pathological consequences, including the development of types of human tumors and fibrogenesis (Syn et al., 2009; Bai et al., 2016).

SHH expression is extremely low and difficult to detect in healthy kidney. It was activated in renal tubular epithelial

cells in models of renal mass ablation, ischemia/reperfusion injury (IRI), and in renal tubules of biopsy specimens of CKD patients. When activated, it was predominantly localized in renal tubular epithelial cells. The sonic hedgehog pathway transcriptional effectors GLI1 and GLI2 are expressed in myofibroblast progenitors (Kramann et al., 2015a). Zhou et al. (2014) identified interstitial fibroblasts to be the targets of renal SHH signaling. Incubation with SHH or SHH overexpression promoted kidney fibroblast proliferation and stimulated expression of numerous proliferation-related genes. One study (Ding et al., 2012) also found that in ureteral obstruction model, SHH localized predominantly to the renal tubular epithelium. After administration of recombinant SHH protein, renal interstitial fibroblasts showed increased α-SMA, desmin, fibronectin, and collagen I expression, suggesting that SHH signaling participates in promoting myofibroblast activation and extracellular matrix accumulation.

SHH signaling might be involved in the process of EMT. Experiments demonstrated that injuries activated hedgehog signaling, resulting in tubular EMT and ECM production (Bai et al., 2014; Lu et al., 2016). Bai found that after ureteral obstruction, epithelial cells undergo G2/M cell cycle arrest and acquire a myofibroblastic phenotype. Meanwhile, the injury also stimulated activation of SHH signaling pathway. SHH-treated renal fibroblasts exhibited a fibrogenic response. Blockade of SHH inhibited fibroblast activation and improved ECM deposition (Bai et al., 2016). These results suggest that tubule-derived SHH activation might target interstitial fibroblasts and mediate epithelial-mesenchymal communication during EMT, thus promoting interstitial fibroblast proliferation and activation. SHH inhibition may be a potential therapeutic strategy to reduce fibroblast activation during kidney fibrosis (Syn et al., 2009).

Wnt/β-Catenin Signaling

The Wnt family is a group of lipid-modified glycoproteins. The most studied Wnt signaling pathway in kidney is the Wnt/β-catenin signaling pathway, which plays an essential role in regulating nephrogenesis and pathogenesis of kidney diseases (Xiao et al., 2013).

Studies have shown a renoprotective effect of wnt/β-catenin in AKI models after either ischemic or nephrotoxic insults. Wnt/β-catenin protein was predominantly expressed in the kidney tubular epithelium. Tubule specific ablation of β-catenin aggravates injuries (Zhou et al., 2012). Nevertheless, chronic and persistent activation of this signaling pathway could lead to development and progression of CKD (Kawakami et al., 2013). Surendran et al. (2005) found that Wnt/β-catenin activation in UUO mice was associated with MMP-7, fibronectin, *Twist*, and c-Myc expression. Xiao et al.'s (2016) investigated the role of Wnt/β-catenin activation in IRI models. Moderate IRI led to acute kidney injury and transient Wnt/β-catenin activation, as a result, normal kidney morphology and function were restored. Severe IRI accompanied sustained and exaggerated Wnt/β-catenin activation resulted in the development of renal fibrotic lesions, suggesting that persistent Wnt/β-catenin signaling activation promoted fibroblast proliferation and renal fibrosis. Epithelium-derived Wnt/β-catenin signaling might disturb normal epithelial-mesenchymal crosstalk and thereby promote fibrosis (Xiao et al., 2016).

Recent evidence has demonstrated Wnt/β-catenin also contributes to the EMT process in tubular cells (Xiao et al., 2013). Hydrogen sulfide inhibits TGF-β1-induced EMT via Wnt/β-catenin pathway (Guo et al., 2016). CTGF induces tubular EMT through the activation of canonical Wnt signaling (Yang et al., 2015). Chronic cadmium exposure induces activation of the Wnt pathway and upregulation of EMT markers in mouse kidney (Chakraborty et al., 2010). It is indicated that Wnt/β-catenin signaling was activated during EMT process, and might alter the regular epithelial-mesenchymal cellular crosstalk.

EPIGENETIC REGULATION OF pEMT IN THE KIDNEY

Epigenetic modification refers to stable heritable changes in gene expression without changes in DNA sequence. It is thought to contribute to the regulation of gene expression under different conditions (Rodriguez-Romo et al., 2015; Hewitson et al., 2017; Monteiro-Reis et al., 2019). The chromatin consists of histone proteins and the DNA wrapped around them. Epigenetic modifications involve selective unwinding of the double helix and exposure of the underlying genetic material (Tampe and Zeisberg, 2014). The modifications are well-balanced in normal cells. Small changes may lead to major consequences and result in cellular dysfunction or malignant outgrowth (Sun and Fang, 2016). Growing evidence suggests the epigenetic regulation of pro-inflammatory and pro-fibrotic gene expression, mediated by DNA methylation, histone modifications or microRNAs, is important in EMT and renal fibrogenesis (Wing et al., 2013; Rodriguez-Romo et al., 2015; Wanner and Bechtel-Walz, 2017; Lin and Wu, 2020).

DNA Methylation

DNA methylation occurs at the 50-position of the cytosine ring (5mC) within CpG dinucleotides of gene promotors (De Chiara and Crean, 2016; Wanner and Bechtel-Walz, 2017). It is catalyzed by DNA methyltransferases (DNMTs). By inhibiting access of transcription factors to the binding sites or promoting the recruitment of methyl-binding domain proteins, gene expression is changed (Lee and Kong, 2016; Sun and Fang, 2016).

Carmona et al. (2014) found altered transcription of EMT-related genes in accordance with the dynamic changes of DNA methylation, reinforcing the role of the epigenetic mechanisms in the development of EMT. Direct methylation of certain transcription factors such as KLF4 and RASAL1 by Dnmt1 contributes to the progression of EMT in renal epithelial cells and is associated with fibrogenesis in the kidneys (Bechtel et al., 2010; Xiao et al., 2015). In arsenic-induced renal fibrosis, treatment with a DNA methylation inhibitor reversed the EMT properties of HK-2 cells, suggesting that the fibrotic changes are mediated by DNA methylation (Chang and Singh, 2019). There is still debate over the role of DNA methylation in renal fibrosis and EMT. By using comprehensive high-throughput arrays for relative

methylation and TGF-β stimulation during EMT in AML12 cells, McDonald et al. (2011) showed no changes in DNA methylation.

Histone Modification

Histone modification may be a key determinant of progression in renal diseases. The histone octamer is composed of a H3-H4 tetramer and two separate H2A-H2B dimers. The modifications, including acetylation, methylation, phosphorylation, ubiquitination, have been proposed to constitute specific biological outcomes (Sun et al., 2010; Wanner and Bechtel-Walz, 2017).

Recent studies show that histone acetylation through histone deacetylases (HDACs) activation mediated several physiological and pathophysiological changes in the kidney. Inhibition of histone deacetylase activity attenuated renal fibroblast activation and interstitial fibrosis in obstructive nephropathy (Pang et al., 2009). Histone 3 lysine 4 acetylation (H3K4Ac) is observed in the promoter regions of EMT marker genes, such as CDH1 and VIM. In hypoxia-induced EMT, HIF-1α induced histone deacetylase and then regulated EMT related gene expression (Wu et al., 2011; Wang et al., 2019). McDonald et al. (2011) investigated epigenetic modifications during EMT mediated by TGF-β, they found a reduction in the heterochromatin marker H3 Lys9 dimethylation (H3K9Me2), an increase in the euchromatin marker H3 Lys4 trimethylation (H3K4Me3) and in the transcriptional mark H3 Lys36 trimethylation (H3K36Me3). This suggests that during the process of EMT, specific chromatin domains across the genome were reprogrammed. In the UUO model, the number of individual histone markers, H3K9 acetylation (H3K9Ac) and tri-methylation (H3K9Me3) in proximal tubules and myofibroblasts, was increased 10 days after UUO (Irifuku et al., 2016; Hewitson et al., 2017). Targeting methyltransferases, such as disruptor of telomeric silencing-1 like (DOT1L) (Liu et al., 2019) and enhancer of zeste homolog 2 (EZH2) (Zhou et al., 2016), attenuates EMT and fibroblast activation by suppressing activation of multiple profibrotic signaling pathways. So, regulation of histone modification could be a strategy to interfere with the EMT process.

MicroRNA

MicroRNA (miRNAs) are small, non-coding nucleotides that regulate diverse biological processes including aggressiveness of cancers and fibrosis. Altered microRNA biosynthesis or regulation contributes to pathological processes including kidney fibrosis (Tampe and Zeisberg, 2014; Wanner and Bechtel-Walz, 2017). Some suggests that microRNA crosstalk may influence epithelial-to-mesenchymal, endothelial-to-mesenchymal, and macrophage-to-mesenchymal transitions in the kidney (Srivastava et al., 2019).

Increasing evidence confirms various microRNAs are involved in the EMT process. Chen et al. (2015) found that after exposure to cyclosporine A (CsA), 46 miRNAs were significantly altered

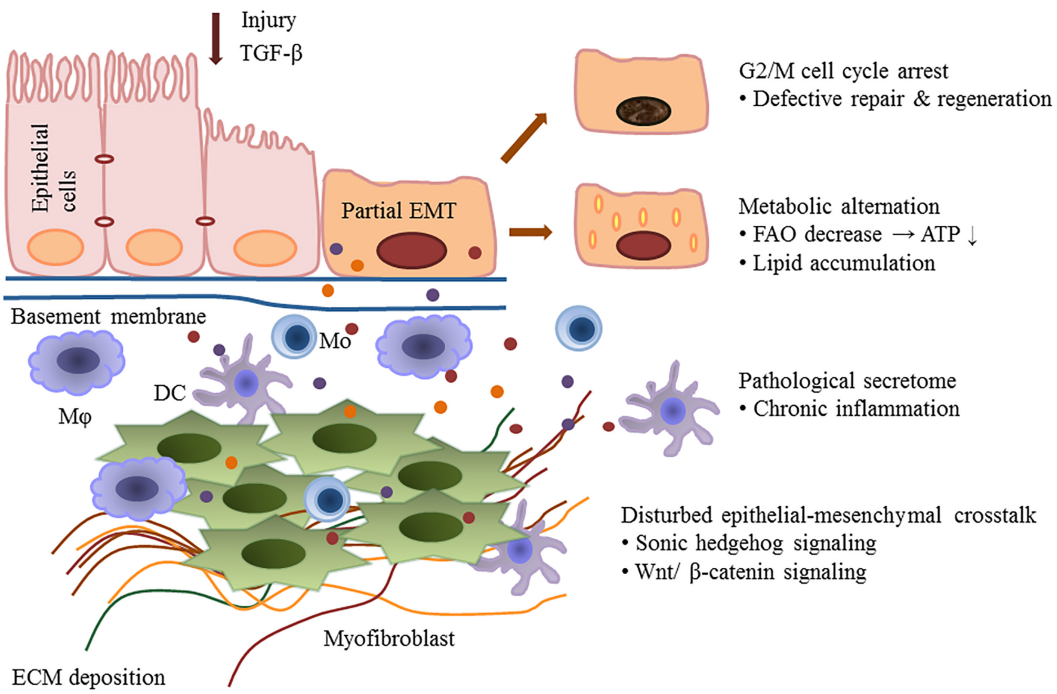

FIGURE 1 | Partial epithelial-mesenchymal transition and renal fibrosis. After injury or TGF-b1 stimulation, epithelial cells undergo a partial EMT and remain attached to the basement membrane. This process leads to G2/M cell cycle arrest, impairing cell regeneration and tissue repair. Injured epithelial cells also display dramatic metabolic rearrangements, with great impacts on regeneration capacity and fibrogenesis. Epithelial cells secret cytokines and chemokines and release extracellular vesicles, followed by the recruitment of inflammatory cells including macrophages (M), monocytes (Mo), and dendritic cells (DC). The partial EMT also leads to a disturbed epithelial-mesenchymal crosstalk by overexpressing growth factors, activating several signaling pathways (such as the Wnts and sonic hedgehog signaling) and epigenetic reprogramming.

in proximal tubular epithelial cells, with alterations in EMT markers including vimentin and a-SMA. Several miRNAs are thought to be able to regulate different transcription factors including Snail, bHLH, and ZEB families are drivers of the epithelial plasticity leading to EMT (Díaz-López et al., 2015). The miR-200 family targets two important transcriptional repressors of the cell adherence (E-cadherin) and cell polarity genes, the ZEB1 and ZEB2 (Davalos et al., 2012; Tang O. et al., 2013). The hypermethylated or unmethylated status of miR-200 can be shifted corresponding to the EMT and MET (mesenchymal–epithelial transition) phenotypes of cells (Chen et al., 2015). Overexpression of miR-141 in HK-2 cells blocked the process of EMT by increasing E-cadherin and decreasing vimentin and FSP1 expression (Huang et al., 2015). And ZEB2 and cadherin-2 were directly regulated by miR-192 and -194 (Kim et al., 2018).

There are also some results suggesting a renal protective role of miRNA in renal injury. Zhao et al. (2017) found that miR-30c inhibited EMT through Snail1-TGF-β1 pathway, and attenuated diabetic nephropathy. In another study, researchers found that miR-152 overexpression inhibited TGF-β1-induced EMT in HK-2 cells (Ning et al., 2018). It is hard to identify which miRNA determines EMT initiation, and some have suggested unbalanced control of several miRNAs.

Role of Extracellular Vesical Communication in the Kidney Injury, Recovery, and Fibrosis

Extracellular vesicles (EVs) such as exosomes are important mediators of cell-cell communication that act by transmitting proteins and genetic information. Vesicles incorporate molecules from their origin cells containing proteins, nucleic acids and lipids (Rigalli et al., 2020). A recent study demonstrated that exosomes are produced in renal proximal tubular epithelium following various fibrotic injury (UUO, ischemia/reperfusion or

TABLE 1 | Main findings related to partial EMT.

Main topics	Subtopics	Principle findings	References
EMT	Concept of EMT	Injured TECs are activated and undergo a phenotypic conversion and acquire the features of matrix-producing fibroblasts or myofibroblasts. A complete phenotype alternation from TECs to myofibroblast is rare, most studies proved evidence for a large population of tubular epithelial cells that co-express epithelial and mesenchymal markers.	Liu, 2010; Lee and Nelson, 2012; LeBleu et al., 2013
Partial EMT	Concept of partial EMT	TECs expressed both markers of epithelial and mesenchymal cells while remained attached to the basement membrane during fibrosis. A partial EMT is sufficient to induce TEC dysfunction.	Grande et al., 2015; Lovisa et al., 2015; Hajarnis et al., 2018
Phenotypic alternation during partial EMT	Cell-cycle arrest	Partial EMT program is associated with p21-mediated G2/M cell cycle arrest, which impairs cell regeneration and halts the following repair, resulting in chronic fibrosis.	Canaud and Bonventre, 2015; Lovisa et al., 2015
	Metabolic alternation	The decrease of FAO along with accumulation of lipids was related to mesenchymal reprogramming of epithelial cells. Upregulation of *Snail*, a major regulator of EMT, correlated with the downregulation of critical genes involved in FAO expression.	Tanaka et al., 2013; Xu et al., 2014; Simon and Hertig, 2015
	Pathological secretome	EMT inhibition resulted in a distinct reduction in immune cells infiltration, as well as the lower levels of proinflammatory factors.	Grande et al., 2015; Lovisa et al., 2015, 2016
Epithelial-mesenchymal crosstalk	Disturbed epithelial-mesenchymal crosstalk	Fibrogenic response of EMT activation may not need complete transition of epithelial cells into myofibroblasts, and cells with partial EMT acquire the ability to produce profibrotic cytokines/growth factors to induce renal fibroblast activation and renal fibrosis. The cellular senescence-initiated EMT program may contribute to renal fibrosis.	Wu et al., 2013; Grande et al., 2015; Lovisa et al., 2015
	Signals mediating partial EMT	Sonic hedgehog signaling; Wnt/β-catenin signaling Tubule-derived SHH and Wnt/β-catenin signaling activation might target interstitial fibroblasts and mediate epithelial-mesenchymal communication during EMT.	Xiao et al., 2013; Bai et al., 2014, 2016; Guo et al., 2016; Lu et al., 2016
Epigenetic regulation of partial EMT	DNA methylation	Directly methylation of certain transcription factors contributes to the progression of EMT in renal epithelial cells and is associated with fibrogenesis in the kidney. DNA methylation inhibitor reversed the EMT properties.	Bechtel et al., 2010; Carmona et al., 2014; Xiao et al., 2015
	Histone modification	Histone modifications including acetylation, methylation activate EMT process and fibroblast activation by activation of multiple profibrotic signaling pathways.	Pang et al., 2009; Wu et al., 2011; Irifuku et al., 2016; Zhou et al., 2016; Hewitson et al., 2017; Liu et al., 2019; Wang et al., 2019
	microRNAs	Several miRNAs are able to regulate multiple transcription factors (i.e., Snail, bHLH, and ZEB), leading to EMT; Some other miRNAs contribute to renal injury by inhibition of EMT process.	Davalos et al., 2012; Tang O. et al., 2013; Chen et al., 2015; Díaz-López et al., 2015; Huang et al., 2015
Extracellular vesicles	EVs mediated cell-cell communication during EMT	Tubule-derived exosomes may play an essential role in driving renal fibroblast activation and fibrogenesis.	Borges et al., 2013; Guan et al., 2020

5/6 nephrectomy) (Liu et al., 2020). Stimulation of cultured renal epithelial cells with TGF-β1 also increased exosome production, and the exosome purified from these cells are able to induce renal interstitial fibroblast activation (Liu et al., 2020). Conversely, pharmacologic inhibition of exosome secretion or depletion of exosome from the conditioned media blocked the ability of TGF-β1 stimulated renal epithelial cells to induce renal fibroblast activation; injection of tubular cell-derived exosomes also enhanced kidney injury and fibrosis (Liu et al., 2020). Given that TGF-β1 is a potent inducer of partial EMT and all three fibrotic injuries cited by Liu et al. (2020) can induce EMT, these results suggest that tubule-derived exosomes play an essential role in driving renal fibroblast activation and fibrogenesis. Since tubule-derived exosomes contain numerous miRNAs and growth factors that are beneficial to renal recovery and repair, TECs may also employ exosomes to regulate renal reparative responses (Borges et al., 2013; Guan et al., 2020). In addition, tubular-derived EVs may regulate inflammatory responses to affect renal injury, fibrosis and repair. In this regard, it has been reported that tail-vein injection of DM mice with EVs from HSA-induced HK-2 cells induces kidney macrophage M1 polarization and accelerate the progression of diabetic kidney disease through miR-199a-5p (Jia et al., 2019). Currently, there is still no direct evidence indicating whether renal epithelial cells undergoing EMT would promote EVs production and release. It has been reported that slug-mediated partial EMT in hepatocellular carcinoma cells can promote exosomal secretion of some proteins that can be considered as potential non-invasive biomarkers (Karaosmanoğlu et al., 2018). Based on the importance of tubular-derived EVs in regulating cellular communication and functional responses, it will be interesting to further elucidate the role and mechanism of extracellular vesicles in inducing partial EMT development and in mediating partial EMT regulated kidney injury and repair. Several recent review articles have described the production, regulation and therapeutic implication of extracellular vesicles in the kidney after acute and chronic injuries (Erdbrügger and Le, 2016; Morrison et al., 2016; Karpman et al., 2017; Lv et al., 2018).

CONCLUSION

Kidney fibrosis is a multi-factorial and multi-cellular disease. All cell types present in the kidney including epithelial cells, endothelial cells, mesangial cells, as well as immune cells contribute to the progression of chronic kidney diseases. EMT has long been recognized as a main mechanism mediating renal interstitial fibrosis. In recent years, the proposal of partial EMT sets a novel insight on generation of epithelium dysfunction and tubulointerstitial fibrosis. According to recent studies, epithelial cell undergoes cell cycle arrest and metabolic alternation, inducing the infiltration of immune cells and disturbed epithelial-mesenchymal crosstalk, initiating and accelerating the process of fibrogenesis (**Figure 1**). Main findings related to partial EMT were listed in **Table 1**. More recent evidence demonstrates a role for epigenetic regulation of EMT. Considerable work still needs to be done to achieve more therapeutic possibilities.

AUTHOR CONTRIBUTIONS

LS wrote the manuscript. SZ edited the manuscript. Both authors contributed to the article and approved the submitted version.

FUNDING

This work was supported by the National Natural Science Foundation of China (81670623 and 81830021 to SZ), the Branch Grant of National Key Grants of the Ministry of Science and Technology (2018YFA0108802 to SZ), and the US National Institutes of Health (1R01DK113256-01A1 to SZ).

ACKNOWLEDGMENTS

We thank Dr. George Bayliss (Rhode Island Hospital and Alpert Medical School, Brown University) for critically reading and editing this manuscript.

REFERENCES

Abbate, M., Zoja, C., Rottoli, D., Corna, D., Tomasoni, S., and Remuzzi, G. (2002). Proximal tubular cells promote fibrogenesis by TGF-beta1-mediated induction of peritubular myofibroblasts. *Kidney Int.* 61, 2066–2077. doi: 10.1046/j.1523-1755.2002.00380.x

Bai, Y., Lu, H., Lin, C., Xu, Y., Hu, D., Liang, Y., et al. (2016). Sonic hedgehog-mediated epithelial-mesenchymal transition in renal tubulointerstitial fibrosis. *Int. J. Mol. Med.* 37, 1317–1327. doi: 10.3892/ijmm.2016.2546

Bai, Y., Lu, H., Wu, C., Liang, Y., Wang, S., Lin, C., et al. (2014). Resveratrol inhibits epithelial-mesenchymal transition and renal fibrosis by antagonizing the hedgehog signaling pathway. *Bioche. Pharmacol.* 92, 484–493. doi: 10.1016/j.bcp.2014.09.002

Bechtel, W., McGoohan, S., Zeisberg, E. M., Müller, G. A., Kalbacher, H., Salant, D. J., et al. (2010). Methylation determines fibroblast activation and fibrogenesis in the kidney. *Nat. Med.* 16, 544–550. doi: 10.1038/nm.2135

Bielesz, B., Sirin, Y., Si, H., Niranjan, T., Gruenwald, A., Ahn, S., et al. (2010). Epithelial Notch signaling regulates interstitial fibrosis development in the kidneys of mice and humans. *J. Clin. Invest.* 120, 4040–4054. doi: 10.1172/JCI43025

Bonventre, J. V. (2014). Primary proximal tubule injury leads to epithelial cell cycle arrest, fibrosis, vascular rarefaction, and glomerulosclerosis. *Kidney Int. Suppl. (2011)* 4, 39–44. doi: 10.1038/kisup.2014.8

Borges, F., Melo, S., Ozdemir, B., Kato, N., Revuelta, I., Miller, C. A., et al. (2013). TGF-β1-containing exosomes from injured epithelial cells activate fibroblasts to initiate tissue regenerative responses and fibrosis. *J. Am. Soc. Nephrol.* 24, 385–392. doi: 10.1681/asn.2012101031

Canaud, G., and Bonventre, J. V. (2015). Cell cycle arrest and the evolution of chronic kidney disease from acute kidney injury. *Nephrol. Dial Transpl.* 30, 575–583. doi: 10.1093/ndt/gfu230

Carew, R. M., Wang, B., and Kantharidis, P. (2012). The role of EMT in renal fibrosis. *Cell Tissue Res.* 347, 103–116. doi: 10.1007/s00441-011-1227-1

Carmona, F. J., Davalos, V., Vidal, E., Gomez, A., Heyn, H., Hashimoto, Y., et al. (2014). A comprehensive DNA methylation profile of epithelial-to-mesenchymal transition. *Cancer Res.* 74, 5608–5619. doi: 10.1158/0008-5472.CAN-13-3659

Chakraborty, P. K., Scharner, B., Jurasovic, J., Messner, B., Bernhard, D., and Thévenod, F. (2010). Chronic cadmium exposure induces transcriptional activation of the Wnt pathway and upregulation of epithelial-to-mesenchymal

transition markers in mouse kidney. *Toxicol. Lett.* 198, 69–76. doi: 10.1016/j.toxlet.2010.05.007

Chang, Y., and Singh, K. P. (2019). Arsenic induces fibrogenic changes in human kidney epithelial cells potentially through epigenetic alterations in DNA methylation. *J. Cell Physiol.* 234, 4713–4725. doi: 10.1002/jcp.27244

Chen, J., Zmijewska, A., Zhi, D., and Mannon, R. B. (2015). Cyclosporine-mediated allograft fibrosis is associated with micro-RNA-21 through AKT signaling. *Transpl. Int.* 28, 232–245. doi: 10.1111/tri.12471

Cianciolo, C. C., Skrypnyk, N. I., Brilli, L. L., Chiba, T., Novitskaya, T., Woods, C., et al. (2013). Histone deacetylase inhibitor enhances recovery after AKI. *J. Am. Soc. Nephrol.* 24, 943–953. doi: 10.1681/ASN.2012111055

Davalos, V., Moutinho, C., Villanueva, A., Boque, R., Silva, P., Carneiro, F., et al. (2012). Dynamic epigenetic regulation of the microRNA-200 family mediates epithelial and mesenchymal transitions in human tumorigenesis. *Oncogene* 31, 2062–2074. doi: 10.1038/onc.2011.383

De Chiara, L., and Crean, J. (2016). Emerging transcriptional mechanisms in the regulation of epithelial to mesenchymal transition and cellular plasticity in the kidney. *J. Clin. Med.* 5:6. doi: 10.3390/jcm5010006

Díaz-López, A., Díaz-Martín, J., Moreno-Bueno, G., Cuevas, E. P., Santos, V., Olmeda, D., et al. (2015). Zeb1 and Snail1 engage miR-200f transcriptional and epigenetic regulation during EMT. *Inter J. Cancer* 136, E62–E73. doi: 10.1002/ijc.29177

Ding, H., Zhou, D., Hao, S., Zhou, L., He, W., Nie, J., et al. (2012). Sonic hedgehog signaling mediates epithelial-mesenchymal communication and promotes renal fibrosis. *J. Am. Soc. Nephrol.* 23, 801–813. doi: 10.1681/ASN.2011060614

Djudjaj, S., and Boor, P. (2018). Cellular and molecular mechanisms of kidney fibrosis. *Mol. Aspects Med.* 65, 16–36. doi: 10.1016/j.mam.2018.06.002

Docherty, M. H., O'Sullivan, E. D., Bonventre, J. V., and Ferenbach, D. A. (2019). Cellular senescence in the kidney. *J. Am. Soc. Nephrol.* 30, 726–736. doi: 10.1681/ASN.2018121251

Eddy, A. A., and Neilson, E. G. (2006). Chronic kidney disease progression. *J. Am. Soc. Nephrol.* 17, 2964–2966. doi: 10.1681/ASN.2006070704

Erdbrügger, U., and Le, T. H. (2016). Extracellular vesicles in renal diseases: more than novel biomarkers? *J. Am. Soc. Nephrol.* 27, 12–26. doi: 10.1681/ASN.2015010074

Farris, A. B., and Colvin, R. B. (2012). Renal interstitial fibrosis. *Curr. Opin. Nephrol. Hypertens.* 21, 289–300. doi: 10.1097/MNH.0b013e3283521cfa

Fine, L. G., Ong, A. C., and Norman, J. T. (1993). Mechanisms of tubulo-interstitial injury in progressive renal diseases. *Eur. J. Clin. Invest.* 23, 259–265. doi: 10.1111/j.1365-2362.1993.tb00771.x

Fragiadaki, M., and Mason, R. M. (2011). Epithelial−mesenchymal transition in renal fibrosis – evidence for and against. *Int. J. Exp. Pathol.* 92, 143–150. doi: 10.1111/j.1365-2613.2011.00775.x

Gonzalez, D. M., and Medici, D. (2014). Signaling mechanisms of the epithelial-mesenchymal transition. *Sci. Signal.* 7:e8. doi: 10.1126/scisignal.2005189

Grande, M. T., Sánchez-Laorden, B., López-Blau, C., De Frutos, C. A., Boutet, A., Arévalo, M., et al. (2015). Snail1-induced partial epithelial-to-mesenchymal transition drives renal fibrosis in mice and can be targeted to reverse established disease. *Nat. Med.* 21, 989–997. doi: 10.1038/nm.3901

Guan, H., Peng, R., Mao, L., Fang, F., Xu, B., and Chen, M. (2020). Injured tubular epithelial cells activate fibroblasts to promote kidney fibrosis through miR-150-containing exosomes. *Exp. Cell Res.* 392:112007. doi: 10.1016/j.yexcr.2020.112007

Guo, L., Peng, W., Tao, J., Lan, Z., Hei, H., Tian L., et al. (2016). Hydrogen sulfide inhibits transforming growth factor-beta1-induced EMT via Wnt/Catenin pathway. *PLoS One* 11:e147018. doi: 10.1371/journal.pone.0147018

Hajarnis, S., Yheskel, M., Williams, D., Brefort, T., Glaudemans, B., Debaix H., et al. (2018). Suppression of microRNA activity in kidney collecting ducts induces partial loss of epithelial phenotype and renal fibrosis. *J. Am. Soc. Nephrol.* 29, 518–531. doi: 10.1681/ASN.2017030334

Hertig, A., Anglicheau, D., Verine, J., Pallet, N., Touzot, M., Ancel, PY., et al. (2008). Early epithelial phenotypic changes predict graft fibrosis. *J. Am. Soc. Nephrol.* 19, 1584–1591. doi: 10.1681/ASN.2007101160

Hewitson, T. D., Holt, S. G., Tan, S., Wigg, B., Samuel, C. S., and Smith, ER. (2017). Epigenetic modifications to H3K9 in renal tubulointerstitial cells after unilateral ureteric obstruction and TGF-β1 stimulation. *Front. Pharmacol.* 8:307. doi: 10.3389/fphar.2017.00307

Huang, Y., Tong, J., He, F., Yu, X., Fan, L., Hu, J., et al. (2015). MiR-141 regulates TGF-beta1-induced epithelial-mesenchymal transition through repression of HIPK2 expression in renal tubular epithelial cells. *Int. J. Mol. Med.* 35, 311–318. doi: 10.3892/ijmm.2014.2008

Humphreys, B. D., Lin, S., Kobayashi, A., Hudson, T. E., Nowlin, B. T., Bonventre, JV., et al. (2010). Fate tracing reveals the pericyte and not epithelial origin of myofibroblasts in kidney fibrosis. *Am. J. Pathol.* 176, 85–97. doi: 10.2353/ajpath.2010.090517

Irifuku, T., Doi, S., Sasaki, K., Doi, T., Nakashima, A., Ueno, T., et al. (2016). Inhibition of H3K9 histone methyltransferase G9a attenuates renal fibrosis and retains klotho expression. *Kidney Int.* 89, 147–157. doi: 10.1038/ki.2015.291

Iwano, M., Plieth, D., Danoff, T. M., Xue, C., Okada, H., and Neilson, EG. (2002). Evidence that fibroblasts derive from epithelium during tissue fibrosis. *J. Clin. Invest.* 110, 341–350. doi: 10.1172/JCI15518

Jenkins, R. H., Davies, L. C., Taylor, P. R., Akiyama, H., Cumbes, B., and Beltrami, C. (2014). MiR-192 induces G2/M growth arrest in aristolochic acid nephropathy. *Am. J. Pathol.* 184, 996–1009. doi: 10.1016/j.ajpath.2013.12.028

Jia, Y., Zheng, Z., Xue, M., Zhang, S., Hu, F., and Li, Y. (2019). Extracellular vesicles from albumin-induced tubular epithelial cells promote the M1 macrophage phenotype by targeting klotho. *Mol. Ther.* 27, 1452–1466. doi: 10.1016/j.ymthe.2019.05.019

Johnson, D. W., Saunders, H. J., Baxter, R. C., Field, M. J., and Pollock, C. A. (1998). Paracrine stimulation of human renal fibroblasts by proximal tubule cells. *Kidney Int.* 54, 747–757. doi: 10.1046/j.1523-1755.1998.00048.x

Kaissling, B., LeHir, M., and Kriz, W. (2013). Renal epithelial injury and fibrosis. *Biochim. Biophys. Acta (BBA)* 1832, 931–939. doi: 10.1016/j.bbadis.2013.02.010

Kalluri, R., and Weinberg, R. A. (2009). The basics of epithelial-mesenchymal transition. *J. Clin. Invest.* 119, 1420–1428. doi: 10.1172/JCI39104

Kang, H. M., Ahn, S. H., Choi, P., Ko, Y., Han, S. H., Chinga, F., et al. (2015). Defective fatty acid oxidation in renal tubular epithelial cells has a key role in kidney fibrosis development. *Nat. Med.* 21, 37–46. doi: 10.1038/nm.3762

Karaosmanoğlu, O., Banerjee, S., and Sivas, H. (2018). Identification of biomarkers associated with partial epithelial to mesenchymal transition in the secretome of slug over-expressing hepatocellular carcinoma cells. *Cell Oncol. (Dordr.)* 41, 439–453. doi: 10.1007/s13402-018-0384-6

Karpman, D., Ståhl, A. L., and Arvidsson, I. (2017). Extracellular vesicles in renal disease. *Nat. Rev. Nephrol.* 13, 545–562. doi: 10.1038/nrneph.2017.98

Kawakami, T., Ren, S., and Duffield, J. S. (2013). Wnt signalling in kidney diseases: dual roles in renal injury and repair. *J. Pathol.* 229, 221–231. doi: 10.1002/path.4121

Kim, D. Y., Woo, Y. M., Lee, S., Oh, S., Shin, Y., Shin, JO., et al. (2018). Impact of miR−192 and miR−194 on cyst enlargement through EMT in autosomal dominant polycystic kidney disease. *FASEB J.* 33, 2870–2884. doi: 10.1096/fj.201800563RR

Kishi, S., Brooks, C. R., Taguchi, K., Ichimura, T., Mori, Y., Akinfolarin, A., et al. (2019). Proximal tubule ATR regulates DNA repair to prevent maladaptive renal injury responses. *J. Clin. Invest.* 129, 4797–4816. doi: 10.1172/JCI122313

Kramann, R., Fleig, S. V., Schneider, R. K., Fabian, S. L., DiRocco, D. P., Maarouf, O., et al. (2015a). Pharmacological GLI2 inhibition prevents myofibroblast cell-cycle progression and reduces kidney fibrosis. *J. Clin. Invest.* 125, 2935–2951. doi: 10.1172/JCI74929

Kramann, R., Schneider, R. K., DiRocco, D. P., Machado, F., Fleig, S., Bondzie, PA., et al. (2015b). Perivascular gli1+ progenitors are key contributors to Injury-Induced organ fibrosis. *Cell Stem Cell* 16, 51–66. doi: 10.1016/j.stem.2014.11.004

Kriz, W., Kaissling, B., and Le Hir, M. (2011). Epithelial-mesenchymal transition (EMT) in kidney fibrosis: fact or fantasy? *J. Clin. Invest.* 121, 468–474. doi: 10.1172/JCI44595

Kumar, S. (2018). Cellular and molecular pathways of renal repair after acute kidney injury. *Kidney Int.* 93, 27–40. doi: 10.1016/j.kint.2017.07.030

Lamouille, S., Xu, J., and Derynck, R. (2014). Molecular mechanisms of epithelial–mesenchymal transition. *Nat. Rev. Mol. Cell Biol.* 15, 178–196. doi: 10.1038/nrm3758

LeBleu, V. S., Taduri, G., O'Connell, J., Teng, Y., Cooke, V. G., Woda, C., et al. (2013). Origin and function of myofibroblasts in kidney fibrosis. *Nat. Med.* 19, 1047–1053. doi: 10.1038/nm.3218

Lee, J., and Kong, G. (2016). Roles and epigenetic regulation of epithelial–mesenchymal transition and its transcription factors in cancer initiation

and progression. *Cell Mol. Life Sci.* 73, 4643–4660. doi: 10.1007/s00018-016-2313-z

Lee, K., and Nelson, C. M. (2012). New insights into the regulation of epithelial-mesenchymal transition and tissue fibrosis. *Int. Rev. Cell Mol. Biol.* 294, 171–221. doi: 10.1016/B978-0-12-394305-7.00004-5

Lewis, M. P., Fine, L. G., and Norman, J. T. (1996). Pexicrine effects of basement membrane components on paracrine signaling by renal tubular cells. *Kidney Int.* 49, 48–58. doi: 10.1038/ki.1996.7

Lin, S., Kisseleva, T., Brenner, D. A., and Duffield, J. S. (2008). Pericytes and perivascular fibroblasts are the primary source of Collagen-Producing cells in obstructive fibrosis of the kidney. *Am. J. Pathol.* 173, 1617–1627. doi: 10.2353/ajpath.2008.080433

Lin, Y., and Wu, K. (2020). Epigenetic regulation of epithelial-mesenchymal transition: focusing on hypoxia and TGF-β signaling. *J. Biomed. Sci.* 27:39. doi: 10.1186/s12929-020-00632-3

Liu, B. C., Tang, T. T., Lv, L. L., and Lan, H. Y. (2018). Renal tubule injury: a driving force toward chronic kidney disease. *Kidney Int.* 93, 568–579. doi: 10.1016/j.kint.2017.09.033

Liu, L., Zou, J., Guan, Y., Zhang, Y., Zhang, W., Zhou, X., et al. (2019). Blocking the histone lysine 79 methyltransferase DOT1L alleviates renal fibrosis through inhibition of renal fibroblast activation and epithelial-mesenchymal transition. *FASEB J.* 33, 11941–11958. doi: 10.1096/fj.201801861R

Liu, X., Miao, J. H., Wang, C., Zhou, S., Chen, S., Ren, Q., et al. (2020). Tubule-derived exosomes play a central role in fibroblast activation and kidney fibrosis. *Kidney Int.* 97, 1181–1195. doi: 10.1016/j.kint.2019.11.026

Liu, Y. (2004). Epithelial to mesenchymal transition in renal fibrogenesis: pathologic significance, molecular mechanism, and therapeutic intervention. *J. Am. Soc. Nephrol.* 15, 1–12. doi: 10.1097/01.ASN.0000106015.29070.E7

Liu, Y. (2010). New insights into epithelial-mesenchymal transition in kidney fibrosis. *J. Am. Soc. Nephrol.* 21, 212–222. doi: 10.1681/ASN.2008121226

Loeffler, I., and Wolf, G. (2015). Epithelial-to-Mesenchymal transition in diabetic nephropathy: fact or fiction? *Cells* 4, 631–652. doi: 10.3390/cells4040631

Lovisa, S., LeBleu, V. S., Tampe, B., Sugimoto, H., Vadnagara, K., Carstens, JL., et al. (2015). Epithelial-to-mesenchymal transition induces cell cycle arrest and parenchymal damage in renal fibrosis. *Nat. Med.* 21, 998–1009. doi: 10.1038/nm.3902

Lovisa, S., Zeisberg, M., and Kalluri, R. (2016). Partial Epithelial-to-Mesenchymal transition and other new mechanisms of kidney fibrosis. *Trends Endocrinol. Metab.* 27, 681–695. doi: 10.1016/j.tem.2016.06.004

Lu, H., Chen, B., Hong, W., Liang, Y., and Bai, Y. (2016). Transforming growth factor-beta1 stimulates hedgehog signaling to promote epithelial-mesenchymal transition after kidney injury. *FEBS J.* 283, 3771–3790. doi: 10.1111/febs.13842

Lv, L. L., Wu, W. J., Feng, Y., Li, Z. L., Tang, T. T., and Liu, B. C. (2018). Therapeutic application of extracellular vesicles in kidney disease: promises and challenges. *J. Cell Mol. Med.* 22, 728–737. doi: 10.1111/jcmm.13407

McDonald, O. G., Wu, H., Timp, W., Doi, A., and Feinberg, A. P. (2011). Genome-scale epigenetic reprogramming during epithelial-to-mesenchymal transition. *Nat. Struct. Mol. Biol.* 18, 867–874. doi: 10.1038/nsmb.2084

Monteiro-Reis, S., Lobo, J., Henrique, R., and Jerónimo, C. (2019). Epigenetic mechanisms influencing epithelial to mesenchymal transition in bladder cancer. *Int. J. Mol. Sci.* 20:297. doi: 10.3390/ijms20020297

Moonen, L., D'Haese, P., and Vervaet, B. (2018). Epithelial cell cycle behaviour in the injured kidney. *Int. J. Mol. Sci.* 19:2038. doi: 10.3390/ijms19072038

Morrison, E. E., Bailey, M. A., and Dear, J. W. (2016). Renal extracellular vesicles: from physiology to clinical application. *J. Physiol.* 594, 5735–5748. doi: 10.1113/JP272182

Nadasdy, T., Laszik, Z., Blick, K. E., Johnson, D. L., and Silva, F. G. (1994). Tubular atrophy in the end-stage kidney: a lectin and immunohistochemical study. *Hum. Pathol.* 25, 22–28. doi: 10.1016/0046-8177(94)90166-x

Ning, Y. X., Wang, X. Y., Wang, J. Q., Zeng, R., and Wang, G. Q. (2018). MiR152 regulates TGFbeta1induced epithelialmesenchymal transition by targeting HPIP in tubular epithelial cells. *Mol. Med. Rep.* 17, 7973–7979. doi: 10.3892/mmr.2018.8842

Ovadya, Y., and Krizhanovsky, V. (2015). A new Twist in kidney fibrosis. *Nat. Med.* 21, 975–977. doi: 10.1038/nm.3938

Pang, M., Kothapally, J., Mao, H., Tolbert, E., Ponnusamy, M., Chin, Y. E., et al. (2009). Inhibition of histone deacetylase activity attenuates renal fibroblast activation and interstitial fibrosis in obstructive nephropathy. *Am. J. Physiol. Renal. Physiol.* 297, F996–F1005. doi: 10.1152/ajprenal.00282.2009

Prunotto, M., Budd, D. C., Gabbiani, G., Meier, M., Formentini, I., Hartmann, G., et al. (2012). Epithelial-mesenchymal crosstalk alteration in kidney fibrosis. *J. Pathol.* 228, 131–147. doi: 10.1002/path.4049

Rigalli, J. P., Barros, E. R., Sommers, V., Bindels, R. J. M., and Hoenderop, J. G. J. (2020). Novel aspects of extracellular vesicles in the regulation of renal physiological and pathophysiological processes. *Front. Cell Dev. Biol.* 15:244. doi: 10.3389/fcell.2020.00244

Rodriguez-Romo, R., Berman, N., Gomez, A., and Bobadilla, N. A. (2015). Epigenetic regulation in the acute kidney injury to chronic kidney disease transition. *Nephrology (Carlton)* 20, 736–743. doi: 10.1111/nep.12521

Simon, N., and Hertig, A. (2015). Alteration of fatty acid oxidation in tubular epithelial cells: from acute kidney injury to renal fibrogenesis. *Front. Med.* 2:52. doi: 10.3389/fmed.2015.00052

Sosa Peña, M. D. P., Lopez-Soler, R., and Melendez, J. A. (2018). Senescence in chronic allograft nephropathy. *Am. J. Physiol. Renal. Physiol.* 315, F880–F889. doi: 10.1152/ajprenal.00195.2016

Srivastava, S. P., Hedayat, A. F., Kanasaki, K., and Goodwin, J. E. (2019). MicroRNA crosstalk influences Epithelial-to-Mesenchymal, Endothelial-to-Mesenchymal, and Macrophage-to-Mesenchymal transitions in the kidney. *Front. Pharmacol.* 10:904. doi: 10.3389/fphar.2019.00904

Sun, G., Reddy, M. A., Yuan, H., Lanting, L., Kato, M., and Natarajan, R. (2010). Epigenetic histone methylation modulates fibrotic gene expression. *J. Am. Soc. Nephrol. JASN* 21, 2069–2080. doi: 10.1681/ASN.2010060633

Sun, L., and Fang, J. (2016). Epigenetic regulation of epithelial–mesenchymal transition. *Cell Mol. Life Sci.* 73, 4493–4515. doi: 10.1007/s00018-016-2303-1

Surendran, K., Schiavi, S., and Hruska, K. A. (2005). Wnt-dependent beta-catenin signaling is activated after unilateral ureteral obstruction, and recombinant secreted frizzled-related protein 4 alters the progression of renal fibrosis. *J. Am. Soc. Nephrol.* 16, 2373–2384. doi: 10.1681/ASN.2004110949

Syn, W. K., Jung, Y., Omenetti, A., Abdelmalek, M., Guy, C. D., Yang, L., et al. (2009). Hedgehog-mediated epithelial-to-mesenchymal transition and fibrogenic repair in nonalcoholic fatty liver disease. *Gastroenterology* 137, 1478–1488. doi: 10.1053/j.gastro.2009.06.051

Tampe, B., and Zeisberg, M. (2014). Evidence for the involvement of epigenetics in the progression of renal fibrogenesis. *Nephrol. Dial Transpl.* 29, i1–i8. doi: 10.1093/ndt/gft361

Tanaka, M., Masaki, Y., Tanaka, K., Miyazaki, M., Kato, M., Sugimoto, R., et al. (2013). Reduction of fatty acid oxidation and responses to hypoxia correlate with the progression of de-differentiation in HCC. *Mol. Med. Rep.* 7, 365–370. doi: 10.3892/mmr.2012.1201

Tang, J., Liu, N., Tolbert, E., Ponnusamy, M., Ma, L., Gong, R., et al. (2013). Sustained activation of EGFR triggers renal fibrogenesis after acute kidney injury. *Am. J. Pathol.* 183, 160–172. doi: 10.1016/j.ajpath.2013.04.005

Tang, O., Chen, X., Shen, S., Hahn, M., and Pollock, C. A. (2013). MiRNA-200b represses transforming growth factor-β1-induced EMT and fibronectin expression in kidney proximal tubular cells. *Am. J. Physiol. Renal Physiol.* 304, F1266–F1273. doi: 10.1152/ajprenal.00302.2012

Tennakoon, A., Izawa, T., Kuwamura, M., and Yamate, J. (2016). Pathogenesis of type 2 epithelial to mesenchymal transition (EMT) in renal and hepatic fibrosis. *J. Clin. Med.* 5:4. doi: 10.3390/jcm5010004

Wang, J. Q., Yan, F. Q., Wang, L. H., Yin, W. J., Chang, T. Y., Liu, J. P., et al. (2019). Identification of new hypoxia−regulated epithelial−mesenchymal transition marker genes labeled by H3K4 acetylation. *Gene Chrom. Cancer* 59, 73–83. doi: 10.1002/gcc.22802

Wanner, N., and Bechtel-Walz, W. (2017). Epigenetics of kidney disease. *Cell Tissue Res.* 369, 75–92. doi: 10.1007/s00441-017-2588-x

Wing, M. R., Ramezani, A., Gill, H. S., Devaney, J. M., and Raj, D. S. (2013). Epigenetics of progression of chronic kidney disease: fact or fantasy? *Semi. Nephrol.* 33, 363–374. doi: 10.1016/j.semnephrol.2013.05.008

Wu, C. F., Chiang, W. C., Lai, C. F., Chang, F. C., Chen, Y. T., Chou, Y. H., et al. (2013). Transforming growth factor beta-1 stimulates profibrotic epithelial signaling to activate pericyte-myofibroblast transition in obstructive kidney fibrosis. *Am. J. Pathol.* 182, 118–131. doi: 10.1016/j.ajpath.2012.09.009

Wu, M., Tsai, Y., Yang, M., Huang, C., Chang, S., Chang C., et al. (2011). Interplay between HDAC3 and WDR5 is essential for Hypoxia-Induced Epithelial-Mesenchymal transition. *Mol. Cell* 43, 811–822. doi: 10.1016/j.molcel.2011.07.012

Xiao, L., Wang, M., Yang, S., Liu, F., and Sun, L. (2013). A glimpse of the pathogenetic mechanisms of wnt/β-Catenin signaling in diabetic nephropathy. *BioMed. Res. Int.* 2013, 1–7. doi: 10.1155/2013/987064

Xiao, L., Zhou, D., Tan, R. J., Fu, H., Zhou, L., Hou, F., et al. (2016). Sustained activation of Wnt/beta-Catenin signaling drives AKI to CKD progression. *J. Am. Soc. Nephrol.* 27, 1727–1740. doi: 10.1681/ASN.2015040449

Xiao, X., Tang, W., Yuan, Q., Peng, L., and Yu, P. (2015). Epigenetic repression of Krüppel-like factor 4 through Dnmt1 contributes to EMT in renal fibrosis. *Int. J. Mol. Med.* 35, 1596–1602. doi: 10.3892/ijmm.2015.2189

Xu, Y., Huang, J., Xin, W., Chen, L., Zhao, X., Lv, Z., et al. (2014). Lipid accumulation is ahead of epithelial-to-mesenchymal transition and therapeutic intervention by acetyl-CoA carboxylase 2 silence in diabetic nephropathy. *Metabolism* 63, 716–726. doi: 10.1016/j.metabol.2014.02.01

Yang, J., Kim, N., Yun, J., Cho, E., Cha, Y., Cho, S., et al. (2020). Snail augments fatty acid oxidation by suppression of mitochondrial ACC2 during cancer progression. *Life Sci. Alliance* 3:e202000683. doi: 10.26508/lsa.202000683

Yang, L., Besschetnova, T. Y., Brooks, C. R., Shah, J. V., and Bonventre, J. V. (2010). Epithelial cell cycle arrest in G2/M mediates kidney fibrosis after injury. *Nat. Med.* 16, 535–543. doi: 10.1038/nm.2144

Yang, Z., Sun, L., Nie, H., Liu, H., Liu, G., Guan G., et al. (2015). Connective tissue growth factor induces tubular epithelial to mesenchymal transition through the activation of canonical Wnt signaling in vitro. *Ren. Fail.* 37, 129–135. doi: 10.3109/0886022X.2014.967699

Zeisberg, M., and Neilson, E. G. (2010). Mechanisms of tubulointerstitial fibrosis. *J. Am. Soc. Nephrol.* 21, 1819–1834. doi: 10.1681/ASN.2010080793

Zhao, Y., Yin, Z., Li, H., Fan, J., Yang, S., Chen C., et al. (2017). MiR-30c protects diabetic nephropathy by suppressing epithelial-to-mesenchymal transition in db/db mice. *Aging Cell* 16, 387–400. doi: 10.1111/acel.12563

Zhou, D., Li, Y., Lin, L., Zhou, L., Igarashi, P., and Liu, Y. (2012). Tubule-specific ablation of endogenous beta-catenin aggravates acute kidney injury in mice. *Kidney Int.* 82, 537–547. doi: 10.1038/ki.2012.173

Zhou, D., Li, Y., Zhou, L., Tan, R. J., Xiao, L., Liang M., et al. (2014). Sonic hedgehog is a novel tubule-derived growth factor for interstitial fibroblasts after kidney injury. *J. Am. Soc. Nephrol.* 25, 2187–2200. doi: 10.1681/ASN.2013080893

Zhou, D., and Liu, Y. (2016). Renal fibrosis in 2015: Understanding the mechanisms of kidney fibrosis. *Nat. Rev. Nephrol.* 12, 68–70. doi: 10.1038/nrneph.2015.215

Zhou, T., Luo, M., Cai, W., Zhou, S., Feng, D., Xu C., et al. (2018). Runt-related transcription factor 1 (RUNX1) promotes TGF-β-induced renal tubular epithelial-to-mesenchymal transition (EMT) and renal fibrosis through the PI3K subunit p110δ. *EBioMedicine* 31, 217–225. doi: 10.1016/j.ebiom.2018.04.023

Zhou, X., Zang, X., Ponnusamy, M., Masucci, M. V., Tolbert, E., Gong R., et al. (2016). Enhancer of zeste homolog 2 inhibition attenuates renal fibrosis by maintaining smad7 and phosphatase and tensin homolog expression. *J. Am. Soc. Nephrol.* 27, 2092–2108. doi: 10.1681/ASN.2015040457

Conflict of Interest: The authors declare that the research was conducted in the absence of any commercial or financial relationships that could be construed as a potential conflict of interest.

frontiers in Physiology

MINI REVIEW
published: 25 September 2020
doi: 10.3389/fphys.2020.586290

Programmed Adult Kidney Disease: Importance of Fetal Environment

Rogério Argeri[1], Fernanda Thomazini[1], Débora Conte Kimura Lichtenecker[1], Karina Thieme[2], Maria do Carmo Franco[1†] and Guiomar Nascimento Gomes[1†]*

[1]Department of Physiology, School of Medicine, Federal University of São Paulo, São Paulo, Brazil, [2]Department of Physiology and Biophysics, Institute of Biomedical Sciences, Universidade de Sao Paulo, São Paulo, Brazil

The Barker hypothesis strongly supported the influence of fetal environment on the development of chronic diseases in later life. Multiple experimental and human studies have identified that the deleterious effect of fetal programming commonly leads to alterations in renal development. The interplay between environmental insults and fetal genome can induce epigenetic changes and lead to alterations in the expression of renal phenotype. In this review, we have explored the renal development and its functions, while focusing on the epigenetic findings and functional aspects of the renin-angiotensin system and its components.

Keywords: renal function, programmed kidney disease, hypertension, nephron number, fetal environment

OPEN ACCESS

Edited by:
Adriana Castello Costa Girardi, University of São Paulo, Brazil

Reviewed by:
Michel Baum, University of Texas Southwestern Medical Center, United States
Patricia Aline Boer, Campinas State University, Brazil
Nilberto Robson Falcão Nascimento, State University of Ceará, Brazil

***Correspondence:**
Guiomar Nascimento Gomes
guiomar.gomes@unifesp.br

[†]These authors have contributed equally to this work

Specialty section:
This article was submitted to Renal and Epithelial Physiology, a section of the journal Frontiers in Physiology

Received: *22 July 2020*
Accepted: *07 September 2020*
Published: *25 September 2020*

Citation:
Argeri R, Thomazini F, Lichtenecker DCK, Thieme K, Franco MdC and Gomes GN (2020) Programmed Adult Kidney Disease: Importance of Fetal Environment. Front. Physiol. 11:586290. doi: 10.3389/fphys.2020.586290

INTRODUCTION

The number of nephrons in humans is highly variable, ranging from 250,000 to 2 million per kidney (Bertram et al., 2011). There is an inverse correlation between the total number of nephrons and the risk of developing kidney disease and hypertension (Brenner et al., 1988; Keller et al., 2003). Nephrons are composed of specialized cells, such as epithelial, endothelial, and stromal cells. The epithelial cells originated from the intermediate mesoderm, which also originates two different progenitor cell populations: the ureteric bud (UB) and the metanephric mesenchyme (Little et al., 2007). Clusters of metanephric mesenchymal cells condense around each ureteric bud to form cap mesenchyme (CM). Then, follows a complex and highly coordinated process that depends on interactions between the UB (which will form the collecting duct system) and surrounding CM (which originates the intermediate progenitor cells that ultimately generate all cell types of the nephron; Costantini and Kopan, 2010; Little and McMahon, 2012; Nicolaou et al., 2015; Hurtado Del Pozo et al., 2018). Grobstein's study was a pioneer in renal development. It showed that kidney development is a multi-stage process, which starts with a primary induction event from the UB, followed by mesenchymal-to-epithelial transition within the CM. The process ends with the completion of nephron patterning and elongation (Grobstein, 1956).

KIDNEY DISEASE AND BARKER HYPOTHESIS: IMPORTANCE OF FETAL ENVIRONMENT

Renal disease is one of the common causes of mortality and morbidity worldwide (Luyckx et al., 2018). Interestingly, this disease can originate in early life (Hoy et al., 1999; Lackland et al., 2000; Eriksson et al., 2018). Barker proposed that insults during critical periods of fetal development can result in a growth deficit, characterized by low birth weight (LBW) and silent morpho-functional changes, that translate into kidney disease in the long term (Hales and Barker, 2001; Langley-Evans et al., 2003).

The human nephrogenesis requires an optimum balance and is completed by around 32–34 weeks of gestation. During this period, the kidneys can be influenced by insults in fetal environment. Evidence suggests that people with LBW have congenital deficit in the number of nephrons and are more susceptible to subsequent renal injury and functional decline in later life (Brenner et al., 1988; Schreuder et al., 2006; Eriksson et al., 2018). Reports that evaluated fetal kidney by ultrasound have supported these findings (Konje et al., 1996; Spencer et al., 2001). Interestingly, other studies have described a positive correlation between birth weight and number of nephrons (Feig et al., 2004; Hoy et al., 2005). Besides, an inverse correlation between the birth weight and glomerular size in the kidney, isolated from neonates, was observed (Mañalich et al., 2000). According to Brenner's theory (Brenner et al., 1988), the reduced number of nephrons limits excretion of fluids and electrolytes, leading to volume expansion and development of hypertension; this alteration, in turn, damages the glomeruli, causing glomerulosclerosis and accelerating the loss of nephrons (Brenner et al., 1988; Hinchliffe et al., 1991; Schreuder et al., 2006). Conversely, the reduction in nephron number, by the reduction in renal mass or of congenital origin, is followed by compensatory renal growth that leads to hypertrophy of both glomeruli and tubules. This structural change, in addition to increasing glomerular filtration, results in the proximal and distal tubules growth favoring the reabsorption of the filtered volume. Thus, renal function is preserved; however, in long term may result in hypertension and kidney damage (Fong et al., 2014; McArdle et al., 2020).

The assessment of renal function is important to detect the extent and progression of renal diseases. Increasing evidence is available about the impact of fetal environment on the decline in renal function (Hoy et al., 1999; Giapros et al., 2007). An inverse correlation has been observed between birth weight and albumin-to-creatinine ratio in individuals from an Australian aboriginal community (Hoy et al., 1998). Other reports have observed a relationship between LBW with lower glomerular filtration rate (GFR) and albuminuria (Hoy et al., 1999, 2005; Keijzer-Veen et al., 2005). It has been described that LBW neonates, as a result of either prematurity or growth restriction, have increased levels of albuminuria (Aisa et al., 2016). Additionally, severe tubular injury, characterized by high levels of cathepsin B and N-acetyl-β-D-glucosaminidase (NAG) activity, was observed in these neonates (Aisa et al., 2016). In a twin study, Gielen et al. (2005) found that LBW population had lower creatinine clearance levels than the high birth weight population. Moderate renal disturbances were found in LBW children from 4 to 12 years of age (Monge et al., 1998). Another study has reported high levels of cystatin C, a marker of renal function, in LBW children (Franco et al., 2008b). Additionally, Barbati et al. (2016) have shown high levels of cystatin C in urine of LBW neonates. These authors observed an inverse correlation between cystatin C levels and renal volume (Barbati et al., 2016).

Several experimental studies were conducted to confirm the human data (Swanson and David, 2015). Studies demonstrated that restricted protein intake during pregnancy led to LBW, reduced nephron number, and glomerular enlargement in offspring (Merlet-Bénichou et al., 1994; Langley-Evans et al., 1999; Woods, 2000; Vehaskari et al., 2004; Mesquita et al., 2010). Additionally, protein restriction also increased: blood urea, urinary output, and urinary albumin excretion in resultant offspring (Nwagwu et al., 2000). It is believed that the renal changes occur in response to inadequate nutrition as adaptations to ensure survival (Langley-Evans, 2015). These adaptations would be adequate if in the postnatal period the nutritional conditions remained the same. However, if in the postnatal period the nutritional offer changes to a better nutritional standard, the occurred adaptations are no longer adequate and become harmful. This discrepancy between the phenotype developed and that suitable for a given environment is called "mismatch" (Gluckman et al., 2019).

Another important prenatal factor contributing to programming of the renal diseases is maternal diabetes mellitus (e.g., pre-existing type 1 or 2 and gestational diabetes). Although it is correlated with high, instead of LBW, is also associated with impairment of both GFR and renal plasma flow (Abi Khalil et al., 2010). The effect of maternal diabetes on fetal kidney volume is not well established (Hokke et al., 2019). In a recent study, instead of nephron number, the total renal and cortical volumes were assessed in newborns. Neonates of diabetic mothers, with inadequate glycemic control, had lower cortical and total renal volume, suggesting a lower nephron number. However, newborns of diabetic mothers, with strict glycemic control, had similar values as control newborns (Aisa et al., 2019). Thus, it is evident that variations in the maternal glycemic status can lead to different outcomes in the offspring's kidneys (Aisa et al., 2019).

The studies about the impact of maternal diabetes on fetal development are of great importance since this metabolic disorder can promote several congenital anomalies (Steel et al., 1990). Some studies have demonstrated a high risk of congenital anomalies of the kidney and urinary tract (CAKUT) in children exposed to maternal diabetes (Shnorhavorian et al., 2011; Hsu et al., 2014). Dart et al. (2015) reported that pre-gestational diabetes increased the risk of CAKUT in infants by 67%. Maternal hyperglycemia is an important threat, as glucose crosses the placenta leading to fetal hyperinsulinemia (Higgins and Mc Auliffe, 2010). In turn, hyperinsulinemia stimulates leptin secretion, resulting in hyperleptinemia (Lepercq et al., 1998). Fetal exposure to non-physiological concentrations of these hormones is associated with hypothalamic dysfunction (Plagemann, 2004). Additionally, generation of reactive oxygen species can occur in response to increased glucose/insulin metabolism (Tozour et al., 2018). Therefore, maternal hyperglycemia can be threatening to the developing fetus by different mechanisms. Hence, it is crucial to maintain optimum blood glucose levels during pregnancy.

Experimental studies in female rats, in which diabetes mellitus was induced before the onset of pregnancy using streptozotocin (STZ), demonstrated that offspring developed glomerular hypertrophy and reduction of both GFR and urinary output (Rocha et al., 2005; Magaton et al., 2007). Additionally, renal vascular resistance and the thickness of interlobular arteries were increased in the offspring of diabetic mothers, suggesting vascular remodeling (Rocco et al., 2008); results recently confirmed by Dib et al. (2018). However, there are controversies

regarding the nephron number in offspring of diabetic mothers (Rocha et al., 2005; Magaton et al., 2007; Rocco et al., 2008). Reduction in nephron number was observed in studies in which diabetes was induced by different protocols after confirmation of pregnancy (Amri et al., 1999; Tran et al., 2008; Hokke et al., 2013). However, in these studies, the fetus was exposed to the direct effects of STZ, in addition to hyperglycemia.

MECHANISMS INVOLVED IN PROGRAMMED KIDNEY DISEASES

Many are the possible mechanisms involved in fetal programming, in **Figure 1** are represented the most studied ones.

Epigenetic Events

The fetal environment can alter the epigenetic landscape, strongly impacting the reprogramming of gene expression (Dressler and Patel, 2015). Epigenetic modification refers to dynamic changes in chromatin that mediates interactions between environmental factors and the genome. These modifications alter chromatin structure, thereby modulating the accessibility of transcription factors and consequently determining the expression or repression of genes (Hurtado Del Pozo et al., 2018; Wanner et al., 2019). Some of the well-known epigenetic modifications are DNA methylation and post-translation modifications of histones (acetylation, methylation, phosphorylation, and ubiquitination; Hilliard and El-Dahr, 2016).

The role of DNA methylation in the nephron development and its function is not yet well defined. Recently, Wanner et al. (2019) reported that DNA methyltransferase 1 (Dnmt1), and not Dnmt3a/b, is the key regulator of prenatal renal programming, representing a fundamental link between nephron number and intrauterine environment. On the other hand, histone marks distinctively dictate nephrogenesis and affect the expression of several developmental genes, some of them involved in renal disease development (Harikumar and Meshorer, 2015). Studies have provided important information about spatiotemporal changes and dynamic functional states of the epigenome during nephrogenesis. These studies have demonstrated that promoter regions of specific genes in nephron progenitor cells are bivalent and carry both "active" (H3K4me3) and "repressive" (H3K9me3 and H3K27me3) histone marks, along with expression of their corresponding methyltransferases (Ash2l, G9a, Ezh2/Suz12, respectively; McLaughlin et al., 2013, 2014). This suggests that differentiation programs are silenced in these cells, however, can be activated in response to external factors that can be determined by maternal nutritional features during fetal life. Dnmt1 and H3K27me3 are critical in nephron progenitor cells (NPCs) self-renewal and differentiation (Huang et al., 2020). NPC express H3K4me3/K9me3/K27me3 but nascent nephrons retain H3K4me3 marks and downregulate H3K9me3/K27me3 (Hilliard and El-Dahr, 2016). Remarkably, alterations in H3K27me3 levels in differentiated cells have been linked to renal diseases (Majumder et al., 2018; Jia et al., 2019).

Gene-environment interactions during fetal development can persist in multiple generations. Some studies have reported that *in utero* exposure can affect fetal germ cells and F2 offspring, resulting in transgenerational programming. Epigenetic changes at birth can be associated with maternal nutrition and in the case of female fetuses they can be transmitted to the next generation, emphasizing that inheritance does not depend only on genetic factors but also involves epigenetic mechanisms (Gluckman et al., 2019). However, still little is known about these effects on kidney disease (Briffa et al., 2020).

Renin-Angiotensin System

It is well established that the renin-angiotensin system (RAS) plays an important role in normal morphological development of the kidney and renal function (Guron and Friberg, 2000). All the components of RAS are expressed in early gestation in both rats and human beings (McMillen and Robinson, 2005). In fact, the pharmacological blockade of RAS during renal development leads to altered renal structures (Machado et al., 2008; Madsen et al., 2010; Kett and Denton, 2011; de Almeida et al., 2017). Mutations and altered expressions in genes coding for RAS components are linked to congenital abnormalities of the kidney, confirming the importance of RAS in renal morphogenesis and metanephric organogenesis (Song et al., 2011). It was demonstrated that angiotensin II stimulates the growth and branching of the UB through its receptors (Yosypiv et al., 2008; Song et al., 2011). Also, angiotensin II stimulates the expression of Pax-2 (homeobox 2 gene), an anti-apoptotic factor, which is essential for renal development and repair

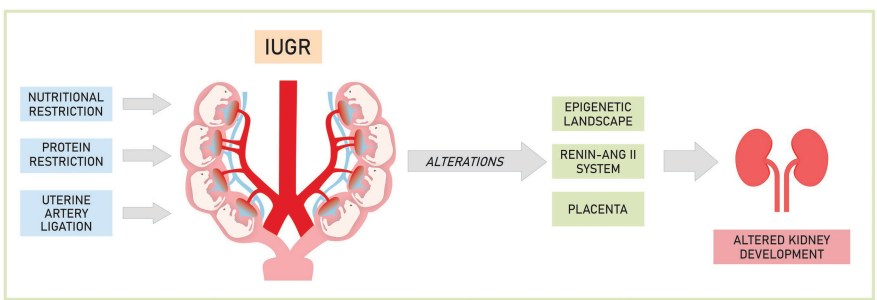

FIGURE 1 | Mechanisms involved in the development of renal changes caused by experimental intrauterine growth restriction (IUGR).

(Hershkovitz et al., 2007). This process occurs through AT_2 receptors (AT2r) and modulates nephrogenesis and renal development (Zandi-Nejad et al., 2006).

The expression of some RAS components could be sensitive to insult during fetal development contributing to later development of renal diseases. Evidence in the literature has demonstrated that fetal programming by several insults promote suppression of the fetal RAS, resulting in altered nephrogenesis (Woods et al., 2001; Dötsch et al., 2009; Mesquita et al., 2010; Moritz et al., 2010). Woods et al. (2001) showed reduction in messenger RNA (mRNA) expression and renin levels in newborns exposed to low protein diet in prenatal life. These authors suggest that such early alteration may be caused by lower intrarenal angiotensin II concentration during nephrogenesis and consequently impair the renal development.

It was observed that fewer ureteral branches sprouted out from the metanephros in the fetus exposed to low protein diet in utero (Mesquita et al., 2010). These changes occurred simultaneously with decreased expression of AT1 receptors (AT1r; on the 17th embryonic day), confirming maladjustment of RAS in the kidneys of these animals (Mesquita et al., 2010).

On the other hand, after the end of nephrogenesis, hyperactivity of RAS was observed in response to fetal programming. There is evidence that exposure to low protein diet, throughout gestation or during specific periods, results in an imbalance in the expression of AT1r and AT2r (Moritz et al., 2010). An increase in AT1r mRNA and protein and a decrease in AT2r gene expression were observed (McMullen et al., 2004; Vehaskari et al., 2004; McMullen and Langley-Evans, 2005). Moreover, it was reported high expression of both mRNA and proteins coding for Angiotensin II 1b receptor (AT_1b-R) in adrenal glands isolated from adult offspring exposed to protein restriction during fetal life; and also, hypo-methylation in the promoter regions ofAT_1b-R gene (Bogdarina et al., 2007). This epigenetic alteration could lead to higher transcriptional activity, thereby promoting higher expression of this receptor.

Considering maternal diabetes models, it has also been described that the expression of the mRNA coding for angiotensin 1–7 was significantly lower in the offspring of diabetic mothers (Magaton et al., 2007). Besides, increased expression of AT1r was observed in the kidneys of offspring from diabetic mothers, suggesting that changes in RAS might have contributed to the renal changes in this model (Yan et al., 2014).

Interestingly, the RAS blockade in early post-natal life seems to offset the negative effects of fetal programming on the kidneys (Manning and Vehaskari, 2005; Hsu et al., 2015; Watanabe et al., 2018). Early administration of aliskiren, a renin inhibitor, reduced angiotensinogen expression associated with increased renal AT2r and Mas protein in offspring exposed to nutrient restriction during gestation (Hsu et al., 2015). Also, post-weaning losartan (AT1r blocker) therapy completely stopped immune cell infiltration and intrarenal RAS activation in the kidneys isolated from adult offspring exposed to protein restriction during fetal life (Watanabe et al., 2018).

Additionally, altered expression of AT1r in areas of the brain involved in the regulation of blood pressure has been found in protein-restricted offspring (Pladys et al., 2004; de Lima et al., 2013). This change is probably associated with the autonomic changes found in these animals. Increased sympathetic tone seems to have an important role in the genesis of arterial hypertension in this experimental model, supporting this hypothesis are the high plasma concentration of catecholamines observed in protein-restricted offspring (Petry et al., 2000); and the fact that renal denervation prevented hypertension confirming the role of renal nerves activation in the offspring with restricted growth (Alexander et al., 2005; Custódio et al., 2017).

Regarding the changes in RAS in humans, Simonetti et al. (2008) observed higher salt sensitivity in LBW children, possibly as a result of increased aldosterone activity or alterations in AT1r expression or affinity. It has also been reported that circulating levels of angiotensin II and angiotensin-converting enzyme (ACE) activity were higher in healthy males with LBW (Franco et al., 2008a). Ajala et al. (2012) found that the presence of DD genotype in the ACE gene is associated with higher ACE activity in children with a history of LBW. Moreover, one study in LBW children has reported hypo-methylation in the promoter region of the ACE gene (Rangel et al., 2014). These authors also observed that LBW children have lower methylation levels along with higher ACE activity (Rangel et al., 2014).

Placental Alterations

The placenta, which forms the functional interface between the maternal and fetal circulations, is important for the normal development of the fetus. Usually, the placenta expresses the enzyme 11 beta-hydroxysteroid dehydrogenase type 2 (11β-HSD2) that inactivates maternal glucocorticoids, protecting the fetus from premature exposure to this hormone. Studies have shown that maternal nutritional restriction significantly reduces placental development and also the expression of 11β-HSD2, thus the fetus may be exposed to these hormones prematurely (Börzsönyi et al., 2012; Chapman et al., 2013).

In rats, premature exposure to corticosterone impacted kidney formation resulting in reduction of the nephron number, confirming the negative effects of early exposure to this hormone (Woods and Weeks, 2005; Singh et al., 2007).

CONCLUSION

Kidney disease is a concerning health problem in the modern world and can be considered as one of the common causes of morbidity and mortality. The fetal environment is an important period for the development of several adaptive mechanisms in various organ systems, leading to an increased risk of development of renal diseases in later life. Several reports from human and animal models suggest that the kidneys can be influenced by insults during fetal development in utero. The impairment in nephrogenesis leads to the process of glomerulosclerosis and loss of renal function in later life. Modifications in the epigenetic characteristics and RAS components are likely involved. Further studies are required to determine relationships between epigenetic alterations and RAS pathway abnormalities, and their ability to influence fetal programming of the kidney diseases.

AUTHOR CONTRIBUTIONS

All authors listed have made a substantial, direct and intellectual contribution to the work, and approved it for publication.

FUNDING

This manuscript is a revision and for its elaboration no funding was received.

REFERENCES

Abi Khalil, C., Travert, F., Fetita, S., Rouzet, F., Porcher, R., Riveline, J. P., et al. (2010). Fetal exposure to maternal type 1 diabetes is associated with renal dysfunction at adult age. *Diabetes* 59, 2631–2636. doi: 10.2337/db10-0419

Aisa, M. C., Cappuccini, B., Barbati, A., Clerici, G., Torlone, E., Gerli, S., et al. (2019). Renal consequences of gestational diabetes mellitus in term neonates: a multidisciplinary approach to the DOHaD perspective in the prevention and early recognition of neonates of GDM mothers at risk of hypertension and chronic renal diseases in later life. *J. Clin. Med.* 8:429. doi: 10.3390/jcm8040429

Aisa, M. C., Cappuccini, B., Barbati, A., Orlacchio, A., Baglioni, M., and Di Renzo, G. C. (2016). Biochemical parameters of renal impairment/injury and surrogate markers of nephron number in intrauterine growth-restricted and preterm neonates at 30-40 days of postnatal corrected age. *Pediatr. Nephrol.* 31, 2277–2287. doi: 10.1007/s00467-016-3484-4

Ajala, A. R., Almeida, S. S., Rangel, M., Palomino, Z., Strufaldi, M. W., Puccini, R. F., et al. (2012). Association of ACE gene insertion/deletion polymorphism with birth weight, blood pressure levels, and ACE activity in healthy children. *Am. J. Hypertens.* 25, 827–832. doi: 10.1038/ajh.2012.50

Alexander, B. T., Hendon, A. E., Ferril, G., and Dwyer, T. M. (2005). Renal denervation abolishes hypertension in low-birth-weight offspring from pregnant rats with reduced uterine perfusion. *Hypertension* 45, 754–758. doi: 10.1161/01.HYP.0000153319.20340.2a

Amri, K., Freund, N., Vilar, J., Merlet-Bénichou, C., and Lelièvre-Pégorier, M. (1999). Adverse effects of hyperglycemia on kidney development in rats: in vivo and in vitro studies. *Diabetes* 48, 2240–2245. doi: 10.2337/diabetes.48.11.2240

Barbati, A., Cappuccini, B., Aisa, M. C., Grasselli, C., Zamarra, M., Bini, V., et al. (2016). Increased urinary cystatin-c levels correlate with reduced renal volumes in neonates with intrauterine growth restriction. *Neonatology* 109, 154–160. doi: 10.1159/000441273

Bertram, J. F., Douglas-Denton, R. N., Diouf, B., Hughson, M. D., and Hoy, W. E. (2011). Human nephron number: implications for health and disease. *Pediatr. Nephrol.* 26, 1529–1533. doi: 10.1007/s00467-011-1843-8

Bogdarina, I., Welham, S., King, P. J., Burns, S. P., and Clark, A. J. (2007). Epigenetic modification of the renin-angiotensin system in the fetal programming of hypertension. *Circ. Res.* 100, 520–526. doi: 10.1161/01.RES.0000258855.60637.58

Börzsönyi, B., Demendi, C., Pajor, A., Rigó, J. Jr., Marosi, K., Agota, A., et al. (2012). Gene expression patterns of the 11β-hydroxysteroid dehydrogenase 2 enzyme in human placenta from intrauterine growth restriction: the role of impaired feto-maternal glucocorticoid metabolism. *Eur. J. Obstet. Gynecol. Reprod. Biol.* 161, 12–17. doi: 10.1016/j.ejogrb.2011.12.013

Brenner, B. M., Garcia, D. L., and Anderson, S. (1988). Glomeruli and blood pressure. Less of one, more the other? *Am. J. Hypertens.* 1, 335–347. doi: 10.1093/ajh/1.4.335

Briffa, J. F., Wlodek, M. E., and Moritz, K. M. (2020). Transgenerational programming of nephron deficits and hypertension. *Semin. Cell Dev. Biol.* 103, 94–103. doi: 10.1016/j.semcdb.2018.05.025

Chapman, K., Holmes, M., and Seckl, J. (2013). 11β-hydroxysteroid dehydrogenases: intracellular gate-keepers of tissue glucocorticoid action. *Physiol. Rev.* 93, 1139–1206. doi: 10.1152/physrev.00020.2012

Costantini, F., and Kopan, R. (2010). Patterning a complex organ: branching morphogenesis and nephron segmentation in kidney development. *Dev. Cell* 18, 698–712. doi: 10.1016/j.devcel.2010.04.008

Custódio, A. H., de Lima, M. C., Vaccari, B., Boer, P. A., and Gontijo, J. A. R. (2017). Renal sodium handling and blood pressure changes in gestational protein-restricted offspring: role of renal nerves and ganglia neurokinin expression. *PLoS One* 12:e0179499. doi: 10.1371/journal.pone.0179499

Dart, A. B., Ruth, C. A., Sellers, E. A., Au, W., and Dean, H. J. (2015). Maternal diabetes mellitus and congenital anomalies of the kidney and urinary tract (CAKUT) in the child. *Am. J. Kidney Dis.* 65, 684–691. doi: 10.1053/j.ajkd.2014.11.017

de Almeida, L. F., Francescato, H. D. C., da Silva, C. G. A., Costa, R. S., and Coimbra, T. M. (2017). Calcitriol reduces kidney development disorders in rats provoked by losartan administration during lactation. *Sci. Rep.* 7:11472. doi: 10.1038/s41598-017-11815-8

de Lima, M. C., Scabora, J. E., Lopes, A., Mesquita, F. F., Torres, D., Boer, P. A., et al. (2013). Early changes of hypothalamic angiotensin II receptors expression in gestational protein-restricted offspring: effect on water intake, blood pressure and renal sodium handling. *J. Renin-Angiotensin-Aldosterone Syst.* 14, 271–282. doi: 10.1177/1470320312456328

Dib, A., Payen, C., Bourreau, J., Munier, M., Grimaud, L., Fajloun, Z., et al. (2018). In utero exposure to maternal diabetes is associated with early abnormal vascular structure in offspring. *Front. Physiol.* 9:350. doi: 10.3389/fphys.2018.00350

Dötsch, J., Plank, C., Amann, K., and Ingelfinger, J. (2009). The implications of fetal programming of glomerular number and renal function. *J. Mol. Med.* 87, 841–848. doi: 10.1007/s00109-009-0507-7

Dressler, G. R., and Patel, S. R. (2015). Epigenetics in kidney development and renal disease. *Transl. Res.* 165, 166–176. doi: 10.1016/j.trsl.2014.04.007

Eriksson, J. G., Salonen, M. K., Kajantie, E., and Osmond, C. (2018). Prenatal growth and CKD in older adults: longitudinal findings from the Helsinki birth cohort study, 1924-1944. *Am. J. Kidney Dis.* 71, 20–26. doi: 10.1053/j.ajkd.2017.06.030

Feig, D. I., Nakagawa, T., Karumanchi, S. A., Oliver, W. J., Kang, D. H., Finch, J., et al. (2004). Hypothesis: uric acid, nephron number, and the pathogenesis of essential hypertension. *Kidney Int.* 66, 281–287. doi: 10.1111/j.1523-1755.2004.00729.x

Fong, D., Denton, K. M., Moritz, K. M., Evans, R., and Singh, R. R. (2014). Compensatory responses to nephron deficiency: adaptive or maladaptive? *Nephrology* 19, 119–128. doi: 10.1111/nep.12198

Franco, M. C., Casarini, D. E., Carneiro-Ramos, M. S., Sawaya, A. L., Barreto-Chaves, M. L., and Sesso, R. (2008a). Circulating renin-angiotensin system and catecholamines in childhood: is there a role for birthweight? *Clin. Sci.* 114, 375–380. doi: 10.1042/cs20070284

Franco, M. C., Nishida, S. K., and Sesso, R. (2008b). GFR estimated from cystatin C versus creatinine in children born small for gestational age. *Am. J. Kidney Dis.* 51, 925–932. doi: 10.1053/j.ajkd.2008.02.305

Giapros, V., Papadimitriou, P., Challa, A., and Andronikou, S. (2007). The effect of intrauterine growth retardation on renal function in the first two months of life. *Nephrol. Dial. Transplant.* 22, 96–103. doi: 10.1093/ndt/gfl550

Gielen, M., Pinto-Sietsma, S. J., Zeegers, M. P., Loos, R. J., Fagard, R., de Leeuw, P. W., et al. (2005). Birth weight and creatinine clearance in young adult twins: influence of genetic, prenatal, and maternal factors. *J. Am. Soc. Nephrol.* 16, 2471–2476. doi: 10.1681/asn.2004030210

Gluckman, P. D., Hanson, M. A., and Low, F. M. (2019). Evolutionary and developmental mismatches are consequences of adaptive developmental plasticity in humans and have implications for later disease risk. *Philos. Trans. R. Soc. Lond. Ser. B Biol. Sci.* 374:20180109. doi: 10.1098/rstb.2018.0109

Grobstein, C. (1956). Trans-filter induction of tubules in mouse metanephrogenic mesenchyme. *Exp. Cell Res.* 10, 424–440. doi: 10.1016/0014-4827(56)90016-7

Guron, G., and Friberg, P. (2000). An intact renin-angiotensin system is a prerequisite for normal renal development. *J. Hypertens.* 18, 123–137. doi: 10.1097/00004872-200018020-00001

Hales, C. N., and Barker, D. J. (2001). The thrifty phenotype hypothesis. *Br. Med. Bull.* 60, 5–20. doi: 10.1093/bmb/60.1.5

Harikumar, A., and Meshorer, E. (2015). Chromatin remodeling and bivalent histone modifications in embryonic stem cells. *EMBO Rep.* 16, 1609–1619. doi: 10.15252/embr.201541011

Hershkovitz, D., Burbea, Z., Skorecki, K., and Brenner, B. M. (2007). Fetal programming of adult kidney disease: cellular and molecular mechanisms. *Clin. J. Am. Soc. Nephrol.* 2, 334–342. doi: 10.2215/cjn.03291006

Higgins, M., and Mc Auliffe, F. (2010). A review of maternal and fetal growth factors in diabetic pregnancy. *Curr. Diabetes Rev.* 6, 116–125. doi: 10.2174/157339910790909431

Hilliard, S. A., and El-Dahr, S. S. (2016). Epigenetics mechanisms in renal development. *Pediatr. Nephrol.* 31, 1055–1060. doi: 10.1007/s00467-015-3228-x

Hinchliffe, S. A., Sargent, P. H., Howard, C. V., Chan, Y. F., and van Velzen, D. (1991). Human intrauterine renal growth expressed in absolute number of glomeruli assessed by the disector method and Cavalieri principle. *Lab. Investig.* 64, 777–784.

Hokke, S. N., Armitage, J. A., Puelles, V. G., Short, K. M., Jones, L., Smyth, I. M., et al. (2013). Altered ureteric branching morphogenesis and nephron endowment in offspring of diabetic and insulin-treated pregnancy. *PLoS One* 8:e58243. doi: 10.1371/journal.pone.0058243

Hokke, S., de Zoysa, N., Carr, B. L., Abruzzo, V., Coombs, P. R., Allan, C. A., et al. (2019). Normal foetal kidney volume in offspring of women treated for gestational diabetes. *Endocrinol. Diabetes Metab.* 2:e00091. doi: 10.1002/edm2.91

Hoy, W. E., Hughson, M. D., Bertram, J. F., Douglas-Denton, R., and Amann, K. (2005). Nephron number, hypertension, renal disease, and renal failure. *J. Am. Soc. Nephrol.* 16, 2557–2564. doi: 10.1681/asn.2005020172

Hoy, W. E., Mathews, J. D., McCredie, D. A., Pugsley, D. J., Hayhurst, B. G., Rees, M., et al. (1998). The multidimensional nature of renal disease: rates and associations of albuminuria in an Australian aboriginal community. *Kidney Int.* 54, 1296–1304. doi: 10.1046/j.1523-1755.1998.00099.x

Hoy, W. E., Rees, M., Kile, E., Mathews, J. D., and Wang, Z. (1999). A new dimension to the Barker hypothesis: low birthweight and susceptibility to renal disease. *Kidney Int.* 56, 1072–1077. doi: 10.1046/j.1523-1755.1999.00633.x

Hsu, C. C., Jhang, H. R., Chang, W. T., Lin, C. H., Shin, S. J., Hwang, S. J., et al. (2014). Associations between dietary patterns and kidney function indicators in type 2 diabetes. *Clin. Nutr.* 33, 98–105. doi: 10.1016/j.clnu.2013.04.010

Hsu, C. N., Lee, C. T., Huang, L. T., and Tain, Y. L. (2015). Aliskiren in early postnatal life prevents hypertension and reduces asymmetric dimethylarginine in offspring exposed to maternal caloric restriction. *J. Renin-Angiotensin-Aldosterone Syst.* 16, 506–513. doi: 10.1177/1470320313514123

Huang, B., Liu, Z., Vonk, A., Zeng, Z., and Li, Z. (2020). Epigenetic regulation of kidney progenitor cells. *Stem Cells Transl. Med.* 9, 655–660. doi: 10.1002/sctm.19-0289

Hurtado Del Pozo, C., Garreta, E., Izpisúa Belmonte, J. C., and Montserrat, N. (2018). Modeling epigenetic modifications in renal development and disease withs organoids and genome editing. *Dis. Model. Mech.* 11:dmm035048. doi: 10.1242/dmm.035048

Jia, Y., Reddy, M. A., Das, S., Oh, H. J., Abdollahi, M., Yuan, H., et al. (2019). Dysregulation of histone H3 lysine 27 trimethylation in transforming growth factor-β1-induced gene expression in mesangial cells and diabetic kidney. *J. Biol. Chem.* 294, 12695–12707. doi: 10.1074/jbc.RA119.007575

Keijzer-Veen, M. G., Schrevel, M., Finken, M. J., Dekker, F. W., Nauta, J., Hille, E. T., et al. (2005). Microalbuminuria and lower glomerular filtration rate at young adult age in subjects born very premature and after intrauterine growth retardation. *J. Am. Soc. Nephrol.* 16, 2762–2768. doi: 10.1681/asn.2004090783

Keller, G., Zimmer, G., Mall, G., Ritz, E., and Amann, K. (2003). Nephron number in patients with primary hypertension. *N. Engl. J. Med.* 348, 101–108. doi: 10.1056/NEJMoa020549

Kett, M. M., and Denton, K. M. (2011). Renal programming: cause for concern? *Am. J. Phys. Regul. Integr. Comp. Phys.* 300, R791–R803. doi: 10.1152/ajpregu.00791.2010

Konje, J. C., Bell, S. C., Morton, J. J., de Chazal, R., and Taylor, D. J. (1996). Human fetal kidney morphometry during gestation and the relationship between weight, kidney morphometry and plasma active renin concentration at birth. *Clin. Sci.* 91, 169–175. doi: 10.1042/cs0910169

Lackland, D. T., Bendall, H. E., Osmond, C., Egan, B. M., and Barker, D. J. (2000). Low birth weights contribute to high rates of early-onset chronic renal failure in the Southeastern United States. *Arch. Intern. Med.* 160, 1472–1476. doi: 10.1001/archinte.160.10.1472

Langley-Evans, S. C. (2015). Nutrition in early life and the programming of adult disease: a review. *J. Hum. Nutr. Diet.* 28(Suppl. 1), 1–14. doi: 10.1111/jhn.12212

Langley-Evans, S. C., Langley-Evans, A. J., and Marchand, M. C. (2003). Nutritional programming of blood pressure and renal morphology. *Arch. Physiol. Biochem.* 111, 8–16. doi: 10.1076/apab.111.1.8.15136

Langley-Evans, S. C., Welham, S. J., and Jackson, A. A. (1999). Fetal exposure to a maternal low protein diet impairs nephrogenesis and promotes hypertension in the rat. *Life Sci.* 64, 965–974. doi: 10.1016/s0024-3205(99)00022-3

Lepercq, J., Cauzac, M., Lahlou, N., Timsit, J., Girard, J., Auwerx, J., et al. (1998). Overexpression of placental leptin in diabetic pregnancy: a critical role for insulin. *Diabetes* 47, 847–850. doi: 10.2337/diabetes.47.5.847

Little, M. H., Brennan, J., Georgas, K., Davies, J. A., Davidson, D. R., Baldock, R. A., et al. (2007). A high-resolution anatomical ontology of the developing murine genitourinary tract. *Gene Expr. Patterns* 7, 680–699. doi: 10.1016/j.modgep.2007.03.002

Little, M. H., and McMahon, A. P. (2012). Mammalian kidney development: principles, progress, and projections. *Cold Spring Harb. Perspect. Biol.* 4:a008300. doi: 10.1101/cshperspect.a008300

Luyckx, V. A., Tonelli, M., and Stanifer, J. W. (2018). The global burden of kidney disease and the sustainable development goals. *Bull. World Health Organ.* 96, 414–422D. doi: 10.2471/BLT.17.206441

Machado, F. G., Poppi, E. P., Fanelli, C., Malheiros, D. M., Zatz, R., and Fujihara, C. K. (2008). AT1 blockade during lactation as a model of chronic nephropathy: mechanisms of renal injury. *Am. J. Physiol. Ren. Physiol.* 294, F1345–F1353. doi: 10.1152/ajprenal.00020.2008

Madsen, K., Marcussen, N., Pedersen, M., Kjaersgaard, G., Facemire, C., Coffman, T. M., et al. (2010). Angiotensin II promotes development of the renal microcirculation through AT1 receptors. *J. Am. Soc. Nephrol.* 21, 448–459. doi: 10.1681/ASN.2009010045

Magaton, A., Gil, F. Z., Casarini, D. E., Cavanal Mde, F., and Gomes, G. N. (2007). Maternal diabetes mellitus-early consequences for the offspring. *Pediatr. Nephrol.* 22, 37–43. doi: 10.1007/s00467-006-0282-4

Majumder, S., Thieme, K., Batchu, S. N., Alghamdi, T. A., Bowskill, B. B., Kabir, M. G., et al. (2018). Shifts in podocyte histone H3K27me3 regulate mouse and human glomerular disease. *J. Clin. Invest.* 128, 483–499. doi: 10.1172/JCI95946

Mañalich, R., Reyes, L., Herrera, M., Melendi, C., and Fundora, I. (2000). Relationship between weight at birth and the number and size of renal glomeruli in humans: a histomorphometric study. *Kidney Int.* 58, 770–773. doi: 10.1046/j.1523-1755.2000.00225.x

Manning, J., and Vehaskari, V. M. (2005). Postnatal modulation of prenatally programmed hypertension by dietary Na and ACE inhibition. *Am. J. Phys. Regul. Integr. Comp. Phys.* 288, R80–R84. doi: 10.1152/ajpregu.00309.2004

McArdle, Z., Schreuder, M. F., Moritz, K. M., Denton, K. M., and Singh, R. R. (2020). Physiology and pathophysiology of compensatory adaptations of a solitary functioning kidney. *Front. Physiol.* 11:725. doi: 10.3389/fphys.2020.00725

McLaughlin, N., Wang, F., Saifudeen, Z., and El-Dahr, S. S. (2014). In situ histone landscape of nephrogenesis. *Epigenetics* 9, 222–235. doi: 10.4161/epi.26793

McLaughlin, N., Yao, X., Li, Y., Saifudeen, Z., and El-Dahr, S. S. (2013). Histone signature of metanephric mesenchyme cell lines. *Epigenetics* 8, 970–978. doi: 10.4161/epi.25753

McMillen, I. C., and Robinson, J. S. (2005). Developmental origins of the metabolic syndrome: prediction, plasticity, and programming. *Physiol. Rev.* 85, 571–633. doi: 10.1152/physrev.00053.2003

McMullen, S., Gardner, D. S., and Langley-Evans, S. C. (2004). Prenatal programming of angiotensin II type 2 receptor expression in the rat. *Br. J. Nutr.* 91, 133–140. doi: 10.1079/bjn20031029

McMullen, S., and Langley-Evans, S. C. (2005). Maternal low-protein diet in rat pregnancy programs blood pressure through sex-specific mechanisms. *Am. J. Phys. Regul. Integr. Comp. Phys.* 288, R85–R90. doi: 10.1152/ajpregu.00435.2004

Merlet-Bénichou, C., Gilbert, T., Muffat-Joly, M., Lelièvre-Pégorier, M., and Leroy, B. (1994). Intrauterine growth retardation leads to a permanent nephron deficit in the rat. *Pediatr. Nephrol.* 8, 175–180. doi: 10.1007/bf00865473

Mesquita, F. F., Gontijo, J. A., and Boer, P. A. (2010). Maternal undernutrition and the offspring kidney: from fetal to adult life. *Braz. J. Med. Biol. Res.* 43, 1010–1018. doi: 10.1590/s0100-879x2010007500113

Monge, M., García-Nieto, V. M., Domenech, E., Barac-Nieto, M., Muros, M., and Pérez-González, E. (1998). Study of renal metabolic disturbances related to renal lithiasis at school age in very-low-birth-weight children. *Nephron* 79, 269–273. doi: 10.1159/000045048

Moritz, K. M., Cuffe, J. S., Wilson, L. B., Dickinson, H., Wlodek, M. E., Simmons, D. G., et al. (2010). Review: sex specific programming: a critical

role for the renal renin-angiotensin system. *Placenta* 31, S40–S46. doi: 10.1016/j.placenta.2010.01.006

Nicolaou, N., Renkema, K. Y., Bongers, E. M., Giles, R. H., and Knoers, N. V. (2015). Genetic, environmental, and epigenetic factors involved in CAKUT. *Nat. Rev. Nephrol.* 11, 720–731. doi: 10.1038/nrneph.2015.140

Nwagwu, M. O., Cook, A., and Langley-Evans, S. C. (2000). Evidence of progressive deterioration of renal function in rats exposed to a maternal low-protein diet in utero. *Br. J. Nutr.* 83, 79–85.

Petry, C. J., Dorling, M. W., Wang, C. L., Pawlak, D. B., and Ozanne, S. E. (2000). Catecholamine levels and receptor expression in low protein rat offspring. *Diabet. Med.* 17, 848–853. doi: 10.1046/j.1464-5491.2000.00392.x

Pladys, P., Lahaie, I., Cambonie, G., Thibault, G., Lê, N. L., Abran, D., et al. (2004). Role of brain and peripheral angiotensin II in hypertension and altered arterial baroreflex programmed during fetal life in rat. *Pediatr. Res.* 55, 1042–1049. doi: 10.1203/01.Pdr.0000127012.37315.36

Plagemann, A. (2004). 'Fetal programming' and 'functional teratogenesis': on epigenetic mechanisms and prevention of perinatally acquired lasting health risks. *J. Perinat. Med.* 32, 297–305. doi: 10.1515/jpm.2004.055

Rangel, M., dos Santos, J. C., Ortiz, P. H., Hirata, M., Jasiulionis, M. G., Araujo, R. C., et al. (2014). Modification of epigenetic patterns in low birth weight children: importance of hypomethylation of the ACE gene promoter. *PLoS One* 9:e106138. doi: 10.1371/journal.pone.0106138

Rocco, L., Gil, F. Z., da Fonseca Pletiskaitz, T. M., de Fátima Cavanal, M., and Gomes, G. N. (2008). Effect of sodium overload on renal function of offspring from diabetic mothers. *Pediatr. Nephrol.* 23, 2053–2060. doi: 10.1007/s00467-008-0884-0

Rocha, S. O., Gomes, G. N., Forti, A. L., do Carmo Pinho Franco, M., Fortes, Z. B., de Fátima Cavanal, M., et al. (2005). Long-term effects of maternal diabetes on vascular reactivity and renal function in rat male offspring. *Pediatr. Res.* 58, 1274–1279. doi: 10.1203/01.pdr.0000188698.58021.ff

Schreuder, M., Delemarre-van de Waal, H., and van Wijk, A. (2006). Consequences of intrauterine growth restriction for the kidney. *Kidney Blood Press. Res.* 29, 108–125. doi: 10.1159/000094538

Shnorhavorian, M., Bittner, R., Wright, J. L., and Schwartz, S. M. (2011). Maternal risk factors for congenital urinary anomalies: results of a population-based case-control study. *Urology* 78, 1156–1161. doi: 10.1016/j.urology.2011.04.022

Simonetti, G. D., Raio, L., Surbek, D., Nelle, M., Frey, F. J., and Mohaupt, M. G. (2008). Salt sensitivity of children with low birth weight. *Hypertension* 52, 625–630. doi: 10.1161/hypertensionaha.108.114983

Singh, R. R., Cullen-McEwen, L. A., Kett, M. M., Boon, W. M., Dowling, J., Bertram, J. F., et al. (2007). Prenatal corticosterone exposure results in altered AT1/AT2, nephron deficit and hypertension in the rat offspring. *J. Physiol.* 579, 503–513. doi: 10.1113/jphysiol.2006.125773

Song, R., Preston, G., and Yosypiv, I. V. (2011). Angiotensin II stimulates in vitro branching morphogenesis of the isolated ureteric bud. *Mech. Dev.* 128, 359–367. doi: 10.1016/j.mod.2011.07.002

Spencer, J., Wang, Z., and Hoy, W. (2001). Low birth weight and reduced renal volume in aboriginal children. *Am. J. Kidney Dis.* 37, 915–920. doi: 10.1016/s0272-6386(05)80006-x

Steel, J. M., Johnstone, F. D., Hepburn, D. A., and Smith, A. F. (1990). Can prepregnancy care of diabetic women reduce the risk of abnormal babies? *BMJ* 301, 1070–1074. doi: 10.1136/bmj.301.6760.1070

Swanson, A. M., and David, A. L. (2015). Animal models of fetal growth restriction: considerations for translational medicine. *Placenta* 36, 623–630. doi: 10.1016/j.placenta.2015.03.003

Tozour, J. N., Delahaye, F., Suzuki, M., Praiss, A., Zhao, Y., Cai, L., et al. (2018). Intrauterine hyperglycemia is associated with an impaired postnatal response to oxidative damage. *Stem Cells Dev.* 27, 683–691. doi: 10.1089/scd.2017.0232

Tran, S., Chen, Y. W., Chenier, I., Chan, J. S., Quaggin, S., Hébert, M. J., et al. (2008). Maternal diabetes modulates renal morphogenesis in offspring. *J. Am. Soc. Nephrol.* 19, 943–952. doi: 10.1681/ASN.2007080864

Vehaskari, V. M., Stewart, T., Lafont, D., Soyez, C., Seth, D., and Manning, J. (2004). Kidney angiotensin and angiotensin receptor expression in prenatally programmed hypertension. *Am. J. Physiol. Ren. Physiol.* 287, F262–F267. doi: 10.1152/ajprenal.00055.2004

Wanner, N., Vornweg, J., Combes, A., Wilson, S., Plappert, J., Rafflenbeul, G., et al. (2019). DNA methyltransferase 1 controls nephron progenitor cell renewal and differentiation. *J. Am. Soc. Nephrol.* 30, 63–78. doi: 10.1681/ASN.2018070736

Watanabe, I. K. M., Jara, Z. P., Volpini, R. A., Franco, M. D. C., Jung, F. F., and Casarini, D. E. (2018). Up-regulation of renal renin-angiotensin system and inflammatory mechanisms in the prenatal programming by low-protein diet: beneficial effect of the post-weaning losartan treatment. *J. Dev. Orig. Health Dis.* 9, 530–535. doi: 10.1017/s2040174418000296

Woods, L. L. (2000). Fetal origins of adult hypertension: a renal mechanism? *Curr. Opin. Nephrol. Hypertens.* 9, 419–425. doi: 10.1097/00041552-200007000-00014

Woods, L. L., Ingelfinger, J. R., Nyengaard, J. R., and Rasch, R. (2001). Maternal protein restriction suppresses the newborn renin-angiotensin system and programs adult hypertension in rats. *Pediatr. Res.* 49, 460–467. doi: 10.1203/00006450-200104000-00005

Woods, L. L., and Weeks, D. A. (2005). Prenatal programming of adult blood pressure: role of maternal corticosteroids. *Am. J. Phys. Regul. Integr. Comp. Phys.* 289, R955–R962. doi: 10.1152/ajpregu.00455.2004

Yan, J., Li, X., Su, R., Zhang, K., and Yang, H. (2014). Long-term effects of maternal diabetes on blood pressure and renal function in rat male offspring. *PLoS One* 9:e88269. doi: 10.1371/journal.pone.0088269

Yosypiv, I. V., Boh, M. K., Spera, M. A., and El-Dahr, S. S. (2008). Downregulation of spry-1, an inhibitor of GDNF/ret, causes angiotensin II-induced ureteric bud branching. *Kidney Int.* 74, 1287–1293. doi: 10.1038/ki.2008.378

Zandi-Nejad, K., Luyckx, V. A., and Brenner, B. M. (2006). Adult hypertension and kidney disease: the role of fetal programming. *Hypertension* 47, 502–508. doi: 10.1161/01.HYP.0000198544.09909.1a

Conflict of Interest: The authors declare that the research was conducted in the absence of any commercial or financial relationships that could be construed as a potential conflict of interest.

frontiers in Physiology

BRIEF RESEARCH REPORT
published: 15 December 2020
doi: 10.3389/fphys.2020.601237

Renal Sensory Activity Regulates the γ-Aminobutyric Acidergic Inputs to the Paraventricular Nucleus of the Hypothalamus in Goldblatt Hypertension

*Maycon I. O. Milanez†, Amanda C. Veiga†, Beatriz S. Martins, Roberto B. Pontes, Cassia T. Bergamaschi, Ruy R. Campos and Erika E. Nishi**

Department of Physiology, Cardiovascular Division, Escola Paulista de Medicina, Universidade Federal de São Paulo, São Paulo, Brazil

OPEN ACCESS

Edited by:
H Della Coletta Francescato, University of São Paulo, Brazil

Reviewed by:
Aline M. A. De Souza, Georgetown University, United States
Oscar Lorenzo, Universidad Autónoma Madrid, Spain

***Correspondence:**
Erika E. Nishi
enishi@unifesp.br

†These authors have contributed equally to this work

Specialty section:
This article was submitted to Renal and Epithelial Physiology, a section of the journal Frontiers in Physiology

Received: *31 August 2020*
Accepted: *27 November 2020*
Published: *15 December 2020*

Citation:
Milanez MIO, Veiga AC, Martins BS, Pontes RB, Bergamaschi CT, Campos RR and Nishi EE (2020) Renal Sensory Activity Regulates the γ-Aminobutyric Acidergic Inputs to the Paraventricular Nucleus of the Hypothalamus in Goldblatt Hypertension. Front. Physiol. 11:601237. doi: 10.3389/fphys.2020.601237

Renal sensory activity is centrally integrated within brain nuclei involved in the control of cardiovascular function, suggesting that renal afferents regulate basal and reflex sympathetic vasomotor activity. Evidence has shown that renal deafferentation (DAx) evokes a hypotensive and sympathoinhibitory effect in experimental models of cardiovascular diseases; however, the underlying mechanisms involved in this phenomenon need to be clarified, especially those related to central aspects. We aimed to investigate the role of renal afferents in the control of γ-aminobutyric acid (GABA)ergic inputs to the paraventricular nucleus (PVN) of the hypothalamus in renovascular hypertensive (2K1C) rats and their influence in the regulation of cardiovascular function. Hypertension was induced by clipping the left renal artery. After 4 weeks, renal DAx was performed by exposing the left renal nerve to a 33 mM capsaicin solution for 15 min. After 2 weeks of DAx, microinjection of muscimol into the PVN was performed in order to evaluate the influence of GABAergic activity in the PVN and its contribution to the control of renal sympathetic nerve activity (rSNA) and blood pressure (BP). Muscimol microinjected into the PVN triggered a higher drop in BP and rSNA in the 2K1C rats and renal DAx mitigated these responses. These results suggest that renal afferents are involved in the GABAergic changes found in the PVN of 2K1C rats. Although the functional significance of this phenomenon needs to be clarified, it is reasonable to speculate that GABAergic alterations occur to mitigate microglia activation-induced sympathoexcitation in the PVN of 2K1C rats.

Keywords: renal denervation, neuroinflammation, γ-aminobutyric acid, renovascular hypertension, afferent innervation

INTRODUCTION

Elevated sympathetic vasomotor activity is implicated in cardiovascular diseases, either experimentally or clinically (Grassi, 2010; Campos et al., 2015). Studies indicate that approaches aimed at reducing sympathetic vasomotor tone are beneficial in these conditions (Nishi et al., 2019; Lopes et al., 2020; Veiga et al., 2020); therefore, the underlying mechanisms by which such

benefits occur have been extensively studied in recent years, especially how the central nervous system (CNS) drives sympathetic vasomotor overactivation in pathophysiological conditions (Oliveira-Sales et al., 2009; Nishi et al., 2019).

It is well-described that phenotypic changes in brain nuclei involved in cardiovascular control contribute to the maintenance of high sympathetic outflow in cardiovascular diseases, such as hypertension or heart failure (Oliveira-Sales et al., 2009; Carillo et al., 2012; Milanez et al., 2020). In this context, hypotensive and sympathoinhibitory effects triggered by the pharmacological blockade of glutamatergic and angiotensinergic pathways in the CNS have been shown in cardiovascular diseases (Bergamaschi et al., 1995; de Oliveira-Sales et al., 2010; Ramchandra et al., 2012; Milanez et al., 2018). In addition, changes in γ-aminobutyric acid (GABA)ergic pathways involved in the control of sympathetic vasomotor activity have also been reported in the Goldblatt model of hypertension, two-kidney, one-clip (2K1C), and chronic kidney disease, suggesting that neurotransmission of an inhibitory nature is also altered in the condition of cardiovascular disease (Biancardi et al., 2010; Nishihara et al., 2017; Milanez et al., 2020). Although it is not fully known what leads sympathetic activation in cardiovascular diseases, recent studies highlight the role of sensory signaling in these alterations, especially the renal sensory system (Nishihara et al., 2017; Zheng et al., 2018).

Currently, it is possible to study the selective role of sensory renal afferents and evaluate the effects evoked by their removal in the course of the disease (Foss et al., 2015). For example, we recently showed that the selective renal nerve deafferentation (DAx) causes a decrease in blood pressure (BP) and renal sympathetic nerve activity (rSNA) in the Goldblatt 2K1C rats and 5/6 nephrectomy model of chronic renal failure, indicating that the renal sensory afferents are centrally integrated and trigger changes in central nuclei involved in the control of cardiovascular function (Lopes et al., 2020; Veiga et al., 2020). In fact, evidences indicate that brain nuclei involved in the cardiovascular control, such as the rostral ventrolateral medulla (RVLM) and the paraventricular nucleus (PVN) of the hypothalamus, receive projections of sensory renal afferents (Nishi et al., 2017; Zheng and Patel, 2017).

In order to clarify the repercussions of renal denervation on neurotransmission in the PVN in mice with chronic renal failure, Nishihara et al. (2017) showed that the removal of total renal nerve, that is both sympathetic and sensory fibers, increased GABAergic activity in the PVN accompanied by a robust hypotensive effect. It is rational to speculate that the improvement in the GABAergic neurotransmission in the PVN was caused, in part, by the absence of renal sensory afferents; however, the underlying mechanisms need to be better explored. A previous study by our group showed that total renal denervation decreased oxidative stress within the RVLM and PVN independently of BP reduction in 2K1C rats (Nishi et al., 2019). However, these studies did not distinguish the specific role of sympathetic or sensory fibers from the kidneys mediating changes in CNS pathways.

Setiadi et al. (2020) showed that inflammation plays a role in maintaining hypertension in the Goldblatt model, as the treatment with pentoxifylline, a tumor necrosis factor-α (TNF-α) synthesis inhibitor, evoked a drop in BP and rSNA, as well as a reduction in neuronal activity in the PVN of 2K1C rats. In addition, evidence suggests that the central GABAergic system can attenuate the release of pro-inflammatory agents from microglia cells, playing an important anti-inflammatory role in the CNS (Lee et al., 2011). Therefore, it is reasonable to speculate that changes in the GABAergic inputs to the PVN triggered by the renovascular hypertension may contribute to inflammation-induced sympathoexcitation in the 2K1C rats.

Thus, considering that we previously reported a robust renal sympathoinhibitory effect caused by DAx in the 2K1C rats (Lopes et al., 2020), we hypothesized in the present study that this phenomenon may be triggered by alterations in the GABAergic inputs into the PVN of 2K1C DAx rats. In addition, in order to analyze the effects of DAx in terms of sympathetic vasomotor activity reflex control, we evaluated the cardiac baroreflex sensitivity in the presence and absence of renal sensory activity in 2K1C rats.

MATERIALS AND METHODS

Animals and Experimental Protocol

All experimental procedures used in this study were conducted according to the guidelines recommended by the National Institutes of Health and were approved by the Ethics in Research Committee of the Escola Paulista de Medicina – Universidade Federal de São Paulo – (3629190314). Male Wistar rats were used at 5 weeks of age (150–180 g) for the induction of renovascular hypertension. In addition, male Wistar rats at 9 weeks of age (300–350 g) were used as the control group. The animals were housed in groups of 3–4 in standard polypropylene cages in a room maintained at 22 ± 1°C, humidity 60% and with a 12:12 h light-dark cycle (lights on at 7 am) and were allowed free access to food and water.

Thirty Wistar rats were distributed into three independent experimental groups: a control group underwent sham surgery for DAx (n = 10), a 2K1C group underwent sham surgery for DAx (n = 10), and a 2K1C group underwent DAx (2K1C DAx; n = 10). To induce renovascular hypertension, a silver clip (gap width 0.2 mm) was implanted around the left renal artery of rats anesthetized with an i.p. injection of ketamine and xylazine (100 and 10 mg/kg, respectively; Vetbrands, Jacareí, SP, Brazil). Age-matched rats were used as controls, which did not undergo clip implantation. After 4 weeks of renal artery clipping, unilateral DAx was performed by exposing the left or ischemic kidney nerve to 33 mM capsaicin (diluted in 0.1% ethanol and 0.1% Tween 80) for 15 min. In the sham groups, rats underwent the same surgical procedure described above, but with vehicle application (0.1% ethanol and 0.1% Tween 80) around the renal artery (Foss et al., 2015). As previously shown in another study by our group, the confirmation of DAx was verified by the reduction in calcitonin gene-related peptide (CGRP) expression by immunohistochemical analysis in the renal pelvis after 2 weeks

of the procedure (Lopes et al., 2020) when all data were collected. Two independent sets of experiments were performed: one set for BP and rSNA responses triggered by muscimol, an agonist of GABA-A receptors, microinjected into PVN and another set for analysis of cardiac baroreflex sensitivity in conscious rats and microglia activation analysis in the PVN.

Direct Measurement of Blood Pressure and Heart Rate and Baroreflex Sensitivity Evaluation in Conscious Rats

After 2 weeks of sham surgery or DAx, control (n = 5), 2K1C (n = 5) and 2K1C DAx (n = 5) rats were respectively anesthetized with ketamine and xylazine (100 and 10 mg/kg i.p., respectively), the femoral artery was catheterized for direct recording of arterial BP, and the femoral vein was catheterized for drug infusions. After surgical recovery (~24 h), pulsatile arterial pressure (PAP) was recorded in conscious rats using a BP signal amplifier (PowerLab System, ADInstruments, Sydney, Australia). The average values of baseline mean arterial pressure (MAP, mmHg), systolic arterial pressure (SAP, mmHg), diastolic arterial pressure (DAP, mmHg), and heart rate (HR, bpm) were obtained from the direct recording of pulsatile BP by 15-min continuous recording. MAP and HR changes to the various stimuli were expressed as the change (Δ) from the baseline value obtained immediately before each test (i.e., a basal record of 10 min).

Reflex bradycardia and tachycardia responses induced by bolus infusion of phenylephrine (3, 5, and 10 μg/rat, i.v.) and sodium nitroprusside (5, 12 e 20 μg/rat, i.v.; Sigma Aldrich Co, St. Louis, MO, United States) were measured, as previously reported (Lincevicius et al., 2017). Cardiac baroreflex sensitivity was evaluated by the mean index relating changes in HR to the changes in MAP and expressed as beats per mmHg (bpm/mmHg, baroreflex function sensitivity).

Evaluation of Microglia Activation by Iba1-Positive Cells Analysis in the PVN by Immunohistochemistry

After deep anesthesia with ketamine and xylazine, control (n = 5), 2K1C (n = 5), and 2K1C DAx (n = 5) rats were perfused transcardially with 400 ml of 0.1 M buffered saline (pH 7.4), followed by 400 ml of 4% (w/v) paraformaldehyde (PFA). Brains were removed and post-fixed in 4% PFA for 4 h followed by cryoprotection in 20% (w/v) sucrose at 4°C until the brains sunk. Then, serial coronal slices at 30 μm were performed according to a brain atlas (1.8–2.10 mm from the bregma; Paxinos and Watson, 2007) in a cryostat. Immunodetection was performed by the free-floating method, and the sections were incubated with anti-Iba1 antibody (1:200, Abcam) overnight at room temperature. Subsequently, the sections were incubated in biotinylated secondary antibody (Jackson ImmunoResearch Laboratories, West Grove, PA, 1:500 dilution in 1% normal horse serum) for 24 h at room temperature. The sections were then incubated in ExtrAvidin-HRP (1:1,500, Sigma-Aldrich) for at least 4 h at room temperature. Subsequently, Iba1-positive cells were visualized using imidazole-intensified diaminobenzidine (DAB) reaction in which peroxide was generated by glucose oxidase. Then, the sections were mounted onto glass microscope slides with 0.5% gelatin and allowed to air-dry. Once dry, the slides were dehydrated in ethanol (70, 90, and 2 × 100%), cleared in xylol and cover-slipped in DPX mountant (Sigma-Aldrich). Tissue sections were inspected using an Eclipse 80i microscope (Nikon Instruments, Melville, NY) and a Nikon digital sight DSRi1 camera with NIS-Elements software. Images were uniformly adjusted for brightness and contrast and photographed under ideal magnification (20× objective) for high resolution photos. Blinded and stereological method for analysis was performed in at least three sections containing the PVN in every fourth section (each section 120 μm apart) that were averaged for each sample. Immunohistochemical control was performed in a set of sections for each group in which either the primary or secondary antibody was omitted. We verified no non-specific staining (data not shown).

Analysis of the Renal Sympathetic Nerve Activity and Microinjection of Muscimol Into the PVN in Urethane-Anesthetized Rats

After recording the cardiovascular parameters in conscious rats, the animals were slowly anesthetized with urethane (1.2 g/kg, i.v.; Sigma-Aldrich Co., St. Louis, MO, United States) to avoid any change in baseline cardiovascular conditions. Tracheotomy was performed to reduce airway resistance. The nerve of the left or ischemic kidney was exposed retroperitoneally for the implantation of bipolar silver electrode, and activity was amplified (20 K) and filtered (100–1,000 Hz; NeuroLog, Digitimer, Welwyn Garden City, Herts, United Kingdom). The raw nerve signal was passed through a spike discriminator using Spike Histogram software (PowerLab, ADInstruments) to remove background noise, and the total nerve activity was expressed in spikes per second (spikes/s), as commonly used by previous studies that compared multifiber nerve recording among different groups (Wei and Felder, 2002; Oliveira-Sales et al., 2009; Veiga et al., 2020). The number of spikes/bursts reflects cardiovascular barosensitive fibers, as previously shown (Malpas and Ninomiya, 1992). The spikes/s changes to the various stimuli were expressed as the change (Δ) from the baseline value obtained immediately before each test (i.e., a basal record of 10 min).

Urethane-anesthetized rats were placed in a stereotaxic apparatus (David Kopf Instruments, Tujunga, CA) for the microinjection procedure. The bregma was exposed, and a craniotomy of approximately 3 × 3 mm was performed dorsally to the bregma with a drill. The PVN was located 1.8 mm caudal to bregma, 0.5 mm lateral to the midline, and 7.8 mm from dorsal surface (bite bar = 3.6 mm). Bilateral microinjections of muscimol (10 mM in 100 nl) into PVN were performed with the use of glass micropipettes with tip diameters of 10–20 μm connected to a nitrogen pressure injector (Channel pressure injector – MicroData

Instruments Inc., United States), as previously reported (Oliveira-Sales et al., 2009; Carillo et al., 2012). At the end of the experiments, the background noise of rSNA was determined by hexamethonium bromide administration (30 mg/kg, i.v.) to select postganglionic sympathetic ongoing nerve activity, and the efficacies of the microinjections were confirmed by administering Evans Blue 2% (100 nl) into the PVN (**Figure 1C**). As previously reported, microinjection of 100 nl is capable of covering approximately 0.3–0.7 mm (spherical pattern of distribution) when applied to hypothalamic tissue (Segura et al., 1992).

Statistical Analysis

Values are presented as the mean ± SEM. Data were analyzed by one-way ANOVA or repeated measures ANOVA followed by Tukey's *post hoc* test was applied to compare data among control, 2K1C e 2K1C DAx groups. A value of $p < 0.05$ was considered statistically significant.

RESULTS

Basal values of SAP, DAP, MAP, and HR in the control, 2K1C and 2K1C DAx groups are exhibited in **Table 1**.

Cardiovascular and Renal Sympathetic Vasomotor Responses Evoked by Muscimol Injection Into the PVN

Muscimol microinjected into the PVN triggered a more intense MAP variation (Δ) in the 2K1C rats (CTL vs. 2K1C: −8 ± 2 vs. −46 ± 9* ΔmmHg, $p < 0.05$; **Figure 1A**). In addition, the magnitude of rSNA reduction was higher in 2K1C rats (CTL vs. 2K1C: −8 ± 1 vs. −36 ± 4* Δspikes/s, $p < 0.05$). DAx attenuated the MAP, and the renal sympathoinhibitory responses evoked by muscimol microinjected into the PVN when compared to 2K1C (2K1C vs. 2K1C DAx: −36 ± 4 vs. −19 ± 2* Δspikes/s, $p < 0.05$; **Figure 1B**). The representative diagram related to these responses is exhibited in **Figure 1D**.

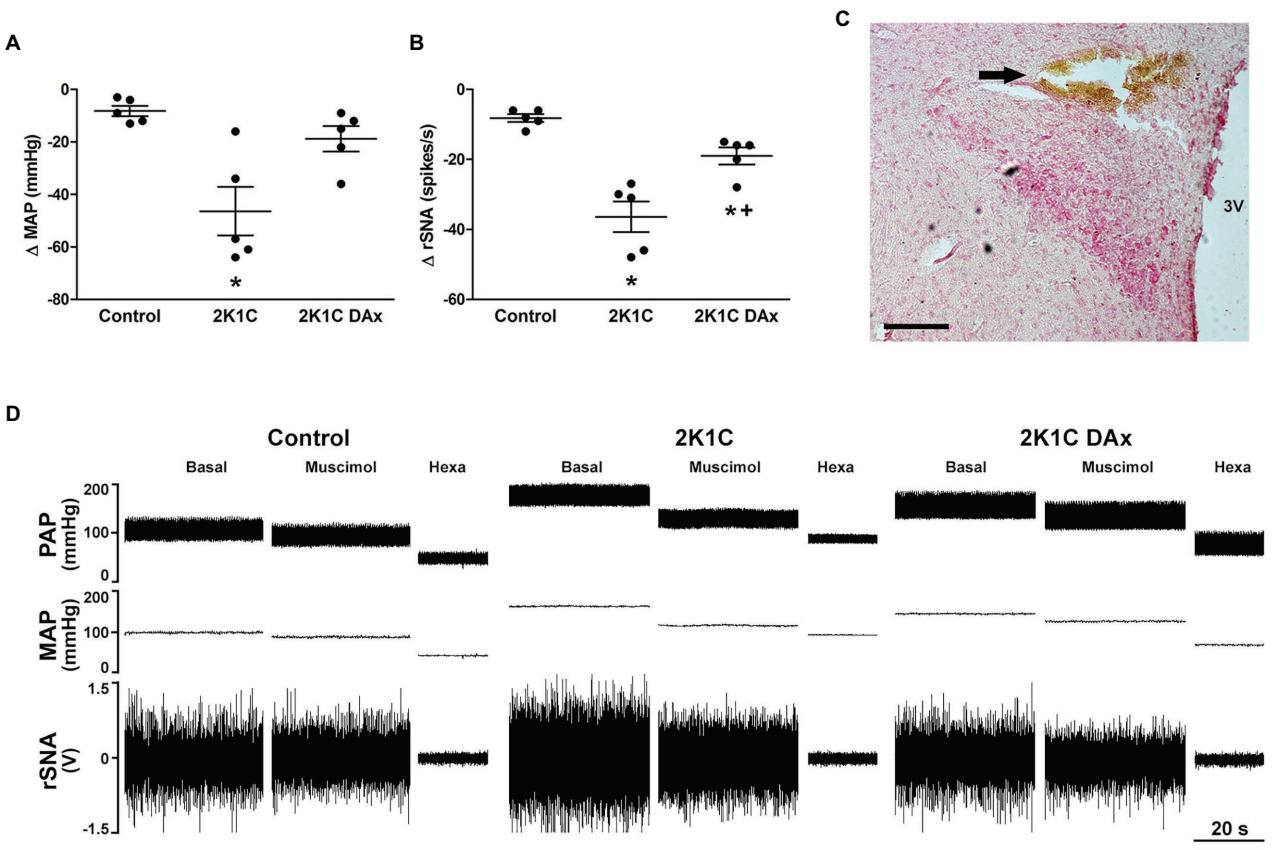

FIGURE 1 | Maximum variation triggered by the microinjection of muscimol into paraventricular nucleus (PVN) of the hypothalamus in terms of **(A)** mean arterial pressure (MAP) and **(B)** renal sympathetic nerve activity (rSNA) in the control, hypertensive (2K1C) and renal deafferented hypertensive (2K1C DAx) rats. *$p < 0.05$ in relation to the control group; +$p < 0.05$ in relation to the 2K1C group (one-way ANOVA followed by Tukey's *post hoc* test). **(C)** Representative histological image: the arrow indicates the site of microinjection into the PVN. Scale bar = 100 μm. 3 V, third ventricle. **(D)** Diagram representing the effect of muscimol microinjected into the PVN in terms of pulsatile arterial pressure (PAP), MAP, and rSNA in the control, hypertensive (2K1C) and renal deafferented hypertensive (2K1C DAx) rats. Microinjection of muscimol into the PVN triggered a higher drop in MAP and rSNA in 2K1C rats and the renal deafferentation blunted these findings. Hexa, hexamethonium.

TABLE 1 | Basal values of systolic arterial pressure (SAP), diastolic arterial pressure (DAP), MAP, and HR in the control, 2K1C and 2K1C DAx obtained from conscious rats.

	Control (n = 5)	2K1C (n = 5)	2K1C DAx (n = 5)
SAP (mmHg)	129 ± 4	228 ± 10*	198 ± 6*+
DAP (mmHg)	91 ± 2	160 ± 8*	133 ± 3*+
MAP (mmHg)	104 ± 2	183 ± 8*	154 ± 4*+
HR (bpm)	379 ± 12	412 ± 9	378 ± 9

*$p < 0.05$ in relation to the control group.
+$p < 0.05$ in relation to the 2K1C group (one-way ANOVA followed by Tukey's post hoc test).

Effects of Selective Renal Nerve Deafferentation on Cardiac Baroreflex Sensitivity

Figure 2 shows the effects of DAx on cardiac baroreflex sensitivity in 2K1C rats. We found that the induction of renovascular hypertension caused an impairment in this parameter and that selective renal deafferentation normalized the cardiac baroreflex response, both for tachycardia and bradycardia responses.

Effects of Selective Renal Nerve Deafferentation on Iba1-Positive Cells in the PVN of 2K1C Rats

Immunohistochemistry analysis revealed that the induction of renovascular hypertension caused an increase in Iba1-positive cells in the PVN (control vs. 2K1C: 4.7 ± 0.4 vs. 7 ± 0.4*, $p < 0.05$). However, DAx normalized this parameter in 2K1C rats (2K1C vs. 2K1C DAx: 7 ± 0.4 vs. 4.7 ± 0.5*, $p < 0.05$; **Figure 3**).

DISCUSSION

The main findings of this study demonstrate that changes in renal sensory activity in 2K1C rats evoke an increase in the GABAergic inputs into the PVN and contribute to impaired cardiac baroreflex sensitivity. In addition, renal afferent activity may be involved in the induction of inflammatory state in the PVN of 2K1C rats.

Although it has been shown that RVLM is an important site integrating renal afferent signaling (Nishi et al., 2017), glutamatergic neurons in the PVN that project into RVLM are activated by stimulation of renal afferents (Xu et al., 2015). We found that stimulation of GABAergic neurons with muscimol microinjected into the PVN of 2K1C rats produced a greater drop in BP and rSNA, suggesting that GABAergic inputs to the PVN may be increased in renovascular hypertension. In fact, increased GABAergic terminal density within the PVN in Goldblatt rats was reported (Biancardi et al., 2010). Similarly, bicuculline, a GABAergic antagonist, intrathecally administered triggered a greater increase in BP and rSNA in renovascular hypertensive rats, indicating that the spinal GABAergic system involved in the control of sympathetic vasomotor activity is also altered in the model (Milanez et al., 2020). In addition, previous studies carried out on renal-wrapped hypertensive rats – another experimental model of renovascular hypertension – reported that, despite a reduction in GABAergic inputs to the PVN in the onset of hypertension, there is a higher GABAergic activity in the PVN in the chronic phase of hypertension (Martin and Haywood, 1998; Haywood et al., 2001). These findings suggest that a higher inhibitory input to CNS regions involved in the control of cardiovascular function act protectively, mitigating an exacerbation of sympathetic vasomotor over activity in the 2K1C model. In fact, both GABAergic and glutamatergic innervation densities are augmented in the PVN of renovascular hypertensive rats (Biancardi et al., 2010). Thus, an imbalance between excitatory and inhibitory inputs to sympathetic premotor neurons leads to increased sympathetic drive in renovascular hypertension.

It is noteworthy that GABA regulates the activity of microglia cells through activation of its Type A receptors; Lee et al. (2011) showed that the release of TNF-α and interleukin-6 induced by lipopolysaccharide from microglia cells is blunted by muscimol, suggesting an anti-inflammatory action of the central GABAergic system. Thus, we cannot rule out the hypothesis that an increase in GABAergic inputs to the PVN occurs in order to mitigate the local inflammatory state and reduce the sympathoexcitation in renovascular hypertension (Wu et al., 2012). This speculation can be strengthened by the fact that the cardiovascular responses evoked by the muscimol microinjected into the PVN were normalized in the 2K1C DAx rats, as well as the Iba-1 percentage area in the PVN.

Nishihara et al. (2017) found a reduction in the sympathoexcitatory effects triggered by the microinjection of bicuculline into the PVN in mice with chronic renal failure, indicating that GABAergic inputs to PVN is reduced in this condition. Interestingly, the authors showed that total renal denervation was able to normalize the sympathetic responses evoked by GABAergic antagonism in the PVN in the chronic renal failure (Nishihara et al., 2017). Such evidence, together with the findings of the present study, brings to light an important aspect regarding the central changes involved in the genesis/maintenance of high sympathetic vasomotor activity, that is, although the sympathoexcitation is a characteristic commonly found in cardiorenal diseases, the neural mechanisms that culminate in this anomaly can be distinct.

In previous studies, we showed that DAx of the ischemic kidney reduced BP partially and decreased sympathetic hyperactivity to both the ischemic and contralateral kidneys (Lopes et al., 2020) and that the total renal denervation improved cardiac and renal, but not lumbar, baroreflex sensitivity in 2K1C rats (Lincevicius et al., 2017). Interestingly, in the present study, we show that renal DAx improves the reflex control of HR by arterial baroreceptors in the 2K1C model, potentially due to the modulatory influence of renal sensory fibers that project to regions involved in the control of baroreflex function, such as the nucleus tractus solitarii, PVN, and RVLM, differently influencing the control of sympathetic vasomotor outflow (Solano-Flores et al., 1997; Xu et al., 2015; Nishi et al., 2017). Moreover, this study suggests that the GABAergic inputs to

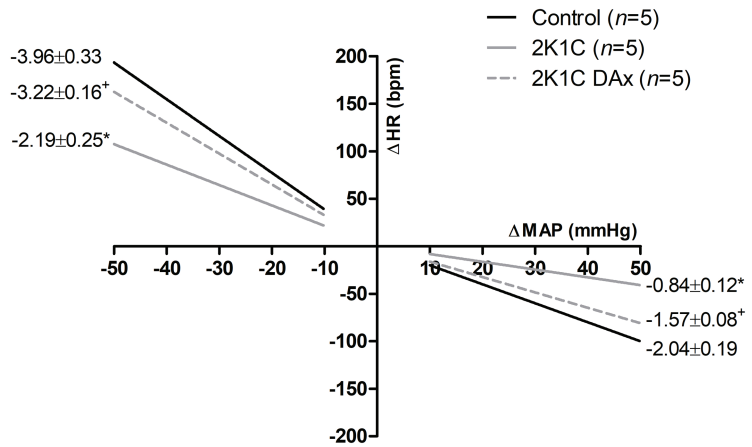

FIGURE 2 | Heart rate (HR) reflex responses induced by unloading or loading of arterial baroreceptors in the control, 2K1C, and 2K1C DAx rats. $^{*}p < 0.05$ in relation to the control group; $^{+}p < 0.05$ in relation to the 2K1C group (repeated measures ANOVA followed by Tukey's *post hoc* test).

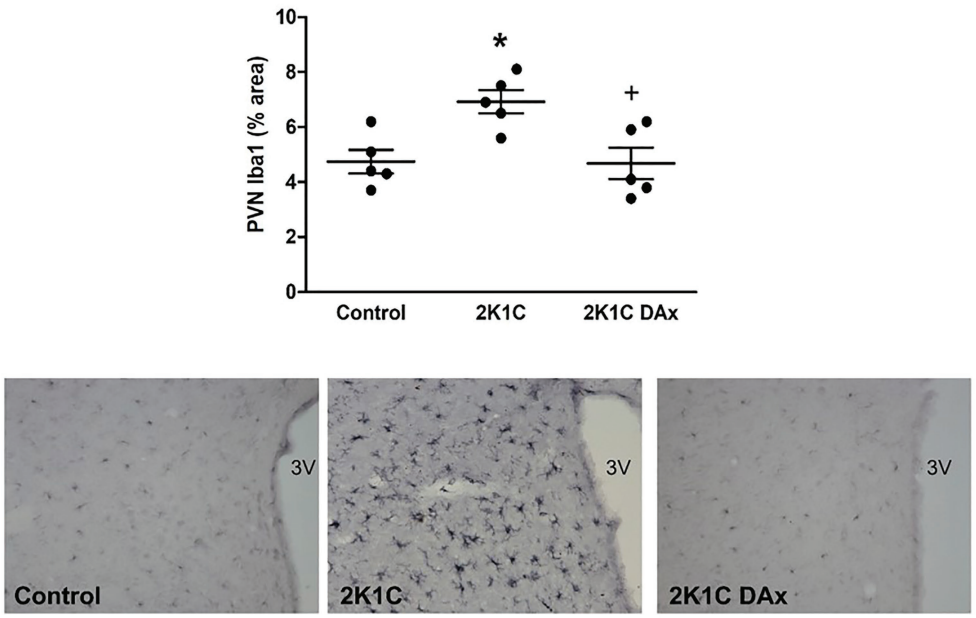

FIGURE 3 | Analysis of ionized calcium binding adaptor molecule 1 (Iba1)-positive cells in the PVN of the hypothalamus in the control, 2K1C, and 2K1C DAx rats **(upper panel)**. $^{*}p < 0.05$ in relation to the control group; $^{+}p < 0.05$ in relation to the 2K1C group (one-way ANOVA followed by Tukey's *post hoc* test). Representative histological section of Iba1 analysis among groups **(lower panel)**. Scale bar = 100 μm. 3 V: third ventricle.

the PVN may exert a tonic inhibitory action on the local neurons involved in controlling the baroreflex function in the 2K1C model, contributing to an impairment in its sensitivity. However, we cannot rule out the possibility that the improvement in the baroreflex control of cardiac function may have occurred by improving the brain oxidative system and/or mitigating the inflammatory process caused by the removal of renal sensory activity (Oliveira-Sales et al., 2009; Fonkoue et al., 2019). In addition to GABA, functional changes in other neurotransmitters/neuromodulators contributing to the impairment in the baroreflex sensitivity have been described in the 2K1C rats; for example, a higher spinal angiotensinergic and glutamatergic activity in the Goldblatt model blunt the reflex control of rSNA by arterial baroreceptors (Milanez et al., 2018). Although not yet fully clarified, the role of baroreflex in the long-term control of BP cannot be ruled out (Thrasher, 2006). Therefore, it is reasonable to assume that part of the hypotensive effect triggered by renal DAx in 2K1C rats was evoked by the improvement in baroreflex control of cardiac function (Tsyrlin et al., 2013). Another possible mechanism by which DAx triggers BP reduction

is attenuating intrarenal angiotensinergic activity in the 2K1C model (Lopes et al., 2020).

Several studies have shown that oxidative imbalance and inflammation in the brain contribute to sympathoexcitation in neurogenic hypertension, especially in medullary and hypothalamic sites. Previous studies showed that oxidative stress induced by angiotensin II-NADPH oxidase pathway in the RVLM and PVN plays a critical role in the development of hypertension in the 2K1C model (Oliveira-Sales et al., 2009; de Oliveira-Sales et al., 2010), and total renal denervation was capable of reversing it (Nishi et al., 2019). In the present study, we show greater activation of microglia in the PVN that was reversed by renal DAx in the 2K1C rats. A previous study related the development of neurogenic hypertension induced by systemic inflammation with increased microglial activity and the generation of reactive oxygen species in the RVLM, given by the increase in the subunits of NADPH oxidase and superoxide anion that contributed to the maintenance of higher BP (Wu et al., 2012). Moreover, angiotensin II-induced microglial activation and hypertension in the PVN were reversed by intracerebroventricular infusion of minocycline, an anti-inflammatory antibiotic, and another study showed that total renal denervation decreased microglial activation and reactive oxygen species in the cortex, white matter, and PVN of stroke prone spontaneously hypertensive rats (SHRSP; Shi et al., 2010; Nakagawa et al., 2013). In accordance with these studies, we show that afferent signaling from the ischemic kidney may contribute to neuroinflammation-induced sympathetic vasomotor overactivity in the PVN of 2K1C rats. However, the underlying mechanisms by which renal DAx attenuated glial activity in the PVN of 2K1C rats need to be further explored, as well as whether this phenomenon is related to the autonomic and cardiovascular effects found in this study.

In the present study, we assessed the inflammatory state of PVN indirectly through the analysis of Iba-1. Although it is a marker widely used for this purpose, it is necessary to evaluate, locally, and systemically, the inflammatory profile through the quantification of pro-inflammatory agents, such as TNF-α and other cytokines. Moreover, BP measurement was performed during the daylight, at the end of the dark cycle. Thus, circadian rhythms and food intake may influence to some degree of the basal level of BP. Although all animals underwent the same experimental protocol, it would be necessary to measure cardiovascular parameters by telemetry over the whole period to detect the influences of light and dark cycles during the course of 2K1C hypertension.

Taken together, these results suggest that renal afferent activity is involved in the changes of the neuronal inputs to the PVN of 2K1C rats, especially those inputs related to inhibitory activity. Although the functional significance of this finding still needs to be clarified, it is likely that the increase in GABAergic inputs to PVN occurs in order to mitigate a higher sympathoexcitation in renovascular hypertension. Moreover, we found that the impairment in baroreflex control of HR in 2K1C rats is mediated, in part, by alterations in the renal sensory system.

DATA AVAILABILITY STATEMENT

The raw data supporting the conclusions of this article will be made available by the authors, without undue reservation.

ETHICS STATEMENT

The animal study was reviewed and approved by Ethics in Research Committee of the Escola Paulista de Medicina – Universidade Federal de São Paulo – (3629190314).

AUTHOR CONTRIBUTIONS

EN, CB, and RC: conception or design of the work. MM, AV, BM, and RP: acquisition, analysis, and interpretation of data for the work. MM and AV: drafting the work. All authors revised the manuscript critically for important intellectual content, approved the final version of the manuscript, agreed to be accountable for all aspects of the work in ensuring that questions related to the accuracy or integrity of any part of the work are appropriately investigated and resolved. All persons designated as authors qualify for authorship. All those who qualify for authorship are listed.

FUNDING

This study was financed in part by the Coordenação de Aperfeiçoamento de Pessoal de Nível Superior – Brasil (CAPES) – Finance Code 001, by the São Paulo Research Foundation (FAPESP 18/02671-3) and by the Brazilian National Research Council (CNPq 406233/2018-7, 0817/2018). AV (17/03905-5, 18/11909-3, 20/02617-9, MIOM (18/01898-4) and BM (15/23809-5) were recipients of FAPESP scholarships. RC and CB are recipients of the CNPq productive research fellowship.

REFERENCES

Bergamaschi, C., Campos, R. R., Schor, N., and Lopes, O. U. (1995). Role of the rostral ventrolateral medulla in maintenance of blood pressure in rats with Goldblatt hypertension. *Hypertension* 26, 1117–1120. doi: 10.1161/01.HYP.26.6.1117

Biancardi, V. C., Campos, R. R., and Stern, J. E. (2010). Altered balance of gamma-aminobutyricacidergic and glutamatergic afferent inputs in rostral ventrolateral medulla-projecting neurons in the paraventricular nucleus of the hypothalamus of renovascular hypertensive rats. *J. Comp. Neurol.* 518, 567–585. doi: 10.1002/cne.22256

Campos, R. R., Oliveira-Sales, E. B., Nishi, E. E., Paton, J. F., and Bergamaschi, C. T. (2015). Mechanisms of renal sympathetic activation in renovascular hypertension. *Exp. Physiol.* 100, 496–501. doi: 10.1113/expphysiol.2014.079855

Carillo, B. A., Oliveira-Sales, E. B., Andersen, M., Tufik, S., Hipolide, D., Santos, A. A., et al. (2012). Changes in GABAergic inputs in the paraventricular

nucleus maintain sympathetic vasomotor tone in chronic heart failure. *Auton. Neurosci.* 171, 41–48. doi: 10.1016/j.autneu.2012.10.005

de Oliveira-Sales, E. B., Nishi, E. E., Boim, M. A., Dolnikoff, M. S., Bergamaschi, C. T., and Campos, R. R. (2010). Upregulation of AT1R and iNOS in the rostral ventrolateral medulla (RVLM) is essential for the sympathetic hyperactivity and hypertension in the 2K-1C wistar rat model. *Am. J. Hypertens.* 23, 708–715. doi: 10.1038/ajh.2010.64

Fonkoue, I. T., Le, N. A., Kankam, M. L., DaCosta, D., Jones, T. N., Marvar, P. J., et al. (2019). Sympathoexcitation and impaired arterial baroreflex sensitivity are linked to vascular inflammation in individuals with elevated resting blood pressure. *Phys. Rep.* 7:e14057. doi: 10.14814/phy2.14057

Foss, J. D., Wainford, R. D., Engeland, W. C., Fink, G. D., and Osborn, J. W. (2015). A novel method of selective ablation of afferent renal nerves by periaxonal application of capsaicin. *Am. J. Phys. Regul. Integr. Comp. Phys.* 308, R112–R122. doi: 10.1152/ajpregu.00427.2014

Grassi, G. (2010). Sympathetic neural activity in hypertension and related diseases. *Am. J. Hypertens.* 23, 1052–1060. doi: 10.1038/ajh.2010.154

Haywood, J. R., Mifflin, S. W., Craig, T., Calderon, A., Hensler, J. G., and Hinojosa-Laborde, C. (2001). Gamma-aminobutyric acid (GABA)--a function and binding in the paraventricular nucleus of the hypothalamus in chronic renal-wrap hypertension. *Hypertension* 37, 614–618. doi: 10.1161/01.hyp.37.2.614

Lee, M., Schwab, C., and McGeer, P. L. (2011). Astrocytes are GABAergic cells that modulate microglial activity. *Glia* 59, 152–165. doi: 10.1002/glia.21087

Lincevicius, G. S., Shimoura, C. G., Nishi, E. E., Oliveira, T., Cespedes, J. G., Bergamaschi, C. T., et al. (2017). Differential effects of renal denervation on arterial baroreceptor function in Goldblatt hypertension model. *Auton. Neurosci.* 208, 43–50. doi: 10.1016/j.autneu.2017.06.002

Lopes, N. R., Milanez, M. I. O., Martins, B. S., Veiga, A. C., Ferreira, G. R., Gomes, G. N., et al. (2020). Afferent innervation of the ischemic kidney contributes to renal dysfunction in renovascular hypertensive rats. *Pflugers Arch.* 472, 325–334. doi: 10.1007/s00424-019-02346-4

Malpas, S. C., and Ninomiya, I. (1992). The amplitude and periodicity of synchronized renal sympathetic nerve discharges in anesthetized cats: differential effect of baroreceptor activity. *J. Auton. Nerv. Syst.* 40, 189–198. doi: 10.1016/0165-1838(92)90200-z

Martin, D. S., and Haywood, J. R. (1998). Reduced GABA inhibition of sympathetic function in renal-wrapped hypertensive rats. *Am. J. Physiol.* 275, R1523–R1529. doi: 10.1152/ajpregu.1998.275.5.R1523

Milanez, M. I. O., Nishi, E. E., Rocha, A. A., Bergamaschi, C. T., and Campos, R. R. (2020). Interaction between angiotensin II and GABA in the spinal cord regulates sympathetic vasomotor activity in Goldblatt hypertension. *Neurosci. Lett.* 728:134976. doi: 10.1016/j.neulet.2020.134976

Milanez, M. I. O., Nishi, É., Sato, A. Y. S., Neto, H. A. F., Bergamaschi, C. T., and Campos, R. R. (2018). Control of renal sympathetic nerve activity by neurotransmitters in the spinal cord in Goldblatt hypertension. *Brain Res.* 1698, 43–53. doi: 10.1016/j.brainres.2018.06.025

Nakagawa, T., Hasegawa, Y., Uekawa, K., Ma, M., Katayama, T., Sueta, D., et al. (2013). Renal denervation prevents stroke and brain injury via attenuation of oxidative stress in hypertensive rats. *J. Am. Heart Assoc.* 2:e000375. doi: 10.1161/JAHA.113.000375

Nishi, E. E., Lopes, N. R., Gomes, G. N., Perry, J. C., Sato, A. Y. S., Naffah-Mazzacoratti, M. G., et al. (2019). Renal denervation reduces sympathetic overactivation, brain oxidative stress, and renal injury in rats with renovascular hypertension independent of its effects on reducing blood pressure. *Hypertens. Res.* 42, 628–640. doi: 10.1038/s41440-018-0171-9

Nishi, E. E., Martins, B. S., Milanez, M. I., Lopes, N. R., de Melo, J. F., Pontes, R. B., et al. (2017). Stimulation of renal afferent fibers leads to activation of catecholaminergic and non-catecholaminergic neurons in the medulla oblongata. *Auton. Neurosci.* 204, 48–56. doi: 10.1016/j.autneu.2017.01.003

Nishihara, M., Takesue, K., and Hirooka, Y. (2017). Renal denervation enhances GABAergic input into the PVN leading to blood pressure lowering in chronic kidney disease. *Auton. Neurosci.* 204, 88–97. doi: 10.1016/j.autneu.2016.09.018

Oliveira-Sales, E. B., Nishi, E. E., Carillo, B. A., Boim, M. A., Dolnikoff, M. S., Bergamaschi, C. T., et al. (2009). Oxidative stress in the sympathetic premotor neurons contributes to sympathetic activation in renovascular hypertension. *Am. J. Hypertens.* 22, 484–492. doi: 10.1038/ajh.2009.17

Paxinos, G., and Watson, C. (2007). *The rat brain in stereotaxic coordinates. 6th Edn.* London: Elsevier Academic Press.

Ramchandra, R., Hood, S. G., Watson, A. M., Allen, A. M., and May, C. N. (2012). Central angiotensin type 1 receptor blockade decreases cardiac but not renal sympathetic nerve activity in heart failure. *Hypertension* 59, 634–641. doi: 10.1161/HYPERTENSIONAHA.111.181131

Segura, T., Martin, D. S., Sheridan, P. J., and Haywood, J. R. (1992). Measurement of the distribution of [3H]bicuculline microinjected into the rat hypothalamus. *J. Neurosci. Methods* 41, 175–186. doi: 10.1016/0165-0270(92)90059-M

Setiadi, A., Korim, W. S., May, C. N., and Yao, S. T. (2020). Systemic administration of pentoxifylline attenuates the development of hypertension in renovascular hypertensive rats. *Hypertens. Res.* 43, 667–678. doi: 10.1038/s41440-020-0412-6

Shi, P., Diez-Freire, C., Jun, J. Y., Qi, Y., Katovich, M. J., Li, Q., et al. (2010). Brain microglial cytokines in neurogenic hypertension. *Hypertension* 56, 297–303. doi: 10.1161/HYPERTENSIONAHA.110.150409

Solano-Flores, L. P., Rosas-Arellano, M. P., and Ciriello, J. (1997). Fos induction in central structures after afferent renal nerve stimulation. *Brain Res.* 753, 102–119. doi: 10.1016/S0006-8993(96)01497-7

Thrasher, T. N. (2006). Arterial baroreceptor input contributes to long-term control of blood pressure. *Curr. Hypertens. Rep.* 8, 249–254. doi: 10.1007/s11906-006-0058-z

Tsyrlin, V. A., Galagudza, M. M., Kuzmenko, N. V., Pliss, M. G., Rubanova, N. S., and Shcherbin, Y. I. (2013). Arterial baroreceptor reflex counteracts long-term blood pressure increase in the rat model of renovascular hypertension. *PLoS One* 8:e64788. doi: 10.1371/journal.pone.0064788

Veiga, A. C., Milanez, M. I. O., Ferreira, G. R., Lopes, N. R., Santos, C. P., De Angelis, K., et al. (2020). Selective afferent renal denervation mitigates renal and splanchnic sympathetic nerve overactivity and renal function in chronic kidney disease-induced hypertension. *J. Hypertens.* 38, 765–773. doi: 10.1097/HJH.0000000000002304

Wei, S. G., and Felder, R. B. (2002). Forebrain renin-angiotensin system has a tonic excitatory influence on renal sympathetic nerve activity. *Am. J. Physiol. Heart Circ. Physiol.* 282, H890–H895. doi: 10.1152/ajpheart.2002.282.3.H890

Wu, K. L., Chan, S. H., and Chan, J. Y. (2012). Neuroinflammation and oxidative stress in rostral ventrolateral medulla contribute to neurogenic hypertension induced by systemic inflammation. *J. Neuroinflammation* 9:212. doi: 10.1186/1742-2094-9-212

Xu, B., Zheng, H., Liu, X., and Patel, K. P. (2015). Activation of afferent renal nerves modulates RVLM-projecting PVN neurons. *Am. J. Physiol. Heart Circ. Physiol.* 308, H1103–H1111. doi: 10.1152/ajpheart.00862.2014

Zheng, H., Katsurada, K., Liu, X., Knuepfer, M. M., and Patel, K. P. (2018). Specific afferent renal denervation prevents reduction in neuronal nitric oxide synthase within the paraventricular nucleus in rats with chronic heart failure. *Hypertension* 72, 667–675. doi: 10.1161/HYPERTENSIONAHA.118.11071

Zheng, H., and Patel, K. P. (2017). Integration of renal sensory afferents at the level of the paraventricular nucleus dictating sympathetic outflow. *Auton. Neurosci.* 204, 57–64. doi: 10.1016/j.autneu.2016.08.008

Conflict of Interest: The authors declare that the research was conducted in the absence of any commercial or financial relationships that could be construed as a potential conflict of interest.

frontiers in Physiology

ORIGINAL RESEARCH
published: 22 April 2021
doi: 10.3389/fphys.2021.658431

Gestational and Breastfeeding Low-Protein Intake on Blood Pressure, Kidney Structure, and Renal Function in Male Rat Offspring in Adulthood

*Gabriela Leme Lamana, Ana Leticia Luchiari Ferrari, José Antonio Rocha Gontijo and Patrícia Aline Boer**

Fetal Programming and Hydroelectrolyte Metabolism Laboratory, Nucleus of Medicine and Experimental Surgery, Department of Internal Medicine, Faculty of Medical Sciences at State University of Campinas, Campinas, Brazil

Background: Our previous studies demonstrated that maternal protein-restricted (low-protein, LP) 16-week-old offspring had pronounced nephron number reduction and arterial hypertension associated with an unchanged glomerular filtration rate (GFR). An enhanced gomerular area may be related to increased glomerular filtration and overflow, which accounts for glomerular filtration barrier breakdown and early glomerulosclerosis. The effect of protein restriction during gestational and breastfeeding periods is unknown.

Method: The functional e-structural kidney evaluation was obtained using lithium and creatinine clearance, kidney morphometry, immunoblotting, and immunostaining analysis in 16 and 24-week-old LP offspring compared to age-matched NP progeny.

Results: Low protein rats' progeny had significantly reduced birth weight, without previous catch-up growth phenomena, in parallel with a decreased adiposity index. Transforming growth factor-beta 1 (TGF-β1) glomerular expression was significantly enhanced in the LP group. Also, the LP offspring had a 38% lower nephron number and an increased glomerular volume. They also presented with a higher cardiac index and arterial blood pressure compared with age-matched NP offspring. The LP rats exhibited augmented Na+/K+-ATPase in the proximal segments, and NOS1 immunoreactivity in whole renal tissue was associated with sodium retention in the proximal nephron segments. We also found significantly enhanced collagen content associated with increased TGFβ1 and ZEB1/2 renal immunoreactivity in LP offspring compared with NP offspring. Increased hypertrophy markers in LP podocytes were associated with an amplified IL-6/STAT3 pathway activity.

Conclusion: To our knowledge, these are the first data demonstrating renal functional and structural changes in protein restriction during gestation and lactation model of fetal programming. The fetal-programmed adult offspring showed pronounced structural glomerular disorders with an accentuated and advanced fibrosis stage, without a change in the GFR. These findings suggest that the glomerular enhanced TGF-β1 action may

OPEN ACCESS

Edited by:
Guiomar Nascimento Gomes, Federal University of São Paulo, Brazil

Reviewed by:
Analia Tomat, University of Buenos Aires, Argentina
Adalberto Vieyra, Federal University of Rio de Janeiro, Brazil

***Correspondence:**
Patrícia Aline Boer
alineboer@yahoo.com.br

Specialty section:
This article was submitted to Renal and Epithelial Physiology, a section of the journal Frontiers in Physiology

Received: *25 January 2021*
Accepted: *23 March 2021*
Published: *22 April 2021*

Citation:
Lamana GL, Ferrari ALL, Gontijo JAR and Boer PA (2021) Gestational and Breastfeeding Low-Protein Intake on Blood Pressure, Kidney Structure, and Renal Function in Male Rat Offspring in Adulthood. Front. Physiol. 12:658431. doi: 10.3389/fphys.2021.658431

induce ZEB1/2 expression that may cause glomeruli epithelial-to-mesenchymal transition. Besides, decreased nephron number in the LP offspring with preserved glomerular function may be related to protective or even attenuate the activated IL-6/STAT3 pathway.

Keywords: fetal programming, low-protein diet, lactation, epithelial-mesenchymal transition, tubular kidney dysfunction, arterial hypertension

INTRODUCTION

Fetal programming by gestational low-protein intake results in reduced birth weight, 28% fewer nephrons, reduced renal salt excretion, and increased risk of cardiovascular and renal disorders in adults (Schreuder et al., 2006; Mesquita et al., 2010a,b; Sene et al., 2013, 2018; Vaccari et al., 2015). Despite the unchanged glomerular filtration rate (GFR), these results were associated with a 17% increment in the glomerular tuft area. Previous studies revealed that protein and caloric intake restriction in rats results in embryonic/fetal growth retardation (IUGR), accompanied by impaired nephron development (Mesquita et al., 2010a,b). The tubular dysfunction associated with enhanced sodium and water reabsorption might, at least in part, be responsible for the programming of adult arterial hypertension. Recent studies on programmed progeny by maternal protein restriction also show that enhanced sympathetic neural activity may involve increased tubular salt and water transport disorders (Vaccari et al., 2015; Custódio et al., 2017). Kidney disorders in maternal protein-restricted offspring may partly be secondary to reduced nephron numbers associated with glomeruli overflow, basal membrane breakdown, and early glomerulosclerosis (Sene et al., 2013, 2018). The lack of nutrients may result in pivotal pathway signaling changes during several stages of fetal development, which, in turn, may cause irreversible organ and system disorders in adulthood (Barker, 1995, 2003; Langley-Evans, 2006, 2009). In rats, nephron development involves a tight control of gene expression, protein synthesis, tissue remodeling, and different compensative challenges to maintain homeostasis from birth to adult life. After delivery, the programmed rats' day-to-day adaptations to maintain body salt and water homeostasis may involve changes in signaling molecular cell pathways' expression. As such, the present study aimed to determine how severe protein restriction during pregnancy and breastfeeding alters kidney function and structure in 16- and 24-week-old male offspring. We studied the blood pressure and tubular sodium handling, evaluated by lithium clearance, in conscious maternal protein-undernourished rats compared with their appropriate healthy maternal food intake controls.

Thus, environmental and genetic interactions interfere with ontogenic cell proliferation and differentiation, leading to structural and dysfunctional organ development effects in distinct organs. The epithelium-mesenchymal transition (EMT) is a critical adaptive phenomenon characterized by the interchangeable cell plasticity process between the epithelial and mesenchymal phenotypic states (Liu, 2004; Kalluri and Weinberg, 2009). These phenotypic changes are accompanied by a reduction in the genetic expression of transcription factors epithelial markers associated with the high expression of mesenchymal markers, such as desmin and nestin (Kalluri and Weinberg, 2009). The evolution of chronic kidney damage is accompanied by irreversible renal parenchymal fibrosis. In this pathophysiological process of renal fibrosis, there is a fundamental involvement of EMT as the typical final route that leads to chronic kidney disease (CKD; Liu, 2010). The transforming growth factor-beta (TGF-β) triggers tubular EMT, and its expression is regulated positively in several types of CKDs (Chung et al., 2010). In isolated glomeruli, we found that adult male children of mothers fed a protein-restricted diet during pregnancy showed reduced miR-200f expression associated with increased expression of TGF-β1 and ZEB2 for glomerular EMT and expression of glomerular fibrosis markers (Sene et al., 2013). Besides, studies have shown that IL-6 plays a crucial role in regulating various physiological and pathological processes. IL-6 is stimulated by the JAK/STAT3 signal transduction cascade, which leads to nuclear phospho-STAT3 translocation, which is implicated in cell growth, proliferation, differentiation, and survival (Postigo and Dean, 2000). Despite several changes observed in the maternal adult LP offspring's renal structure and function, the renal functional and structural patterns in the progeny restricted to proteins during pregnancy and breastfeeding remain unknown. The current study evaluates whether maternal protein intake restriction during whole pregnancy and breastfeeding alters kidney functional and morphological response beyond 16-week of life in male rats. Therefore, we also verified the renal expression of protein markers of fibrosis and inflammation during the severe restriction of protein maternal and breastfeeding ingestion periods in adult offspring compared with appropriate controls.

MATERIALS AND METHODS

Experimental Animals

The experiments were conducted on age-matched Wistar Hannover rats (0.250–0.300 kg), which were allowed free access to water and standard rat chow. The Institutional Ethics Committee on the Use of Animals (CEUA/UNICAMP) approved the experimental protocol according to the general guidelines established by the Brazilian College of Animal Experimentation (COBEA), and the NIH Guide for the Care and Use of Laboratory Animals was followed throughout the study (protocol number #4242-1). Our local colonies originated from a breeding stock supplied by CEMIB/Unicamp, Campinas, SP, Brazil. Immediately after weaning at 3 weeks of age, the animals were maintained under controlled temperatures (25°C) and lighting conditions (7:00–19:00), with free access to tap water

and standard rodent laboratory chow (Nuvital, Curitiba, PR, Brazil) and followed up to 12 weeks of age. The animals were mated using the permanent polygamous system; the day that sperm were seen in the vaginal smear was designated as day 1 of pregnancy. The dams were singly caged and randomly assigned into two groups: daily food supply of regular protein diet (NP, 17% protein) or low-protein diet (LP, 6% protein) chow ad libitum throughout pregnancy and lactation. The NP and LP maternal food consumption were determined daily and later normalized for body weight, also recorded daily in both groups. The NP and LP maternal food consumption were determined daily (subsequently normalized for body weight), and the bodyweight of dams was recorded weekly in both groups. The dams' body weight and food consumption were determined daily and weekly (subsequently normalized for body weight). Male pups from the NP and LP litters were weighed at birth. Post-weaning was followed and maintained with normoprotein standard rodent laboratory chow weekly until the 24th week of life. The NP and LP offspring were euthanized and sampled at 16 and 24 weeks of age. For sampling, a cohort of pups was euthanized at 16- and 24-week-old with a mixture of ketamine (75 mg kg^{-1} body weight, i.p.) and xylazine (10 mg kg^{-1} body weight, i.p.), and the level of anesthesia was controlled by corneal reflex monitoring. The animals (n = 60) were then perfused *via* transcardiac perfusion with saline containing heparin (5%) for 15 min under constant pressure, followed by 0.1 M phosphate-buffered saline (PBS, pH 7.4) containing 4% (w/v) paraformaldehyde and 0.1 M sucrose for 25 min. After perfusion, the kidneys were removed, weighed, and representative samples were fixed in 4% phosphate-buffered formalin for 24 h for paraffin embedding. The retroperitoneal and perigonadal adipose tissues were collected from the 24-week-old NP, and LP offspring (n = 49) after 5% isoflurane inhalation anesthesia was administered. The adiposity index was calculated as the ratio of total adipose tissue weight to body weight. The kidneys were excised, weighed, and tissue samples were collected for histology, immunohistochemistry, and immunoblotting tests.

Blood Pressure Measurement

The systolic blood pressure (SBP) of the NP offspring (n = 18–20) and LP (n = 12–20) was measured from 8 to 24 weeks in conscious rats using an indirect tail-cuff method. Blood pressure was assessed using an electrosphygmomanometer (BP-2000 Blood Pressure Analysis System, Visitech Systems, Austin, TX, United States) combined with a pneumatic pulse transducer/amplifier. This indirect approach allowed repeated measurements with a close correlation (correlation coefficient = 0.975) compared with direct intra-arterial recording. The mean of 10 consecutive SBP readings represented the measured blood pressure. Measurements were performed under controlled temperature and luminosity at the same time during the day. The double product (DP) was calculated as the heart rate product (HR) × SBP, and the units for HR and blood pressure were beats per minute and mmHg, respectively.

Renal Function Test

Renal function was tested on the last day at 24 weeks of age in awake and unrestrained NP (n = 15) and LP (n = 11) male offspring. Renal clearance of creatinine (CCr) and lithium (CLi) was calculated using the standard formula (C = UV/P) based on urinary and plasma creatinine and lithium levels. CCr was used to estimate GFR, and CLi+ was used to assess proximal tubule output. Fractional urinary sodium excretion (FENa+) and fractional potassium excretion (FEK+) were calculated as CNa+/CCr and CK+/CCr, respectively. Fractional proximal sodium excretion (FEPNa +) and fractional post-proximal sodium excretion (FEPPNa +) were calculated as CLi+/CCr × 100 and CNa+/CLi+ × 100, respectively (Mesquita et al., 2010a; Vaccari et al., 2015; Custódio et al., 2017). Plasma and urinary sodium, potassium, and lithium concentrations were measured using flame photometry (B262; Micronal, São Paulo, Brazil). Creatinine was determined spectrophotometrically (362; Micronal, São Paulo, Brazil) using the alkaline picrate method. The results are reported as mean ± SD per 100 g body weight.

Morphometric Analysis and Stereological Estimation of Kidney Volume, Glomerular Number, and Glomerular Volume

Renal stereology estimates the glomerular volume, and the total number of renal corpuscles per kidney was performed in 12-day old offspring using the combination of dissector/fractionator technique as described by Mandarim-de-Lacerda (2003; Erratum in 2007). Total offspring body and kidney masses were determined for both the NP (n = 5) and LP (n = 5) offspring obtained from different litters. We used the fractionator method to estimate the number of glomeruli. Briefly, NP and LP offspring were anesthetized (ketamine, 75 mg kg^{-1} body weight, and xylazine 10 mg kg^{-1} body weight, i.p.). The left kidney was removed, weighed, and the Cavalieri principle estimated the volume. Each group's kidney was sliced longitudinally in two halves; this preliminary procedure, using one-half kidney, was used as a pilot to determine the average diameter of glomeruli in the subsequent studies. The material was fixed, included in paraplast, the entire kidney was exhaustively sliced into serial sections of 5 μm, and ordered sequentially. The 4-mm-slices were processed and stained with hematoxylin-eosin, analyzed in an Olympus® microscope, photographed, and posteriorly submitted to study by the Image-Pro Express 6.0® software. The glomerular diameter was evaluated by taking kidney sections passing through the macula densa, and the average of glomeruli diameters was obtained for each experimental group. The necessary spacing kidney section was established, considering the prior glomeruli diameter study. In another kidney half portion, the isotropic samples from NP and LP groups were obtained through two consecutive cuts, where the first cut was made at a random angle. Then, the cut kidney surface was sectioned again at a random angle. In this way, we could admit that the obtained fragment presented tissue in an isotropic form. The material was then processed and sliced according to the spacing previously determined in

the pilot diameter study for its respective group (NP: 23 cuts dispensed/LP: 28 cuts issued). The histological renal slices were stained with hematoxylin-eosin, and glomeruli were counted. The total number of glomeruli was calculated as: N (gl) = N (count) × fractionation, where fractionation = kidney weight (g) /slice weight (g).

The cortex's volume was determined. The material was photographed in 100x magnification using a grid system of central points of squares; a count was made, taking into account how many points pass through the renal cortex. The cortex's volume was then obtained, calculated as the sum of these points, multiplied by the cut's thickness (5 μm) So, Vcortex = $\sum$A × spacing × 5 μm.

The total volume of glomeruli [V(gl)] was then determined using the same software. A dot mask was inserted in glomeruli photos, and the number of points that touched the glomeruli was counted. Thus, VV(gl) = Pp/Pt where, Pp = points counted and Pt = total points, such as V (gl) = VV(gl) × Vcortex.

Additionally, the total glomerular volume [V(gl)] was calculated using the average glomerular volume times glomeruli number by the followed equation: V (average gl) = V (gl) × N (gl), where N is the number of glomeruli.

Immunohistochemistry Study: Tissue Processing, Histology, and Immunohistochemical Procedures

Twenty-four-week-old NP (n = 5) and LP (n = 5) male offspring were anesthetized with 5% isoflurane inhalation. The level of anesthesia was controlled by corneal reflex monitoring. The animals were then perfused with saline containing heparin (5%) for 15 min under constant pressure, followed by 0.1 M phosphate buffer (pH 7.4) containing 4% (w/v) paraformaldehyde and 0.1 M sucrose for 25 min. After perfusion, the kidneys were removed, weighed, and representative samples were fixed in 4% phosphate-buffered formalin for 24 h for paraffin embedding. The paraffin blocks were cut into 5 μm-thick sections. For immunohistochemical analysis, paraffin sections were incubated overnight at 4°C with primary antibodies for anti-Na/K-ATPase (Santa Cruz Biotechnology, Inc., CA, United States, 1:100 dilution), anti-TGF-β1 (Santa Cruz Biotech, Inc., CA, United States, 1:250 dilution), anti-desmin (Santa Cruz Biotech, Inc., CA, United States, 1: 200 dilution), anti-nestin (Santa Cruz Biotech, Inc., CA, United States, 1: 600 dilution), anti-collagen I (Sigma-Aldrich Co., St. Louis, MO, United States, 1:400 dilution), and anti-ZEB1 (Santa Cruz Biotech, Inc., CA, United States, 1:400 dilution). Secondary antibodies were used following the primary antibody host. Proteins were immunohistochemically detected using the avidin-biotin-peroxidase method. Briefly, 5 μm-thick deparaffinized kidney sections on poly-L-lysine-coated slides were treated with 3% H2O2 in PBS for 15 min, nonfat milk for 60 min, primary antibodies for 60 min, and avidin-biotin-peroxidase solution (Vector Laboratories Inc., CA, United States, 1:50 dilution). The kidney sections were finally stained with 3,3'-diaminobenzidine tetrahydrochloride substrate (Sigma-Aldrich Co., St. Louis, MO, United States) to demonstrate the sites of peroxidase binding. The slides were counterstained with Harris' hematoxylin.

Five cortical and medullar fields of each histological section were analyzed, and the average immunoreactivity reading was determined. Images were captured with a photomicroscope and analyzed using Leica Qwin 3.1 for Windows. No immunoreactivity was observed in the control experiments in which one of the primary antibodies was omitted.

Immunoblotting

Twenty-four-week-old NP (n = 5) and LP (n = 5) male offspring were anesthetized with 5% isoflurane inhalation. Anesthesia was controlled by monitoring the corneal reflex, and the animal's abdominal cavity was opened for kidney removal. The tissue was minced coarsely and homogenized immediately in 10 volumes of solubilization buffer [10 ml/L Triton-X 100, 100 mM Tris(hydroxymethyl)amino-methane (Tris) pH 7.4, 10 mM sodium pyrophosphate, 100 mM sodium fluoride, 10 mM ethylenediaminetetraacetic acid, 10 mM sodium vanadate, 2 mM phenylmethylsulfonyl fluoride, and 0.1 mg/ml of aprotinin] at 4°C, using a polytron PTA 20S generator (model PT 10/35, Brinkmann Instruments, Westbury, NY, United States) operated at maximum speed for 20 s. The tissue extracts were centrifuged at 11,000 rpm at 4°C for 40 min, and the supernatants were used as samples. Protein quantitation was performed using the Bradford method. The tissue extract samples (250 μg of protein) were subjected to sodium dodecyl sulfate-polyacrylamide gel (SDS-PAGE) electrophoresis. After electrophoretic separation, proteins were transferred to nitrocellulose membranes and blotted with a specific antibody. The samples were treated with Laemmli buffer containing 100 mM dithiothreitol, heated in a boiling water bath for 4 min, and subjected to 8% SDS-PAGE in a Bio-Rad mini gel apparatus (Mini-Protean, Bio-Rad). The protein was transferred from the gel to the nitrocellulose membranes for 90 min at 120 V (constant) using a Bio-Rad miniature transfer apparatus (Mini-Protean). Nonspecific protein binding to the nitrocellulose was reduced by pre-incubation at 22°C for 2 h in a blocking buffer (5% nonfat dry milk, 10 mM Tris, 150 mM NaCl, and 0.02% Tween 20). Nitrocellulose blots were incubated at 4°C overnight with primary antibodies diluted in a blocking buffer (3% nonfat dry milk, 10 mM Tris, 150 mM NaCl, and 0.02% Tween 20) as follows: AT1R (Santa Cruz Biotech, Inc., CA, United States, 1:1000 dilution), AT2R (Santa Cruz Biotech, Inc., CA, United States, 1:1000), JAK2 (Santa Cruz Biotech, Inc., CA, United States, 1:1000 dilution), STAT3 (Santa Cruz Biotech, Inc., CA, United States, 1:1000 dilution) NOS1 (Santa Cruz Biotech, Inc., CA, United States, 1:1000 dilution), NOS2 (Santa Cruz Biotech, Inc., CA, United States, 1:1000 dilution), SOD2 (Santa Cruz Biotech, Inc., CA, United States, 1:1000 dilution), IL-6 (Santa Cruz Biotech, Inc., CA, United States, 1:1000 dilution), pJAK2 (Cell Signaling Technology, Inc., MA, United States, 1:1000 dilution), pSTAT3 (Cell Signaling Technology, Inc., MA, United States, 1:1000 dilution), ERK1/ERK2 (Cell Signaling Technology, Inc., MA, United States, 1:1000 dilution), and β-actin (Cell Signaling Technology, Inc., MA, United States, 1:1000 dilution). Membranes were stained with Coomassie Brilliant

Blue dye before blotting to ensure equal protein loading. All membranes were incubated with β-actin antibodies to avoid possible inconsistencies in protein loading and transfer. Only homogeneously stained membranes were used in this study. Immunoreactive bands were detected using the chemiluminescence method (SuperSignal West Pico Chemiluminescent Substrate, Thermo Scientific, United States). Images of the developed radiographs were scanned (HP DeskJet Ink Advantage 4625), and the band intensities were quantified using optical densitometry (Scion Image Corporation).

Data Presentation and Statistical Analysis

All data are reported as mean ± SD. Data obtained over time were analyzed using one-way ANOVA. *Post hoc* comparisons between means were performed using Bonferroni's contrast test when one-way ANOVA analysis indicated statistical differences between groups. Comparisons between the two groups throughout the weeks were performed using two-way ANOVA for repeated measurements. The first factor was the protein content in the pregnant dam's diet, and the second factor was time. When an interaction was significant, the mean values were compared using Tukey's posthoc analysis. Student's t-test evaluated studies involving only two independent samples, within or between groups. The Brown-Forsythe and Welch's tests and ANOVA tests were used to correct situations characterized by heteroscedasticity (different variances between groups). GraphPad Prism was used for data analysis (GraphPad 8.0 Software, Inc., La Jolla, CA, United States). The level of significance was set at $p \leq 0.05$.

RESULTS

Body Mass, Adiposity Index, and Kidney Morphometry

Gestational and breastfeeding protein restriction intake did not significantly change the body mass of pregnant dams (NP: 278.5 ± 6.239 g, $n = 24$; LP: 266.5 ± 3.794 g, $n = 39$). Besides, it did not affect the number of offspring (NP: 9.7 ± 3, $n = 178$; LP: 8.6 ± 4, $n = 246$; $p = 0.28$) and the proportion of male and female offspring ($p = 0.3245$) per litter. The birth weight of LP male pups (body mass relative to that of the entire litter; $n = 117$) was significantly reduced compared with that of NP pups ($n = 84$; NP: 6.854 ± 0.5928 g vs. LP: 6.491 ± 0.6820 g; $p = 0.0001$; **Figure 1**). The body mass of 24-week-old LP offspring (471.9 ± 34.91 g, $n = 18$) remained lower than that of age-matched NP progeny (531.3 ± 48.49 g, $n = 27$, $p = 0.0001$). It was associated with a reduced adiposity index in the LP offspring (3.242 ± 0.8214) relative to the NP group (4.962 ± 1.413; $p = 0.0015$; **Figure 1**). Additionally, at 16 weeks after birth, both the left and right kidney masses of LP offspring (1.098 ± 0.1201 g, $n = 5$) were significantly reduced compared with that of age-matched NP offspring (1.302 ± 0.1021 g, $n = 5$, $p = 0.0100$; **Figure 2**).

The present study evaluated the glomerular number in 16-week-old LP offspring kidney compared to age-matched controls by stereological analyses. In gestational and breastfeeding protein-restricted animals, a significant reduction in the number of glomeruli was observed in the LP progeny [about 36%; LP ($n = 5$): 9850 ± 2587; NP ($n = 5$): 15.940 ± 1926; $p = 0.0015$, **Figure 2**]. Simultaneously, an increase in glomerular volume accompanied by a reduced nephron number in the LP group compared with the control group [LP ($n = 5$): 263.270 ± 67.108; NP ($n = 5$): 162.600 ± 49.017; $p = 0.0134$, **Figure 2**] was observed with no change in renal cortex volume ($p = 0.4352$). As shown in **Figure 3**, the SBP increased progressively, being significant from the 17th to 24th weeks of age (17th week of age, LP: 157.4 ± 8.2 mmHg vs. NP: 146.1 ± 8.6 mmHg, $p < 0.02$; 24th week of age, LP: 164.4 ± 13.4 mmHg vs. NP: 139 ± 7.0 mmHg, $p = 0.001$). A higher calculated DP accompanied the increment in blood pressure in LP ($p = 0.001$) than in NP progeny (**Figure 3**).

Renal Function Data

The data for renal function performed on the last day at 24 weeks of age in male offspring of both the NP and LP

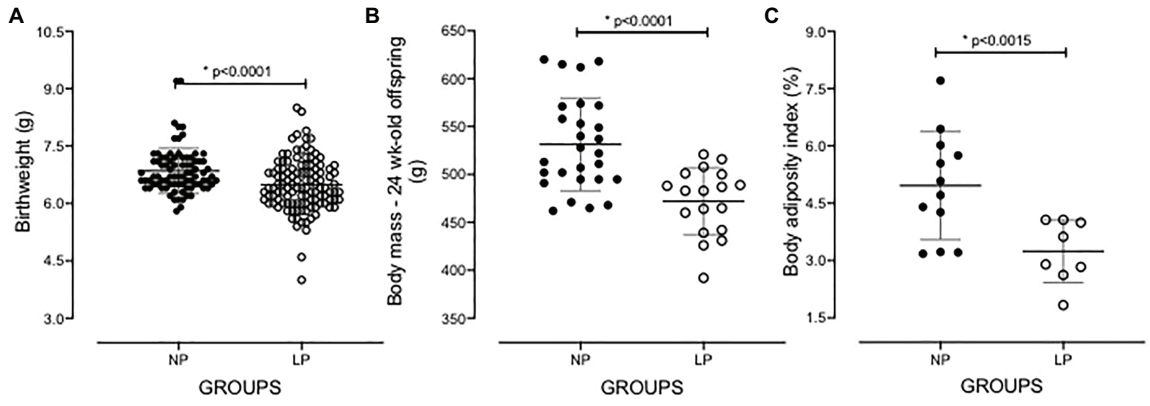

FIGURE 1 | The low-protein (LP) and NP birthweight (**A**; LP: $n = 117$; NP: $n = 84$), and body weight (**B**; LP: $n = 18$; NP: $n = 27$) and body adiposity index (**C**; LP: 18; NP: $n = 27$), in grams, of 24-week-old protein-restricted (LP) progeny compared with age-matched standard (NP) progeny. Data are presented as scatter dot plots; Welch's *t*-test was used for data analysis. The level of significance was set at $p < 0.05$.

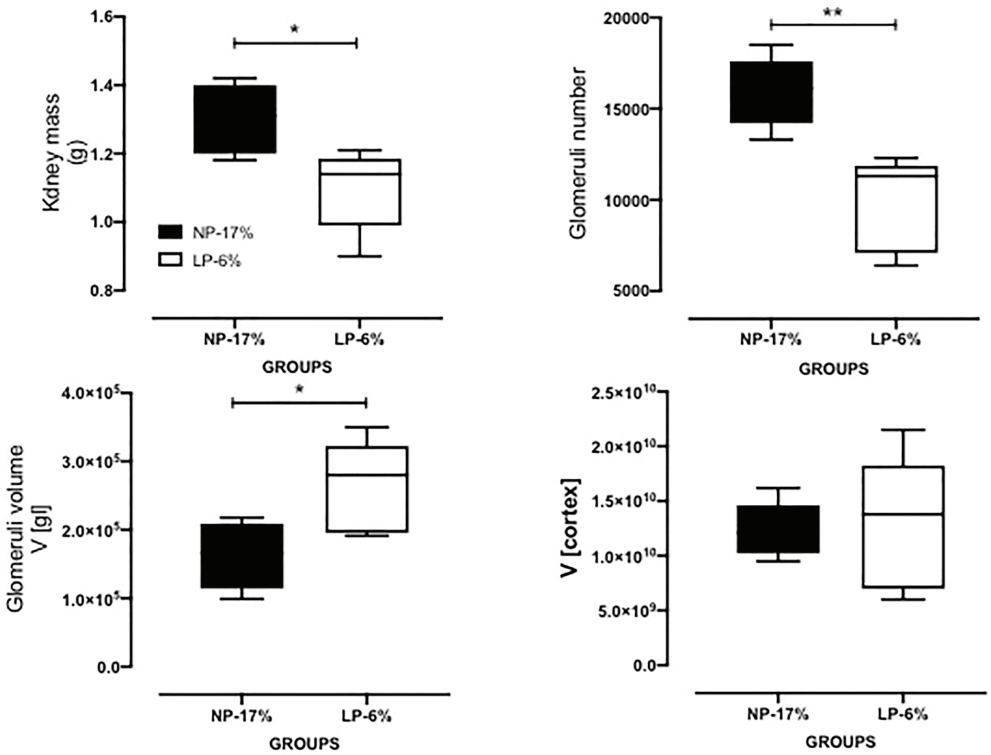

FIGURE 2 | The kidney mass (in grams), glomeruli number and volume, and cortical volume of 24-week-old LP progeny (n = 5) compared to age-matched NP offspring (n = 5). Data are presented as scatter dot plots; unpaired Welch's t-test was used for data analysis. The level of significance was set at $^{*}p$ = 0.01; $^{**}p$ = 0.0015.

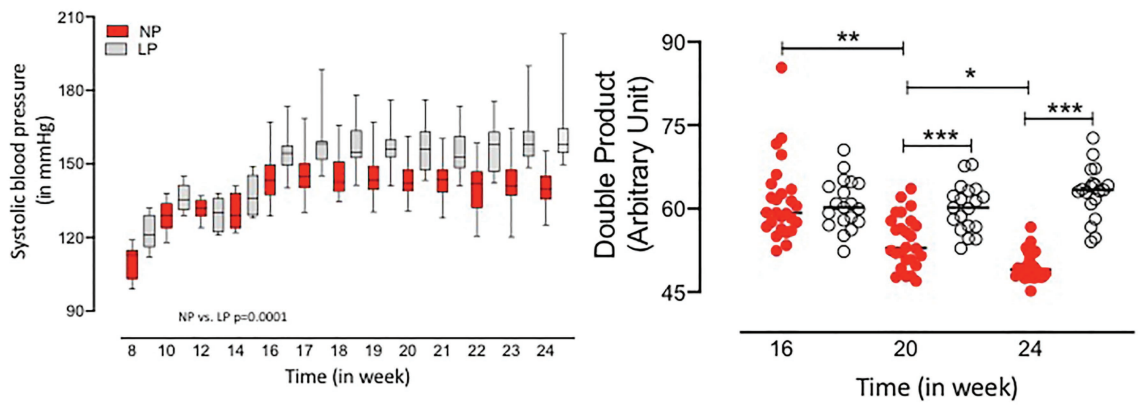

FIGURE 3 | Systolic blood pressure (SBP; in mmHg) and double product (DP) index (in arbitrary unit) from 8 to 24 weeks of age in LP (n = 12–20) progeny compared to age-matched NP offspring (n = 18–20). Data are presented as boxes and whiskers (minimum and maximum values); Welch's ANOVA test was used for data analysis. The level of significance was set at $^{*}p$ = 0.0256; $^{**}p$ = 0.0117; $^{***}p$ = 0.001.

groups are summarized in **Figure 4**. The plasma sodium (LP: 147 ± 4.8 mM vs. NP: 144 ± 4.5 mM), plasma potassium (LP: 4.7 ± 0.9 mM vs. NP: 4.5 ± 0.9 mM), plasma lithium (LP: 86 ± 19 mM vs. NP: 78 ± 23 mM), urinary flow rates and glomerular filtration rates, estimated by CCr, did not significantly differ between the groups during the renal tubule sodium handling studies (LP: 187.5 ± 30.85 µl/min/100 g body weight (b.w.) vs. NP: 157.4 ± 56.15 µl/min/100 g b.w., p = 0.2103). FENa+ was significantly lower in the LP offspring (0.06407 ± 0.018%, n = 7) than in the NP age-matched offspring (0.1186 ± 0.077%, n = 9; p = 0.0461). The decreased FENa+ occurred in parallel with a significant reduction in FEPNa+ (LP: 24.13 ± 5.031% vs. NP: 41.84 ± 17.29%, p = 0.0103; **Figure 4**). The decreased FENa+ in the LP progeny was also

accompanied by unchanged FEPPNa+ (LP: 0.2918 ± 0.1584% vs. NP: 0.3475 ± 0.1656%, p = 0.2527) and FEK+ (LP: 0.9794 ± 0.4357% vs. NP: 0.7464 ± 0.2981%, p = 0.0534) compared with the NP age-paired control group (**Figure 4**).

Immunohistochemistry and Immunoblotting Analyses

The current study showed that the Na/K-ATPase expression in the basolateral membrane tubule proximal segments of the 24-week-old LP (**Figure 5**) considerably increased compared with that of the age-matched NP. In the 24-week-old LP offspring, TGF-β1 was slightly expressed in the glomerular basement membrane delimiting the glomerular capillaries, as well as in the proximal tubule (**Figure 6**). The current study also demonstrated an increased glomerular TGF-β1 immunostain and the basal portion of the proximal and post-proximal tubular cells.

The increased TGF-β1 immunomarker was associated with high ZEB1 staining in LP rats compared with NP rats of the same age (**Figure 6**). The findings also indicated a high and extensive tubular and glomerular type I collagen immunoreactivity in the LP offspring relative to the NP offspring (**Figure 7**). A higher desmin and nestin immunoreactivity was observed in the glomeruli podocyte and renal tubules of 24-week-old LP rats compared to age-matched NP progeny (**Figures 8, 9**). Significant enhancement of both JAK-2 and pSTAT-3 levels (Dot plots chart) were also verified in the whole kidney of 24-week-old LP rats through Western blotting. It was associated with reduced pJAK-2 and unchanged STAT-3 levels (**Figure 10**) compared with the NP age-matched offspring. Additionally, NOS1 and IL-6 expression was enhanced in the whole kidney of the 24-week-old LP offspring compared with that of the NP offspring (**Figure 11**). No changes were observed in NOS2, SOD, and GH immunoblotting analyses.

DISCUSSION

The role of the kidney in the genesis of arterial hypertension has long been established. Brenner et al. (1998) proposed that some individuals are susceptible to hypertension and renal injury because of reduced nephron number. A reduction in nephron number and, therefore, in the whole kidney glomerular filtration area would result in decreased salt excretory capacity, enhanced susceptibility to hypertension, and reduced renal reserve upon excessive sodium intake (Schor et al., 1980). Embryonic and fetal protein restriction may lead to a long-term disorder in renal sodium and water handling and structural changes that may be associated with arterial hypertension onset in male adult progeny (Mesquita et al., 2010a,b; Sene et al., 2013, 2018; Vaccari et al., 2015). Therefore, the limiting compensation for renal injury may, at least in part, explain the higher prevalence of hypertension and renal disease observed in populations with a high prevalence of low birth weight (Barker, 1995, 2003; Lackland et al., 2000, 2002; Hsu et al., 2003). However, despite several kidney morphological and functional disorders in the maternal restricted-protein intake model, the effect of protein restriction on gestational and breastfeeding low-protein ingestion (LP) remains unknown. Herein, we focused on hypertension development as an outcome and its association with nephron number and structure changes and reduced urinary sodium excretion in LP offspring. It is essential to state that sex hormones determine sexual phenotype dimorphism in the

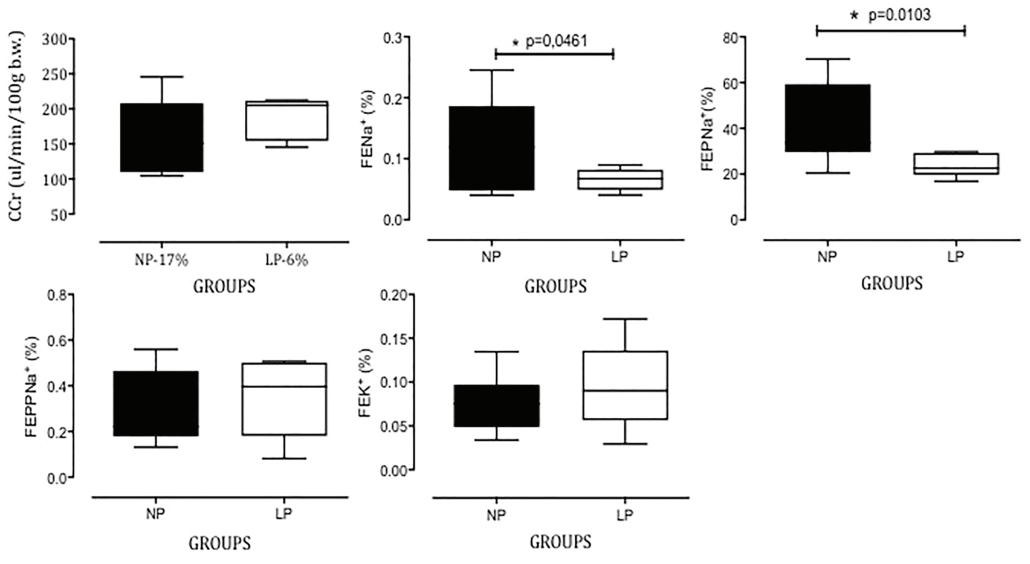

FIGURE 4 | Renal function; creatinine clearance (CCr), fractional sodium excretion (FENa+), proximal (FEPNa+), and post-proximal (FEPPNa+) fractional sodium excretion, and fractional potassium excretion (FEK+) in 16-week-old LP offspring (n = 11) compared to age-matched NP progeny (n = 15). Data are presented as boxes and whiskers (minimum and maximum values); unpaired Welch's t-test was used for data analysis. The level of significance was set at $p < 0.05$.

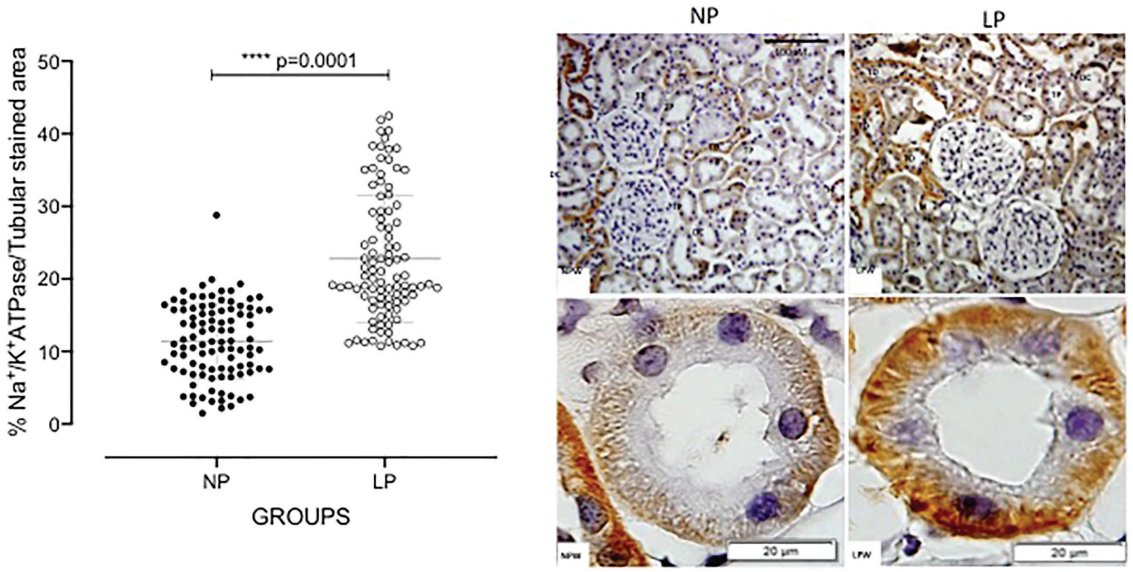

FIGURE 5 | Kidney Na/K-ATPase expression by immunohistochemistry in 24-week-old LP progeny (n = 5) compared with age-matched NP progeny (n = 5). A magnification of 400× and 1000× was used. The scale bar can be found at the bottom right of each figure. Five cortical and medullar fields of each histological section were analyzed, and the average immunoreactivity reading was determined. Data are presented as scatter dot plots on the left; unpaired Welch's t-test was used for data analysis. The level of significance was set at $p < 0.05$.

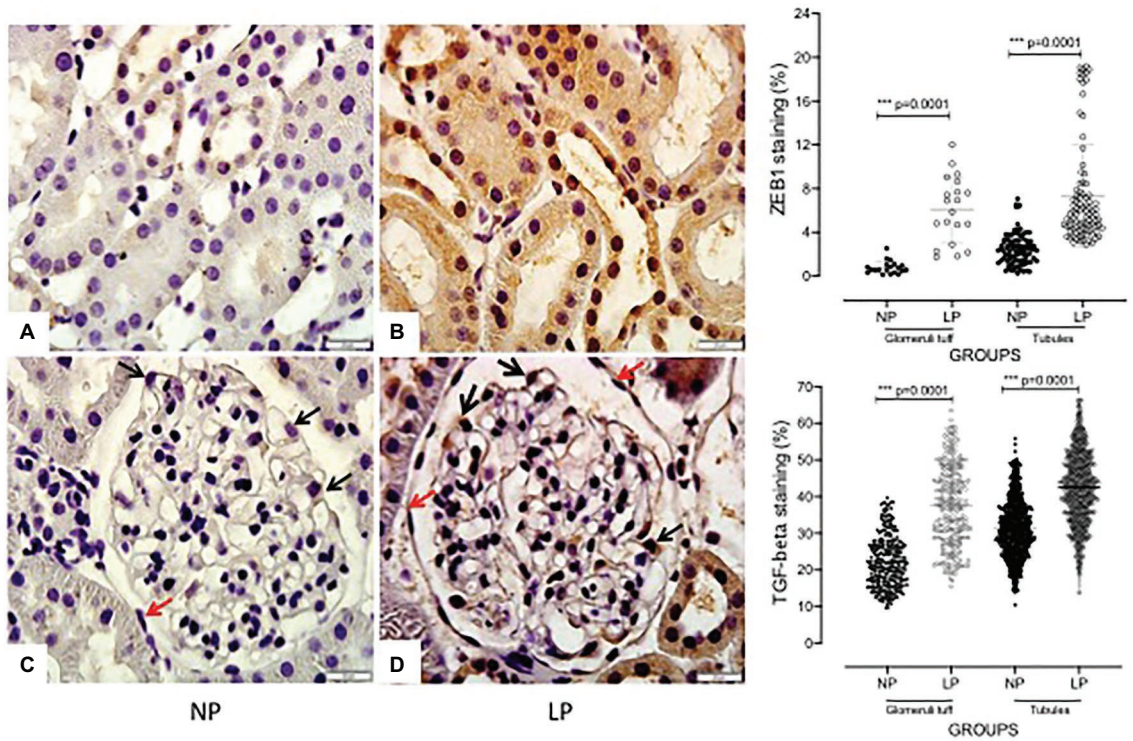

FIGURE 6 | Glomerular and tubular TGFβ1 and ZEB1 immunoperoxidase labeling in 24-week-old male NP offspring (**A/C**; n = 5) compared with age-matched LP progeny (**B/D**; n = 5). A red arrow indicates perivascular epithelial cell (PEC); a black arrow characterizes podocyte. A 400× and 1000× magnification was used in the tubular area **(A,B)** and glomerular area **(C,D)**, respectively. The scale bar can be found at the bottom right of each figure. Five cortical and medullar fields of each histological section were analyzed, and the average immunoreactivity reading was determined. Data are presented as scatter dot plots on the right; the unpaired Welch' ANOVA test was used for data analysis. The level of significance was set at $p < 0.05$.

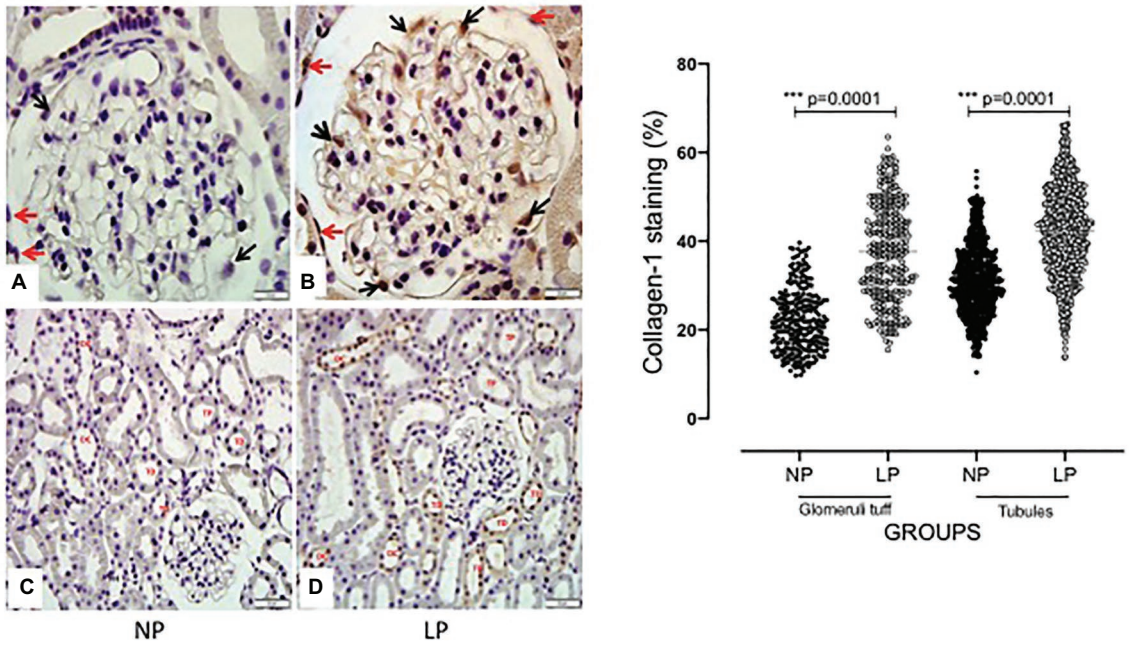

FIGURE 7 | Glomerular and tubular collagen-1 immunoperoxidase staining in 24-week-old male NP offspring (n = 5; **A/C**) compared with age-matched LP progeny (n = 5; **B/D**). A 400× and 1000× magnification was used in the tubular area **(A,B)** and glomerular area **(C,D)**, respectively. The scale bar can be found at the bottom right of each figure. Five cortical and medullar fields of each histological section were analyzed, and the average immunoreactivity reading was determined. Data are presented as scatter dot plots on the right; the unpaired Welch' ANOVA test was used for data analysis. The level of significance was set at $p < 0.05$.

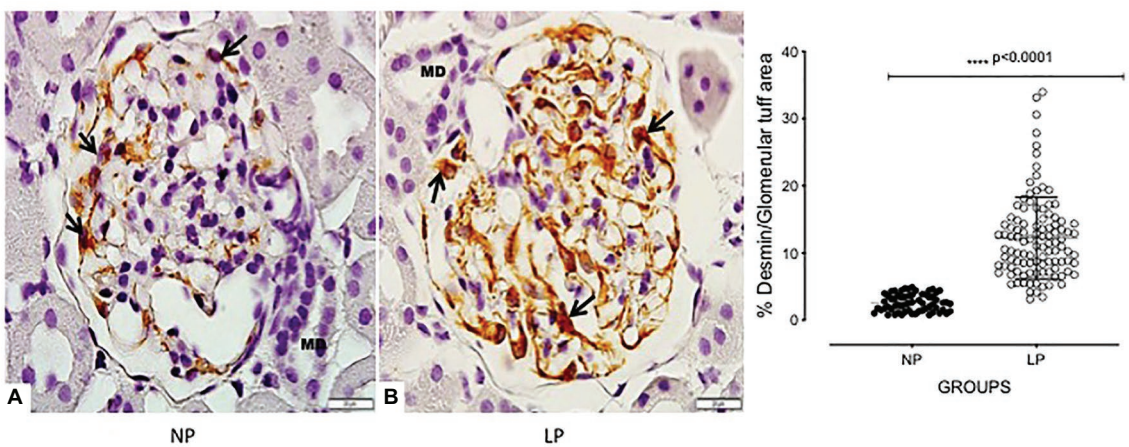

FIGURE 8 | Glomerular tuff desmin immunoperoxidase staining in 24-week-old male NP offspring (n = 5; **A**) compared with age-matched LP progeny (n = 5; **B**). The black arrow indicates podocytes, and the *macula densa* is shown as MD. A 1000× magnification was used in the glomerular area. The scale bar can be found at the bottom right of each figure. Five cortical and medullar fields of each histological section were analyzed, and the average immunoreactivity reading was determined. Data are presented as scatter dot plots on the right; unpaired Welch's t-test was used for data analysis. The level of significance was set at $p < 0.05$.

fetal-programmed disease model in adulthood by changes in the long-term control of neural, cardiac, and endocrine functions. Thus, the present study was performed in male rats considering the findings above to eliminate interferences due to gender differences (Kwong et al., 2000; Gillette et al., 2017). The current study confirmed that low birth weight (approximately 13%) might reflect the influence of inappropriate protein intake during pregnancy and lactation on embryonic/fetal growth and development. Unpredictably, LP offspring's body mass, beyond the second week of age, remained lower than that of age-matched NP progeny during the allover follow-up. The phenomenon known as catch-up growth was

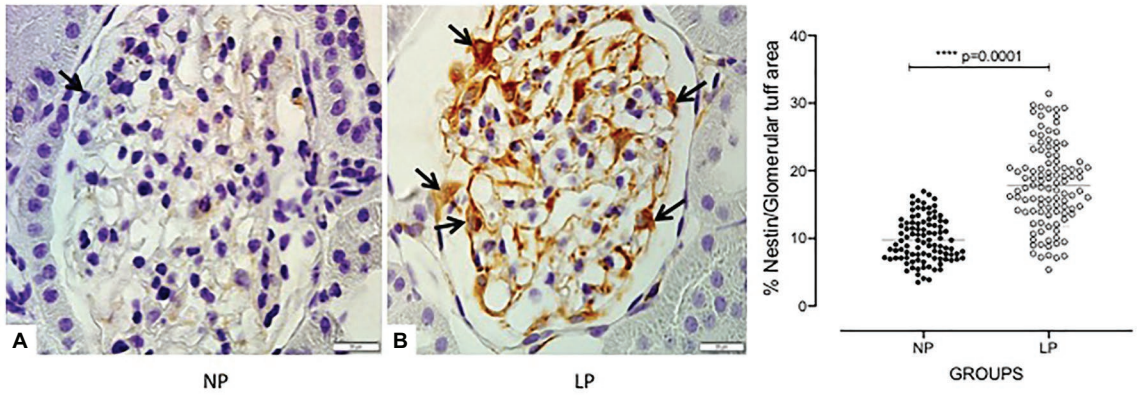

FIGURE 9 | Glomerular tuff nestin immunoperoxidase staining in 24-week-old male NP offspring (n = 5; **A**) compared with age-matched LP progeny (n = 5; **B**). The black arrow indicates podocytes. A 1000X magnification was used in the glomerular area. The scale bar can be found at the bottom right of each figure. Five cortical and medullar fields of each histological section were analyzed, and the average immunoreactivity reading was determined. Data are presented as scatter dot plots on the right; unpaired Welch's t-test was used for data analysis. The level of significance was set at $p < 0.05$.

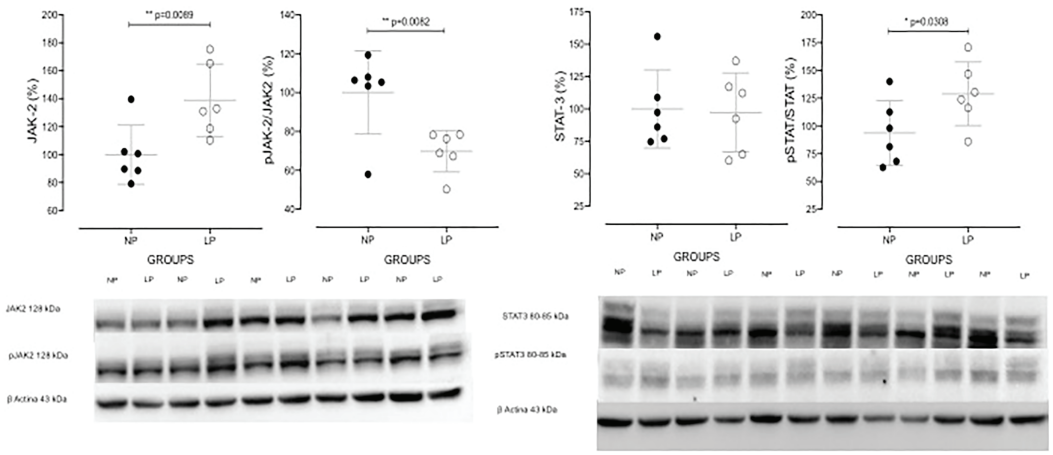

FIGURE 10 | Western blot analyses of JAK-2, pJAK-2, STAT-3, and pSTAT-3 protein expression in the whole kidneys of 24-week-old NP (n = 5) and LP (n = 5) offspring. Data are presented as scatter dot plots; unpaired Welch's t-test was used for data analysis. The level of significance was set at $p < 0.05$.

not observed in this model, unlike the observed mass recovery observed in mothers' offspring subjected to protein restriction supply only during the gestational period. Although the placenta is capable of self-regulation, the compensatory mechanism does not seem sufficient in protein restriction cases, especially in the final pregnancy period, where fetal growth is predominant and accelerated (Fowden et al., 2006). A previous study in rodent fetal programming models demonstrated that impairment in placental transport of nutrients, mainly involving amino acids, may be related, at least in part, to the decline in placental vascularization (Burdge and Lillycrop, 2010). Barker (1995) presented the theory that the maternal environment could induce adult diseases based on observed epidemiological associations between low birth weight and an increased risk for ischemic heart diseases and, particularly, arterial hypertension. Although it seemed that the relationship is not invariant, the bulk of evidence suggested a meaningful direct or indirect interaction between low birth weight and subsequent hypertension (Barker, 1995, 2003). As such, our results confirmed the findings of previous studies, which demonstrated a marked and sustained rise in arterial blood pressure associated with a decreased urinary sodium excretion in low-birth-weight LP compared with that in age-matched NP offspring (Mesquita et al., 2010a,b). However, unlike previous findings in the gestational protein-restricted model that demonstrated an enhanced arterial pressure beyond 7 weeks of age in LP relative to NP counterparts, the present study extended the protein restriction throughout lactation and revealed a consistent onset delay of hypertension at adulthood. The reduced glomeruli number in this model, including protein intake reduction and breastfeeding, was higher than observed previously for us. A 36% reduction in nephron number was also confirmed in the gestational and breastfeeding

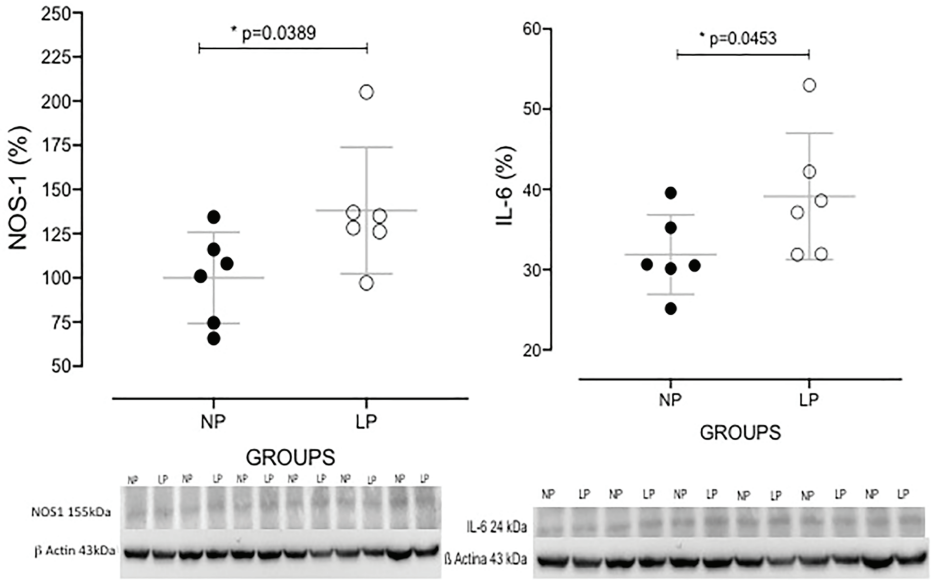

FIGURE 11 | Western blot analyses of NOS1 and IL-6 protein expression in the whole kidneys of 24-week-old NP (n = 5) and LP (n = 5) offspring. Data are presented as scatter dot plots; unpaired Welch's t-test was used for data analysis. The level of significance was set at $p < 0.05$.

protein-restricted model compared with a 27% reduction when restriction occurred only during the gestational period (Mesquita et al., 2010a,b; Sene et al., 2013). Additionally, a pronounced decline in FENa+ was observed in the 24-week-old maternal protein-restricted male offspring. This effect was accompanied by intensive sodium reabsorption in the nephron's proximal segments despite unchanged CCr, FEK+, and post-proximal sodium handle FEPPNa+ (**Figure 4**). The present study confirmed previous findings from our laboratory, demonstrating that even when associated with decreased nephron number units, maternal food-restricted offspring maintain normal whole GFR estimated by creatinine clearance. Herein, a reduced remaining glomerular number was associated with an increased glomerular volume, probably by enhancing glomerular volume with compensatory enhanced blood flow and glomerular hyperfiltration despite a loss of efficiency on the filter barrier (Mesquita et al., 2010a,b; Sene et al., 2013, 2018; Vaccari et al., 2015). The renal results and the increased blood pressure in the maternal low protein diet intake model corroborated hypothesis of Brenner et al. (1998). Hyperfiltration in low birth weight leads to subsequent glomerular hypertension, resulting in sustained renal function disorder. Once the glomerular filtration rate does not change significantly due to protein restriction in LP offspring, compensatory poorly adapted nephron functional changes may have occurred intrinsically when nephrogenesis was compromised. A previous study suggested that the late-onset arterial hypertension induced by maternal low-protein intake is associated, at least in part, with an increased renal neural activity. An explanation for a reduced renal sodium excretion maybe explain by decreasing the proximal tubule sodium rejection, associated with unchanged creatinine clearance, and sodium was usually filtered (Custódio et al., 2017). In the present study, the persistent and enhanced DP in the LP progeny strongly suggested an increased sympathetic activity in the LP group relative to the control group.

The reduced urinary sodium excretion is significantly attenuated by renal denervation (Custódio et al., 2017). Experimental studies have supported the hypothesis that fetal programming correlates with the deregulation of sodium transporters in different nephron segments (Manning et al., 2002; Alwasel and Ashton, 2009; Baum, 2010). To the best of our knowledge, the present data demonstrated for the first time that a decreased urinary sodium excretion in gestational and breastfeeding LP offspring was associated with a reduction in proximal tubular sodium reabsorption that was incompletely compensated by distal nephron segments. do Carmo Pinho et al. (2003), in a study of renal function and Na+ transporters in male rats born to low-protein diet dams, showed that the transcriptional upregulation of Na+ transport could have contributed to hypertension. Interestingly, by Western blot analysis, the present study found that Na/K-ATPase protein was upregulated in the low-protein diet male progeny compared with the standard diet intake offspring (**Figure 5**). Considering a study showing that AngII AT2R is an effective inhibitor of Na/K-ATPase (De Souza et al., 2004; Alwasel and Ashton, 2009), we previously demonstrated that the downregulation of the renin-angiotensin system, found in 16-week-old LP male offspring, might also explain the lack of inhibition of Na/K-ATPase (Mesquita) in this model. The finding may support the results obtained here by western blot analysis and the low sodium excretion rate because Na/K-ATPase participates in Na+ reabsorption in the basolateral membrane of the proximal segments of the nephron (**Figure 5**). Fekete et al. (2008) demonstrated that AngII promotes Na/K-ATPase-α1 subunit translocation from the cytoskeletal fraction into the cytosol

under experimental conditions, which must be taken into account. Prolonged elevated glomerular filtration and blood flow processes may cause the reduced nephron number manifested as an accelerated renal function loss and glomerulosclerosis. These findings were highly prevalent among adult LP offspring with low birth weight (Mesquita et al., 2010a,b; Sene et al., 2013). Glomeruli overflow may be an initial insult that initiates a cascade of events, including an early inflammatory phase followed by a fibrotic response. Irreversible renal fibrosis is a common consequence of most renal injuries (Liu, 2010; Zeisberg and Neilson, 2010). TGF-β regulates extracellular matrix protein deposition in renal tissue (Lee, 2012). To our knowledge, these are the first data showing renal morphological and protein expression changes in the gestational and lactation protein restriction model of fetal programming. In the current study, the protein-restricted fetal-programmed adult rats showed structural glomerular and tubular disorders with remarkable TGF-β1 and collagen-1 immunoreactivity, suggesting an advanced fibrosis stage. These findings led us to speculate that the renal TGF-β1 upregulation may induce ZEB 2 expression, which may cause glomerular EMT as evidenced by increased nestin and desmin expression.

Epithelium-mesenchymal transition is associated with fibrosis progression (Carew et al., 2012). Studies have implicated TGF-β1 and ZEB2 overexpression with the phenotypic changes during EMT in progressive renal development of fibrosis (Kato et al., 2007; Wang et al., 2010, 2011). The glomerular corpuscle is composed of different mesenchymal and epithelial cell types, and the EMT process may be uneven throughout the renal parenchyma. Four resident cell types constitute the renal corpuscles: mesangial cells, endothelial cells, visceral cells (podocytes), parietal epithelial cells (PECs) with specific glomerular functions and protein expressions. Podocytes are terminally differentiated epithelial cells with a low proliferation capacity (Kriz, 1996); thus, injury and loss of these cells can lead to glomerular scarring (Liu, 2010; Zeisberg and Neilson, 2010). The present study verified strikingly enhanced glomerular and tubular expressions of TGF-β1 and type I collagen, intrinsically related to the fibrotic process, by immunohistochemistry. We hypothesized that the hemodynamic glomerular overload in the LP progeny compared with the NP progeny associated with an enhanced blood flow in the remaining nephrons stimulated fibrous processes by enhancing TGF-β1 collagen 1. In parallel, an altered cellular corpuscles phenotype to EMT occurred by expressing mesenchymal markers, namely nestin and desmin. Thus, earlier findings indicated that glomerular podocytes might undergo phenotypic conversion, characterized by the loss of podocyte-specific markers and gain of transitional features, a process reminiscent of EMT (Li et al., 2008). TGF-β triggers EMT, and its expression is upregulated in virtually every type of chronic kidney disease (Yang and Liu, 2001; Bottinger and Bitzer, 2002), including in the diseased LP programmed model.

In the present study, we speculated that EMT, a process induced by TGF-β1 and ZEB 2 overexpression, plays a significant role in imparting PEC plasticity. PEC plasticity results in non-differentiated progenitor cell glomerular migration, an early and ruling response of nephron cells in the LP renal pathological process. Glomerular insults are potent inducers for the generation of IL6 by the tubular epithelial cells functioning as a cross-talk between the glomerulus and the tubule (Su et al., 2017). IL-6 may induce type-I collagen by tubular epithelial cells and accelerate tubulointerstitial fibrosis, which has been associated with increased STAT3 phosphorylation (Nechemia-Arbely et al., 2008; Ranganathan et al., 2013). This study observed a significant increase in IL-6 (23%) and the phosphorylated fraction of STAT3 (28%) in the LP progeny compared with the age-matched NP progeny. Although JAK2 increased by 40%, the phosphorylated JAK fraction decreased by 23%. Thus, we assumed that the high expression of JAK might be responsible for the phosphorylation of STAT3. Renal cells, including podocytes, endothelial cells, mesangial cells, and tubular epithelial cells, secrete IL-6. Thus, IL6 over-reactivity may induce mesangial dysfunction, increase cell proliferation, increase mesangial matrix deposition, and glomerular sclerosis (Coletta and Polentarutti, 2000; Gohda et al., 2001; Lu, 2008; Nechemia-Arbely et al., 2008). Studies suggested that fetal programming and chronic kidney disease in adult offspring are associated with increased maternal ROS production and high oxidative stress in fetal tissues (Halliwell, 2013; de Brito Alves et al., 2016). The present study did not demonstrate significant renal changes in the SOD and ROS levels. However, we observed an unprecedented increase of 32% in the NOS1 content in the renal of 24-week-old LP, relating to the kidney tubular O_2 consumption in parallel with increased sodium and water reabsorption stimulation the proximal tubule. This effect, particularly in the proximal segments of nephrons, was associated with a determining factor, which was the basolateral expression of the Na/K-ATPase pump. As observed in the laboratory LP model (Mesquita et al., 2010b), our study revealed a quantitative increase in Na/K-ATPase in the 24th week of life in LP offspring. The elevated Na/K-ATPase in the 24-week-old LP offspring's proximal tubules may involve an increase in NOS1 expression associated with increased reabsorption of sodium and water.

In conclusion, it is plausible to deduce an association between accentuated reduction of the nephron numbers, decreased natriuresis, and reciprocal changes in tubular Na/K-ATPase with the development of arterial hypertension found in severe gestational and breastfeeding protein-restricted progeny compared with age-matched NP rats. After birth, the overload of an economic kidney may result in an increased glomerular overflow. This overload in fetal-programmed rats can result in pronounced structural glomerular disorders and accentuated and advanced stage of fibrosis promoted by TGF-β1 action inducing ZEB 2 expression, which may cause premature nephron senescence in parallel with functional loss.

DATA AVAILABILITY STATEMENT

The raw data supporting the conclusions of this article will be made available by the authors, without undue reservation.

ETHICS STATEMENT

The animal study was reviewed and approved by Committee on the Use of Animals (CEUA/UNICAMP) according to COBEA (protocol number #4242-1).

AUTHOR CONTRIBUTIONS

GL: data curation, investigation, formal analysis, methodology, visualization, and writing–original draft. AF: methodology. JG: formal analysis, methodology, visualization, and writing–review and editing. PB: conceptualization, formal analysis, funding acquisition, methodology, resources, supervision, visualization, writing–original draft, and writing–review and editing. All authors contributed to the article and approved the submitted version.

FUNDING

This work was supported by Fundação de Amparo à Pesquisa do Estado de São Paulo (FAPESP, 2013/12486-5 and 15/00360-2), Coordenação de Aperfeiçoamento de Pessoal de Nível Superior (CAPES) and Conselho Nacional de Desenvolvimento Científico e Tecnológico (CNPq, 465699/2014-6).

REFERENCES

Alwasel, S. H., and Ashton, N. (2009). Prenatal programming of renal sodium handling in the rat. *Clin. Sci.* 117, 75–84. doi: 10.1042/CS20080294

Barker, D. J. (1995). Intrauterine programming of adult disease. *Mol. Med. Today* 1, 418–423. doi: 10.1016/S1357-4310(95)90793-9

Barker, D. (2003). The midwife, the coincidence, and the hypothesis. *BMJ* 327, 1428–1430. doi: 10.1136/bmj.327.7429.1428

Baum, M. (2010). Role of the kidney in the prenatal and early postnatal programming of hypertension. *Am. J. Phys.* 298, F235–F247. doi: 10.1152/ajprenal.00288.2009

Bottinger, E. P., and Bitzer, M. (2002). TGF-beta signaling in renal disease. *J. Am. Soc. Nephrol.* 13, 2600–2610. doi: 10.1097/01.asn.0000033611.79556.ae

Brenner, B. M., Garcia, D. L., and Anderson, S. (1998). Glomeruli and blood pressure: less of one, more the other? *Am. J. Hypertens.* 1, 335–347.

Burdge, G. C., and Lillycrop, K. A. (2010). Nutrition, epigenetics, and developmental plasticity: implications for understanding human disease. *Annu. Rev. Nutr.* 30, 315–339. doi: 10.1146/annurev.nutr.012809.104751

Carew, R. M., Wang, B., and Kantharidis, P. (2012). The role of EMT in renal fibrosis. *Cell Tissue Res.* 347, 103–116. doi: 10.1007/s00441-011-1227-1

Chung, A. C. K., Huang, X. R., Meng, X., and Lan, H. Y. (2010). miR-192 mediates TGF-β/Smad3-driven renal fibrosis. *J. Am. Soc. Nephrol.* 21, 1317–1325. doi: 10.1681/ASN.2010020134

Coletta, I., and Polentarutti, N. (2000). Selective induction of MCP-1 in human mesangial cells by the IL-6/sIL-6R complex. *Exp. Nephrol.* 8, 37–43. doi: 10.1159/000059327

Custódio, A. H., de Lima, M. C., Vaccari, B., Boer, P. A., and Gontijo, J. A. R. (2017). Renal sodium handling and blood pressure changes in gestational protein-restricted offspring: role of renal nerves and ganglia neurokinin expression. *PLoS One* 12:e0179499. doi: 10.1371/journal.pone.0179499

de Brito Alves, J. L., de Oliveira, J. M. D., Ferreira, D. J. S., Barros, M. A. d. V., Nogueira, V. O., Alves, D. S., et al. (2016). Maternal protein restriction-induced hypertension is associated with oxidative disruption at transcriptional and functional levels in the medulla oblongata. *Clin. Exp. Pharmacol. Physiol.* 43, 1177–1184. doi: 10.1111/1440-1681.12667

De Souza, A. M., Lopes, A. G., Pizzino, C. P., Fossari, R. N., Miguel, N. C., Cardozo, F. P., et al. (2004). Angiotensin II and angiotensin-(1-7) inhibit the inner cortex Na^+-ATPase activity through the AT2 receptor. *Regul. Pept.* 120, 167–175. doi: 10.1016/j.regpep.2004.03.005

do Carmo Pinho, F. M., Nigro, D., Fortes, Z. B., Tostes, R. C., Carvalho, M. H., Lucas, S. R., et al. (2003). Intrauterine undernutrition - renal and vascular origin of hypertension. *Cardiovasc. Res.* 60, 228–234. doi: 10.1016/s0008-6363(03)00541-8

Fekete, A., Rosta, K., Wagner, L., Prokai, A., Degrell, P., Ruzicska, E., et al. (2008). Na^+, K^+/-ATPase is modulated by angiotensin II in diabetic rat kidney - another reason for diabetic nephropathy? *J. Physiol.* 586, 5337–5348. doi: 10.1113/jphysiol.2008.156703

Fowden, A. L., Ward, J. W., Wooding, F. P. B., Forhead, A. J., and Constancia, M. (2006). Programming placental nutrient transport capacity. *J. Physiol.* 572, 5–15. doi: 10.1113/jphysiol.2005.104141

Gillette, R., Reilly, M. P., Topper, V. Y., Thompsom, L. M., Crews, D., and Gore, A. C. (2017). Anxiety-like behaviors in adulthood are altered in male but not female rats exposed to low dosages of polychlorinated biphenyls in utero. *Horm. Behav.* 87, 8–15. doi: 10.1016/j.yhbeh.2016.10.011

Gohda, T., Makita, Y., Shike, T., Funabiki, K., and Elisa, I. (2001). Dilazep hydrochloride, an antiplatelet drug inhibits lipopolysaccharide-induced mouse mesangial cell IL-6 secretion and proliferation. *Kidney Blood Press. Res.* 24, 33–38. doi: 10.1159/000054203

Halliwell, B. (2013). The antioxidant paradox: less paradoxical now? *Br. J. Clin. Pharmacol.* 75, 637–644. doi: 10.1111/j.1365-2125.2012.04272.x

Hsu, C. Y., Lin, F., Vittinghoff, E., and Shlipak, M. G. (2003). Racial differences in the progression from chronic renal insufficiency to end-stage renal disease in the United States. *J. Am. Soc. Nephrol.* 14, 2902–2907. doi: 10.1097/01.asn.0000091586.46532.b4

Kalluri, R., and Weinberg, R. A. (2009). The basics of epithelial-mesenchymal transition. *J. Clin. Invest.* 119, 1420–1428. doi: 10.1172/JCI39104

Kato, M., Zhang, J., Wang, M., Lanting, L., Yuan, H., Rossi, J. J., et al. (2007). MicroRNA-192 in diabetic kidney glomeruli and its function in TGF-beta-induced collagen expression via inhibition of E-box repressors. *Proc. Natl. Acad. Sci. U. S. A.* 104, 3432–3437. doi: 10.1073/pnas.0611192104

Kriz, W. (1996). Progressive renal failure-inability of podocytes to replicate, and the consequences for the development of glomerulosclerosis. *Nephrol. Dial. Transplant.* 11, 1738–1742.

Kwong, W. Y., Wild, A. E., Roberts, P., Willis, A. C., and Fleming, T. P. (2000). Maternal undernutrition during the preimplantation period of rat development causes blastocyst abnormalities and programming of postnatal hypertension. *Development* 127, 4195–4202.

Lackland, D. T., Bendall, H. E., Osmond, C., Egan, B. M., and Barker, D. J. (2000). Low birth weights contribute to high rates of early-onset chronic renal failure in the southeastern United States. *Arch. Intern. Med.* 160, 1472–1476. doi: 10.1001/archinte.160.10.1472

Lackland, D. T., Egas, B. M., Syddall, H. E., and Barker, D. J. (2002). Associations between birth weight and antihypertensive medication in black and white medicaid recipients. *Hypertension* 39, 179–183. doi: 10.1161/hy0102.100545

Langley-Evans, S. C. (2006). Developmental programming of health and disease. *Proc. Nutr. Soc.* 65, 97–105. doi: 10.1079/PNS2005478

Langley-Evans, S. C. (2009). Nutritional programming of disease: unraveling the mechanism. *J. Anat.* 215, 36–51. doi: 10.1111/j.1469-7580.2008.00977.x

Lee, H. S. (2012). Mechanisms and consequences of TGF-b overexpression by podocytes in progressive podocyte disease. *Cell Tissue Res.* 347, 129–140. doi: 10.1007/s00441-011-1169-7

Li, Y., Kang, Y. S., and Dai, C. (2008). Epithelial-to-mesenchymal transition is a potential pathway leading to podocyte dysfunction and proteinuria. *Am. J. Pathol.* 172, 299–308. doi: 10.2353/ajpath.2008.070057

Liu, Y. (2004). Epithelial to Mesenchymal transition in renal fibrogenesis. Pathologic significance, molecular mechanism, and therapeutic intervention. *J. Am. Soc. Nephrol.* 15, 1–12. doi: 10.1097/01.asn.0000106015.29070.e7

Liu, Y. (2010). New insights into epithelial-mesenchymal transition in kidney fibrosis. *J. Am. Soc. Nephrol.* 21, 212–222. doi: 10.1681/ASN.2008121226

Lu, H. (2008). HBV X gene transfection Upregulates IL-1 β and IL-6 gene. *J. Huazhong Univ. Sci. Technol. Med. Sci.* 28, 247–250. doi: 10.1007/s11596-008-0304-5

Mandarim-de-Lacerda, C. A. (2003). Stereological tools in biomedical research. *An. Acad. Bras. Cienc.* 75, 469–486. doi: 10.1590/S0001-37652003000400006

Manning, J., Beutler, K., Knepper, M. A., and Matti, V. V. (2002). Upregulation of renal BSC1 and TSC in prenatally programmed hypertension. *Am. J. Phys.* 283, F202–F206. doi: 10.1152/ajprenal.00358.2001

Mesquita, F. F., Gontijo, J. A., and Boer, P. A. (2010a). Expression of renin-angiotensin system signaling compounds in maternal protein-restricted rats: effect on renal sodium excretion and blood pressure. *Nephrol. Dial. Transplant.* 25, 380–388. doi: 10.1093/ndt/gfp505

Mesquita, F. F., Gontijo, J. A., and Boer, P. A. (2010b). Maternal undernutrition and the offspring kidney: from fetal to adult life. *Braz. J. Med. Biol. Res.* 43, 1010–1018. doi: 10.1590/s0100-879x2010007500113

Nechemia-Arbely, Y., Barkan, D., Pizov, G., Shriki, A., Rose-john, S., Galun, E., et al. (2008). IL-6/IL-6R Axis plays a critical role in acute kidney injury. *J. Am. Soc. Nephrol.* 19, 1106–1115. doi: 10.1681/ASN.2007070744

Postigo, A. A., and Dean, D. C. (2000). Differential expression and function of members of the zfh-1 family of zinc finger/homeodomain repressors. *Proc. Natl. Acad. Sci. U. S. A.* 12, 6391–6396. doi: 10.1073/pnas.97.12.6391

Ranganathan, P., Jayakumar, C., and Ramesh, G. (2013). Chronic kidney disease and fibrosis proximal tubule-specific overexpression of netrin-1 suppresses acute kidney injury-induced interstitial fibrosis and glomerulosclerosis through suppression of IL-6/STAT3 signaling. *Am. J. Physiol. Ren. Physiol.* 304, F1054–F1065. doi: 10.1152/ajprenal.00650.2012

Schor, N., Ichikawa, I., and Brenner, B. M. (1980). Glomerular adaptations to chronic dietary salt restriction or excess. *Am. J. Phys.* 238, F428–F436. doi: 10.1152/ajprenal.1980.238.5.F428

Schreuder, M., Delemarre-van de Waal, H. A., and van Wijk, A. (2006). Consequences of intrauterine growth restriction for the kidney. *Kidney Blood Press. Res.* 29, 108–125. doi: 10.1159/000094538

Sene, L. d. B., Mesquita, F. F., de Moraes, L. N., Santos, D. C., Carvalho, R., Gontijo, J. A., et al. (2013). Involvement of renal corpuscle microRNA expression on epithelial-to-mesenchymal transition in maternal low protein diet in adult programmed rats. *PLoS One* 19:e71310. doi: 10.1371/journal.pone.0071310

Sene, L. B., Rizzi, V. H. G., Gontijo, J. A. R., and Boer, P. A. (2018). Gestational low-protein intake enhances whole-kidney miR-192 and miR-200 family expression and epithelial-to-mesenchymal transition in rat adult male offspring. *J. Exp. Biol.* 221:jeb171694. doi: 10.1242/jeb.171694

Su, H., Lei, C., Zhang, C., and Whiteford, J. R. (2017). Interleukin-6 signaling pathway and its role in kidney disease: an update. *Front. Immunol.* 8:405. doi: 10.3389/fimmu.2017.00405

Vaccari, B., Mesquita, F. F., Gontijo, J. A., and Boer, P. A. (2015). Fetal kidney programming by severe food restriction: effects on structure, hormonal receptor expression, and urinary sodium excretion in rats. *J. Renin-Angiotensin-Aldosterone Syst.* 16, 33–46. doi: 10.1177/1470320313481081

Wang, B., Herman-Edelstein, M., Koh, P., Burns, W., Jandeleit-Dahm, K., Watson, A., et al. (2010). E-Cadherin expression is regulated by miR-192/215 by a mechanism that is independent of the profibrotic effects of transforming growth factor-b. *Diabetes* 59, 1794–1802. doi: 10.2337/db09-1736

Wang, B., Koh, P., Winbanks, C., Coughlan, M. T., McClelland, A., Watson, A., et al. (2011). miR200a prevents renal fibrogenesis through repression of TGF-{beta}2 expression. *Diabetes* 60, 280–287. doi: 10.2337/db10-0892

Yang, J., and Liu, Y. (2001). Dissection of key events in tubular epithelial to myofibroblast transition and its implications in renal interstitial fibrosis. *Am. J. Pathol.* 159, 1465–1475. doi: 10.1016/S0002-9440(10)62533-3

Zeisberg, M., and Neilson, E. G. (2010). Mechanisms of tubulointerstitial fibrosis. *J. Am. Soc. Nephrol.* 21, 1819–1834. doi: 10.1681/ASN.2010080793

Conflict of Interest: The authors declare that the research was conducted in the absence of any commercial or financial relationships that could be construed as a potential conflict of interest.

frontiers in Physiology

ORIGINAL RESEARCH
published: 14 May 2021
doi: 10.3389/fphys.2021.642409

The Angiotensin II Type 1 Receptor-Associated Protein Attenuates Angiotensin II-Mediated Inhibition of the Renal Outer Medullary Potassium Channel in Collecting Duct Cells

*Juliano Zequini Polidoro[1], Nancy Amaral Rebouças[2] and Adriana Castello Costa Girardi[1]**

[1]Heart Institute (InCor), University of São Paulo Medical School, São Paulo, Brazil, [2]Department of Physiology and Biophysics, Institute of Biomedical Sciences, University of São Paulo, São Paulo, Brazil

OPEN ACCESS

Edited by:
Minolfa C. Prieto, Tulane University, United States

Reviewed by:
Tianxin Yang, The University of Utah, United States
Carsten Alexander Wagner, University of Zurich, Switzerland

***Correspondence:**
Adriana Castello Costa Girardi
adriana.girardi@incor.usp.br

Specialty section:
This article was submitted to Renal and Epithelial Physiology, a section of the journal Frontiers in Physiology

Received: *16 December 2020*
Accepted: *16 April 2021*
Published: *14 May 2021*

Citation:
Polidoro JZ, Rebouças NA and Girardi ACC (2021) The Angiotensin II Type 1 Receptor-Associated Protein Attenuates Angiotensin II-Mediated Inhibition of the Renal Outer Medullary Potassium Channel in Collecting Duct Cells. Front. Physiol. 12:642409. doi: 10.3389/fphys.2021.642409

Adjustments in renal K^+ excretion constitute a central mechanism for K^+ homeostasis. The renal outer medullary potassium (ROMK) channel accounts for the major K^+ secretory route in collecting ducts during basal conditions. Activation of the angiotensin II (Ang II) type 1 receptor (AT1R) by Ang II is known to inhibit ROMK activity under the setting of K^+ dietary restriction, underscoring the role of the AT1R in K^+ conservation. The present study aimed to investigate whether an AT1R binding partner, the AT1R-associated protein (ATRAP), impacts Ang II-mediated ROMK regulation in collecting duct cells and, if so, to gain insight into the potential underlying mechanisms. To this end, we overexpressed either ATRAP or β-galactosidase (LacZ; used as a control), in M-1 cells, a model line of cortical collecting duct cells. We then assessed ROMK channel activity by employing a novel fluorescence-based microplate assay. Experiments were performed in the presence of 10^{-10} M Ang II or vehicle for 40 min. We observed that Ang II-induced a significant inhibition of ROMK in LacZ, but not in ATRAP-overexpressed M-1 cells. Inhibition of ROMK-mediated K^+ secretion by Ang II was accompanied by lower ROMK cell surface expression. Conversely, Ang II did not affect the ROMK-cell surface abundance in M-1 cells transfected with ATRAP. Additionally, diminished response to Ang II in M-1 cells overexpressing ATRAP was accompanied by decreased c-Src phosphorylation at the tyrosine 416. Unexpectedly, reduced phospho-c-Src levels were also found in M-1 cells, overexpressing ATRAP treated with vehicle, suggesting that ATRAP can also downregulate this kinase independently of Ang II-AT1R activation. Collectively, our data support that ATRAP attenuates inhibition of ROMK by Ang II in collecting duct cells, presumably by reducing c-Src activation and blocking ROMK internalization. The potential role of ATRAP in K^+ homeostasis and/or disorders awaits further investigation.

Keywords: K^+ homeostasis, K^+ channels, angiotensin II type 1 receptor, c-Src, angiotensin II type 1 receptor-associated protein, kidney

INTRODUCTION

Appropriate regulation of K^+ content in the extracellular fluid is critical for cell function, especially for excitable tissues, since the K^+ gradient largely determines resting membrane potential (Unwin et al., 2011). Accordingly, many different acute and chronic mechanisms are now recognized to play a role in K^+ homeostasis (Mcdonough and Youn, 2017) in such a way that blood K^+ levels tend to vary slightly throughout the day (Moore-Ede, 1986). The task of maintaining short- and long-term K^+ balance is mainly achieved by kidneys, which properly regulate K^+ content in urine in response to the physiological status. Indeed, kaliuresis can be as high as ~150% or as low as ~2% of total filtered potassium (Unwin et al., 2011). By doing so, kidneys can respond to critical situations of ion excess or restriction.

Seminal studies by Giebisch, Malnic, and Klose during the 1960s have shown the crucial role of distal nephron to the regulated kaliuresis under different experimental conditions (Malnic et al., 1964). They have found that the proximal tubule and the Henle of Loop segments reabsorb ~90% of all filtered K^+, regardless of the amount of K^+ contained in the diet. On the other hand, the appropriate regulation of renal losses occurs in the downstream segments by further K^+ reabsorption or secretion from the peritubular space (Malnic et al., 1964).

The renal outer medullary potassium (ROMK) channel comprises the major constitutive pathway for renal K^+ secretion (Wang and Giebisch, 2009; Welling and Ho, 2009), thereby playing an essential role in K^+ homeostasis. Under the setting of K^+ restriction, K^+ homeostasis can be maintained at least in part by inhibition of ROMK in the collecting duct *via* coupling of angiotensin II (Ang II) to its Ang II type 1 receptor (AT1R; Wei et al., 2007). Ang II/AT-1R induces oxidative stress and enhances the levels of total and phosphorylated c-Src, which ultimately inhibits ROMK by its phosphorylation at a tyrosine residue (Wei et al., 2007; Yue et al., 2011). Accordingly, AT1R is locally upregulated in collecting ducts during low K^+-diets (LK; Wei et al., 2007), and AT1R inhibition during LK diets impairs renal K^+ conservation (Jin et al., 2009), underlining the importance of renin-angiotensin-system for K^+ homeostasis.

Several studies have pointed out that AT1R signaling is modulated by associated proteins, particularly the AT1R-associated protein (ATRAP). ATRAP colocalizes *in vivo* with AT1R in all nephron segments, from the Bowman's capsule to the inner medullary collecting duct cells (Tsurumi et al., 2006). It has been shown that ATRAP is often an inhibitory partner of AT1R by, at least in part, impairing G-protein coupling to the receptor (Lopez-Ilasaca et al., 2003). However, it has also been reported that ATRAP can potentiate, instead of inhibiting, AT1R-mediated effects (Barro-Soria et al., 2012) and that ATRAP may also induce AT1R-independent actions (Mederle et al., 2016). The impact of ATRAP on AT1R/Ang II-mediated sodium homeostasis has been previously shown (Wakui et al., 2013; Ohsawa et al., 2014).

However, the potential role of ATRAP on Ang II-regulation of K^+ homeostasis remains to be established. Therefore, the present study aimed to test the hypothesis that ATRAP impacts Ang II-mediated ROMK regulation and if so, to gain insight into the potential underlying mechanisms.

MATERIALS AND METHODS

Reagents and Antibodies

Reagents were obtained from ThermoFisher Scientific (Rockford, IL, United States) unless otherwise noted. VU591, a specific ROMK inhibitor (Bhave et al., 2011), and dexamethasone were acquired from Sigma-Aldrich (St. Louis, MO, United States). Ang II was purchased from Tocris Bioscience (Bristol, United Kingdom). Anti-α-epithelial sodium channel (ENaC; C-20), anti-β-ENaC (E-10), and anti-γ-ENaC (H-110) antibodies were obtained from Santa Cruz Biotechnology (Santa Cruz, CA, United States). Anti-ROMK (SAB2501215), anti-V5 (R960-25), and anti-phospho-c-Src (#2101) antibodies were acquired from Sigma-Aldrich, ThermoFisher Scientific, and Cell Signaling (Beverly, MA, United States), respectively. Anti-GAPDH antibodies (Ab8245 and sc-20357) were obtained from Abcam and Santa Cruz Biotechnology. Horseradish peroxidase-conjugated antibodies were obtained from Jackson ImmunoResearch (West Grove, PA, United States).

Cell Culture

M-1 collecting duct cells (ATCC CRL-2038) were kindly provided by Dr. Per Svenningsen (University of South Denmark, Denmark) and maintained in 25-cm^2 tissue culture flasks in a 1:1 mixture of Dulbecco's modified Eagle's medium/Ham's F12 medium (DMEM/F12) supplemented by 100 U/ml penicillin, 100 μg/ml streptomycin, 0.5 mM sodium pyruvate, 5 μM dexamethasone, and 5% (v/v) heat-inactivated fetal bovine serum (FBS) as recommended by the supplier. Cultures were incubated in a humidified 95% air-5% CO_2 atmosphere at 37°C and subcultured by 0.25% trypsin-EDTA. Cells were seeded onto 24-well microplates for immunoblotting experiments or 96-well microplates for FluxOR assay experiments. Non-transfected cells were grown to confluence and then serum-starved for at least 72 h. Lysates from M-1 cells were immunoblotted with antibodies against the α subunit of ENaC and ROMK for cell line characterization (**Figures 1A,B**). Band sizes were predicted based on previous evidence (Hu et al., 2009; Murthy et al., 2016; Shimizu et al., 2017).

ATRAP Overexpression in M-1 Cells

M-1 ATRAP coding sequence was amplified using 5' primer and 3' primer containing Hind III and Not I restriction sequences, respectively (5'-ACACAAGCTTGGGATGGAGCTGCCTGCCGTGAAC-3' and 5'-ACACGCGGCC-GCGGTACCCCCGGGGGGCAGCTTG-3') and cloned into pcDNA6/V5-His vector (ThermoFisher). pAcGFP1-C1 (Clontech) was used to assess lipotransfection efficiency. Cultures were serum-deprived at ~90% confluence and lipotransfected with pcDNA6/V5-His/galactosidase (LacZ) control vector, encoding a β-galactosidase protein, or with pcDNA6/V5-His/ATRAP vector, both of them

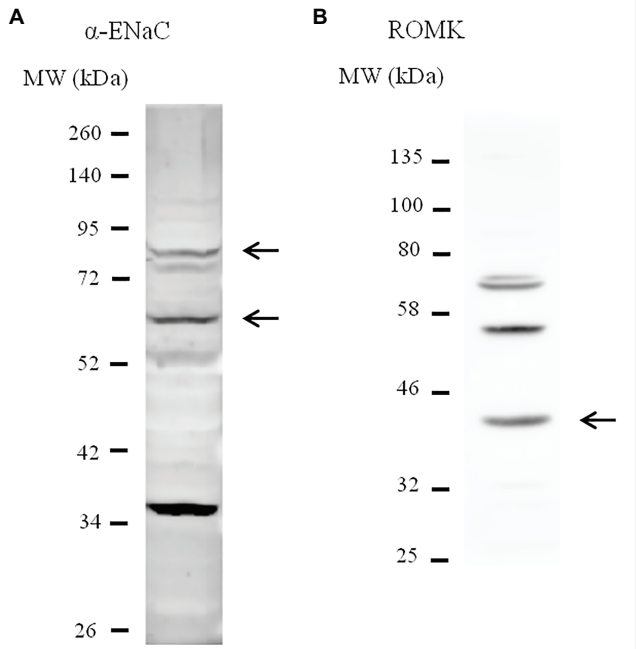

FIGURE 1 | Characterization of M-1 cell line by immunoblotting. Lysates from M-1 cells were immunoblotted with antibodies against anti-α-epithelial sodium channel (ENaC; **A**)and anti-renal outer medullary potassium (ROMK; **B**) for cell line characterization. Arrows indicate the predicted bands that represent each protein, including full-length and the cleaved form of α-ENaC.

tagged to V5-His at their C-termini. For every 2 cm^2 of cell culture, 2 μg of plasmid DNA and 1-2 μl lipofectamine 2000 were added to the serum-free medium for 24 h. Cells were then maintained in a serum-free medium for at least more 48 h before conducting functional experiments.

FluxOR Assay

Renal outer medullary potassium channel activity was assessed by a fluorescence-based microplate assay (FluxOR II Green Potassium Ion Channel Assay). The assay is based on the fact that thallium influx serves as a surrogate for K^+ channel and transporter activity and takes advantage of recently developed thallium-sensitive fluorophores (Beacham et al., 2010). The FluxOR assay was performed using the washing method recommended by the supplier, and bottom fluorescence intensity was assessed by end-point readout in the SynergyH1 microplate reader (Biotek, Winooski, VT).

SDS-PAGE and Immunoblotting

M-1 cells were solubilized by radioimmunoprecipitation assay (RIPA) buffer (140 mM NaCl, 1% Triton X-100, 0.1% sodium deoxycholate, 0.1% sodium dodecyl sulfate (SDS), and 10 mM Tris-HCl pH 8.0), supplemented with 5 mM EDTA, 1 mM EGTA, 0.2 mM PMSF, and protease cocktails [cOmplete, Mini, EDTA-free protease inhibitor cocktail (Roche) or Protease Inhibitor Cocktail P8340 (Sigma-Aldrich)]. Phosphatases inhibitor cocktails [P5726 and P0044 (Sigma-Aldrich)], at 1:150 dilution, were also added to RIPA buffer when assessing phospho-c-Src expression. Protein supernatants were obtained by centrifuging cell lysates at 14,000 rpm for 20 min. Protein quantification was performed using the BCA or Lowry assay. The appropriate amount of lysate was denatured by Laemmli buffer (2% SDS, 20% glycerol, 100 mM β-mercaptoethanol, and 0.1% bromophenol blue, and 50 mM Tris, pH 6.8). About 7.5–12%, SDS polyacrylamide gel electrophoresis (SDS-PAGE) was performed as described previously (Crajoinas et al., 2016). Proteins were transferred to polyvinylidene difluoride (PVDF) membranes (Millipore Immobilon-P, Bedford, MA) by the semi-dry system [Owl HEP-1 (ThermoFisher)] for 3 h at 400 mA or by wet transfer systems [TE 62 (GE Healthcare, Little Chalfont, United Kingdom)] overnight at 350 mA, 4°C. Western-immunoblotting experiments using V5 and phospho-c-Src antibodies were performed following the supplier's recommendations. For the remaining antibodies, PVDF membranes were blocked with TBST solution (5% nonfat dry milk and 0.1% Tween 20 in Tris-Buffered Saline (TBS), pH 7.4) for 1 h, and then incubated with the appropriate primary antibody overnight. Primary antibody dilutions were 1:500 for anti-ROMK, 1:1,000 for anti-phospho-c-Src, 1:1,000 for sc-20357, and 1:5,000 for Ab8245 and anti-V5. Membranes were then washed five times for 10 min and incubated with the respective secondary antibody at 1:2,000 dilution for 1 h. Densitometry analyses of digitized bands were performed by ImageJ software (National Institutes of Health, Bethesda, MD, United States).

Cell Surface Biotinylation

Cell surface biotinylation was performed to assess ROMK expression in the plasma membrane, as previously described (Carraro-Lacroix et al., 2010). LacZ- and ATRAP-overexpressing M-1 cells cultivated in six-well plates were treated with 10^{-10} M Ang II for 40 min before biotinylation protocol as previously described in detail (Carneiro De Morais et al., 2015). Biotinylated cells were then lysed by a modified RIPA buffer (150 mM NaCl, 50 mM Tris·HCl, 1% Triton X-100, 0.5% sodium deoxycholate, and 5 mM EDTA, pH 7.4) and 300 μg of the total cellular extract were incubated with 50 μl streptavidin-coupled agarose beads (#20347, ThermoFisher). After overnight incubation, streptavidin beads were washed with RIPA buffer for 15 min, followed by centrifugation at 10.000 rpm for 5 min. This washing step was repeated three times. Biotinylated proteins were then denatured from streptavidin beads by adding modified Laemmli buffer (2% SDS, 20% glycerol, 100 mM DTT, 0.1% bromophenol blue, 50 mM Tris, and pH 6.8) and heating samples at 98°C for 3 min. Solubilized biotinylated proteins were submitted to SDS-PAGE. Finally, we have also used 10 μg of the total cellular extract from each sample to assess total ROMK and GAPDH expression.

Statistical Analysis

Data are presented as mean ± SE. Statistical analyses were performed using GraphPad Prism 7.04. Groups were tested for normality by the Shapiro-Wilk test and homoscedasticity by the Brown-Forsythe test. When comparing three or more

groups, we used a parametric ANOVA test followed by Bonferroni *post hoc* test or nonparametric Kruskal-Wallis followed by Dunn's *post hoc* test. For comparison between two groups, we used an unpaired *t*-test.

RESULTS

Ang II Inhibits ROMK Activity in M-1 Cells

To assess whether K^+ transport in M-1 cells was responsive to Ang II, we employed the FluxOR assay, as described in Materials and Methods. Experiments were conducted in the presence or absence of the ROMK inhibitor VU591. As seen in **Figure 2A**, the K^+ conductance in non-transfected M-1 cells, measured as the thallium-induced fluorescence, was similarly reduced by Ang II at concentrations ranging from 10^{-9} to 10^{-12} M. The concentration of 10^{-10} M Ang II was chosen to be used in the subsequent experiments, an average urinary concentration of Ang II (Wang et al., 2003).

In order to assess whether the Ang II-mediated effect on K^+ conductance was induced by AT1R activation, M-1 cells were then pretreated with telmisartan (10^{-8} M) before exposing cells to vehicle or Ang II (10^{-10} M). As observed in **Figure 2B**, telmisartan pretreatment abrogates Ang II-induced inhibition of K^+ conductance. Finally, M-1 cells were also treated with Ang II or vehicle for 40 min in the presence or absence of 10 μM VU591. As illustrated in **Figure 2C**, the VU591 compound reduced K^+ conductance by ~45 ± 3% in comparison with vehicle-treated cells, underlining the critical role of the ROMK channel in apical K^+ conductance in M-1 cells. Similar to the findings of **Figure 2A**, Ang II decreased K^+ conductance by ~30 ± 6% compared to vehicle-treated M-1 cells. Importantly, VU591 and Ang II cotreatment did not induce an additive inhibitory effect on K^+ conductance, supporting the notion that Ang II-mediated modulation of K^+ transport in M-1 cells is due to the regulation of ROMK activity.

ATRAP Overexpression Attenuates the Ang II Inhibitory Effect on ROMK

The efficiency of M-1 transfection was evaluated by the emission of fluorescence in mock- or GFP-transfected M-1 cells and the efficacy of overexpression of ATRAP and recombinant β-LacZ was confirmed by immunoblotting using an anti-V5 antibody (**Figures 3A,B**). We then sought to examine the effect of overexpressing ATRAP in the Ang II-mediated ROMK inhibition in M-1 cells. As seen in **Figure 3C**, Ang II significantly reduced ROMK activity in control LacZ-M-1 cells (~29 ± 9%, $p < 0.05$), but not in ATRAP-overexpressing cells (~15 ± 2%), when compared to vehicle-treated LacZ-overexpressing M-1 cells.

Interestingly, a significant part of this discrete inhibitory effect in K^+ conductance observed in ATRAP-overexpressing M-1 cells is present at baseline conditions (8 ± 3% inhibition vs. vehicle-treated LacZ-overexpressing cells). In fact, when this difference at basal levels is taken into account, the magnitude of ROMK inhibition mediated by Ang II in ATRAP-overexpressing cells is only 7 ± 3% when compared to vehicle-treated ATRAP-overexpressing cells, an effect significantly smaller than that observed in LacZ-overexpressing cells (**Figure 3D**). These data collectively suggest that ATRAP overexpression attenuates Ang II-inhibition of ROMK but does not increase K^+ conductance at basal conditions.

ATRAP Overexpression Blunts Ang II-Induced Decrease of Cell Surface ROMK Expression

To assess whether the decrease of Ang II-induced inhibition of ROMK in ATRAP-overexpressing cells was associated with a reduction in ROMK expression at the plasma membrane, we evaluated ROMK expression plasma membrane by cell surface biotinylation. As presented in **Figures 4A,B**, after acute treatment with Ang II, Lac-Z overexpressing cells, but not ATRAP-overexpressing cells, showed a significant decrease in the ratio of surface ROMK to total ROMK expression, when compared to vehicle-treated LacZ-overexpressing cells (43 ± 8%, $p < 0.05$). It was observed that Ang II treatment caused a reduction of

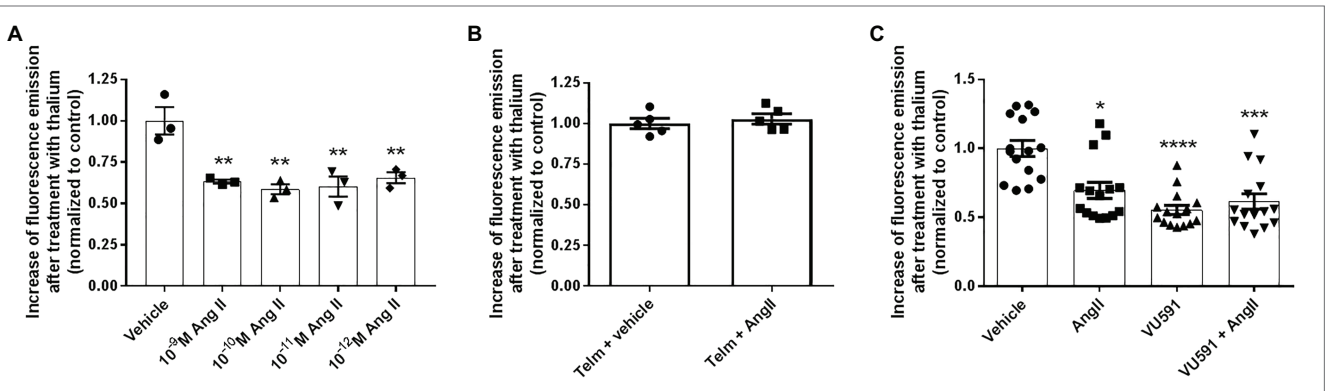

FIGURE 2 | Angiotensin II (Ang II) inhibits ROMK-mediated K^+ conductance in M-1 cells. **(A)** M-1 cells were treated with different Ang II concentrations or vehicle for 30 min ($n = 3$). $^{**}p < 0.01$ vs. vehicle-treated M-1 cells. The *p* value was calculated using ANOVA followed by the Bonferroni *post hoc* test. **(B)** M-1 cells were pretreated with telmisartan for 60 min and then treated with vehicle or Ang II (10^{-10} M) for 40 min. **(C)** M-1 cells were treated with Ang II (10^{-10} M) or vehicle in the presence or absence of the selective ROMK inhibitor VU591 (10 μM) for 40 min ($n = 15$). $^{*}p<0.05$; $^{***}p<0.001$; $^{****}p<0.0001$ vs. vehicle-treated M-1 cells. The *p* value was calculated by using the Kruskal-Wallis test, followed by Dunn's *post hoc* test.

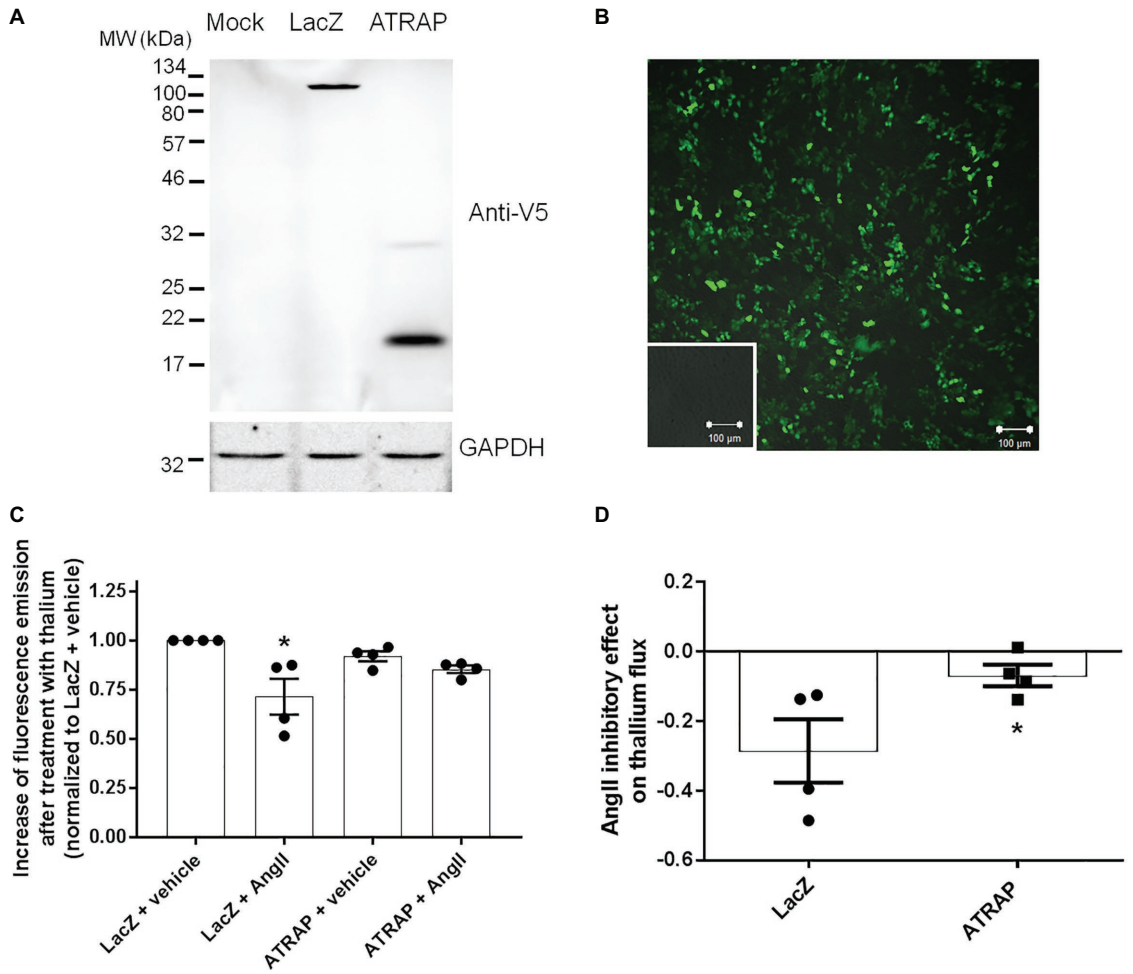

FIGURE 3 | Angiotensin II type 1 receptor-associated protein (ATRAP)-overexpression attenuates Ang II-mediated ROMK inhibition in M-1 cells. **(A)** Representative immunoblot of M-1 cells transfected with galactosidase (LacZ-V5) and ATRAP-V5 vectors probed with an anti-V5 antibody. **(B)** Evaluation of lipotransfection protocol efficiency in M-1 cells that were transfected with a GFP-encoding vector. Green fluorescence emission in M-1 cells was detected using a 505–550 nm filter in a confocal microscope after exciting GFP-transfected and mock-transfected M-1 cells at 488 nm laser light. Images were captured at 10x magnification. Mock-transfected M-1 cells are displayed in the inset. **(C)** K^+ conductance was determined as the increase of fluorescence emission after thallium incubation in M-1 cells overexpressing LacZ or ATRAP treated with 10^{-10} M Ang II or vehicle for 40 min ($n = 4$). *$p < 0.05$ vs. vehicle-treated LacZ M-1 cells. The p value was calculated by the Kruskal-Wallis test, followed by Dunn's *post hoc* test. **(D)** K^+ conductance inhibition by Ang II treatment in LacZ- and ATRAP-overexpressing M-1 cells. *$p < 0.05$ vs. LacZ-overexpressing M-1 cells, using unpaired t-test.

ROMK cell surface expression in only one out of four samples from ATRAP-overexpressing cells. As seen in **Figure 4C**, the mean Ang II-induced effect on reducing plasma membrane ROMK expression was just 6 ± 10% in the ATRAP-overexpressing group ($p < 0.05$ vs. LacZ-overexpressing cells). Finally, we also assessed total ROMK expression normalized to GAPDH expression, and no difference was observed among experimental groups (**Figure 4D**).

ATRAP Attenuates Activation of c-Src in the Presence and Absence of Ang II

The activation of the c-Src kinase by phosphorylation of the tyrosine 416 residue constitutes the central molecular mechanism of ROMK inhibition by Ang II (Yue et al., 2011). Thus, we next assessed whether modulation of c-Src activation could underlie the diminished response to Ang II in M-1 cells overexpressing ATRAP compared with LacZ- overexpressing M-1 cells. The representative immunoblot of phospho-c-Src in ATRAP and Lac-Z-overexpressed M-1 cells treated or not with 10^{-10} M Ang II is shown in **Figure 5A**. The phospho-c-Src levels were significantly elevated in LacZ-overexpressing M-1 cells treated with Ang II vs. vehicle-treated LacZ-overexpressing M-1 cells (**Figures 5A,B**). In contrast, phosphorylation of c-Src at tyrosine 416 significantly decreased in both vehicle- and Ang II-treated ATRAP-overexpressing M-1 cells compared to LacZ-overexpressing M-1 cells (**Figures 5A,B**).

DISCUSSION

Understanding kaliuresis regulation is crucial since plasma K^+ levels need to be kept within a narrow range for vital cellular functions.

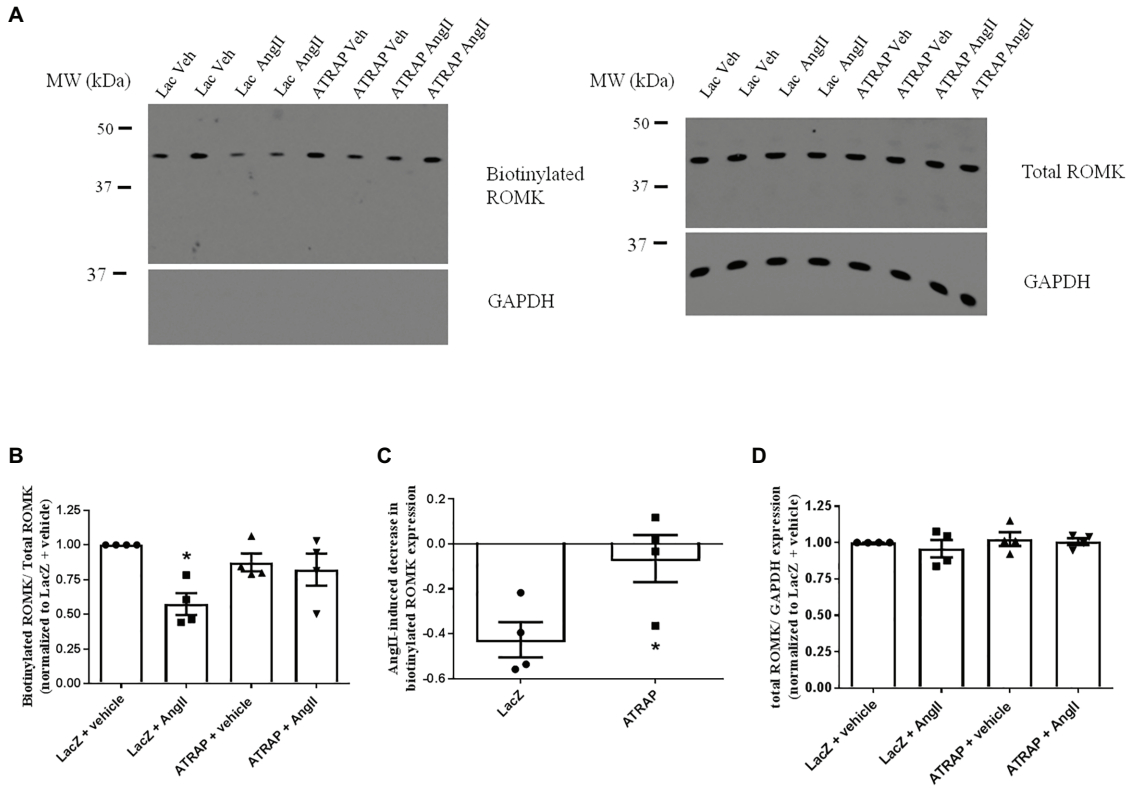

FIGURE 4 | AT1R-associated protein-overexpression blunts Ang II-mediated decrease of plasma membrane ROMK expression. M-1 cells overexpressing LacZ-V5 or ATRAP-V5 were treated with vehicle or 10^{-10} M Ang II for 30–40 min before assessing plasma membrane ROMK expression by biotinylation protocol. **(A)** Representative immunoblot image of biotinylated ROMK, total ROMK, and GAPDH. GAPDH was also used as a control to assess purity in biotinylated samples (**Supplementary Material**). **(B)** Densitometry analysis of bands from biotinylated ROMK (~45-kda) normalized to total ROMK expression ($n = 4$). As biotinylation protocol was performed in six-well plates, band intensities were normalized to each plate's respective control (vehicle-treated LacZ sample). *$p < 0.05$ vs. vehicle-treated LacZ-overexpressing M-1 cells, using Kruskal-Wallis test followed by Dunn's *post hoc* test. **(C)** Ang II-mediated reduction of ROMK expression at the plasma membrane in LacZ- and ATRAP-overexpressing M1-cells. *$p < 0.05$ vs. LacZ-overexpressing M-1 cells, using unpaired *t*-test. **(D)** Densitometry analysis of bands from total ROMK normalized to GAPDH expression ($n = 4$).

As the median K^+ consumption in modern western diets is ~50% of the recommended intake (Chen et al., 2006), understanding how kidneys are able to decrease kaliuresis is particularly important. It is well established that AT1R upregulation in collecting duct cells with consequent ROMK inhibition constitutes an essential mechanism for K^+ conservation during low-K^+ diets. Indeed, it has been demonstrated that rats fed a low K^+ diet and simultaneously treated with losartan do not exhibit a decrease in the number of ROMK-like channels in their collecting ducts and exhibit a higher reduction in plasma potassium levels during potassium restriction (Jin et al., 2009). Our study provides new evidence that the angiotensin receptor-associated protein ATRAP impacts K^+ conductance in collecting duct cells. More specifically, ATRAP counteracts the Ang II-mediated ROMK internalization and consequent inhibition in a collecting cell culture model. This effect is accompanied by decreases in c-Src Y416 phosphorylation, a critical signaling pathway for ROMK inhibition by Ang II.

Although p38 and ERK1/2 pathways seem to be part of AT1R-dependent inhibition of ROMK channels during LK diets (Babilonia et al., 2006; Jin et al., 2009), tyrosine phosphorylation of ROMK by c-Src is the most important signaling pathway directly responsible for ROMK inhibition during potassium restriction. While collecting ducts from rats fed LK diets do not show relevant ROMK-like small conductance K^+ currents, these same collecting ducts presented a significant increase in the number of ROMK-like channels in patch-clamp recordings when the collecting duct cells were acutely treated with c-Src inhibitor herbimicyn A for 30 min, an effect that does not occur in rats receiving HK diets (Wang et al., 2000, 2010). Also, in the collecting ducts from animals receiving LK diets, the acute treatment with c-Src inhibitor herbymicin A majorly abolishes the Ang II inhibitory effect over ROMK activity (Wei et al., 2007). Accordingly, in the present study, diminished response to Ang II in M-1 cells overexpressing ATRAP was accompanied by a decrease in c-Src phosphorylation at the tyrosine 416. Interestingly, we have observed lower activation of c-Src even in the vehicle-treated ATRAP-M1 cells, suggesting that ATRAP not only inhibits Ang II-mediated c-Src signaling but also evokes Ang II/AT1R-independent modulation of this kinase. It has been previously shown that ATRAP can regulate signaling pathways in the absence of Ang II. Interestingly, ATRAP interacts with the multiscaffolding RACK1 (Wang et al., 2002), a protein that is also detected in AT1R immunocomplexes (Parent et al., 2008) and is associated with c-Src sequestration (Kiely et al., 2005). Since

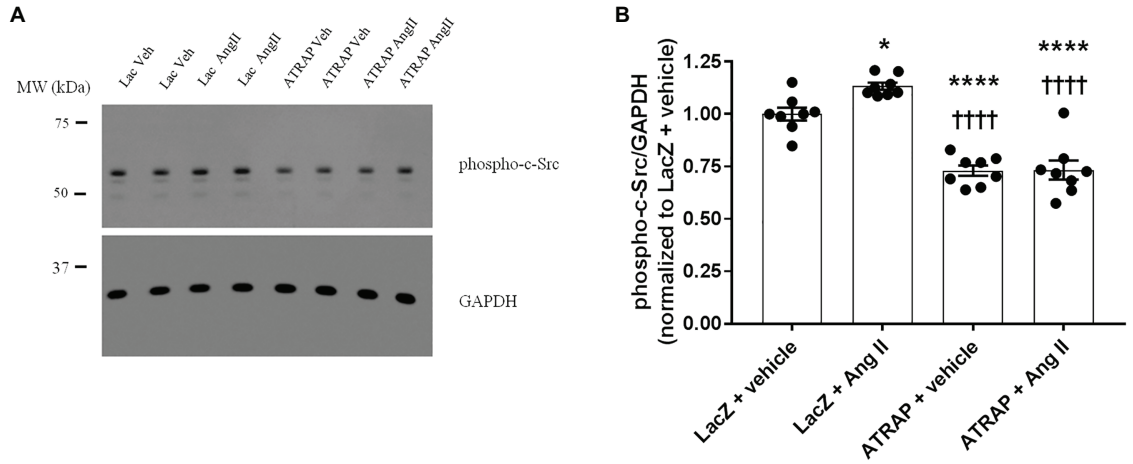

FIGURE 5 | The effect of Ang II on the levels of phospho-c-Src in radioimmunoprecipitation assay (RIPA)-soluble lysates from M-1 cells overexpressing LacZ and ATRAP protein. M-1 cells overexpressing LacZ-V5 and ATRAP-V5 were acutely treated with vehicle or 10^{-10} M Ang II for 15 min and assessed for c-Src phosphorylation status. **(A)** Representative immunoblot of phospho-c-Src (**Supplementary Material**). **(B)** Graphical representation of the ratio of phosphorylated Src to GAPDH ($n = 8$). *$p < 0.05$; ****$p < 0.0001$ vs. vehicle-treated LacZ-M-1 cells. ††††$p < 0.0001$ vs. Ang II-treated-LacZ-M-1 cells. All statistical analyses were performed using ANOVA, followed by Bonferroni *post hoc* test.

RACK1 is not an integral membrane protein, ATRAP might recruit RACK1 to the plasma membrane, which would favor c-Src inactivation, even without Ang II involvement.

Albeit ATRAP overexpression *per se* decreased c-Src phosphorylation, we did not observe increased ROMK activity in the vehicle-treated ATRAP overexpressed-M1 cells. This finding could be expected considering the effect of c-Src inhibition by herbymicin A in collecting duct cells from animals fed an LK diet. Other AT1R-independent effects mediated by ATRAP or cellular compensatory mechanisms might take place in such a way that K^+ channel activity does not change in cells overexpressing ATRAP despite the reduction in c-Src activation. This observation resembles what was observed for the ATRAP-mediated effect on cardiomyocyte Ca^{2+} signaling (Mederle et al., 2016). The authors found that ATRAP stimulates SERCA2a and accelerates calcium sequestration into the endoplasmic reticulum *in vitro*, which improves ventricular relaxing and filling. However, ATRAP knockout cells also had an unexpectedly lower basal intracellular Ca^{2+} concentration, which led the authors to postulate that ATRAP could regulate other calcium homeostasis mechanisms at basal conditions. When these basal differences were not considered, the ATRAP effect over physiological relevant calcium transients was somewhat masked. Accordingly, when we take into account the modest basal variations of K^+ conductance between LacZ and ATRAP-overexpressing cells, the inhibitory effect of Ang II on ROMK is even lower in the ATRAP-overexpressing M-1 cells (7% inhibition in ATRAP-overexpressing group, in comparison to a 29% inhibitory effect of Ang II in LacZ-overexpressing cells).

It is known that ROMK inhibition by c-Src is not directly caused by channel phosphorylation. Previous studies demonstrated that ROMK inhibition by exogenous c-Src was only seen in cell-attached patches but not in isolated patches. This inhibitory effect was associated with phosphorylation of tyrosine 337 of the channel and was abolished by agents that inhibit endocytosis (Wang et al., 2000; Moral et al., 2001). Therefore, ROMK inhibition by c-Src is mediated by phosphorylation and consequent internalization of the channel. In line with these observations, we observed that Ang II treatment induced a significant decrease in plasma membrane expression of ROMK in LacZ-overexpressing cells, but not in ATRAP-overexpressing cells, and the level of changes observed in ROMK activity assay somehow resembles what we have observed in biotinylation experiments. It is worth mentioning that previous studies assessing ROMK inhibition by AT1R/Ang II have deduced ROMK internalization by single-channel patch-clamp experiments and further analysis of NPo products (Wei et al., 2007; Jin et al., 2009; Wang et al., 2010). Therefore, the present study provides novel molecular evidence that Ang II reduces ROMK cell surface expression in collecting duct cells.

Whereas the ATRAP's impact on sodium balance and volemic homeostasis has been shown in different studies, particularly during Ang II-induced hypertension (Ohsawa et al., 2014), its implications for kaliuresis regulation are unknown. K^+ conservation through ROMK inhibition is an essential mechanism for K^+ homeostasis without evoking other electrolyte imbalances. When such a regulatory mechanism is not enough to maintain K^+ balance during LK diets, the consequent decreases of extracellular K^+ levels induce hyperactivation of NCC transporter, thus linking K^+ restriction to hypertension (Terker et al., 2015). Therefore, it is possible that differential regulation of ROMK by Ang II/AT1R and ATRAP in collecting ducts that we found here may have consequences in serum K^+ levels and could impact not only K^+ homeostasis but also pressure outcomes in K^+-restricted diets. In this regard, Yap et al. (2017) have observed that the polymorphism A1166C at the 3'-UTR of the AT1R gene correlates with alterations in blood pressure that seems dependent on K^+ intake in healthy Malaysian adults. Subjects with the genotype AA, associated with lower

expression of AT1R (Sethupathy et al., 2007; Chandra et al., 2014), showed higher systolic and diastolic blood pressure when their K^+ intakes were low. Also, He et al. (2011) observed that this genotype was also associated with higher blood pressure decline after potassium supplementation in Chinese subjects. It remains to be established whether such changes in blood pressure during dietary K^+ restriction may also be associated with genetic variations in other RAS components, including ATRAP.

The impact of differential regulation of ATRAP on ROMK regulation and, consequently, on K^+ homeostasis and blood pressure control could resemble some effects of losartan treatment observed during poor-K^+ diets (Jin et al., 2009). As aforementioned, losartan treatment increases kaliuresis and exacerbates hypokalemia during the LK diet in rats (Jin et al., 2009). This condition could also upregulate NCC activity and, by doing so, attenuate the natriuretic effect of such a drug. Interestingly, the K^+-rich DASH diet amplifies losartan treatment response, particularly in African-American subjects, so that the combined treatment is more than additive (Conlin et al., 2003). It is known that African-Americans represent a population that has diminished blood pressure response to AT1 receptor blockers and, at the same time, increased blood pressure response to thiazides (Brewster and Seedat, 2013). Notably, a genetic study reported that, for African-American women, such increased thiazide response was associated with the genotype AA of the polymorphism A1166C (Frazier et al., 2004). Taking these studies into account and considering ATRAP effects on ROMK regulation, the classical hypotensive effect of ATRAP reported in normal-K^+ diets could be blunt during diets with a modest or more severe K^+ restriction.

On the other hand, during HK diets, ATRAP might be an important component determining the K^+ secretion capacity of collecting ducts. Interestingly, Wei et al. (2014) observed that CCDs from rats submitted to HK rats and pretreated with AT2R antagonists did not show a decreased ROMK activity after AngII treatment. This observation suggests that collecting duct AT1R during HK settings is not responsive to modulate ROMK activity. Notably, AT1R expression, assessed at the transcriptional level, was not decreased during the HK diet. It would be interesting to evaluate further whether ATRAP is upregulated in CCDs during HK diets, which might explain these previous observations made by Wei and colleagues. Although our *in vitro* observations give us direct evidence of ATRAP's ability to attenuate AT1R-mediated ROMK inhibition, further *in vivo* works will be important for assessing how ATRAP is modulated during changes in potassium intake and how CCD-specific ATRAP transgenic animals respond to potassium dietary changes, for instance. These analyses will address ATRAP's physiological impact on potassium balance and might help us to explain previous physiological observations in this field.

In conclusion, our study demonstrates that ATRAP can counteract Ang II-mediated inhibition of ROMK activity and might then be a relevant protein regulating K^+ handling. As depicted in **Figure 6**, K^+ conductance is inhibited in

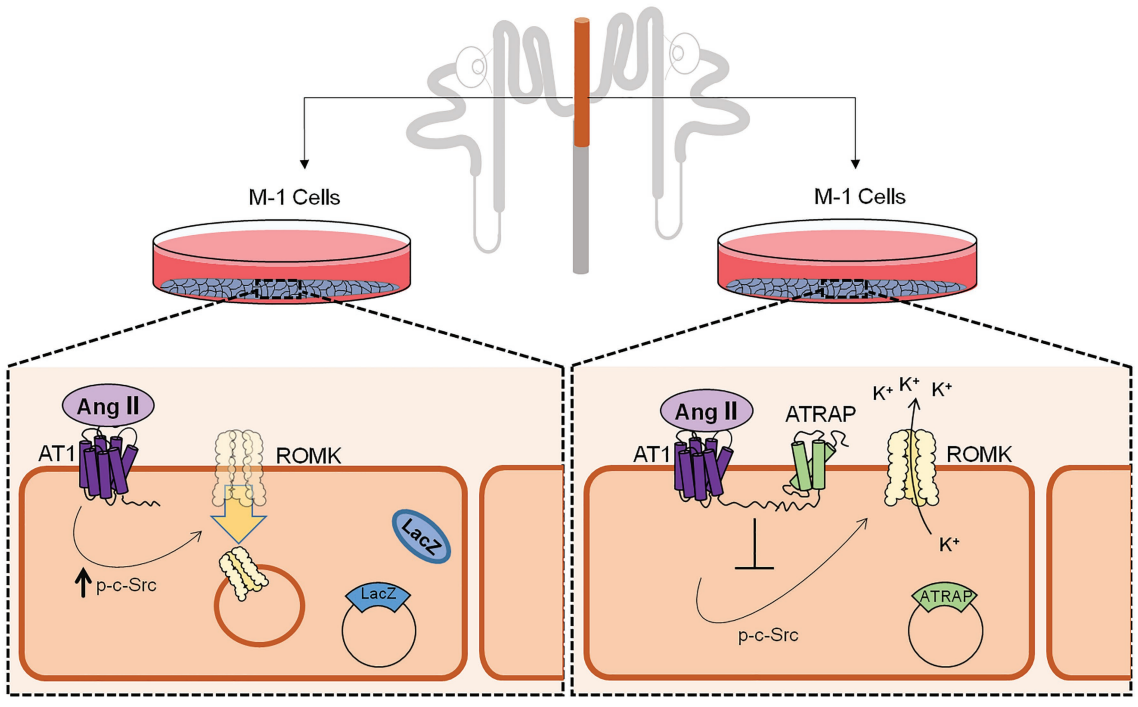

FIGURE 6 | Schematic representation of ATRAP-mediated actions on c-Src phosphorylation status, ROMK expression at the plasma membrane, and ROMK activity. M-1 cells overexpressing control LacZ protein has a decreased K^+ conductance after Ang II treatment, an effect that was associated with lower expression of ROMK at the plasma membrane and induction of c-Src phosphorylation, the classical signaling pathway for ROMK inhibition by Ang II. Conversely, M-1 cells overexpressing the ATRAP do not show significant decreases in K^+ conductance after Ang II treatment and plasma membrane ROMK expression, which was also associated with a blunted response of c-Src phosphorylation.

LacZ-overexpressing M-1 cells treated with Ang II. In contrast, this response is blunted in M1 cells overexpressing ATRAP. Accordingly, this differential response is accompanied by a decrease in the expression of ROMK channels at the plasma membrane of LacZ-overexpressing M-1 cells, but not in ATRAP-overexpressing cells. Finally, blunted response to Ang II in ATRAP-overexpressing M1 cells is associated with diminished c-Src phosphorylation signaling, a pathway that seems to be critically involved in ROMK endocytosis. Future studies should be performed in animal models to evaluate the impact of differential ATRAP expression in K^+ homeostasis during different changes of K^+ dietary content. Moreover, it would be interesting to assess how polymorphisms in ATRAP could be associated with changes in plasma K^+ levels and/or in blood pressure during K^+-poor diets in different human populations.

DATA AVAILABILITY STATEMENT

The raw data supporting the conclusions of this article will be made available by the authors, without undue reservation.

AUTHOR CONTRIBUTIONS

AG and NR designed the study. JP carried out the experiments, analyzed the data, wrote the manuscript, and prepared the figures. All authors contributed to the article and approved the submitted version.

FUNDING

This work was supported by grants 2013/11093-0 and 2016/22140-7 from the São Paulo Research Foundation (FAPESP) and by the Coordination for the Improvement of Higher Education Personnel (CAPES) – Finance Code 001.

SUPPLEMENTARY MATERIAL

The Supplementary Material for this article can be found online at: https://www.frontiersin.org/articles/10.3389/fphys.2021.642409/full#supplementary-material

REFERENCES

Babilonia, E., Li, D., Wang, Z., Sun, P., Lin, D. H., Jin, Y., et al. (2006). Mitogen-activated protein kinases inhibit the ROMK (Kir 1.1)-like small conductance K channels in the cortical collecting duct. *J. Am. Soc. Nephrol.* 17, 2687–2696. doi: 10.1681/ASN.2006050426

Barro-Soria, R., Stindl, J., Müller, C., Foeckler, R., Todorov, V., Castrop, H., et al. (2012). Angiotensin-2-mediated Ca2+ signaling in the retinal pigment epithelium: role of angiotensin-receptor-associated-protein and TRPV2 channel. *PLoS One* 7:e49624. doi: 10.1371/journal.pone.0049624

Beacham, D. W., Blackmer, T., O'Grady, M., and Hanson, G. T. (2010). Cell-based potassium ion channel screening using the FluxOR assay. *J. Biomol. Screen.* 15, 441–446. doi: 10.1177/1087057109359807

Bhave, G., Chauder, B. A., Liu, W., Dawson, E. S., Kadakia, R., Nguyen, T. T., et al. (2011). Development of a selective small-molecule inhibitor of Kir1.1, the renal outer medullary potassium channel. *Mol. Pharmacol.* 79, 42–50. doi: 10.1124/mol.110.066928

Brewster, L. M., and Seedat, Y. K. (2013). Why do hypertensive patients of African ancestry respond better to calcium blockers and diuretics than to ACE inhibitors and β-adrenergic blockers? A systematic review. *BMC Med.* 11:141. doi: 10.1186/1741-7015-11-141

Carneiro De Morais, C. P., Polidoro, J. Z., Ralph, D. L., Pessoa, T. D., Oliveira-Souza, M., Barauna, V. G., et al. (2015). Proximal tubule NHE3 activity is inhibited by beta-arrestin-biased angiotensin II type 1 receptor signaling. *Am. J. Phys. Cell Phys.* 309, C541–C550. doi: 10.1152/ajpcell.00072.2015

Carraro-Lacroix, L. R., Lessa, L. M. A., Bezerra, C. N. A., Pessoa, T. D., Souza-Menezes, J., Morales, M. M., et al. (2010). Role of CFTR and ClC-5 in modulating vacuolar H+-ATPase activity in kidney proximal tubule. *Cell. Physiol. Biochem.* 26, 563–576. doi: 10.1159/000322324

Chandra, S., Narang, R., Sreenivas, V., Bhatia, J., Saluja, D., and Srivastava, K. (2014). Association of angiotensin II type 1 receptor (A1166C) gene polymorphism and its increased expression in essential hypertension: a case-control study. *PLoS One* 9:e101502. doi: 10.1371/journal.pone.0101502

Chen, P., Guzman, J. P., Leong, P. K., Yang, L. E., Perianayagam, A., Babilonia, E., et al. (2006). Modest dietary K+ restriction provokes insulin resistance of cellular K+ uptake and phosphorylation of renal outer medulla K+ channel without fall in plasma K+ concentration. *Am. J. Phys. Cell Phys.* 290, C1355–C1363. doi: 10.1152/ajpcell.00501.2005

Conlin, P. R., Erlinger, T. P., Bohannon, A., Miller, E. R., Appel, L. J., Svetkey, L. P., et al. (2003). The DASH diet enhances the blood pressure response to losartan in hypertensive patients. *Am. J. Hypertens.* 16, 337–342. doi: 10.1016/S0895-7061(03)00056-6

Crajoinas, R. O., Polidoro, J. Z., Carneiro De Morais, C. P. A., Castelo-Branco, R. C., and Girardi, A. C. C. (2016). Angiotensin II counteracts the effects of cAMP/PKA on NHE3 activity and phosphorylation in proximal tubule cells. *Am. J. Phys. Cell Phys.* 311, C768–C776. doi: 10.1152/ajpcell.00191.2016

Frazier, L., Turner, S. T., Schwartz, G. L., Chapman, A. B., and Boerwinkle, E. (2004). Multilocus effects of the renin-angiotensin-aldosterone system genes on blood pressure response to a thiazide diuretic. *Pharm. J.* 4, 17–23. doi: 10.1038/sj.tpj.6500215

He, J., Gu, D., Kelly, T. N., Hixson, J. E., Rao, D. C., Jaquish, C. E., et al. (2011). Genetic variants in the renin-angiotensin-aldosterone system and blood pressure responses to potassium intake. *J. Hypertens.* 29, 1719–1730. doi: 10.1097/HJH.0b013e32834a4d1f

Hu, J. C., Bengrine, A., Lis, A., and Awayda, M. S. (2009). Alternative mechanism of activation of the epithelial na+ channel by cleavage. *J. Biol. Chem.* 284, 36334–36345. doi: 10.1074/jbc.M109.032870

Jin, Y., Wang, Y., Wang, Z. J., Lin, D. H., and Wang, W. H. (2009). Inhibition of angiotensin type 1 receptor impairs renal ability of K conservation in response to K restriction. *Am. J. Physiol. Ren. Physiol.* 296, F1179–F1184. doi: 10.1152/ajprenal.90725.2008

Kiely, P. A., Leahy, M., O'gorman, D., and O'connor, R. (2005). RACK1-mediated integration of adhesion and insulin-like growth factor I (IGF-I) signaling and cell migration are defective in cells expressing an IGF-I receptor mutated at tyrosines 1250 and 1251. *J. Biol. Chem.* 280, 7624–7633. doi: 10.1074/jbc.M412889200

Lopez-Ilasaca, M., Liu, X., Tamura, K., and Dzau, V. J. (2003). The angiotensin II type I receptor-associated protein, ATRAP, is a transmembrane protein and a modulator of angiotensin II signaling. *Mol. Biol. Cell* 14, 5038–5050. doi: 10.1091/mbc.e03-06-0383

Malnic, G., Klose, R. M., and Giebisch, G. (1964). Micropuncture study of renal potassium excretion in the rat. *Am. J. Phys.* 206, 674–686.

Mcdonough, A. A., and Youn, J. H. (2017). Potassium homeostasis: the knowns, the unknowns, and the health benefits. *Physiology* 32, 100–111. doi: 10.1152/physiol.00022.2016

Mederle, K., Gess, B., Pluteanu, F., Plackic, J., Tiefenbach, K. J., Grill, A., et al. (2016). The angiotensin receptor-associated protein Atrap is a stimulator of the cardiac Ca2+-ATPase SERCA2a. *Cardiovasc. Res.* 110, 359–370. doi: 10.1093/cvr/cvw064

Moore-Ede, M. C. (1986). Physiology of the circadian timing system: predictive versus reactive homeostasis. *Am. J. Phys.* 250, R737–R752. doi: 10.1152/ajpregu.1986.250.5.R737

Moral, Z., Dong, K., Wei, Y., Sterling, H., Deng, H., Ali, S., et al. (2001). Regulation of ROMK1 channels by protein-tyrosine kinase and -tyrosine phosphatase. *J. Biol. Chem.* 276, 7156–7163. doi: 10.1074/jbc.M008671200

Murthy, M., Kurz, T., and O'shaughnessy, K. M. (2016). ROMK expression remains unaltered in a mouse model of familial hyperkalemic hypertension caused by the CUL3Δ403-459 mutation. *Phys. Rep.* 4:e12850. doi: 10.14814/phy2.12850

Ohsawa, M., Tamura, K., Wakui, H., Maeda, A., Dejima, T., Kanaoka, T., et al. (2014). Deletion of the angiotensin II type 1 receptor-associated protein enhances renal sodium reabsorption and exacerbates angiotensin II-mediated hypertension. *Kidney Int.* 86, 570–581. doi: 10.1038/ki.2014.95

Parent, A., Laroche, G., Hamelin, E., and Parent, J. L. (2008). RACK1 regulates the cell surface expression of the G protein-coupled receptor for thromboxane A(2). *Traffic* 9, 394–407. doi: 10.1111/j.1600-0854.2007.00692.x

Sethupathy, P., Borel, C., Gagnebin, M., Grant, G. R., Deutsch, S., Elton, T. S., et al. (2007). Human microRNA-155 on chromosome 21 differentially interacts with its polymorphic target in the AGTR1 3' untranslated region: a mechanism for functional single-nucleotide polymorphisms related to phenotypes. *Am. J. Hum. Genet.* 81, 405–413. doi: 10.1086/519979

Shimizu, A., Shiratori, I., Horii, K., and Waga, I. (2017). Molecular evolution of versatile derivatives from a GFP-like protein in the marine copepod *Chiridius poppei*. *PLoS One* 12:e0181186. doi: 10.1371/journal.pone.0181186

Terker, A. S., Zhang, C., Mccormick, J. A., Lazelle, R. A., Meermeier, N. P., Siler, D. A., et al. (2015). Potassium modulates electrolyte balance and blood pressure through effects on distal cell voltage and chloride. *Cell Metab.* 21, 39–50. doi: 10.1016/j.cmet.2014.12.006

Tsurumi, Y., Tamura, K., Tanaka, Y., Koide, Y., Sakai, M., Yabana, M., et al. (2006). Interacting molecule of AT1 receptor, ATRAP, is colocalized with AT1 receptor in the mouse renal tubules. *Kidney Int.* 69, 488–494. doi: 10.1038/sj.ki.5000130

Unwin, R. J., Luft, F. C., and Shirley, D. G. (2011). Pathophysiology and management of hypokalemia: a clinical perspective. *Nat. Rev. Nephrol.* 7, 75–84. doi: 10.1038/nrneph.2010.175

Wakui, H., Tamura, K., Masuda, S.-I., Tsurumi-Ikeya, Y., Fujita, M., Maeda, A., et al. (2013). Enhanced angiotensin receptor-associated protein in renal tubule suppresses angiotensin-dependent hypertension. *Hypertension* 61, 1203–1210. doi: 10.1161/HYPERTENSIONAHA.111.00572

Wang, W. H., and Giebisch, G. (2009). Regulation of potassium (K) handling in the renal collecting duct. *Pflugers Arch.* 458, 157–168. doi: 10.1007/s00424-008-0593-3

Wang, W., Huang, Y., Zhou, Z., Tang, R., Zhao, W., Zeng, L., et al. (2002). Identification and characterization of AGTRAP, a human homolog of murine angiotensin II receptor-associated protein (Agtrap). *Int. J. Biochem. Cell Biol.* 34, 93–102. doi: 10.1016/S1357-2725(01)00094-2

Wang, W., Lerea, K. M., Chan, M., and Giebisch, G. (2000). Protein tyrosine kinase regulates the number of renal secretory K channels. *Am. J. Physiol. Ren. Physiol.* 278, F165–F171. doi: 10.1152/ajprenal.2000.278.1.F165

Wang, C. T., Navar, L. G., and Mitchell, K. D. (2003). Proximal tubular fluid angiotensin II levels in angiotensin II-induced hypertensive rats. *J. Hypertens.* 21, 353–360. doi: 10.1097/00004872-200302000-00027

Wang, Z. J., Sun, P., Xing, W., Pan, C., Lin, D. H., and Wang, W. H. (2010). Decrease in dietary K intake stimulates the generation of superoxide anions in the kidney and inhibits K secretory channels in the CCD. *Am. J. Physiol. Ren. Physiol.* 298, F1515–F1522. doi: 10.1152/ajprenal.00502.2009

Wei, Y., Liao, Y., Zavilowitz, B., Ren, J., Liu, W., Chan, P., et al. (2014). Angiotensin II type 2 receptor regulates ROMK-like K^+ channel activity in the renal cortical collecting duct during high dietary K^+ adaptation. *Am. J. Physiol. Ren. Physiol.* 307, F833–F843. doi: 10.1152/ajprenal.00141.2014

Wei, Y., Zavilowitz, B., Satlin, L. M., and Wang, W. H. (2007). Angiotensin II inhibits the ROMK-like small conductance K channel in renal cortical collecting duct during dietary potassium restriction. *J. Biol. Chem.* 282, 6455–6462. doi: 10.1074/jbc.M607477200

Welling, P. A., and Ho, K. (2009). A comprehensive guide to the ROMK potassium channel: form and function in health and disease. *Am. J. Physiol. Ren. Physiol.* 297, F849–F863. doi: 10.1152/ajprenal.00181.2009

Yap, R. W. K., Shidoji, Y., Yap, W. S., and Masaki, M. (2017). Association and interaction effect of AGTR1 and AGTR2 gene polymorphisms with dietary pattern on metabolic risk factors of cardiovascular disease in malaysian adults. *Nutrients* 9:853. doi: 10.3390/nu9080853

Yue, P., Sun, P., Lin, D. H., Pan, C., Xing, W., and Wang, W. (2011). Angiotensin II diminishes the effect of SGK1 on the WNK4-mediated inhibition of ROMK1 channels. *Kidney Int.* 79, 423–431. doi: 10.1038/ki.2010.380

Conflict of Interest: The authors declare that the research was conducted in the absence of any commercial or financial relationships that could be construed as a potential conflict of interest.

frontiers in Physiology

ORIGINAL RESEARCH
published: 09 June 2021
doi: 10.3389/fphys.2021.656460

Antiproteinuric and Hyperkalemic Mechanisms Activated by Dual Versus Single Blockade of the RAS in Renovascular Hypertensive Rats

*José Wilson N. Corrêa[1,2], Karoline R. Boaro[1], Letícia B. Sene[1], Juliano Z. Polidoro[1], Thiago A. Salles[1], Flavia L. Martins[1], Lusiane M. Bendhack[3] and Adriana C. C. Girardi[1]**

[1] Laboratory of Genetics and Molecular Cardiology, Heart Institute (InCor) University of São Paulo Medical School, São Paulo, Brazil, [2] Department of Physiological Sciences, Institute of Biological Sciences, Federal University of Amazonas, Manaus, Brazil, [3] Faculty of Pharmaceutical Sciences of Ribeirão Preto, University of São Paulo, Ribeirão Preto, Brazil

This study aimed to investigate the antiproteinuric and hyperkalemic mechanisms activated by dual renin-angiotensin system (RAS) blockade in renovascular hypertensive rats (2-kidney 1-clip model [2K-1C]). Six weeks after clipping the left renal artery or sham operation (2K), rats were treated with losartan, enalapril, or both drugs for two weeks. We found that 2K-1C rats displayed higher tail-cuff blood pressure (BP), increased non-clipped kidney Ang II concentration, and more pronounced urinary albumin excretion than 2K. BP was decreased by the treatment with either enalapril or losartan, and the combination of both drugs promoted an additional antihypertensive effect in 2K-1C rats. Renal Ang II content and albuminuria were reduced by either enalapril or losartan in monotherapy and restored to control levels by dual RAS blockade. Albuminuria in 2K-1C rats was accompanied by downregulation of the glomerular slit protein podocin, reduction of the endocytic receptors megalin and cubilin, and a marked decrease in the expression of the ClC-5 chloride channel, compared to 2K animals. Treatment with losartan and enalapril in monotherapy or combination increased the expression of podocin, cubilin, and ClC-5. However, only the combined therapy normalized podocin, cubilin, and ClC-5 protein abundance in the non-clipped kidney of 2K-1C rats. Renovascular hypertensive 2K-1C rats had a lower concentration of plasma potassium compared to 2K rats. Single RAS blockade normalized potassium plasma concentration, whereas 2K-1C rats treated with dual RAS blockade exhibited hyperkalemia. Hypokalemia in 2K-1C rats was accompanied by an increase in the cleaved activated forms of α-ENaC and γ-ENaC and the expression of β-ENaC. Combined RAS blockade but not monotherapy significantly reduced the expression of these ENaC subunits in 2K-1C rats. Indeed, double RAS blockade reduced the abundance of cleaved-α-ENaC to levels lower than those of 2K rats. Collectively, these results demonstrate that the antiproteinuric effect of dual RAS blockade in 2K-1C rats is associated with the restored abundance of podocin and cubilin, and ClC-5. Moreover, double RAS blockade-induced hyperkalemia may be due, at least partially, to an exaggerated downregulation of cleaved α-ENaC in the non-clipped kidney of renovascular hypertensive rats.

Keywords: proteinuria, hypertension, podocin, cubilin, ClC-5 chloride channel, epithelial sodium channel, hyperkalemia, angiotensin II

OPEN ACCESS

Edited by:
Guiomar Nascimento Gomes, Federal University of São Paulo, Brazil

Reviewed by:
Lisa M. Harrison-Bernard, Louisiana State University Health Sciences Center New Orleans, United States
Oleh Pochynyuk, University of Texas Health Science Center at Houston, United States

****Correspondence:***
Adriana C. C. Girardi
adriana.girardi@incor.usp.br

Specialty section:
This article was submitted to Renal and Epithelial Physiology, a section of the journal Frontiers in Physiology

Received: *20 January 2021*
Accepted: *09 April 2021*
Published: *09 June 2021*

Citation:
Corrêa JWN, Boaro KR, Sene LB, Polidoro JZ, Salles TA, Martins FL, Bendhack LM and Girardi ACC (2021) Antiproteinuric and Hyperkalemic Mechanisms Activated by Dual Versus Single Blockade of the RAS in Renovascular Hypertensive Rats. Front. Physiol. 12:656460. doi: 10.3389/fphys.2021.656460

INTRODUCTION

The renin-angiotensin system (RAS) plays a crucial role in blood pressure (BP) control. However, abnormal stimulation of RAS components, ultimately leading to the upregulation of angiotensin II (Ang II) and activation of its angiotensin receptor type 1 (AT1R), contribute to the development and progression of hypertension (Crowley et al., 2005, 2006). Not surprisingly, pharmacological antagonists of the RAS, such as angiotensin-converting enzyme inhibitors (ACEi) or AT1R blockers (ARBs), constitute classical therapeutic approaches to control hypertension and end-organ damage, including the kidney (Carson et al., 2001; Dahlof et al., 2002; Viazzi et al., 2016). Interestingly, because of the "escape phenomenon" (Athyros et al., 2007), ACEi and ARB alone may not be sufficient to fully block the RAS. Indeed, evidence suggests that the combined use of ACEi and ARBs is superior to monotherapy for BP control and proteinuria reduction (Kunz et al., 2008; Mann et al., 2008). Nevertheless, it may also be associated with increased adverse effects (Doulton et al., 2005; Mann et al., 2008).

Proteinuria is a well-documented risk factor and predictor of progression to end-stage renal disease and cardiovascular disease (Lassila et al., 2004). The regulation of the expression of key proteins of the glomerular filtration barrier and the apical endocytic machinery in the renal proximal tubule is impaired in hypertension, producing increased urinary protein excretion (Tanaka and Nakaki, 2004; Inoue et al., 2013; Arruda-Junior et al., 2014; Berger et al., 2015; Seccia et al., 2017; Lopes et al., 2020). Lesions in the glomerular slit diaphragm, an intercellular junction between podocytes' foot processes, are particularly important for establishing proteinuria (Wharram et al., 2005; Grahammer et al., 2013). Accordingly, renovascular-hypertensive rats exhibit increased proteinuria compared to normotensive rats, which is associated with downregulation of the podocin expression (Lopes et al., 2020). RAS status also seems important for glomerular integrity fate, as evidenced by studies with rats receiving Ang II chronic pressor doses. These animals presented podocyte apoptosis, reduction of nephrin protein abundance, and, as a result, proteinuria (Jia et al., 2008). Nonetheless, proteinuria in hypertensive models such as the spontaneously hypertensive rat (SHR) appears to be, at least in part, caused by a dysregulation of the proximal tubule endocytic machinery (Tanaka and Nakaki, 2004; Inoue et al., 2013). This macromolecular complex, comprised of megalin, cubilin, and the chloride channel ClC-5 (Gekle, 2005; Birn and Christensen, 2006; Hryciw et al., 2006; Pollock and Poronnik, 2007; Nielsen et al., 2016), among other components, is responsible for internalizing low molecular weight proteins capable of passing through the slit diaphragm. In this regard, SHRs exhibit lower expression of cubilin, megalin, ClC-5, and vH^+-ATPase B2 subunit in the renal cortex compared to age-matched normotensive rats (Inoue et al., 2013). RAS upregulation might be important in the pathophysiology of proximal tubular proteinuria beyond high BP since the treatment of SHRs with losartan versus hydralazine produced upregulation of megalin expression in the renal proximal tubule, an effect that was accompanied by a much greater reduction in proteinuria. However, both antihypertensives displayed similar BP effects (Arruda-Junior et al., 2014). Despite the evidence of RAS modulating glomerular and proximal tubule handling of proteins, the molecular mechanisms that mediate the additive antiproteinuric effects of dual versus single blockade of the RAS remain to be established.

Clinical studies designed to evaluate the effects of the combination of ACEi and ARBs revealed additional side effects such as hyperkalemia and hypotension (Pfeffer et al., 2003; Phillips et al., 2007; Saglimbene et al., 2018), so there is a current contraindication for using dual RAS blockade in the management of hypertension. However, in terms of kidney disease prognosis, existing data regarding dual RAS blockade inhibition is still a matter of debate. Indeed, the result of a current meta-analysis demonstrates that dual RAS blockade may be suitable for hypertensive patients with diabetic kidney nephropathy and albuminuria (Feng et al., 2019). Noteworthy, the mechanisms by which the double combination of ARBs and ACEi may cause hyperkalemia have not been fully elucidated. The main proposed mechanisms include decreased aldosterone concentrations, reduced glomerular filtration rate, and/or abnormal collecting duct function (Raebel, 2012).

In light of the above, the present study aimed to investigate the underlying molecular mechanisms associated with the additive antiproteinuric and hyperkalemic effects activated by dual versus single blockade of the RAS in an experimental model of hypertension. We hypothesized that the dual blockade of RAS could better preserve both glomerular and proximal tubular components responsible for protein handling than monotherapy and that the increased risk of hyperkalemia could be established by exaggerated downregulation of sodium epithelial channel (ENaC) in collecting ducts.

MATERIALS AND METHODS

Animal Protocols, Surgical Procedures, and Drug Treatment

All animal procedures were approved by the Institutional Animal Care and Use Committee of the University of São Paulo, Ribeirão Preto, SP, Brazil (Protocol n° 07.1.607.53.1) and were carried out following the ethical principles of the Brazilian College of Animal Experimentation. Experiments were performed on male Wistar rats (8 weeks old, 180–200 g) purchased from the University of São Paulo (São Paulo, SP, Brazil). The animals were housed at the Heart Institute animal facility under a constant temperature and a 12:12-h dark-light cycle and had free access to food and water. The two-kidney one-clip (2K-1C) renovascular-hypertension was induced as described previously (Corrêa et al., 2020). Briefly, rats were anesthetized with tribromoethanol (50 mg/kg i.p.) and, after a midline laparotomy, a silver clip with an internal diameter of 0.20 mm was placed around the left renal artery. Normotensive two-kidney (2K) rats were subjected to the same surgical procedure except for the clip implantation. Tail-cuff BP was measured 6 weeks after surgery (pretreatment measurement) by plethysmography (BP-2000 Blood Pressure Analysis System, Visitech System, Apex, NC, United States),

as previously described (Martins et al., 2020). Only 2K−1C rats that displayed tail-cuff BP higher than 160 mm Hg were included in the study (**Figure 1A**). The 2K−1C rats were then randomly divided into four groups and treated for 14 days with vehicle (water, 1 ml/kg), enalapril (20 mg/kg/day), losartan (30 mg/kg/day), or enalapril (20 mg/kg/day) plus losartan (30 mg/kg/day) by gavage. Vehicle-treated 2K rats were used as controls. Tail-cuff BP was also measured at the end of the treatment. Rats were anesthetized with ketamine and xylazine (50 and 10 mg/kg, respectively, i.p.). Blood samples were collected from the abdominal aorta and transferred into vacutainer tubes to obtain plasma. Subsequently, rats were euthanized by cervical displacement, and the kidneys were immediately removed and weighed. The left and right kidney weights were normalized by their respective tibial length. The non-clipped kidney was used to isolate renal cortical membrane and total proteins or tissue fixation for histological analysis.

Renal Function Evaluation

The rats were individually housed and placed in metabolic cages (Tecniplast, Buguggiate, VA, Italy) throughout the last 4 days of treatment, as previously described (Inoue et al., 2013). Urine samples were collected for 24 h and used to determine urinary flow, sodium, potassium, glucose, creatinine, proteinuria, and albuminuria. Creatinine clearance was used to estimate the glomerular filtration rate (GFR).

Plasma and Urine Analysis

Plasma and urinary sodium and potassium concentrations were measured by flame photometry (Digimed DM-62, São Paulo, Brazil). Plasma and urinary creatinine concentrations were measured using a kinetic method (Labtest, Lagoa Santa, MG, Brazil) and a ThermoPlate Analyzer Plus (ThermoPlate, São Paulo, SP, Brazil). The urinary glucose concentration was measured by the hexokinase method using a commercial kit (Labtest). Total urinary protein excretion was measured using a commercial kit based on the pyrogallol red-molybdate method (Labtest). The urinary albumin concentration was determined using an enzyme-linked immunosorbent assay (ELISA) kit specific for rat urine albumin (Nephrat II kit; Ethos Biosciences, Newtown Square, PA, United States). The experiments were carried out following the manufacturer's instructions.

Preparation of Renal Homogenate and Cortical Membrane Proteins

Kidney cortices were isolated at 4°C and homogenized in phosphate buffer saline (PBS) containing protease [1 mM pepstatin, 1 mM leupeptin, 230 mM PMSF and 1 tablet/50 ml of Complete protease inhibitor cocktail tablets (Roche, Mannheim, Germany)] and phosphatase inhibitors (50 mM NaF and 15 mM sodium pyrophosphate) at pH 7.4. Aliquots of the homogenate were saved for ELISA. The remaining renal cortical homogenate was centrifuged at 4,000 rpm for 15 min at 4°C. The supernatant was removed and subjected to a further 90 min centrifugation at 28,000 rpm at 4°C to pellet the membrane fraction. The supernatant was discarded; the renal cortical membranes were resuspended in fresh PBS containing protease and phosphatase inhibitors. The total protein concentration was determined using the Lowry method (Lowry et al., 1951).

SDS-PAGE and Immunoblotting

Renal cortical samples containing an equivalent amount of protein and volumes of urine containing 5 μg of creatinine were solubilized in Laemmli sample buffer and resolved using 7.5 or 10% SDS-PAGE gels, respectively. Following electrophoresis, gels containing proteins from urine samples were silver stained using the ProteoSilver Plus kit (Merck, Darmstadt, Germany) to detect urinary proteins. Renal homogenate and urine proteins were transferred from SDS-PAGE gels to polyvinylidene difluoride

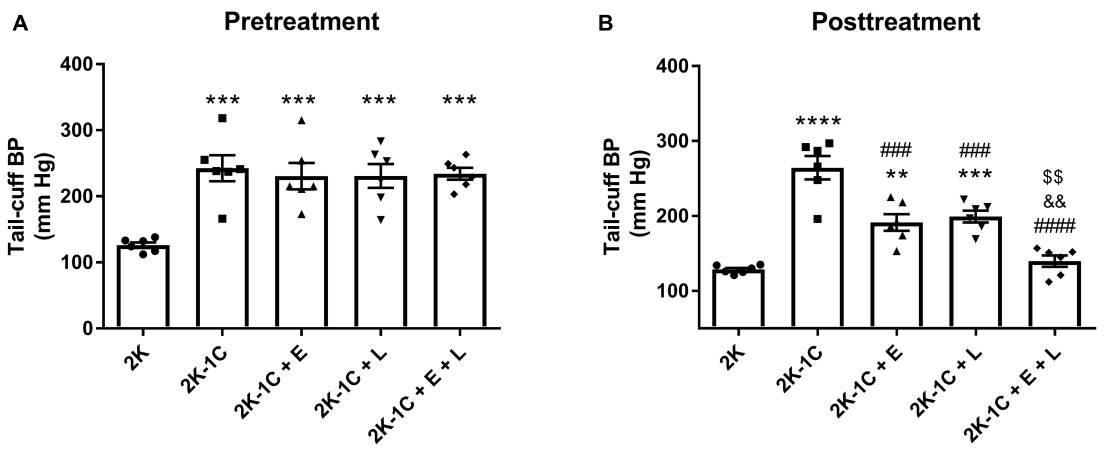

FIGURE 1 | Dual RAS blockade, but not losartan or enalapril alone, normalizes blood pressure in renovascular hypertensive rats. Blood pressure was measured using tail-cuff plethysmography in two-kidney one-clip (2K-1C) renovascular-hypertensive rats and controls (2K). Experiments were conducted **(A)** before and **(B)** 14 days after treatment with enalapril (2K-1C + E, 20 mg/kg/day), losartan (2K-1C + L, 30 mg/kg/day), enalapril plus losartan (2K-1C + E + L, 30 and 20 mg/kg/day, respectively), or vehicle (2K and 2K-1C, water: 1 ml/kg). The values represent individual measurements and the means ± SEM. $^{**}P < 0.01$, $^{***}P < 0.001$, and $^{****}P < 0.0001$ vs. 2K; $^{\#\#\#}P < 0.001$ and $^{\#\#\#\#}P < 0.0001$ vs. 2K-1C; $^{\&\&}P < 0.01$ vs. 2K-1C + E; $^{\$\$}P < 0.01$ vs. 2K-1C + L.

(PVDF) membranes (Immobilon-P; Merck). Then, the PVDF membranes were incubated with blocking solution (5% non-fat dry milk or 5% bovine serum albumin and 0.1% Tween 20 in PBS, pH 7.4) for 1 h and the following specific primary antibodies overnight (4°C): polyclonal antibody against podocin (1:1,000; Santa Cruz Biotech, sc-21009), polyclonal antibody against nephrin (1:1,000; Abcam, Cambridge, MA, Ab 58968), polyclonal antibody against megalin (1:50,000; a gift from Dr. Daniel Biemesderfer) (Li et al., 2008), polyclonal antibody against cubilin (1:1,000; Santa Cruz Biotech, sc-20609), polyclonal antibody against the ClC-5, H^+/Cl^- exchange transporter 5 (1:1,000; Alpha Diagnostic International, CLC51-A, San Antonio, TX, United States) (Carraro-Lacroix et al., 2010), polyclonal antibody against α-ENaC (1:1,000; Alomone Labs, ASC-030, Jerusalem, Israel), polyclonal antibody against β-ENaC (1:1,000; StressMarq Biosciences, SPC-404, Victoria, British Columbia, Canada), polyclonal antibody against cleaved γ-ENaC (1:1,000; Alomone Labs, ASC-011), or actin (1:5,000; Abcam ab179467). Actin was used as a loading control. Proteins were detected using horseradish peroxidase-conjugated secondary antibodies (1:2,000; Jackson ImmunoResearch, West Grove, PA, United States). The bound antibodies were detected using an enhanced chemiluminescence system (GE HealthCare, Chicago, IL, United States) according to the manufacturer's protocols. The visualized bands were digitized using an image scanner (GE HealthCare) and quantified using Scion Image software (Scion Corporation, Frederick, MD, United States).

Histological Analysis

The non-clipped kidney from five rats per group was fixed in 10% phosphate buffered-formalin, pH 7.3, for 24 h. After the fixation, the renal tissue was transferred into 70% vol/vol ethanol and stored at room temperature until processing into paraffin. The paraffin blocks were sectioned at 4 μm thickness using a microtome (Leica RM 2035, Leica Biosystems, Wetzlar, Hesse, Germany) and placed on silanized slides. Then, the sections were stained with Picrosirius red to detect collagen fiber deposition. Fifteen fields from each section were chosen at random, and the images were acquired under a 400× magnification light microscope using the Leica Qwin Plus Software (Leica Biosystems). The red-stained collagen fibers were quantified by Image J software, and the degree of fibrosis was expressed as the average percentage of the total area. A single examiner, blinded to the experimental groups, performed all histological measures.

Determination of Renal Cortical Ang II and TGF-β and Plasma Aldosterone Concentrations

The Ang II and TGF-β concentrations in renal homogenates and the plasma aldosterone concentration were measured using competitive ELISA (Biomatik Corporation, Kitchener, ON, Canada), (Abcam), and (Enzo Life Sciences, New York, NY, United States), respectively, according to the manufacturers' instructions, including sample collection and storage.

Statistical Analysis

The results are reported as the mean ± standard error of the mean (SEM). Comparisons among the groups were performed using one-way ANOVA followed by the Tukey *post hoc* test. $P < 0.05$ was considered significant.

RESULTS

Effect of Dual Versus Single RAS Blockade on Biometric Parameters, Blood Pressure, Renal Function, and Non-Clipped Kidney Ang II Concentration

The biometric characteristics of the animals are shown in **Table 1**. The final mean body weights were similar among the five groups

TABLE 1 | Biometrical and renal function parameters, non-clipped kidney Ang II content and plasma aldosterone concentration in two-kidney one-clip (2K-1C) renovascular-hypertensive rats and controls (2K).

	2K (*n* = 6)	2K-1C (*n* = 6)	2K-1C + E (*n* = 6)	2K-1C + L (*n* = 6)	2K-1C + E + L (*n* = 6)
Body weight (g)	430 ± 9	376 ± 13	386 ± 22	375 ± 21	388 ± 20
LKW/TL (mg/mm)	0.40 ± 0.01	0.29 ± 0.04	0.33 ± 0.03	0.34 ± 0.03	0.29 ± 0.02
RKW/TL (mg/mm)	0.41 ± 0.01	0.61 ± 0.04**	0.53 ± 0.04	0.54 ± 0.04	0.44 ± 0.04
Urinary flow (ml/24h/kg)	35 ± 1	194 ± 19***	111 ± 18*##	118 ± 18*#	63 ± 9###
Plasma Cr (mg/dl)	0.43 ± 0.01	0.56 ± 0.03	0.59 ± 0.03	0.52 ± 0.07	0.53 ± 0.04
Cr Clearance (ml/min/kg)	9.1 ± 0.6	5.9 ± 0.5**	6.4 ± 0.5**	6.0 ± 0.3**	6.6 ± 0.3**
Plasma Na^+ (mM)	141 ± 1	144 ± 3	143 ± 2	143 ± 3	142 ± 1
FE Na^+ (%)	0.51 ± 0.04	0.72 ± 0.13	0.89 ± 0.02	0.87 ± 0.04	0.64 ± 0.11
Glycosuria (mg/24h/kg)	21 ± 1	16 ± 2	279 ± 28***###	200 ± 22***###	217 ± 16***###
Non-clipped kidney Ang II (pg/g)	133 ± 6	1422 ± 93***	337 ± 17*###	422 ± 22***###	93 ± 8###,&&,$$$
Plasma Aldosterone (pg/ml)	224 ± 14	881 ± 26***	445 ± 87##	489 ± 74#	310 ± 89###

*Values are means ± SEM with the number of rats of each group in parenthesis. *P < 0.05, **P < 0.01, and ***P < 0.01 vs. 2K; #P < 0.05, ##P < 0.01, and ###P < 0.001 vs. 2K-1C; &&P < 0.01 vs. 2K-1C + E, $$$P < 0.001 vs. 2K-1C + L, assessed by ANOVA one-way followed by Tukey's post hoc test. Urinary output was measured gravimetrically. Fractional excretion (FE) of Na^+ was expressed in percentage and calculated as C_{Na}/C_{Cr} where C_{Na} is the Na^+ clearance, and C_{Cr} is creatinine clearance. Ang II, angiotensin II; Cr, creatinine; LKW, left kidney weight; RKW, right kidney weight; TL, tibia length.*

of rats. Vehicle-treated 2K-1C rats displayed higher right kidney (non-clipped) weight to tibia length (TL) than normotensive 2K rats. In contrast, enalapril and losartan alone or in combination prevented non-clipped kidney hypertrophy. The left kidney (clipped) weight (LKW) to TL did not significantly vary among the five groups of rats, despite a trend toward a reduction in LKW/TL in vehicle-treated and drug-treated 2K-1C.

As shown in **Figure 1A**, the tail-cuff BP of 2K-1C rats was higher than that observed in 2K rats (242 ± 20 mmHg vs. 126 ± 4 mm Hg, $P < 0.001$). Before starting treatments, animals randomized to enalapril and losartan alone or in combination exhibited tail-cuff BP levels similar to that of 2K-1C rats (**Figure 1A**). After 14 days of treatment (**Figure 1B**), the BP levels of 2K-1C rats remained remarkably high compared to 2K rats (264 ± 15 mm Hg vs. 128 ± 2 mm Hg, $P < 0.0001$). Treatment with enalapril (191 ± 11 mm Hg) or losartan (199 ± 8 mm Hg) promoted a significant reduction in BP of 2K-1C rats ($P < 0.01$ and $P < 0.001$ vs. 2K-1C, respectively). In addition, the combination of enalapril and losartan exerted an antihypertensive effect, bringing the tail-cuff BP of double blockaded treated 2K-1C rats to levels non-significantly different from normotensive 2K control rats (140 ± 7 vs. 128 ± 2 mm Hg).

Vehicle-treated 2K-1C rats displayed higher urinary flow than 2K rats (**Table 1**). A reduction in urinary flow was observed in 2K-1C treated with enalapril or losartan. The enalapril/losartan combination promoted an additional decrease in 2K-1C urinary flow. Vehicle-treated 2K-1C rats also exhibited lower creatinine clearance than normotensive 2K rats. None of the treatments with ACEi and ARB alone or in combination could prevent/revert the decline in creatinine clearance (**Table 1**). 2K-1C rats with or without treatments did not show differences in plasma levels of creatinine and sodium and on fractional sodium excretion compared to 2K rats. Although 2K-1C rats did not show differences in urinary glucose excretion than 2K rats, it was observed that enalapril and losartan alone or in combination similarly increased glycosuria in 2K-1C hypertensive rats.

In addition, 2K-1C renovascular hypertensive rats showed a marked increase in Ang II content in the non-clipped kidney over 2K rats (**Table 1**). The treatment with losartan or enalapril reduced non-clipped kidney Ang II levels. The reduction of renal Ang II concentration was even more prominent when enalapril and losartan were used in combination.

Effect of Dual Versus Single RAS Blockade on Urinary Protein and Albumin Excretion

The urine analysis revealed that 2K-1C rats presented remarkably higher proteinuria (995 ± 70 vs. 54 ± 5 mg/24 h/Kg, $P < 0.0001$) (**Figure 2A**) and albuminuria levels (431 ± 36 vs. 12 ± 2 mg/24 h/kg, $P < 0.0001$) (**Figure 2B**) than 2K rats. The treatment with enalapril or losartan reduced both total protein excretion (enalapril: 219 ± 7 mg/24 h/kg, $P < 0.0001$; losartan: 287 ± 72 mg/24 h/kg, $P < 0.0001$) and albuminuria (enalapril: 129 ± 14 mg/24 h/kg, $P < 0.0001$; losartan:152 ± 4 mg/24 h/Kg, $P < 0.0001$), respectively, in 2K-1C rats. An additional reduction in proteinuria (72 ± 10 mg/24 h/kg) and albuminuria (48 ± 5 mg/24 h/kg) excretion were observed after treating 2K-1C rats with the combination of enalapril and losartan in comparison with monotherapy ($P < 0.05$) (**Figures 2A,B**). Dual RAS blockade restored proteinuria and albuminuria in 2K-1C to the same levels of normotensive 2K rats (**Figures 2A,B**). The profile of urinary proteins excreted by the five groups of rats was evaluated by SDS-PAGE (**Figure 2C**). Analysis of the pattern of proteins excreted by vehicle-treated 2K-1C rats suggested proteinuria of mixed origin, i.e., glomerular and tubular proteinuria, since both high- and low-molecular-weight proteins were present in the urine of these animals (Waller et al., 1989). The treatment of 2K-1C rats with enalapril or losartan reduced the protein excretion of high and low molecular weight. A much greater reduction was observed in the group of hypertensive 2K-1C rats that received the combined treatment. The results from these experiments are consistent with those shown in **Figures 2A,B**.

Effect of Dual Versus Single RAS Blockade on the Expression of Components of the Glomerular Filtration Barrier

Given that enalapril and losartan alone or combined seemed to reduce glomerular proteinuria, we next sought to examine whether RAS inhibition could modulate nephrin and podocin expression (**Figure 3**). As noted, there was a ∼55% reduction in podocin expression in 2K-1C rats in comparison with 2K rats ($P < 0.0001$) (**Figure 3A**). Losartan and enalapril in monotherapy partially prevented podocin downregulation. The treatment of 2K-1C rats with enalapril combined with losartan was superior to monotherapy ($P < 0.05$) and normalized podocin expression levels to those of 2K rats. The expression of nephrin remained unchanged among the groups (**Figure 3B**).

Effect of Dual Versus Single RAS Blockade on the Expression of Selected Key Components of the Proximal Tubular Endocytic Machinery

Enalapril and losartan alone or combined also appeared to reduce tubular proteinuria, suggesting that RAS inhibition may upregulate the expression of components of the proximal tubular endocytic machinery. There was a 30% reduction in megalin expression in 2K-1C rats than 2K rats (**Figure 4A**). Treatment of 2K-1C rats with enalapril, losartan, or enalapril with losartan combined further and similarly reduced megalin expression (**Figure 4A**). On the other hand, the reduction in cubilin expression observed in 2K-1C rats compared to 2K rats (60 ± 4 vs. 100 ± 4%, $P < 0.0001$) was similarly attenuated by the treatment with enalapril and losartan and restored to control 2K levels when both drugs were combined (**Figure 4B**). Interestingly, 2K-1C rats showed a marked reduction (12 ± 5 vs. 100 ± 3%, $P < 0.0001$) in the relative expression of CIC-5 compared to 2K rats ($P < 0.0001$) (**Figure 4C**). The therapy with either enalapril or losartan alone attenuated the decrease in ClC-5 protein abundance. In contrast, treatment of 2K-1C rats with the

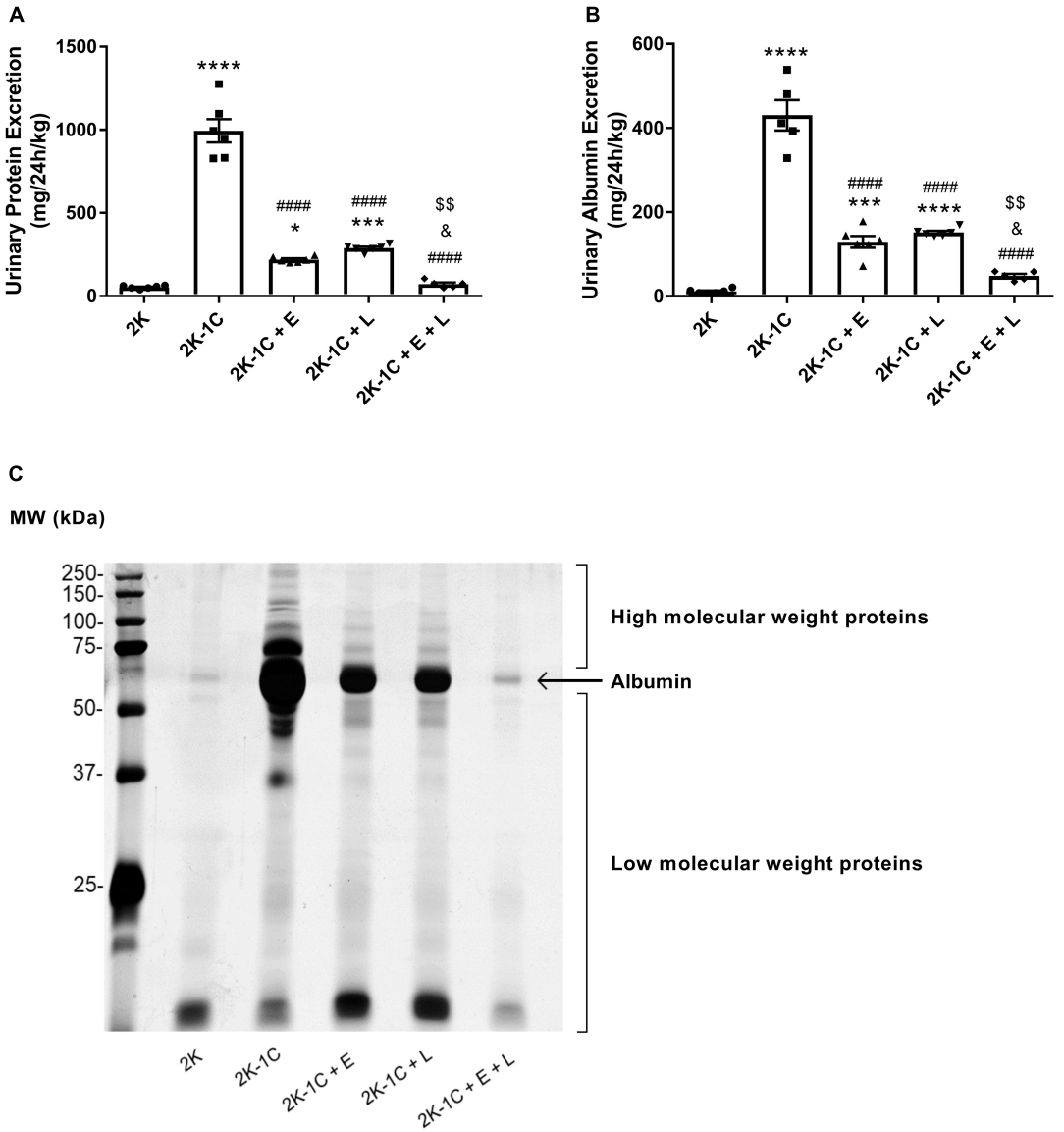

FIGURE 2 | Dual RAS blockade, but not losartan or enalapril alone, normalizes proteinuria and albuminuria in renovascular hypertensive rats. Two-kidney one-clip (2K-1C) renovascular-hypertensive rats treated with enalapril (2K-1C + E, 20 mg/kg/day), losartan (2K-1C + L, 30 mg/kg/day), enalapril plus losartan (2K-1C + E + L, 30 and 20 mg/kg/day, respectively), or vehicle (2K-1C) and vehicle-treated control rats (2K) were placed into metabolic cages for 24-h urine collection. **(A)** Urinary protein excretion was measured using a commercially available kit based on the pyrogallol red-molybdate method. **(B)** Urinary albumin concentration was determined by ELISA. The values represent individual measurements and the means ± SEM. $^{*}P < 0.05$,$^{***}P < 0.001$, and $^{****}P < 0.0001$ vs. 2K; $^{\#\#\#\#}P < 0.0001$ vs. 2K-1C; $^{\&}P < 0.05$ vs. 2K-1C + E; $^{\$\$}P < 0.01$ vs. 2K-1C + L. **(C)** Profile of urine proteins excreted by the five groups of rats. The 24-h urine samples (volume equivalent to 5.0 μg of creatinine) were subjected to 10% SDS-PAGE. Following electrophoresis, the gels were silver stained. The urinary excretion of proteins of a size smaller than albumin (low molecular weight proteins) and higher than albumin (high molecular weight proteins) is indicated in the representative gel.

combined therapy completely restored ClC-5 renal expression to the levels of 2K rats (**Figure 4C**).

Effect of Dual Versus Single RAS Blockade on Renal Fibrosis

Figure 5A shows a representative histological image of non-clipped kidney tissue sections from each group of rats stained with Picrossirius Red. The percentage of collagen deposition was significantly higher in the non-clipped kidney of 2K-1C than 2K rats (**Figure 5B**). The degree of renal fibrosis in vehicle-treated 2K-1C rats was accompanied by a higher content of TGF-β (150 ± 12 ng/g vs. 28 ± 7 ng/g in 2K rats, $P < 0.0001$) (**Figure 5C**). The treatment of 2K-1C rats with RAS inhibitors effectively reduced collagen accumulation. An additional effect was observed for losartan or its combination with enalapril in comparison with enalapril alone ($P < 0.005$) (**Figure 5B**). When compared with the 2K-1C group, the levels

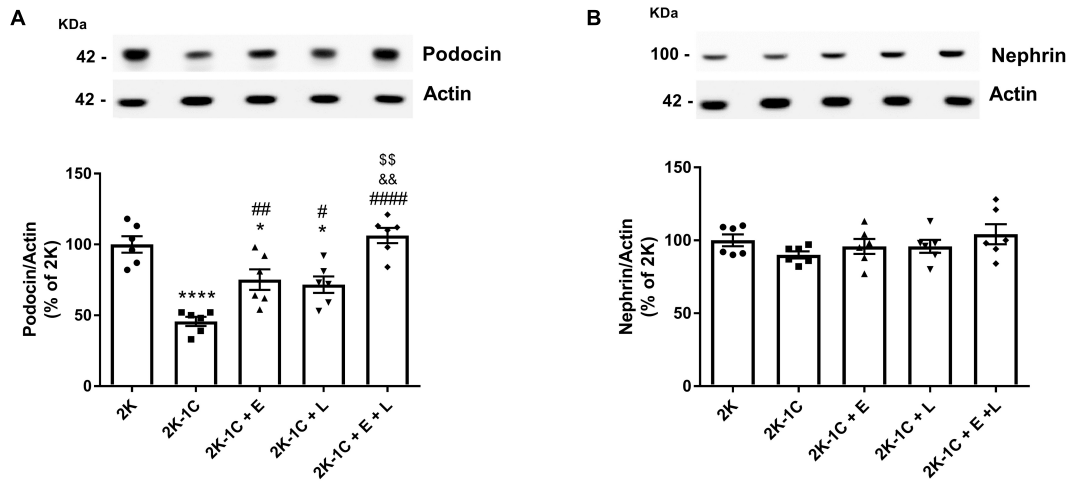

FIGURE 3 | Effect of dual versus single RAS blockade on the expression of components of the glomerular filtration barrier in the non-clipped kidney of renovascular hypertensive rats. Samples isolated from the non-clipped kidney of renovascular-hypertensive rats treated with enalapril (2K-1C + E, 20 mg/kg/day), losartan (2K-1C + L, 30 mg/kg/day), enalapril plus losartan (2K-1C + E + L, 30 and 20 mg/kg/day, respectively), or vehicle (2K-1C) and vehicle-treated control rats (2K) containing equal amounts of membrane proteins (20 μg for podocin and nephrin and 5 μg for actin) were subjected to SDS-PAGE, after which the proteins were transferred to a PVDF membrane and incubated with primary antibodies. Actin was used as a loading control. Representative immunoblots of electrophoresed renal membrane proteins and graphical representation of the relative expression of **(A)** podocin and **(B)** nephrin. The values represent individual measurements and the means ± SEM. $^{*}P < 0.05$ and $^{****}P < 0.0001$ vs. 2K; $^{\#}P < 0.05$, $^{\#\#}P < 0.01$, and $^{\#\#\#\#}P < 0.0001$ vs. 2K-1C; $^{\&\&}P < 0.01$ vs. 2K-1C + E; $^{\$\$}P < 0.01$ vs. 2K-1C + L.

of TGF-β was also reduced ($P < 0.0001$) by the treatment with enalapril (78 ± 12 ng/g), losartan (74 ± 5 ng/g), or by the combination enalapril/losartan (39 ± 6 ng/g). A superior reduction of TGF-β levels was observed in 2K-1C rats treated with losartan or by its combination with enalapril when compared to monotherapy with enalapril ($P < 0.05$) (**Figure 5C**).

Effect of Dual Versus Single RAS Blockade on Potassium Homeostasis

Figure 6 shows that 2K-1C hypertensive rats had a lower concentration of plasma potassium compared to 2K rats (3.4 ± 0.1 vs. 4.5 ± 0.2 mEq, $P < 0.05$) (**Figure 6A**), which is associated with an increase in the fractional potassium excretion (78 ± 9 vs. 17 ± 3%, $P < 0.0001$) (**Figure 6B**). No differences were found in plasma potassium concentration between 2K-1C rats treated with either enalapril or losartan (4.1 ± 0.2 and 4.3 ± 0.3 mEq, respectively) and 2K normotensive rats (4.5 ± 0.2 mEq) (**Figure 6A**). Similarly, no differences were found in the fractional potassium excretion (**Figure 6B**) between 2K-1C rats treated with enalapril or losartan and 2K rats. Conversely, when 2K-1C rats were treated with the combination of enalapril and losartan, their plasma potassium concentration raised to a level higher than 2K rats (5.8 ± 0.4 vs. 4.5 ± 0.2 mEq, $P < 0.05$) (**Figure 6A**). This hyperkalemic status in 2K-1C rats treated with the combined therapy was accompanied by a non-significant decrease in fractional excretion of potassium (9 ± 1 vs. 17 ± 3% in 2K rats) (**Figure 6B**). Lower plasma potassium concentration in 2K-1C rats was accompanied by a higher plasma concentration of aldosterone (**Table 1**). The plasma aldosterone concentration did not vary significantly between 2K rats and 2K-1C rats treated with enalapril or losartan as monotherapy or the combination of enalapril and losartan (**Table 1**).

Potential Role of ENaC in Mediating Potassium Disturbances in Response to Dual RAS Blockade

The epithelial Na^+ channel (ENaC) mediates the passive sodium entry across the apical membrane of the principal cells in the late distal tubule and collecting ducts and consists of a heterotrimer with a single α, β, and γ subunit (Bhalla and Hallows, 2008). Proteolytic processing of α and γ subunits are markers for apical membrane ENaC activation (Kleyman et al., 2009; Palmer et al., 2012). When the apical membrane potential becomes depolarized by increased sodium entry through activated ENaC, potassium secretion across this membrane increases, and potassium is lost to the urine (Bubien, 2010). We then tested the hypothesis that the hyperkalemia induced by double RAS blockade in 2K-1C rats could be associated with ENaC subunits' downregulation (**Figure 7**). As seen in **Figure 7A**, full-length α-ENaC expression was ∼50% reduced in vehicle-treated 2K-1C rats and 2K-1C rats treated with enalapril or losartan compared to 2K animals. No difference was found in full-length α-ENaC expression in the non-clipped kidneys of 2K-1C rats treated with the combined therapy and 2K rats (**Figure 7A**). In contrast, the abundance of the active cleaved α-ENaC levels was 62% increased in vehicle-treated 2K-1C, and it was also higher in 2K-1C rats treated with enalapril than in 2K rats (**Figure 7B**). The combined enalapril and losartan treatment considerably reduced the abundance of the active form of α-ENaC compared with vehicle-treated 2K-1C and 2K-1C rats treated with either enalapril or losartan alone (**Figure 7B**).

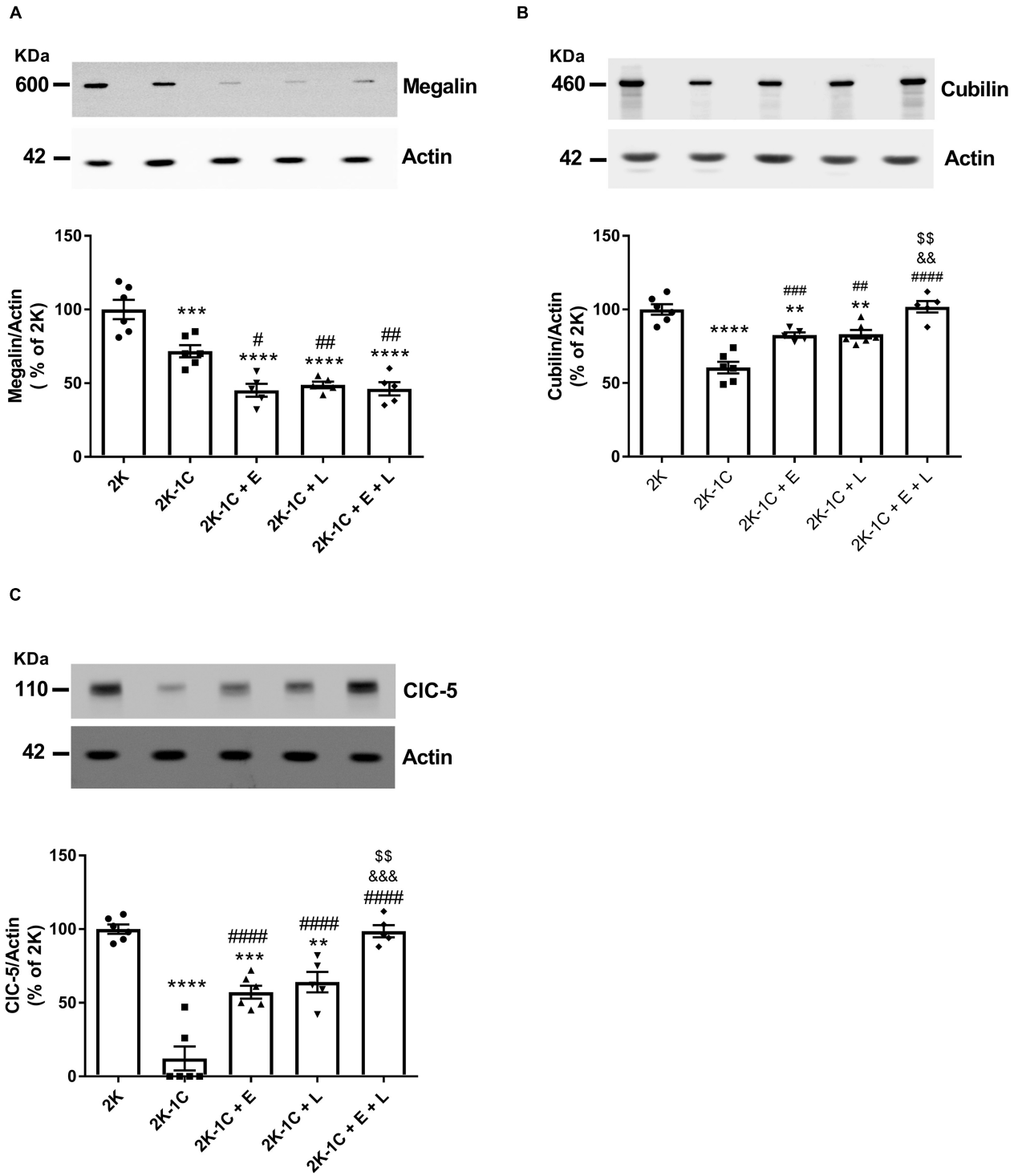

FIGURE 4 | Effect of dual versus single RAS blockade on the expression of selected key components of the proximal tubular endocytic machinery in the non-clipped kidney of renovascular hypertensive rats. Samples isolated from the non-clipped kidney of renovascular-hypertensive rats treated with enalapril (2K-1C + E, 20 mg/kg/day), losartan (2K-1C + L, 30 mg/kg/day), enalapril plus losartan (2K-1C + E + L, 30 and 20 mg/kg/day, respectively), or vehicle (2K-1C) and vehicle-treated control rats (2K) containing equal amounts of membrane proteins (10 μg for megalin, 20 μg for cubilin and ClC-5 nephrin and 5 μg for actin) were subjected to SDS-PAGE, after which the proteins were transferred to a PVDF membrane and incubated with primary antibodies. Actin was used as a loading control. Representative immunoblots of electrophoresed renal membrane proteins and graphical representation of the relative expression of **(A)** megalin, **(B)** cubilin, and **(C)** ClC-5. The values represent individual measurements and the means ± SEM. $^{**}P < 0.01$, $^{***}P < 0.001$, and $^{****}P < 0.0001$ vs. 2K; $^{\#}P < 0.05$, $^{\#\#}P < 0.01$, $^{\#\#\#}P < 0.001$, and $^{\#\#\#\#}P < 0.0001$ vs. 2K-1C; $^{\&\&}P < 0.01$ and $^{\&\&\&}P < 0.001$ vs. 2K-1C + E; $^{\$\$}P < 0.01$ vs. 2K-1C + L.

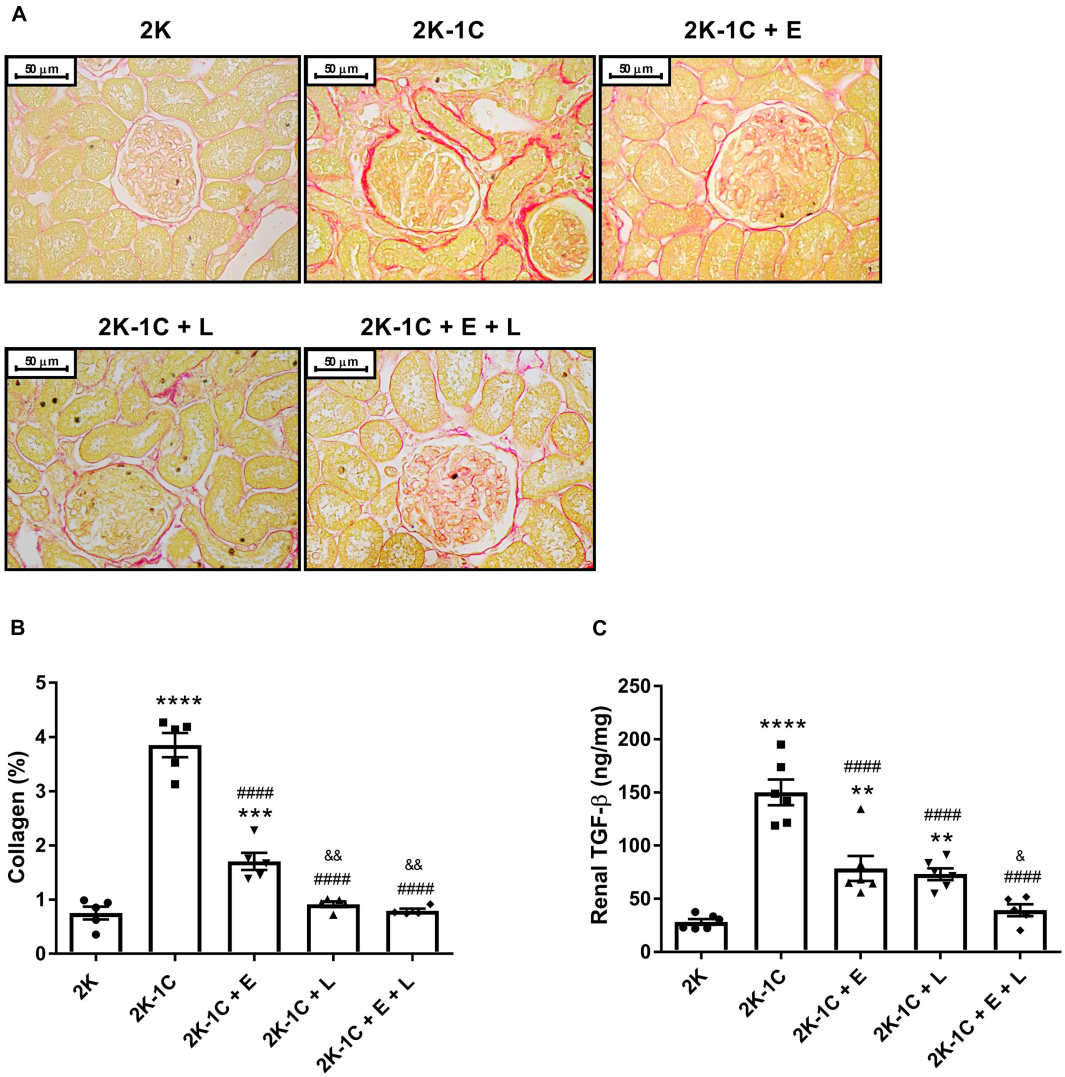

FIGURE 5 | Effect of dual versus single RAS blockade on fibrosis of the non-clipped kidney of renovascular hypertensive rats. **(A)** Representative images of Picrosirius Red staining non-clipped kidney sections (400 × magnification) from renovascular-hypertensive rats treated with enalapril (2K-1C + E, 20 mg/kg/day), losartan (2K-1C + L, 30 mg/kg/day), enalapril plus losartan (2K-1C + E + L, 30 and 20 mg/kg/day, respectively), or vehicle (2K-1C) and vehicle-treated control rats (2K). The scale bar shows 50 µm. **(B)** Quantification of Picrossiuris Red staining kidney sections. The levels of non-clipped kidney collagen were expressed as percent of the total cross-section area. **(C)** The concentration of TGF-β was measured in non-clipped kidneys homogenate by ELISA. The values represent individual measurements and the means ± SEM. $^{**}P < 0.01$, $^{***}P < 0.001$, and $^{****}P < 0.0001$ vs. 2K; $^{\#\#\#\#}P < 0.0001$ vs. 2K-1C; $^{\&}P < 0.05$ and $^{\&\&}P < 0.01$ vs. 2K-1C + E.

Indeed, dual RAS blockade lowered the abundance of cleaved α-ENaC to levels lower than those of 2K control rats (38 ± 9 vs. 100 ± 5%, $P < 0.05$) (**Figure 7B**). The β-ENaC subunit was ∼75% more expressed in the non-clipped kidney of vehicle-treated 2K-1C rats than in 2K rats ($P < 0.05$) (**Figure 7C**). The combined therapy of enalapril and losartan but not the monotherapy effectively reduced the β-ENaC subunit expression in 2K-1C rats (**Figure 7C**). The expression of the active cleaved form of γ-ENaC was increased in the non-clipped kidney of vehicle-treated 2K-1C rats compared to 2K rats (144 ± 8 vs. 100 ± 9%, $P < 0.01$). Only the combined therapy could restore the cleaved γ-ENaC abundance to the levels of 2K rats (**Figure 7D**).

DISCUSSION

This study explored the potential molecular mechanisms underlying the antiproteinuric and hyperkalemic effects of dual RAS blockade in renovascular hypertensive rats. We found that the better management of proteinuria of 2K-1C rats in response to the combination of enalapril with losartan was associated with higher protein abundance of podocin and cubilin in the non-clipped kidney relative to either enalapril- or losartan -treated 2K-1C rats. Additionally, we showed that higher plasma potassium concentration in 2K-1C rats treated with the combination of enalapril and losartan exhibited downregulation of the cleaved/activated forms of

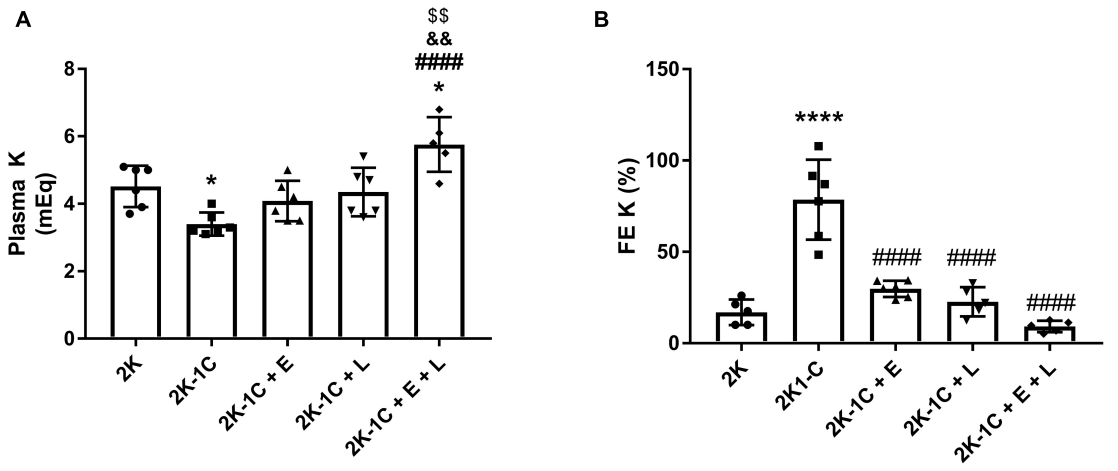

FIGURE 6 | Dual RAS blockade, but not losartan or enalapril alone, induces hyperkalemia in renovascular hypertensive rats. **(A)** The plasma potassium concentration (Plasma K^+) and **(B)** the Fractional excretion of potassium (FE K^+) were determined in normotensive (2K) and renal hypertensive (2K-1C) rats treated for 14 days with enalapril (2K-1C + E, 20 mg/kg/day), losartan (2K-1C + L, 30 mg/kg/day), enalapril plus losartan (2K-1C + E + L, 30 and 20 mg/kg/day, respectively), or vehicle (2K and 2K-1C, water: 1 ml/kg). The values represent individual measurements and the means ± SEM. $^{*}P < 0.05$ and $^{****}P < 0.0001$ vs. 2K, $^{\#\#\#\#}P < 0.0001$ vs. 2K-1C; $^{\&\&}P < 0.01$ vs. 2K-1C + E; $^{\$\$}P < 0.01$ vs. 2K-1C + L.

α-ENaC and γ-ENaC in the non-clipped kidney, suggesting that posttranslational modification of these ENaC subunits in the collecting duct may contribute to dual RAS blockade-induced hyperkalemia.

Hyperactivation of the renal RAS limits the kidney's ability to maintain sodium balance at normal arterial pressures and contributes to hypertension development (Crowley et al., 2006; Navar et al., 2011). Renovascular hypertension in the 2K-1C model is initially induced by renin secretion stimulation caused by decreased renal perfusion, leading to increased systemic Ang II concentration. Interestingly, despite circulating Ang II levels return to normal at the hypertensive state, hypertension becomes stable as renal RAS is maintained abnormally overactive (Navar et al., 1998). We found that the Ang II content in the non-clipped kidney of renovascular hypertensive 2K-1C rats was markedly elevated. We also observed that either enalapril or losartan treatment reduced Ang II levels in the non-clipped kidney of 2K-1C, potentially favoring the natriuretic ability in these animals and setting an intermediate hypertensive state. However, the dual RAS blockade that blunts both AT1R activation and Ang II production by ACE was capable of restoring the renal concentration of Ang II to normotensive rats' levels and, therefore, the ability of the kidneys to maintain sodium balance. As a result, the combined therapy of enalapril and losartan was more effective than either drug alone in reducing BP in 2K-1C.

Ang II can substantially modulate proteinuria and albuminuria through effects on BP, and independently thereof, through changes of intraglomerular hemodynamics and modulation of critical components of the glomerular filtration barrier and the apical endocytic machinery in the renal proximal tubule (Langham et al., 2004; Long et al., 2004; Mann and Böhm, 2015; Aroor et al., 2016). The relative contribution of elevated BP versus Ang II on the induction of renal injury has been previously quantified by Mori and Cowley (2004) in the experimental model of Ang II-induced hypertension. Using servo-controlled kidneys that eliminated the hypertensive environment from one kidney, these authors observed that kidney injury markers were mainly induced by hypertension. Nevertheless, the servo-controlled kidney still has higher levels of injury markers than the sham group, which supports that RAS overactivation can affect kidney integrity by a pressure-independent mechanism and, plausibly, by direct local activation of Ang II production and signaling. As expected, 2K-1C rats presented overt proteinuria and albuminuria, which were attenuated by monotherapy with either enalapril and losartan and restored to control levels normotensive rats by the combined treatment. Considering previous evidence, such normalization would involve not only the control of BP by the combination of enalapril and losartan but also its underlying suppression of overactive local RAS.

Podocin and nephrin are two essential components of the glomerular filtration barrier, whose integrity is responsible for restricting the loss of high-molecular proteins in the urine. We observed that, whereas nephrin expression is not changed in 2K-1C rats, the protein abundance of podocin is significantly downregulated. It is known that Ang II and mechanical forces induce autophagy and apoptosis in podocyte culture (Yadav et al., 2010; Huang et al., 2012; Zhao et al., 2018), which could cause a generalized loss of both nephrin and podocin expression. At the same time, Ang II treatment can regulate nephrin and podocin transcription. Ang II treatment decreases podocin mRNA levels *in vitro* (Yang et al., 2017), which would favor podocin expression reduction in Ang II-dependent hypertensive settings. Accordingly, ACEi and ARB treatment partially reverted, and combined treatment completely reverted downregulation of podocin expression, which is in line with the efficiency of BP control and normalization of renal RAS obtained by such therapies. On the other hand, Ang II regulation of nephrin expression seems more complex. Rats receiving Ang

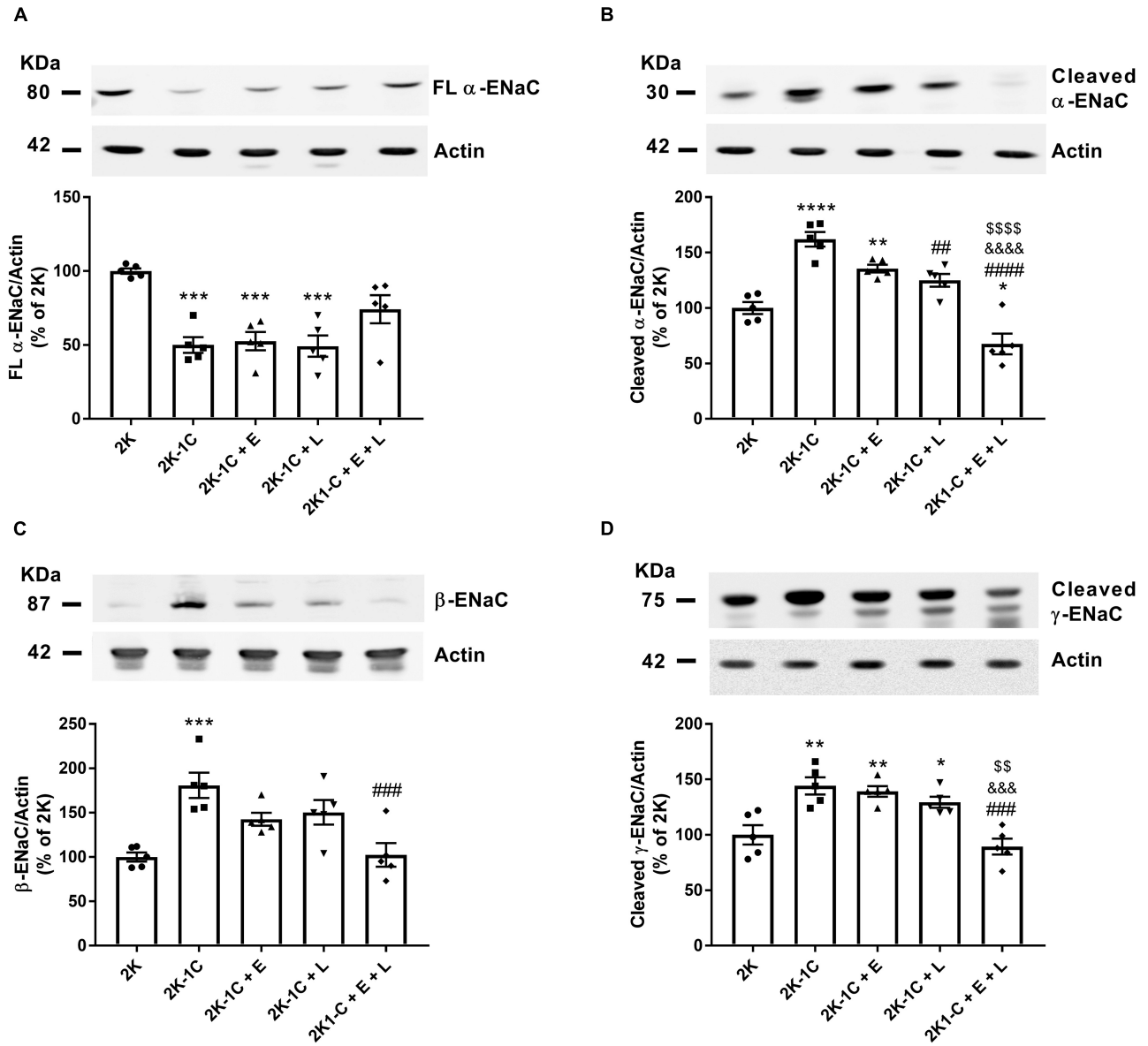

FIGURE 7 | Effect of dual versus single RAS blockade on the expression of total and cleaved ENaC subunits in the non-clipped kidney of renovascular hypertensive rats. Samples isolated from the non-clipped kidney of renovascular-hypertensive rats treated with enalapril (2K-1C + E, 20 mg/kg/day), losartan (2K-1C + L, 30 mg/kg/day), enalapril plus losartan (2K-1C + E + L, 30 and 20 mg/kg/day, respectively), or vehicle (2K-1C) and vehicle-treated control rats (2K) containing equal amounts of membrane proteins (75 μg for α-ENaC, β-ENaC, and γ-ENaC and 20 μg for actin) were subjected to SDS-PAGE, after which the proteins were transferred to a PVDF membrane and incubated with primary antibodies. Actin was used as a loading control. Representative immunoblots of electrophoresed renal membrane proteins and graphical representation of the relative expression of **(A)** Full-length (FL) α-ENaC, **(B)** cleaved α-ENaC, **(C)** β-ENaC, **(D)** cleaved γ-ENaC. The values represent individual measurements and the means ± SEM. $^{*}P < 0.05$, $^{**}P < 0.01$, $^{***}P < 0.001$ and $^{****}P < 0.0001$ vs. 2K; $^{\#\#}P < 0.01$, $^{\#\#\#}P < 0.001$, and $^{\#\#\#\#}P < 0.0001$ vs. 2K-1C; $^{\&\&\&}P < 0.001$ and $^{\&\&\&\&}P < 0.0001$ vs. 2K-1C + E; $^{\$\$}P < 0.01$ and $^{\$\$\$\$}P < 0.0001$ vs. 2K-1C + L.

II pressor doses of Ang II during 10–14 days showed increased nephrin expression at mRNA (Langham et al., 2004; Jia et al., 2008) and protein levels (Jia et al., 2008). However, after 28 days of Ang II infusion, nephrin mRNA and protein abundance start to decline in comparison with basal levels, and such reduction was associated with the appearance of apoptosis in podocytes. The absence of differences in nephrin expression in 2K-1C rats in comparison with sham rats may reflect the balance between these opposite regulatory processes, i.e., induction of nephrin transcription by increases in renal Ang II levels and downregulation of podocyte proteins due to apoptosis induced, directly or indirectly, by chronic Ang II stimulus.

Renovascular hypertensive 2K-1C rats also exhibited increased low-molecular-weight proteins in the urine, suggesting abnormal handling of filtrated smaller proteins by the renal tubule. Endocytic receptors in the proximal tubule (megalin and

cubilin) are involved in handling, internalizing filtrated proteins, and avoiding their urine loss. In line with the analysis of the pattern of proteinuria, cubilin and megalin expressions in the cortical membranes of the non-clipped kidney were reduced in 2K-1C rats. Such reductions might be partly caused by tubular injury observed in Ang II-dependent hypertensive models (Mori and Cowley, 2004). Nevertheless, Ang II-dependent local signaling and fine control of protein expression are probably also involved. Aroor and colleagues (Aroor et al., 2016) observed that decreased megalin expression in rats receiving Ang II infusion is associated with increased kidney DPP4 activity since DPP4 inhibition partially restored megalin expression in these animals. Moreover, such regulation of megalin expression was also observed in proximal tubule cells *in vitro*. Another critical molecular mechanism regulating the expression of endocytic receptors in the proximal tubule is TGF-β (Gekle et al., 2003), a factor that we found to be upregulated in the non-clipped kidney of 2K-1C rats. Proximal tubule-like OKP cell line treated with TGF-β have lower levels of both megalin and cubilin and lower protein endocytosis capacity. This regulation seems dependent on the induction of the transcription factors Smad2/3.

Dual RAS blockade reverted cubilin downregulation, which is expected by attenuation of kidney injury, TGF-β levels, and local RAS signaling in treated rats. Unexpectedly, RAS inhibitors further decreased megalin expression in the non-clipped kidney of 2K-1C treated rats. Such downregulation of megalin may be associated with the glycosuria presented in hypertensive rats treated with enalapril and/or losartan. Notably, cumulative evidence demonstrates the existence of an interplay between Ang II and sodium-glucose cotransporter 2 (SGLT2)-mediated glucose uptake in the renal proximal tubule (Silva Dos Santos et al., 2020). Accordingly, Bautista and colleagues (Bautista et al., 2004) have shown that renovascular hypertensive rats display higher activity in renal brush border membrane vesicles, an effect that was inhibited by treatment with ACEi or ARB. These findings suggest that the glycosuria observed in 2K-1C treated with RAS inhibitors might be induced by SGLT2 downregulation. Interestingly, there is evidence that SGLT2 modulates megalin cell surface expression in the renal proximal tubule. Using an animal model of diabetic nephropathy, Otomo and colleagues (Otomo et al., 2020) observed that SGLT2 inhibition suppressed O-GlcNAcylation of megalin, contributing to megalin internalization. Regardless of the mechanism responsible for further reducing megalin in 2K-1C treated with RAS inhibitors either in monotherapy or combination, the normalization of cubilin and podocin expression by dual RAS blockade seems sufficient to abrogate the overt proteinuria observed in 2K-1C untreated rats.

In the present study, we observed for the first time that another critical component of the apical endocytic machinery in the renal proximal tubule, the ClC-5, is remarkably downregulated in the non-clipped kidney of renovascular hypertensive 2K-1C rats. Cultures of proximal tubule cells from ClC-5 knockout mice showed that ClC-5 is critical for proper acidification of early endosomes, thus explaining why Dent's disease, caused by ClC-5 mutations, is characterized by low-molecular-weight proteinuria (Günther et al., 1998). It was reported previously that microalbuminuric SHR displays reduced renal cortical ClC-5 protein abundance compared to WKY rats. This reduction was attenuated by ACEi treatment, suggesting that Ang II downregulates ClC-5 expression by a pressure mechanism and/or by a local RAS signaling (Tanaka and Nakaki, 2004). Accordingly, we observed that renal cortical expression of ClC-5 was reverted, at least in part, by ACEi and ARB treatment and normalized by dual RAS blockade.

We also assessed how ACEi and ARB treatment alone or in combination impacts fibrosis in the non-clipped kidney of 2K-1C rats. TGF-β is recognized as a vital mediator in kidney fibrosis. Mechanical forces are known to induce TGF-β signaling and neutralization of TGF-β with antibodies abrogates the increase in collagen synthesis in vascular smooth muscle cells (O'Callaghan and Williams, 2000). Therefore, upregulation of TGF-β and collagen deposition observed in the non-clipped kidney of 2K-1C rats might be at least partially attributed to the hypertensive state, and these mechanisms are blunted by ACEi and ARB treatments that reduce BP levels. Moreover, Ang II is involved in direct signaling pathways triggering TGF-β secretion (Wolf, 2006) in such a way that ACEi and ARBs might also attenuate TGF-β signaling by a pressure-independent mechanism. Interestingly, collagen deposition differs between enalapril-treated and losartan-treated 2K-1C rats, despite similar TGF-β levels, suggesting that other molecular factors may contribute to kidney fibrosis under these conditions. Losartan-mediated blockade of AT1R might be more efficient in normalizing collagen deposition since losartan treatment not only decreases renal Ang II synthesis, as ACEi treatment does, but also directly blocks AT1R signaling. It is known that AT2R stimulation induces a decrease in collagen synthesis (Danyel et al., 2013), and losartan-treated kidneys might switch from an Ang II signaling to an AT2R-dependent pathway, thus further reducing collagen deposition.

Even though dual RAS therapy is superior to monotherapy for BP control and proteinuria, such superiority does not translate into improvements in long-term clinical outcomes. Moreover, dual blockade of the RAS is associated with a higher prevalence of hyperkalemia in patients with hypertension. As potassium net secretion is defined by modulation of ion transport at the distal nephron (Malnic et al., 1964), we assessed the effect of dual RAS blockade on the modulation of a critical channel that indirectly favors potassium secretion, the epithelial sodium channel (ENaC). Indeed, the inhibition of ENaC impairs renal potassium secretion and causes hyperkalemia, whereas the stimulation of ENaC increases renal potassium secretion and leads to hypokalemia. Accordingly, we observed that 2K-1C rats presented lower levels of plasma potassium associated with higher fractional excretion of potassium and increased expression of the active cleaved forms of α-ENaC and γ-ENaC and upregulation of β-ENaC. On the other hand, 2K-1C rats treated with either ACEi or ARB alone had lower markers of ENaC activation compared to vehicle-treated 2K-1C rats, and K^+ excretion was attenuated. The combined therapy of ACEi and ARB normalized the abundance of β-ENaC and cleaved γ-ENaC in the non-clipped kidney of 2K-1C rats. Notably, dual RAS

blockade decreased the renal cortical content of cleaved α-ENaC to levels that were even lower than those of 2K normotensive rats, which may explain, at least in part, the presence of hyperkalemia.

It is known that both α- and γ-ENaC are activated by double cleavage of N-terminal sites and consequent release of auto-inhibitory peptides (Carattino et al., 2008; Passero et al., 2010). α-ENaC is cleaved twice by furin, an intracellular protease that resides in the trans-Golgi network (TGN) (Carattino et al., 2008). On the other hand, γ-ENaC is cleaved once by furin and then cleaved at another site by other collecting duct membrane proteases (Frindt et al., 2016). It is also known that ENaC in rat kidneys can bypass TGN trafficking and, thus, furin cleavage step, resulting in a heterogeneous population of cleaved and non-cleaved ENaC channels plasma membrane. Evidence suggests that ENaC trafficking through TGN is regulated positively by a low-salt diet, implicating the involvement of RAS (Frindt et al., 2016). In this regard, Dooley and colleagues (Dooley et al., 2013) observed that aldosterone treatment in collecting duct cells induces a protein complex at TGN that is essential for ENaC induced exocytosis. As far as we know, it is not clear whether Ang II can also directly modulate similar regulatory processes at TGN. Our observations that α-ENaC cleavage is upregulated in hypertensive 2K-1C rats and then downregulated by combined treatment are in line with these previous observations. These findings suggest that Ang II signaling upregulates, either directly or indirectly, the cleavage of α-ENaC and, consequently, the activity of the channel.

Moreover, the β-ENaC expression is also upregulated in some hypertension models, such as SHR and Dahl salt-sensitive rats (Haloui et al., 2013; Pavlov et al., 2013). Although previous studies have not shown evidence for direct stimulation of β-ENaC expression by Ang II or aldosterone (Masilamani et al., 1999; Loffing et al., 2001; Beutler et al., 2003), recent work demonstrated that a non-pressor dose of Ang II is able to upregulate β-ENaC protein expression, even in mineralocorticoid receptor-knockout mice (Wu et al., 2020). This is in line with our results that showed higher β-ENaC expression in cortical membranes of 2K-1C rats, partial normalization by ACEi or ARB treatment, and normalization to control levels in combined therapy.

Other mechanisms for modulation of potassium excretion during ACEi and ARB therapy may not be ruled out. Indeed, ACEi treatment seems to considerably reduce the fractional excretion of potassium compared to vehicle-treated 2K-1C rats, despite modest changes in ENaC regulation. It is known that BK channels in the distal nephron can be activated by flow, thus increasing potassium secretion (Liu et al., 2009). We have observed that 2K-1C rats had significantly increased urinary flow, and that was attenuated by ACEi and ARB treatments. Such diuresis reduction might also be important to attenuate potassium excretion in ACEi- and ARB-treated 2K-1C rats. Lee and colleagues (Lee et al., 2001) have observed that the increase in urinary flow observed in 2K-1C rats was associated with a decreased expression of AQP2 in the clipped kidney, especially in the outer medulla region. Interestingly, the downregulation of AQP2 was reverted when the kidney was unclipped for 24 h. They also observed that clipped kidney medulla is less responsive to vasopressin, an effect that was also reverted by 1-day unclipping. These observations suggest that decreased kidney perfusion might blunt AVP response and, then, antidiuretic mechanisms. Accordingly, collecting duct cells chronically treated with activators of AMPK, a protein that is activated by hypoxia, reduces the cell ability to AQP2 upregulation in response to forskolin (Al-Bataineh et al., 2016). Dual RAS blockade may ameliorate renal perfusion, thus improving antidiuresis. It is known that cortical and medullary perfusion in 2K-1C is decreased even in unclipped kidneys compared to sham rat kidneys, despite a higher BP (Wickman et al., 2001). This event might be associated with Ang II-induced hemodynamic changes in afferent and efferent arterioles. Accordingly, it is reported that peritubular capillary perfusion is reduced by Ang II administration in rats and patients (Nangaku and Fujita, 2008). Reducing renal RAS status by ACEi and ARB therapy attenuates vasoconstriction in glomeruli, thus improving perfusion to downstream vascular beds.

In conclusion, we demonstrate that dual RAS blockade may ameliorate proteinuria by preventing downregulation of components of the glomerular filtration barrier and the apical endocytic machinery in the renal proximal tubule. While dual RAS blockade normalized the expression of podocin, cubilin, and ClC-5, the single blockade of the RAS only attenuated the Ang II and/or BP-induced downregulation of these proteins may explain the superior antiproteinuric effect of dual vs. single RAS blockade in renovascular hypertensive rats. Additionally, we show that dual vs. single RAS blockade differentially impacts renal ENaC modulation at both translational and posttranslational levels. Moreover, we observed that dual RAS blockade-induced hyperkalemia is associated with exacerbated downregulation of the active cleaved form of α-ENaC.

DATA AVAILABILITY STATEMENT

The raw data supporting the conclusions of this article will be made available by the authors, without undue reservation.

ETHICS STATEMENT

The animal study was reviewed and approved by the Institutional Animal Care and Use Committee of the University of São Paulo, Ribeirão Preto, SP, Brazil.

AUTHOR CONTRIBUTIONS

JC, LB, and AG designed the study. JC, KB, LS, TS, and FM carried out the experiments. JC, KB, LS, JP, and FM analyzed the data. JC, JP, and AG wrote the manuscript. JC and LS prepared the

figures. All authors contributed to the article and approved the submitted version.

FUNDING

This work was supported by the São Paulo State Research Foundation (FAPESP) Grant 2016/22140-7, National Council for Scientific Grant 307156/2018-4, and Technological Development and Coordination for the Improvement of Higher Education Personnel (CAPES) – Finance Code 001.

ACKNOWLEDGMENTS

We thank Maria Elena Riul from the Department of Pathology, Ribeirão Preto Medical School, University of São Paulo, for expert technical assistance.

REFERENCES

Al-Bataineh, M. M., Li, H., Ohmi, K., Gong, F., Marciszyn, A. L., Naveed, S., et al. (2016). Activation of the metabolic sensor AMP-activated protein kinase inhibits aquaporin-2 function in kidney principal cells. *Am. J. Physiol. Renal Physiol.* 311, F890–F900.

Aroor, A., Zuberek, M., Duta, C., Meuth, A., Sowers, J. R., Whaley-Connell, A., et al. (2016). Angiotensin II stimulation of DPP4 activity regulates megalin in the proximal tubules. *Int. J. Mol. Sci.* 17:780. doi: 10.3390/ijms17050780

Arruda-Junior, D. F., Virgulino, S. G., and Girardi, A. C. (2014). Reduced tubular proteinuria in hypertensive rats treated with losartan is associated with higher renal cortical megalin expression. *Horm. Mol. Biol. Clin. Investig.* 18, 105–112.

Athyros, V. G., Mikhailidis, D. P., Kakafika, A. I., Tziomalos, K., and Karagiannis, A. (2007). Angiotensin II reactivation and aldosterone escape phenomena in renin-angiotensin-aldosterone system blockade: is oral renin inhibition the solution? *Expert Opin. Pharmacother.* 8, 529–535. doi: 10.1517/14656566.8.5.529

Bautista, R., Manning, R., Martinez, F., Avila-Casado, M. E. C., Soto, V., Medina, A., et al. (2004). Angiotensin II-dependent increased expression of Na+-glucose cotransporter in hypertension. *Am. J. Physiol. Renal Physiol.* 286, F127–F133.

Berger, R. C., Vassallo, P. F., Crajoinas, R. E. O., Oliveira, M. L., Martins, F. L., Nogueira, B. V., et al. (2015). Renal effects and underlying molecular mechanisms of long-term salt content diets in spontaneously hypertensive rats. *PLoS One* 10:e0141288. doi: 10.1371/journal.pone.0141288

Beutler, K. T., Masilamani, S., Turban, S., Nielsen, J., Brooks, H. L., Ageloff, S., et al. (2003). Long-term regulation of ENaC expression in kidney by angiotensin II. *Hypertension* 41, 1143–1150. doi: 10.1161/01.hyp.0000066129.12106.e2

Bhalla, V., and Hallows, K. R. (2008). Mechanisms of ENaC regulation and clinical implications. *J. Am. Soc. Nephrol.* 19, 1845–1854. doi: 10.1681/asn.2008020225

Birn, H., and Christensen, E. I. (2006). Renal albumin absorption in physiology and pathology. *Kidney Int.* 69, 440–449. doi: 10.1038/sj.ki.5000141

Bubien, J. K. (2010). Epithelial Na+ channel (ENaC), hormones, and hypertension. *J. Biol. Chem.* 285, 23527–23531. doi: 10.1074/jbc.r109.025049

Carattino, M. D., Passero, C. J., Steren, C. A., Maarouf, A. B., Pilewski, J. M., Myerburg, M. M., et al. (2008). Defining an inhibitory domain in the alpha-subunit of the epithelial sodium channel. *Am. J. Physiol. Renal Physiol.* 294, F47–F52.

Carraro-Lacroix, L. R., Lessa, L. M. A., Bezerra, C. N. A., Pessoa, T. D., Souza-Menezes, J., Morales, M. M., et al. (2010). Role of CFTR and ClC-5 in modulating vacuolar H+-ATPase activity in kidney proximal tubule. *Cell. Physiol. Biochem.* 26, 563–576. doi: 10.1159/000322324

Carson, P., Giles, T., Higginbotham, M., Hollenberg, N., Kannel, W., and Siragy, H. M. (2001). Angiotensin receptor blockers: evidence for preserving target organs. *Clin. Cardiol.* 24, 183–190. doi: 10.1002/clc.4960240303

Corrêa, J. W. D. N., Prado, C. M., Riul, M. E., Araújo, A. V., Rossi, M. A., and Bendhack, L. M. (2020). Reversion of cardiovascular remodelling in renovascular hypertensive 2K-1C rats by renin-angiotensin system inhibitors. *Clin. Exp. Pharmacol. Physiol.* 47, 1965–1977.

Crowley, S. D., Gurley, S. B., Herrera, M. J., Ruiz, P., Griffiths, R., Kumar, A. P., et al. (2006). Angiotensin II causes hypertension and cardiac hypertrophy through its receptors in the kidney. *Proc. Natl. Acad. Sci. U.S.A.* 103, 17985–17990. doi: 10.1073/pnas.0605545103

Crowley, S. D., Gurley, S. B., Oliverio, M. I., Pazmino, A. K., Griffiths, R., Flannery, P. J., et al. (2005). Distinct roles for the kidney and systemic tissues in blood pressure regulation by the renin-angiotensin system. *J. Clin. Invest.* 115, 1092–1099. doi: 10.1172/jci23378

Dahlof, B., Devereux, R. B., Kjeldsen, S. E., Julius, S., Beevers, G., De Faire, U., et al. (2002). Cardiovascular morbidity and mortality in the Losartan Intervention For Endpoint reduction in hypertension study (LIFE): a randomised trial against atenolol. *Lancet* 359, 995–1003. doi: 10.1016/s0140-6736(02)08089-3

Danyel, L. A., Schmerler, P., Paulis, L., Unger, T., and Steckelings, U. M. (2013). Impact of AT2-receptor stimulation on vascular biology, kidney function, and blood pressure. *Integr. Blood Press. Control* 6, 153–161. doi: 10.2147/ibpc.s34425

Dooley, R., Angibaud, E., Yusef, Y. R., Thomas, W., and Harvey, B. J. (2013). Aldosterone-induced ENaC and basal Na+/K+-ATPase trafficking via protein kinase D1-phosphatidylinositol 4-kinaseIIIβ trans Golgi signalling in M1 cortical collecting duct cells. *Mol. Cell. Endocrinol.* 372, 86–95. doi: 10.1016/j.mce.2013.03.011

Doulton, T. W., He, F. J., and Macgregor, G. A. (2005). Systematic review of combined angiotensin-converting enzyme inhibition and angiotensin receptor blockade in hypertension. *Hypertension* 45, 880–886. doi: 10.1161/01.hyp.0000161880.59963.da

Feng, Y., Huang, R., Kavanagh, J., Li, L., Zeng, X., Li, Y., et al. (2019). Efficacy and safety of dual blockade of the renin-angiotensin-aldosterone system in diabetic kidney disease: a meta-analysis. *Am. J. Cardiovasc. Drugs* 19, 259–286. doi: 10.1007/s40256-018-00321-5

Frindt, G., Gravotta, D., and Palmer, L. G. (2016). Regulation of ENaC trafficking in rat kidney. *J. Gen. Physiol.* 147, 217–227. doi: 10.1085/jgp.201511533

Gekle, M. (2005). Renal tubule albumin transport. *Annu. Rev. Physiol.* 67, 573–594. doi: 10.1146/annurev.physiol.67.031103.154845

Gekle, M., Knaus, P., Nielsen, R., Mildenberger, S., Freudinger, R., Wohlfarth, V., et al. (2003). Transforming growth factor-beta1 reduces megalin- and cubilin-mediated endocytosis of albumin in proximal-tubule-derived opossum kidney cells. *J. Physiol.* 552, 471–481. doi: 10.1113/jphysiol.2003.048074

Grahammer, F., Schell, C., and Huber, T. B. (2013). The podocyte slit diaphragm–from a thin grey line to a complex signalling hub. *Nat. Rev. Nephrol.* 9, 587–598. doi: 10.1038/nrneph.2013.169

Günther, W., Lüchow, A., Cluzeaud, F., Vandewalle, A., and Jentsch, T. J. (1998). ClC-5, the chloride channel mutated in Dent's disease, colocalizes with the proton pump in endocytotically active kidney cells. *Proc. Natl. Acad. Sci. U.S.A.* 95, 8075–8080. doi: 10.1073/pnas.95.14.8075

Haloui, M., Tremblay, J., Seda, O., Koltsova, S. V., Maksimov, G. V., Orlov, S. N., et al. (2013). Increased renal epithelial na channel expression and activity correlate with elevation of blood pressure in spontaneously hypertensive rats. *Hypertension* 62, 731–737. doi: 10.1161/hypertensionaha.113.01295

Hryciw, D. H., Ekberg, J., Pollock, C. A., and Poronnik, P. (2006). ClC-5: a chloride channel with multiple roles in renal tubular albumin uptake. *Int. J. Biochem. Cell Biol.* 38, 1036–1042. doi: 10.1016/j.biocel.2005.09.009

Huang, C., Bruggeman, L. A., Hydo, L. M., and Miller, R. T. (2012). Shear stress induces cell apoptosis via a c-Src-phospholipase D-mTOR signaling pathway in cultured podocytes. *Exp. Cell Res.* 318, 1075–1085. doi: 10.1016/j.yexcr.2012.03.011

Inoue, B. H., Arruda-Junior, D. F., Campos, L. C. G., Barreto, A. L. T., Rodrigues, M. V., Krieger, J. E., et al. (2013). Progression of microalbuminuria in SHR is associated with lower expression of critical components of the apical endocytic machinery in the renal proximal tubule. *Am. J. Physiol. Renal Physiol.* 305, F216–F226.

Jia, J., Ding, G., Zhu, J., Chen, C., Liang, W., Franki, N., et al. (2008). Angiotensin II infusion induces nephrin expression changes and podocyte apoptosis. *Am. J. Nephrol.* 28, 500–507. doi: 10.1159/000113538

Kleyman, T. R., Carattino, M. D., and Hughey, R. P. (2009). ENaC at the cutting edge: regulation of epithelial sodium channels by proteases. *J. Biol. Chem.* 284, 20447–20451. doi: 10.1074/jbc.r800083200

Kunz, R., Friedrich, C., Wolbers, M., and Mann, J. F. (2008). Meta-analysis: effect of monotherapy and combination therapy with inhibitors of the renin angiotensin system on proteinuria in renal disease. *Ann. Intern. Med.* 148, 30–48. doi: 10.7326/0003-4819-148-1-200801010-00190

Langham, R. G., Kelly, D. J., Cox, A. J., Gow, R. M., Holthofer, H., and Gilbert, R. E. (2004). Angiotensin II-induced proteinuria and expression of the podocyte slit pore membrane protein, nephrin. *Nephrol. Dial. Transplant.* 19, 262–263. doi: 10.1093/ndt/gfg509

Lassila, M., Cooper, M. E., and Jandeleit-Dahm, K. (2004). Antiproteinuric effect of RAS blockade: new mechanisms. *Curr. Hypertens. Rep.* 6, 383–392. doi: 10.1007/s11906-004-0058-9

Lee, J., Oh, Y., and Kim, S. W. (2001). Altered renal expression of aquaporin-2 water channels in rats with experimental two-kidney, one clip hypertension. *J. Korean Med. Sci.* 16, 462–466. doi: 10.3346/jkms.2001.16.4.462

Li, Y., Cong, R., and Biemesderfer, D. (2008). The COOH terminus of megalin regulates gene expression in opossum kidney proximal tubule cells. *Am. J. Physiol. Cell Physiol.* 295, C529–C537.

Liu, W., Wei, Y., Sun, P., Wang, W. H., Kleyman, T. R., and Satlin, L. M. (2009). Mechanoregulation of BK channel activity in the mammalian cortical collecting duct: role of protein kinases A and C. *Am. J. Physiol. Renal Physiol.* 297, F904–F915.

Loffing, J., Zecevic, M., Féraille, E., Kaissling, B., Asher, C., Rossier, B. C., et al. (2001). Aldosterone induces rapid apical translocation of ENaC in early portion of renal collecting system: possible role of SGK. *Am. J. Physiol. Renal Physiol.* 280, F675–F682.

Long, D. A., Price, K. L., Herrera-Acosta, J., and Johnson, R. J. (2004). How does angiotensin II cause renal injury? *Hypertension* 43, 722–723. doi: 10.1161/01.hyp.0000120964.22281.3e

Lopes, N. R., Milanez, M. I. O., Martins, B. S., Veiga, A. C., Ferreira, G. R., Gomes, G. N., et al. (2020). Afferent innervation of the ischemic kidney contributes to renal dysfunction in renovascular hypertensive rats. *Pflugers Arch.* 472, 325–334. doi: 10.1007/s00424-019-02346-4

Lowry, O. H., Rosebrough, N. J., Farr, A. L., and Randall, R. J. (1951). Protein measurement with the Folin phenol reagent. *J. Biol. Chem.* 193, 265–275. doi: 10.1016/s0021-9258(19)52451-6

Malnic, G., Klose, R. M., and Giebisch, G. (1964). Micropuncture study of renal potassium excretion in the rat. *Am. J. Physiol.* 206, 674–686. doi: 10.1152/ajplegacy.1964.206.4.674

Mann, J. F., and Böhm, M. (2015). Dual renin-angiotensin system blockade and outcome benefits in hypertension: a narrative review. *Curr. Opin. Cardiol.* 30, 373–377. doi: 10.1097/hco.0000000000000173

Mann, J. F., Schmieder, R. E., Mcqueen, M., Dyal, L., Schumacher, H., Pogue, J., et al. (2008). Renal outcomes with telmisartan, ramipril, or both, in people at high vascular risk (the ONTARGET study): a multicentre, randomised, double-blind, controlled trial. *Lancet* 372, 547–553. doi: 10.1016/s0140-6736(08)61236-2

Martins, F. L., Bailey, M. A., and Girardi, A. C. C. (2020). Endogenous activation of glucagon-like peptide-1 receptor contributes to blood pressure control: role of proximal tubule Na +/H + exchanger isoform 3, renal angiotensin II, and insulin sensitivity. *Hypertension* 76, 839–848. doi: 10.1161/hypertensionaha.120.14868

Masilamani, S., Kim, G. H., Mitchell, C., Wade, J. B., and Knepper, M. A. (1999). Aldosterone-mediated regulation of ENaC alpha, beta, and gamma subunit proteins in rat kidney. *J. Clin. Invest.* 104, R19–R23.

Mori, T., and Cowley, A. W. (2004). Role of pressure in angiotensin II-induced renal injury: chronic servo-control of renal perfusion pressure in rats. *Hypertension* 43, 752–759. doi: 10.1161/01.hyp.0000120971.49659.6a

Nangaku, M., and Fujita, T. (2008). Activation of the renin-angiotensin system and chronic hypoxia of the kidney. *Hypertens. Res.* 31, 175–184. doi: 10.1291/hypres.31.175

Navar, L. G., Prieto, M. C., Satou, R., and Kobori, H. (2011). Intrarenal angiotensin II and its contribution to the genesis of chronic hypertension. *Curr. Opin. Pharmacol.* 11, 180–186. doi: 10.1016/j.coph.2011.01.009

Navar, L. G., Zou, L., Von Thun, A., Tarng Wang, C., Imig, J. D., and Mitchell, K. D. (1998). Unraveling the mystery of Goldblatt hypertension. *News Physiol. Sci.* 13, 170–176. doi: 10.1152/physiologyonline.1998.13.4.170

Nielsen, R., Christensen, E. I., and Birn, H. (2016). Megalin and cubilin in proximal tubule protein reabsorption: from experimental models to human disease. *Kidney Int.* 89, 58–67. doi: 10.1016/j.kint.2015.11.007

O'Callaghan, C. J., and Williams, B. (2000). Mechanical strain-induced extracellular matrix production by human vascular smooth muscle cells: role of TGF-beta(1). *Hypertension* 36, 319–324. doi: 10.1161/01.hyp.36.3.319

Otomo, H., Nara, M., Kato, S., Shimizu, T., Suganuma, Y., Sato, T., et al. (2020). Sodium-glucose cotransporter 2 inhibition attenuates protein overload in renal proximal tubule via suppression of megalin O-GlcNacylation in progressive diabetic nephropathy. *Metabolism* 113;154405. doi: 10.1016/j.metabol.2020.154405

Palmer, L. G., Patel, A., and Frindt, G. (2012). Regulation and dysregulation of epithelial Na+ channels. *Clin. Exp. Nephrol.* 16, 35–43. doi: 10.1007/s10157-011-0496-z

Passero, C. J., Carattino, M. D., Kashlan, O. B., Myerburg, M. M., Hughey, R. P., and Kleyman, T. R. (2010). Defining an inhibitory domain in the gamma subunit of the epithelial sodium channel. *Am. J. Physiol. Renal Physiol.* 299, F854–F861.

Pavlov, T. S., Levchenko, V., O'Connor, P. M., Ilatovskaya, D. V., Palygin, O., Mori, T., et al. (2013). Deficiency of renal cortical EGF increases ENaC activity and contributes to salt-sensitive hypertension. *J. Am. Soc. Nephrol.* 24, 1053–1062. doi: 10.1681/asn.2012080839

Pfeffer, M. A., Mcmurray, J. J., Velazquez, E. J., Rouleau, J. L., Køber, L., Maggioni, A. P., et al. (2003). Valsartan, captopril, or both in myocardial infarction complicated by heart failure, left ventricular dysfunction, or both. *N. Engl. J. Med.* 349, 1893–1906. doi: 10.1056/nejmoa032292

Phillips, C. O., Kashani, A., Ko, D. K., Francis, G., and Krumholz, H. M. (2007). Adverse effects of combination angiotensin II receptor blockers plus angiotensin-converting enzyme inhibitors for left ventricular dysfunction: a quantitative review of data from randomized clinical trials. *Arch. Intern. Med.* 167, 1930–1936. doi: 10.1001/archinte.167.18.1930

Pollock, C. A., and Poronnik, P. (2007). Albumin transport and processing by the proximal tubule: physiology and pathophysiology. *Curr. Opin. Nephrol. Hypertens.* 16, 359–364. doi: 10.1097/mnh.0b013e3281eb9059

Raebel, M. A. (2012). Hyperkalemia associated with use of angiotensin-converting enzyme inhibitors and angiotensin receptor blockers. *Cardiovasc. Ther.* 30, e156–e166.

Saglimbene, V., Palmer, S. C., Ruospo, M., Natale, P., Maione, A., Nicolucci, A., et al. (2018). The long-term impact of renin-angiotensin system (RAS) inhibition on cardiorenal outcomes (LIRICO): a randomized, controlled trial. *J. Am. Soc. Nephrol.* 29, 2890–2899. doi: 10.1681/asn.2018040443

Seccia, T. M., Caroccia, B., and Calò, L. A. (2017). Hypertensive nephropathy. moving from classic to emerging pathogenetic mechanisms. *J. Hypertens.* 35, 205–212. doi: 10.1097/hjh.0000000000001170

Silva Dos Santos, D., Polidoro, J. Z., Borges-Júnior, F. A., and Girardi, A. C. C. (2020). Cardioprotection conferred by sodium-glucose cotransporter 2 inhibitors: a renal proximal tubule perspective. *Am. J. Physiol. Cell Physiol.* 318, C328–C336.

Tanaka, K., and Nakaki, T. (2004). Reduced renal ClC-5 Cl- channel expression in spontaneously hypertensive rats with microalbuminuria. *Eur. J. Pharmacol.* 501, 185–189. doi: 10.1016/j.ejphar.2004.08.012

Viazzi, F., Bonino, B., Cappadona, F., and Pontremoli, R. (2016). Renin-angiotensin-aldosterone system blockade in chronic kidney disease: current strategies and a look ahead. *Intern. Emerg. Med.* 11, 627–635. doi: 10.1007/s11739-016-1435-5

Waller, K. V., Ward, K. M., Mahan, J. D., and Wismatt, D. K. (1989). Current concepts in proteinuria. *Clin. Chem.* 35, 755–765. doi: 10.1093/clinchem/35.5.755

Wharram, B. L., Goyal, M., Wiggins, J. E., Sanden, S. K., Hussain, S., Filipiak, W. E., et al. (2005). Podocyte depletion causes glomerulosclerosis: diphtheria toxin-induced podocyte depletion in rats expressing human diphtheria toxin receptor transgene. *J. Am. Soc. Nephrol.* 16, 2941–2952. doi: 10.1681/asn.2005010055

Wickman, A., Andersson, I. J., Jia, J., Hedin, L., and Bergström, G. (2001). Endothelial nitric oxide synthase protein is reduced in the renal medulla of two-kidney, one-clip hypertensive rats. *J. Hypertens.* 19, 1665–1673. doi: 10.1097/00004872-200109000-00020

Wolf, G. (2006). Renal injury due to renin-angiotensin-aldosterone system activation of the transforming growth factor-beta pathway. *Kidney Int.* 70, 1914–1919. doi: 10.1038/sj.ki.5001846

Wu, P., Gao, Z. X., Zhang, D. D., Duan, X. P., Terker, A. S., Lin, D. H., et al. (2020). Effect of angiotensin II on ENaC in the distal convoluted tubule and in the cortical collecting duct of mineralocorticoid receptor deficient mice. *J. Am. Heart Assoc.* 9:e014996.

Yadav, A., Vallabu, S., Arora, S., Tandon, P., Slahan, D., Teichberg, S., et al. (2010). ANG II promotes autophagy in podocytes. *Am. J. Physiol. Cell Physiol.* 299, C488–C496.

Yang, Y., Yang, Q., Yang, J., Ma, Y., and Ding, G. (2017). Angiotensin II induces cholesterol accumulation and injury in podocytes. *Sci. Rep.* 7:10672.

Zhao, M., Bai, M., Ding, G., Zhang, Y., Huang, S., Jia, Z., et al. (2018). Angiotensin II stimulates the NLRP3 inflammasome to induce podocyte injury and mitochondrial dysfunction. *Kidney Dis. (Basel)* 4, 83–94. doi: 10.1159/000488242

Conflict of Interest: The authors declare that the research was conducted in the absence of any commercial or financial relationships that could be construed as a potential conflict of interest.

frontiers in Physiology

ORIGINAL RESEARCH
published: 22 June 2021
doi: 10.3389/fphys.2021.648056

Gestational Low Protein Diet Modulation on miRNA Transcriptome and Its Target During Fetal and Breastfeeding Nephrogenesis

*Letícia de Barros Sene[1], Gabriela Leme Lamana[2], Andre Schwambach Vieira[3], Wellerson Rodrigo Scarano[1], José Antônio Rocha Gontijo[2] and Patrícia Aline Boer[2]**

[1] Department of Structural and Functional Biology, Institute of Biosciences, São Paulo State University (UNESP), Botucatu, Brazil, [2] Fetal Programming and Hydroelectrolyte Metabolism Laboratory, Nucleus of Medicine and Experimental Surgery, Department of Internal Medicine, FCM, Campinas, Brazil, [3] Department of Structural and Functional Biology, Biology Institute, State University of Campinas (UNICAMP), Campinas, Brazil

OPEN ACCESS

Edited by:
Guiomar Nascimento Gomes, Federal University of São Paulo, Brazil

Reviewed by:
Egberto Gaspar Moura, Rio de Janeiro State University, Brazil
Jacqueline Ho, University of Pittsburgh School of Medicine, United States

***Correspondence:**
Patrícia Aline Boer
alineboer@yahoo.com.br; boer@fcm.unicamp.br

Specialty section:
This article was submitted to Renal and Epithelial Physiology, a section of the journal Frontiers in Physiology

Received: *31 December 2020*
Accepted: *22 April 2021*
Published: *22 June 2021*

Citation:
de Barros Sene L, Lamana GL, Schwambach Vieira A, Scarano WR, Gontijo JAR and Boer PA (2021) Gestational Low Protein Diet Modulation on miRNA Transcriptome and Its Target During Fetal and Breastfeeding Nephrogenesis. Front. Physiol. 12:648056. doi: 10.3389/fphys.2021.648056

Background: The kidney ontogenesis is the most structurally affected by gestational protein restriction, reducing 28% of their functional units. The reduced nephron number is predictive of hypertension and cardiovascular dysfunctions that are generally observed in the adult age of most fetal programming models. We demonstrate miRNAs and predict molecular pathway changes associated with reduced reciprocal interaction between metanephros cap (CM) and ureter bud (UB) and a 28% decreased nephron stem cells in the 17 gestational days (17GD) low protein (LP) intake male fetal kidney. Here, we evaluated the same miRNAs and predicted targets in the kidneys of 21GD and at 7 days of life (7DL) LP offspring to elucidate the molecular modulations during nephrogenesis.

Methods: Pregnant Wistar rats were allocated into two groups: NP (regular protein diet-17%) or LP (diet-6%). miRNA transcriptome sequencing (miRNA-Seq) was performed on the MiSeq platform from 21GD and 7DL male offspring kidneys using previously described methods. Among the top 10 dysfunctional regulated miRNAs, we validated 7 related to proliferation, differentiation, and apoptosis processes and investigated predicted target genes and proteins by RT-qPCR and immunohistochemistry.

Results: In 21GD, LP fetuses were identified alongside 21 differently expressed miRNAs, of which 12 were upregulated and 9 downregulated compared to age-matched NP offspring. In 7-DL LP offspring, the differentially expressed miRNAs were counted to be 74, of which 46 were upregulated and 28 downregulated. The curve from 17-GD to 7-DL shows that mTOR was fundamental in reducing the number of nephrons in fetal kidneys where the mothers were subjected to a protein restriction. IGF1 and TGFβ curves also seemed to present the same mTOR pattern and were modulated by miRNAs 181a-5p, 181a-3p, and 199a-5p. The miRNA 181c-3p modulated SIX2 and Notch1 reduction in 7-DL but not in terms of the enhanced expression of both in the 21-GD, suggesting the participation of an additional regulator. We found enhanced Bax

in 21-GD; it was regulated by miRNA 298-5p, and Bcl2 and Caspase-3 were controlled by miRNA (by 7a-5p and not by the predicted 181a-5p). The miRNA 144-3p regulated BCL6, which was enhanced, as well as Zeb 1 and 2 induced by BCL6. These results revealed that in 21GD, the compensatory mechanisms in LP kidneys led to the activation of UB ramification. Besides, an increase of 32% in the CM stem cells and a possible cell cycle halt of renal progenitor cells, which remaining undifferentiated, were observed. In the 7DL, much more altered miRNA expression was found in LP kidneys, and this was probably due to an increased maternal diet content. Additionally, we verified the activation of pathways related to differentiation and consumption of progenitor cells.

Keywords: fetal programming, gestational low-protein intake, nephrogenesis, metanephric mesenchyme, low nephron number, miRNA

INTRODUCTION

Maternal nutritional restriction results in several critical changes in the fetal organ and system during the development stages, which may cause irreversible disorders in adult life (Langley-Evans, 2006). Fetal programming is characterized as any psychological and nutritional stress during development, which leads to long-term effects on kidney structure and function disorders with an increasing predictive chance to develop chronic renal disease (Lucas, 1998). Disturbance in fetal programming results in low birth weight, fewer nephrons, and increased risk of cardiovascular and renal disorders in adulthood (Mesquita et al., 2010a,b; Sene et al., 2013, 2018, 2021). The low nephron number is related to hypertension, and in hypertensive patients, approximately 46% of the number of nephrons is reduced (Mackenzie et al., 1996). Prior experimental studies from our lab and other authors have demonstrated lower birth weight, 28% fewer nephrons, reduced renal salt excretion, chronic renal failure, and enhanced systolic pressure from 8 to 16 weeks of life in gestational low-protein (LP) intake compared to standard (NP) protein intake offspring in adulthood (Schreuder et al., 2006; Mesquita et al., 2010a,b; Sene et al., 2013, 2018, 2021). However, information regarding the molecular mechanisms of the etiopathogenesis of nephrogenesis cessation is still scarce. Recently, Huang et al. showed evidence indicating epigenetic mechanisms controlling the nephrogenesis process.

Nephrogenesis involves fine control of gene expression, protein synthesis, tissue remodeling, and cell fates of the different kidney progenitor cells (Huang et al., 2020). During renal ontogenesis, nephron stem cell renewal and differentiation are too controlled to generate an adequate number of nephrons. These kidney nephron numbers are defined by a closed interaction among ureter bud (UB) and metanephros mesenchyme (MM) progenitor cells (Grobstein, 1955; Saxen and Sariola, 1987; Pan et al., 2017). Signals from MM induce UB-stimulated growth and branching of the tubule system. In turn, MM proliferation and differentiation, constituting a mesenchymal cap (CM), is mediated by UB ends (Phua et al., 2015). There has been serious interest in the role of epigenetic changes, concerning the long-term effects of prenatal stress, on fetal development (Monk et al., 2012). MicroRNAs (miRNAs) are genome-encoded small non-coding RNAs of approximately 22 nucleotides in length, and they play an essential role in the post-transcriptional regulation of target gene expression (Ambros, 2004; Bartel, 2004; Nilsen, 2007). Studies indicate that miRNAs are involved in many regulatory biological networks during development and cell physiology. Deregulation in their expression has been observed in several pathologies (Bushati and Cohen, 2007; Chang and Mendell, 2007). Thus, miRNA characterization is indispensable for nephron development and may help us understand gene regulation and cellular proliferation, differentiation, and apoptosis and explain pathophysiology, including kidney disorders (Chu and Rana, 2007; Harvey et al., 2008; Kim et al., 2009; Li et al., 2010; Chu et al., 2014). However, reduced miRNA expression in MM progenitor cells may decrease cell proliferation, resulting in early differentiation and a reduced number of nephrons (Ho et al., 2011; Nagalakshmi et al., 2011). This phenomenon is characterized by increased apoptosis and high Bim expression in progenitor cells. Thus, miRNAs modulate the balance between apoptosis and proliferation of these metanephric primary cells (Ho et al., 2011). We recently demonstrated in the fetus at 17 days of gestation (GD) protein-restricted male fetus changes in metanephros miRNAs and predicted mRNA expression that encodes proteins related to nephrogenesis a 28% reduction in nephrogenic stem cells in the cap metanephric (CM). We suggested that miRNAs, mRNAs, and protein disruption could have reduced proliferation and promote early cell differentiation

Abbreviations: Bax, Apoptosis regulator; Bcl2, B-cell lymphoma 2; Bcl6, B-cell lymphoma 6; Bim, or Bcl-2-like protein 11; BSA, Bovine serum albumin; cDNA, complementary deoxyribonucleic acid; CEUA/UNESP, Institutional Ethics Committee; c-Myc, regulator genes and MYC proto-oncogenes; CM, metanephros cap; c-ret, rearranged during transfection; DAB - 3,3′, diaminobenzidine tetrahydrochloride; DNA, deoxyribonucleic acid; GD, gestational days; GAPDH, Glyceraldehyde 3-phosphate dehydrogenase; GDNF, Glial cell line-derived neurotrophic factor; IGF1, Insulin-like growth factor 1; Ki67, a nuclear protein associated with cellular proliferation; let-7, lethal-7 (let-7) gene; Lin28b, Lin-28 Homolog B, suppressor of microRNA (miRNA) biogenesis; LP, gestational low-protein intake; Map2k2, mitogen-activated protein kinase kinase 2; *miRNA (miR)*, a small non-coding RNA molecule; *miRNA-Seq*, *miRNA sequencing*; mRNA, messenger ribonucleic acid; mTOR, mammalian target of rapamycin; NGS, Next Generation Sequencing; NOTCH1, single-pass transmembrane receptor protein; NP, normal protein intake; PCNA, Proliferating cell nuclear antigen; PRDM1, PR domain zinc finger protein 1; RIN, RNA Integrity Number; RT-qPCR, reverse transcription-polymerase chain reaction quantitative real-time; Six2, SIX homeobox 2; TGFβ-1, transforming growth factor-beta 1; UB, ureter bud; U6 and U87, internal reference gene; Zeb1 and Zeb2, Zinc finger E-box-binding homeobox 1 and 2; 21GD, 21th gestational day; 7DL, 7 days of life kidney.

(Sene et al., 2021). The rats are remaining the nephrogenesis after birth. Brown et al. (2016) showed in Sprague-Dawley rats that renal papilla is mature on day 7 of life (7DL), but cortex and medulla maturation occur, respectively, on 21 and 30DL. Additionally, Schreuder et al. (2006) demonstrated a 25% reduced nephron number over the breastfeeding period in offspring submitted to nutritional stress. Thus, in the present study, we evaluated during the last gestational day and during breastfeeding the miRNAs transcriptome and predicted targets of those more altered on the kidney of male offspring submitted to gestational low protein diet to elucidate the time-course of molecular modulations during nephrogenesis.

MATERIALS AND METHODS

Animal and Diets

The experiments were conducted on age-matched female and male rats of sibling-mated Wistar *HanUnib*rats (250–300 g) that were allowed free access to water and standard rodent chow (Nuvital, Curitiba, PR, Brazil). The Institutional Ethics Committee (#446-CEEA/UNESP) approved the experimental protocol, and the general guidelines established by the Brazilian College of Animal Experimentation were followed throughout the investigation. At 12 weeks of age, the animals were mated, and the day that sperm were seen in the vaginal smear was designated as day 1 of pregnancy. Then, dams were maintained *ad libitum* throughout the entire pregnancy on an isocaloric rodent laboratory chow with either standard protein content [NP, $n = 20$] (17% protein) or low protein content [LP, $n = 20$] (6% protein) diets. The NP and LP maternal food consumption were determined daily (subsequently normalized for body weight), and the body weight of dams was recorded weekly in both groups. At 21 days of gestation (GD), in the dams on anesthesia (75 mg/kg ketamine and 10 mg/kg xylazine), the fetuses were removed and sacrificed. The fetuses were weighed, and the kidneys were collected, weighed, and processed for Next Generation Sequencing (NGS), RT-qPCR, and immunohistochemistry analyses. An additional group of dams was maintained on the NP and LP diets throughout the entire pregnancy. After delivery, the male pups were weighed at the birth, and NP and LP dams returned to standard protein content chow intake. At 21 GD, the kidneys from male NP and LP offspring were removed, weighed, and processed for NGS, RT-qPCR, and morphological analyses.

Sexing Determination

The present study was performed only in male 17-GD offspring, and the sexing was determined by Sry conventional PCR (Polymerase Chain Reaction) sequence analysis. The DNA was extracted by enzymatic lysis with proteinase K and Phenol-Chloroform. For reaction, the Master Mix Colorless—Promega was used, with the manufacturer's cycling conditions. The Integrated DNA Technologies (IDT) synthesized the primer following sequences below:

1. Forward: 5′-TACAGCCTGAGGACATATTA-3′
2. Reverse: 5′-GCACTTTAACCCTTCGATTAG-3′.

Total RNA Extraction

RNA was extracted from NP (21GD, $n = 4$ and 7DL $n = 4$, from different mothers) and LP (21GD, $n = 4$ and 7DL $n = 4$, from different mothers) whole kidneys using Trizol reagent (Invitrogen), according to the instructions specified by the manufacturer. Total RNA quantity was determined by the absorbance at 260 nm using a nanoVue spectrophotometer (GE Healthcare, United States). RNA Integrity was ensured by obtaining an RNA Integrity Number - RIN > 8 with Agilent 2100 Bioanalyzer (Agilent Technologies, Germany).

miRNA-Seq and Data Analysis

Sequencing was performed on the MiSeq platform (Illumina). The protocol followed the manufacturer's instructions available in http://www.illumina.com/documents//products/datasheets/datasheet_truseq_sample_prep_kits.pdf. Briefly, the sequencing includes library construction, and this used 1μg total RNA. In this step, the adapters are connected (3′ and 5′). After ligation of adapters, a reverse transcription reaction was performed to create cDNA. It was then amplified by a standard PCR reaction, which uses primers containing a sequence index for sample identification—this cDNA library, subjected to agarose gel electrophoresis for miRNA isolation. After quantitation, the library concentration was normalized to 2 nM using 10 nM Tris-HCl, pH 8.5, and transcriptome sequencing was performed by MiSeq Reagent Kit v2 (50 cycles). The library construction used the TruSeq Small RNA Library Preparation Kit (catalog number RS-200-0012). Approximately 530,000 reads/samples (21DG and 7DPN) were obtained with a size of 1.35GB. The study has used Genome Reference version rn5 from the UCSC Genome Browser or (UCSC rn5) for *Rattus norvegicus*. The miRNA sequences were acquired from miRBase v21. The alignment was done by Bowtie software (version 0.12.8), and the Differential Expression was obtained by way of the Small RNA software (BaseSpace Workflow) version 1.0.0.0. and the list of all sequenced miRNAs defined by DESeq2 (version 1.0.17). Also, the sequencing data were deposited in the Bioproject repository https://www.ncbi.nlm.nih.gov/bioproject/PRJNA694197 (NCBI) with the access number: PRJNA694197. Data analysis was performed in collaboration with Tao Chen, Ph.D., from the Division of Genetic and Molecular Toxicological, National Center for Toxicological Research, Jefferson, AR, United States. The data from the Next Generation Sequencing (NGS) of miRNAs were generated in a FASTAQ format and imported into BaseSpace.com (Illumina, United States). The data quality was evaluated using the base calling CASAVA software developed by the manufacturer (Illumina). The analyses were carried out using a BaseSpace miRNA Analysis (from the University of Toronto, Canada) and the sequence mapping of different miRNAs carried out by Small RNA (Illumina, United States) for the rat genome. The differentially expressed miRNA study was analyzed using Ingenuity Pathway Analysis software (Ingenuity, United States).

miRNA Expression Validation

Among the most differentially expressed miRNA, we selected seven (miR-127-3p, -144-3p, -298-5p, let-7a-5p, Lin28b, -181a-5p, -181c-3p, and -199a-5p) for expression analysis. Briefly, 450

ng RNA was reverse transcribed, without pre-amplification, using a TaqMan® MicroRNA Reverse Transcription Kit according to the manufacturer's guidelines. Complementary DNA (cDNA) was amplified using TaqMan MicroRNA Assays (Life Technologies, United States) with *TaqMan® Universal PCR Master Mix, No AmpErase® UNG* (2x) on StepOnePlusTM Real-Time PCR System (Applied BiosystemsTM) according to the manufacturer's instructions. Data analysis was performed using relative gene expression evaluated using the comparative quantification method (Pfaffl, 2001). The U6 and U87 gene was used as a reference gene. All relative quantifications were evaluated using the DataAssist software, v 3.0, using the ΔΔCT method. miRNA data have been generated following the MIQE guidelines (Bustin et al., 2009).

RT-qPCR of Predicted Target and ZEB1/2 Genes

For the cDNA synthesis, the High Capacity cDNA reverse transcription kit (Life Technologies, United States) was used. To analyze the level of expression of 22 genes (Bax, Bim, Caspase-3, Collagen 1, GDNF, PCNA, TGFβ-1, Bcl-2, Bcl-6, c-myc, c-ret, cyclin A, Map2k2, PRDM1, Six-2, Ki67, MTOR, β-catenin, ZEB1, ZEB2, NOTCH1, and IGF1), the reaction of RT-qPCR was performed with SYBR Green Master Mix (Life Technologies, United States), using primers specific for each gene, provided by IDT® Integrated DNA Technologies (**Table 1**). The reactions were done in a total volume of 20 μL using 2 μL of cDNA (diluted 1:30), 10 μL SYBER Green Master Mix (Life Technologies, United States), and 4 μL of each specific primer (5 nM). Amplification and detection were performed using the StepOnePlusTM Real-Time PCR System (Applied BiosystemsTM). Ct values were converted to relative expression values using the ΔΔCt method with offspring kidneys data normalized to GAPDH as a reference gene.

Area and Cells Quantification

Hematoxylin-eosin stained paraffin sections (5NP and 5LP from different mothers) were used to measure renal, cortical, and medullar areas in the kidneys from 21GD and 7DL animals. The CAP areas and cell analysis were performed by microscopic fields digitized (Olympus BX51) using CellSens Dimension or *ImageJ* software evaluating images of the histological section in HE. The relative percentages of the cortical and medullary area relative to the total renal area, previously determined, were also determined. The whole kidney area corresponds to the determination of measures of the entire cut, that is, the sum of cortical and medullary area. Therefore, we reiterate that the histological section's whole CAP regions were evaluated for each animal ($n = 4$) in both groups. For this procedure, the kidneys were sectioned longitudinally in half and embedded in paraffin each half. Then, the microtome cuts were made after the block was trimmed and stained in HE. The studies were carried out blindly and similarly for both groups of animals (NP and LP).

TABLE 1 | Dilution of antibodies used in immunohistochemistry.

Antibody	Dilution	Company
Anti-Six2 (11562-1-AP)	1:50	Proteintech
Anti-c-myc (NBP1-19671)	1:150	Novus Biologicals
Anti-Ki67 (ab16667)	1:100	Abcam
Anti-Bcl2 (ab7973)	1:100	Abcam
Anti-TGFβ-1 (sc-146)	1:50	Santa Cruz
Anti-B-catenina (ab32572)	1:500	Abcam
Anti-Zeb1 (sc-10572)	1:50	Santa Cruz
Anti-Zeb2 (sc-48789)	1:50	Santa Cruz
Anti-VEGF (NB100-664)	1:50	Novus Biologicals
Anti-Caspase-3 clivada (9664)	1:200	Cell Signaling
Anti-Ciclina A (sc-31085)	1:50	Santa Cruz
Anti-WT1 (sc-192)	1:50	Santa Cruz
Anti-mTOR	1:100	Abcam

Immunohistochemistry

After euthanasia, the kidneys from NP (21GD, $n = 5$ and 7DL $n = 5$, from different mothers) and LP (21GD, $n = 5$ and 7DL $n = 5$, from different mothers) were removed and fixed (4% paraformaldehyde in 0.1 M phosphate buffer pH 7.4) for 4 h. After, they were washed in running water and followed by 70% alcohol until processed. The materials were dehydrated, diaphanized, and included in the paraplast. The paraplast blocks were cut into 5-μm-thickness sections. Histological sections were deparaffinized and processed for immunoperoxidase. The slides were hydrated, and after being washed in PBS pH 7.2 for 5 min, the antigenic recovery was made with citrate buffer pH 6.0 for 25 min in the pressure cooker. The slides were washed in PBS and, endogenous peroxidase blockade with hydrogen peroxide and methanol was performed for 10 min in the dark. The sections were rewashed in PBS. Blocking of non-specific binding was then followed, and the slides were incubated with a blocking solution (5% skimmed milk powder in PBS) for 1 h. The sections were incubated with the primary antibody (**Table 2**), diluted in 1% BSA overnight in the refrigerator. After washing with PBS, the sections were exposed to the specific secondary antibody, diluted in 1% BSA, for 2 hours at room temperature. The slides were washed with PBS. The cuts were revealed with DAB (3,3′- diaminobenzidine tetrahydrochloride, Sigma - Aldrich CO®, United States). After successive washing with running water, the slides were counterstained with hematoxylin, dehydrated, and mounted with a coverslip using Entellan®. The images were obtained using the photomicroscope (Olympus BX51).

Statistical Analysis

The Kolmogorov-Smirnov normality test with Dallal-Wilkinson-Lillefor *p*-Values was used to evaluate the Gaussian distribution of data values. The *t*-test was used, and the values were expressed as mean ± standard deviation (SD). $p \leq 0.05$ was considered significant. GraphPad Prisma v. 01 software (GraphPad Software, Inc., United States) was used for statistical analysis and graph construction.

TABLE 2 | Sequence of the primers used for RT-qPCR, designed by the company IDT.

Gene	Forward sequence	Reverse sequence
Six2	5′-GCCGAGGCCAAGGAAAGGGAG-3′	5′-GAGTGGTCTGGCGTCCCCGA-3′
c-myc	5′-AGCGTCCGAGTGCATCGACC-3′	5′-ACGTTCCAAGACGTTGTGTG-3′
c-ret	5′-GTTTCCCTGATGAGAAGAAGTG-3′	5′-GTGGACAGCAGGACAGATA-3′
Bcl-2	5′-ACGGTGGTGGAGGAACTCTT-3′	5′-GTCATCCACAGAGCGATGTTG-3′
Col-1	5′-ACCTGTGTGTTCCCCACT-3′	5′-CTTCTCCTTGGGGTTTGGGC-3′
TGFB-1	5′-GGACTCTCCACCTGCAAGAC-3′	5′-GACTGGCGAGCCTTAGTTTG-3′
Ciclin A	5′-GCC TTCACCATTCATGTGGAT-3′	5′-TTGCTGCGGGTAAAGAGACAG-3′
Bax	5′-TTCAGTGAGACAGGAGCTGG-3′	5′-GCATCTTCCTTGCCTGTGAT-3′
Bim	5′-CAATGAGACTTACACGAGGAGG-3′	5′CCAGACCAGACGGAAGATGAA-3′
Casp 3	5′-ACGGGACTTGGAAAGCATC-3′	5′-TAAGGAAGCCTGGAGCACAG-3′
GDNF	5′-CAGAGGGAAAGGTCGCAGAG-3′	5′-TCGTAGCCCAAACCCAAGTC-3′
Ki67	5′-GTCTCTTGGCACTCACAG-3′	5′-TGGTGGAGTTACTCCAGGAGAC-3′
mTOR	5′-ACGCCTGCCATACTTGAGTC-3′	5′-TGGATCTCCAGCTCTCCGAA-3′
VEGF	5′-CGGGCCTCTGAAACCATGAA-3′	5′-GCTTTCTGCTCCCCTTCTGT-3′
GAPDH	5′-CAACTCCCTCAAGATTGTCAGCAA-3′	5′-GGCATGGACTGTGGTCATGA-3′
B-catenin	5′-AGTCCTTTATGAGTGGGAGCAA-3′	5′-GTTTCAGCATCTGTGACGGTTC-3′
Map2K2	5′-ACCGGCACTCACTATCAACC-3′	5′-TTGAGCTCACCGACCTTAGC-3′
Bcl-6	5′-CCAACCTGAAGACCCACACTC-3′	5′-GCGCAGATGGCTCTTCAGAGTC-3′
PCNA	5′-TTTGAGGCACGCCTGATCC-3′	5′-GGAGACGTGAGACGAGTCCAT-3’
PRDM1	5′-CTTGTGTGGTATTGTCGGGAC-3′	5′-CACGCTGTACTCTCTCTTGG-3′
NOTCH1	5′-ACTGCCCTCTGCCCTATACA-3′	5′-GACACGGGCTTTTCACACAC-3′
IGF1	5′-AAGCCTACAAAGTCAGCTCG-3′	5′-GGTCTTGTTTCCTGCACTTC-3′
ZEB1	5′-CATTTGATTGAGCACATGCG-3′	5′-AGCGGTGATTCATGTGTTGAG-3′
ZEB2	5′-CCCTTCTGCGACATAAATACGA-3′	5′-TGTGATTCATGTGCTGCGAGT-3′

RESULTS

Body Mass, Renal Area, and CM Cells Number

The male offspring of the LP group presented a significant reduction in the body mass in the 21GD and 7DL compared to the NP group (**Figure 1**). The kidney/body mass was also reduced in both 21GD and 7DL (**Figure 1**). In the 21GD LP animals, the nephrogenic cortical area was 31% reduced (LP = 27.5 ± 1 vs. NP = 58.1 ± 1.6, $n = 4$ of each, $p < 0.0001$) and the medullar 34% enhanced (LP = 72.5 ± 1 vs. NP = 42 ± 1.6, $n = 4$ of each, $p < 0.0001$) when compared to that observed in NP group. The CMs presented an increase in both areas (103%) and several Six2 positive cells (32%) in the 21GD LP kidneys (**Figure 2**). In the 7DL LP animals, the renal areas, as well as the percentage of the two renal areas were not altered (cortical: LP = 56 ± 3 vs. 69 ± 9, $n = 4$; medullar: LP = 44 ± 3 vs. NP = 39 ± 2, $n = 4$).

Expression of miRNAs by miRNA-Seq

By expressing a global miRNA profiling analysis, we founded 21 differently expressed miRNAs, of which 12 were upregulated and 9 downregulated in 21-GD, LP fetuses, compared to age-matched NP offspring (**Table 3**). In 7-DL LP offspring, there were 74 differentially expressed miRNAs, 46 were upregulated, and 28 were downregulated (**Table 3**). The top expressed miRNAs and their functions, pathways, and networks were identified using Ingenuity Software (**Table 4**). After obtaining a list of differential expressed miRNAs, the software Ingenuity Pathways Analysis (IPA) was used to determine the functions, pathways, and networks involved with these differentially expressed miRNAs. In this analysis, an experimental target is used, instead of a putative one, as it is more reliable. Having obtained these pathways, we analyzed those that we were interested in concerning the processes of cell proliferation, apoptosis, and differentiation. We then selected, from the top 10, the miRNAs that were involved in these pathways. Afterwards, we also checked the miRTarBase database, which shows target microRNA interactions. Cross-referencing the data from Ingenuity and mirTarBase, we selected the target miRNAs and genes that we would validate by RT-PCR.

Validation of miRNA Expression

In the animals of 21GD from the LP group, miR-127-3p, miR-298-5p, let-7a-5p, miR-181a-5p, and miR-181c-3p were upregulated in the kidneys compared to NP animals. The results do not show any difference in miR-144-3p and miR-199a-5p expression, comparing both groups (**Figure 3A**). Only miR-181a-5p was upregulated, and let-7a-5p was downregulated *in* the kidneys from 7DL LP compared to age-matched NP offspring (**Figure 3B**). **Table 5** and additional data showed in the **Supplementary Material file** revealed the values obtained by miRNAs sequencing with the RT-qPCR validation data. Although significant miRNA expression difference was observed in LP

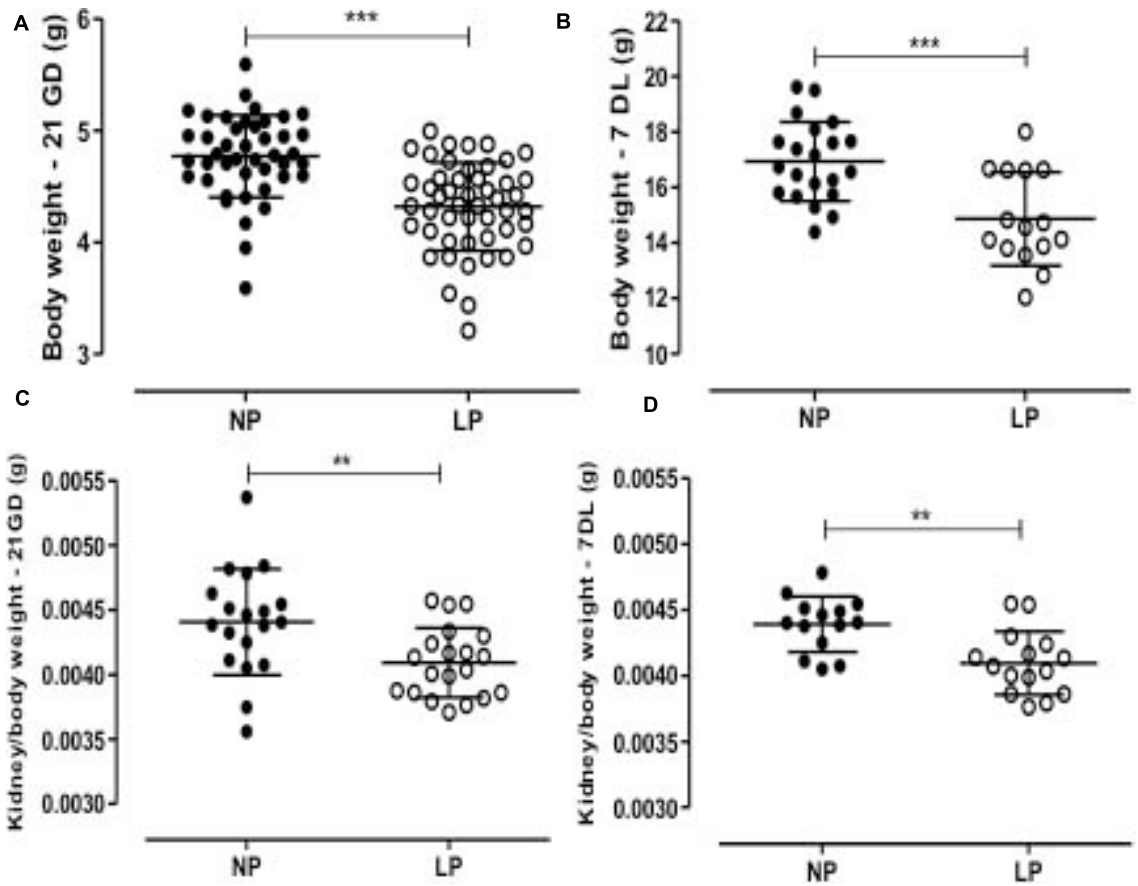

FIGURE 1 | The graphics represent the male pups' weight of body (**A**: 21GD, **B**:7DL) and kidney/body (**C**: 21GD, **D**:7DL). Mean ± SD, $^{**}p < 0.005$ and $^{***}p < 0.0001$.

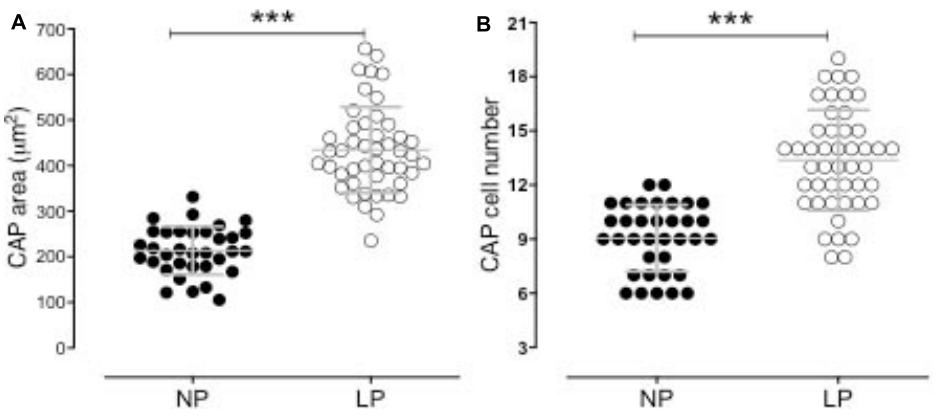

FIGURE 2 | The graphics represent the CM area **(A)** and Six2 positive cells in CM **(B)**. $^{***}p < 0.0001$.

relative to NP offspring, the fold change (FC) of the validated miRNAs was similar to both techniques.

miRNA Targets and ZEB1/2 Expression

The mRNA expression of the most elected predicted targets of miRNAs and ZEB1/2 were enhanced in 21GD and 7DL kidneys LP compared to NP. Thus, Bax, Caspase-3, GDNF, Collagen 1, TGFβ, Bcl-2, Bcl-6, PRDM1, β-catenin, and IGF1. At 7DV, Bim, cyclin A, and Map2k2 mRNA expression were enhanced, and mTOR was reduced in LP. At 21GD, PCNA and c-myc mRNA expression was downregulated (**Figure 4**) in maternal protein-restricted offspring. Using results obtained in the 17GD

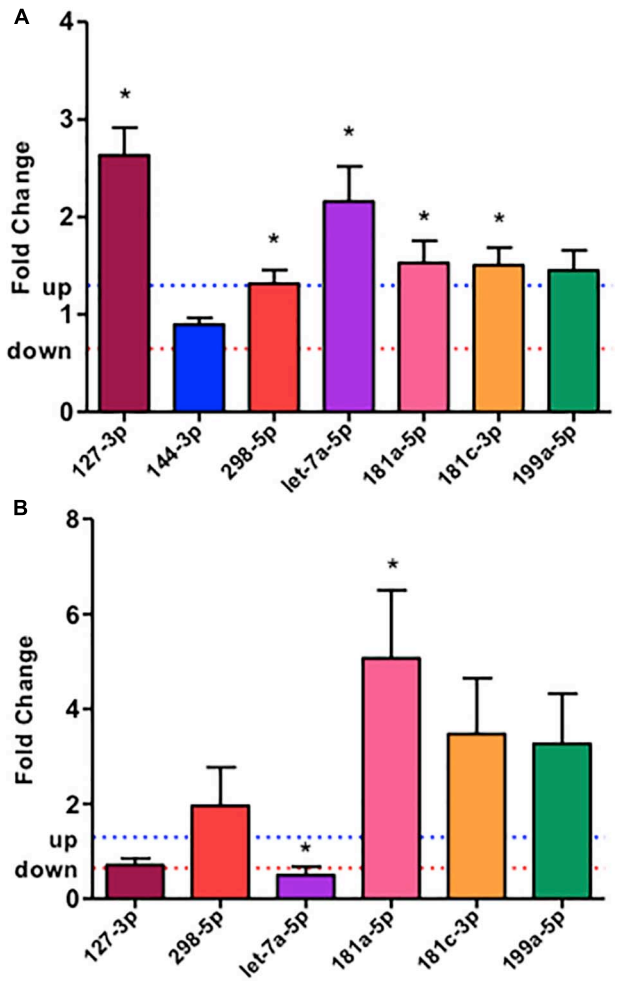

FIGURE 3 | Expression of miRNAs in the LP kidneys from 21 GD **(A)** and 7DL **(B)** rats compared to the level of expression in the NP group. The expression of each miRNA was normalized with U6 and U87. The cutoff point variation of 1.3 (upwards) or 0.65 (downwards) was established, and data are expressed as fold change (mean ± SD, $n = 4$) concerning the control group. *$p \leq 0.05$: statistical significance versus NP.

metanephros using the same model presented here (Sene et al., 2021) and 21GD and 7DL kidneys, we have traced curves where we can observe the more detailed and comparative view of mRNAs expression control by microRNAs (**Figure 4**).

Immunohistochemistry

Results in 21GD: In a general view of Six2 labeled LP kidney, we verified more intensive reactivity and more cells labeled in comparison whit that observed in NP. These labeled cells are present in both CM and differentiated LP structures and not in NP (**Figures 5A,B**). In a more detailed view, we can observe that the more intensive Six2 reactivity is present in CM cells whose number is raised in LP (**Figures 6A-E**). In a more reduced pattern, Six2-positive cells are migrating from CM and present in differentiating vesicles only in the LP kidney (**Figures 6B,E**). We can also see that all cells are more extensive than those present in NP and enlarged nuclei with loose chromatin and evident nucleolus (typical of interphases' nuclei). Simultaneously, in NP, we can observe more intense hematoxylin-labeled nuclei, indicating condensed chromatin (**Figures 6A-E**). The cMyc reactivity was remarkably reduced in the nephrogenic zone but not so expressive in the medulla in LP compared to NP (**Figures 6C,D**). Already, LP kidneys presented much more Ki67 reactive cells than NP in all tissue (**Figures 5E,F**). In the highest magnification, we can see Ki67-positive cells, and in LP, the majority have their nucleoli evident, whereas, in NP, this is not visible (**Figures 6H,I**). The cyclin A reactivity was the same in NP and LP kidneys and was only found in tubular segments below the nephrogenic zone (**Figures 5G,H**) being absent in this zone (**Figures 6F,G**). In the highest magnification, we observed that in LP kidneys, the UB epithelial cells have round nuclei, representing their cubic shape, while in NP, we can keep elongated nuclei, characteristic of cylindrical epithelia (**Figure 6**). By the immunolocalization of β-catenin, we observe that this protein was present in many more LP kidney structures than observed in NP (**Figures 7A,B**). mTor was present in tubular segments below the nephrogenic zone and was increased in LP (**Figures 7C,D**). The intensity of TGFβ1 reactivity was significantly enhanced in all renal tissue in LP than in NP (**Figures 7E-H**). The VEGF was more intensive and present in the higher area of extracellular matrix in LP than in NP (**Figures 7I,J**). All cells of LP kidneys presented the anti-apoptotic Bcl2 protein, and in NP, this protein was present in a low number of cells (**Figures 8A,B**). Activated caspase-3 distribution was not different from NP and LP kidneys (**Figures 8C,D**). Zeb 1 and 2 were present in a higher number of cells from a nephrogenic LP zone than NP (**Figure 8**).

By the immunoperoxidase, the data has shown that c-Myc positive cells were more numerous in the extracellular matrix of the 7-DL NP nephrogenic zone when compared to LP. In the medulla, the tubular cells are labeled in a similar pattern in both groups (**Figures 9A,B**). Although not so apparent, the number of Ki67 positive cells in LP was higher than in NP (**Figures 9C,D**). Cyclin A was intensely increased in all renal tissue from LP than that viewed in NP (**Figures 9E,F**). Elevated β-catenin and mTor reactivity were obtained in tubular segments of LP renal tissue compared to NP (**Figures 10A-D**). TGF-β1 was increased, more prominent in the outer cortex of LP than NP (**Figures 10E,F**). LP kidneys have elevated VEGF immunoreactivity in cytosolic and apical tubular cells' compartments (**Figures 10G,H**). Bcl2 was more intensely labeled and distributed in the tubular cells of LP, and cleaved caspase-3 reactivity was raised in the medulla of LP (**Figures 11A-H**). LP kidneys presented a much higher number of cells showing Zeb 2 reactivity than NP (**Figures 11I,J**).

DISCUSSION

During perinatal kidney development in rats, nephrogenesis depends on adequate progenitor cells' self-renewal, survival, and differentiation capacity. Newborn rats maintain active nephrogenesis. There exists a consensus that miRNAs drive renal development regulating gene expression of proteins involved in

TABLE 3 | Lists of the deregulated miRNAs obtained by miRNA-Seq.

miRNAs up-regulated – 21 DG	FC	miRNAs downregulated – 21 DG	FC
25_TACCCTGTAGATCCTAATTTGT_rno-mir-10b	1.92	7_TGAGGTAGTAGATTGTATAGT_rno-let-7f-2	0.72
53_TGTGCAAATCCATGCAAAACTG_rno-mir-19b-1	1.56	52_TCAGTGCATGACAGAACT_rno-mir-152	0.63
14_TCTGGCTCCGTGTCTTCACTCC_rno-mir-149	1.72	rno-let-7f-5p	0.80
rno-miR-326-3p	1.70	5_TGAGGTAGTAGTTTGTGCTGTTA_rno-let-7i	0.78
rno-miR-615	1.67	rno-let-7g-5p	0.85
10_GGCAGAGGAGGGCTGTTCTTC_rno-mir-298	1.53	rno-miR-98-5p	0.83
15_TAGGTAGTTTCCTGTTGTTGGGT_rno-mir-196b-2	1.44	rno-miR-103-3p	0.79
56_TCGGATCCGTCTGAGCTTGGC_rno-mir-127	1.57	rno-miR-451-5p	0.63
rno-let-7e-3p	1.56	15_TAGGTAGTTTCCTGTTGTTGGGAT_rno-mir-196b-2	0.64
rno-miR-127-3p	1.48		
10_TGAGGGGCAGAGAGCGAGACTTT_rno-mir-423	1.39		
51_AGCAGCATTGTACAGGGCTATGT_rno-mir-103-1	1.57		
miRNAs up-regulated – 7 DL	**FC**	**miRNAs downregulated – 7 DL**	**FC**
50_CTAGACTGAGGCTCCTTGAGGA_rno-mir-151	1.80	25_TACCCTGTAGATCCGAATTCGT_rno-mir-10b	0.41
69_TACAGCAGGCACAGACAGGCAG_rno-mir-214	2.43	60_TCAGTGCACTACAGAACTTTGT_rno-mir-148a	0.64
rno-miR-298-5p	1.94	59_TGAGATGAAGCACTGTAGCTCTT_rno-mir-143	0.72
15_TCCCTGAGGAGCCCTTTGAGCCTG_rno-mir-351-1	1.70	25_TACCCTGTAGATCCTAATTTGT_rno-mir-10b	0.43
rno-miR-1249	2.4	59_TGAGATGAAGCACTGTAGCTCT_rno-mir-143	0.72
47_TATTGCACTTGTCCCGGCCTGTAA_rno-mir-92a-1	1.64	rno-miR-199a-3p	0.73
15_TCCCTGAGGAGCCCTTTGAGCCTG_rno-mir-351-2	1.78	rno-miR-26b-5p	0.63
8_AGACCCTGGTCTGCACTCTGTCT_rno-mir-504	2.33	rno-miR-143-3p	0.74
11_TGTAAACATCCCCGACTGGAAGCT_rno-mir-30d	1.59	15_TAGGTAGTTTCCTGTTGTTGGGT_rno-mir-196b-2	0.53
14_AACATTCAACGCTGTCGGTGAGTT_rno-mir-181a-1	1.39	5_TGAGGTAGTAGTTTGTGCTGTTAT_rno-let-7i	0.48
14_AACATTCATTGCTGTCGGTGGGTT_rno-mir-181b-2	1.53	rno-let-7a-5p	0.69
rno-miR-181a-5p	1.28	22_AAAGTTCTGAGACACTCTGACT_rno-mir-148a	0.64
47_TATTGCACTTGTCCCGGCCTGTAAA_rno-mir-92a-1	1.69	rno-miR-148a-3p	0.51
61_AGCTACATCTGGCTACTGGGTCTCT_rno-mir-222	1.84	59_TGAGATGAAGCACTGTAGCTC_rno-mir-143	0.73
rno-miR-125a-5p	1.70	15_TCTTTGGTTATCTAGCTGTAT_rno-mir-9a-2	0.54
rno-miR-486	1.77	25_TACCCTGTAGAACCGAATTTGTGTGT_rno-mir-10b	0.55
47_CTGGCCCTCTCTGCCCTTCCGTTT_rno-mir-328a	2.13	rno-miR-196b-5p	0.69
15_TCCCTGAGGAGCCCTTTGAGCCT_rno-mir-351-1	1.69	14_TGAGGTAGGAGGTTGTATAGT_rno-let-7e	0.67
11_TGTAAACATCCCCGACTGGAAGC_rno-mir-30d	1.58	rno-miR-17-1-3p	0.60
6_CACCCGTAGAACCGACCTTGCGA_rno-mir-99b	1.62	15_TAGGTAGTTTCCTGTTGTTGGGT_rno-mir-196b-1	0.57
47_TATTGCACTTGTCCCGGCCTGTTAT_rno-mir-92a-1	1.68	22_CAGCAGCAATTCATGTTTTGGAT_rno-mir-322-1	0.60
69_TACAGCAGGCACAGACAGGCAGT_rno-mir-214	1.67	24_TAGGTAGTTTCATGTTGTTGGGT_rno-mir-196a	0.64
32_TCCTTCATTCCACCGGAGTCTG_rno-mir-205	1.88	21_TACCCTGTAGAATCGAATTTGT_rno-mir-10a	0.57
48_TACTAGACTGAGGCTCCTTGAG_rno-mir-151	1.92	48_TGTGACAGATTGATAACTGAAAGT_rno-mir-542-3	0.60
70_ACAGCAGGCACAGACAGGCAGT_rno-mir-214	1.66	15_TCTTTGGTTATCTAGCTGTATG_rno-mir-9a-1	0.57
14_TCCCTGAGACCCTTTAACCTGTG_rno-mir-125a	1.64	rno-miR-146b-5p	0.66
rno-miR-151-3p	1.60	5_TGAGGTAGTAGTTTGTGCTG_rno-let-7i	0.57
14_TCCCTGAGACCCTTTAACCTG_rno-mir-125a	1.64	21_TACCCTGTAGAACCGAATTTGA_rno-mir-10a	0.61
14_TCCCTGAGACCCTTTAACCTGTGG_rno-mir-125a	1.65	14_TTCAAGTAATTCAGGATAGGTT_rno-mir-26b	0.79
rno-miR-125b-5p	1.48		
16_TGTAAACATCCTACACTCTCAGCT_rno-mir-30c-1	1.17		
11_TGTAAACATCCCCGACTGGA_rno-mir-30d	1.39		
46_AGCTCGGTCTGAGGCCCCTCAGA_rno-mir-423	1.87		
45_TCAGGCTCAGTCCCCTCCCGATT_rno-mir-484	1.86		
54_TATTGCACTTGTCCCGGCCTGAAA_rno-mir-92a-2	1.80		
3_TCCTGTACTGAGCTGCCCCGA_rno-mir-486	1.64		
45_ATCACATTGCCAGGGATTTCCAA_rno-mir-23a	1.80		
24_AAGTTCTGTTATACACTCAGGCT_rno-mir-148b	1.73		
60_CTATACAACCTACTGCCTTCCT_rno-let-7b	1.78		
15_TCCCTGAGGAGCCCTTTGAGCC_rno-mir-351-1	1.52		
10_GGCAGAGGAGGGCTGTTCTTCC_rno-mir-298	1.56		
15_TCCCTGAGGAGCCCTTTGAGCCT_rno-mir-351-2	1.50		
15_TCCCTGAGGAGCCCTTTGAGCCTGT_rno-mir-351-1	1.54		
rno-miR-149-5p	1.73		
14_AACATTCAACGCTGTCGGTGAG_rno-mir-181a-1	1.22		

TABLE 4 | Top canonical pathways affected by differentially expressed miRNAs in 21 DG and 7 DL metanephros.

21 GD	Pathway analysis results (IPA)	Number of miRNAs	*p*-Value/score
NP vs LP	**Top Molecular and Cellular Functions**		
	Cellular Development	64	4.77E-02 – 5.79E-14
	Cellular Growth and Proliferation	64	4.43E-02 – 5.79E-14
	Cellular Movement	36	4.77E-02 – 1.07E-08
	Cell Cycle	23	4.76E-02 – 1.65E-06
	Cell Death and Survival	38	4.29E-02 – 5.29E-05
	Top Networks		
	Cancer, Organismal Injury and Abnormalities, Reproductive System Disease		54
	Top Tox Lists		
	Renal Ischemia-Reperfusion Injury microRNA Biomarker Panel (Mouse)		2.88E-17
	Top 10 highly expressed miRNAs		
	miR-10b-5p; miR-148a-3p; miR-330-5p; miR-615-5p let-7a-5p; miR-298-5p; miR-127-3p; let-7e-3p miR-103-3p; miR-423-3p		
7 DL	**Pathway analysis results (IPA)**	**Number of miRNAs**	***p*-Value/score**
NP vs LP	**Top Molecular and Cellular Functions**		
	Cellular Development	18	4.71E-02 – 4.76E-08
	Cellular Growth and Proliferation	15	3.44E-02 – 4.76E-08
	Cell Cycle	07	3.98E-02 – 5.81E-06
	Cellular Movement	11	4.83E-02 – 5.81E-06
	Cell Death and Survival	13	4.50E-02 – 6.10E-05
	Top Networks		
	Cancer, Gastrointestinal Disease, Organismal Injury and Abnormalities		28
	Top Tox Lists		
	Renal Ischemia-Reperfusion Injury microRNA Biomarker Panel (Mouse)		1.01E-07
	Top 10 highly expressed miRNAs		
	miR-10b-5p; miR-214-3p; miR-298-5p; miR-143-3p miR-1249-3p; miR-504-5p; miR30c-5p; miR-181a-5p miR-199a-5p; miR-221-3p		

key signaling pathways (Lv et al., 2014; Marrone and Ho, 2014; Wei et al., 2014; Phua et al., 2015). Recently, we established miRNA and elected target mRNA expression in maternal low-protein intake 17GD male metanephros (Sene et al., 2021). In the current study, we performed a similar evaluation, ensuring UB branching and mesenchymal to epithelial transformation in 21GD fetus and 7DL kidneys from LP progeny compared to NP offspring. Thus, we depicted a time-course curve of most altered miRNAs and elected mRNAs transcripts during nephrogenesis in the maternal low protein intake model by data from these ages. This observation aims to elucidate particular pathways related to the reduced nephron number observed in this model (Mesquita et al., 2010a,b).

Surprisingly, as the discussion below, the present study data showed some discrepancies between miRNAs and their predicted targets' expected expression.

These findings confirm prior studies demonstrate that miRNAs could act as positive transcription factors (Vasudevan et al., 2007; Zhang et al., 2014). Furthermore, the algorithms could not find all miRNA-gene interactions, and it has been demonstrated that they detect 60% of all available targets (Reczko et al., 2012; Vlachos and Hatzigeorgiou, 2013).

The present data found 12 upregulated and 9 downregulated miRNAs in 21GD, and 46 were upregulated and 28 downregulated in 7DL LP progeny compared to age-matched NP offspring kidneys in the present study. The current data identified the top 10 deregulated miRNAs in 17 GD and 21 GD fetuses and 7DL offspring. Here, we have selected 7 miRNAs involved in the protein synthesis that are key regulators during renal ontogenesis.

The miR-181a has been related to the critical developmental process of cell proliferation, migration, and apoptosis (Chen et al., 2010). The current study showed an increased expression of miR-181a-5p in 21GD and 7DL LP rats relative to age-matched NP offspring. In the 21GD, both Bcl2 and caspase-3 mRNA are also enhanced, but as a previous study shows, Bcl2 inhibits Caspase-3 activation, reducing cellular apoptosis (Scorrano and Korsmeyer, 2003).

The present study shows an enhanced Bcl2 reactivity in 21GD LP progeny by immunohistochemistry compared to age-matched NL offspring. However, the cleaved Caspase-3 was not altered. Thus, although overexpressed miR-181a has been related to decreased Bcl2 protein levels (Li et al., 2016), here, we do not find an undoubted association.

In our model, the Bcl2 mRNA was not modulated by miR-181a-5p, considering the depicted expression curve. Also, TGFβ1 mRNA, another known predicted target of miR-181a-5p, no observed association was identified in the present study.

TABLE 5 | Comparison between the values obtained in the miRNA sequencing and the validation by RT-qPCR.

miRNA (21 GD)	RNA-Seq logFC	Fold Change	*p-Value*	miRNA (21GD)	Fold Change	qPCR logFC	*p-Value*
miR-127-3p	0.565173065	1.4796	0.04442707	miR-127-3p	2.6333	1.3969	6.02E-03
miR-144-3p				miR-144-3p	0.8974	−0.1562	0.1723848
miR-298-5p	0.613353841	1.5298	0.03299593	miR-298-5p	1.3170	0.3972	0.0402289
let-7a-5p				let-7a-5p	2.1660	1.1150	0.0059875
miR-181a-5p				miR-181a-5p	1.5286	0.6122	0.0421524
miR-181c-3p				miR-181c-3p	1.5058	0.5906	0.0228443
miR-199a-5p				miR-199a-5p	1.4513	0.5373	0.0604275
miRNA(7 DL)	**RNA-Seq logFC**	**Fold Change**	***p-value***	**miRNA (7 DL)**	**Fold Change**	**qPCR logFC**	***p-value***
miR-127-3p				miR-127-3p	0.730578	−0.4529	6.01E-02
miR-144-3p				miR-144-3p	No expressed		
miR-298-5p	0.958238445	1.9429	0.00055761	miR-298-5p	1.9583	0.9696	0.3025506
let-7a-5p	−0.537048101	0.6892	0.01533047	let-7a-5p	0.4997	−1.0008	0.0269524
miR-181a-5p	0.357437752	1.2811	0.00498333	miR-181a-5p	5.0680	2.3414	0.0217739
miR-181c-3p				miR-181c-3p	3.4746	1.7968	0.0731242
miR-199a-5p				miR-199a-5p	3.2639	1.7066	0.0858642

GDNF-RET signaling is the primary regulator of the ureteric bud branching process (Schuchardt et al., 1994; Moore et al., 1996; Pichel et al., 1996; Sanchez et al., 1996), and both GDNF and c-ret mRNA are described how the target of miR-181a-5p. Here, the results showed a negative and reciprocal relationship between miR-181a-5p and c-ret mRNA expression. By the curve of expression, GDNF mRNA was not modulated by miR-181a-5p but, GDNF and c-ret mRNA were upregulated in LP at 21GD fetus, indicating an active induction of UB ramification. In the 7DL, the LP progeny kidneys also showed an enhanced GDNF expression but associated with decreased c-ret mRNA expression, indicating a reduction in the UB ramification in this age.

During kidney development in LP 17GD offspring, we have demonstrated that miR-181c enhanced the expression of Six2 and negatively regulates cell proliferation (Sene et al., 2021), confirming results by Lv et al. (2014).

The present results demonstrated in 21GD LP kidney, upregulation of ki67 and Six2 mRNAs in parallel with raised miR-181c-3p expression. In the 7DL, the miR-181c-3p expression was enhanced in LP compared to the NP offspring kidney, which is compatible with the reduced Six2 expression in this age.

As demonstrated in **Figure 12**, the variations in miR-181c-3p expression were not causally associated with results observed to Bcl2, casp3, NOTCH1, and mTOR mRNA in the LP relative NP group at the same age. Concerning proliferation, we observed that miR-181c-3p negatively regulated ki67 and positively cyclin-A and PCNA mRNAs in LP kidneys. The present study has shown unexpected discrepancies concerning cell cycle markers; in such a way that ki67 mRNA expression and protein reactivity were significantly upregulated; however, PCNA was unaltered. Cyclin-A mRNA and protein were reduced in 21GD kidneys LP when compared to age-matched NP progeny. Considering 21GD kidneys in NP fetus, an enhanced ki67 reactivity was observed in developing nephrons, but, unprecedently, cyclin-A immunoreactivity was not present. In this way, the cyclin-A reactivity was only present in tubular segments below the nephrogenic zone.

The upregulation of miR-127 has been related to increased cell proliferation (Pan et al., 2012). As we observed here, the ki67 mRNA expression and protein reactivity were elevated in the nephrogenic zone of maternal protein-restricted offspring kidney. The CAP area and the number of Six 2 expressing cells in the CAPs were also elevated (103 and 32%, respectively) in 21GD LP kidneys.

The depicted curves of miR and mRNAs expression in the different studied ages showed that miRNAs 127-3p, 144-3p, and Let7a-5p regulated positively Ki67 and negatively cyclin-A and PCNA mRNA expression. Conversely, such as mentioned anteriorly, miR-181c-3p downregulated ki67 associated with increased cyclin-A and PCNA mRNAs expression in LP kidneys.

Unprecedentedly, in 21GD LP kidneys, the UB epithelial cells have round nuclei, representing their cubic shape, with loose chromatin and evident nucleolus (typical of interphases' nuclei). Simultaneously, in 21GD NP, we found elongated nuclei, characteristic of cylindrical epithelia, with dense chromatin (**Figure 7**). The CM and disperse mesenchyme cell nuclei have the same aspects observed in UB in both NP and LP at a similar age.

Despite raised ki67 expression in the nephrogenic zone in the 21GD LP, the nuclear characteristics described above are incompatible with cells in the mitosis process. Thus, we cannot exclude a possible cell-cycle arrest in these structures. However, Ki67 is expressed throughout the cell cycle, including G1, and some non-proliferative cells can poise at G1 for an extended period without cell division (Alvarez et al., 2019).

IGF-1R is a plasma membrane receptor with tyrosine kinase activity, whose inhibitors have been used to treat carcinoma cell lines, with a strong non-proliferative effect (Fuentes-Baile et al., 2020). The IGF-1R elevated expression has also been associated with inhibition of apoptosis and increased proliferation rate and angiogenesis in patients with cancer (Matsubara et al., 2009; Valsecchi et al., 2012). The upregulation of miR 127-3p in the

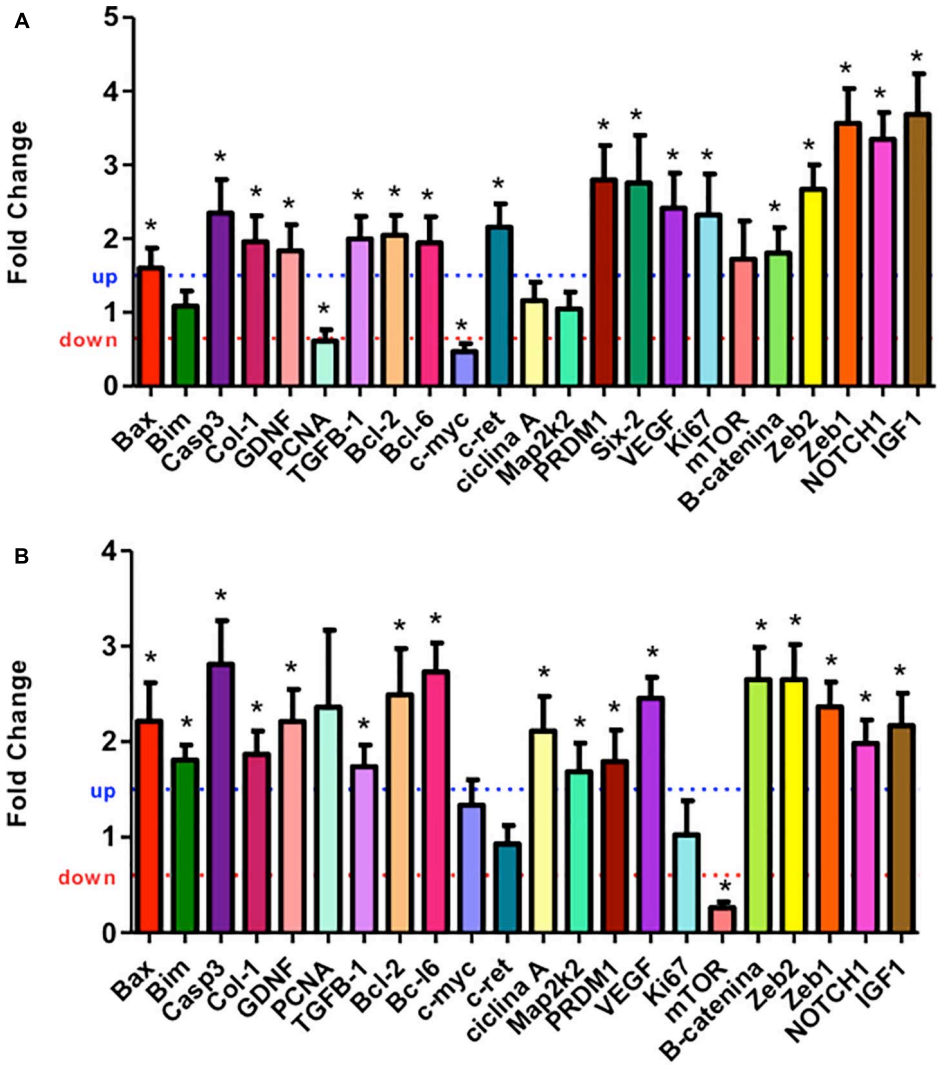

FIGURE 4 | Renal expression estimated by SyBR green RT-qPCR of mRNA from 21GD **(A)** to 7DL **(B)** LP rats. The expression was normalized with GAPDH. The authors established a cutoff point variation of 1.3 (upwards) or 0.65 (downwards), and data are expressed as fold change (mean ± SD, $n = 4$) concerning the control group. *$p \leq 0.05$: statistical significance versus NP.

21GD kidneys from LP animals was accompanied by enhanced IGF1 expression. The rise of ki67 and the decrease of activated caspase-3 in the 21GD LP nephrogenic zone coincide with the activities described previously. The study also showed that miR 127-3p negatively modulated map2k2 mRNA expression, which is in direct contrast to the Ki67 expression.

We may infer that enhanced Ki67 and Bcl-6 mRNA expression in the 17GD LP mesenchymal metanephros compared to age-matched NP progeny is also associated with miR-127-3p downregulation expression. These results may be related to the cell proliferative process (Sene et al., 2021). We found an increased miR-127-3p expression in the 21GD LP kidneys accompanied by enhanced Ki67 expression compared to 17DG LP. Thus, we may suppose that counter-regulatory mechanisms acted by other pathways preventing cell proliferation. At 7DL progeny, the miR-127-3p and Ki67 mRNA encodings in the LP kidneys were reduced compared to 21GD, and the Ki67 immunoreactivity was remarkably like NP offspring kidneys.

A previous study using human cancer cell culture incubated in propidium iodide found a reduction in the proportion of cells in the G2/M phase of the cycle and consequent suppression of renal carcinoma proliferation induced by enhanced miR-144 (Xiang et al., 2016). These authors suggest S/G2 cell cycle arrest. Here the miR-144-3p expression was unaltered in 21GD LP relative to NP; however, its curve of expression showed a positive control of Ki67 associated with the reduced encoding of cyclin A and PCNA. The current study was not able to detect the miR-144-3p expression at 7DL kidneys. In prior research, the authors demonstrated mTOR inhibition by miR-144 overexpression (Xiang et al., 2016). Here, the miR-144-3p expression does not influence mTOR expression.

Recently, Sun et al. (2020) demonstrated that miR-144-3p inhibits cell proliferation and delays the G1/S phase

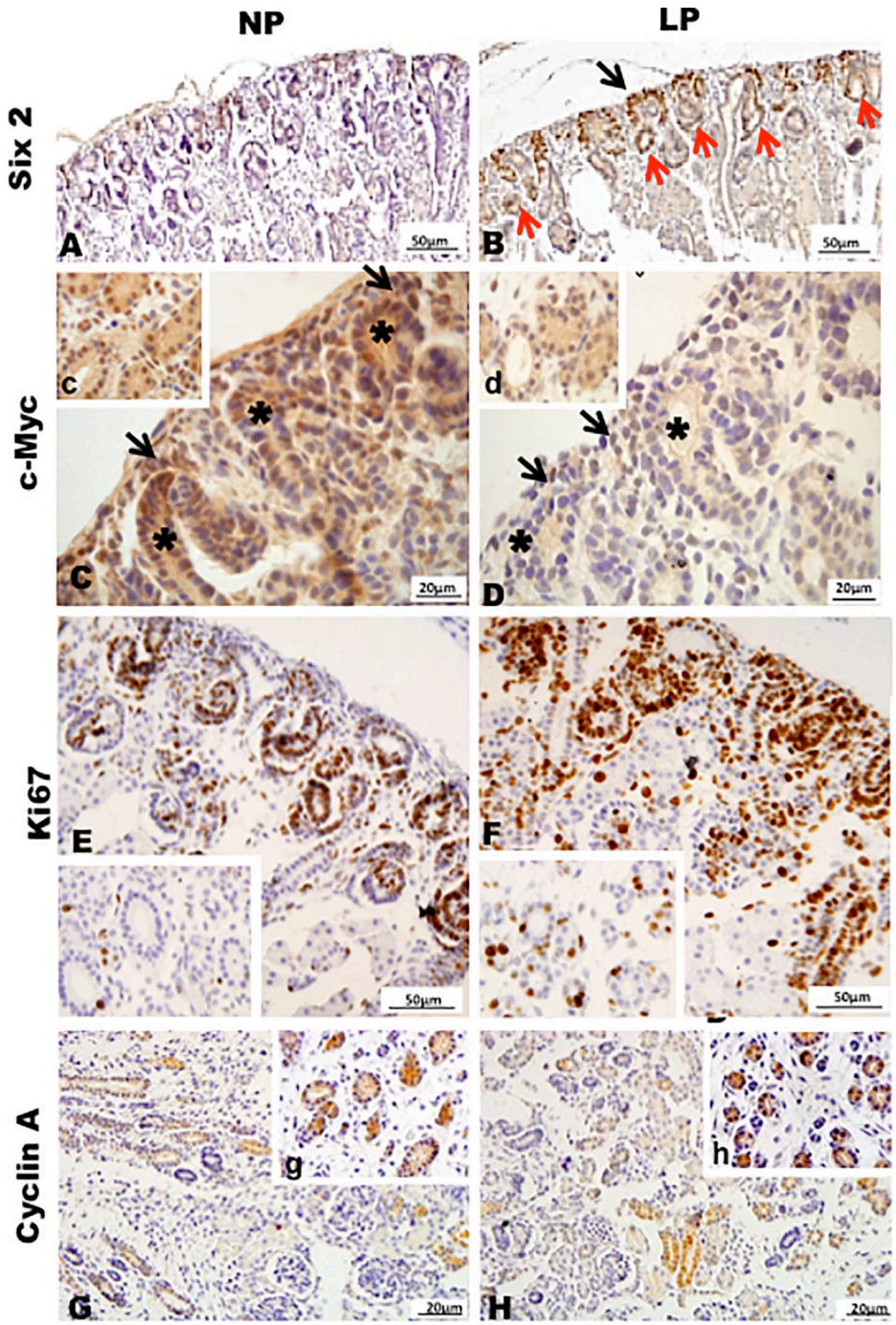

FIGURE 5 | Immunoperoxidase in kidneys of 21GD rats for **(A,B)** Six 2, (C,D) c-Myc, **(E,F)** Ki67, and **(G,H)** cyclin A for the NP **(A,C,E,G)** and LP **(B,D,F,H)** groups. CM (black arrow); UB (*) renal structures in differentiation (red arrow). The inserts represent a medullar area.

transition of colorectal cancer cells. Additionally, the authors determined Bcl6 as a new target of miR-144-3p, suggesting that miR-144-3p/Bcl6 repressed cell proliferation possibly through Wnt/β-catenin signaling.

They found that miR-144-3p downregulated the expression of β-catenin, c-myc, and cyclin D1 (Sun et al., 2020). In the present study, the Bcl6, β-catenin, and miR-144-3p analysis depicted curves of expression in LP revealed remarkably similar curves negatively regulated by their miR.

In this way, the results showing unaltered cyclin-A and Map2k2 in the 21GD LP kidneys and downregulated PCNA mRNAs may be associated with reducing mitosis activity.

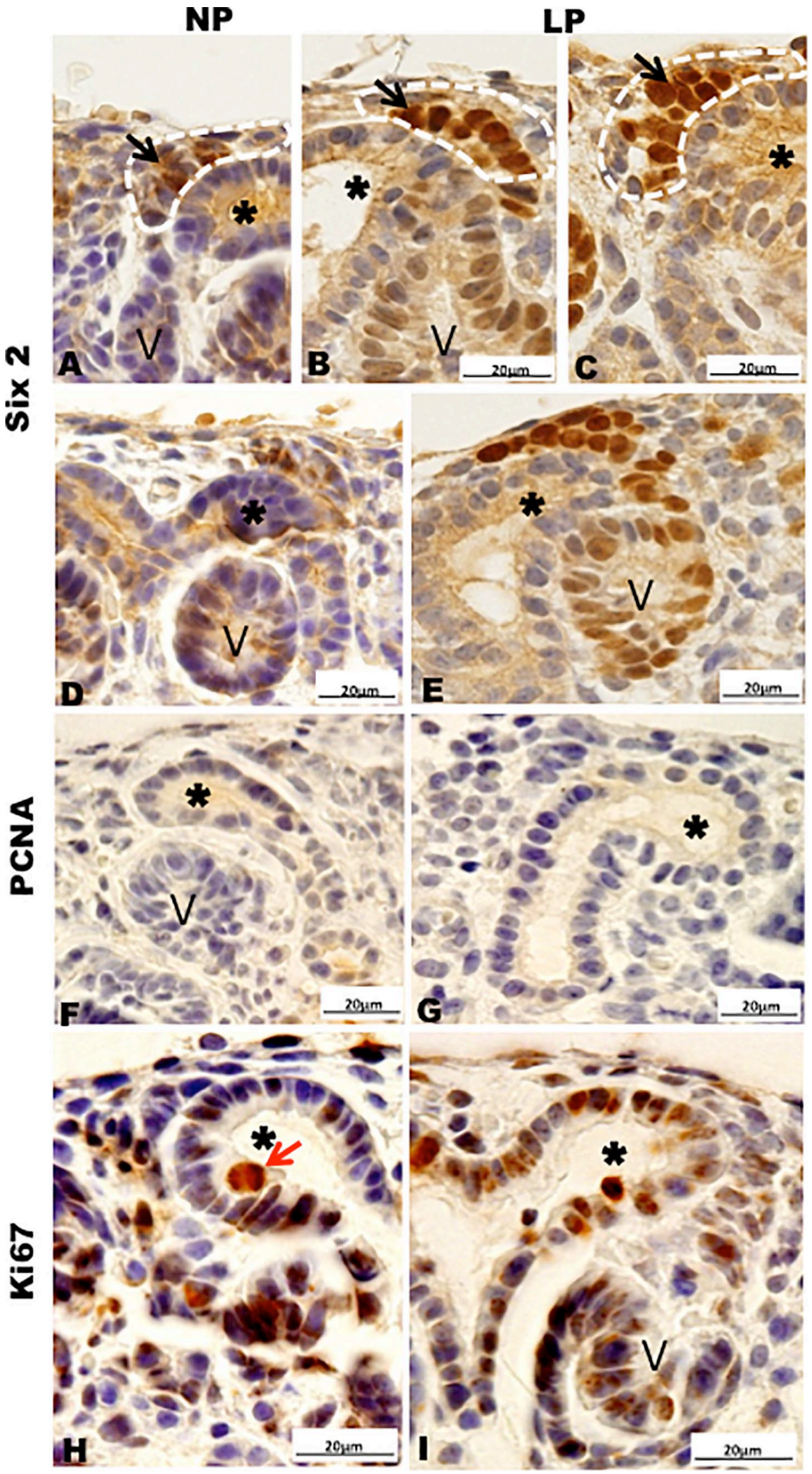

FIGURE 6 | Immunoperoxidase in kidneys of 21GD rats for **(A–E)** Six 2, **(F,G)** PCNA, **(H,I)** Ki67 for the NP **(A,B,D,F,H)** and LP **(C,E,G,I)** groups. CM (black arrow); UB (*) renal vesicles (V); cell in late anaphase (red arrow).

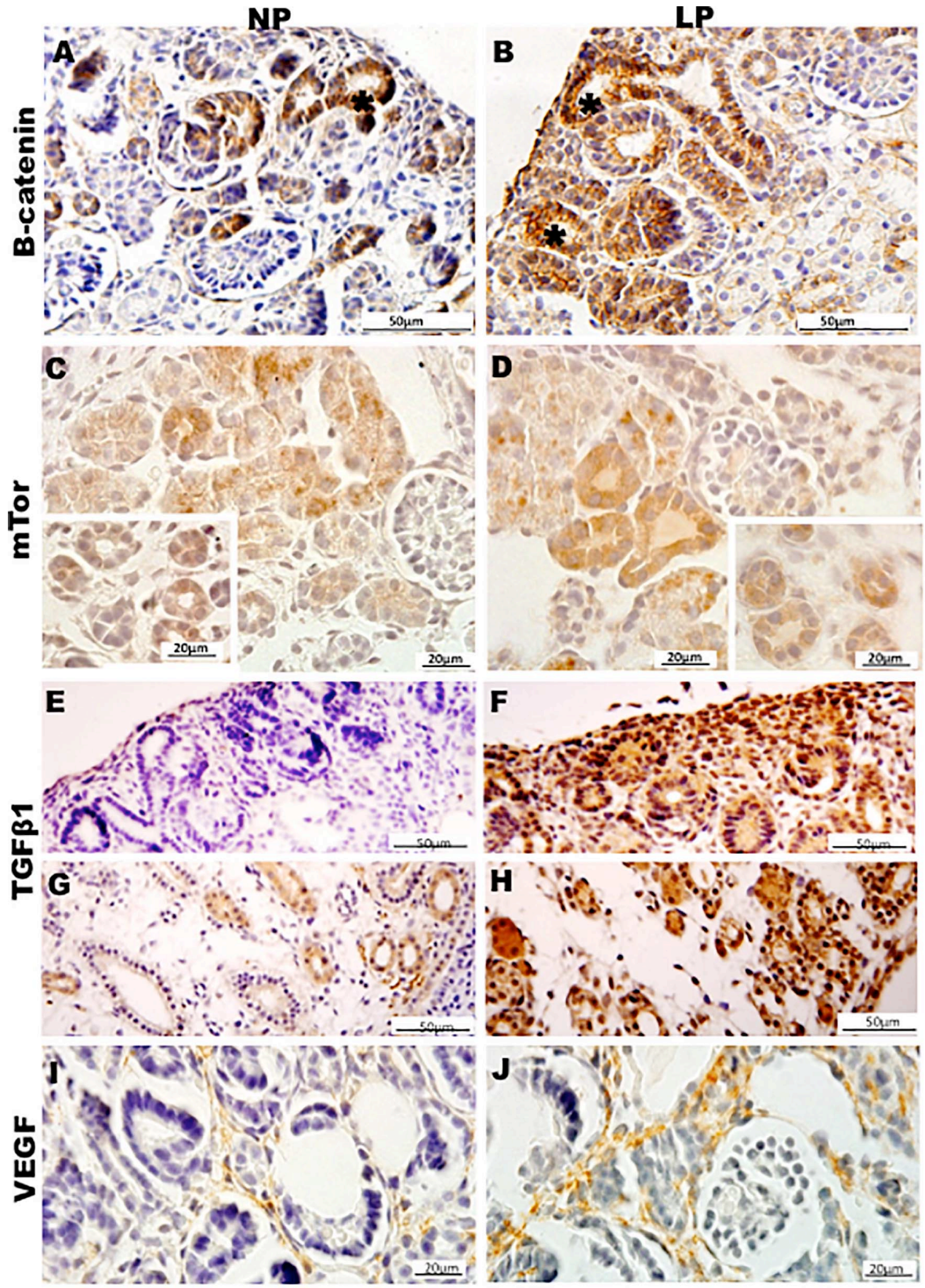

FIGURE 7 | Immunoperoxidase in kidneys of 21GD rats for **(A,B)** B-catenin, **(C,D)** mTor, **(E–H)** TGFb1, and **(I,J)** VEGF for the NP **(A,C,E,G,I)** and LP **(B,D,F,H,J)** groups. The inserts represent the medullar area. UB (*) renal vesicles.

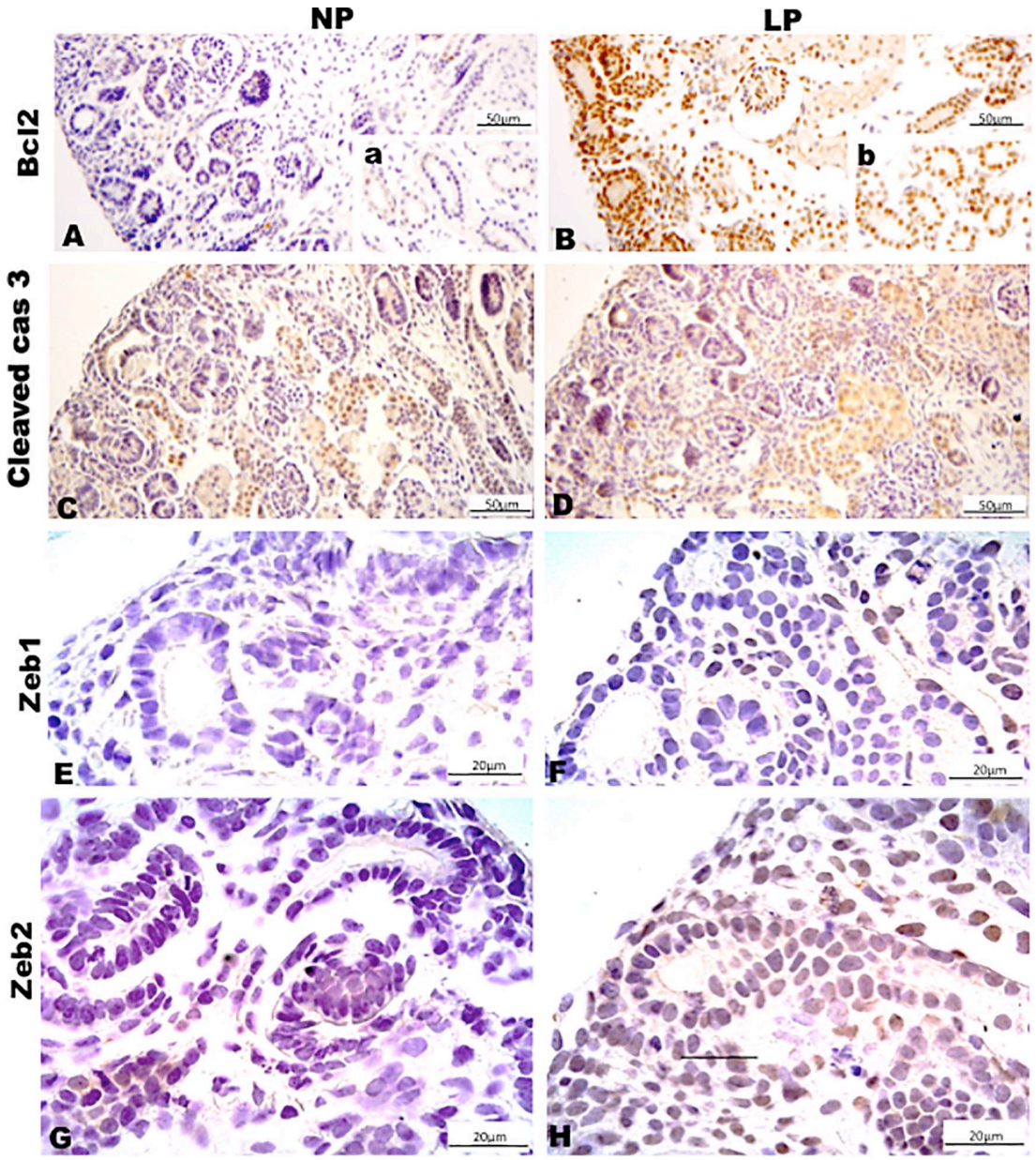

FIGURE 8 | Immunoperoxidase in kidneys of 21GD rats for **(A,B)** Bcl2, **(C,D)** cleaved cas 3, **(E,F)** Zeb1, and **(G,H)** Zeb2 for the NP **(A,C,E,G)** and LP **(B,D,F,H)** groups. The inserts represent the medullar area.

However, by the enhanced mRNA and protein content of Ki67 at the same time, we supposed a compensatory elevation in cell proliferation stimuli. From our perspective, persists unexplained the discrepancy in proliferative cell markers found in NP kidneys, being necessary for additional studies to elucidate each protein's role.

Although inhibition of miR-199a-5p has been related to a reduction in cell proliferation and enhanced apoptosis (Sun et al., 2015), the expression curves showed an uncorrelated miR expression, cell cycle, and apoptosis-related proteins. The miR-199a-5p encoding and its predicted target, IGF1 mRNA, showed a similar modulation with upregulated expression of IGF1 mRNA in the different age times studied.

In the present work, among miRs, the miR-199a-5p expression was the most significantly related to mTOR mRNA encoding and protein immunoreactivity. The mTOR mRNA expression has a pronounced reduction in the time course from 17GD to 7DL LP offspring kidney. The upstream of mTOR mRNA signaling and the IGF1 were upregulated at the LP compared to NP beyond 17GD of age, but mTOR mRNA expression was unchanged. Conversely, in the 7DL LP kidney, the mTOR mRNA was significantly reduced compared to age-matched NP progeny.

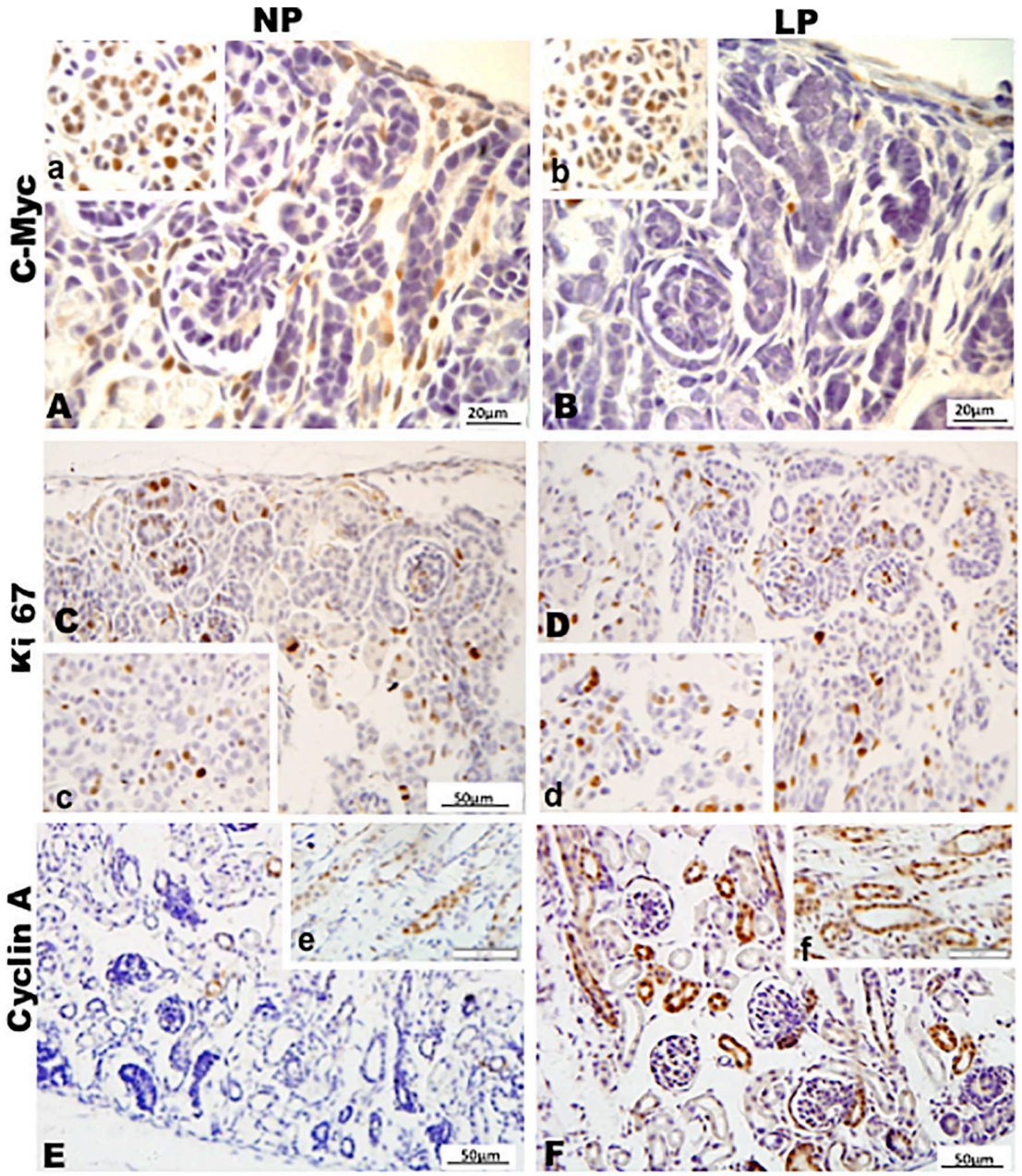

FIGURE 9 | Immunoperoxidase in kidneys of 7DL rats for **(A,B)** c-Myc, **(C,D)** Ki67, and **(E,F)** cyclin A for the NP **(A,C,E)** and LP **(B,D,F)** groups. The inserts represent the medullar area.

On the other hand, mTOR immunoreactivity in 21GD and 7DL kidneys was notably enhanced compared to NP offspring. Thus, we can suppose that a post-translational factor can be maintaining the raised protein level.

The miR-298-5p and its predicted targets showed a positive regulation of Bcx and negative of IGF1 mRNA. In this way, the miR-298-5p acted to enhance IGF1 and, consequently, mTOR signaling. mTOR signaling plays a central role in sensing response to intracellular nutrient availability (Marshall, 2006; Nijland et al., 2007). The kidneys transcriptome from a fetal baboon, whose mothers are submitted to regular content or nutrient-restricted (70% reduced fed), demonstrated that the mTOR signaling pathway is central to induce a reduction in the nephron number in this model (Nijland et al., 2007). Although it is widely known that mTORC1 has an essential role in embryo development, keep completely unclear the complex mechanisms in stress conditions (Gürke et al., 2016).

Nakagawa et al., 2015 have shown that miR 199a-5p is related to activation of the WNT pathway regulating vascular and nephron development. Here, we can suppose that miR-199a-5p

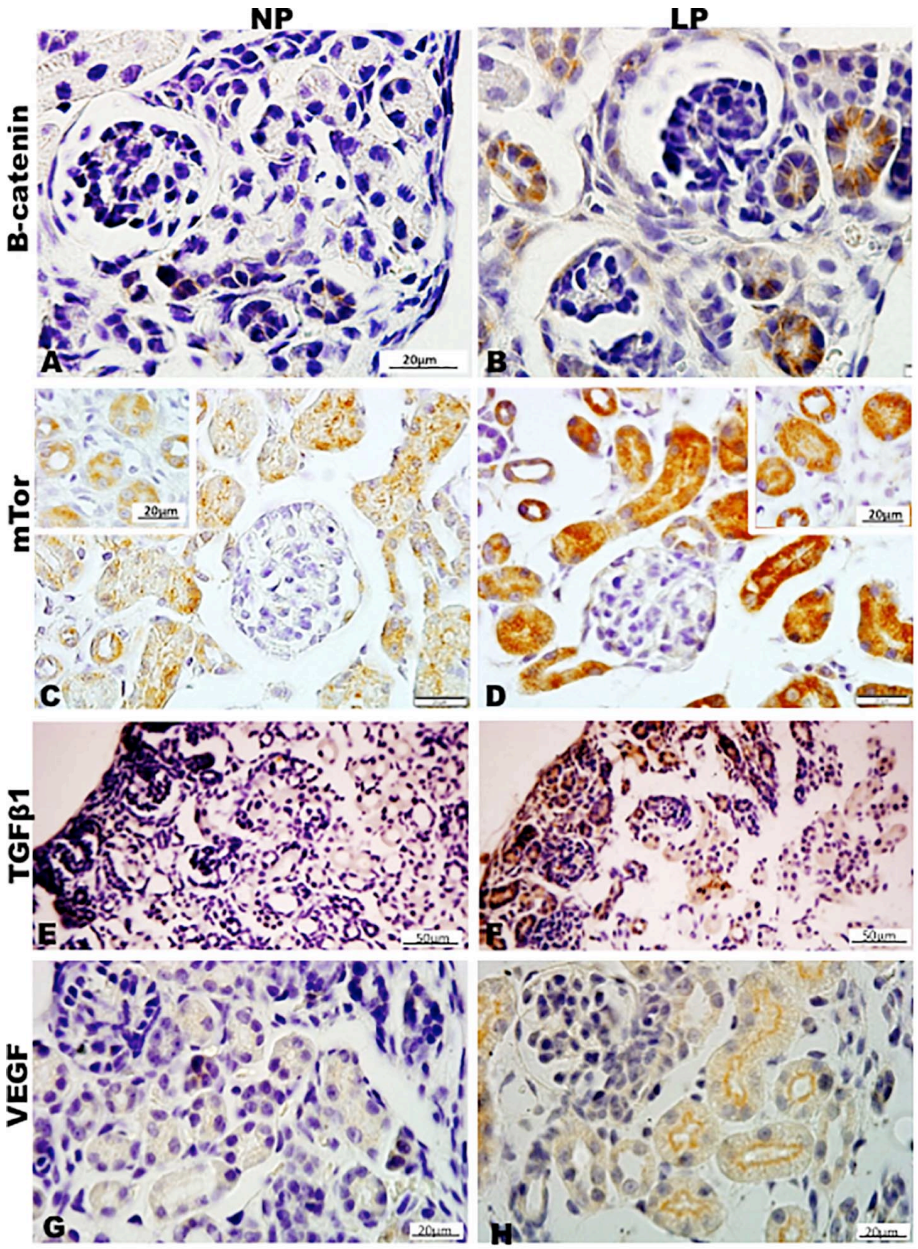

FIGURE 10 | Immunoperoxidase in kidneys of 7DL rats for **(A,B)** B-catenin, **(C,D)** mTor, **(E,F)** TGFb1, and **(G,H)** VEGF for the NP **(A,C,E,G)** and LP **(B,D,F,H)** groups. The inserts represent the medullar area.

positively modulated VEGF expression (mRNA and protein) in the LP kidneys. VEGF signaling is a downstream event of the mTOR pathway, but, in the present study, the VEGF mRNA was not accompanied by the mTOR mRNA encoding; however, it occurs in parallel to VEGF immunoreaction. Kitamoto et al. (1997) studied *in vivo* the role of VEGF in kidney development by blocking the endogenous VEGF activity in newborn mice. They showed a reduced nephron number and abnormal glomeruli. The increased VEGF reactivity observed in 21GD, and 7DL kidneys from the LP progeny indicate a possible compensation of peritubular and glomerular capillary development; once in the 17GD LP kidneys, the low expression could impair vascular development.

The present study of miR let7a-5p and its predicted mRNA targets observed a reciprocal behavior of downregulated c-myc and Six2 upbeat mRNA encoding in 21GD LP kidneys fetus. Besides the 32% increase, Six2 was expressing cells in the CM of 21GD LP kidneys, a 70% significantly enhanced CM area cannot be explained only by cell number. Beyond the interphase nuclei characteristics, the cells at LP CM from

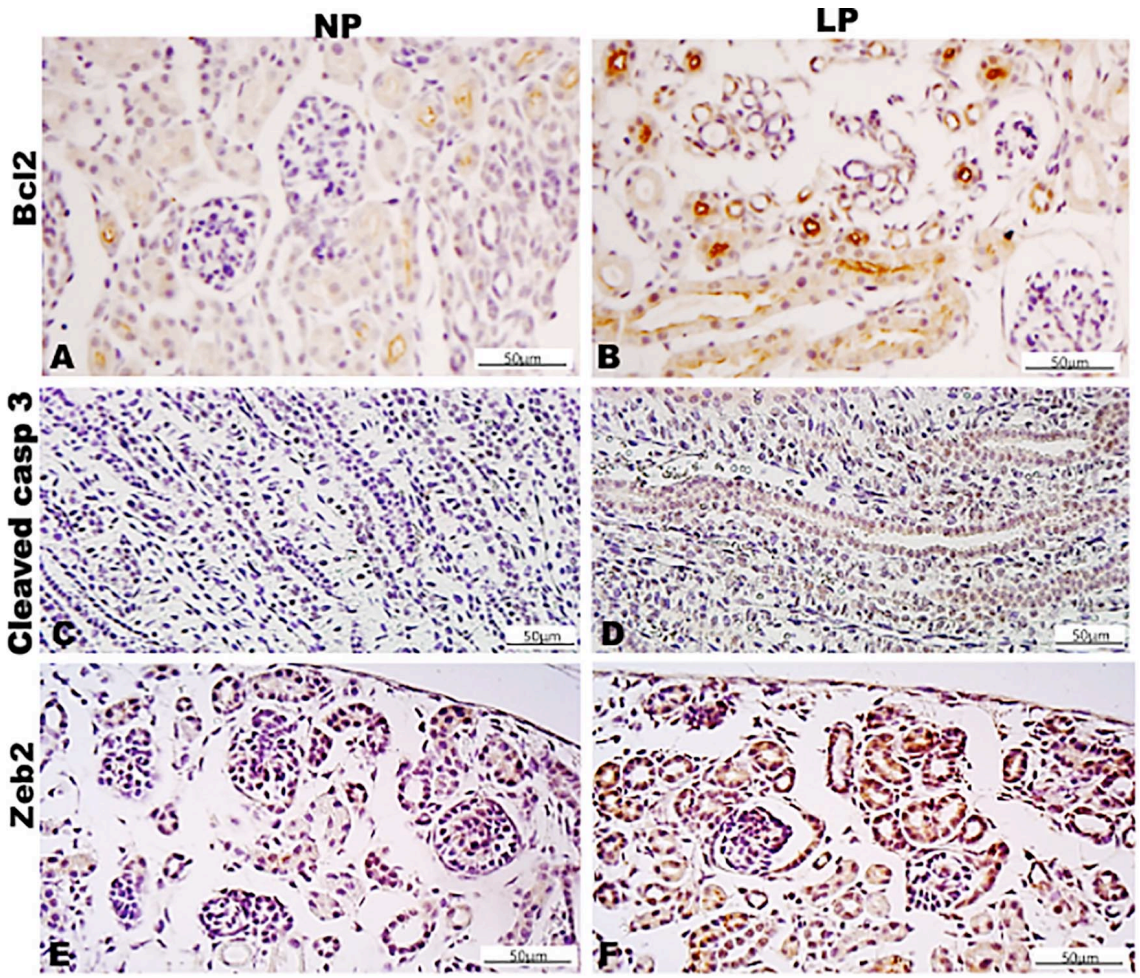

FIGURE 11 | Immunoperoxidase in kidneys of 7DL rats for **(A,B)** Bcl2, **(C,D)** cleaved casp 3, and **(E,F)** Zeb2 for the NP **(A,C,E)** and LP **(B,D,F)** groups.

21GD kidneys are more prominent than those observed in the NP progeny. When in the G1 phase, the cells increase protein synthesis for DNA replication (S phase) and growth, and then, in the G2 phase, cells grow before mitosis. After mitogenic stimuli of cells in G1, cyclin D bind to cyclin-dependent kinases (CKD) and activate a downstream process that led to the S phase, which is regulated by the cyclin E-CDK2 complex, while the G2/M transition is under control of cyclin B-CDK1 complex (Mens and Ghanbari, 2018). Thus, in 21GD LP kidneys, we can modulate other cyclins (D, E, or E), leading to a possible cell cycle arrest. Another intriguing observation in the 21GD LP kidneys is the strong reactivity of Six2, a marker of undifferentiated state, in cells of vesicles. Our results demonstrate a progenitor cell proliferation and self-renewal pathways activation, in the whole-kidney tissue, with cells supposedly in the interphases. These LP fetus cells are significant increased than observed in NP progeny following upregulated growth and protein synthesis. The upregulation of the cell differentiation and consumption was verified in 21GD LP kidneys. This result is incomprehensive, considering the increased Six2 positive cells in the CM and non-differentiated cells migrating to vesicles. Why and how a CM progenitor cell migrates to differentiating nephron structures remains unanswered.

We may suppose that miRNAs regulate stem cells' mitotic cycle, and the let-7 miRNAs suppress their self-renewal (J Melton et al., 2010; Shim and Nam, 2016). The Lin28-Let-7 axis forms a crucial feedback loop in stem cell development (Zhou et al., 2015). The 21GD LP fetus kidneys presented upregulated miR let7a-5p and reduced c-myc mRNA expression and protein reactivity, which is permissive to increased Six2 expression observed. We could suggest that both proliferation and differentiation of stem cells may have been blocked. Reinforcing this hypothesis, the miR 127-3p and let7a-5p in 21GD LP fetus kidneys up-regulated PRDM1 mRNA, a predicted target of the miRNAs. Prdms promote and maintain stem and primordial germ cell identity (To review, Hohenauer and Moore, 2012). Prdm can repress TGFβ downstream signaling (Alliston et al., 2005), and Prdm1 directly suppresses the proliferation factor *Myc* (Yu et al., 2000). Bcl6 also acts as a transcriptional

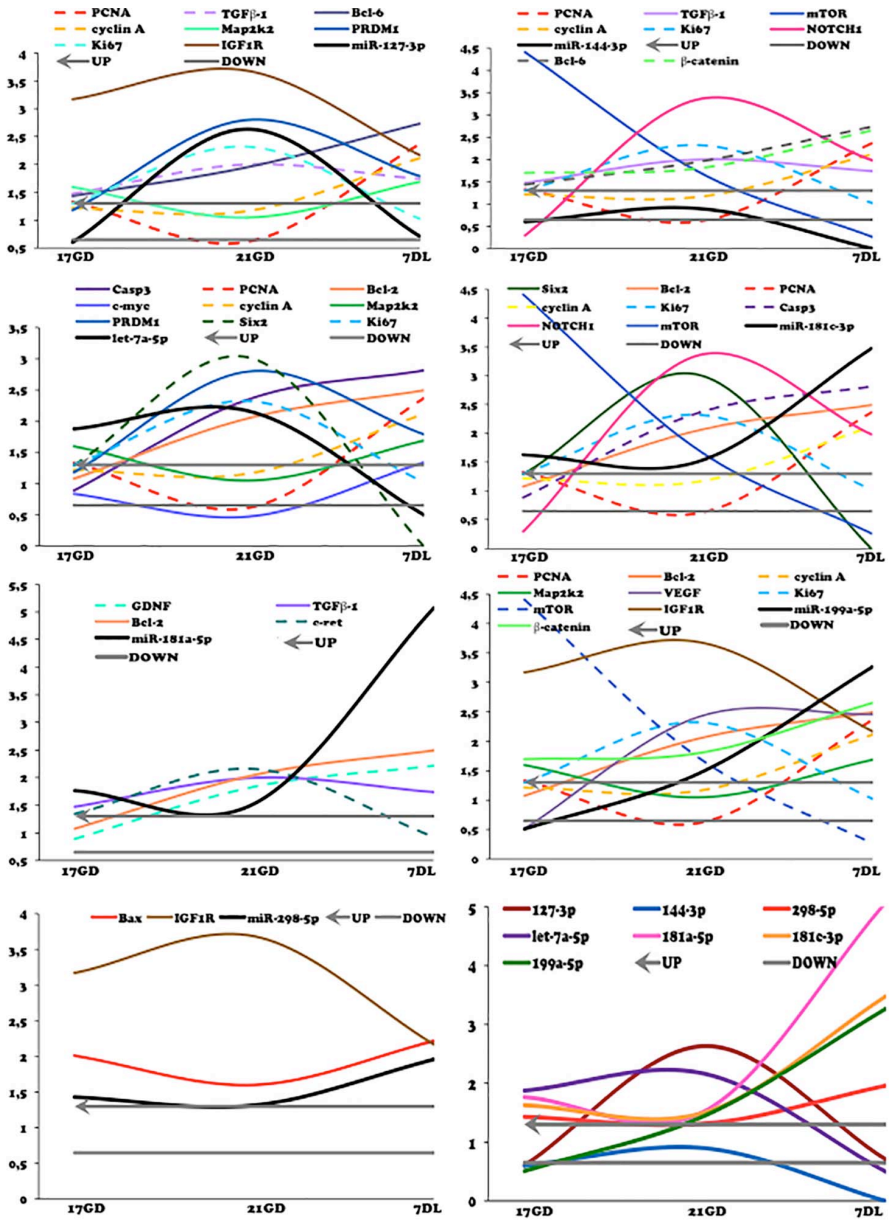

FIGURE 12 | Curves of validated miRNAs and their predicted target mRNAs obtained by miRTarBase and Ingenuity (solid lines) and from literature (dashed line). The expression was normalized with GAPD. The authors established a cutoff point variation of 1.3 (upwards) or 0.65 (downwards), and data are expressed as fold change (mean) concerning the control group.

repressor by a negative-feedback loop with Prdm1 (reviewed by Crotty et al., 2010). These components can also be performed to reduce stem cell differentiation and proliferation in the nephrogenic zone of 21GD LP kidneys.

In the 7DL offspring from both experimental groups, higher altered miRNA expression was found due to raised nutrient content that led to the activation of pathways related to differentiation and progenitor cells' consumption. Studies concerning the developmental origins of health and disease (DOHaD) have shown that the incompatibility between the environmental insults in the intrauterine phase and those conditions found after birth may result in health problems in adulthood (Gluckman et al., 2005; Gluckman and Hanson, 2006). In the present model, after delivery, the rat's dams are fed with chow with standard protein supply, which leads to offspring catch-up growth extremely harmful to health in adult age. By the way, we hypothesize that a high number of miRNAs altered at 7DL LP kidneys concerning NP offspring are related to that accelerated growth. Thus, postnatal unrestricted food intake may induce nephron differentiation fastly and kidney vasculogenesis followed by mRNA and proteins overexpressed in 7DL LP compared to NP progeny.

In conclusion, the gestational protein-restricted intake induced differential kidney miRNA expression in the fetal and breastfeeding period. Considering these results seem to have a modulatory function on expressing specific genes and proteins associated with impaired nephrogenesis observed in this model.

We found clues to future in-depth analysis. It is essential to consider a complex and intricate gene expression network that miRNAs can regulate during development, integrating regulation and handling a large part of the transcriptome (Zhao and Srivastava, 2008). The cell cycle control and migration of CM undifferentiated cells need more investigations. VEGF protein expression and signaling also require focused future analysis. Whole-tissue homogenates do not reflect what can be found within the developing kidney's different compartments. They are necessary studies in isolated cells from CM and BU for specifying where modulations are occurring.

DATA AVAILABILITY STATEMENT

The miRNA sequencing data has been deposited into the Sequence Read Archive repository (accession: PRJNA694197).

ETHICS STATEMENT

The animal study was reviewed and approved by the Institutional Ethics Committee (CEUA/UNESP, Protocol #446). The general guidelines established by the Brazilian College of Animal Experimentation were followed throughout the investigation.

AUTHOR CONTRIBUTIONS

LB contributed to the data curation, investigation, formal analysis, methodology, visualization, and writing the original draft. GL contributed to the methodology and visualization. WS contributed to the methodology and supervision. AS contributed to the methodology and supervision. JG contributed to the formal analysis, methodology, visualization, and writing, review, and editing the manuscript. PB contributed to the conceptualization, formal analysis, funding acquisition, methodology, resources, supervision, visualization, and writing the original draft, and review and editing the manuscript. All authors contributed to the article and approved the submitted version.

FUNDING

This work was supported by Fundação de Amparo à Pesquisa do Estado de São Paulo (FAPESP, 05/54362-4, 12/18492-4, 13/12486-5, and 14/50938-8), Coordenação de Aperfeiçoamento de Pessoal de Nível Superior (CAPES), and Conselho Nacional de Desenvolvimento Científico e Tecnológico (CNPq, 465699/2014-6).

ACKNOWLEDGMENTS

Data analysis was partial and generously performed in collaboration with Tao Chen, Ph.D. from the Division of Genetic and Molecular Toxicological, National Center for Toxicological Research, Jefferson, AR, United States.

SUPPLEMENTARY MATERIAL

The Supplementary Material for this article can be found online at: https://www.frontiersin.org/articles/10.3389/fphys.2021.648056/full#supplementary-material

REFERENCES

Alliston, T., Ko, T. C., Cao, Y., Liang, Y. Y., Feng, X. H., Chang, C., et al. (2005). Repression of bone morphogenetic protein and activin inducible transcription by Evi-1. *J. Biol. Chem.* 280, 24227–24238. doi: 10.1074/jbc.m414305200

Alvarez, R. Jr., Wang, B. J., Quijada, P. J., Avitabile, D., and Ho, T. (2019). Cardiomyocyte cell cycle dynamics and proliferation revealed through cardiac-specific transgenesis of fluorescent ubiquitinated cell cycle indicator (FUCCI). *J. Mol. Cell Cardiol.* 127, 154–164. doi: 10.1016/j.yjmcc.2018.12.007

Ambros, V. (2004). The functions of animal microRNAs. *Nature* 431, 350–355. doi: 10.1038/nature02871

Bartel, D. P. (2004). MicroRNAs: genomics, biogenesis, mechanism, and function. *Cell* 116, 281–297. doi: 10.1016/s0092-8674(04)00045-5

Brown, D. L., Walling, B. E., and Mattix, M. E. (2016). "Urinary system," in *Atlas of Histology of the Juvenile Rat*, eds G. A. Parker and C. A. Picut (San Diego, CA: Elsevier).

Bushati, N., and Cohen, S. M. (2007). microRNA functions. *Annu. Rev. Cell Dev. Biol.* 23, 175–205. doi: 10.1146/annurev.cellbio.23.090506.123406

Bustin, S. A., Benes, V., Garson, J. A., Hellemans, J., Huggett, J., Kubista, M., et al. (2009). The MIQE guidelines: minimum information for publication of quantitative real-time PCR experiments. *Clin. Chem.* 55, 611–622. doi: 10.1373/clinchem.2008.112797

Chang, T. C., and Mendell, J. T. (2007). microRNAs in vertebrate physiology and human disease. *Annu. Rev. Genomics Hum. Genet.* 8, 215–239. doi: 10.1146/annurev.genom.8.080706.092351

Chen, G., Zhu, W., Shi, D., Lv, L., Zhang, C., Liu, P., et al. (2010). MicroRNA-181a sensitizes human malignant glioma U87MG cells to radiation by targeting Bcl-2. *Oncol. Rep.* 23, 997–1003. doi: 10.3892/or_00000725

Chu, C., and Rana, T. M. (2007). Small RNAs: regulators and guardians of the genome. *J. Cell. Physiol.* 213, 412–419. doi: 10.1002/jcp.21230

Chu, J. Y. S., Sims-Lucas, S., Bushnell, D. S., Bodnar, A. J., Kreidberg, J. A., and Ho, J. (2014). Dicer function is required in the metanephric mesenchyme for early kidney development. *AJP Renal Physiol.* 306, F764–F772.

Crotty, S., Johnston, R. J., and Schoenberger, S. P. (2010). Effectors and memories: Bcl-6 and Blimp-1 in T and B lymphocyte differentiation. *Nat. Immunol.* 11, 114–120. doi: 10.1038/ni.1837

Fuentes-Baile, M., Ventero, M. P., Encinar, J. A., García-Morales, P., Poveda-Deltell, M., and Pérez-Valenciano, E. (2020). Differential effects of IGF-1R small molecule tyrosine kinase inhibitors BMS-754807 and OSI-906 on human cancer cell lines. *Cancers (Basel)* 12:3717. doi: 10.3390/cancers12123717

Gluckman, P. D., and Hanson, M. A. (2006). The consequences of being born small–an adaptive perspective. *Horm. Res.* 65 (Suppl. 3), 5–14. doi: 10.1159/000091500

Gluckman, P. D., Hanson, M. A., and Spencer, H. G. (2005). Predictive adaptive responses and human evolution. *Trends Ecol. Evol.* 20, 527–533. doi: 10.1016/j.tree.2005.08.001

Grobstein, C. (1955). Inductive interaction in the development of the mouse metanephros. *J. Exp. Zool.* 130, 319–339. doi: 10.1002/jez.1401300207

Gürke, J., Schindler, M., Pendzialek, S. M., Thieme, R., Grybel, K. J., Heller, R., et al. (2016). Maternal diabetes promotes mTORC1 downstream signaling in rabbit preimplantation embryos. *Soc. Reprod. Fertil.* 151, 465–476. doi: 10.1530/REP-15-0523

Harvey, S. J., Jarad, G., Cunningham, J., Goldberg, S., Schermer, B., Harfe, B. D., et al. (2008). Podocyte-specific deletion of dicer alters cytoskeletal dynamics and causes glomerular disease. *J. Am. Soc. Nephrol.* 19, 2150–2158. doi: 10.1681/ASN.2008020233

Ho, J., Pandey, P., Schatton, T., Sims-Lucas, S., Khalid, M., Frank, M. H., et al. (2011). The pro-apoptotic protein Bim is a microRNA target in kidney progenitor cells. *J. Am. Soc. Neph.* 22, 1053–1063.

Hohenauer, T., and Moore, A. W. (2012). The Prdm family: expanding roles in stem cells and development. *Development* 139, 2267–2282. doi: 10.1242/dev.070110

Huang, B., Liu, Z., Vonk, A., Zeng, Z., and Li, Z. (2020). Epigenetic regulation of kidney progenitor cells. *Stem Cells Transl. Med.* 9, 655–660. doi: 10.1002/sctm.19-0289)

Kim, V., Han, J., and Siomi, M. (2009). Biogenesis of small RNAs in animals. *Nat. Rev. Mol. Cell Biol.* 10, 126–139. doi: 10.1038/nrm2632

Kitamoto, Y., Tokunaga, H., and Tomita, K. (1997). Vascular endothelial growth factor is an essential molecule for mouse kidney development: glomerulogenesis and nephrogenesis. *J. Clin. Invest.* 99, 2351–2357. doi: 10.1172/jci119416

Langley-Evans, S. C. (2006). Developmental programming of health and disease. *Proc. Nutr. Soc.* 65, 97–105. doi: 10.1079/pns2005478

Li, J. Y., Yong, T. Y., Michael, M. Z., and Gleadle, J. M. (2010). The role of microRNAs in kidney disease. *Nephrology (Carlton)* 15, 599–608. doi: 10.1111/j.1440-1797.2010.01363.x

Li, W., Qiu, X., Jiang, H., Han, Y., Wei, D., and Liu, J. (2016). ScienceDirect downregulation of miR-181a protects mice from LPS-induced acute lung injury by targeting Bcl-2. *Biomed. Pharmacother.* 84, 1375–1382. doi: 10.1016/j.biopha.2016.10.065

Lucas, A. (1998). Symposium: the effects of childhood diet on adult health and disease psychological influences on childhood diet 1. *J. Nutr.* 128, 401S–406S. doi: 10.1093/jn/128.2.401S

Lv, X., Mao, Z., Lyu, Z., Zhang, P., Zhan, A., Wang, J., et al. (2014). miR181c promotes apoptosis and suppresses the proliferation of metanephric mesenchyme cells by targeting Six2 in vitro. *Cell Biochem. Funct.* 32, 571–579. doi: 10.1002/cbf.3052

Mackenzie, H. S., Lawler, E. V., and Brenner, B. M. (1996). Congenital oligonephropathy: the fetal flaw in essential hypertension? *Kidney Int. Suppl.* 55, S30–S34.

Marrone, A. K., and Ho, J. (2014). MicroRNAs: potential regulators of renal development genes that contribute to CAKUT. *Pediatr. Nephrol.* 29, 565–574. doi: 10.1007/s00467-013-2599-0

Marshall, S. (2006). Role of insulin, adipocyte hormones, and nutrient-sensing pathways in regulating fuel metabolism and energy homeostasis: a nutritional perspective of diabetes, obesity, and cancer. *Sci. STKE* 2006:re7. doi: 10.1126/stke.3462006re7

Matsubara, J., Takashima, A., Kato, K., Hamaguchi, T., Shirao, K., Shimada, Y., et al. (2009). Relationships of insulin-like growth factor-1 receptor and epidermal growth factor receptor expression to clinical outcomes in patients with colorectal cancer. *Oncology* 76, 42–48. doi: 10.1159/000178164

Melton, C., Judson, R. L., and Blelloch, R. (2010). Opposing microRNA families regulate self-renewal in mouse embryonic stem cells. *Nature* 463, 621–626. doi: 10.1038/nature08725

Mens, M. M. J., and Ghanbari, M. (2018). Cell cycle regulation of stem cells by microRNAs. *Stem Cell Rev. Rep.* 14, 309–322. doi: 10.1007/s12015-018-9808-y

Mesquita, F. F., Gontijo, J. A., and Boer, P. A. (2010a). Expression of renin-angiotensin system signalling compounds in maternal protein-restricted rats: effect on renal sodium excretion and blood pressure. *Nephrol. Dial. Transplant.* 25, 380–388. doi: 10.1093/ndt/gfp505

Mesquita, F. F., Gontijo, J. A. R., and Boer, P. A. (2010b). Maternal undernutrition and the offspring kidney: from fetal to adult life. *Braz. J. Med. Biol. Res.* 43, 1010–1018. doi: 10.1590/s0100-879x2010007500113

Moore, M. W., Klein, R. D., Farinas, I., Sauer, H., Armanini, M., Phillips, H., et al. (1996). Renal and neuronal abnormalities in mice lacking GDNF. *Nature* 382, 76–79. doi: 10.1038/382076a0

Monk, C., Spicer, J., and Champagne, F. A. (2012). Linking prenatal maternal adversity to developmental outcomes in infants: the role of epigenetic pathways. *Dev. Psychopathol.* 24, 1361–1376. doi: 10.1017/S0954579412000764

Nagalakshmi, V. K., Ren, Q., Pugh, M. M., Valerius, M. T., McMahon, A. P., and Yu, J. (2011). Dicer regulates the development of nephrogenic and ureteric compartments in the mammalian kidney. *Kidney Int.* 79, 317–330. doi: 10.1038/ki.2010.385

Nakagawa, N., Xin, C., Roach, A. M., Naiman, N., Shankland, S. J., Ligresti, G., et al. (2015). Dicer1 activity in the stromal compartment regulates nephron differentiation and vascular patterning during mammalian kidney organogenesis. *Kidney Int.* 87, 1125–1140. doi: 10.1038/ki.2014.406

Nijland, M. J., Schlabritz-loutsevitch, N. E., Hubbard, G. B., Nathanielsz, P. W., and Cox, L. A. (2007). Non-human primate fetal kidney transcriptome analysis indicates the mammalian target of rapamycin (mTOR) is a central nutrient-responsive pathway. *J. Physiol.* 579, 643–656. doi: 10.1113/jphysiol.2006.122101

Nilsen, T. W. (2007). Mechanisms of microRNA-mediated gene regulation in animal cells. *Trends Genet.* 23, 243–249. doi: 10.1016/j.tig.2007.02.011

Pan, C., Chen, H., Wang, L., Yang, S., Fu, H., Zheng, Y., et al. (2012). Down-regulation of MiR-127 facilitates hepatocyte proliferation during rat liver regeneration. *PLoS One* 7:e39151. doi: 10.1371/journal.pone.0039151

Pfaffl, M. W. (2001). A new mathematical model for relative quantification in real-time RT–PCR. *Nucleic Acids Res.* 29:e45. doi: 10.1093/nar/29.9.e45

Pan, X., Karner, C. M., and Carroll, T. J. (2017). Myc cooperates with beta-catenin to drive gene expression in the nephron progenitor cells. *Development* 144, 4173–4182. doi: 10.1242/dev.153700

Phua, Y. L., Chu, J. Y. S., Marrone, A. K., Bodnar, A. J., Sims-Lucas, S., and Ho, J. (2015). Renal stromal miRNAs are required for normal nephrogenesis and glomerular mesangial survival. *Physiol. Rep.* 3:e12537. doi: 10.14814/phy2.12537

Pichel, J. G., Shen, L., Sheng, H. Z., Granholm, A. C., Drago, J., Grinberg, A., et al. (1996). Defects in enteric innervation and kidney development in mice lacking GDNF. *Nature* 382, 73–76. doi: 10.1038/382073a0

Reczko, M., Maragkakis, M., Alexiou, P., Grosse, I., and Hatzigeorgiou A. G. (2012). Functional microRNA targets in protein coding sequences. *Bioinformatics* 28, 771–776. doi: 10.1093/bioinformatics/bts043

Sanchez, M. P., Silos-Santiago, I., Frisen, J., He, B., Lira, S. A., and Barbacid, M. (1996). Renal agenesis and the absence of enteric neurons in mice lacking GDNF. *Nature* 382, 70–73. doi: 10.1038/382070a0

Saxen, L., and Sariola, H. (1987). Early organogenesis of the kidney. *Pediatr. Nephrol.* 1, 385–392. doi: 10.1007/BF00849241

Schreuder, M., Delemarre-Van De Waal, H., and Van Wijk, A. (2006). Consequences of intrauterine growth restriction for the kidney. *Kidney Blood Press. Res.* 29, 108–125. doi: 10.1159/000094538

Schuchardt, A., D'Agati, V., Larsson-Blomberg, L., Costantini, F., and Pachnis, V. (1994). Defects in the kidney and enteric nervous system of mice lacking the tyrosine kinase receptor Ret. *Nature* 367, 380. doi: 10.1038/367380a0

Scorrano, L., and Korsmeyer, S. J. (2003). Mechanisms of cytochrome c release by proapoptotic BCL-2 family members. *Biochem. Biophys. Res. Commun.* 304, 437–444. doi: 10.1016/s0006-291x(03)00615-6

Sene, L. B., Mesquita, F. F., de Moraes, L. N., Santos, D. C., Carvalho, R., Gontijo, J. A., et al. (2013). Involvement of renal corpuscle microRNA expression on epithelial-to-mesenchymal transition in maternal low protein diet in adult programmed rats. *PLoS One* 19:e71310. doi: 10.1371/journal.pone.0071310

Sene, L. B., Rizzi, V. H. G., Gontijo, J. A. R., and Boer, P. A. (2018). Gestational low-protein intake enhances whole-kidney miR-192 and miR-200 family expression and epithelial-to-mesenchymal transition in rat adult male offspring. *J. Exp. Biol.* 22:221. doi: 10.1242/jeb.171694

Sene, L. B., Scarano, W. R., Zapparoli, A., Gontijo, J. A. R., and Boer, P. A. (2021). Impact of gestational low-protein intake on embryonic kidney microRNA expression and in nephron progenitor cells of the male fetus. *PLoS One* 16:e0246289. doi: 10.1371/journal.pone.0246289

Shim, J., and Nam, J. W. (2016). The expression and functional roles of microRNAs in stem cell differentiation. *BMB Rep.* 49, 3–10. doi: 10.5483/bmbrep.2016.49.1.217

Sun, H., Zhou, C., and Fu, L. (2015). Inhibition of MiR-199a-5p reduced cell proliferation in autosomal dominant polycystic kidney disease through targeting CDKN1C. *Med. Sci. Monit.* 21, 195–200. doi: 10.12659/MSM.892141

Sun, N., Zhang, L., Zhang, C., and Yuan, Y. (2020). miR-144-3p inhibits cell proliferation of colorectal cancer cells by targeting BCL6 via inhibition of Wnt/β-catenin signaling. *Cell Mol. Biol. Lett.* 17:19. doi: 10.1186/s11658-020-00210-3

Valsecchi, M. E., McDonald, M., Brody, J. R., Hyslop, T., Freydin, B., and Yeo, C. J. (2012). Epidermal growth factor receptor and insulinlike growth factor 1 receptor expression predict poor survival in pancreatic ductal adenocarcinoma. *Cancer* 118, 3484–3493. doi: 10.1002/cncr.26661

Vasudevan, S., Tong, Y., and Steitz, J. A. (2007). Switching from repression to activation: microRNAs can up-regulate translation. *Science* 318, 1931–1934. doi: 10.1126/science.1149460

Vlachos, I. S., and Hatzigeorgiou, A. G. (2013). Online resources for miRNA analysis. *Clin. Biochem.* 46, 879–900. doi: 10.1016/j.clinbiochem.2013.03.006

Wei, J., Zhang, Y., Luo, Y., Wang, Z., Bi, S., Song, D., et al. (2014). Aldose reductase regulates miR-200a-3p/141-3p to coordinate Keap1-Nrf2, Tgf1/2, and Zeb1/2 signaling in renal mesangial cells and the renal cortex of diabetic mice. *Free Radic. Biol. Med.* 67, 91–102. doi: 10.1016/j.freeradbiomed.2013.10.811

Xiang, C., Cui, S., and Ke, Y. (2016). MiR-144 inhibits cell proliferation of renal cell carcinoma by targeting mTOR. *J. Huazhong Univ. Sci Technolog. Med. Sci.* 36, 186–192. doi: 10.1007/s11596-016-1564-0

Yu, J., Angelin-Duclos, C., Greenwood, J., Liao, J., and Calame, K. (2000). Transcriptional repression by blimp-1 (PRDI-BF1) involves recruitment of histone deacetylase. *Mol. Cell. Biol.* 20, 2592–2603. doi: 10.1128/mcb.20.7.2592-2603.2000

Zhang, Y., Miaomiao, F., Zhang, X., Huang, F., Wu, K., Zhang, J., et al. (2014). Cellular microRNAs up-regulate transcription via interaction with promoter TATA-box motifs. *RNA* 20, 1878–1889. doi: 10.1261/rna.045633.114

Zhao, Y., and Srivastava, D. (2008). A developmental view of microRNA function. *Trends Biochem. Sci.* 32, 189–197. doi: 10.1016/j.tibs.2007.02.006

Zhou, Y., Li, Y. S., Bandi, S. R., Tang, L., Shinton, S. A., Hayakawa, K., et al. (2015). Hard Lin28b promotes fetal B lymphopoiesis through the transcription factor Arid3a. *J. Exp. Med.* 212, 569–580. doi: 10.1084/jem.20141510

Conflict of Interest: The authors declare that the research was conducted in the absence of any commercial or financial relationships that could be construed as a potential conflict of interest.

frontiers in Physiology

ORIGINAL RESEARCH
published: 28 June 2021
doi: 10.3389/fphys.2021.630933

Tsc Gene Locus Disruption and Differences in Renal Epithelial Extracellular Vesicles

Prashant Kumar[1†], Fahad Zadjali[1,2†], Ying Yao[1], Brian Siroky[1], Aristotelis Astrinidis[1], Kenneth W. Gross[3] and John J. Bissler[1,4]*

[1] Department of Pediatrics, University of Tennessee Health Science Center and Le Bonheur Children's Hospital, Memphis, TN, United States, [2] Department of Clinical Biochemistry, College of Medicine & Health Sciences, Sultan Qaboos University, Muscat, Oman, [3] Department of Molecular and Cellular Biology, Roswell Park Comprehensive Cancer Center, Buffalo, NY, United States, [4] Department of Pediatrics, St. Jude Children's Research Hospital, Memphis, TN, United States

In tuberous sclerosis complex (TSC), *Tsc2* mutations are associated with more severe disease manifestations than *Tsc1* mutations and the role of extracellular vesicles (EVs) in this context is not yet studied. We report a comparative analysis of EVs derived from isogenic renal cells except for *Tsc1* or *Tsc2* gene status and hypothesized that in spite of having similar physical characteristics, EVs modulate signaling pathways differently, thus leading to TSC heterogenicity. We used mouse inner medullary collecting duct (mIMCD3) cells with the *Tsc1* (T1G cells) or *Tsc2* (T2J cells) gene disrupted by CRISPR/CAS9. EVs were isolated from the cell culture media by size-exclusion column chromatography followed by detailed physical and chemical characterization. Physical characterization of EVs was accessed by tunable resistive pulse sensing and dynamic light scattering, revealing similar average sizes and zeta potentials (at pH 7.4) for EVs from mIMCD3 (123.5 ± 5.7 nm and −16.3 ± 2.1 mV), T1G cells (131.5 ± 8.3 nm and −19.8 ± 2.7 mV), and T2J cells (127.3 ± 4.9 nm and −20.2 ± 2.1 mV). EVs derived from parental mIMCD3 cells and both mutated cell lines were heterogeneous (>90% of EVs < 150 nm) in nature. Immunoblotting detected cilial Hedgehog signaling protein Arl13b; intercellular proteins TSG101 and Alix; and transmembrane proteins CD63, CD9, and CD81. Compared to *Tsc2* deletion, *Tsc1* deletion cells had reduced EV production and release rates. EVs from *Tsc1* mutant cells altered mTORC1, autophagy, and β-catenin pathways differently than EVs from *Tsc2*-mutated cells. Quantitative PCR analysis revealed the down regulation of miR-212a-3p and miR-99a-5p in EVs from *Tsc2*-mutated cells compared to EVs from *Tsc1*-mutant cells. Thus, EV-derived miR-212-3p and mIR-99a-5p axes may represent therapeutic targets or biomarkers for TSC disease.

Keywords: tuberous sclerosis complex, extracellular vesicles, miRNA, autophagy, cell signaling

OPEN ACCESS

Edited by:
H. Della Coletta Francescato, University of São Paulo, Brazil

Reviewed by:
Joost Hoenderop, Radboud University Nijmegen Medical Centre, Netherlands
Fiona McDonald, University of Otago, New Zealand

****Correspondence:***
John J. Bissler
jbissler@uthsc.edu

[†] These authors have contributed equally to this work

Specialty section:
This article was submitted to Renal and Epithelial Physiology, a section of the journal Frontiers in Physiology

Received: *18 November 2020*
Accepted: *29 March 2021*
Published: *28 June 2021*

Citation:
Kumar P, Zadjali F, Yao Y, Siroky B, Astrinidis A, Gross KW and Bissler JJ (2021) Tsc Gene Locus Disruption and Differences in Renal Epithelial Extracellular Vesicles. Front. Physiol. 12:630933. doi: 10.3389/fphys.2021.630933

INTRODUCTION

Tuberous sclerosis complex (TSC) affects over one million people worldwide, and the disease manifests from abnormalities in embryonic and postpartum cell growth control that can impact every organ system. The *TSC* genes encode proteins that heterodimerize to repress mTORC1 activity. The *TSC1* gene encodes hamartin, and the *TSC2* gene encodes tuberin. Loss of either

TSC1 or *TSC2* locus function results in upregulated mTORC1 activity associated with disease (Nathan et al., 2017). Though excellent advances have been made in understanding the genetics and involvement of the mTORC1 pathway, how the disease manifestations develop is unclear.

Given that the TSC gene products interact to regulate the mTORC1 pathway, the human disease phenotype is unexpectedly different for patients with *TSC1*-associated disease compared to those with *TSC2*-associated disease (Dabora et al., 2001; Sancak et al., 2005; Aronow et al., 2012; Kothare et al., 2014). This genotype–phenotype difference is also observed in *Tsc* mouse models of neurological disease. *Tsc1*-associated disease is less severe than *Tsc2*-associated disease (Zeng et al., 2011; Magri et al., 2013), and evidence indicates this is not due to changes in mTORC1 activity (Magri et al., 2013). Murine renal solid tumor disease also exhibits a differential effect based on which *Tsc* gene is affected (Kobayashi et al., 2001). Loss of either gene leads to increased mTORC1 activity, but the mechanism for the disease severity difference is unknown.

Although a somatic mutation, or "second hit" mechanism, is involved in disease development, the steps leading to disease manifestation appears to be nuanced in organ systems like the brain and kidney. Central nervous system pathologies in TSC include cortical tubers, subependymal giant cell astrocytomas, and focal cortical dysplasia (Niida et al., 2001; Ramesh, 2003). Inconsistent with the somatic mutation mechanism of TSC, these lesions may lack identifiable somatic mutations (Jozwiak and Jozwiak, 2007), raising the question of whether these tumors contain a mixture of wild-type and *Tsc*-null cells (Au et al., 1999; Napolioni and Curatolo, 2008). The genomic heterogeneity of TSC lesions is further supported by the varied clonality within samples from angiomyolipoma, hamartoma, or tuber or subependymal giant cell astrocytoma (Niida et al., 2001; Ramesh, 2003). Analyses performed on tubers and microdissected giant cells showed equal expression of both TSC alleles; however, giant cells exhibited increased phospho-S6, indicating mTORC1 activation (Ramesh, 2003; Baybis et al., 2004), and rare giant cells within tubers have also lost TSC function (Crino et al., 2010). A possible explanation for this genotype–phenotype difference may involve extracellular vesicles (EVs). Patel et al. (2015) examined the impact of the loss of *Tsc1* on the function on surrounding normal cells using the *in vivo* mouse embryo-neural tube model. Based on their cell phenotype results, they posited that cells without *Tsc1* might secrete EVs that alter surrounding cells with a preserved *Tsc1* locus such that mutant cells disseminate the TSC disease phenotype. However, they did not isolate EVs (Patel et al., 2015).

To better understand renal cystic disease in TSC, we recently used immunofluorescence, immunohistochemistry, and fluorescent lineage-tracing experiments and identified a cell non-autonomous mechanism between TSC-deficient cells and TSC-intact cells (Bissler et al., 2019). This mechanism relies on EVs as the inductive signal and is reminiscent of the morphogen transport model involving primary cilia and left–right asymmetry [for perspective, see Vogel et al. (2010)]. EVs are known to be involved in normal renal collecting duct physiological adaption (Street et al., 2011; Oosthuyzen et al., 2016). The loss of the *Tsc2* gene in renal epithelial cells significantly increases EV production and alters the EV proteome (Zadjali et al., 2020). Thus, the role of EVs in renal development and physiology is becoming clearer. EVs are also involved in renal tubular changes in a von Hippel–Lindau zebrafish model (van Rooijen et al., 2018). Such a cell non-autonomous mechanism may explain why murine models of *Tsc* renal cystic disease fail to show a convincing "second hit" mechanism (Onda et al., 1999; Wilson et al., 2006) and human TSC-associated cysts robustly express hamartin and tuberin (Bonsib et al., 2016).

We reasoned that if the TSC disease involved EV signaling, we might be able to identify a difference in the effects of EVs based on the genetic mutation in the *Tsc* axis. Here we report the EV differences between *Tsc1* and *Tsc2* mutant renal collecting duct cells.

MATERIALS AND METHODS

Cell Lines and Development of *Tsc1* Knockout Cell Lines

We used murine kidney-derived principal cell lines, i.e., mIMCD3, purchased from ATCC (ATCC® CRL-2123™, Manassas, VA, United States). We previously developed derivative isogenic cell lines by knocking out the *Tsc1* or *Tsc2* gene by CRISPR/Cas9, and the derivative lines were designated T1G and T2J, respectively (Bissler et al., 2019). The *Tsc1* gene was knocked out by targeting exon 4 (Bissler et al., 2019). Cystic kidney-derived epithelial cells, i.e., M1 cells, were also purchased from ATCC® (CRL-2038™, Manassas, VA, United States). mIMCD3, T1G, and T2J cells were maintained in DMEM/F12 with 10% FBS, whereas M1 cells were maintained with DMEM/F12 with 5% FBS and supplemented with 5 μM dexamethasone. Cultures were maintained at 37°C in a humidified 95% air and 5% CO_2 atmosphere.

Protein Isolation and Western Blot

Proteins were isolated from cultured cells using Mammalian Protein Extraction Reagent (M-PER, Thermo Fisher Scientific #78501) with PhosSTOP (Sigma-Aldrich, 4906845001) and Complete protease inhibitor cocktail (Sigma-Aldrich, 11697498001) as per the manufacturer's protocol. Isolated proteins were quantified using Bradford assay. Western blot analysis was done to identify EV-related protein markers. For this experiment, proteins isolated from EVs were separated by SDS-PAGE, followed by electrophoretic transfer of proteins to a nitrocellulose membrane. The membrane was blocked with 5% non-fat dry milk or 5% bovine serum albumin in TBST (Tris-buffered saline, 0.5% Tween 20) for 1 h. Then, the membrane was probed with an appropriate primary antibody and incubated for 16 h at 4°C, followed by incubation with horseradish peroxidase-conjugated secondary antibodies for 1 h at room temperature. The primary and secondary antibodies were diluted in 5% milk or 5% BSA from 1:00 to 1:1,000 and 1:5,000, respectively. The specific antibodies used for each protein (manufacturer, code, or clone number) as well as the specific concentration used for each

antibody and whether milk or BSA was used as blocking agent can be found in **Table 1**.

Isolation of Extracellular Vesicles by Column Chromatography

Extracellular vesicles were isolated from the conditioned media derived from mIMCD3, T1G, and T2J cells per our published protocol with minor modifications (Zadjali et al., 2020). Briefly, cells were grown in complete growth media, with 10% FBS up to 75–80% confluency. Then, the cells were washed three times with sterile phosphate-buffered saline (PBS) to remove any traces of serum and replaced with conditioned DMEM/F12 media without serum for 24 h. The isolated conditioned media were centrifuged at 2,000 x *g* for 20 min at 4°C to remove cells and debris. The supernatant was further loaded on a Millipore Amicon® Ultra 15-ml 10K centrifugal filter (Cat# UFC901008, Burlington, MA, United States) and concentrated to 0.5 ml. The sample was applied to a qEV column (Izon Sciences, New Zealand) and immediately eluted with 0.5 ml of 0.2 μM filtered PBS. Initial fractions (1st–6th) were not expected to contain EVs and were thus discarded. The latter three fractions, i.e. 7th, 8th, and 9th, were considered EV-rich fractions and were collected as per the manufacturer's instructions. Finally, these fractions were pooled together and concentrated up to 0.5 ml using an Amicon® Ultra 2-mL Concentration device (Millipore).

Characterization of EVs

Transmission Electron Microscopy

Extracellular vesicles were negatively stained and observed for size and surface morphology using a TEM. Briefly, 8 μl of freshly isolated EV suspension was dried on the top of a carbon mesh 200 grid at room temperature. The sample was then negatively stained by 2% uranyl acetate followed by washing with water to remove excess stain. The grids were visualized by TEM JEOL 2000EXII (JEOL, Peabody, MA, United States; access provided by the Neuroscience Institute, The University of Tennessee Health Science Center).

Tunable Resistive Pulse Sensing (TRPS) Analysis of EVs

Extracellular vesicles were further characterized by TRPS analysis using qNano Gold (Izon Sciences) as described by the manufacturer's instructions. During this process, EVs were driven through a polyurethane nanopore (NP150, Part No #A54186) under a 15-millibar pressure and a voltage of 0.30 mV. Polystyrene beads CPC100 (Batch #B8748S) with a stock concentration of 1.2×10^{13} and a working dilution of 1:500 were used as a standard. EV samples (35 μl) were applied on top of the nanopore under the abovementioned conditions, and a minimum of 500 particle blockade signals were recorded. The data were processed and analyzed by Izon control suite v3.0.

Dynamic Light Scattering

The particle size distribution of EVs was examined using DLS. For analysis, EV samples (50 μl) were mixed with 950 μl milliQ water. The samples were loaded into a disposable polystyrene cuvette, and five measurements were recorded; the mean value of the measurements was documented.

pH Effect on EV Zeta Potential

This experiment was performed to elucidate the effect of cyst microenvironmental pH on the zeta potential of EVs derived from cell lines. Equal numbers of EVs, i.e., 5×10^7, derived from mIMCD3, T1G, and T2G cells, were incubated with 500 μL PBS at pH 7.4 (physiological pH) or pH 6.0 (renal cystic pH) for 15 min followed by zeta potential measurement by qNano. Initially, the qNano was calibrated using the standard beads (CPC100) and zeta potential was measured at three different applied voltages, i.e., 0.20, 0.18, and 0.16 mV, in the presence of a constant stretch for all measurements. The samples were measured at the same setting at either of the voltages as per manufacturer protocol. For each reading, a minimum of 200 particles were measured and the raw data were analyzed using Izon control suite v3.0.

Release and Uptake of EVs

Equal numbers of mIMCD3 and T1G cells were transfected with eGFP-tagged CD63 (pcDNA3-EGFP, Addgene) using Lipofectamine plus reagent (Thermo Fisher Scientific, Waltham, MA, United States). Transfection efficiency was measured by calculating the ratio of the GFP signal to the nuclear stain DAPI signal. The images were captured using a Leica DMi8 fluorescence microscope (Leica, Germany). To measure eGFP-EV release, debris-free cell media were collected 48 h after transfection. Fluorescence intensity was measured at

TABLE 1 | List of antibodies used in the study.

Antibodies	Manufacture	Catalog #	Clone #	Dilution	Blocking agent
Alix	Proteintech	12422-1-AP	Polyclonal	100	5% BSA
ARL 13B	Neuroma	75287020	N295B/66	500	5% MILK
CD63	MBL International	D263-3	R5G2	300	5% BSA
CD81	Cell Signaling	10037S	D5O2Q	1000	5% BSA
CD9	Invitrogen	10626D	Ts9	500	5% MILK
GAPDH	Proteintech	10494-1-AP	Polyclonal	10,000	5% BSA
p-S6K	Cell Signaling	2211S	Ser235/236	5000	5% BSA
S6K	Cell Signaling	2317S	54D2	1000	5% MILK
TSG101	Millipore sigma	MABC786	4A10	1000	5% MILK

480 nm (excitation) and 510 nm (emission). Mean fluorescence intensities were normalized to total protein in cell media. EVs were isolated from eGFP-CD63-transfected mIMCD3, T1G, and T2J cells and quantified. Equal numbers of EVs were then added to recipient cells (M1 cells) for 24 h to measure EV uptake as the number of GFP foci normalized to the number of DAPI-stained nuclei.

Effect of EVs on mTOR and Autophagy

Briefly, 5×10^6 M1 cells per well were cultured in DMEM/F12 serum-starved media in a 10-cm dish and treated with 50×10^6 EVs derived from mIMCD3, T1G, or T2J cells for 24 h. Next, cell lysates were obtained, and western blots were performed using mTOR markers pS6-K and S6K. Western blots were quantified using ImageJ (NIH, Bethesda, MD, United States) and normalized to GAPDH.

Total RNA Isolation From EVs and Transfection

Equal amounts of EVs ($\sim 20 \times 10^6$ particles) from mIMCD3, T1G, or T2J cells were used to isolate total RNA using a total exosomal RNA isolation kit (Invitrogen, Lithuania). For miRNA transfection, a Lipofectamine RNAiMAX transfection kit was used (Thermo Fisher Scientific). For control scramble transfection, mirVana^{TM} miRNA Mimic Negative Control was used (Thermo Fisher Scientific).

RT-PCR and miRNA Analysis

Total cellular RNA was isolated from cells (miRNeasy Mini, Qiagen, Germany), and DNA was removed using DnaseI digestion. cDNAs were generated by reverse transcription (High Capacity cDNA Reverse Transcription Kit, Applied Biosystems, Foster City, CA, United States). SYBR Green-based real-time PCR was performed (PowerUp SYBR Master Mix, Thermo Fisher Scientific) with the following primer sequences; m_Rps6kb: GGTAAAGGGGGCTATGGAAA (forward) and GGTCCACAATGAAAGGGTGT (reverse), m_@ Actin: CCAGTTGGTAACAATGCCATGT (forward) and CCAGTTGGTAACAATG-CCATGT (reverse). Results are expressed as a relative unit from the relative standard curve.

To predict the miRNA targeting mouse p70-S6K (Rps6kb1) mRNA, we followed a strategy similar to that performed on the human p70-S6K gene (Razaviyan et al., 2018). Here we used multiple algorithms and mouse miRNA search databases. The databases included miRBase, TargetScan, miRanda, miRDB, mIRtarBASE, DIANA-microT, PicTar, EIMMo3, and TargetS. All miRNAs from TargetScan prediction were tabulated, and matches from other databases were scored. miRNAs identified from three or more databases were selected. Selected miRNAs were aligned to mouse Rps6kb1 mRNA 5' and 3' untranslated regions (Utr) and coding sequences of isoform 1 (NM_001114334) and isoform 2 (NM_028259). Western blot analysis of mIMCD3 cells shows isoform 2 of the gene (*S6K*) with a protein band around 35 kDa. Therefore, we selected miRNAs targeting this isoform.

For miRNA quantification, total RNA was extracted from EVs of the three cell lines (total of 1×10^8 particles) and 30 ng RNA was then reverse transcribed using a locked nucleic acid approach (miRCURY LNA RT Kit, Qiagen). Selected miRNAs were quantified using SYBR Green-based real-time PCR (miRCURY LNA SYBR Green PCR Kit, Qiagen) using a pre-designed primer assay from Qiagen. Expression was normalized using the global mean of three snRNA loading controls: *U6*, *Rnu1a1*, and *Rnu5g*. The relative fold changes in miRNA expression levels were calculated with the $2\text{-}\Delta\Delta Ct$ method.

Statistical Analysis

All studies were performed in triplicate for all groups, and results are presented as mean ± standard deviation. Statistical analyses were done using Student's *t*-test. Multiple values between groups were analyzed using ANOVAs. The level of statistical significance (p) was set at $p < 0.05$.

RESULTS

Tsc1 and *Tsc2* Deleted Renal Collecting Duct Cells Produce EVs *in vitro* Differentially

Extracellular vesicles were isolated from the conditioned media of murine renal collecting duct cells (mIMCD3) and *Tsc1*-deleted mIMCD3 designated as T1G, as per our previous paper (Bissler et al., 2019). EVs were biophysically characterized using transmission electron microscopy (TEM; **Figure 1A**), tunable resistive pulse sensing (TRPS; **Figure 1B-i**), and dynamic light scattering (DLS; **Figure 1C**). The isolated EVs possessed a unique cup-shaped characteristic (**Figure 1A**) and heterogeneous size distribution which were similar to EVs derived from the *Tsc2*-deleted mIMCD3 cell line (Zadjali et al., 2020). TRPS showed a size of 123.5 ± 5.7 nm and 131.5 ± 8.3 nm for mIMCD3- and T1G-derived EVs, respectively. These EVs were in a similar size range as the EVs derived from the *Tsc2*-deleted mIMCD3 cell line at 127.3 ± 4.9 nm (T2J) (Zadjali et al., 2020).

Our data suggest a significant increase in the mean EV production value derived from T1G ($1.65 \times 10^8 \pm 2.8 \times 10^7$) and T2J ($2.3 \times 10^8 \pm 3.5 \times 10^7$) as compared to that in the parental mIMCD3 ($1.10 \times 10^8 \pm 2.1 \times 10^7$) cells (**Figure 1B-ii**). At physiological pH 7.4, the zeta potentials of mIMCD3-, T1G-, and T2J-derived EVs were recorded in a range of −15 to −20 mV (**Figure 2B**). At the renal cystic pH 6.0, the zeta potential of T1G-derived EVs and mIMCD3-derived EVs increased to −1.8 and −8.3 mV, respectively. There were no significant changes observed in the zeta potential for T2J-derived EVs. The majority of EVs from all three cell lines exhibited a similar small size (**Figure 2A**). To further verify that the isolated structures were EVs, we used western blot analysis to identify EV markers. Western blots of proteins isolated from the EVs identified the cellular proteins Alix and TSG101; the transmembrane proteins CD63, CD81, and CD9; and the cilia protein ARL13b (**Figure 2C**). We previously identified these EV markers in EVs from the *Tsc2*-deleted mIMCD3 cell line (Zadjali et al., 2020).

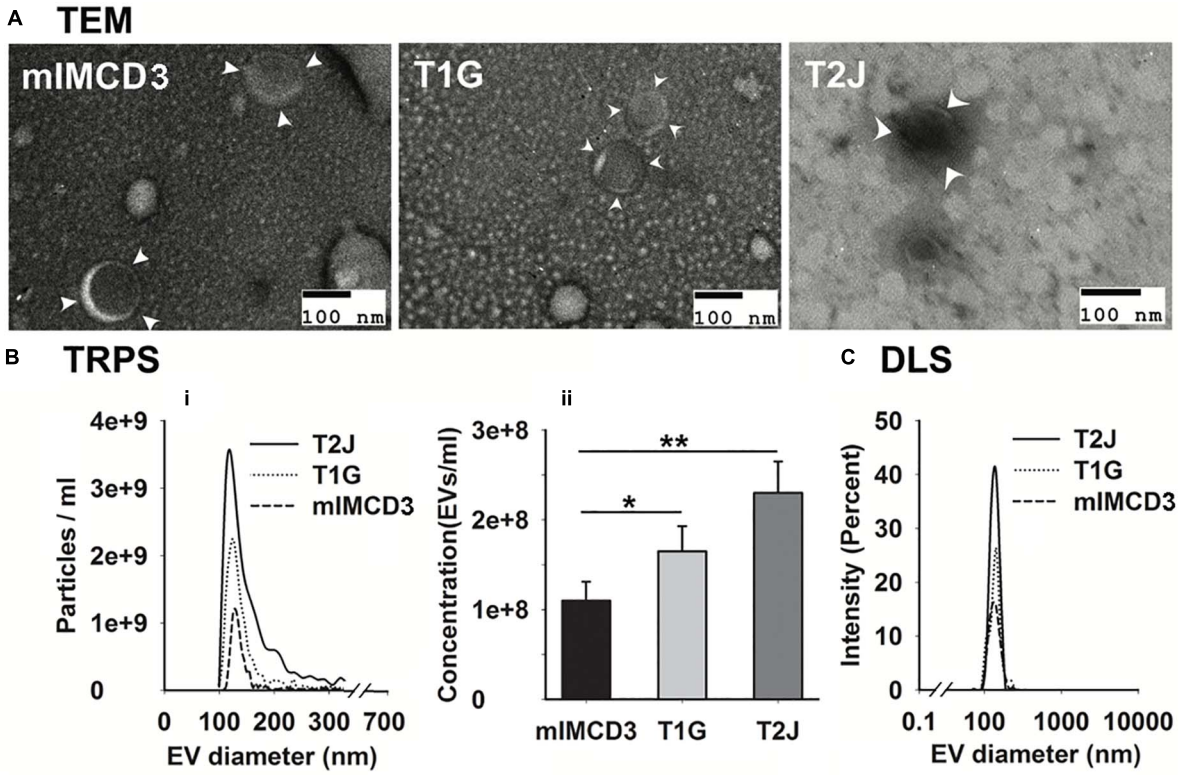

FIGURE 1 | Characterization of mIMCD3, T1G, and T2J cells derived EVs. **(A)** Representation of transmission electron microscopy confirmed the rounded cup-shaped structure of EVs (indicated with white arrowhead) isolated from the cell culture media of all three cell lines (scale bar 100 nm). **(B-i,ii,C)** Tunable resistive pulse sensing (TRPS) and dynamic light scattering (DLS) analysis of purified EVs. Data ($n = 3$) were represented as mean ± SD. *Significant difference analyzed by *t*-test (*$p < 0.05$, **$p < 0.01$).

Differences in EV Flux

To better understand how the *Tsc* gene status impacted the turnover of EVs, we examined EV release and uptake rates. We transfected mIMCD3, T1G, and T2J cells with a CD63-green fluorescent protein (GFP) construct and collected cell media to measure release post-transfection. This approach allowed us to assess EV production in the presence of fetal bovine serum (FBS). Experiments in **Figure 1** were performed in the absence of FBS to avoid contamination with EVs from FBS. The transfection efficiency for the cell lines was equivalent (**Figure 3A**). The EV release rate (**Figure 3B**) was increased in the *Tsc2*-disrupted T2J cell line compared to that in the parental mIMCD3 cell line. T1G EVs had a release rate similar to that of mIMCD3 EVs. This is somewhat different from that seen in **Figure 1**, likely because in the absence of FBS, the cells were stressed and produced more EVs (Eguchi et al., 2020). We used EVs from these cells to treat intercalated M1 cells and measure the uptake rate. A higher uptake rate was observed with EVs from T2J cells, while T1G EV uptake was similar to mIMCD3 EV uptake (**Figure 3C**).

Tsc Locus Modulates Different EV Effects on Target Renal Epithelial Cells

Because the release and uptake rates are different for EVs derived from isogenic cell lines except for their *Tsc* gene status, we wished to understand if the different EV populations also had different effects on target collecting duct cells. We previously reported that EVs from *Tsc*-deleted cells induced more mTORC1 activity (S6K phosphorylation) (Bissler et al., 2019). Because EVs can transduce signals that affect transcription and translation, we wished to understand if this S6K effect was mediated by a change in gene expression. To assess this effect, we assayed M1 target cell RNA using RT-PCR normalized using β-*actin* after exposure to EVs. *RPS6KB1 (p70S6K)* mRNA expression was decreased in M1 cells treated with EVs from T2J cells but not from mIMCD3 cells ($p < 0.05$, **Figure 4A**). Paradoxically, EVs isolated from T1G cells induced an increased *RPS6KB1* mRNA expression, providing a further difference between the cell lines and their EVs at the RNA level, ($p < 0.05$, **Figure 4A**). These data suggest that EVs from T1G and T2J exert different effects and these differences may influence the phenotype severity between the genotypes.

EV RNA Cargo Alter mTORC1 Activity in Recipient Cells

We have previously identified that when cells are exposed to EVs from the T2J cell line, the total S6K protein is decreased, while pS6K is increased, making the standard pS6k/S6K ratio change (Bissler et al., 2019). To investigate this further, we again exposed the M1 tubule cell line to EVs from the mIMCD3, T1G, and

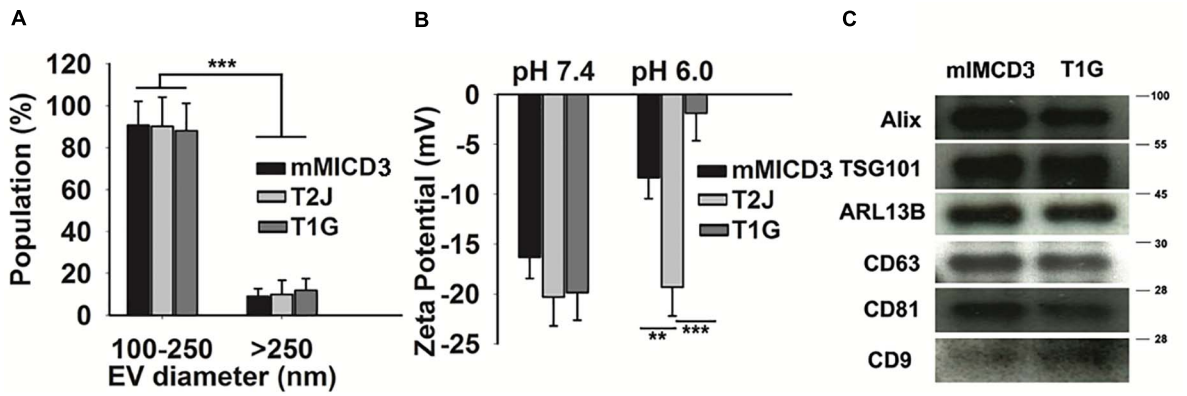

FIGURE 2 | Particle population characteristics, zeta potential, and western blot analysis of cell-derived EVs. **(A)** Categorization of EV populations by size distribution by TRPS. The majority of EVs belong to a size range of 100–250 nm. *t-test* was performed between their counterparts. **(B)** pH affects the zeta potential of EVs: Compared to physiological pH (7.4), cyst microenvironmental pH (6.0) showed a drastic change in the zeta potential (measured by TRPS) of EVs derived from T1G cells. **(C)** Western blot analysis of EVs. Classical EV markers such as Alix, TSG 101, ARL13b, CD63, CD81, and CD9 were present in EVs derived from mIMCD3 and T1G cells. Data ($n = 3$) were represented as mean ± SD. Significant difference analyzed by *t*-test (*$p < 0.05$, **$p < 0.01$, ***$p < 0.001$).

T2J cell lines and again observed the expected increase in the pS6K/S6K ratio for the T2J cell line and noted that the T1G and mIMCD3 lines did not exhibit this increase in pS6K and decrease in S6K that drives the ratio higher (**Figure 4A**). We wanted to see if the target M1 cell transcription had changed to help explain the change in the ratio. We used rtPCR to look at the transcriptional level for S6K protein and found that, in fact, the T2J cell line exhibited a reduced S6K gene expression, which was not observed in cells treated with EVs from the mIMCD3 (**Figure 4B**, $p < 0.01$). We also identified that the T1G cell line exhibited a significant increase in the S6K gene expression (**Figure 4B**), though protein levels are not different from the mIMCD3 cell line and the pS6K/S6K ratio is the same as mIMCD3 (**Figure 4A**).

Because EVs can transduce signals through proteins, mRNA, miRNA, lncRNA, and lipids, we wished to focus on the role of the EV RNA component. To investigate the role of RNA in these effects, we isolated EV RNA from $\sim 5 \times 10^8$ EVs derived from mIMCD3, T1G, and T2J cell lines and used these RNA samples to transfect M1 cells. We used a commercially available scrambled RNA as a control and found that the RNA from the EVs seemed to drive the change in transcription for the *Tsc* mutant cell line. The T1G cell line exhibited an increase while the T2J cell line exhibited a decrease (**Figure 4C**).

Extracellular Vesicle miRNA Targeting S6K Expression

The alterations in *RPS6KB1* gene expression upon transfection of EV isolated RNA derived from *Tsc* mutant T2J cell line EVs implicated an miRNA effect. Based on the changes we identified, we used the extracted total RNA from the EVs for quantitative PCR of the top 3 predicted miRNAs that target *RPS6KB1* mRNA. We identified three candidate miRNAs: miR-212-3p, miR-216b-3p, and miR-7116-5p. These miRNAs were most frequently identified by greater than three prediction tools. We also included a previously validated miRNA, miR-99a-5p, that reduces *RPS6KB1* gene expression (Tsai et al., 2018). miR-99a-5p and miR-212-3p expression levels were lower ($p < 0.01$) in EVs shed by T2J cells, but T1G-EVs induced a significantly higher expression of both miRNAs (**Figure 4C**). We failed to detect the expression of miR-216b-3p and miR-7116-5p in EVs.

DISCUSSION

Patients with *TSC2* mutations often have more severe disease manifestations than patients with *TSC1* mutations. Compared with *TSC1* deletion, *TSC2* deletion is linked to not only greater disease severity but also earlier symptom development (Kothare et al., 2014). Despite the significant progress in the understanding of TSC, a substantial gap in knowledge remains regarding why the disease severity is different depending on the locus involved. We previously reported that loss of the *Tsc2* gene resulted in renal cystic disease via a novel EV-mediated pathway (Bissler et al., 2019), and the mutant cells produced more EVs with an altered proteome (Zadjali et al., 2020). In this study, we hypothesize that the differences in EV characteristics, derived from *TSC1* and *TSC2* knocked out cells, may be dependent on the gene locus and thus affect the disease phenotype.

We isolated EVs from mIMCD3, T1G, and T2J conditioned (without serum, as serum contains an abundance of EVs) media by size-exclusion chromatography. Size-exclusion chromatography (SEC) is an easy-to-use and proven method to isolate EVs from a variety of clinical samples (Lobb et al., 2015). We preferred to use serum-free culture media instead of exosome-depleted media for EV isolation. Our cells (mIMCD3, T1G, and T2J) can tolerate and remain viable up to 48–56 h without serum, as assessed by cell viability MTT assay (data not included). Further, the column chromatography is a well-established and highly reproducible EV isolation method which elutes EVs with maximum purity and high yield (Lobb et al., 2015; Welton et al., 2015). To meet the criteria of the International

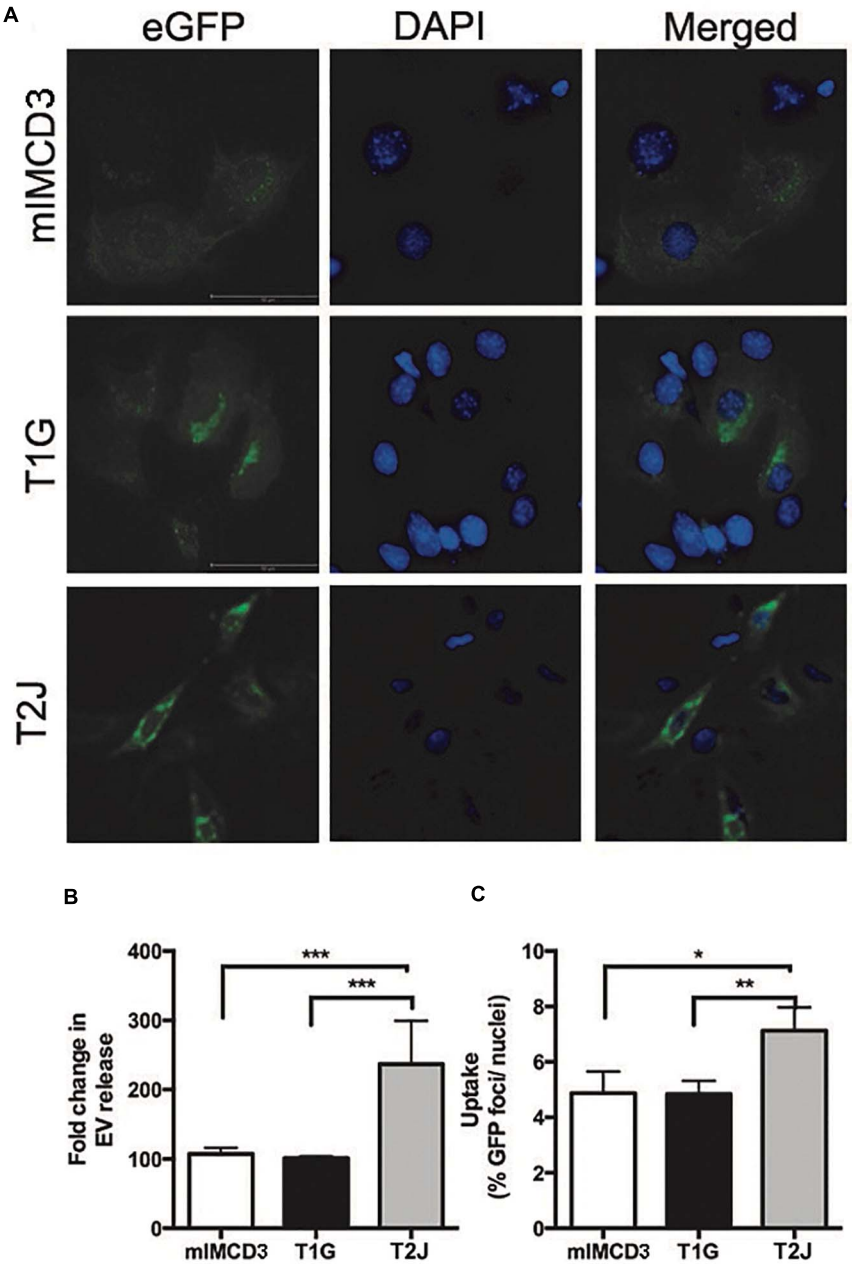

FIGURE 3 | Release and uptake of extracellular vesicles. mIMCD3, T1G, and T2J cells were transfected with green fluorescent protein (eGFP)-tagged CD63, a marker of extracellular vesicles (EVs). **(A)** Immunofluorescence images of eGFP-transfected mIMCD3, T1G, and T2J cells with blue nuclear DAPI stain. **(B)** Fold difference in release in reference to mIMCD3 EV-release ($n = 4$) and **(C)** uptake of EVs from mIMCD3 (reference), T1G, and T2J cells. Cells were transfected with eGFP-CD63 plasmid. After 48 h, transfection media were collected, and cells were lysed. Mean fluorescence intensities (MFIs) normalized to protein content were quantified in cell media (to measure EV release). For uptake of GFP-positive EVs by intercalated M1 cell - EVs isolated from the culture media of mIMCD3, T1G, and T2J cells were used to treat M1 cells at a dose of 50 million EVs/ml in a microscopic slide chamber for 24 h. Slides were imaged, and the number of GFP positive foci was counted and normalized to the number of DAPI-positive nuclei. Mean ± SD data of total of 15–20 images were analyzed from two experiments. Student's *t*-test was performed (*$p < 0.05$, **$p < 0.01$, ***$p < 0.001$).

Society for Extracellular Vesicles (ISEV), we characterized the EVs according to the standard guidelines (Théry et al., 2018). We further characterized EVs for their concentration and size distribution using TRPS and DLS. Although TRPS and DLS work on significantly different principles, both provided a similar size distribution, i.e., 123.5 ± 5.7 nm, 131.5 ± 8.3 nm, and 127.3 ± 4.9 nm, for mIMCD3-EVs, T1G-EVs, and T2J-EVs, respectively (**Figures 1B,C**).

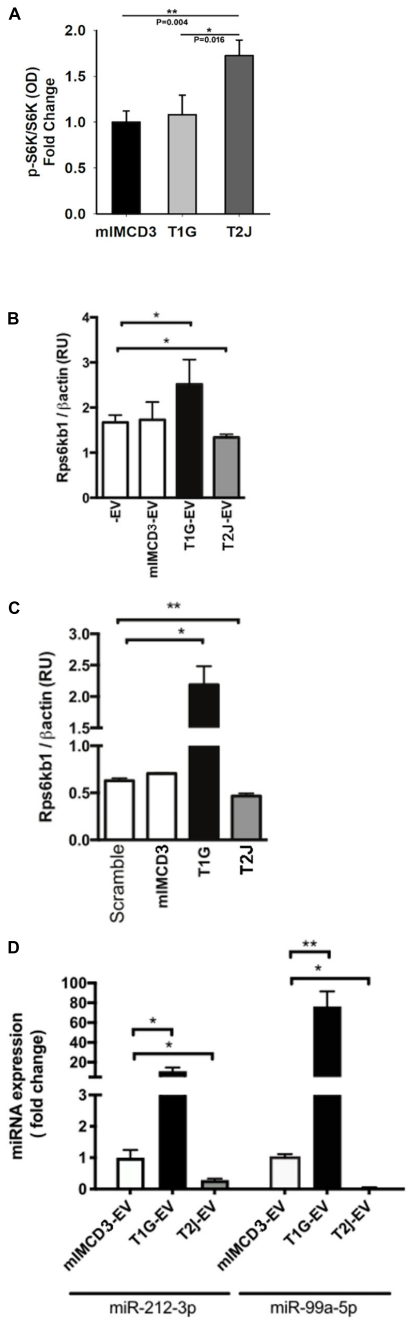

FIGURE 4 | Cellular effects of EVs from *Tsc1*- or *Tsc2*-deleted cells on recipient cells. **(A)** Effect of EV treatment on mTORC1 signaling on the pS6K/S6K ratio. All values normalized to mIMCD3 and reported as fold change. **(B)** Effect of EV treatment on S6K mRNA (*Rps6kb1*) expression normalized to the expression of β-Actin. -EV means no EVs, and the cell type that produced the EVs is indicated. **(C)** Effect of total RNA (isolated from EVs) transfection on S6K mRNA expression. RNA extracted from mIMCD3, T1G, and T2J-EVs was transfected into serum-starved M1 cells. For the control, scrambled RNA was used ($n = 3$). S6K (*Rps6kb1*) gene expression was normalized to β-actin expression (RU: relative expression unit). **(D)** miRNA expression in mIMCD3, T1G, and T2J cells. Gene expression was normalized to the global mean of three loading controls. All experiments were performed in triplicate ($n = 3$), and statistical analysis was performed using one-way ANOVA followed by Tukey's test (*$p < 0.05$, **$p < 0.01$).

The zeta potential of mIMCD3- and T1G-derived EVs at physiological pH (pH 7.4) was -16.3 ± 2.1 mV and -19.8 ± 2.7 mV, respectively. We observed a drastic drop in the zeta potential of T1G-EVs at cystic pH (pH 6.0) and interestingly no change in the zeta potential of T2J-EVs. Microenvironmental pH plays a very important role in EV trafficking. Generally, low pH facilitates EV release and uptake as described in melanoma cells (Parolini et al., 2009). The drop in zeta potential and pH could lead to a physical interaction between the vesicles: exosome–exosome interaction ("mitosis like" phenotype) (Beit-Yannai et al., 2018). These types of interactions are selective and might have an inhibitory effect on incoming signals, which could influence the EV-mediated signal modulation in various biological processes such as homeostasis and cancer metastasis (Beit-Yannai et al., 2018). Apart from physical characterization of EVs by TRPS, DLS, and TEM, western blot was performed to confirm the expression of EV-associated protein markers. As per the ISEV guidelines, EVs must be characterized for the presence of at least one transmembrane protein (CD63, CD81, or CD9) and one cytosolic protein (Alix or TSG101).

EVs can influence disease manifestation by regulating multiple signaling pathways. We found that EVs regulated mTORC1, and this pathway is known to regulate downstream Wnt/β-catenin and autophagy signaling pathways. We recently reported a cell non-autonomous involvement of mTORC1 in *Tsc* renal manifestation (Bissler et al., 2019; Barone et al., 2021). mTORC1 promotes the phosphorylation of an array of downstream effectors such as S6K, ULK1, TFEB, and 4EBP1, which further regulate various cellular processes such as cell proliferation, nucleotide synthesis, autophagy, and other growth-related signaling pathways (Zadjali et al., 2020). Furthermore, mTORC1 signaling cell autonomously suppresses Wnt/β-catenin signaling by promoting Dishevelled–clathrin AP-2 adaptor interaction and enhancing Dishevelled-mediated frizzled internalization (Zeng et al., 2018). In fact, the TSC1/TSC2 (hamartin/tuberin) complex can be associated with GSK3β and Axin and can therefore regulate the β-catenin degradation complex (Mak, 2003). In addition, autophagy plays a very crucial role in the development and homeostasis of normal tubular epithelial cells. Autophagy dysregulation is associated with renal manifestations including diabetic nephropathy, polycystic kidney diseases, acute kidney injury, and obstructive nephropathy (Huber et al., 2012; Kume et al., 2012). We posit that *Tsc*-mutant renal epithelial cells suppress autophagy and this feature may be involved in proliferation into cysts.

miRNA plays an important role in the development and progression of different types of cancer as well as in TSC (Volinia et al., 2006; Bagla et al., 2018). Identifying the responsible miRNA in TSC could lead to the development of novel biomarkers and therapeutic targets. In our current study, the qRT-PCR data showed the EV-mediated differential expression of miRNA-212-3p and miRNA-99a-5p. Deletion of the *Tsc1* gene leads to dramatically higher levels of miR-212-3p (approximately 20-fold change) compared to the control parental cell line (**Figure 4D**). By contrast, *Tsc2* gene deletion triggered the down regulation of miR-212-3p. Increased levels of miR-212-3p negatively regulate hepatocellular carcinoma by suppressing the connective tissue

growth factor (Chen et al., 2019). miRNA-212 suppresses the X-linked inhibitor of apoptosis protein that constrains renal cancer invasion and proliferation, raising questions about a possible role in TSC-associated lymphangioleiomyomatosis. Furthermore, a low level of miR-212 is highly linked to T-stage and TNM-stage of renal cell carcinoma (Gu et al., 2017), which is related to cellular stress (Potter et al., 2017). In this study, we also identified changes in miRNA-99a-5p, which followed the same trend of expression as miRNA-212-3p. Compared to EVs from control mIMCD3 cells, EVs from *Tsc1* knockout cells facilitated a >80-fold increase in the expression of miRNA-99a-5p, whereas EVs from *Tsc2* knockout cells completely silenced the expression of miRNA-99a-5p. miRNA-99a-5p plays an important role in the pathogenesis of various types of cancer such as ovarian cancer (Yoshimura et al., 2018), oral cancer (Shi et al., 2017), and bladder cancer (Tsai et al., 2018). Downregulation of miRNA-99a-5p may contribute to the more severe disease phenotype in *TSC2*-associated disease than in *TSC1*-associated disease. For example, in bladder cancer tissue, overexpression of miR-99a-5p triggered the dual inhibition of the mTORC1 and mTORC2 signaling axis by the PI3K/AKT pathway (Tsai et al., 2018). Perhaps this activity may be leveraged to develop a combination therapy by combining miRNA-99a-5p and the mTOR inhibitor TSC in other cancers (Trelinska et al., 2016).

In conclusion, we demonstrate that EVs released from T1G and T2J cells possess different physical characteristics as well as different release and uptake rates. These differences in EV characteristics are due to the deletion of the *Tsc1* or *Tsc2* gene, and these differences may contribute to the differences in locus-associated disease severity. We demonstrate that the EVs from these isogenic cell lines except for their *Tsc* gene were responsible for the differential expression of the miR-212-3p/mTORC1 and mIR-99a-5p/mTORC1 axis and regulated S6K expression differently. These differences may impact TSC-associated cell proliferation. Our findings suggest that miRNA-212-3p and miRNA-99a-5p may be potential biomarkers and possible therapeutic targets for TSC disease.

DATA AVAILABILITY STATEMENT

The raw data supporting the conclusions of this article will be made available by the authors, without undue reservation.

AUTHOR CONTRIBUTIONS

FZ, JB, PK, and YY: conceptualization, methodology, investigation, and data curation. BS and JB: resources. AA, FZ, JB, KG, PK, and YY: writing—original draft preparation. AA, FZ, JB, KG, and PK: writing—review and editing. JB: supervision and funding acquisition. All authors contributed to the article and approved the submitted version.

FUNDING

This work was supported by DoD grant W81XWH-14-1-0343 (JB), Federal Express Chair of Excellence (JB), and Children's Foundation Research Institute (JB).

REFERENCES

Aronow, M. E., Nakagawa, J. A., Gupta, A., Traboulsi, E. I., and Singh, A. D. (2012). Tuberous sclerosis complex: genotype/phenotype correlation of retinal findings. *Ophthalmology* 119, 1917–1923. doi: 10.1016/j.ophtha.2012.03.020

Au, K. S., Hebert, A. A., Roach, E. S., and Northrup, H. (1999). Complete inactivation of the TSC2 gene leads to formation of hamartomas. *Am. J. Hum. Genet.* 65, 1790–1795. doi: 10.1086/302648

Bagla, S., Cukovic, D., Asano, E., Sood, S., Luat, A., Chugani, H. T., et al. (2018). A distinct microRNA expression profile is associated with α[11C]-methyl-L-tryptophan (AMT) PET uptake in epileptogenic cortical tubers resected from patients with tuberous sclerosis complex. *Neurobiol. Dis.* 109, 76–87. doi: 10.1016/j.nbd.2017.10.004

Barone, S., Zahedi, K., Brooks, M., Henske, E. P., Yang, Y., Zhang, E., et al. (2021). Kidney intercalated cells and the transcription factor FOXi1 drive cystogenesis in tuberous sclerosis complex. *Proc. Natl. Acad. Sci. U. S. A.* 118:e2020190118. doi: 10.1073/pnas.2020190118

Baybis, M., Yu, J., Lee, A., Golden, J. A., and Weiner, H. (2004). McKhann 2nd G, et al. mTOR cascade activation distinguishes tubers from focal cortical dysplasia. *Ann. Neurol.* 56, 478–487. doi: 10.1002/ana.20211

Beit-Yannai, E., Tabak, S., and Stamer, W. D. (2018). Physical exosome:exosome interactions. *J. Cell Mol. Med.* 22, 2001–2006.

Bissler, J. J., Zadjali, F., Bridges, D., Astrinidis, A., Barone, S., Yao, Y., et al. (2019). Tuberous sclerosis complex exhibits a new renal cystogenic mechanism. *Physiol. Rep.* 7:e13983. doi: 10.14814/phy2.13983

Bonsib, S. M., Boils, C., Gokden, N., Grignon, D., Gu, X., Higgins, J. P. T., et al. (2016). Tuberous sclerosis complex: hamartin and tuberin expression in renal cysts and its discordant expression in renal neoplasms. *Pathol. Res. Pract.* 212, 972–979. doi: 10.1016/j.prp.2016.04.005

Chen, J. Q., Ou, Y. l, Huang, Z. P., Hong, Y. G., Tao, Y. P., and Wang, Z. G. (2019). MicroRNA-212-3p inhibits the Proliferation and Invasion of Human Hepatocellular Carcinoma Cells by Suppressing CTGF expression. *Sci. Rep.* 9, 1–10. doi: 10.3892/ol.2020.11956

Crino, P. B., Aronica, E., Baltuch, G., and Nathanson, K. L. (2010). Biallelic TSC gene inactivation in tuberous sclerosis complex. *Neurology* 74, 1716–1723. doi: 10.1212/wnl.0b013e3181e04325

Dabora, S. L., Jozwiak, S., Franz, D. N., Roberts, P. S., Nieto, A., Chung, J., et al. (2001). Mutational analysis in a cohort of 224 tuberous sclerosis patients indicates increased severity of TSC2, compared with TSC1, disease in multiple organs. *Am. J. Hum. Genet.* 68, 64–80. doi: 10.1086/316951

Eguchi, T., Sogawa, C., Ono, K., Matsumoto, M., Tran, M. T., Okusha, Y., et al. (2020). Cell Stress Induced Stressome Release Including Damaged Membrane Vesicles and Extracellular HSP90 by Prostate Cancer Cells. *Cells* 9:755. doi: 10.3390/cells9030755

Gu, C., Wang, Z., Jin, Z., Li, G., Kou, Y., Jia, Z., et al. (2017). MicroRNA-212 inhibits the proliferation, migration and invasion of renal cell carcinoma by targeting X-linked inhibitor of apoptosis protein (XIAP). *Oncotarget* 8, 92119–92133. doi: 10.18632/oncotarget.20786

Huber, T. B., Edelstein, C. L., Hartleben, B., Inoki, K., Jiang, M., Koya, D., et al. (2012). Emerging role of autophagy in kidney function, diseases and aging. *Autophagy* 8, 1009–1031. doi: 10.4161/auto.19821

Jozwiak, J., and Jozwiak, S. (2007). Giant cells: contradiction to two-hit model of tuber formation? *Cell Mol. Neurobiol.* 27, 251–261. doi: 10.1007/s10571-006-9106-0

Kobayashi, T., Minowa, O., Sugitani, Y., Takai, S., Mitani, H., Kobayashi, E., et al. (2001). A germ-line Tsc1 mutation causes tumor development and embryonic lethality that are similar, but not identical to, those caused by Tsc2 mutation in mice. *Proc. Natl. Acad. Sci. U. S. A.* 98, 8762–8767. doi: 10.1073/pnas.151033798

Kothare, S. V., Singh, K., Chalifoux, J. R., Staley, B. A., Weiner, H. L., Menzer, K., et al. (2014). Severity of manifestations in tuberous sclerosis complex in relation to genotype. *Epilepsia* 55, 1025–1029. doi: 10.1111/epi.12680

Kume, S., Thomas, M. C., and Koya, D. (2012). Nutrient sensing, autophagy, and diabetic nephropathy. *Diabetes* 61, 23–29. doi: 10.2337/db11-0555

Lobb, R. J., Becker, M., Wen, S. W., Wong, C. S. F., Wiegmans, A. P., Leimgruber, A., et al. (2015). Optimized exosome isolation protocol for cell culture supernatant and human plasma. *J. Extracell. Vesicles* 4:27031. doi: 10.3402/jev.v4.27031

Magri, L., Cominelli, M., Cambiaghi, M., Cursi, M., Leocani, L., Minicucci, F., et al. (2013). Timing of mTOR activation affects tuberous sclerosis complex neuropathology in mouse models. *DMM Dis. Model Mech.* 6, 1185–1197. doi: 10.1242/dmm.012096

Mak, B. C. (2003). The Tuberin-Hamartin Complex Negatively Regulates beta - Catenin Signaling Activity. *J. Biol. Chem.* 278, 5947–5951. doi: 10.1074/jbc.C200473200

Napolioni, V., and Curatolo, P. (2008). Genetics and molecular biology of tuberous sclerosis complex. *Curr. Genomics.* 9, 475–487. doi: 10.2174/138920208786241243

Nathan, N., Keppler-Noreuil, K. M., Biesecker, L. G., Moss, J., and Darling, T. N. (2017). Mosaic Disorders of the PI3K/PTEN/AKT/TSC/mTORC1 Signaling Pathway. *Dermatol. Clin.* 35, 51–60. doi: 10.1016/j.det.2016.07.001

Niida, Y., Stemmer-Rachamimov, A. O., Logrip, M., Tapon, D., Perez, R., Kwiatkowski, D. J., et al. (2001). Survey of somatic mutations in tuberous sclerosis complex (TSC) hamartomas suggests different genetic mechanisms for pathogenesis of TSC lesions. *Am. J. Hum. Genet.* 69, 493–503. doi: 10.1086/321972

Onda, H., Lueck, A., Marks, P. W., Warren, H. B., and Kwiatkowski, D. J. (1999). Tsc2(+/-) mice develop tumors in multiple sites that express gelsolin and are influenced by genetic background. *J. Clin. Invest.* 104, 687–695. doi: 10.1172/jci7319

Oosthuyzen, W., Scullion, K. M., Ivy, J. R., Morrison, E. E., Hunter, R. W., Lewis, P. J. S., et al. (2016). Vasopressin regulates extracellular vesicle uptake by kidney collecting duct cells. *J. Am. Soc. Nephrol.* 27, 3345–3355. doi: 10.1681/asn.2015050568

Parolini, I., Federici, C., Raggi, C., Lugini, L., Palleschi, S., De Milito, A., et al. (2009). Microenvironmental pH is a key factor for exosome traffic in tumor cells. *J. Biol. Chem.* 284, 34211–34222. doi: 10.1074/jbc.m109.041152

Patel, B., Patel, J., Cho, J.-H., Manne, S., Bonala, S., Henske, E., et al. (2015). Exosomes mediate the acquisition of the disease phenotypes by cells with normal genome in tuberous sclerosis complex. *Oncogene* 35, 1–10.

Potter, S. L., Venkatramani, R., Wenderfer, S., Graham, B. H., Vasudevan, S. A., Sher, A., et al. (2017). Renal cell carcinoma harboring somatic TSC2 mutations in a child with methylmalonic acidemia. *Pediatr. Blood Cancer* 64, 1–4.

Ramesh, V. (2003). Aspects of tuberous sclerosis complex (TSC) protein function in the brain. *Biochem. Soc. Trans.* 31, 579–583. doi: 10.1042/bst0310579

Razaviyan, J., Hadavi, R., Tavakoli, R., Kamani, F., Paknejad, M., and Mohammadi-Yeganeh, S. (2018). Expression of miRNAs Targeting mTOR and S6K1 Genes of mTOR Signaling Pathway Including miR-96, miR-557, and miR-3182 in Triple-Negative Breast Cancer. *Appl. Biochem. Biotechnol.* 186, 1074–1089. doi: 10.1007/s12010-018-2773-8

Sancak, O., Nellist, M., Goedbloed, M., Elfferich, P., Wouters, C., Maat-Kievit, A., et al. (2005). Mutational analysis of the TSC1 and TSC2 genes in a diagnostic setting: genotype – phenotype correlations and comparison of diagnostic DNA techniques in Tuberous Sclerosis Complex. *Eur. J. Hum. Genet.* 13, 731–741. doi: 10.1038/sj.ejhg.5201402

Shi, Y., Bo, Z., Pang, G., Qu, X., Bao, W., Yang, L., et al. (2017). MiR-99a-5p regulates proliferation, migration and invasion abilities of human oral carcinoma cells by targeting NOX4. *Neoplasma* 64, 666–673. doi: 10.4149/neo_2017_503

Street, J. M., Birkhoff, W., Menzies, R. I., Webb, D. J., Bailey, M. A., and Dear, J. W. (2011). Exosomal transmission of functional aquaporin 2 in kidney cortical collecting duct cells. *J. Physiol.* 589, 6119–6127. doi: 10.1113/jphysiol.2011.220277

Théry, C., Witwer, K. W., Aikawa, E., Alcaraz, M. J., Anderson, J. D., Andriantsitohaina, R., et al. (2018). Minimal information for studies of extracellular vesicles 2018 (MISEV2018): a position statement of the International Society for Extracellular Vesicles and update of the MISEV2014 guidelines. *J. Extracell. Vesicles* 7:1535750. doi: 10.1080/20013078.2018.1535750

Trelinska, J., Fendler, W., Dachowska, I., Kotulska, K., Jozwiak, S., Antosik, K., et al. (2016). Abnormal serum microRNA profiles in tuberous sclerosis are normalized during treatment with everolimus: possible clinical implications. *Orphanet J. Rare Dis.* 11, 1–7. doi: 10.1186/s13023-016-0512-1

Tsai, T. F., Lin, J. F., Chou, K. Y., Lin, Y. C., Chen, H. E., and Hwang, T. I. S. (2018). miR-99a-5p acts as tumor suppressor via targeting to mTOR and enhances RARAD001-induced apoptosis in human urinary bladder urothelial carcinoma cells. *Onco Targets Ther.* 11, 239–252. doi: 10.2147/ott.s114276

van Rooijen, E., van de Hoek, G., Logister, I., Ajzenberg, H., Knoers, N. V. A. M., van Eeden, F., et al. (2018). The von Hippel-Lindau Gene Is Required to Maintain Renal Proximal Tubule and Glomerulus Integrity in Zebrafish Larvae. *Nephron* 138, 310–323. doi: 10.1159/000484096

Vogel, P., Read, R., Hansen, G. M., Freay, L. C., Zambrowicz, B. P., and Sands, A. T. (2010). Situs inversus in Dpcd/Poll-/-, Nme7-/-, and Pkd1l1-/- mice. *Vet. Pathol.* 47, 120–131. doi: 10.1177/0300985809353553

Volinia, S., Calin, G. A., Liu, C.-G., Ambs, S., Cimmino, A., Petrocca, F., et al. (2006). A microRNA expression signature of human solid tumors defines cancer gene targets. *Proc. Natl. Acad. Sci. U. S. A.* 103, 2257–2261. doi: 10.1073/pnas.0510565103

Welton, J. L., Webber, J. P., Botos, L. A., Jones, M., and Clayton, A. (2015). Ready-made chromatography columns for extracellular vesicle isolation from plasma. *J. Extracell. Vesicles* 4, 1–9.

Wilson, C., Bonnet, C., Guy, C., Idziaszczyk, S., Colley, J., Humphreys, V., et al. (2006). Tsc1 haploinsufficiency without mammalian target of rapamycin activation is sufficient for renal cyst formation in Tsc1+/- mice. *Cancer Res.* 66, 7934–7938. doi: 10.1158/0008-5472.can-06-1740

Yoshimura, A., Sawada, K., Nakamura, K., Kinose, Y., Nakatsuka, E., Kobayashi, M., et al. (2018). Exosomal miR-99a-5p is elevated in sera of ovarian cancer patients and promotes cancer cell invasion by increasing fibronectin and vitronectin expression in neighboring peritoneal mesothelial cells. *BMC Cancer* 18:1065.

Zadjali, F., Kumar, P., Yao, Y., Johnson, D., Astrinidis, A., Vogel, P., et al. (2020). Tuberous Sclerosis Complex Axis Controls Renal Extracellular Vesicle Production and Protein Content. *Int. J. Mol. Sci.* 21, 1729–1744. doi: 10.3390/ijms21051729

Zeng, H., Lu, B., Zamponi, R., Yang, Z., Wetzel, K., Loureiro, J., et al. (2018). mTORC1 signaling suppresses Wnt/β-catenin signaling through DVL-dependent regulation of Wnt receptor FZD level. *Proc. Natl. Acad. Sci. U. S. A.* 115, E10362–E10369. doi: 10.1073/pnas.1808575115

Zeng, L. H., Rensing, N. R., Zhang, B., Gutmann, D. H., Gambello, M. J., and Wong, M. (2011). Tsc2 gene inactivation causes a more severe epilepsy phenotype than Tsc1 inactivation in a mouse model of Tuberous Sclerosis Complex. *Hum. Mol. Genet.* 20, 445–454. doi: 10.1093/hmg/ddq491

Conflict of Interest: The authors declare that the research was conducted in the absence of any commercial or financial relationships that could be construed as a potential conflict of interest.

frontiers in Physiology

ORIGINAL RESEARCH
published: 17 September 2021
doi: 10.3389/fphys.2021.680544

A-Lipoic Acid Alleviates Folic Acid-Induced Renal Damage Through Inhibition of Ferroptosis

*Xue Li[1,2], Yu Zou[1], Yuan-Yuan Fu[1], Jia Xing[1], Kai-Yue Wang[1], Peng-Zhi Wan[3] and Xiao-Yue Zhai[1,4]**

[1]Department of Histology and Embryology, Basic Medical College, China Medical University, Shenyang, China, [2]Department of Nephrology, Shengjing Hospital of China Medical University, Shenyang, China, [3]Department of Nephrology, First Affiliated Hospital of China Medical University, Shenyang, China, [4]Institute of Nephropathology, China Medical University, Shenyang, China

OPEN ACCESS

Edited by:
Karina Thieme,
University of São Paulo, Brazil

Reviewed by:
Nilberto Robson Falcão Nascimento,
State University of Ceará, Brazil
Erika E. Nishi,
Universidade Federal de São Paulo, Brazil

***Correspondence:**
Xiao-Yue Zhai
xyzhai@cmu.edu.cn

Specialty section:
This article was submitted to Renal and Epithelial Physiology, a section of the journal Frontiers in Physiology

Received: 14 March 2021
Accepted: 20 August 2021
Published: 17 September 2021

Citation:
Li X, Zou Y, Fu Y-Y, Xing J, Wang K-Y, Wan P-Z and Zhai X-Y (2021) A-Lipoic Acid Alleviates Folic Acid-Induced Renal Damage Through Inhibition of Ferroptosis. Front. Physiol. 12:680544. doi: 10.3389/fphys.2021.680544

Folic acid (FA)-induced acute kidney injury (AKI) is characterized by the disturbance of redox homeostasis, resulting in massive tubular necrosis and inflammation. A-lipoic acid (LA), as an antioxidant, has been reported to play an important role in renal protection, but the underlying mechanism remains poorly explored. The aim of this study is to investigate the protective effect of LA on FA-induced renal damage. Our findings showed that LA could ameliorate renal dysfunction and histopathologic damage induced by FA overdose injection. Moreover, FA injection induced severe inflammation, indicated by increased release of pro-inflammatory cytokines tumor necrosis factor (TNF)-α and IL-1β, as well as infiltration of macrophage, which can be alleviated by LA supplementation. In addition, LA not only reduced the cellular iron overload by upregulating the expressions of Ferritin and ferroportin (FPN), but also mitigated reactive oxygen species (ROS) accumulation and lipid peroxidation by increasing the levels of antioxidant glutathione (GSH) and glutathione peroxidase-4 (GPX4). More importantly, we found that LA supplementation could reduce the number of Terminal deoxynucleotidyl transferase dUTP nick end labeling (TUNEL)-positive tubular cells caused by FA, indicating that the tubular cell death mediated by ferroptosis may be inhibited. Further study demonstrated that LA supplementation could reverse the decreased expression of cystine/glutamate antiporter xCT (SLC7A11), which mediated GSH synthesis. What is more, mechanistic study indicated that p53 activation was involved in the inhibitory effect of SLC7A11 induced by FA administration, which could be suppressed by LA supplementation. Taken together, our findings indicated that LA played the protective effect on FA-induced renal damage mainly by inhibiting ferroptosis.

Keywords: A-lipoic acid, ferroptosis, p53, folic acid, renal damage

INTRODUCTION

Acute Kidney Injury (AKI) is referred as a transient decline of renal function, which confers the severe clinical syndrome associated with high mortality (Bellomo et al., 2012). It has been reported that AKI affected more than 13.3 million patients with about 1.7 million deaths around the world each year, and the mortality was AKI stage-dependent (Brown et al., 2016). The in-hospital mortality was 5.1% for patients with stage 1 AKI, 13.7% for patients with stage 2 AKI, and 24.8% for patients with stage 3 AKI (Pinheiro et al., 2019). In addition, studies have shown that the 30- and 90-day mortality of the patients with AKI in ICU was much higher than that of the patients without AKI (Santos et al., 2019). Moreover, it has been estimated that nearly 2 million AKI patients each year cannot fully recover and have a high risk of progressing to chronic kidney disease (CKD; de Seigneux and Martin, 2017).

It is well-known that AKI can arise in various pathological conditions, such as drugs, toxicants, ischemia/reperfusion (I/R), obstruction, or sepsis, resulting in acute tubular necrosis (Ronco et al., 2019). Despite unpredictable in most cases, the occurrence of AKI is significantly higher in severe I/R injury after kidney transplant surgery, cisplatin for tumor chemotherapy, or contrast media for radiography and so on, especially for the susceptible individuals, including old age and patients with diabetes mellitus or CKD (Zhang et al., 2020). This highlighted the urgent need for novel therapeutic approaches that aims at preventing and/or reversing its sequelae (Zhao et al., 2018). Folic acid (FA)-induced AKI is one of the typical models simulating drug or toxicant-induced tubular injury, which is closely related to crystal formation in the tubule lumen and cellular oxidative stress, leading to massive inflammatory reaction and eventually tubular cell death (Martin-Sanchez et al., 2018).

Ferroptosis is a recently described form of programmed cell death caused by uncontrolled iron dependent lipid peroxidation that distinguishes it from traditional modalities of regulated cell death including apoptosis, necrosis, and autophagy (Li et al., 2020a). Moreover, ferroptosis is a critical pathophysiological event in FA-induced AKI, characterized by the imbalance of redox homeostasis and lethal lipid-based reactive oxygen species (ROS) generation (Martin-Sanchez et al., 2017). Normally, iron is indispensable for many physiological functions in organisms and can be stored in Ferritin, including Ferritin heavy chain (FTH) and Ferritin light chain (FTL; Hu et al., 2019). FTH, a ferroxidase enzyme, can convert Fe^{2+} to the ferric form (Fe^{3+}) that sequesters free iron (Mumbauer et al., 2019). While under pathological conditions, oxygen reacts with excess labile iron and generates ROS that attacks lipid membrane, implicated in lipid peroxidation (Han et al., 2020). It has been demonstrated that proximal tubule cells expressing FTH could store iron and effectively limit free iron-mediated toxicity (Swaminathan, 2018). In contrast, the specific FTH gene knockout of the mouse proximal tubules could exacerbate renal damage in rhabdomyolysis or cisplatin-induced AKI (Zarjou et al., 2013). Moreover, iron overload could be alleviated by the only known iron exporter, ferroportin (FPN) that promotes iron transport out of cells and inhibits the production of ROS (Geng et al., 2018).

Additionally, the accumulation of lipid ROS is triggered when the endogenous antioxidant status is compromised. Glutathione (GSH) is an important antioxidant that protects against ferroptosis and it can be synthesized *via* cystine uptake mediated by cystine/glutamate antiporter xCT (Lim et al., 2019). Studies have shown that system xCT was mainly located in tubular cells, and its inhibition resulted in a rapid decline in GSH levels, which may accelerate AKI (Su et al., 2019). Inhibition of xCT by Class 1 ferroptosis inducers, such as erastin, may induce ferroptotic cell death mainly by depletion of cellular GSH content, and subsequently lead to inactivation of glutathione peroxidase-4 (GPX4; Yu et al., 2017). GPX4 is an essential lipid hydro-peroxide detoxifying enzyme, which can be directly inhibited by Class 2 ferroptosis inducers without affecting intracellular GSH. The inactivation of GPX4 in the proximal tubules could cause ferroptosis and further induce AKI (Yang et al., 2014). Apart from the features of ferroptosis mentioned above, TUNEL assay was often used to evaluate ferroptotic cells, labeling cells with DNA breakage (Cao et al., 2020).

P53, a tumor suppressor protein, is a critical regulator in various cell biological processes, mainly including cell cycle arrest and apoptosis, which is closely associated with AKI progression (Tang et al., 2019). P53 can also be induced in the oxidative stress response, sensitizing cells to ferroptosis *via* inhibiting system xCT (Zhang et al., 2018).

Lipoic acid (LA), a well-known antioxidant, has been reported to exert the protective effect on I/R-induced AKI by scavenging ROS (Bae et al., 2009). In addition, LA could alleviate oxidative damage to DNA through downregulation of p53 in Parkinson's diseases (Chang et al., 2012). Moreover, LA was proved to chelate excess iron ions, thereby decreasing the risk of Alzheimer's disease (Zhang et al., 2018). So far, we have known that the inhibition of oxidative stress is beneficial for alleviating FA-induced AKI, but the role of LA in this pathological process remains largely unknown. Therefore, the present study aimed to examine the effects of LA on FA-induced AKI and the underlying regulatory mechanisms. We observed that LA could prevent from FA-induced renal damage mainly by reducing ferroptosis.

MATERIALS AND METHODS

Animals

The animal experiments were performed in accordance to the NIH Criteria for the Use of Laboratory Animals, and this study was approved by the ethics committee of the China Medical University Institutional Animal Care and Use Committee (protocol no. 2011037). C57BL/6J mice (male, 6–8 week-old) were acquired from China Medical University (Liaoning, China). The animals were kept in housing facility at the temperature of 22°C with a 12-12 h light–dark cycle. Mice were allocated into four groups randomly ($n = 6$ per group): Control group, FA (250 mg/kg at the concentration of 12.5 mg/ml, dissolved in 300 mM sodium bicarbonate) group, FA + LA-L (50 mg/kg,

dissolved in saline) group, and FA + LA-H (100 mg/kg, dissolved in saline) group. Animals of the FA group were intraperitoneally injected with FA once. Animals of the treatment groups received oral medications of LA 24 h before FA injection and continued afterward for 2 days. On the second day after FA injection, samples of kidney specimens and blood were harvested for further examination. The mice were housed in the metabolic cage in the last 24 h, allowing quantitative urine collection.

Reagents and Antibodies

Folic acid and LA were provided by Dalian Meilun Biotechnology Co. (Dalian, China). Antibodies to F4/80, IL-1β, and p53 were obtained from CST (Danvers, United States). Antibodies to kidney injury molecule KIM-1, 4-HNE 4-hydroxynonenal, GPX4, xCT, Ferritin, FPN, and β-actin were purchased from Abcam (Cambridge, United States). Antibodies to TNF-α was obtained from Proteintech (Wuhan, China).

Assays for Renal Function, ROS, GSH, and Iron

Blood Urea Nitrogen (BUN) and creatinine were measured following manufacturer's instructions (Jian Cheng, Nanjing, China). ROS levels in kidney tissues were measured by DCFH-DA test kit. In brief, tissue homogenates were diluted 1:20 in cold buffer to obtain a concentration of 5 mg tissue/ml. The reaction mixture containing the homogenate and DCFH-DA (5 mmol/L) was incubated for 15 min at room temperature. After 30 min of further incubation, the conversion of DCFH-DA to the fluorescent product DCF was measured by a confocal laser scanning microscope with excitation at 488 nm and an emission at 525 nm to determine the concentration of ROS in the samples. Then ROS formation was quantified. Urinary sodium and potassium levels were determined using Quantichrom Assay Kits (BioAssay Sytems) and then fractional excretion of sodium (FENa) and fractional excretion of potassium (FEK) were calculated using the corresponding formulas (Ashour et al., 2016). Urinary osmolality were measured by the 5,004 Micro-Osmette (Precision Systems). Kidneys were homogenized to measure the levels of ROS (Solarbio, Beijing, China), GSH (Solarbio, Beijing, China), and iron content (Jian Cheng, Nanjing, China) according to manufacturer's instructions.

TUNEL Assay

To assess tubular cell death, TUNEL assay was used on kidney section embedded in paraffin according to the product's protocols (Roche, Basel, Switzerland).

Renal Histopathology

The paraffin-embedded kidneys were cut in 3-μm-thick slices for hematoxylin and eosin (H&E) and Periodic acid-Schiff (PAS) staining to evaluate the histopathologic injury. Furthermore, H&E-stained slices were used to assess acute tubular injury in a blinded way, including tubular epithelial vacuolization, dilation of tubular lumen, brush border loss, or cast formation. The criteria were based on semi-qualification as follows: (0) none; (1) <20%; (2) <20–50%; (3) <50–70%; and (4) >70% (Brooks et al., 2009).

Prussian Iron Staining

Iron deposits in tubular cells were detected by Prussian iron staining (Abcam, Cambridge, MA, United States), as depicted in the book (American Registry of Pathology, Prophet, Edna B, 1992).

Immunohistochemical Staining

Immunohistochemical (IHC) staining was performed in paraffin-embedded sections of 3-um thickness. The sections were deparaffinized, hydrated, antigen retrieved, and then probed with primary antibodies against KIM-1, IL-1β, TNF-α, F4/80, 4-HNE, GPX4, Ferritin, and p53 at the dilution of 1:200, followed by the incubation with the secondary antibodies for 60 min on the second day. The sections were visualized with diaminobenzidine and counterstained with hematoxylin. Images were viewed using Nikon microscope (90i, Nikon, Tokyo, Japan).

Western Blotting Analysis

Proteins from the whole kidney lysates were separated on a 10% SDS-polyacrylamide gel, transferred onto PVDF membrane, blocked in 5% BSA for 60 min, and then primary antibodies against KIM-1, IL-1β, TNF-α, Ferritin, FPN, xCT, and p53 at the dilution of 1:1,000, as well as 4-HNE, GPX4, and β-actin at the dilution of 1:4,000 were probed at 4°C overnight. On the second day, peroxidase-conjugated secondary antibodies were probed for 60 min at room temperature. The bands were visualized *via* chemiluminescence (ECL) system. Quantitative densitometry was used that the target proteins were analyzed using the Image software 6.0. The expression levels of proteins were normalized to that of β-actin.

Real-Time PCR

Total RNA of kidney tissue was extracted by TRIzol method. The cDNA was synthesized through reverse transcription from RNA with PrimeScript RT reagent kit (Vazyme). Then PCR was performed using the SYBR-Green Master PCR Mix (Vazyme). The sequence of the primers used was as follows:

KIM-1 forward: 5'-ATCCCATCCCATACTCCTACAG-3' and reverse: 5'CGGAAGGCAACCACGCTTA;
p53 forward: 5'-TGCTCACCCTGGCTAAAGTT-3'and reverse: 5'-GTCCATGCAGTGAGGTGATG-3';
β-actin forward: 5'-GGCTGTATTCCCCTCCATCG-3' and reverse: 5'-CCAGTTGGTAATGCCATGT-3'.

The relative gene expression level was assessed using the $2^{-\Delta\Delta Ct}$ method.

Statistical Analysis

The data were presented as means ± SDs. Statistical analysis was performed with the statistical software, SPSS version 21.0. Comparisons were analyzed using one-way ANOVA followed by Bonferroni test. Statistical significance of difference was defined as a value of $p < 0.05$.

RESULTS

LA Supplementation Ameliorated Histopathologic Damage and Renal Dysfunction in FA-Induced AKI

To determine whether LA supplementation could protect against FA-induced renal damage, histological analysis was evaluated with H&E and PAS staining. As observed in H&E staining, FA injection induced severe tubular damage, indicated by detachment of tubular cells, dilation of tubules, swelling of tubular cells, degeneration of epithelial cells, and interstitial inflammatory cells infiltration. In line with this tubular damage, the kidney in the FA group also showed aggravated pathological damage by PAS staining, characterized by necrotic tubular epithelial cells, tubular cast, and ablation of brush. While these tubular damage were alleviated by LA supplementation. Moreover, tubular injuries were assessed by quantification of HE-stained sections and revealed significantly increased tubulointerstitial injury scores in mice injected with FA injection, which were reduced by LA supplementation in a dose-dependent manner, but without statistical significance. In addition, renal function was measured to investigate the protective effect of LA on FA-induced AKI. Consistently, the FA injection induced dramatic increases in serum creatinine and BUN levels, indicating impaired renal function, while these functional parameters associated with AKI were reduced by LA supplementation, indicating the amelioration of renal function. The results above are summarized in **Figure 1**.

In addition, to fully determine the impact of LA on renal dysfunction induced by FA, the direct evaluation of renal function was determined with the indicators as displayed in **Supplementary Table 1**, FA injection markedly decreased urine volume, glomerular filtration rate (GFR), and filtration fraction compared with control mice, but these indexes could be reversed partially by LA supplementation, without obvious difference between the two dose groups. Moreover, the FENa, FEK, and urinary osmolarity were significantly reduced in FA-induced mice, which were remarkably reversed by LA supplementation.

KIM-1, a biomarker of renal tubular damage, was examined by IHC staining. The results showed that the expression of KIM-1 in the tubular cells was upregulated after FA injection,

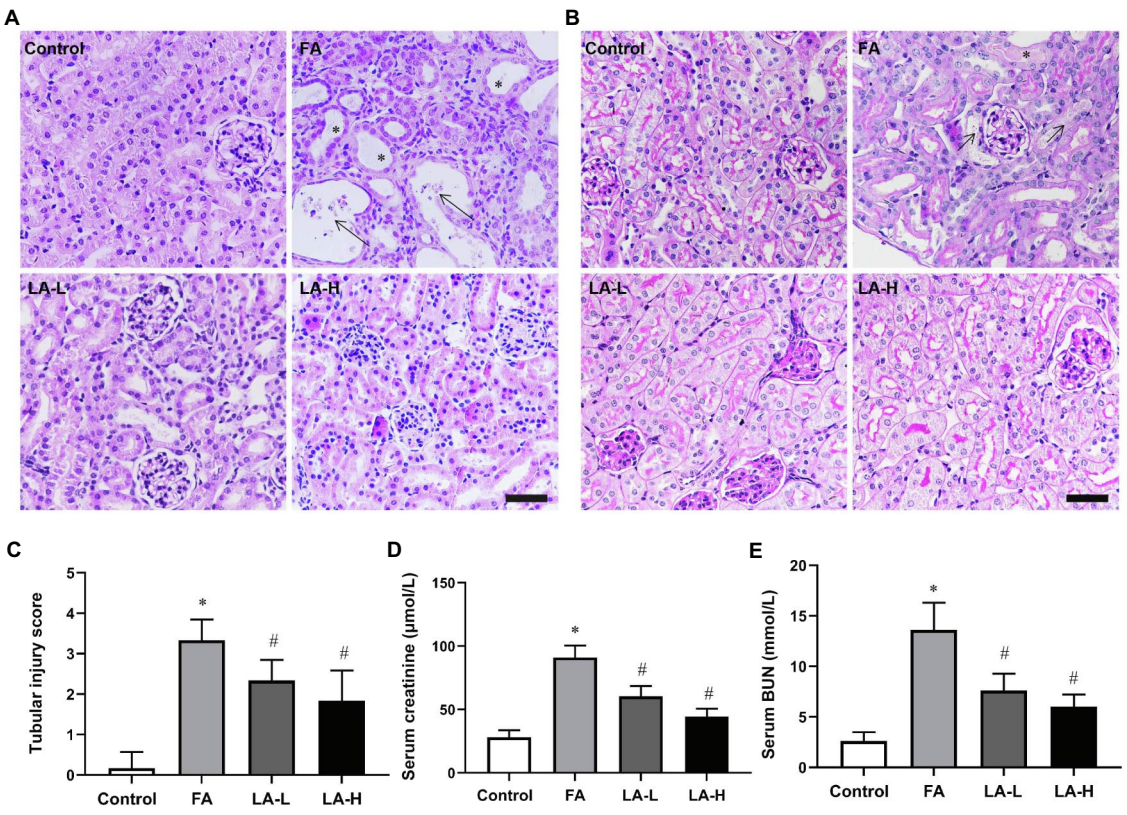

FIGURE 1 | The protective effects of lipoic acid (LA) supplementation on folic acid (FA)-induced acute kidney injury (AKI). FA group mice are given an intraperitoneal injection of FA at 250 mg/kg body weight once, without or with LA-L (50 mg/kg body weight) or LA-H (100 mg/kg body weight) supplementation. **(A)** Representative images of hematoxylin and eosin (H&E) staining, showing the histological changes in FA-induced AKI and the LA-treated groups. Bar = 50 μm. Asterisks for dilated tubule; arrows for necrotic tubular epithelial cells. **(B)** Renal damage is assessed by Periodic acid-Schiff (PAS) staining. Bar = 50 μm. Asterisks for tubular ectasia and arrows for tubules with cells in necrosis and cellular debris. **(C)** Renal tubular injury scores on the basis of H&E staining. The renal function is evaluated by **(D)** serum creatinine and **(E)** serum blood urea nitrogen (BUN) levels. For the FA group vs. the control group, *indicates $p < 0.05$, and **indicates $p < 0.01$. For the LA-treated groups vs. the FA group, #indicates $p < 0.05$, and ##indicates $p < 0.01$.

while the effect was blocked by LA supplementation. Moreover, western blotting data confirmed that FA injection induced the increased expression of KIM-1, which was alleviated by LA supplementation in a dose-dependent manner, but no particular preference for the higher-dose group. Consistent with the protein levels, gene expression studies disclosed increased mRNA level of KIM-1 after FA injection, which was inhibited by LA supplementation. The results are summarized in **Figure 2**.

LA Supplementation Alleviated Inflammation in FA-Induced AKI

Considering the key role of inflammation in FA-induced AKI, we evaluated the release of pro-inflammatory factors and the infiltration of inflammatory cells using IHC staining. The results showed that FA injection markedly enhanced the secretion of TNF-α and IL-1β in the tubular epithelium, together with the increased infiltration of macrophage in the interstitial space, whereas LA supplementation downregulated the levels of these molecules. To corroborate our IHC data, western blotting experiments for TNF-α and IL-1β showed that their expressions were significantly increased after FA injection, which were alleviated by LA supplementation but without significant difference between the two dose groups, shown in **Figure 3**.

Effect of LA Supplementation on Iron Accumulation in FA-Induced AKI

Disorder of iron metabolism was the main cause of FA-induced AKI (Martin-Sanchez et al., 2017). To validate the protective effect of LA supplementation, iron deposits and distribution in the kidney was assessed. With iron staining where the deposits of iron were visualized, there were more iron-positive cells in the tubule of FA-injected kidney, while LA-treated kidney showed less iron-positive cells, compared to those normal cells in control group; But there was no statistical difference between the two LA-treated groups. Consistently, the content of iron in the kidney of LA-treated mice was less as compared to that in FA-injected mice.

To explore the possible mechanism associated with the altered iron accumulation, the levels of Ferritin and FPN were analyzed. IHC staining revealed that Ferritin was diffusely distributed in the cytoplasm of tubular epithelial cells of the control mice,

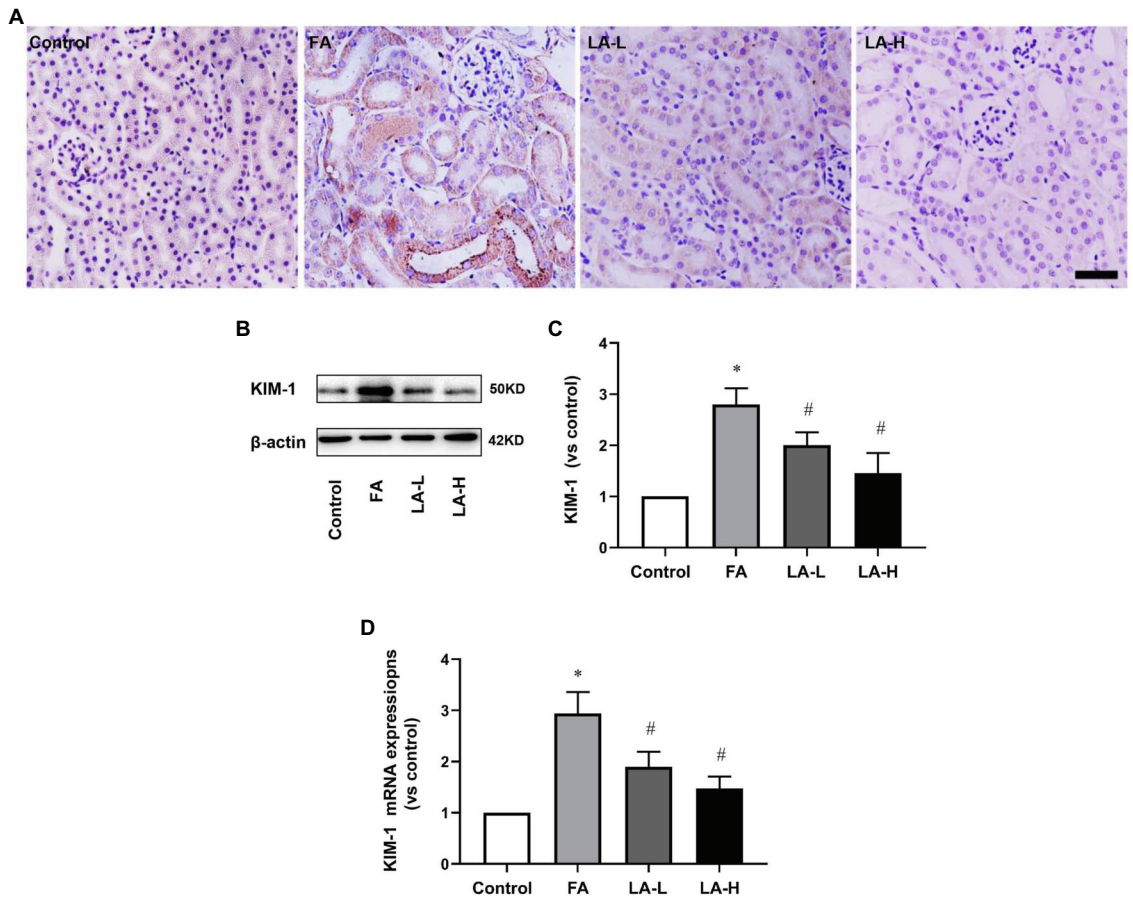

FIGURE 2 | The effect of LA supplementation on acute tubular damage caused by FA injection. Mice are treated as described in **Figure 1**. **(A)** Representative images of immunohistochemical (IHC) staining for KIM-1. Bar = 50 μm. **(B)** Renal tubular damage marker, KIM-1 expression, as determined by western blotting. **(C)** Semi-quantitative assessments of KIM-1. **(D)** The expression of KIM-1 gene, as determined by relative mRNA expression. For the FA group vs. the control group, *indicates $p < 0.05$, and **indicates $p < 0.01$. For the LA-treated groups vs. the FA group, #indicates $p < 0.05$, and ##indicates $p < 0.01$.

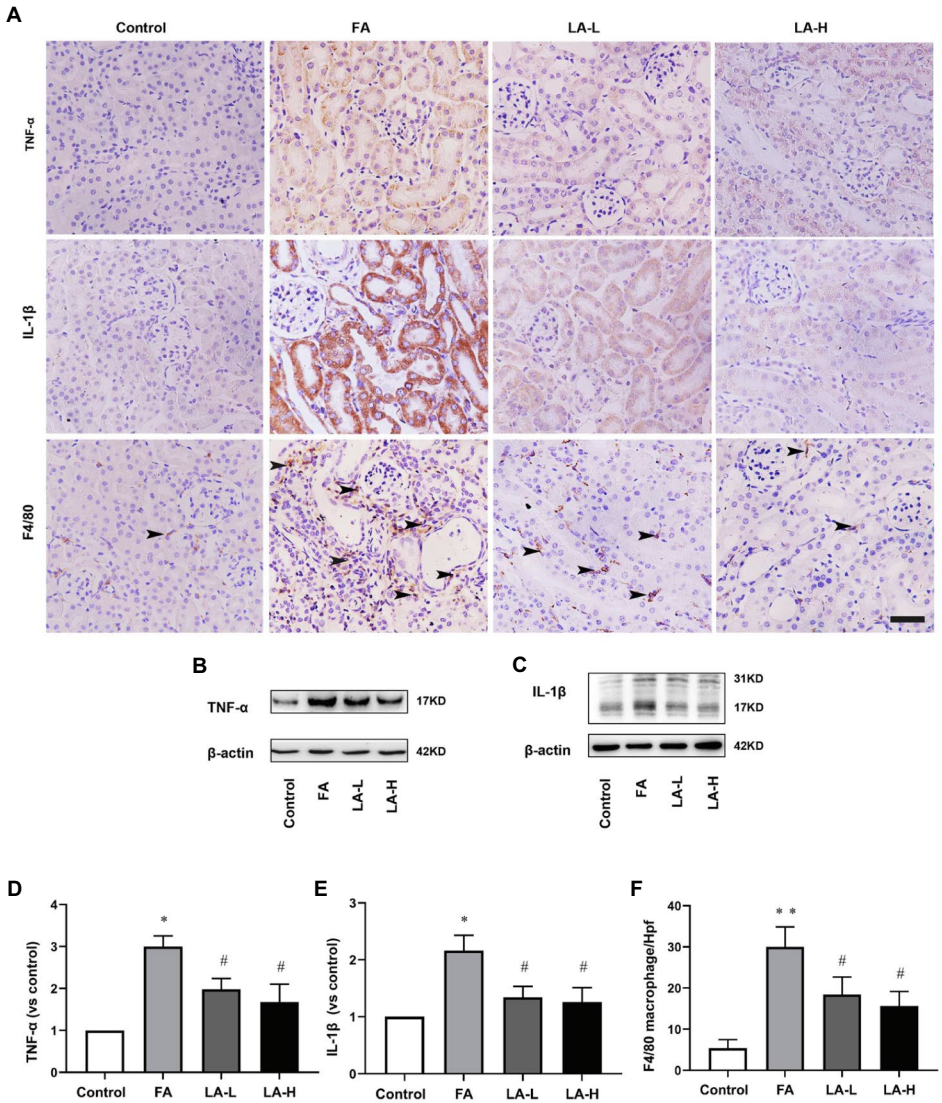

FIGURE 3 | Lipoic acid supplementation reduces release of TNFα and IL-1β, as well as macrophage infiltration caused by FA injection. Mice are treated as described in **Figure 1**. **(A)** Representative images of IHC staining for TNF-α (brown), IL-1β (brown), and macrophages (brown). Bar = 50 μm. Black arrow heads for F4/80-positive interstitial macrophages. **(B)** The expression of inflammatory marker TNF-α, as determined by western blotting. **(C)** The expression of inflammatory marker IL-1β, as determined by western blotting. **(D)** Semi-quantitative assessments of TNF-α. **(E)** Semi-quantitative assessments of IL-1β. **(F)** The number of macrophages per high-power field (Hpf). For the FA group vs. the control group, *indicates $p < 0.05$, and **indicates $p < 0.01$. For the LA-treated groups vs. the FA group, #indicates $p < 0.05$, and ##indicates $p < 0.01$.

while Ferritin was significantly downregulated in FA-injected mice, which was reversed by LA supplementation. A similar result was observed in western blotting analysis that LA treated-mice in a dose-dependent trend increased Ferritin expression compared with FA-injected mice, but without obvious statistical significance between the two dose groups. Meanwhile, western blotting analysis showed that FA injection decreased the expression of FNP, which could be restored by LA supplementation. These results revealed that LA supplementation might enhance iron storage and promote iron turnover by upregulating Ferritin and FPN, therefore reducing iron accumulation, as shown in **Figure 4**.

Effect of LA Supplementation on Anti-oxidative Stress in FA-Induced AKI

Oxidative stress has been demonstrated to be the key element to induce AKI (Li et al., 2020b), therefore, we further evaluated the levels of ROS in the kidney. The results showed that the production of ROS in LA-treated mice was lower than that in FA-injected mice. In addition, IHC staining demonstrated that the intensity of 4-HNE, reflecting the lipid perioxidation, was higher after FA injection, while LA supplementation significantly downregulated the intensity of 4-HNE. To address the issue, western blotting analysis was

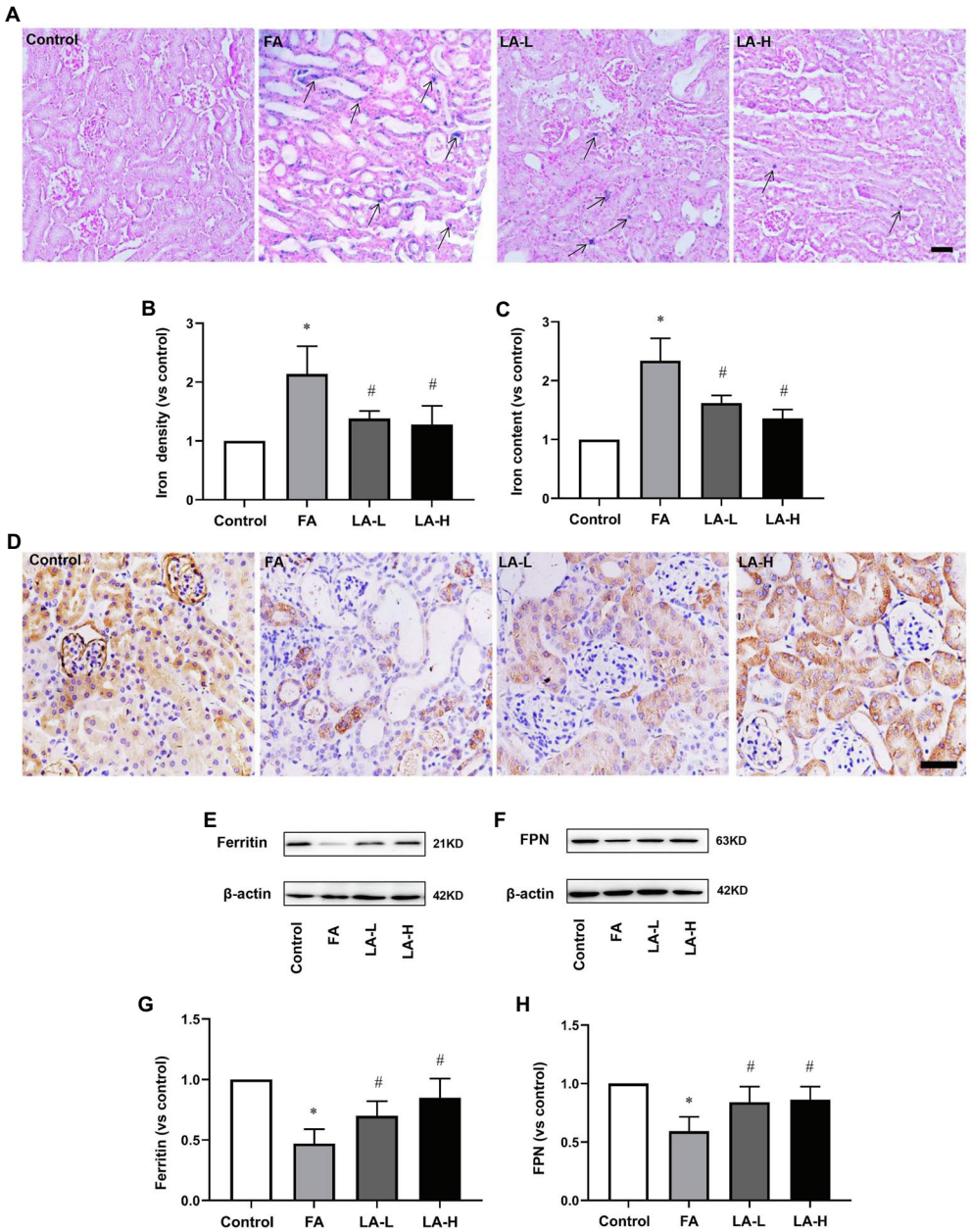

FIGURE 4 | Lipoic acid supplementation alleviates iron accumulation caused by FA injection. Mice are treated as described in **Figure 1**. **(A)** Representative images of Perl's staining. Arrows for iron accumulation. Bar = 50 μm. **(B)** Quantitative assessment of iron staining. **(C)** Iron content of kidney tissue. **(D)** Representative images of IHC staining for Ferritin (brown). **(E)** The expression of iron storage marker Ferritin, as determined by western blotting. **(F)** The expression of iron exporter marker ferroportin (FPN), as determined by western blotting. **(G)** Semi-quantitative assessments of Ferritin. **(H)** Semi-quantitative assessments of FPN. For the FA group vs. the control group, *indicates $p < 0.05$, and **indicates $p < 0.01$. For the LA-treated groups vs. the FA group, #indicates $p < 0.05$, and ##indicates $p < 0.01$.

further performed to confirm that there were obvious decreased level of 4-HNE in LA-treated mice, compared with FA-injected ones, but no significant difference between the high- and low-dose groups was observed, as shown in **Figure 5**.

We further examined the levels of GPX4 and xCT, two important antioxidants related to anti-oxidative stress. IHC staining analyses showed that GPX4 and xCT were mostly expressed in tubular epithelium, while FA injection reduced the levels of GPX4 and xCT, which can be reversed by LA supplementation. Similarly, western blotting analysis confirmed that the expression of GPX4 in LA treated-mice was upregulated in a dose-dependent manner, compared with downregulation in FA injected-mice, although there was no significant statistical difference between two dose groups. In addition, the xCT activity of mice treated with high-dose LA was enhanced

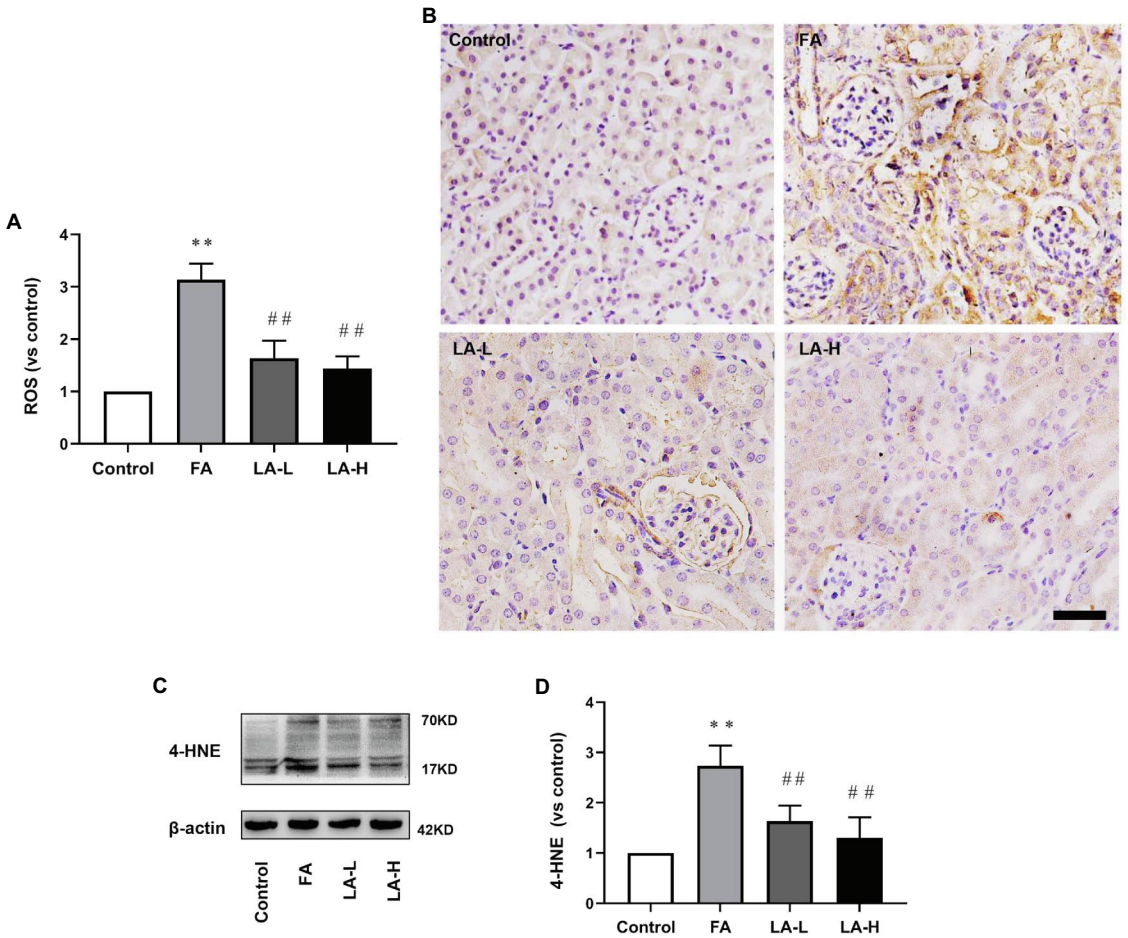

FIGURE 5 | Lipoic acid supplementation decreases oxidative stress caused by FA injection. Mice are treated as described in **Figure 1**. **(A)** Reactive oxygen species (ROS) level in the kidney. **(B)** Representative images of IHC staining for 4-HNE (brown). Bar = 50 μm. **(C)** The expression of lipid peroxidation marker 4-HNE, as determined by western blotting. **(D)** Semi-quantitative assessments of 4-HNE. For the FA group vs. the control group, *indicates $p < 0.05$, and **indicates $p < 0.01$. For the LA-treated groups vs. the FA group, #indicates $p < 0.05$, and ##indicates $p < 0.01$.

compared with mice injected with FA, but there was no significant increase in activity compared with mice treated with low-dose LA. Furthermore, we evaluated the effect of LA on the content of GSH, the synthesis of which was mediated by xCT. The results showed a downregulated level of GSH in FA injection, and this effect was blocked by LA supplementation, consistent with the level of xCT, as shown in **Figure 6**.

Altogether, the results indicated that LA protected the kidney from FA-induced oxidative stress damage, which may be closely related to the maintenance of the antioxidant defenses system.

Effect of LA Supplementation on Ferroptosis in FA-Induced AKI

Iron-dependent lipid perioxidation could cause cell necrosis in tubular epithelium (Conrad et al., 2018). We further explored FA-induced tubular cell death using TUNEL staining. As depicted in **Figure 7**, we found that there were more TUNEL-positive tubular cells in the FA group, and the number of TUNEL-positive tubular cells in the low-dose and high-dose LA treatment groups was significantly reduced, while there was no particular preference for the higher-dose group. This indicated that LA could reduce ferroptosis-mediated tubular cell death without significant dose dependence.

LA Supplementation Prevented FA-Induced xCT Reduction by Inhibiting p53 Activation

P53 served as a major factor of cellular ferroptosis that respond to various injuries, and we further examined whether LA can protect from ferroptosis that was associated with p53 activation in tubular epithelial cells. As shown in **Figure 8**, western blotting analyses indicated that FA injection elevated the expression of p53, which could be declined by LA supplementation in a dose-dependent manner. Meanwhile, the level of p53 mRNA displayed a similar response. Moreover, IHC staining showed that FA not only induced the expression of p53 but also promoted p53 abundance in nucleus. As compared to the FA group, LA supplementation significantly

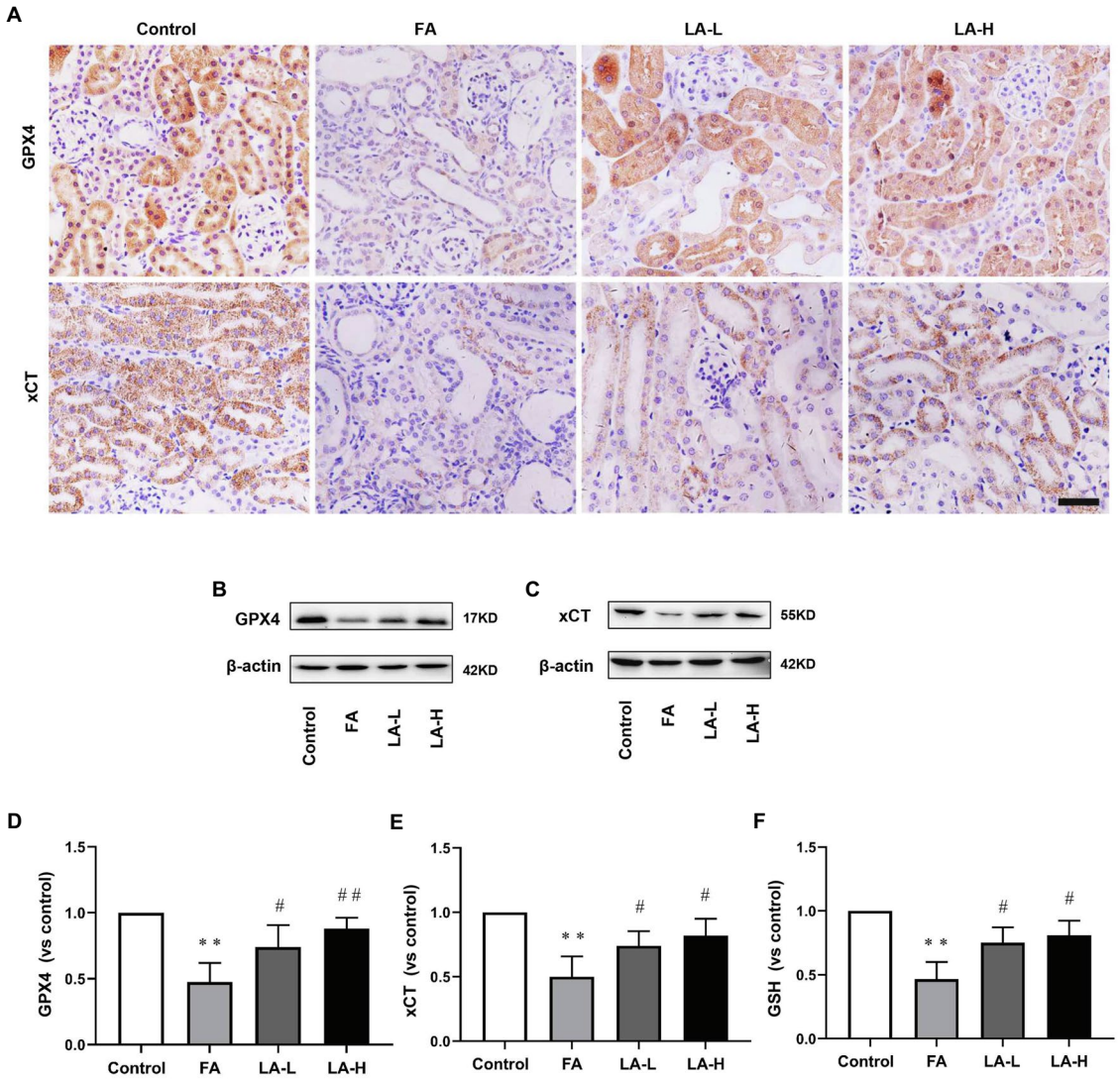

FIGURE 6 | Lipoic acid supplementation increases FA-induced reduction in antioxidants. Mice are treated as described in **Figure 1**. **(A)** Representative images of IHC staining for GPX4 (brown) and xCT (brown). Bar = 50 μm. **(B)** The expression of anti-oxidative enzyme marker GPX4, as determined by western blotting. **(C)** The expression of cystine/glutamate transporter xCT, as determined by western blotting. **(D)** Semi-quantitative assessments of GPX4. **(E)** Semi-quantitative assessments of xCT. **(F)** The levels of antioxidant glutathione (GSH) content. For the FA group vs. the control group, *indicates $p < 0.05$, and **indicates $p < 0.01$. For the LA-treated groups vs. the FA group, #indicates $p < 0.05$, and ##indicates $p < 0.01$.

downregulated the trans-location of p53 into the nuclei. This implied that LA supplementation may increase xCT expression by inhibiting p53 activation.

DISCUSSION

A growing evidence has suggested that regulated necrosis could induce numerous inflammation and serves as a therapeutic target of AKI (Lin and Hsu, 2020). Ferroptosis, an oxidative stress-dependent programmed cell death, played an important role in FA-induced AKI (Martin-Sanchez et al., 2017; Li et al., 2020). Moreover, FA-induced AKI was the main model of nephrotoxic AKI that was usually established by intraperitoneally injected FA at the dose of 250 mg/kg (Diego et al., 2017), but the concentration was not demonstrated. In our study, FA 250 mg/kg at the concentration of 12.5 mg/ml was selected to induce AKI due to the higher concentration of FA (25 or 50 mg/ml) could induce the death of mice.

Lipoic acid is a well-known antioxidative agent that can be used clinically to treat DM and neurodegenerative diseases, closely related to reducing the risk of occurrence of complication and mortality (Singh and Jialal, 2008; Molz and Schroder, 2017; Liakopoulos et al., 2019). What is more, LA has been used to protect against LPS or I/R induced AKI *via* anti-inflammation (Bae et al., 2009; Li et al., 2015; Zhang and McCullough, 2016). However, whether LA could exert the protective role in FA-induced AKI, its dosage and underlying

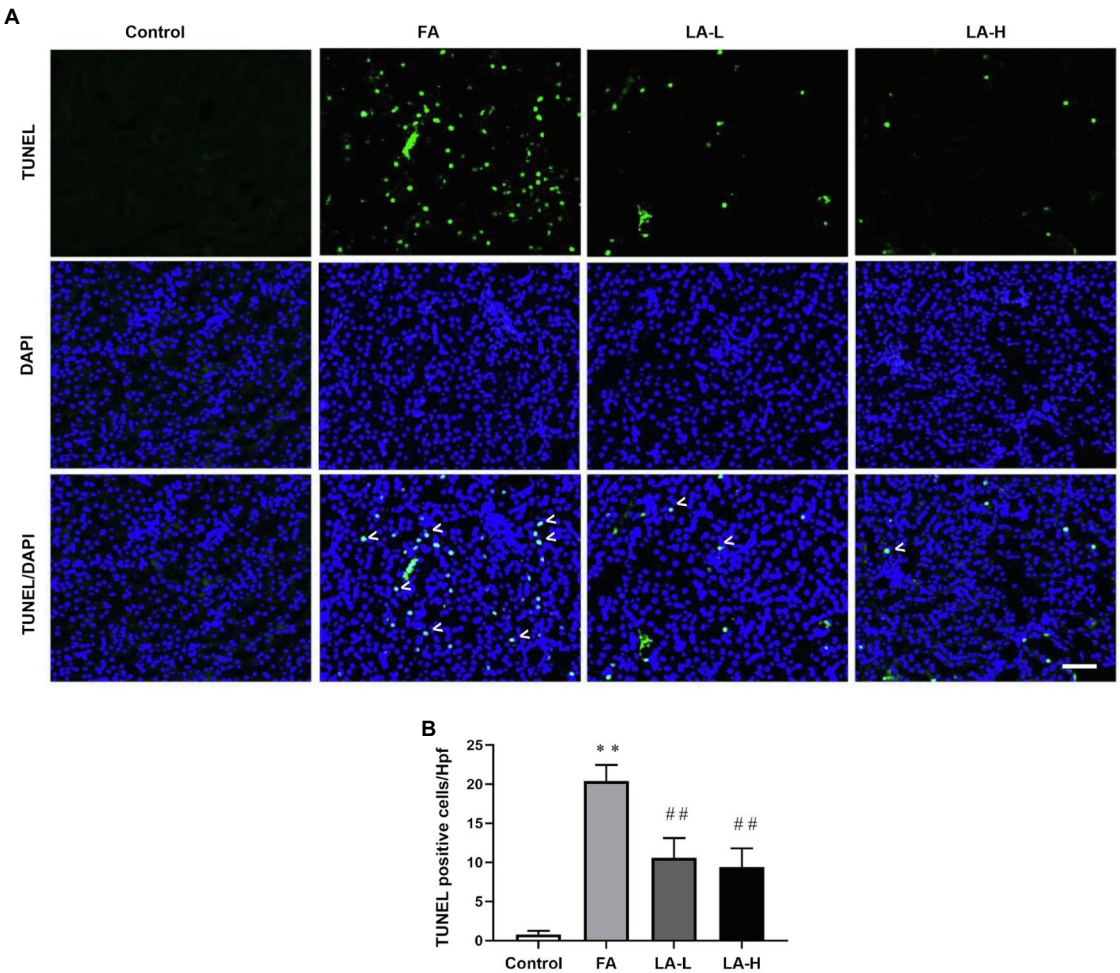

FIGURE 7 | Lipoic acid supplementation decreases ferroptosis-mediated tubular cells death caused by FA injection. Mice are treated as described in **Figure 1**. **(A)** Representative images by TUNEL staining, showing the ferroptosis-mediated tubular cell death. White arrowheads for TUNEL-positive tubular cells (green) on kidney tissue sections; nuclei are labeled with DAPI (blue). Bar = 50 μm. **(B)** The number of TUNEL-positive nuclei per high-power field (Hpf). For the FA group vs. the control group, *indicates $p < 0.05$, and **indicates $p < 0.01$. For the LA-treated groups vs. the FA group, #indicates $p < 0.05$, and ##indicates $p < 0.01$.

mechanism remained unknown. In the present study, FA injection induced the production of massive inflammation. Meanwhile, FA administration could significantly increase the levels of FEK and FENa, probably due to the damage to proximal tubular cells and impaired Na^+/K^+-ATPase. In addition, a decrease was seen in urinary volume, GFR, and filtration fraction in the FA group, followed by an increase in the concentrations of BUN and Cr. While LA (50 or 100 mg/kg) supplementation could significantly reduce histological damage and inflammation, and alters tubular water, sodium, and potassium handling, improving the renal function. It was in conjunction with the previous findings that treatment with LA (50 mg/kg) could suppress UUO-induced tubular interstitial fibrosis in mice by ameliorating the epithelial mesenchymal transition (Hyun et al., 2016). In contrast, lower dose of LA (25 mg/kg) was not found to ameliorate renal dysfunction in our study. Furthermore, the effect of LA (50 mg/kg or 100 mg/kg) on healthy animals was evaluated in the preliminary experiment, and no changes of renal morphology and function were found in the healthy mice after oral medications of LA (shown in **Supplementary Figure 1**).

Ferroptosis was the main tubular cell death that can significantly amplify inflammation. It is characterized by increased iron accumulation, leading to toxic ROS generation by the Fenton reaction (Lei et al., 2019). In our study, there was a large number of iron-positive staining tubular epithelial cells after FA over-injection. At the same time, the iron content in the kidney of FA-injected mice was statistically increment. Importantly, LA supplementation ameliorated renal injury accompanied with decreased iron accumulation. Furthermore, we demonstrated that the levels of Ferritin (a protein complex involved in intracellular iron storage) in the kidney were decreased after FA injection, while LA supplementation reversed the decreased levels. This indicated that the protective effects of LA on FA-induced AKI may increase iron storage by upregulation of Ferritin. Our study was in line with the previous

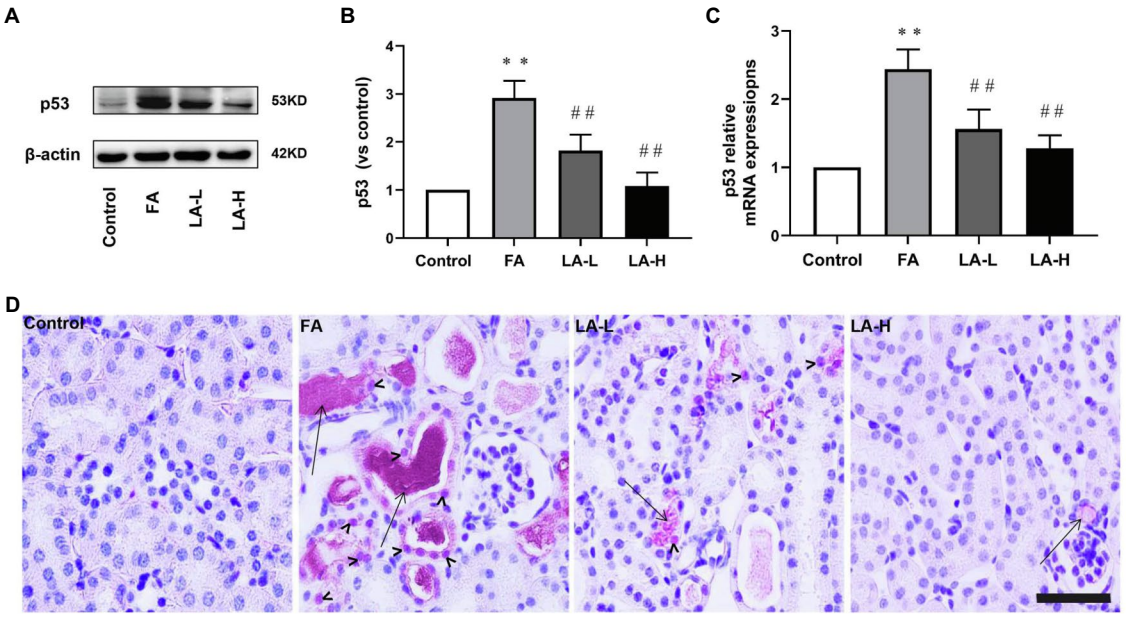

FIGURE 8 | Lipoic acid supplementation inhibits the activation of p53 caused by FA injection. Mice are treated as described in **Figure 1**. **(A)** The expression for p53, as determined by western blotting. **(B)** Semi-quantitative assessments of p53. **(C)** The expression of p53 gene, as determined by relative mRNA expression. **(D)** Representative images of IHC staining for p53 activation. Bar = 50 μm. Black arrow heads for p53 nuclear staining; black arrows for folic acid crystals in tubular lumen. For the FA group vs. the control group, *indicates $p < 0.05$, and **indicates $p < 0.01$. For the LA-treated groups vs. the FA group, #indicates $p < 0.05$, ##indicates $p < 0.01$.

study that upregulation of FTH could alleviate cisplatin induced HK2 cell injury through anti-ferroptosis (Hu et al., 2020). In addition, it has been reported that Ferritin degradation caused by increased autophagy can promote ferroptosis in fibroblasts and cancer cells (Hou et al., 2016). In addition, excessive iron could be exported through the iron efflux pump, FPN, thereby reducing intracellular iron overload (Geng et al., 2018). Accumulating evidences suggested the critical role of FPN in preventing neurodegenative disease caused by ferroptosis (Raha et al., 2013). Down this line, we observed that FA administration induced a transient decrease in FPN expression, while LA supplementation significantly upregulated FPN levels, thereby accelerating mobilization of excessive iron out of tubular cells and reducing intracellular iron overload. In this regard, LA may exert the effect of anti-ferroptosis through chelating intracellular excess iron and mediating iron turnover in tubule of the mouse kidney.

Of note, LA has been reported to act as a direct free radical scavenger that alleviated oxidative stress (Aruoma, 1998). In support of this, we demonstrated that LA supplementation could scavenge ROS and mitigate lipid peroxidation, which further reduced number of ferroptotic tubular cells. Furthermore, we found that LA could elevate the level of GSH, which was consistent with the research that macrophage migration inhibitory factor (MIF) increased intracellular GSH content which protected against oxidative damage of tubular epithelial cell *in vivo* and *in vitro* (Unruh et al., 2019). In addition, another study showed that deferoxamine could alleviate ferroptosis to promote recovery of traumatic spinal cord injury through upregulation of GSH (Yao et al., 2019). On the other hand, several investigators found that treatment with erastin could inhibit system xCT, thereby reducing extracellular cystine import for GSH synthesis and increasing the sensitivity to ferroptosis (Wang et al., 2020). Consistently, we found that the expression of xCT in the kidney was significantly downregulated induced by FA injection, which was closely related to the decrease in GSH levels. Moreover, inhibition of system xCT could lower the activity of GPX4, the vital antioxidant enzyme which allowed for blocking ferroptosis through reducing lipid hydroperoxides (Liu et al., 2017). It has been reported that GPX4 knockout mice could increase the sensitivity of the kidney to ferroptosis caused by IRI (Linkermann et al., 2014). Recovery of the expression of GPX4 has been demonstrated to alleviate ferroptosis in cardiomyocytes and neurons caused by I/R (Seibt et al., 2019; Stamenkovic et al., 2019). Correspondingly, our study found that ferroptosis induced by FA injection was accompanied by downregulation of system xCT, leading to the depletion of GSH, which in turn decreased the expression of GPX4.

Several studies indicated that p53 activation was associated with the inhibition of system xCT (Jiang et al., 2015). It was generally considered that p53 activity exerted anti-tumor effect by regulating apoptosis or cell-cycle arrest (Chen, 2016). In addition, the document has implicated that p53 expression was induced in response to cellular insults, which could accelerate neuron cell death (Morrison and Kinoshita, 2000). Emerging evidence validated that p53 activation played a critical role in mediating ferroptosis (Wang et al., 2016). Ling et al. discovered that inhibition of p53 could defend against liver fibrosis *via*

reducing ferroptosis (Krstic et al., 2018). What is more, p53 activation in renal tubular epithelial cells was closely related to the deterioration of AKI (Zhang et al., 2014). As mentioned above, we explored the potential mechanisms of FA-induced system xCT suppression and found higher p53 activation in tubular cells induced by FA administration, while LA supplementation blocked the activity of p53 and abrogated the pro-ferroptosis effects. Therefore, p53-mediated ferroptosis in tubular epithelial cell may be a therapeutic target for alleviating AKI.

Taken together, our study demonstrated that ferroptosis played an important role in AKI induced by FA overdose injection in mice, which could be alleviated by LA supplementation, indicating that LA may be used as a potential therapeutic approach to ameliorate AKI caused by drugs or toxicants in the clinic. In our study, LA could be used as an anti-ferroptosis agent to reduce iron overload caused by FA injection through upregulation of Ferritin and FPN. Besides, LA supplementation could restore of the expression of system xCT, thereby promoting the synthesis of GSH and subsequently enhancing the activity of GPX4. Finally, we identified that inactivation of p53 was the key mechanism involved in restoring the expression of system xCT, thus suggesting the beneficial effects of LA on anti-ferroptosis in FA-induced AKI.

DATA AVAILABILITY STATEMENT

The raw data supporting the conclusions of this article will be made available by the authors, without undue reservation.

ETHICS STATEMENT

The animal study was reviewed and approved by China Medical University.

AUTHOR CONTRIBUTIONS

XL wrote the manuscript. X-YZ conceived and designed the experiments. YZ analyzed the data. Y-YF collected and provided the sample for this study. JX revised this manuscript. K-YW did the statistics. All authors contributed to the article and approved the submitted version.

FUNDING

The work was financially supported by the National Natural Science Foundation of China (contract no. 31971115).

ACKNOWLEDGMENTS

We would like to acknowledge the reviewers for their helpful comments on this study.

SUPPLEMENTARY MATERIAL

The Supplementary Material for this article can be found online at: https://www.frontiersin.org/articles/10.3389/fphys.2021.680544/full#supplementary-material

Supplementary Table 1 | Changes in renal function parameters due to FA overdose injection in mice and effect of LA supplementation. Data are collected after housing the mice in metabolic cages for the last 24 h. Urinary volume are obtained in individual metabolic cage. GFR mean glomerular filtration rate; Flitration fraction = GFR/plasma flow; and FENa mean fractional excretion of sodium and FEK mean fractional excretion of potassium. Data are presented as mean ± SE ($N = 5$). For the FA group vs. the control group, *indicates $p < 0.05$, and **indicates $p < 0.01$. For the LA-treated groups vs. the FA group, #indicates $p < 0.05$, and ##indicates $p < 0.01$.

Supplementary Figure 1 | No changes of renal morphology and function in the healthy mice after oral medications of LA (50 or 100 mg/kg). The healthy mice are given an oral administration of LA at 50 mg/kg (LA-50) or 100 mg/kg (LA-100). **(A)** Representative images of H&E staining, showing histological changes of healthy mice without or with LA 50 mg/kg (LA-50) or LA 100 mg/kg (LA-100) oral administration. **(B)** Representative images of PAS staining, showing histological changes of healthy mice without or with LA 50 mg/kg (LA-50) or LA 100 mg/kg (LA-100) oral administration. The renal function is evaluated by **(C)** serum creatinine and **(D)** serum BUN levels.

Supplementary Figure 2 | The original data of the western blotting.

REFERENCES

Aruoma, O. I. (1998). Free radicals, oxidative stress, and antioxidants in human health and disease. *J. Am. Oil Chem. Soc.* 75, 199–212. doi: 10.1007/s11746-998-0032-9

Ashour, R. H., Saad, M. A., Sobh, M. A., Al-Husseiny, F., Abouelkheir, M., Awad, A., et al. (2016). Comparative study of allogenic and xenogeneic mesenchymal stem cells on cisplatin-induced acute kidney injury in Sprague-Dawley rats. *Stem Cell Res. Ther.* 7:126. doi: 10.1186/s13287-016-0386-0

Bae, E. H., Lee, J., Ma, S. K., Kim, I. J., Frokiaer, J., Nielsen, S., et al. (2009). Alpha-Lipoic acid prevents cisplatin-induced acute kidney injury in rats. *Nephrol. Dial. Transplant.* 24, 2692–2700. doi: 10.1093/ndt/gfp176

Bellomo, R., Kellum, J. A., and Ronco, C. (2012). Acute kidney injury. *Lancet* 380, 756–766. doi: 10.1016/S0140-6736(11)61454-2

Brooks, C., Wei, Q., Cho, S. G., and Dong, Z, . (2009). Regulation of mitochondrial dynamics in acute kidney injury in cell culture and rodent models. *J. Clin. Invest.* 119, 1275–1285.

Brown, J. R., Hisey, W. M., Marshall, E. J., Likosky, D. S., Nichols, E. L., Everett, A. D., et al. (2016). Acute kidney injury severity and long-term readmission and mortality After cardiac surgery. *Ann. Thorac. Surg.* 102, 1482–1489. doi: 10.1016/j.athoracsur.2016.04.020

Cao, J., Chen, X., Jiang, L., Lu, B., Yuan, M., Zhu, D., et al. (2020). DJ-1 suppresses ferroptosis through preserving the activity of S-adenosyl homocysteine hydrolase. *Nat. Commun.* 11:1251. doi: 10.1038/s41467-020-15109-y

Chang, J. R., Ghafouri, M., Mukerjee, R., Bagashev, A., Chabrashvili, T., and Sawaya, B. E. (2012). Role of p53 in neurodegenerative diseases. *Neurodegener. Dis.* 9, 68–80. doi: 10.1159/000329999

Chen, J. (2016). The cell-cycle arrest and apoptotic functions of p53 in tumor initiation and progression. *Cold Spring Harb. Perspect. Med.* 6:a026104. doi: 10.1101/cshperspect.a026104

Cho, H. S., Kim, J. H., Jang, H. N., Lee, T. W., Jung, M. H., Kim, T. H., et al. (2017). Alpha-lipoic acid ameliorates the epithelial mesenchymal transition induced by unilateral ureteral obstruction in mice. *Sci. Rep.* 7:46065

Conrad, M., Kagan, V. E., Bayir, H., Pagnussat, G. C., Head, B., Traber, M. G., et al. (2018). Regulation of lipid peroxidation and ferroptosis in diverse species. *Genes Dev.* 32, 602–619. doi: 10.1101/gad.314674.118

de Seigneux, S., and Martin, P. Y. (2017). Preventing the progression of AKI to CKD: the role of mitochondria. *J. Am. Soc. Nephrol.* 28, 1327–1329. doi: 10.1681/ASN.2017020146

Geng, N., Shi, B. J., Li, S. L., Zhong, Z. Y., Li, Y. C., Xua, W. L., et al. (2018). Knockdown of ferroportin accelerates erastin-induced ferroptosis in neuroblastoma cells. *Eur. Rev. Med. Pharmacol. Sci.* 22, 3826–3836. doi: 10.26355/eurrev_201806_15267

Han, C., Liu, Y., Dai, R., Ismail, N., Su, W., and Li, B. (2020). Ferroptosis and its potential role in human diseases. *Front. Pharmacol.* 11:239. doi: 10.3389/fphar.2020.00239

Hou, W., Xie, Y., Song, X., Sun, X., Lotze, M. T., Zeh, H. J. 3rd, et al. (2016). Autophagy promotes ferroptosis by degradation of ferritin. *Autophagy* 12, 1425–1428. doi: 10.1080/15548627.2016.1187366

Hu, Z., Zhang, H., Yang, S. K., Wu, X., He, D., Cao, K., et al. (2019). Emerging role of Ferroptosis in acute kidney injury. *Oxidative Med. Cell. Longev.* 2019:8010614. doi: 10.1155/2019/8010614

Hu, Z., Zhang, H., Yi, B., Yang, S., Liu, J., Hu, J., et al. (2020). VDR activation attenuate cisplatin induced AKI by inhibiting ferroptosis. *Cell Death Dis.* 11:73. doi: 10.1038/s41419-020-2256-z

Jiang, L., Kon, N., Li, T., Wang, S. J., Su, T., Hibshoosh, H., et al. (2015). Ferroptosis as a p53-mediated activity during tumour suppression. *Nature* 520, 57–62. doi: 10.1038/nature14344

Krstic, J., Galhuber, M., Schulz, T. J., Schupp, M., and Prokesch, A. (2018). p53 as a dichotomous regulator of liver disease: the dose makes the medicine. *Int. J. Mol. Sci.* 19:921. doi: 10.3390/ijms19030921

Lei, P., Bai, T., and Sun, Y. (2019). Mechanisms of Ferroptosis and relations With regulated cell death: A review. *Front. Physiol.* 10:139. doi: 10.3389/fphys.2019.00139

Li, G., Fu, J., Zhao, Y., Ji, K., Luan, T., and Zang, B. (2015). Alpha-lipoic acid exerts anti-inflammatory effects on lipopolysaccharide-stimulated rat mesangial cells via inhibition of nuclear factor kappa B (NF-kappaB) signaling pathway. *Inflammation* 38, 510–519. doi: 10.1007/s10753-014-9957-3

Li, Y., Xia, W., Wu, M., Yin, J., Wang, Q., Li, S., et al. (2020b). Activation of GSDMD contributes to acute kidney injury induced by cisplatin. *Am. J. Physiol. Ren. Physiol.* 318, F96–F106. doi: 10.1152/ajprenal.00351.2019

Li, X., Zou, Y., Xing, J., Fu, Y. Y., Wang, K. Y., Wan, P. Z., et al. (2020a). Pretreatment with Roxadustat (FG-4592) attenuates folic acid-induced kidney injury through Antiferroptosis via Akt/GSK-3beta/Nrf2 pathway. *Oxidative Med. Cell. Longev.* 2020:6286984. doi: 10.1155/2020/6286984

Liakopoulos, V., Roumeliotis, S., Bozikas, A., Eleftheriadis, T., and Dounousi, E. (2019). Antioxidant supplementation in renal replacement therapy patients: is there evidence? *Oxidative Med. Cell. Longev.* 2019:9109473. doi: 10.1155/2019/9109473

Lim, J. K. M., Delaidelli, A., Minaker, S. W., Zhang, H. F., Colovic, M., Yang, H., et al. (2019). Cystine/glutamate antiporter xCT (SLC7A11) facilitates oncogenic RAS transformation by preserving intracellular redox balance. *Proc. Natl. Acad. Sci. U. S. A.* 116, 9433–9442. doi: 10.1073/pnas.1821323116

Lin, T. Y., and Hsu, Y. H. (2020). IL-20 in acute kidney injury: role in pathogenesis and potential as a therapeutic target. *Int. J. Mol. Sci.* 21:1009. doi: 10.3390/ijms21249751

Linkermann, A., Skouta, R., Himmerkus, N., Mulay, S. R., Dewitz, C., De Zen, F., et al. (2014). Synchronized renal tubular cell death involves ferroptosis. *Proc. Natl. Acad. Sci. U. S. A.* 111, 16836–16841. doi: 10.1073/pnas.1415518111

Liu, D. S., Duong, C. P., Haupt, S., Montgomery, K. G., House, C. M., Azar, W. J., et al. (2017). Inhibiting the system xC(−)/glutathione axis selectively targets cancers with mutant-p53 accumulation. *Nat. Commun.* 8:14844. doi: 10.1038/s41467-017-02320-7

Martin-Sanchez, D., Fontecha-Barriuso, M., Carrasco, S., Sanchez-Nino, M. D., Massenhausen, A. V., Linkermann, A., et al. (2018). TWEAK and RIPK1 mediate a second wave of cell death during AKI. *Proc. Natl. Acad. Sci. U. S. A.* 115, 4182–4187. doi: 10.1073/pnas.1716578115

Martin-Sanchez, D., Ruiz-Andres, O., Poveda, J., Carrasco, S., Cannata-Ortiz, P., Sanchez-Nino, M. D., et al. (2017). Ferroptosis, but not Necroptosis, is important in nephrotoxic folic acid-induced AKI. *J. Am. Soc. Nephrol.* 28, 218–229. doi: 10.1681/ASN.2015121376

Molz, P., and Schroder, N. (2017). Potential therapeutic effects of Lipoic acid on memory deficits related to aging and Neurodegeneration. *Front. Pharmacol.* 8:849. doi: 10.3389/fphar.2017.00849

Morrison, R. S., and Kinoshita, Y. (2000). The role of p53 in neuronal cell death. *Cell Death Differ.* 7, 868–879. doi: 10.1038/sj.cdd.4400741

Mumbauer, S., Pascual, J., Kolotuev, I., and Hamaratoglu, F. (2019). Ferritin heavy chain protects the developing wing from reactive oxygen species and ferroptosis. *PLoS Genet.* 15:e1008396. doi: 10.1371/journal.pgen.1008396

Pinheiro, K. H. E., Azedo, F. A., Areco, K. C. N., and Laranja, S. M. R. (2019). Risk factors and mortality in patients with sepsis, septic and non septic acute kidney injury in ICU. *J. Bras. Nefrol.* 41, 462–471. doi: 10.1590/2175-8239-JBN-2018-0240

Raha, A. A., Vaishnav, R. A., Friedland, R. P., Bomford, A., and Raha-Chowdhury, R. (2013). The systemic iron-regulatory proteins hepcidin and ferroportin are reduced in the brain in Alzheimer's disease. *Acta Neuropathol. Commun.* 1:55. doi: 10.1186/2051-5960-1-55

Ronco, C., Bellomo, R., and Kellum, J. A. (2019). Acute kidney injury. *Lancet* 394, 1949–1964. doi: 10.1016/S0140-6736(19)32563-2

Santos, R. P. D., Carvalho, A. R. S., Peres, L. A. B., Ronco, C., and Macedo, E. (2019). An epidemiologic overview of acute kidney injury in intensive care units. *Rev. Assoc. Med. Bras.* 65, 1094–1101. doi: 10.1590/1806-9282.65.8.1094

Seibt, T. M., Proneth, B., and Conrad, M. (2019). Role of GPX4 in ferroptosis and its pharmacological implication. *Free Radic. Biol. Med.* 133, 144–152. doi: 10.1016/j.freeradbiomed.2018.09.014

Singh, U., and Jialal, I. (2008). Alpha-lipoic acid supplementation and diabetes. *Nutr. Rev.* 66, 646–657. doi: 10.1111/j.1753-4887.2008.00118.x

Stamenkovic, A., Pierce, G. N., and Ravandi, A. (2019). Phospholipid oxidation products in ferroptotic myocardial cell death. *Am. J. Physiol. Heart Circ. Physiol.* 317, H156–H163. doi: 10.1152/ajpheart.00076.2019

Su, L., Jiang, X., Yang, C., Zhang, J., Chen, B., Li, Y., et al. (2019). Pannexin 1 mediates ferroptosis that contributes to renal ischemia/reperfusion injury. *J. Biol. Chem.* 294, 19395–19404. doi: 10.1074/jbc.RA119.010949

Swaminathan, S. (2018). Iron homeostasis pathways as therapeutic targets in acute kidney injury. *Nephron* 140, 156–159. doi: 10.1159/000490808

Tang, C., Ma, Z., Zhu, J., Liu, Z., Liu, Y., Liu, Y., et al. (2019). P53 in kidney injury and repair: mechanism and therapeutic potentials. *Pharmacol. Ther.* 195, 5–12. doi: 10.1016/j.pharmthera.2018.10.013

Unruh, M., Wagner, B., and Hallows, K. R. (2019). MIF matters: the macrophage migration inhibitory factor and kidney injury. *Am. J. Kidney Dis.* 73, 429–431. doi: 10.1053/j.ajkd.2018.07.003

Wang, S. J., Li, D., Ou, Y., Jiang, L., Chen, Y., Zhao, Y., et al. (2016). Acetylation is crucial for p53-mediated Ferroptosis and tumor suppression. *Cell Rep.* 17, 366–373. doi: 10.1016/j.celrep.2016.09.022

Wang, L., Liu, Y., Du, T., Yang, H., Lei, L., Guo, M., et al. (2020). ATF3 promotes erastin-induced ferroptosis by suppressing system xc(.). *Cell Death Differ.* 27, 662–675. doi: 10.1038/s41418-019-0380-z

Yang, W. S., SriRamaratnam, R., Welsch, M. E., Shimada, K., Skouta, R., Viswanathan, V. S., et al. (2014). Regulation of ferroptotic cancer cell death by GPX4. *Cell* 156, 317–331. doi: 10.1016/j.cell.2013.12.010

Yao, X., Zhang, Y., Hao, J., Duan, H. Q., Zhao, C. X., Sun, C., et al. (2019). Deferoxamine promotes recovery of traumatic spinal cord injury by inhibiting ferroptosis. *Neural Regen. Res.* 14, 532–541. doi: 10.4103/1673-5374.245480

Yu, H., Guo, P., Xie, X., Wang, Y., and Chen, G. (2017). Ferroptosis, a new form of cell death, and its relationships with tumourous diseases. *J. Cell. Mol. Med.* 21, 648–657. doi: 10.1111/jcmm.13008

Zarjou, A., Bolisetty, S., Joseph, R., Traylor, A., Apostolov, E. O., Arosio, P., et al. (2013). Proximal tubule H-ferritin mediates iron trafficking in acute kidney injury. *J. Clin. Invest.* 123, 4423–4434. doi: 10.1172/JCI67867

Zhang, W., Gai, C., Ding, D., Wang, F., and Li, W. (2018a). Targeted p53 on small-molecules-induced Ferroptosis in cancers. *Front. Oncol.* 8:507. doi: 10.3389/fonc.2018.00507

Zhang, R., Ji, J., Zhou, X., and Li, R. (2020). Irisin Pretreatment protects kidneys against acute kidney injury induced by ischemia/reperfusion via Upregulating the expression of uncoupling protein 2. *Biomed. Res. Int.* 2020:6537371. doi: 10.1155/2020/3170927

Zhang, D., Liu, Y., Wei, Q., Huo, Y., Liu, K., Liu, F., et al. (2014). Tubular p53 regulates multiple genes to mediate AKI. *J. Am. Soc. Nephrol.* 25, 2278–2289. doi: 10.1681/ASN.2013080902

Zhang, J., and McCullough, P. A. (2016). Lipoic acid in the prevention of acute kidney injury. *Nephron* 134, 133–140. doi: 10.1159/000448666

Zhang, Y. H., Wang, D. W., Xu, S. F., Zhang, S., Fan, Y. G., Yang, Y. Y., et al. (2018b). Alpha-Lipoic acid improves abnormal behavior by mitigation of oxidative stress, inflammation, ferroptosis, and tauopathy in P301S tau transgenic mice. *Redox Biol.* 14, 535–548. doi: 10.1016/j.redox.2017.11.001

Zhao, W., Zhang, L., Chen, R., Lu, H., Sui, M., Zhu, Y., et al. (2018). SIRT3 protects Against acute kidney injury via AMPK/mTOR-regulated autophagy. *Front. Physiol.* 9:1526. doi: 10.3389/fphys.2018.01526

Conflict of Interest: The authors declare that the research was conducted in the absence of any commercial or financial relationships that could be construed as a potential conflict of interest.

Publisher's Note: All claims expressed in this article are solely those of the authors and do not necessarily represent those of their affiliated organizations, or those of the publisher, the editors and the reviewers. Any product that may be evaluated in this article, or claim that may be made by its manufacturer, is not guaranteed or endorsed by the publisher.

Advantages of publishing in Frontiers

OPEN ACCESS
Articles are free to read for greatest visibility and readership

FAST PUBLICATION
Around 90 days from submission to decision

HIGH QUALITY PEER-REVIEW
Rigorous, collaborative, and constructive peer-review

TRANSPARENT PEER-REVIEW
Editors and reviewers acknowledged by name on published articles

Frontiers
Avenue du Tribunal-Fédéral 34
1005 Lausanne | Switzerland

Visit us: www.frontiersin.org
Contact us: frontiersin.org/about/contact

REPRODUCIBILITY OF RESEARCH
Support open data and methods to enhance research reproducibility

DIGITAL PUBLISHING
Articles designed for optimal readership across devices

FOLLOW US
@frontiersin

IMPACT METRICS
Advanced article metrics track visibility across digital media

EXTENSIVE PROMOTION
Marketing and promotion of impactful research

LOOP RESEARCH NETWORK
Our network increases your article's readership